LIFE IN EXTREME ENVIRONMENTS: LANTHANIDE-BASED DETECTION OF BACTERIAL SPORES AND OTHER SENSOR DESIGN PURSUITS

Thesis by

Morgan L. Cable

In Partial Fulfillment of the Requirements

for the Degree of

Doctor of Philosophy

California Institute of Technology

Pasadena, California

2010

(Defended May 3, 2010)

"Lanthanons – these elements perplex us in our researches, baffle us in our speculations, and haunt us in our very dreams. They stretch like an unknown sea before us; mocking, mystifying and murmuring strange revelations and possibilities."

Sir William Crookes, in an address to the Royal Society, February 1887

ACKNOWLEDGMENT

The work presented in this dissertation would not have been possible if not for the guidance and support of many; for any I have inadvertently omitted here, I sincerely apologize. First I must thank my better half Josh for his endless understanding, patience, encouragement and love. My life would not be complete without my triplet siblings, Casey and Matt, who helped me evolve into who I am, and made me realize who I want to be. I must also thank my parents, Ron and Nancy, who raised their Sandpipers with an innate love of science and learning, and who always encouraged me to reach for the stars.

From the science world, my most sincere gratitude and respect go to Adrian and Harry, the best advisors I could have asked for – what a team! I am also the rigorous scientist I am today due to JP Kirby – mentor, idea machine, surfing buddy and friend. And what is graduate school without the friends you make along the way? Thanks to Kyle, my surrogate brother and best friend, for being there from the beginning through to LFT and beyond, and to Gretchen, my surrogate sister and the best roommate ever! Wanwan and Shannon, two of my closest friends, have been my support group through some frustrating experiments and long lab nights. I am grateful to Bert Lai for taking me under his wing as a first-year graduate student, and for teaching me how to survive grad school at Caltech! Thanks to Chase, a great neighbor and friend, from soccer games to turkey basting between episodes of Futurama. Of course I must thank all Ponce and Gray Group members, past and present, for their intellectual and emotional support. In particular, thanks to Doug Yung, Hannah Shafaat, Don Obenhuber and Stephanie Connon. We have had many summer students as well, who have made us remember why we got into science in the first place. Thanks to Mike Ikeda, Blake Sullivan, Oana Ursu,

Jeff Chen, Emma Crow-Willard, Christine Tarleton, Kevin Hartman, William Fan, Margot Kimura and Wilson Sung. Also, the Bercaw Group has provided much distraction from research in terms of soccer and Christmas parties – thanks to Steve Baldwin, Dave Weinberg and the rest of the crew. Finally, I should thank the other important scientists in my life that helped me become a grad student at Caltech in the first place; thank you Dr. Mark Rupright and Dr. Eugene Smith, for pushing me all the way through undergrad, and Mark Tormoen (Mr. T) and Janet Gabrielski (Mrs. G) for doing the same thing in middle school and helping me find my true niche: life on Mars!

In terms of the research described in this thesis, many students, postdocs, faculty and staff have played integral parts in discoveries about lanthanides and guided our choices for target analytes. I would like to thank Dana Levine, Micah Manary and Taran Esplin, for valuable contributions to this work. Thanks to Larry Henling and Mike Day for everything related to X-ray crystallography. John Keith, a postdoc at the University of Ulm in Germany, also gave DFT calculations of lanthanides (not an easy task) his best shot. Aaron Noell, our newest postdoc in the Ponce Group, has provided helpful discussions and proofread both my propositions and thesis. Thanks also to Christine Pelletier, for her analytical rigor and mad racquetball skills, and to Matt Hartings for helping me search for the nonexistent fluorescence of dipicolinate. I would also like to acknowledge Bruce Brunschwig for helpful discussions on Stark splitting. Thanks to Brian Leigh, the titan of Titan and master of many things chemical, for enlightening discussions and help with molecular modeling.

There were also numerous people in staff positions at Caltech and JPL who helped this work become possible. Thanks to Bill Badboy, Tony and Mike at JPL for

getting our lab through the many safety audits and letting us get work done. I am also grateful to Cora, diva of VWR, for great conversation and not billing me for lab goggles for the summer students until we finally got a charge number! Steve Gould at Caltech was also quite efficient at placing orders for rush items at inconvenient times. Joe and Ron in the mailing room also deserve some credit for good company and keeping the squirrels on Caltech's campus fat and happy. Finally, thanks to Jack Sawicki at Horiba Jobin-Yvon, for teaching me the inner workings of the all-powerful fluorimeter.

I have grown not only as a scientist in the past five years, but also as a person and an athlete. Thanks to David Werntz of the Aero Association of Caltech, for helping me realize my dream of becoming a pilot. In that same vein, my gratitude to Bill and Sally Hurt, for welcoming me into their home for almost 2 years and helping me afford flight school. I must also thank John Long, for being larger than life and encouraging me as a mountain unicyclist and a writer. Cheers to Eyal, Hans and the rest of the Santa Barbara Mountain Unicycle Club, for encouragement on and off the trails. Speaking of trailblazing and amazing journeys, I should thank Nicanor, our guide in the driest desert in the world, for his kindness and humor. Also, 'asante sana' to Simon Mtuy, Emmanuel, Frederick and all of the thirty-some-odd porters that helped us summit Mt. Kilimanjaro and do science on the Roof of Africa!

Thanks again to everyone! I love you all!

ABSTRACT

Bacterial spores, or endospores, are produced by certain genera of bacteria under stress and are considered to be one of the most resilient forms of life on Earth. Detection of endospores is vital in areas ranging from bioburden reduction to homeland security. Rapid bacterial spore detection is achieved by targeting dipicolinic acid (DPA), a chemical marker unique to endospores. An improvement on the current bacterial spore detection assay based on sensitized lanthanide luminescence is presented through the implementation of a dipicolinate-specific Tb^{3+} receptor site. The use of a chelating ligand such as DO2A (*1,4,7,10*-tetraazacyclododecane-*1,7*-bisacetate) can increase both the sensitivity and selectivity of the assay. The luminescent series of $Ln(DO2A)(DPA)^-$ complexes (Ln = Sm, Eu, Tb and Dy) is fully characterized in terms of structure, photophysics and stability, and the $Tb(DO2A)^+$ binary complex in particular is investigated as a sensing complex for bacterial spores. The 'ligand enhancement' observed in all cases improves dipicolinate binding affinity by approximately one order of magnitude over the lanthanide ion alone. Binding of the DO2A ligand also appears to generate a 'gadolinium break' effect, creating a discrepancy in binding affinity in the lanthanide series and rendering the terbium complex the most effective dipicolinate receptor site of all investigated. We have also extended the application of this receptor site design technology to the targeted detection of other aromatic analytes of biological relevance, such as salicylates and catecholamines. Our work indicates that construction of effective receptor site complexes is not governed by net electrostatic considerations, and that local charge variations from the ligand-induced perturbation of lanthanide electron density may play a significant role. This work sets the stage for the development

of the next-generation terbium(macrocycle) complex for bacterial spore detection, with the aim of constructing a solid-state endospore microsensor for applications ranging from sterilization validation to life detection in extreme environments.

TABLE OF CONTENTS

LIST OF ILLUSTRATIONS

LIST OF TABLES

LIST OF EQUATIONS

LIST OF ABBREVIATIONS

acac	Acetylacetonate
AETE	Absorption-Energy Transfer-Emission
ARCSS	Arctic System Science
BAC	Binding Affinity by Competition
ben	Benzoate
bpy	*2,2'*-bipyridine
BSSE	Basis set superposition error
CA	Catecholamine
Cat	Catechol, or *1,2*-dihydroxybenzene, or *o*-benzenediol
CCDC	Cambridge Crystallographic Data Centre
Cl-DPA	*4*-chloro-dipicolinic acid, or *4*-chloro-*2,6*-pyridinedicarboxylic acid
DA	Dopamine
DFT	Density functional theory
DMABA	p-dimethyl amino benzoic acid
DO2A	*1,4,7,10*-tetraazacyclododecane-*1,7*-bisacetate
DO3A	*1,4,7,10*-tetraazacyclododecane-*1,4,7*-trisacetate
L-DOPA	L-dihydroxyphenylalanine
DOTA	*1,4,7,10*-tetrakiscarboxymethyl-*1,4,7,10*-tetraazacyclododecane
DPA	Dipicolinic acid, or pyridine-*2,6*-dicarboxylic acid
2,4-DPA	Pyridine-*2,4*-dicarboxylic acid
3,5-DPA	Pyridine-*3,5*-dicarboxylic acid
DTPA	Diethylenetriaminepentaacetic acid
EDTA	Ethylenediaminetetraacetic acid
Epi	Epinephrine (Adrenaline)
ESI-MS	Electrospray ionization mass spectrometer
μEVA	Microscopic Endospore Viability Assay
F-DPA	*4*-fluoro-dipicolinic acid, or *4*-fluoro-*2,6*-pyridinedicarboxylic acid
FRET	Förster Resonance Energy Transfer
GISP2	Greenland Ice Sheet Project 2

HBA	Hydroxybenzoic acid
HFA	Hexafluoroacetylacetonate
hexacyclen	Hexamine, or 18-azacrown-6, or *1,4,7,10,13,16*-hexaazacyclooctadecane
HOMO	Highest occupied molecular orbital
HPLC	High-performance liquid chromatography
IC	Internal conversion
ISC	Intersystem crossing
IUPAC	International Union of Pure and Applied Chemistry
Nd :YAG	Neodymium-doped yttrium aluminum garnet
NE	Norepinephrine (Noradrenaline)
OPP	Office of Polar Programs
PDMS	Polydimethylsiloxane
PES	Polyethersulfone
phen	*1,10*-phenanthroline
Pic	Picolinic acid (pyridine-*2*-carboxylic acid)
PMT	Photomultiplier tube
Pyr	Pyridine
rcf	Relative centrifugal force
ROHF	Restricted open-shell Hartree-Fock
SA	Salicylic acid
SCRF	Self-consistent reaction field
SU	Salicyluric acid, or *2*-hydroxyhippuric acid, or ortho-hydroxyhippuric acid
TFA	Trifluoroacetic acid
THF	Tetrahydrofuran
TLC	Thin layer chromatography
TPEN	*N,N,N',N'*-tetrakis(*2*-pyridylmethyl)ethylenediamine
UHF	Unrestricted Hartree-Fock

DEFINITIONS AND NOMENCLATURE

In this dissertation the conventions of photophysics and photochemistry as described in *Principles of Fluorescence Spectroscopy* (J. R. Lakowicz) and *Modern Molecular Photochemistry* (N. J. Turro) will be followed. 'Fluorescence' is defined as the process of "allowed" radiative emission that occurs from a singlet excited state to a singlet ground state ($S_1 \rightarrow S_0 + h\upsilon$). 'Phosphorescence' is defined as the "forbidden" transition from a triplet excited state to a singlet ground state ($T_1 \rightarrow S_0 + h\upsilon$). 'Luminescence' is an all-encompassing term that refers to emission of light from any substance, and occurs from electronically excited states. Therefore 'luminescence' will be used to describe any radiative transition that cannot be defined as either fluorescence or phosphorescence, such as lanthanide luminescence.

Electronic states are represented according to the Russel-Saunders coupling scheme by the expression

$$^{2S+1}L_J$$

where L is the total angular momentum, S is spin multiplicity and J is the total angular quantum number. Electron spins are coupled together separately from the orbital angular momenta, and the orbital moment is unquenched.

CHAPTER 1

Introduction to Sensitized Lanthanide Luminescence and the Detection of Bacterial Spores

1.1 Lanthanides – Relevance and History

The lanthanides, or lanthanoids in IUPAC terminology, comprise the fifteen elements of the top row in the 'f-block' of the periodic table and have the electronic configuration [Xe] $4f^n 5s^2 5p^6$ where *n* varies from 0 to 14. Also known as 'rare earth elements' due to the etymology of the term 'lanthanide' (derived from the Greek *lanthanein*, meaning 'to lie hidden') and the uncommon oxides from which they were first isolated, lanthanides are in actuality neither 'rare' nor 'earths', an old term used to describe certain metal oxides such as lime and magnesia.[1] Even the rarest lanthanides – thullium and lutetium – are nearly 200 times more abundant than gold (Figure 1.1).[2] Yet, the name 'rare earths' has persisted, perhaps due to the enigmatic nature of these unusual metals, and their ability to 'hide' behind each other in minerals. Indeed, the similar chemical properties of lanthanides make their separation quite difficult, even today.

Lanthanides have found uses in a wide variety of industries and materials, such as catalysts, glasses, ceramics, permanent magnets, optics and electronics.[3, 4] Solid phosphors containing europium, cerium and terbium are major contributors to commercial markets in fluorescent lighting and color displays. Various lanthanide ions can be used in lasers, with neodymium as the most famous in yttrium aluminum garnet (Nd-YAG). The green, blue and red luminescent bands in Euro banknotes are attributed to europium complexes.[5] Certain lanthanides (Eu, La, Lu, Nd, Pr, Sm, Th, Tm and Yb) are used as tracers in wine chemistry to discriminate wines according to geographical region.[6] The ratio of europium, which is almost entirely (~ 97%) formed in stars, to other rare earth elements in meteorites has helped us decipher much of the history of processes in our solar system, such as the early development of the feldspar-rich lunar crust.[7]

In aqueous solution, lanthanides are most stable in the +3 oxidation state, leading to high coherent behavior and hence making them difficult to separate and purify. The preference for the trivalent oxidation state is due in part to the energy of the 4f electrons being below those of the 5d and 6s electrons (except in the cases of La and Ce). When forming ions, electrons from the 6s and 5d orbitals are lost first, so that all Ln^{3+} ions have [Xe] $4f^n$ electronic configurations. This, coupled to the high enthalpies of hydration for trivalent lanthanides, results in the stability of the +3 oxidation state. In reducing conditions, europium, samarium and ytterbium can be stable in the divalent form; cerium has also been known to adopt a +4 oxidation state.

Lanthanide ions possess relatively high charge densities and have a strong electrostatic nature in their bonding, as the ions are polarizing and can be classified as hard Lewis acids. The 4f orbitals in Ln^{3+} ions are well shielded by the 5s and 6p orbitals, and therefore do not participate directly in bonding (Figure 1.2). Therefore, π-bonding is not possible, and no Ln=O or Ln≡N multiple bonds are known for lanthanide complexes.

Coordination to trivalent lanthanides tends to be more ionic in character, which leads to a strong preference for negatively charged or neutral donor groups possessing large ground state dipole moments. Therefore, combinations of amines and carboxylic acid groups are often used in lanthanide complexation.[8, 9] This ionic character of binding also means lanthanide complexes tend to undergo facile exchange of ligands.[5] Coordination geometries in lanthanides are determined by ligand steric factors as opposed to orbital overlap or crystal field effects.[10, 11] In aqueous solution, donor groups containing neutral oxygen or nitrogen atoms generally bind when present in multidentate ligands (podands, crown ethers, cryptates, etc.).[12-15] Relatively few complexes of

monodentate nitrogen donors exist, reinforcing the oxophilic tendency of lanthanide binding. This preference for oxygen donors also makes lanthanides quite lithophilic, and explains their occurrence in silicates as opposed to metallic or sulphidic minerals.[16]

The coordination number of $[Ln(H_2O)_n]^{3+}$ is normally 9 for the early lanthanides (La-Eu) and 8 for those later in the series (Dy-Lu), with the intermediate metals (Sm-Dy) exhibiting a mixture of species. However, the coordination number can be dictated by the steric bulk of the coordinating ligands, and species with coordination numbers as low as 2 and as high as 12 are known.[5, 17]

As the 4f electrons of the lanthanides are well shielded from the environment, the spectroscopic and magnetic properties of these ions (e.g., electronic spectra and crystal-field splittings) are largely independent of environment (solvent, coordinated ligands, etc.). The number of configurations for *n* electrons rapidly increases with the number of unpaired electrons:

$$\frac{14!}{n!(14-n)!} \qquad [1.1]$$

where $0 \leq n \leq 14$, with the lowest energy term for each ion consistent with the predictions of Hund's first and second rules.[18, 19] Since all configurations have different energies, the lanthanides tend to exhibit rich and complex energy level structure (Figure 1.3).[20] Due to spin-orbit coupling, the excited states of the lanthanides are well separated from the ground state manifold. Thus, the excited states are thermally inaccessible and ideal for electronic transitions. With the exceptions of the $4f^0$, $4f^1$, $4f^{13}$ and $4f^{14}$ species (La^{3+}, Ce^{3+}, Yb^{3+} and Lu^{3+}, respectively), all lanthanide ions absorb electromagnetic radiation, primarily in the visible region, which is manifested in f-electrons from the partially filled

4f subshell being excited from the ground state to an excited state. These f–f transitions can be excited by both magnetic dipole and electric dipole radiation. Magnetic dipole transitions are Laporte (parity) allowed, while electric dipole transitions are Laporte-forbidden.[21, 22] Electric dipole transitions are much weaker in lanthanides ($\varepsilon \sim 0.1$ mol^{-1} dm^3 cm^{-1}) than in the transition metals, meaning magnetic dipole transitions can often be seen.[5, 23] Electronic transitions must involve promotion of an electron without a change in its spin ($\Delta S = 0$) and with a variation of either the total angular momentum and the total angular quantum number of one unit at most ($\Delta L = \pm 1,0$; $\Delta J = \pm 1,0$). Though absorption of radiation can in theory promote the lanthanide ion to any energetically accessible state, emission normally occurs only from the lowest lying spectroscopic level of the first excited term due to rapid internal conversion.[19] In cases of low symmetry or vibronic coupling, the f–f transitions can gain intensity through f- and d-state mixing with higher electronic states of opposite parity. Broad $4f^n \rightarrow 4f^{n-1}\ 5d^1$ transitions can also be seen in the infrared region for some lanthanides.

The electronic configuration of lanthanides is split due to a variety of interactions. The initial configuration is split into spectroscopic terms by electronic repulsion, with separations on the order of 10^4 cm^{-1}.[24] These terms can be further split into spectroscopic levels, or J states, due to spin-orbit coupling effects. The energy differences between split J states lies in the range of 10^3 cm^{-1}.[25] These levels, in turn, can be split again into what are termed Stark sublevels due to ligand field effects from the coordination sphere around the lanthanide; Stark sublevel splitting is on the order of 10^2 cm^{-1} (Figure 1.4).[26] This results in the overall emission peak position remaining largely unchanged as the f-electrons remain shielded, but the emission profile of a lanthanide (defined as the

relative intensity and degree of splitting of emission peaks) can vary greatly depending on modulation of these influences.[27, 28] The number of Stark sublevels depends on the site symmetry of the lanthanide ion, and these can be thermally populated at room temperature, yielding more complex emission spectra.

Filling of the inner 4f electron shell across the lanthanide series results in a diminuation of the ionic radius by as much as 15% from lanthanum to lutetium, referred to as the lanthanide contraction.[29] Though atomic radius contraction is not unique across a series (i.e., the actinides and the first two rows of the d-block), the fact that all lanthanides primarily adopt the trivalent oxidation state means that this particular row of elements exhibits a traceable change in properties in a way that is not observed elsewhere in the periodic table. Lanthanides behave similarly in reactions as long as the number of 4f electrons is conserved.[30] Thus, we can use lanthanide substitution as a tool to tune the ionic radius in a lanthanide complex without changing its chemistry, to better understand how the size of the metal cation affects various properties.

1.2 Sensitized Lanthanide Luminescence

Though alone lanthanide ions have very low molar absorptivities and can only be effectively excited by lasers, lanthanide luminescence can be significantly enhanced by chelating ligands in a process called ‘sensitization’. The first demonstration of sensitized lanthanide luminescence was due to the efforts of Bhaumik and El-Sayed, who showed that if the lowest triplet level of europium tris hexafluoroacetylacetonate, or $Eu(HFA)_3$, was excited by triplet-to-triplet intermolecular energy transfer from another donor (benzophenone), the energy could be transferred to the lanthanide cation.[31, 32] This

indirect sensitization bypasses the selection rules that normally limit f–f excitation in lanthanides, and can result in luminescence enhancement by three orders of magnitude or more.[24, 33, 34]

In sensitized lanthanide luminescence, the chromophore is normally an aromatic or unsaturated organic molecule that is either anionic or has a strong dipole moment to coordinate to the Ln^{3+} ion. In order to act as an efficient energy harvester or 'antenna' as they are often termed,[35] the chromophore must absorb radiation effectively and pass as much of this energy as possible, nonradiatively, to the lanthanide for emission. This process, known as the absorption-energy transfer-emission (AETE) mechanism, has several steps. First, the light-harvesting ligand is excited from the ground state S_0 to the singlet excited state S_1 (Figure 1.5). Some chromophores have several singlet excited states; nonradiative relaxation from these higher singlet excited states (S_2, S_3, etc.) to the lowest singlet excited state (S_1) via internal conversion (IC) can occur readily. Second, a triplet excited state (T_1) is formed through intersystem crossing (ISC), a process that is more efficient near heavy atoms such as lanthanides, which promote spin-orbit coupling.[36] Third, intramolecular energy transfer (ET) from the ligand triplet excited state to the lanthanide excited state occurs, resulting in a populated emittive level in the lanthanide. The efficiency of this step, the intramolecular energy transfer from chromophore to lanthanide, is the most important factor influencing the luminescence properties of rare earth complexes.[37] The final step is the luminescence observed as the excited state in the lanthanide decays radiatively to the ground state manifold.[38, 39]

However, there are other pathways, both radiative and nonradiative, that can reduce the efficiency of sensitized lanthanide luminescence. Chromophores can lose

energy from the singlet excited state by two mechanisms: (1) fluorescence, where they radiatively decay from the singlet excited state to the ground state; or (2) the excited state can be nonradiatively quenched by photoinduced electron transfer or other means.[12] The triplet excited state of the chromophore can also radiatively decay as phosphorescence, or be nonradiatively quenched by oxygen, though oxygen has been found to have little or no quenching effect on visible-emitting luminescent lanthanide complexes.[40, 41] These mechanisms can be mitigated or minimized by judicial choice of chromophore.

The greatest vulnerability of sensitized lanthanide luminescence lies in nonradiative deactivation or relaxation due to solvent interactions, which can reduce emission intensity significantly through energy dissipation by vibronic modes.[24, 42] Typically, this occurs by harmonic oscillators in the lanthanide coordination sphere, though outer-sphere quenching has also been observed.[40] Vibronic quenching depends on both the number of oscillators close to the first coordination sphere and the R parameter:

$$R = \frac{\Delta E}{\hbar\omega} = \frac{\Delta E}{\hbar}\sqrt{\frac{\mu}{\kappa}} \qquad [1.2]$$

where ΔE is the energy gap between the emitting state and the higher energy J state of the ground multiplet, $\hbar\omega$ is the oscillator vibrational quantum, μ is the oscillator reduced mass and κ is the oscillator force constant.[43, 44] The R parameter represents the number of vibrational quanta between ΔE; the lower the value of R, the higher the rate of vibronic coupling and the more pronounced the emission quenching will be.

The most common and efficient quencher of lanthanide luminescence is the O–H oscillator.[45] For the four lanthanides that luminesce in the visible region (Sm, Eu, Tb and

Dy), the R parameter lies in the range of 3 to 6, meaning quenching by OH vibrations is a significant mode of radiationless transitions.[44] Gadolinium, in contrast, which is relatively unquenched by OH vibrational overtones, has an R value of ~10. In order to reduce or eliminate this pathway for nonradiative decay, the lanthanide ion must be effectively shielded from the solvent. This can be accomplished using various chelating ligands containing hard donors that bind to the lanthanide ion with high affinity and contain a cavity to encapsulate the ion and prevent solvent coordination. The first 'insulating sheath' for lanthanide ions was developed by Halverson in 1964 using fluorinated 1-diketonates.[46] Since then a variety of successful ligands have been identified for this purpose, including cyclodextrins, cryptands, podands, calixarenes, porphyrins, crown ethers, and aza-crown macrocyclic and bicylic ligands (Figure 1.6).[12, 13, 47-51]

Triplet-mediated energy transfer in sensitized lanthanide luminescence has two proposed mechanisms. The Dexter energy transfer mechanism involves the transfer of an electron from donor (D) to acceptor (A). In the Dexter model, a resonant transfer of energy can be obtained between an allowed transition in the donor and a forbidden transition in the acceptor.[52] The acceptor can therefore be made to luminesce after exposure to a given region of radiation where it would not normally, due to energy transfer from the donor. The Dexter mechanism is highly dependent on orbital overlap, and therefore efficient energy transfer is only seen at very small distances (~ 10 Å).[53] The other proposed mechanism is the Förster, or Coulombic, energy transfer mechanism, in which energy transfer is dipole-induced and the electrons do not physically transfer.[54] Energy transfer in the Förster model is highly dependent on the spectral overlap of the

emission spectrum of the donor and the absorbance spectrum of the acceptor, and can occur over longer distances. (Figure 1.7). However, it must be noted that both the Dexter and Förster mechanisms describe only single-step, photoinduced, nonradiative energy transfers, whereas sensitized lanthanide luminescence often involves multiple steps such as intersystem crossing and internal conversion prior to energy transfer.

The AETE mechanism depends on appropriate alignment of the ligand donating triplet energy level and the lanthanide accepting excited level for efficient energy transfer. The intramolecular energy transfer efficiency depends mainly on two energy transfer processes: Dexter resonant exchange interaction theory and thermal deactivation.[55] The first describes the rate of energy transfer from the lowest triplet state to the resonant energy level as follows:[56]

$$\begin{aligned} k_{ET} &= KP_{da}\exp\left(-2R_{da}/L\right) \\ P_{da} &= \left(2\pi Z^2/R\right)\int F_d(E)E_a(E)dE \end{aligned} \qquad [1.3]$$

where k_{ET} is rate constant of intermolecular energy transfer (ET), P_{da} is the transition probability of the resonant exchange interaction, $F_d(E)$ is the experimental luminescence spectrum of E-donor (ligand), $E_a(E)$ is the experimental absorption spectrum of the E-acceptor (Ln^{3+}), R_{da} is the intermolecular distance between donor and acceptor atoms, L is the Van der Waals radius and $2\pi Z^2/R$ is a constant relating to the specific mutual distance between the E-acceptor (Ln^{3+}) and coordinated atoms (N and O). This is in competition with the reverse energy transition due to thermal deactivation:[52]

$$k(T) = A\exp\left(-\Delta E/RT\right) \qquad [1.4]$$

In other words, the donor and acceptor levels must be close enough to allow for efficient energy transfer, but if they are too close energy is lost due to thermal deactivation. The

optimal energy gap between chromophore triplet state and lanthanide excited state is approximately 4000 ± 500 cm^{-1}, meaning that the pairing of lanthanide and chromophore is of the utmost importance for achieving efficient energy transfer.[37, 57]

Sensitized lanthanide luminescence is a unique process, and as such these lanthanide complexes demonstrate some interesting features not found in other species that are known to luminesce. Emission spectra tend to exhibit narrow line-like bands because both excited and ground states have the same f^n configuration.[12, 24] These electronic f–f transitions are also largely independent of the chemical environment of the lanthanide ion, though the peak splitting and relative intensities can vary significantly in some cases. Due to the various energy transfer steps that occur in lanthanide luminescence (internal conversion, intersystem crossing, etc.), there is usually a very large difference between the absorption and emission maxima in these complexes, known as the Stokes shift.[40, 58] The larger the Stokes shift, the less overlap between absorbance and emission bands and less energy is lost to reabsorption. Further, as the major transitions in these complexes are electric dipole 'forced' and normally forbidden, the excited state lifetimes tend to be very long, on the order of micro- to milliseconds.[27] The triplet state of the ligand can have its own lifetime on the order of nano- to microseconds, so the energy transfer step from ligand to lanthanide can also lengthen the observed lifetime.[59] Though the property of long luminescence lifetime is not necessarily unique, the fact that this occurs under ambient conditions for lanthanides is unusual. Most organic species that exhibit phosphorescence only do so at low temperatures and/or in the absence of oxygen.[19] The observed excited state lifetime (τ) of a luminescent lanthanide complex can be expressed as follows:

$$\tau = \frac{1}{k_r + k_{nr}} \qquad [1.5]$$

where k_r is the rate constant for radiative transition of the lanthanide ion and k_{nr} is the sum of rate constants for all nonradiative relaxation processes, which can include energy back-transfer and vibronic coupling. The excited state lifetime can also be regarded as a function of luminescence quantum yield (Φ_{Lum}):

$$\Phi_{Lum} = \frac{k_r}{k_r + k_{nr}} \qquad [1.6]$$

The overall quantum yield is dependent on the energy transfer efficiency (probability) from the ligand to the lanthanide ion (see equations 1.3 and 1.4).

Due to these unique properties, sensitized lanthanide luminescence has found a variety of applications.[60] Europium and terbium chelates, due to their line-type emissions and long decay times, are used in time-resolved fluorescence resonance energy transfer (TR-FRET) immunoassays.[61, 62] The lanthanide chelate is used as a donor, with some visible-absorbing dye such as Alexa® 647 or a rhodamine derivative used as the acceptor. Quenching of emission due to donor-acceptor proximity then operates as a tool to determine, for instance, protein-protein interaction or enzymatic reaction time. When concentrated as phosphors or in beads, lanthanides have been used in imaging microscopy in the millisecond time domain.[63] Use of two or more lanthanides simultaneously is advantageous for PCR detection of diabetes risk,[64] gene detection of bacterial toxins[65] and an assay of papilloma virus.[66] Sensitized lanthanide luminescence also has drug discovery applications, such as high-throughput screening or pharmacokinetic analysis of drug transportation and accumulation.[40] However, the use of lanthanide complexes as tailored receptor sites has not been fully explored.

1.3 Lanthanides, Dipicolinic Acid and Bacterial Spores

Dipicolinic acid (DPA, pyridine-*2,6*-dicarboxylic acid) was originally used in a fluorescence spectroscopy method to detect trace amounts of terbium for probing alkaline earth metal ion interactions in biological systems.[67] It was realized over twenty years later that this detection technique based on intense luminescence could be used in *reverse* – to detect dipicolinate as a marker of bacterial spores.

Bacterial spores, also known as endospores, are dormant microbial structures that exhibit remarkable resistance to chemical and physical environmental stresses and are considered to be one of the toughest forms of life on Earth.[68] Discovered in 1876, endospores are formed inside the vegetative cells of certain species of *Bacillus*, *Clostridium*, and *Sporosarcina* (hence the 'endo' prefix) in a process called sporulation.[69-72] Sporulation is often triggered when the cells are exposed to adverse environmental conditions, such as desiccation or starvation. Bacterial spores house the cell DNA within the spore core, comprised of calcium dipicolinate (CaDPA), and a tough coat composed of protein layers (Figure 1.8). Endospores can remain dormant with no detectable metabolism for potentially millions of years.[73-76] When conditions become favorable again, as indicated by the presence of water, nutrients or specific germinants, endospores undergo germination and outgrowth to become vegetative cells, completing the cycle.[77, 78]

In the dormant spore state, endospores are resistant to a wide variety of chemical and physical stresses, such as UV and gamma radiation, desiccation, temperature and pressure extremes, and attack by a number of toxic agents.[79-82] Bacterial spores are 10,000 times more resistant to heat and 100 times more resistant to UV radiation than

their active bacterial cell counterparts.[83, 84] As they are resilient to most sterilization procedures, bacterial spores are used in several industries as biological indicators.[85, 86] Certain species can even survive the vacuum, extreme temperatures and radiation of space,[87, 88] and are the focus of research concerning planetary protection, panspermia (transfer of life from one planetary body to another via meteoritic impacts), and life in extreme environments.[89, 90] In addition, detection of bacterial spores became a national priority after the anthrax attacks of 2001, as *Bacillus anthracis* spore powders are the vectors of the anthrax bioweapon.[91-94] Certain species of anaerobic endospores, such as *Clostridium botulinum* and *C. perfringens*, are pathogenic and the causative agents of food poisoning or serious disease.[95]

Due to its applications in homeland security, sterilization validation and astrobiology, bacterial spore detection has become a rather extensive field. The classical measurement of bacterial spores involves culture-based methods, and is used as the NASA Standard Assay for ascertaining spacecraft sterility.[96, 97] This procedure involves swabbing the surface, suspending any collected endospores in water, and then plating this suspension on growth media. Any bacterial spores will germinate in the favorable conditions and produce colonies. However, colony formation requires at least 20 cycles of cell replication, a process that requires 2 to 3 days.[97] This method also cannot discriminate between endospores and vegetative cells. Thus, the NASA Standard Assay is not viable as a rapid endospore detection technique.

Direct detection of bacterial spores can be challenging, for the same reasons that make endospores difficult to irradicate. The tough spore coat is impermeable to staining techniques, so most microscopy and flow cytometry methods are unsuccessful.

Endospores are also highly resistant to lysis, meaning DNA extraction protocols are ineffective. The lack of measurable metabolism renders microcalorimetry and cellular respiration techniques inadequate. In order to detect bacterial spores, we must instead consider what makes them unique and take advantage of these factors to produce a highly specific assay.

Bacterial spores contain a unique chemical marker – dipicolinic acid, or DPA. DPA is present in nearly all bacterial spores and comprises about 10–15 % of a spore's dry weight, or approximately 10^8 molecules per spore.[84, 98, 99] Some endospore mutants do not contain DPA, but these are rare, and DPA has never been detected in vegetative cells.[95] Detection of this chemical marker can therefore serve as a positive signal for the presence of bacterial spores, and the amount of DPA detected can be used to estimate the approximate endospore concentration.[95, 100]

There are several theories regarding the functionality of such a high concentration of dipicolinate in the endospore. First, this dianion serves in the storage of divalent cations such as calcium and magnesium, which are important for cell function.[98] Second, as DPA is an excellent absorber of UV radiation, it appears to play a major role in the UV photochemistry and protection of endospore DNA.[101, 102] The high concentration of dipicolinate salts in the core also displaces water and confers additional resistance to desiccation and wet heat.[103] Finally, DPA is metabolized in the early stages of germination, and therefore serves as a nutrient source for the growing cell.[104, 105]

Detection of DPA as an indicator of bacterial spores was first proposed in 1955, in a protocol involving UV absorption of the dipicolinate following acid digestion of the spores, isolation by ether extraction, separation by paper chromatography and finally

elution of the DPA-containing spots.[106] A much simpler spectroscopic method of dipicolinate detection was published in 1958, in the form of a colorimetric assay with ferrous iron.[107] DPA extracted from endospores was detected via a color change from pale green to red-brown upon complexation with Fe^{2+} in acidic conditions (pH 4–6). Following this work, many methods for dipicolinate detection have been published, including fluorescence of CaDPA, UV absorbance spectrophotometry, anti-Stokes Raman spectroscopy, surface-enhanced Raman spectroscopy, gas chromatography, mass spectrometry and high performance liquid chromatography (HPLC).[95, 108-111]

The application of lanthanides to bacterial spore detection began in 1997 with a method using terbium to detect dipicolinate with fluorescence spectrophotometry.[112] Addition of terbium chloride to a suspension of lysed endospores causes the formation of $[Tb(DPA)_n]^{3-2n}$ complexes, where n varies from 1 to 3, as the Tb^{3+} displaces the Ca^{2+} of CaDPA. Dipicolinate is an effective absorber of ultraviolet radiation due to the delocalized π-electrons of the aromatic pyridine ring. The triplet excited state of the DPA anion (26,600 cm^{-1}) is also in the appropriate regime to effectively sensitize the Tb^{3+} cation via energy transfer to the $^5D_4$ emitting level of the terbium (20,500 cm^{-1}) through the AETE mechanism.[113-115] There is some evidence against an intramolecular heavy atom effect in some 4-substituted dipicolinate ligands coordinated to Tb^{3+}, which argues for a singlet-to-metal mechanism for intersystem crossing to the lanthanide.[41, 116, 117] However, the contribution of this pathway is most likely very small, so we treat this system in the usual manner and assume the excited dipicolinate singlet state decays to the triplet via internal conversion prior to energy transfer to the lanthanide. The end result is

intense luminescence under UV excitation that is more than three orders of magnitude greater than that of terbium alone (Figure 1.9).[95, 118-122]

Although the method is rapid and straightforward, there is much room for improvement in the detection of bacterial spores with the Tb-DPA luminescence assay. The potential for false positives or false negatives through complexation of anionic interferents to the trivalent terbium cation is a serious concern when the method is applied to environmental samples. Previous studies indicate that phosphate in particular can inhibit DPA binding or decrease luminescence intensity.[123, 124] Further, in environmental samples with low endospore concentrations where the $Tb(DPA)^{+}$ species predominates, the six coordinated water molecules can quench the luminescence by nearly an order of magnitude due to radiationless deactivation.[125] Finally, the propensity of dipicolinate to form up to three complexes with terbium, namely $Tb(DPA)^{+}$, $Tb(DPA)_2^{-}$ and $Tb(DPA)_3^{3-}$, each with different luminescence intensities and lifetimes, precludes a direct correlation between intensity and DPA concentration. This dissertation will focus on methods to mitigate these detrimental factors using a macrocyclic helper ligand to generate a dipicolinate-specific lanthanide-based receptor site.

1.4 Lanthanides and Lanthanide Complexes as Sensors

Lanthanides demonstrate several advantages over traditional organic fluorophores, quantum dots and other fluorescent species commonly used as sensors and switches. They feature significant spectral resolution due to their large Stokes shifts and narrow emission lines, and temporal resolution due to long lifetimes. This allows for the use of time-gated techniques and bandpass filters to reduce interference from native or

auto-fluorescence in the sample, which occurs on the nanosecond timescale.[23, 58] Lanthanide complexes also do not suffer from photobleaching as organic dyes do, because lanthanides are effective quenchers of triplet states.[126] These qualities allow for the construction of robust sensors for a variety of applications.

Of all the lanthanides, Eu^{3+}, Tb^{3+} and Gd^{3+} are the best ions in terms of efficient excited state population, with energy gaps of 12,300 cm^{-1} ($^5D_0 \rightarrow {}^7F_6$), 14,800 cm^{-1} ($^5D_4 \rightarrow {}^7F_0$) and 32,200 cm^{-1} ($^6P_{7/2} \rightarrow {}^8S_{7/2}$), respectively.[12] However, while europium and terbium both emit in the visible region, gadolinium emits in the ultraviolet, making it unfeasible for use in most sensing applications due to significant absorption and emission interference of these high-energy wavelengths. Though not suitable as luminescent sensors, Gd^{3+} complexes do have a large number of unpaired electrons ([Xe] $4f^7$) and isotropic magnetic properties. These properties, coupled to a long electron spin relaxation time of 10^{-9} s, makes this lanthanide highly NMR-active.[127] When coordinated to one or more water molecules, Gd^{3+} enhances the water proton relaxation efficiency by lengthening the rotational correlation time.[128] Thus, many gadolinium complexes with one free binding site for solvent coordination, such as Gd(DTPA) and Gd(DOTA), have been developed for use as MRI contrast agents.[129-131]

Luminescent lanthanide complexes designed for use as sensors and switches can be classified into three types, based on the position of the chromophore and the state of the lanthanide before and after analyte binding (Figure 1.10). More complex systems have been designed containing two or more lanthanides for multicolor detection in imaging applications, but these are out of the scope of this dissertation and will not be discussed here.[132]

The type A sensor is the most simple; the receptor site is the lanthanide complex, and the analyte is the chromophore. Binding of the aromatic analyte to the receptor site results in emission due to sensitization. This type of sensor is most effective in cases where the two states – analyte bound or unbound – must be very easily distinguished, as in samples with very low amounts of analyte or where the background noise is high. Type A sensors have been used with amide-modified DO3A (*1,4,7,10*-tetraazacyclo-dodecane-*1,4,7*-trisacetate) ligands bound to Tb^{3+} to selectively bind the bidentate analytes p-dimethyl amino benzoic acid (DMABA) or salicylic acid (SA).[133-135] The binary complex of Tb^{3+} and ethylenediaminetetraacetic acid (EDTA) can effectively detect salicylic acid, *4*-aminosalicylic acid, *5*-fluorosalicylic acid.[136] The Tb(EDTA) complex has also been used to detect catalysis of hydroxybenzoic acid (HBA) by hemin via formation of a ternary complex with the HBA oxidation product.[137] Detection of tetracyclines was realized using sensitized europium luminescence post-column following liquid chromatography; the authors noted a dependence on EDTA concentration but did not hypothesize any ternary complex formation, though this is the likely result.[138] Diaza-crown ethers have been utilized with Tb^{3+} and Eu^{3+} to detect phthalate, benzoate, dibenzoylmethide and picolinate.[139] A pH sensor was developed due to the pH-dependence of a europium ternary complex containing a β-diketonate as the chromophore. When the pH shifted out of physiological range, the chromophore dissociated and sensitization was lost.[12] The future of these types of sensors lies in the development of receptor sites with greater analyte affinity, perhaps via stronger host-guest interactions such as π-stacking or modification of receptor site topology to generate a ‘lock and key’ style of hydrophobic pocket.

The type B sensor involves a change in luminescence upon analyte binding. In this case the receptor site is composed of the lanthanide complex with a chromophore already attached, but the complex is unsaturated. This results in labile solvent molecules in the lanthanide coordination sphere, so luminescence is quenched due to nonradiative deactivation. Binding of the analyte displaces these quenchers and produces a change (usually an increase) in emission. This method is most useful in anion sensing, where the anion (acetate, fluoride, etc.) can coordinate well to the lanthanide but is not capable of absorbing UV radiation and sensitizing the lanthanide. For example, several types of Tb^{3+} and Eu^{3+} podand complexes have been developed with sensitivity to Cl^- and NO_3^-, respectively, when detected in acetonitrile.[140, 141] A binary complex composed of a bis-bpy-phenyl phosphine ligand chelated to Eu^{3+} was able to detect NO_3^-, Cl^-, AcO^- and F^- with varying sensitivities by displacing acetonitrile solvent molecules in the Eu^{3+} coordination sphere.[142, 143] Europium bound to a tri-N-substituted DO3A ligand was able to detect hydrogen carbonate in aqueous solution,[144, 145] and when coordinated to a cryptate with a poly-N-methylated flexible arm can act as a sensitive pH sensor over a fairly wide range.[146] Conversely, quenching of terbium acetylacetonate (acac) luminescence allowed for a sub-micromolar detection limit of chromate in aqueous solution when coupled to ion chromatography.[147] Though sensitive ion detectors have been developed, the selectivity of such receptor sites is still in need of improvement, in particular when discriminating between ions of similar size and/or charge.

The final sensor design motif, type C, also starts with the lanthanide complex and chromophore already bound. In this case, however, the lanthanide coordination sphere is already saturated, so the analyte is not required to chelate the Ln^{3+} to be detected.

Instead, association of the analyte with the *chromophore* causes a change in emission due to an alteration of the antenna properties (i.e., change in degree of sensitization, quantum yield, lifetime, etc.). The first examples of these types of sensing complexes were to detect cations such as H^+, Na^+ and K^+ via suppression of luminescence in europium aza-crown ethers.[148] Other water-soluble complexes have been developed to detect dO_2, halide and hydroxide by quenching of luminescence through various means (protonation, charge transfer, etc.) or decreasing the absorption of the chromophore.[39, 149] Detection of Zn^{2+} using Tb^{3+} and Eu^{3+} diethylenetriaminetetraacetic acid (DTPA) bis-amide complexes has also been proposed, where two *N*,*N*,*N'*,*N'*-tetrakis(*2*-pyridylmethyl) ethylenediamine (TPEN) groups on the DTPA ligand are brought into closer proximity to the lanthanide upon zinc binding, allowing for sensitized luminescence.[150] This sensor demonstrated selectivity over Ca^{2+} and Mg^{2+} ions and an apparent dissociation constant for Zn^{2+} of 2.6 nM, but Cu^{2+} interfered significantly and luminescence intensity was low due to the large lanthanide-chromophore distance. Sensors based on this strategy are still in their infancy, though many applications can be envisioned following sufficient improvement of stability and sensitivity.

This dissertation summarizes work to improve the Tb-DPA luminescence assay for bacterial spore detection by designing a dipicolinate-specific receptor site in the form of a lanthanide binary complex. Since dipicolinate is both our analyte and chromophore, this assay follows the Type A paradigm, with the receptor site comprising the terbium ion protected by an encapsulating helper ligand. However, dipicolinate is not the only aromatic anion capable of sensitizing lanthanide luminescence (Figure 1.11). We will also investigate receptor site designs for various salicylates and catecholamines with

physiological relevance to generate more robust, rapid sensing technologies for highly sensitive in situ detection.

A number of factors must be considered when designing lanthanide-containing receptor sites. The choice of lanthanide is paramount. The ionic radius varies across the lanthanide series, and the size of this cation can influence the relative binding affinity of the target analyte. The lanthanide excited state must also align correctly with the triplet excited state of the target analyte; if the energy difference is too great, the energy transfer efficiency will be low, but if it is too small, quenching effects such as back-transfer will predominate. The emission properties of the lanthanide, such as luminescence lifetime and quantum yield, must also be considered to produce an adequate signal.

Almost as important as the choice of lanthanide is the choice of helper ligand, which turns the lanthanide into a receptor site. This ligand must bind to the lanthanide with high affinity to prevent solvent coordination, which can severely quench luminescence via nonradiative decay pathways. However, the ligand must not interfere with binding of the target analyte, or the lanthanide loses all functionality as a sensor. Finally, pH and temperature effects must be considered, such that the receptor site is stable in the pH range where the target analyte is most soluble and/or sufficiently deprotonated to bind effectively.

We will be using a hexadentate macrocyclic ligand, DO2A (*1,4,7,10*-tetraazacyclododecane-*1,7*-bisacetate), as our helper ligand, as this chelator meets our initial criteria for designing a terbium-containing dipicolinate receptor site. Macrocyclic ligands are molecules – usually heteroatomic – with a semirigid ring structure as the backbone. These ligands vary in terms of ring diameter and the extent of

functionalization of substituents on or attached to the ring scaffold. Most macrocyclics have a hydrophilic cavity in which an ionic substrate such as a metal ion can nest and be shielded from the environment by its lipophilic envelope.[3, 151] Macrocyclic ligands such as the octadentate DOTA (*1,4,7,10*-tetrakiscarboxymethyl-*1,4,7,10*-tetraazacyclo-dodecane) have found a convenient niche in the field of bioimaging as magnetic resonance contrast agents due to their tendency to bind gadolinium with high affinity.[152, 153] In fact, most macrocyclic ligands seem to exhibit an unprecedented selectivity for lanthanide ions, and the dissociation of these lanthanide-macrocycle complexes appears to be independent of foreign metal ion concentration.[154] Lanthanide complexes involving macrocyclic ligands are highly water-soluble, thermodynamically stable, kinetically inert at physiological pH, cell-permeable and nontoxic, making them ideal for use in vivo as bioprobes. The facile derivatization of ligands bound to lanthanides also makes them easily tailored to bind specific biomolecules such as antigens or proteins.

We are therefore interested in constructing receptor sites composed of a lanthanide ion encapsulated by a macrocyclic ligand that confers stability, solubility and high analyte specificity for a target molecule. Binding of the aromatic analyte to this binary complex results in intense luminescence gain upon UV excitation due to the absorbance-energy transfer-emission (AETE) mechanism that is orders of magnitude greater in intensity than the lanthanide alone is capable. We will investigate various binary complexes composed of a luminescent lanthanide (Sm^{3+}, Eu^{3+}, Tb^{3+} and Dy^{3+}) and a macrocyclic ligand to optimize detection of a particular analyte of interest. These investigations will involve complete analysis of structure, photophysics, stability and resistance to interferents. The optimal receptor site will demonstrate superior

spectroscopic and thermodynamic properties, such as intense luminescence, high quantum yield, long luminescence lifetime, high binding affinity and resistance to a variety of chemical and physical conditions (temperature, pH, ionic strength, etc.). The receptor site with the best performance will be used as a sensor in environmental samples to detect the analyte of interest.

1.5 Outline of Thesis

This dissertation is centered around the design of tailored lanthanide receptor sites for target analytes (Figure 1.12). In **Chapter 1**, the various unique properties and applications of lanthanides were discussed, including the use of lanthanides and lanthanide complexes as sensors. The importance of bacterial spore detection was also described, and the qualities of an ideal receptor site identified. **Chapter 2** covers the complete spectroscopic and structural characterization of the Ln(DO2A)(DPA)$^{-}$ ternary complexes, where Ln = Sm, Eu, Gd, Tb and Dy. Relevant discussions concerning the crystal structures and quantum yields of these complexes are included, as well as lifetime studies to determine the number of coordinated solvent molecules and a brief summary of attempted density functional theory (DFT) calculations. In **Chapter 3**, the Ln(DO2A)$^{+}$ complex is investigated as a first-generation bacterial spore receptor site. Experiments involve binding studies, temperature and pH dependence studies, exposure to various cationic and anionic interferents, and examination of DPA analogues to better understand binding geometry and selectivity. The Tb(DO2A)$^{+}$ complex is chosen as the optimal dipicolinate sensor, and is tested with bacterial spore samples. **Chapter 4** discusses recent work on the next generation dipicolinate receptor site, where the DO2A ligand is

modified to append to a solid substrate for future sensor design. This novel Tb(DOAAM)(DPA) complex is characterized and compared to the Tb(DO2A)(DPA)$^-$ complex. In **Chapter 5**, we expand our investigation to include other analytes of interest, such as salicylates and catecholamines. Salicylates, such as salicylic acid (SA) and salicyluric acid (SU), are of medical relevance due to their association with certain metabolic imbalances and disease. Similarly, catecholamines including epinephrine (Epi), norepinephrine (NE) and dopamine (DA) are neurotransmitters of significant importance in normal body function. We apply our sensor design technique in an attempt to improve detection capability for these medically significant analytes. We end this chapter with conclusions drawn during the course of this work, including two important discoveries regarding the effects of helper ligands on lanthanide-based receptor sites. The various appendices at the end of this dissertation include complete derivations of models used to fit competition experimental data and the crystallographic information on all solved crystal structures.

REFERENCES

(1) Holden, N. E. In *IUPAC General Assembly*; US Department of Energy: Brisbane, Australia, 2001.

(2) Haxel, G. B.; Hedrick, J. B.; Orris, G. J.; US Geological Survey, 2002, pp 1-4.

(3) Arnaudneu, F. *Chemical Society Reviews* **1994**, *23*, 235-241.

(4) Bünzli, J.-C. G. *Journal Of Alloys And Compounds* **2006**, *408-412*, 934-944.

(5) Cotton, S. *Lanthanide and Actinide Chemistry*; John Wiley & Sons Ltd.: West Sussex, England, 2006.

(6) Galgano, F.; Favati, F.; Caruso, M.; Scarpa, T.; Palma, A. *LWT - Food Science and Technology* **2008**, *41*, 1808-1815.

(7) Taylor, S. R.; McLennan, S. M. In *Metal Ions in Biological Systems: The Lanthanides and Their Interrelations with Biosystems*; Sigel, A., Sigel, H., Eds.; Marcel Dekker, Inc.: New York, 2003; Vol. 40, pp 1-38.

(8) Faulkner, S.; Matthews, J. L. *Applications of coordination chemistry: Comprehensive coordination chemistry II*, 2nd ed.; Elsevier: Amsterdam, 2003.

(9) Petoud, S.; Cohen, S. M.; Bünzli, J.-C. G.; Raymond, K. N. *Journal Of The American Chemical Society* **2003**, *125*, 13324-13325.

(10) Gritmon, T. F.; Goedken, M. P.; Choppin, G. R. *Journal of Inorganic and Nuclear Chemistry* **1977**, *39*, 2021-2023.

(11) Gritmon, T. F.; Goedken, M. P.; Choppin, G. R. *Journal of Inorganic and Nuclear Chemistry* **1977**, *39*, 2025-2030.

(12) Leonard, J. P.; Nolan, C. B.; Stomeo, F.; Gunnlaugsson, T. *Topics in Current Chemistry* **2007**, *281*, 1-43.

(13) Suarez, S.; Mamula, O.; Scopelliti, R.; Donnio, B.; Guillon, D.; Terazzi, E.; Piguet, C.; Bunzli, J. C. G. *New Journal Of Chemistry* **2005**, *29*, 1323-1334.

(14) Horrocks Jr., W. D. *Science* **1979**, *206*, 1194-1196.

(15) Bunzli, J. C. G.; Wessner, D. *Helvetica Chimica Acta* **1981**, *64*, 582-598.

(16) Bulman, R. A. In *Metal Ions in Biological Systems: The Lanthanides and Their Interrelations with Biosystems*; Sigel, A., Sigel, H., Eds.; Marcel Dekker, Inc.: New York, 2003; Vol. 40, pp 39-67.

(17) Cotton, F. A.; Wilkinson, G. *Advanced Inorganic Chemistry*; John Wiley and Sons: New York, 1988.

(18) van der Ende, B.; Aarts, L.; Meijerink, A. *Physical Chemistry Chemical Physics* **2009**, *11*, 11081-11095.

(19) Parker, D.; Williams, J. A. G. In *Metal Ions in Biological Systems: The Lanthanides and Their Interrelations with Biosystems*; Sigel, A., Sigel, H., Eds.; Marcel Dekker, Inc.: New York, 2003; Vol. 40, pp 233-280.

(20) Dieke, G. H.; Crosswhite, H. M. *Applied Optics* **1963**, *2*, 675-686.

(21) Parker, D.; Dickins, R. S.; Puschmann, H.; Crossland, C.; Howard, J. A. K. *Chemical Reviews* **2002**, *102*, 1977-2010.

(22) Parker, D.; Williams, J. A. G. *Journal Of The Chemical Society-Dalton Transactions* **1996**, *18*, 3613-3628.

(23) Bünzli, J.-C. G. *Lanthanide probes in life, chemical and earth sciences: Theory and practice*; Elsevier: New York, 1989.

(24) Sabbatini, N.; Guardigli, M.; Lehn, J. M. *Coordination Chemistry Reviews* **1993**, *123*, 201-228.
(25) Carnall, W. T. In *Handbook on the Physics and Chemistry of Rare Earths*; Gschneider, K. A., Eyring, L., Eds.; North Holland Publishing Co.: Amsterdam, 1998; Vol. 25, pp 508.
(26) Walsh, B. M. In *Advances in Spectroscopy for Lasers and Sensing*; Di Bartolo, B., Forte, O., Eds.; Springer: The Netherlands, 2006, pp 403-433.
(27) Bünzli, J.-C. G.; Chopin, G. R. *Lanthanide Probes in Life, Chemical and Earth Sciences: Theory and Practice*; Elsevier: New York, 1989.
(28) Richardson, F. S. *Chemical Reviews* **1982**, *82*, 541-552.
(29) Bunzli, J. C. G. In *Metal Ions in Biological Systems*; Sigel, A., Sigel, H., Eds.; Marcel Dekker: Zurich, 2004; Vol. 42, pp 39.
(30) Johnson, D. A. *Journal of Chemical Education* **1980**, *57*, 475-477.
(31) El-Sayed, M. A.; Bhaumik, M. L. *Journal Of Chemical Physics* **1963**, *39*, 2391-2393.
(32) Bhaumik, M. L.; El-Sayed, M. A. *Journal Of Physical Chemistry* **1965**, *69*, 275-280.
(33) Sammes, P. G.; Yahioglu, G. *Natural Product Reports* **1996**, *13*, 1-28.
(34) Stryer, L.; Thomas, D. D.; Meares, C. F. *Annual Review of Biophysics and Bioengineering* **1982**, *11*, 203-222.
(35) Lehn, J. M. *Angewandte Chemie-International Edition* **1990**, *29*, 1304-1319.
(36) de Silva, A. P.; Gunaratne, H. Q. N.; Rice, T. E. *Angewandte Chemie-International Edition* **1996**, *35*, 2116-2118.
(37) Sato, S.; Wada, M. *Bulletin of the Chemical Society of Japan* **1970**, *43*, 1955-1962.
(38) Leonard, J. P.; Gunnlaugsson, T. *Journal Of Fluorescence* **2005**, *15*, 585-595.
(39) Parker, D. *Coordination Chemistry Reviews* **2000**, *205*, 109-130.
(40) Hemmila, I.; Laitala, V. *Journal Of Fluorescence* **2005**, *15*, 529-542.
(41) Prendergast, F. G.; Lu, J.; Callahan, P. J. *Journal of Biological Chemistry* **1983**, *258*, 4075-4078.
(42) Carnall, W. T. In *Handbook on the Physics and Chemistry of Rare Earths*; Gschneider, K. A., Eyring, L., Eds.; North-Holland: Amsterdam, 1979; Vol. 3, pp 171.
(43) Sabbatini, N.; Guardigli, M.; Manet, I. *Antenna effect in encapsulation complexes of lanthanide ions*; Elsevier: Amsterdam, 1996.
(44) Stein, G.; Würzberg, E. *Journal Of Chemical Physics* **1975**, *62*, 208-213.
(45) Horrocks Jr., W. D.; Sudnick, D. R. *Journal Of The American Chemical Society* **1979**, *101*, 334-340.
(46) Halverson, F.; Brinen, J. S.; Leto, J. R. *Journal Of Chemical Physics* **1964**, *41*, 157-163.
(47) Tsukube, H.; Shinoda, S.; Tamiaki, H. *Coordination Chemistry Reviews* **2002**, *226*, 227-234.
(48) Tsukube, H.; Shinoda, S. *Chemical Reviews* **2002**, *102*, 2389-2403.
(49) Rudzinski, C. M.; Hartmann, W. K.; Nocera, D. G. *Coordination Chemistry Reviews* **1998**, *171*, 115-123.
(50) Armaroli, N.; Accorsi, G.; Barigelletti, F.; Couchman, S. M.; Fleming, J. S.; Harden, N. C.; Jeffrey, J. C.; Mann, K. L. V.; McCleverty, J. A.; Rees, L. H.; Starling, S. R.; Ward, M. D. *Inorganic Chemistry* **1999**, *38*, 5769-5776.
(51) Horrocks Jr., W. D.; Wong, C.-P. *Journal Of The American Chemical Society* **1976**, *98*, 7157-7162.
(52) Dexter, D. L. *Journal Of Chemical Physics* **1953**, *21*, 836-850.
(53) Courrol, L. C.; de Oliveira Silva, F. R.; Gomes, L.; Vieira Junior, N. D. *Journal of Luminescence* **2007**, *122-123*, 288-290.

(54) Förster, T. *Annalen der Physik* **1948**, *437*, 55-75.
(55) Wu, S. L.; Wu, Y. L.; Yang, Y. S. *Journal Of Alloys And Compounds* **1992**, *180*, 399-402.
(56) Brown, T. D.; Shepherd, T. M. *Journal Of The Chemical Society-Dalton Transactions* **1973**, 336-341.
(57) Wang, Q.; Yan, B. *Journal Of Materials Chemistry* **2004**, *14*, 2450-2454.
(58) Lakowicz, J. R. *Principles of Fluorescence Spectroscopy*, 3 ed.; Springer Science+Business Media, LLC: Singapore, 2006.
(59) Lemmetyinen, H.; Vuorimaa, E.; Jutila, A.; Mukkala, V. M.; Takalo, H.; Kankare, J. *Journal of Luminescence* **2000**, *15*, 341-350.
(60) Lis, S.; Elbanowski, M.; Makowska, B.; Hnatejko, Z. *Journal Of Photochemistry And Photobiology A-Chemistry* **2002**, *150*, 233-247.
(61) Mathis, G. *Clinical Chemistry* **1993**, *39*, 1953-1959.
(62) Li, M.; Selvin, P. R. *Bioconjugate Chemistry* **1997**, *8*, 127-132.
(63) Soini, A. E.; Kuusisto, A.; Meltola, N. J.; Soini, E.; Seveus, L. *Microsc. Res. Technol.* **2003**, *62*, 396-407.
(64) Sjoroos, M.; Ilonen, J.; Reijonen, H.; Lovgren, T. *Dis. Markers* **1998**, *14*, 9-19.
(65) Watanabe, K.; Arakawa, H.; Maeda, M. *Luminescence* **2002**, *17*, 123-129.
(66) Samiotaki, M.; Kwiatkowski, M.; Ylitalo, N.; Landegren, U. *Analytical Biochemistry* **1997**, *253*, 156-161.
(67) Barela, T. D.; Sherry, A. D. *Analytical Biochemistry* **1976**, *71*, 351-352.
(68) Roberts, T. A.; Hitchins, A. D. In *The Bacterial Spore*; Gould, G. W., Hurst, A., Eds.; Academic Press, 1969; Vol. 1, pp 611-670.
(69) Cohn, F. *Beitr. Biol. Pflanz.* **1876**, *2*, 249-276.
(70) Koch, R. *Beitr. Biol. Pflanz.* **1876**, *2*, 277-310.
(71) Koch, R. *Beitr. Biol. Pflanz.* **1877**, *2*, 399-434.
(72) Tyndall, J. *Phil. Trans. Royal Soc.* **1877**, *167*, 149-206.
(73) Church, B. D.; Halvorson, H. *Nature* **1959**, *183*, 124-125.
(74) Berg, P. E.; Greez, N. *Journal of Bacteriology* **1970**, *103*, 517-519.
(75) Cano, R. J.; Borucki, M. K. *Science* **1995**, *268*, 1060-1064.
(76) Vreeland, R. H.; Rosenzweig, W. D.; Powers, D. W. *Nature* **2000**, *407*, 897-900.
(77) Johnstone, K. *Journal of Applied Bacteriology* **1994**, *76*, 17-24.
(78) Setlow, P. *Current Opinion in Microbiology* **2003**, *6*, 550-556.
(79) Byrne, A. F.; Burton, T. H.; Koch, R. B. *Journal of Bacteriology* **1960**, *80*, 139-140.
(80) Aronson, A. I.; Fitz-James, P. *Bacteriological Reviews* **1976**, *40*, 360-402.
(81) Bisset, K. A. *Nature* **1950**, *166*, 431-432.
(82) Driks, A. *Proceedings of the National Academy of Sciences of the United States of America* **2003**, *100*, 3007-3009.
(83) Lim, D. V. *Microbiology*; WCB/McGraw-Hill: Boston, Massachusetts, 1998.
(84) Gould, G. W.; Hurst, A. *The Bacterial Spore*; Academic Press, 1969.
(85) Albert, H.; Davies, D. J. G.; Woodson, L. P.; Soper, C. J. *Journal Of Applied Microbiology* **1998**, *85*, 865-874.
(86) Yung, P. T.; Ponce, A. *Applied and Environmental Microbiology* **2008**, *74*, 7669-7674.
(87) NIcholson, W. L.; Munakata, N.; Horneck, G.; Melosh, H. J.; Setlow, P. *Microbiol. Mol. Biol. Rev.* **2000**, *64*, 548-572.
(88) Horneck, G.; Bucker, H.; Reitz, G. *Adv. Space Res.* **1994**, *14*, 41-45.
(89) NIcholson, W. L. *Orig. Life Evol. Biosph.* **2003**, *33*, 621-631.
(90) Shafaat, H. S.; Ponce, A. *Applied and Environmental Microbiology* **2006**, *72*, 6808-6814.

(91) Jernigan, J. A.; Stephens, D. S.; Ashford, D. A.; Omenaca, C.; Topiel, M. S.; Galbraith, M.; Tapper, M.; Fisk, T. L.; Zaki, S.; Popovic, T.; Meyer, R. F.; Quinn, C. P.; Harper, S. A.; Fridkin, S. K.; Sejvar, J. J.; Shepard, C. W.; McConnell, M.; Guarner, J.; Shieh, W. J.; Malecki, J. M.; Gerberding, J. L.; Hughes, J. M.; Perkins, B. A. *Emerging Infectious Diseases* **2001**, *7*, 933-944.
(92) Sanderson, W. T.; Stoddard, R. R.; Echt, A. S.; Piacitelli, C. A.; Kim, D.; Horan, J.; Davies, M. M.; McCleery, R. E.; Muller, P.; Schnorr, T. M.; Ward, E. M.; Hales, T. R. *Journal of Applied Microbiology* **2004**, *96*, 1048-1056.
(93) Yung, P. T.; Lester, E. D.; Bearman, G.; Ponce, A. *Biotech. Bioeng.* **2007**, *84*, 864-871.
(94) Sharp, R. J.; Roberts, A. G. *J. Chem. Technol. Biotechnol.* **2006**, *81*, 1612-1625.
(95) Hindle, A. A.; Hall, E. A. H. *Analyst* **1999**, *124*, 1599-1604.
(96) Science, O. o. S., Ed.; Jet Propulsion Laboratory, 1980.
(97) Yung, P. T.; Kempf, M. J.; Ponce, A. In *IEEE Aerospace Conference*; IEEE: Big Sky, Montana, 2006.
(98) Gerhardt, P.; Marquis, R. E. In *Regulation of prokaryotic development*; Smith, I., Slepecky, R. A., Setlow, P., Eds.; American Society for Microbiology: Washington, D.C., 1989, pp 43-63.
(99) Murrell, W. G. *The Bacterial Spore*; Academic Press: New York, 1969.
(100) Slepecky, R.; Foster, J. W. *Journal of Bacteriology* **1959**, *78*, 117-123.
(101) Douki, T.; Setlow, B.; Setlow, P. *Photochemical & Photobiological Sciences* **2005**, *4*, 893-896.
(102) Setlow, B.; Setlow, P. *Applied and Environmental Microbiology* **1993**, *59*, 640-643.
(103) Setlow, B.; Atluri, S.; Kitchel, R.; Koziol-Dube, K.; Setlow, P. *Journal of Bacteriology* **2006**, *188*, 3740-3747.
(104) Vary, J. C. *Journal of Bacteriology* **1973**, *116*, 797-802.
(105) Prasad, C.; Diesterhaft, M.; Freese, E. *Journal of Bacteriology* **1972**, *110*, 321-328.
(106) Perry, J. J.; Foster, J. W. *Journal of Bacteriology* **1955**, *69*, 337-346.
(107) Janssen, F. W.; Lund, A. J.; Anderson, L. E. *Science* **1958**, *127*, 26-27.
(108) Yung, P. T., California Institute of Technology, Pasadena, 2008.
(109) Raymond Ooi, C. H.; Beadie, G.; Kattawar, G. W.; Reintjes, J. F.; Rostovtsev, Y.; Suhail Zubairy, M.; Scully, M. O. *Physical Review A* **2005**, *72*, 023807.
(110) Pestov, D.; Zhi, M. C.; Sariyanni, Z. E.; Kalugin, N. G.; Kolomenskii, A. A.; Murawski, R.; Paulus, G. G.; Sautenkov, V. A.; Schuessler, H.; Sokolov, A. V.; Welch, G. R.; Rostovtsev, Y. V.; Siebert, T.; Akimov, D. A.; Graefe, S.; Kiefer, W.; Scully, M. O. *Proceedings of the National Academy of Sciences of the United States of America* **2005**, *102*, 14976-14981.
(111) Ghiamati, E.; Manoharan, R.; Nelson, W. H.; Sperry, J. F. *Applied Spectroscopy* **1992**, *46*, 357-364.
(112) Rosen, D. L.; Sharpless, C.; McGown, L. B. *Reviews in Analytical Chemistry* **1999**, *18*, 1-21.
(113) Arnaud, N.; Vaquer, E.; Georges, J. *Analyst* **1998**, *123*, 261-265.
(114) Latva, M.; Takalo, H.; Mukkala, V. M.; Matachescu, C.; RodriguezUbis, J. C.; Kankare, J. *Journal of Luminescence* **1997**, *75*, 149-169.
(115) Carnall, W. T.; Fields, P. R.; Rajnak, K. *Journal Of Chemical Physics* **1968**, *49*, 4447-&.
(116) Kleinerman, M. *Journal Of Chemical Physics* **1969**, *51*, 2370-2381.
(117) Lamture, J. B.; Hong Zhou, Z.; Kumar, S.; Wensel, T. G. *Inorganic Chemistry* **1995**, *34*, 864-869.
(118) Horrocks Jr., W. D.; Sudnick, D. R. *Accounts of Chemical Research* **1981**, *14*, 384-392.
(119) Horrocks Jr., W. D.; Albin, M. *Progress in Inorganic Chemistry* **1984**, *31*, 1-104.

(120) Balzani, V. *Pure and Applied Chemistry* **1990**, *62*, 1099-1102.
(121) Balzani, V.; Decola, L.; Prodi, L.; Scandola, F. *Pure and Applied Chemistry* **1990**, *62*, 1457-1466.
(122) Lehn, J. M. *Angewandte Chemie-International Edition In English* **1988**, *27*, 89-112.
(123) Pellegrino, P. M.; Fell, N. F.; Rosen, D. L.; Gillespie, J. B. *Analytical Chemistry* **1998**, *70*, 1755-1760.
(124) Jones, G.; Vullev, V. I. *Journal of Physical Chemistry A* **2002**, *106*, 8213-8222.
(125) Cable, M. L.; Kirby, J. P.; Levine, D. J.; Manary, M. J.; Gray, H. B.; Ponce, A. *Journal Of The American Chemical Society* **2009**, *131*, 9562-9570.
(126) Gassner, A.-L.; Duhot, C.; Bunzli, J. C. G.; Chauvin, A. S. *Inorganic Chemistry* **2008**, *47*, 7802-7812.
(127) Bottrill, M.; Kwok, L.; Long, N. J. *Chemical Society Reviews* **2006**, *35*, 557-571.
(128) Eisinger, J.; Shulman, R. G.; Blumberg, W. E. *Nature* **1961**, *192*, 963-964.
(129) Lauffer, R. B. *Chemical Reviews* **1987**, *87*, 901-927.
(130) Sherry, A. D.; Brown, R. D.; Geraldes, C. F. G. C.; Koenig, S. H.; Kuan, K.-T.; Spiller, M. *Inorganic Chemistry* **1989**, *28*, 620-622.
(131) Bousquet, J. C.; Saini, S.; Stark, D. D.; Hahn, P. F.; Nigam, M.; Wittenberg, J.; Ferrucci, J., J. T. *Radiology* **1988**, *166*, 693-698.
(132) Brunet, E.; Juanes, O.; Rodriguez-Ubis, J. C. *Current Chemical Biology* **2007**, *1*, 11-39.
(133) Gunnlaugsson, T.; Leonard, J. P.; Mulready, S.; Nieuwenhuyzen, M. *Tetrahedron* **2004**, *60*, 105-113.
(134) Gunnlaugsson, T.; Harte, A. J.; Leonard, J. P.; Nieuwenhuyzen, M. *Supramolecular Chemistry* **2003**, *15*, 505-519.
(135) Gunnlaugsson, T.; Harte, A. J.; Leonard, J. P.; Nieuwenhuyzen, M. *Chemical Communications* **2002**, 2134-2135.
(136) Arnaud, N.; Georges, J. *Analyst* **1999**, *124*, 1075-1078.
(137) Zheng, X.-Y.; Lu, J.-Z.; Zhu, Q.-Z.; Xu, J.-G.; Li, Q.-G. *Analyst* **1997**, *122*, 455-458.
(138) Wenzel, T. J.; Collette, L. M.; Dahlen, D. T.; Hendrickson, S. M.; Yarmaloff, L. W. *Journal of Chromatography* **1988**, *433*, 149-158.
(139) Magennis, S. W.; Craig, J.; Gardner, A.; Fucassi, F.; Cragg, P. J.; Robertson, N.; Parsons, S.; Pikramenou, Z. *Polyhedron* **2003**, *22*, 745-754.
(140) Yamada, T.; Shinoda, S.; Sugimoto, H.; Uenishi, J.-I.; Tsukube, H. *Inorganic Chemistry* **2003**, *42*, 7932-7937.
(141) Yamada, T.; Shinoda, S.; Tsukube, H. *Chemical Communications* **2002**, 1218-1219.
(142) Charbonniere, L. J.; Ziessel, R.; Montalti, M.; Prodi, L.; Zaccheroni, N.; Boehme, C.; Wipff, G. *Journal Of The American Chemical Society* **2002**, *124*, 7779-7788.
(143) Montalti, M.; Prodi, L.; Zaccheroni, N.; Charbonniere, L.; Douce, L.; Ziessel, R. *Journal Of The American Chemical Society* **2001**, *123*, 12694-12695.
(144) Bruce, J. I.; Dickins, R. S.; Govenlock, L. J.; Gunnlaugsson, T.; Lopinski, S.; Lowe, M. P.; Parker, D.; Peacock, R. D.; Perry, J. J. B.; Aime, S.; Botta, M. *Journal of the American Chemical Society* **2000**, *122*, 9674-9684.
(145) Dickins, R. S.; Gunnlaugsson, T.; Parker, D.; Peacock, R. D. *Chemical Communications* **1998**, 1643-1644.
(146) Bazzicalupi, T. C.; Bencini, A.; Bianchi, A.; Giorgi, C.; Fusi, V.; Masotti, A.; Valtancoli, B.; Roque, A.; Pina, F. *Chemical Communications* **2000**, 561-562.
(147) Schreurs, M.; Somsen, G. W.; Gooijer, C.; Velthorst, N. H.; Frei, R. W. *Journal of Chromatography A* **1989**, *482*, 351-359.

(148) deSilva, A. P.; Gunaratne, H. Q. N.; Rice, T. E.; Stewart, S. *Chemical Communications* **1997**, 1891-1892.
(149) Parker, D.; Senanayake, P. K.; Williams, J. A. G. *Journal Of The Chemical Society-Perkin Transactions 2* **1998**, 2129-2139.
(150) Hanaoka, K.; Kikuchi, K.; Kojima, H.; Urano, Y.; Nagano, T. *Angewandte Chemie-International Edition* **2003**, *42*, 2996-2999.
(151) Lehn, J. M. *Structure and Bonding* **1973**, *16*, 1-69.
(152) Merbach, A. E.; Toth, E., Eds. *The chemistry of contrast agents in medical magnetic resonance imaging*; Wiley: West Sussex, England, 2001.
(153) Aime, S.; Botta, M.; Fasano, M.; Marques, M. P. M.; Geraldes, C.; Pubanz, D.; Merbach, A. E. *Inorganic Chemistry* **1997**, *36*, 2059-2068.
(154) Chang, C. A.; Chen, Y.-H.; Chen, H.-Y.; Shieh, F.-K. *Journal Of The Chemical Society-Dalton Transactions* **1998**, 3243-3248.

FIGURES

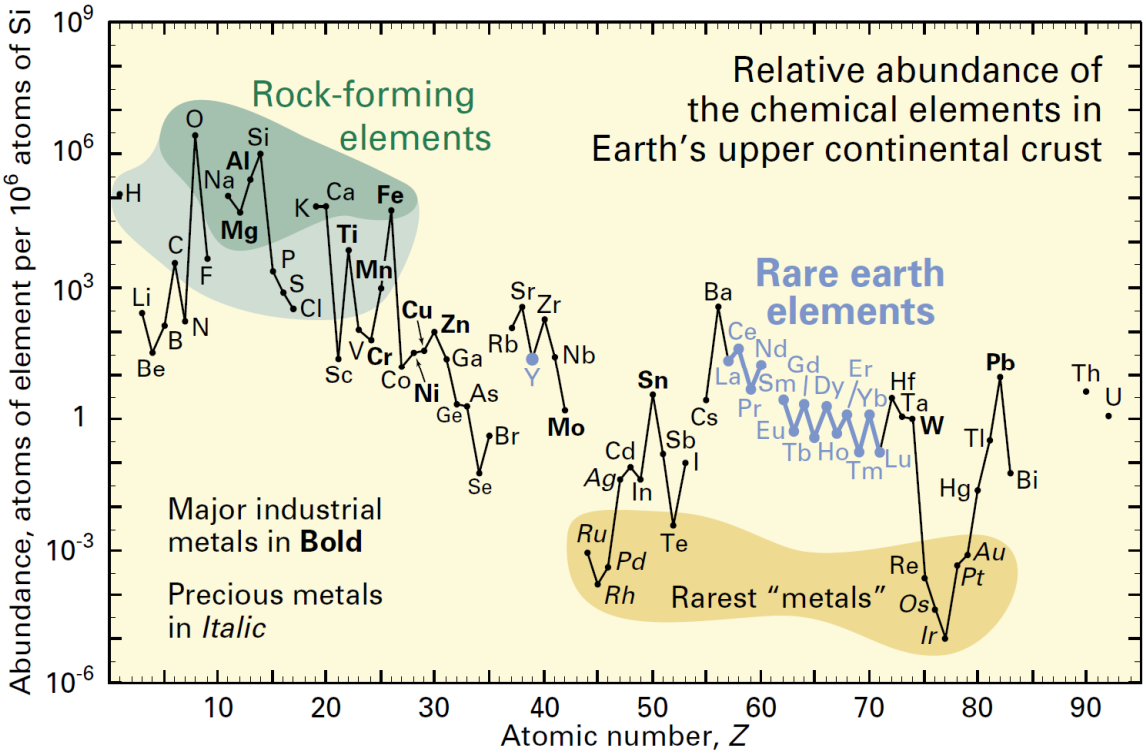

Figure 1.1. Abundance (atom fraction) of the chemical elements in the upper continental crust of the Earth as a function of atomic number. Many elements are classified according to categories: (1) rock-forming elements (major elements in dark green field, minor in light green); (2) major industrial metals (global production ≥3x10^7 kg/year, in **bold**); (3) precious metals and metalloids (*italic*); (4) the nine rarest metals (in orange field); and (5) the rare earth elements (labeled in blue). Reprinted from USGS Fact Sheet 087-02 (reference 2).

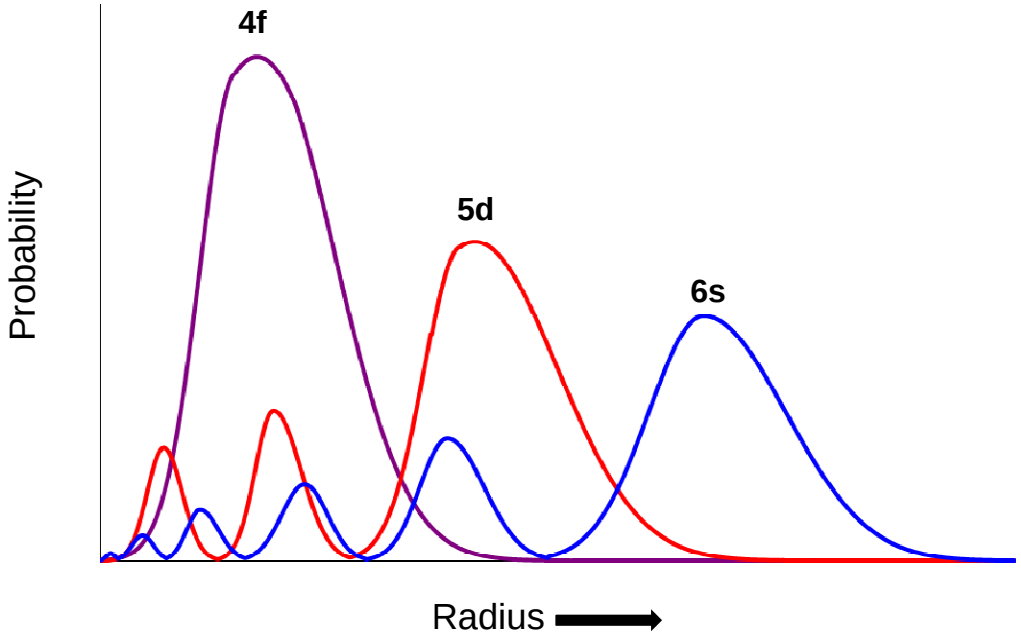

Figure 1.2. The radial portion of the hydrogenic wavefunctions for the 4f, 5d and 6s orbitals, showing the extent of shielding of the 4f orbitals. Redrawn from reference 5.

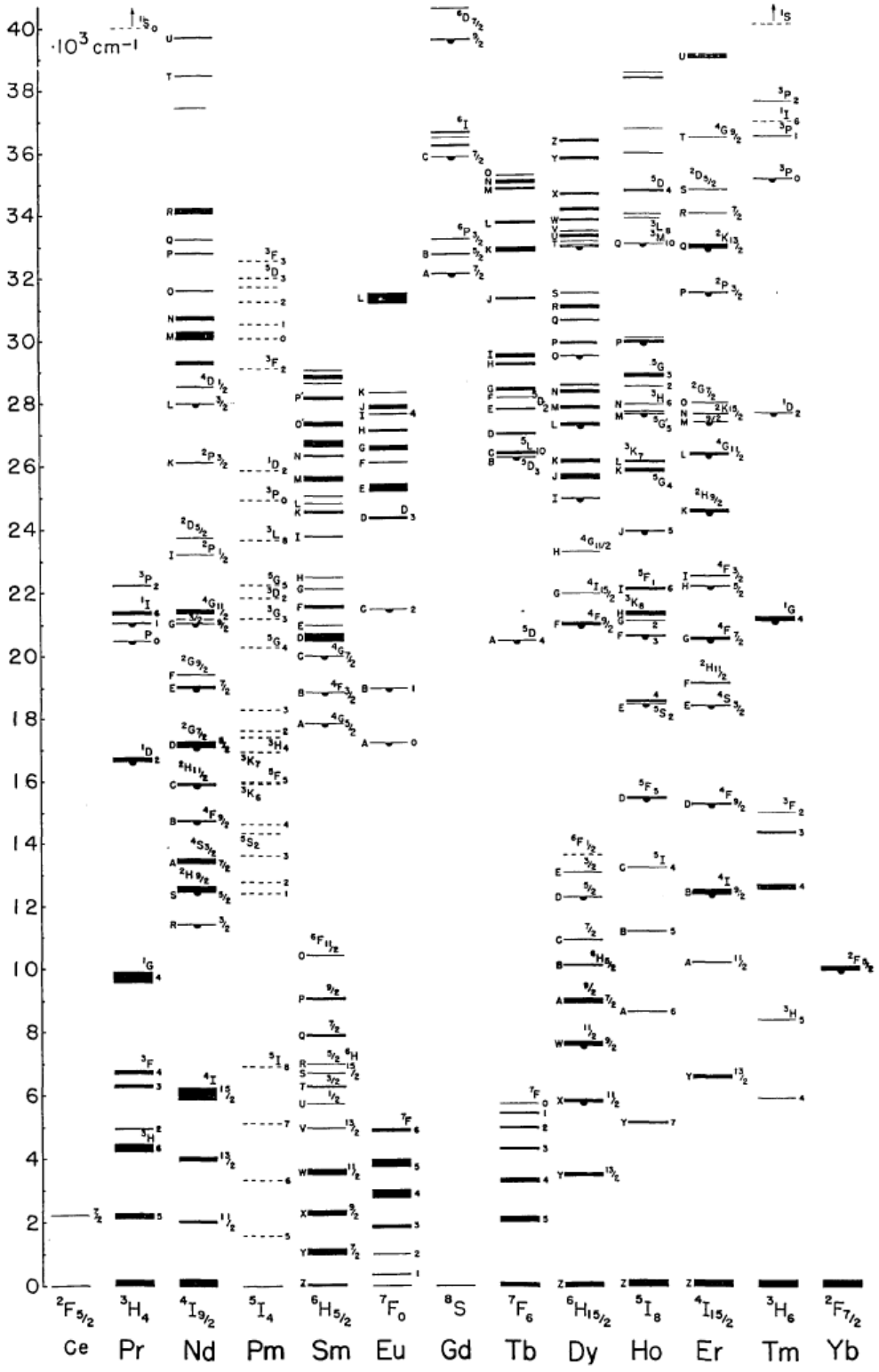

Figure 1.3. Energy level diagram, also known as a Dieke Diagram, depicting the free ion energy levels of the trivalent lanthanide ions from Ce^{3+} ($4f^1$) to Yb^{3+} ($4f^{13}$). Reprinted with permission from reference 20.

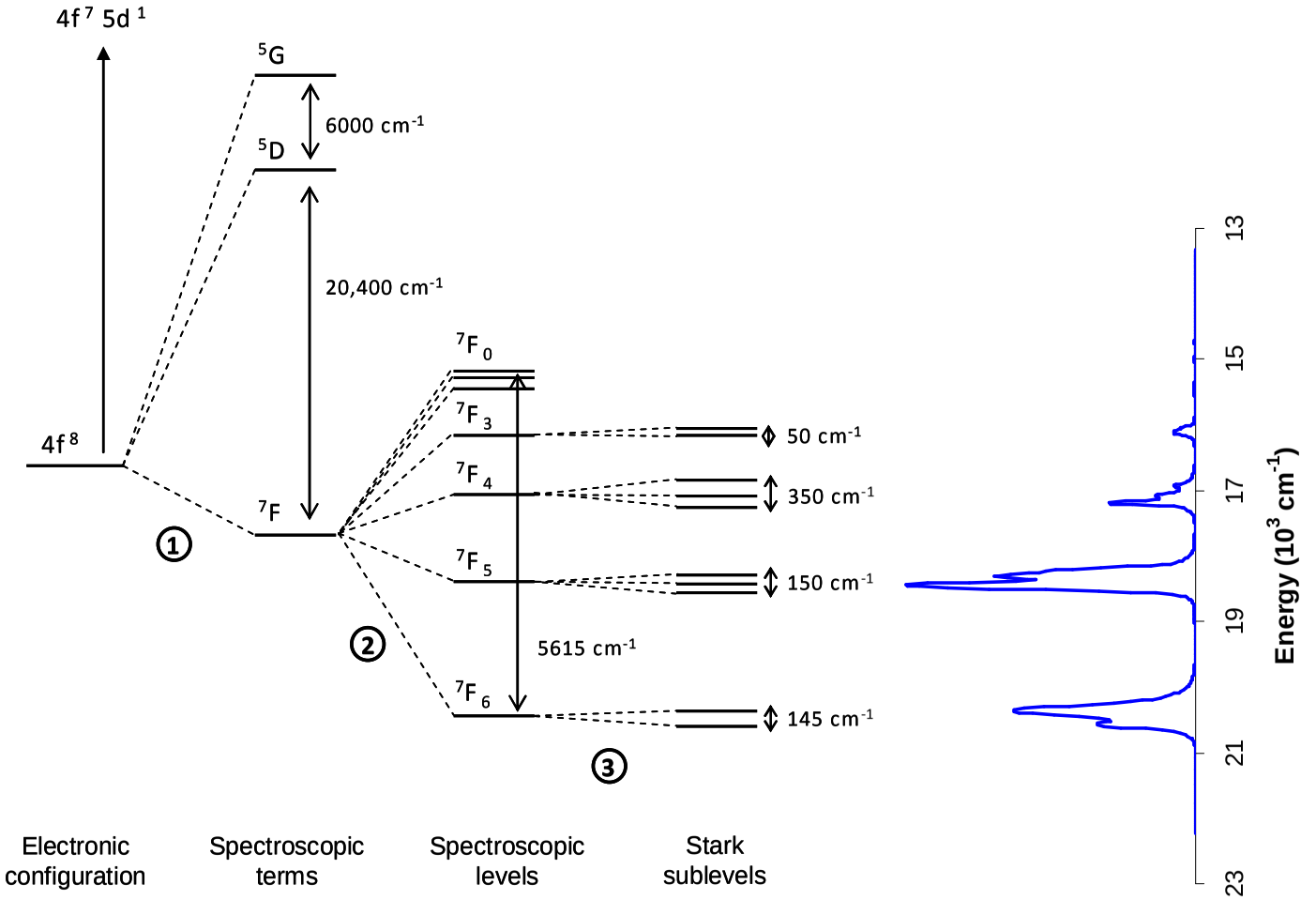

Figure 1.4. Splitting of lanthanide electronic configuration, with Tb^{3+} ($4f^8$) as an example, due to (1) interelectronic repulsion, (2) spin-orbit coupling, and (3) ligand-field effects. The emission spectrum of $Tb(DPA)_3$ at right illustrates the qualitative effect of such splitting.

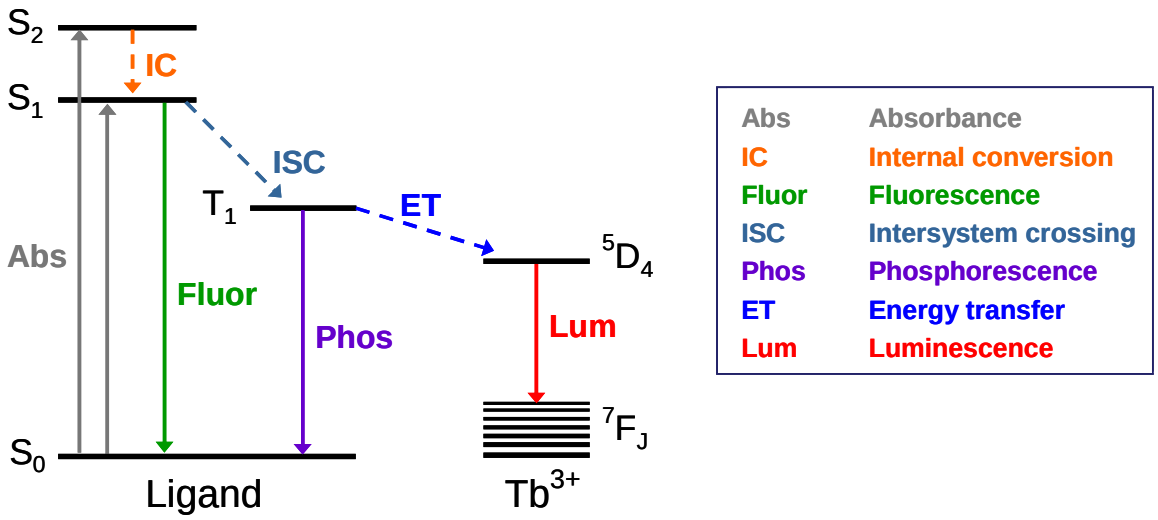

Figure 1.5. Jablonski diagram of the absorption-energy transfer-emission (AETE) mechanism from an aromatic donor ligand to Tb^{3+}. Radiative transitions are shown in solid arrows; nonradiative transfers are depicted with dashed arrows. UV radiation is absorbed by the conjugated π-electron system of the aromatic ligand leading to a singlet excited state; this energy transfers to the ligand triplet excited state via intersystem crossing (ISC) and then to the emittive level ($^5D_4$) of the Tb^{3+} ion. Luminescence is observed through radiative decay from the excited state to the seven energy levels of the Tb^{3+} heptet ground state (^7F_J). Note that fluorescence and phosphorescence are not always observed for aromatic donor ligands.

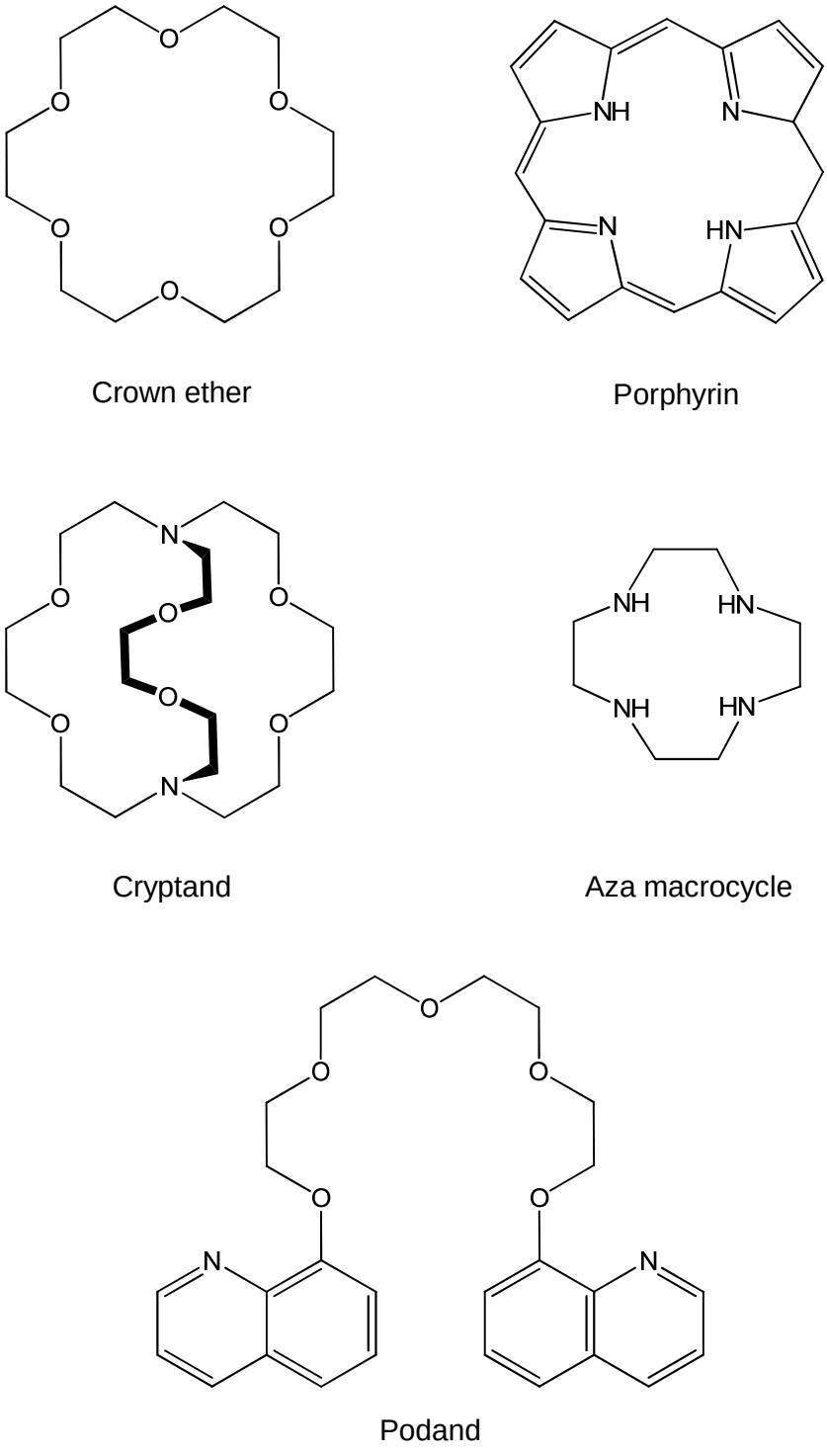

Figure 1.6. Structures of various chelating ligands used to encapsulate lanthanide ions. These ligands bind to lanthanide ions with high affinity and act as a shield against quenching due to coordinating solvent molecules.

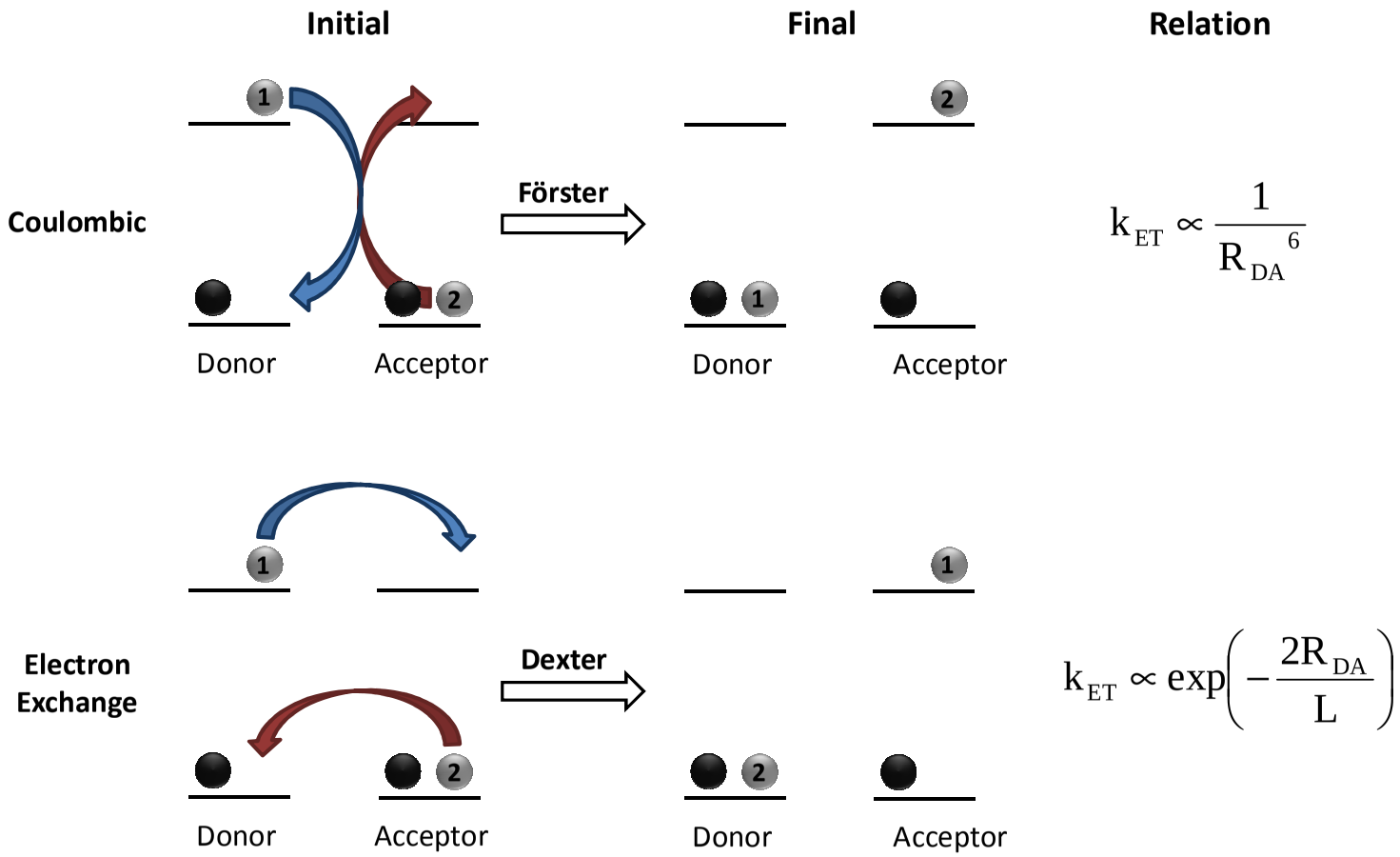

Figure 1.7. Comparison of Förster (Coulombic) and Dexter (electron exchange) energy transfer mechanisms. In the Förster mechanism, no electrons are transferred. Energy is exchanged via Coulombic interaction and is dipole-induced. The rate of energy transfer (k_{ET}) decreases as the intermolecular distance between donor and acceptor (R_{DA}) is increased. In the Dexter mechanism, orbital overlap is needed as electrons are transferred, so the rate of energy transfer drops off even more quickly with distance.

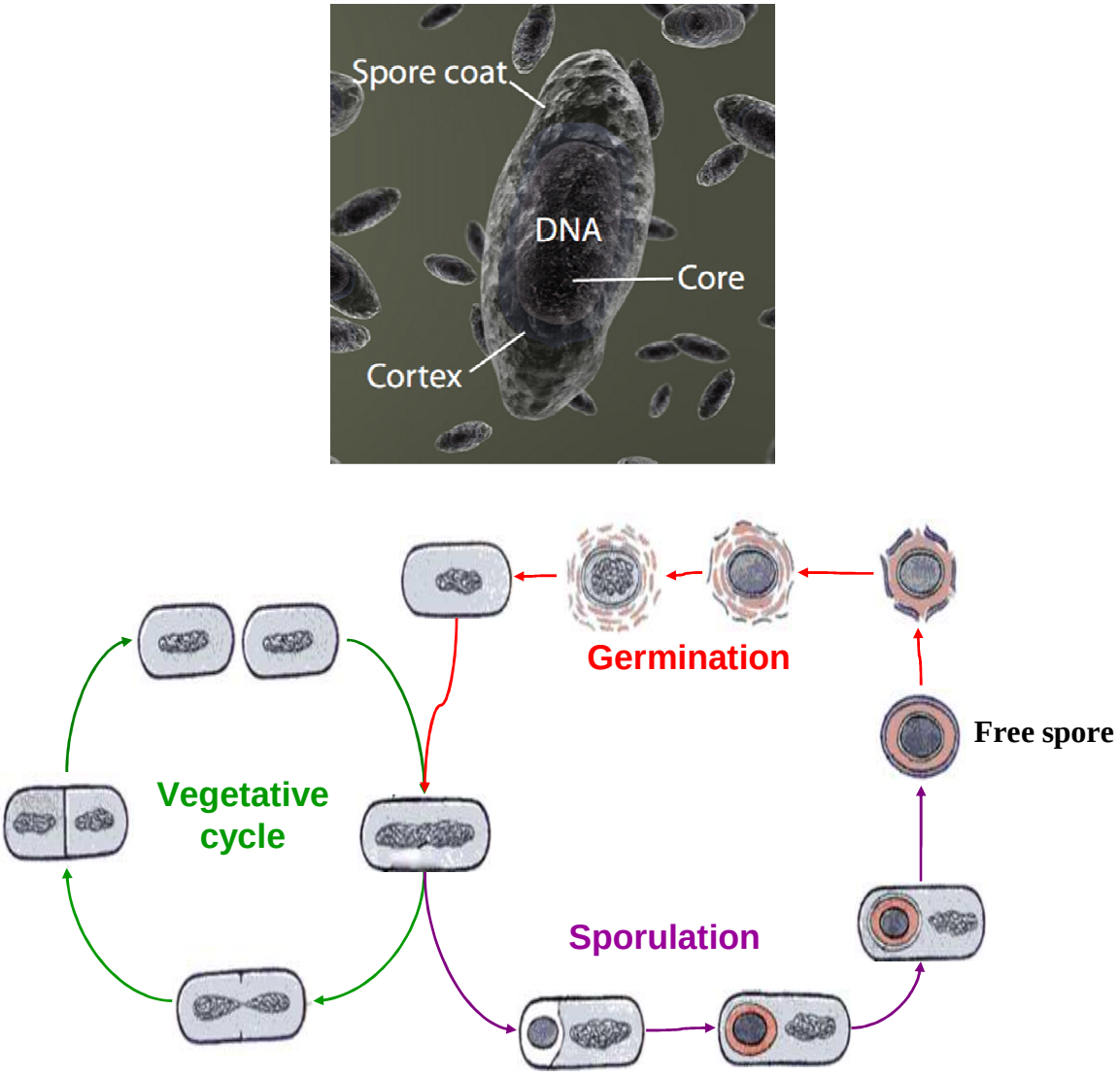

Figure 1.8. Composition and origins of the bacterial spore. Above: Artists' rendering of a typical bacterial spore, showing spore coat, cortex, and core. Below: Cell cycle of a spore-former, depicting normal vegetative cycle (green), which can be disrupted due to adverse environmental conditions triggering sporulation (purple). The free spore will remain dormant until water, nutrients or germinants induce germination (red), producing a vegetative cell.

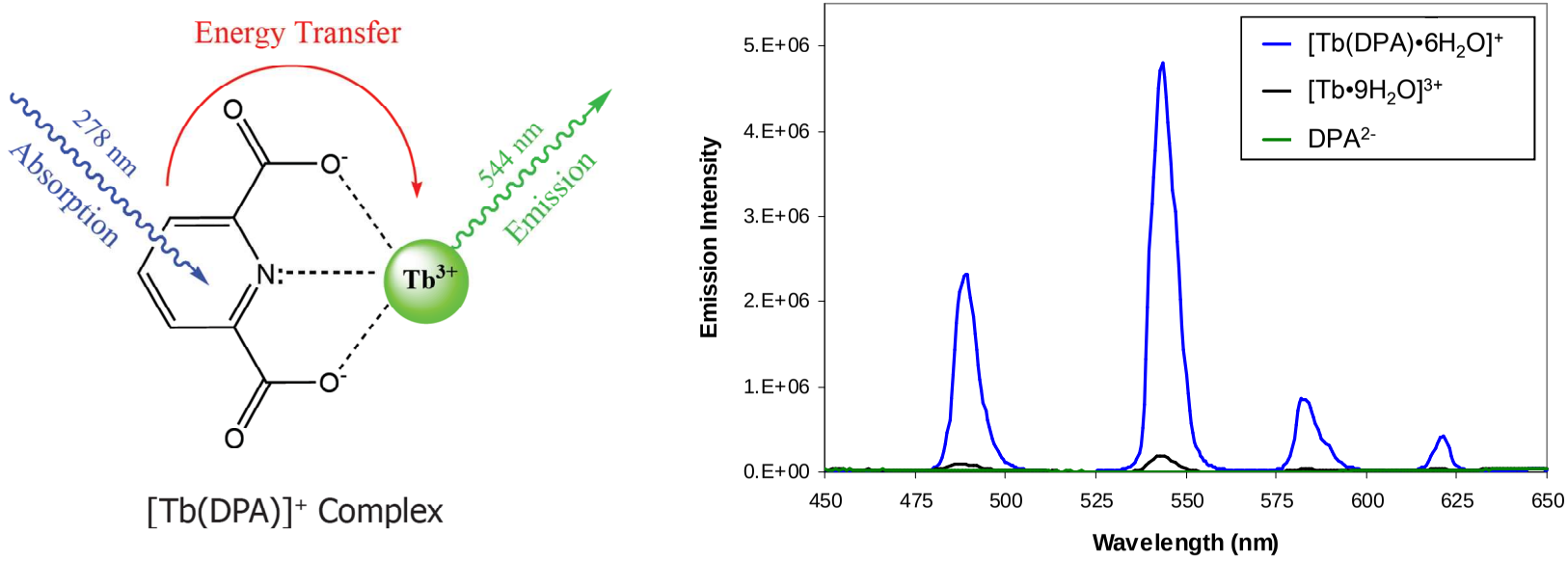

Figure 1.9. The method of bacterial spore detection using terbium. Dipicolinic acid (DPA) is released from endospores via lysis or germination, and binds to Tb^{3+} with high affinity (left). The resulting $[Tb(DPA)]^{+}$ complex exhibits intense luminescence in the visible region (544 nm) under UV excitation (278 nm) that is much greater than Tb^{3+} alone, as shown in the emission spectra at right.

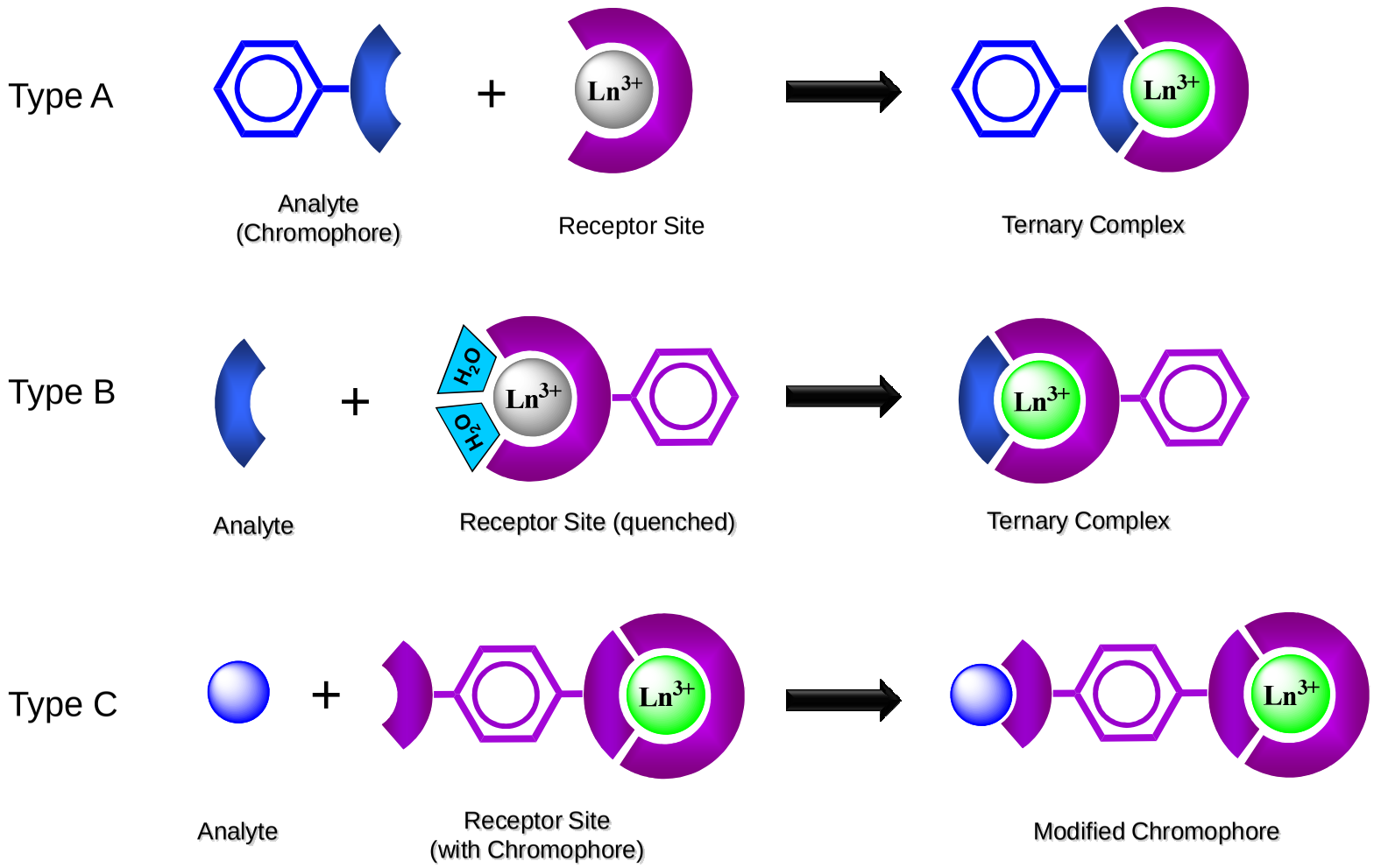

Figure 1.10. The three types of luminescent lanthanide sensors. In Type A, the analyte is also the chromophore, so binding results in sensitization and therefore luminescence turn-on. In Type B, the receptor site is quenched by solvent molecules, so binding of the analyte results in an increase in luminescence. In Type C, the receptor site is already luminescent, and binding of the analyte modifies this luminescence in some way (change in lifetime, intensity, quantum yield, etc.).

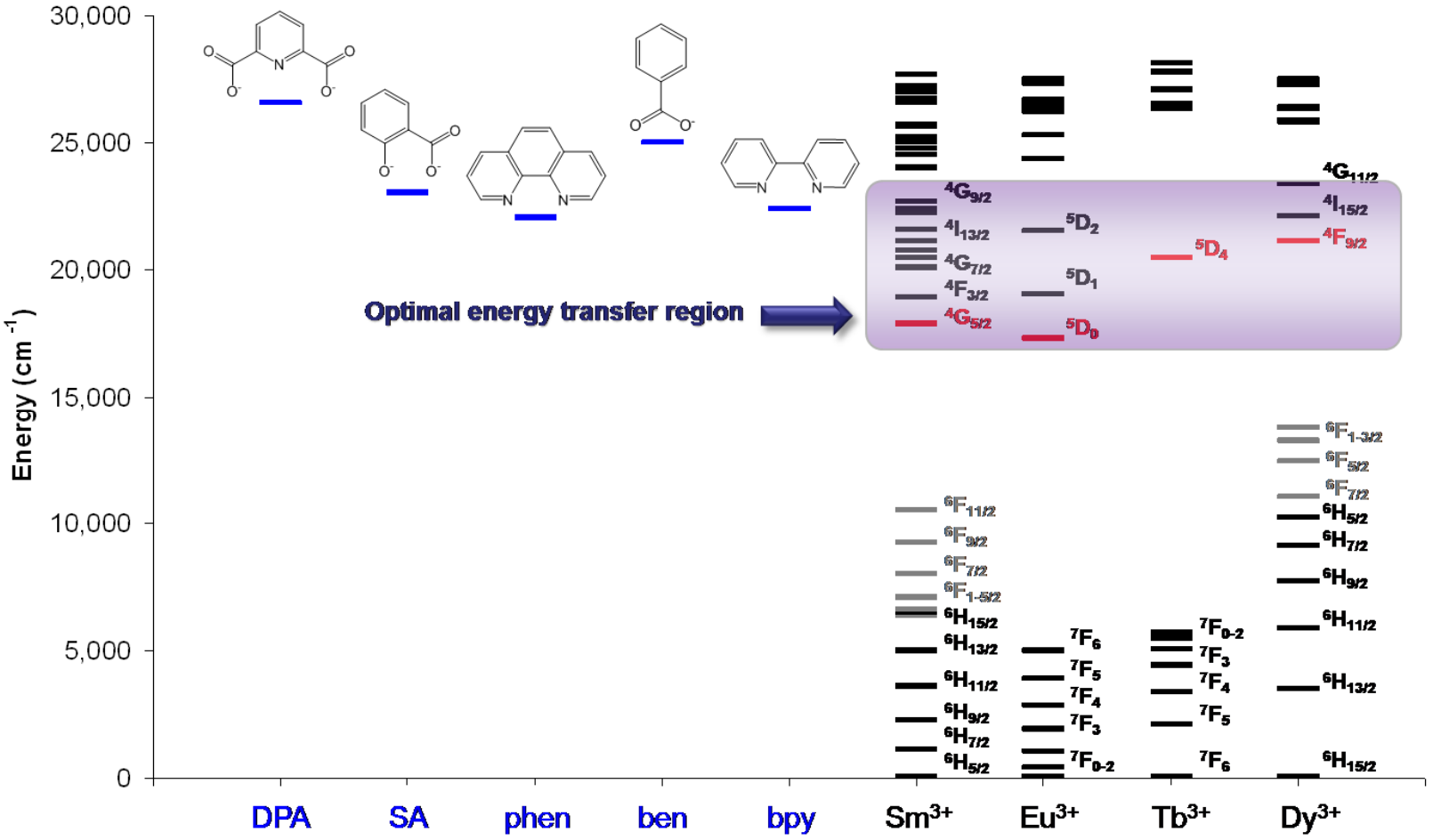

Figure 1.11. Energy level diagram depicting the triplet excited states of various aromatic ligands (blue) along with the excited and ground states of the four luminescent lanthanides (black). Lowest excited states are shown in red; ground states that do not contribute to luminescence are shown in gray. The area highlighted in purple illustrates the region where the energy gap between ligand triplet state and lanthanide excited state is optimal for efficient energy transfer (4000 500 cm^{-1} less than the ligand triplet state[57]). Aromatic ligands: dipicolinic acid (DPA); salicylic acid (SA); 1,10-phenanthroline (phen); benzoate (ben); 2,2'-bipyridine (bpy).

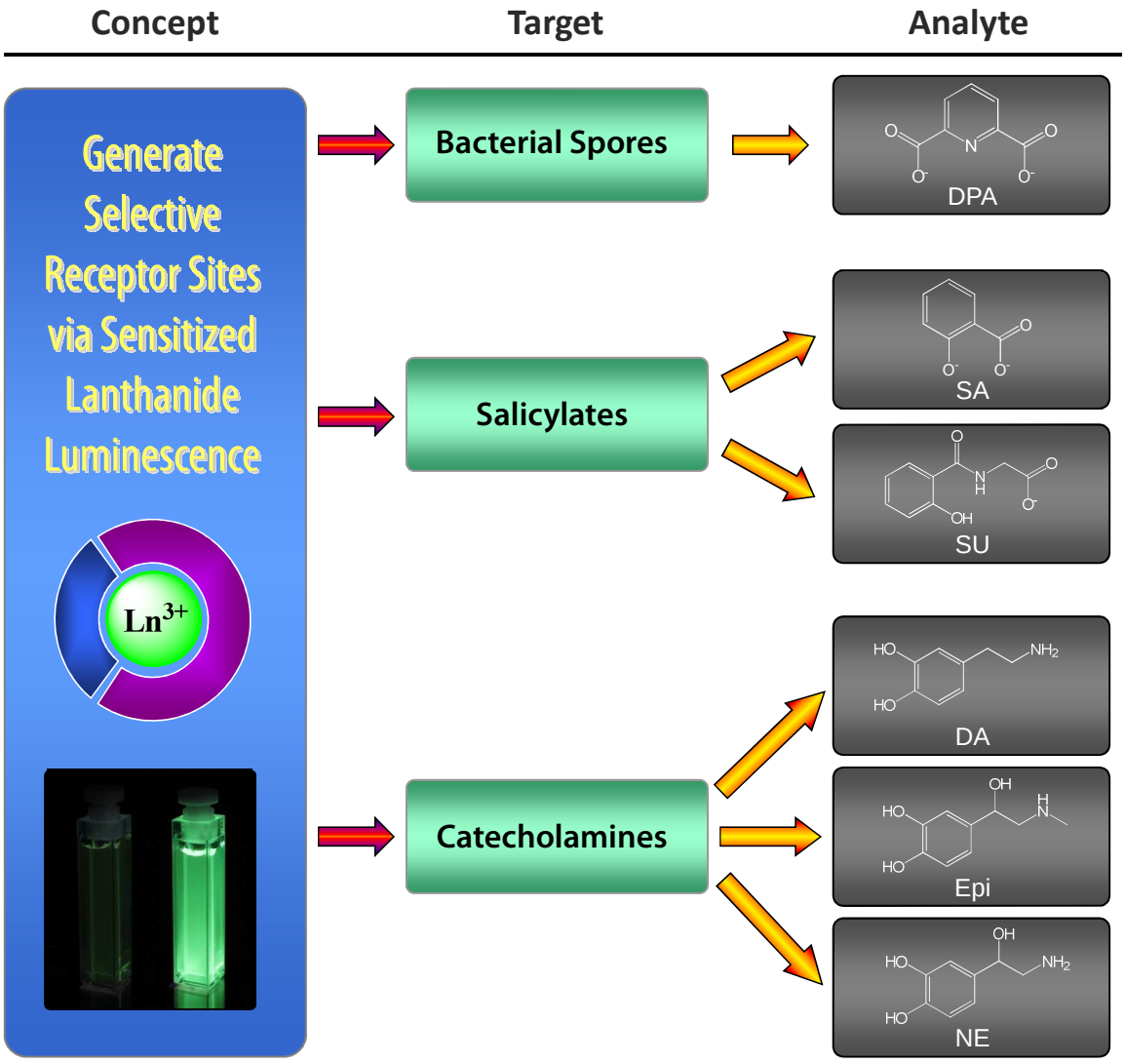

Figure 1.12. General design of thesis, illustrating the application of the receptor site design concept to three target areas, each with specific analyte(s) of interest.

CHAPTER 2

Ternary Complex Characterization: Crystal Structures, Photophysics and Theory

2.1 Introduction

Our goal is to generate a receptor site for the detection of bacterial spores using a dipicolinate-specific lanthanide binary complex. We have chosen DO2A (*1,4,7,10*-tetraazacyclododecane-*1,7*-bisacetate) as the chelating ligand because this macrocycle binds lanthanides with high affinity and leaves three adjacent coordination sites available on the Ln^{3+} ion for the tridentate DPA to bind. Prior to qualifying our lanthanide complexes as dipicolinate receptor sites, we must fully characterize the corresponding $Ln(DO2A)(DPA)^-$ ternary complexes for the various luminescent lanthanides (samarium, europium, terbium and dysprosium). This will involve structural and spectroscopic analyses to determine how parameters such as ligand bond length, luminescence quantum yield and hydration number vary across the series, in addition to theoretical studies to better understand any trends we may find. We expect that structural variations will follow with lanthanide ionic radius, but that the terbium and europium complexes will exhibit the greatest luminescence intensities due close coupling between the DPA triplet energy level and the lanthanide excited state.

2.2 Structural Characterization

2.2.1 Crystallization

Crystallization of the ternary $Ln(DO2A)(DPA)^-$ complexes (Ln = Sm, Eu, Gd, Tb and Dy) is necessary to produce pure compound for accurate quantum yield calculation and analysis of binding properties, as well as to confirm complex formation through crystallographic analysis. The energy gaps between the emissive excited states and the ground state manifolds for Sm^{3+} and Dy^{3+} are 7,400 cm^{-1} and 7,850 cm^{-1}, respectively,

significantly less than those of Tb^{3+} and Eu^{3+}.[1] However, these lanthanides are still capable of sensitized emission in the visible range, and due to their difference in ionic radii (nearly 5 pm difference from Sm^{3+} to Dy^{3+}) are of interest in structural characterization and binding studies.[2] Similarly, though gadolinium complexes cannot be used in luminescence experiments, crystals of $Gd(DO2A)(DPA)^{-}$ will provide additional structural information in terms of any trends due to lanthanide ionic radius. Reported here are the first structurally characterized ternary lanthanide(macrocycle)(dipicolinate) complexes.

Experimental Section

Materials. The following chemicals were purchased and used as received: acetone (J. T. Baker), acetonitrile (Fluka Biochemika), ammonium hydroxide (28.0–30.0% in water) (J. T. Baker), DPA (dipicolinic acid, pyridine-*2,6*,-dicarboxylic acid) (Aldrich), dysprosium(III) chloride hydrate (Alfa Aesar), ether anhydrous (Acros Organics), ethyl alcohol (200-proof) (Acros Organics), europium(III) chloride hexahydrate (Aldrich), hydrochloric acid (36.5–38.0% in water) (EMD Chemicals), methanol (J. T. Baker), samarium(III) chloride (Alfa Aesar), sodium hydroxide (NaOH 50% in water) (Mallinckrodt), terbium(III) chloride hexahydrate (Alfa Aesar), terbium(III) nitrate hexahydrate (Aldrich), tetrabutylammonium chloride hydrate (Aldrich), tetrabutylammonium hydroxide (TBAOH 10% in *2*-propanol) (TCI America), tetrabutylammonium hydroxide (TBAOH 40% in water) (TCI America), and tetraphenyl-arsonium(V) chloride hydrate (Aldrich). All lanthanide salts were 99.9% pure or greater, all solvents were ACS certified or HPLC grade, and all other salts were 97% pure or

greater. Water was deionized to a resistivity of 18.2 MΩ-cm using a Purelab® Ultra laboratory water purification system (Siemens Water Technologies, Warrendale, PA).

The *1,4,7,10*-tetraazacyclododecane-*1,7*-diacetate (DO2A) ligand was prepared by hydrolysis of *1,4,7,10*-tetraazacyclododecane-*1,7*-di(*tert*-butyl acetate) (DO2A-tBu-ester) (Macrocyclics, Dallas, TX).[3] The DO2A-tBu-ester (4.8334 g, 12.07 mmol), a slightly off-white powder, was dissolved in 120 mL of 20% hydrochloric acid in a roundbottom flask and refluxed for 24 hours with stirring in an oil bath (115 °C). The hydrochloric acid was removed by rotary evaporation under vacuum (~ 50 mbar) in a hot water bath (55 °C) for approximately 5 hours to give a white solid. The deprotected ligand was then rinsed using a fine frit (Pyrex, 15 mL, ASTM 4-5.5F, No. 36060) and vacuum filtration with the following in sequence: 50 mL of absolute ethanol (200-proof), 10 mL of diethyl ether, 20 mL of an ethanol-ether (1:1) mixture, and three 20-mL aliquots of ether. The solid was dried in a dessicator under vacuum for five days to produce DO2A·2.80HCl·0.85H_2O (4.6745 g, 11.53 mmol) in 94.84% yield. Anal. Calcd (found) for $C_{12}H_{24}N_4O_4$·2.80HCl·0.85H_2O (fw = 405.57): C, 35.54 (35.54); H, 7.08 (6.72); N, 13.81 (13.25); Cl, 24.43 (25.10).

Methods. Initial crystallization attempts of the Tb(DO2A)$(DPA)^-$ ternary complex involved addition of equimolar amounts of terbium chloride hexahydrate, dipicolinic acid and DO2A to a small volume (5.0 mL) of nanopure water (18.2 MΩ-cm resistivity). The pH was adjusted to ~ 8 with 50% sodium hydroxide added dropwise. The solution was vortexed and sonicated for approximately 1 minute until fully dissolved, filtered using a sterile Acrodisc® 25 mm syringe filter with a 0.2 μm Supor® membrane (Pall Corporation, Ann Arbor, MI), separated into 1-mL aliquots and set aside

for crystal formation. Though crystals were observed, the high solubility of the Tb(DO2A)(DPA) sodium salt in aqueous solution led to crystal formation only as the solution evaporated to dryness. The resulting crystals therefore had a white surface residue, presumably excess reactants and sodium chloride, which caused elemental and mass spectrometry analyses to be inconsistent with the solved crystal structure. Attempts to remove the residue with washing steps completely dissolved the crystals. Substitution of terbium nitrate for terbium chloride, or sodium dipicolinate (Na_2DPA) for dipicolinic acid, produced similar results. New solvent systems had to be explored.

Subsequent crystallization attempts included experimentation with various solvents (methanol, ethanol, acetonitrile), counterions (sodium hydroxide, ammonium hydroxide, tetraphenylarsonium chloride, tetrabutylammonium chloride), filters (0.2 μm syringe filters, glass wool, Pyrex fine and medium frits) and reaction conditions (pH, temperature). Components were combined in aqueous solution, and following confirmation of ternary complex formation by fluorescence spectroscopy, the solutions were lyophilized using a MicroModulyo Freeze Dryer (Thermo Electron Corporation, Waltham, MA) to dryness. The solid was then resuspended in the desired solvent and filtered prior to slow evaporation at a specified temperature. In all cases, only precipitates were observed. As with the aqueous case, the high solubility of the ternary complex salts in methanol resulted in precipitation only upon going to dryness, so this solvent was abandoned as well.

It was hypothesized that the use of both a strong base and a counterion salt to adjust solution pH and provide a cation for Tb(DO2A)(DPA)$^-$, respectively, was forming other salts with greater propensities to crystallize or form a precipitate. Therefore, the pH

adjustment base and counterion salt were combined into one reagent to minimize the extraneous ions in solution. Instead of using sodium hydroxide in conjunction with tetrabutylammonium chloride to produce the tetrabutylammonium (TBA) salt of Tb(DO2A)(DPA), for example, only tetrabutylammonium hydroxide (TBAOH) was added, eliminating the potential to form sodium salts that might interfere with crystallization of the ternary complex. It should also be noted that *only* the TBAOH in isopropanol resulted in crystal formation; performing the identical procedure with TBAOH in water resulted in precipitation. This may indicate that isopropanol is a critical component in the unit cell (see Section 2.2.2). Fluorescence and gravimetric studies revealed that the TBA·Tb(DO2A)(DPA) salt had greater solubility in acetone than in acetonitrile, ethanol, or mixtures of acetonitrile and ethanol (5%, 10% and 20% ethanol). Acetone therefore became the solvent of choice, and ultimately produced crystals of sufficient size and quality for high resolution diffraction studies. It should finally be noted that only *new* frits produced crystals of high quality; a previously-used frit, even if only used once under identical conditions for the same crystallization, would result in poor quality crystals or a precipitate. Attempts to clean the frits using exhaustive rinsing in several solvents, various acid digests or kilning did not resolve the issue. It is therefore recommended that the procedure be performed with care and adjusted to produce sufficient sample, as a new frit must be used each time.

Equimolar aliquots of $TbCl_3 \cdot 6H_2O$ (0.18974 g, 0.508 mmol) and DO2A·2.80HCl·1.00H_2O (0.20738 g, 0.508 mmol) were dissolved in 3.00 mL of nanopure water (18.2 MΩ-cm resistivity) using gentle heating (40 °C) and sonication. The white cloudy mixture became clear and colorless upon clarification. The pH of the solution was

adjusted to ~ 6 with tetrabutylammonium hydroxide (TBAOH, 10% in 2-propanol) added dropwise, and the solution was allowed to equilibrate with stirring and gentle heating for at least 2 hours to promote complete formation of the $Tb(DO2A)^+$ complex. A slightly smaller aliquot of DPA (0.08176 g, 0.489 mmol) was then added to the solution, along with 11.00 mL of nanopure H_2O. This is to prevent formation of any $Tb(DPA)_n$ species ($1 \leq n \leq 3$). The pH of the solution was adjusted to 8.5 with TBAOH, added dropwise. Addition of the yellow TBAOH solution caused formation of a white precipitate, but clarification was observed with stirring and gentle heating in under 5 minutes. The clear, yellow solution was lyophilized using a MicroModulyo Freeze Dryer for 6 days, and 20.0 mL of acetone was added to the resulting orange solid, which was sonicated and vortexed to solubilize as much of the ternary complex as possible. The mixture was centrifuged at 8000 rpm (25 ºC) for 20 minutes (Model 5810 R, Eppendorf, Hamburg, Germany), and the yellow/orange supernatant was quickly and carefully decanted from the white pellet. The supernatant was filtered through a new fine frit (Pyrex, 15 mL, ASTM 4-5.5F) under vacuum with a bell jar directly into a clean scintillation vial (rinsed 3 times with filtered acetone to remove any particulates that might cause multiple nucleation sites). Crystal formation was observed after sitting at room temperature for 24 hours. Suitable crystals were utilized for X-ray diffraction studies at the Beckman Institute X-ray Crystallography Facility (Caltech), while the rest were dried over P_2O_5 under vacuum for 7 days and delivered to: (1) Desert Analytics Transwest Geochem for elemental analysis, and (2) the mass spectrometer facility at Caltech.

Elemental analysis. Elemental analysis was performed in duplicate with determination of carbon, hydrogen, nitrogen and the lanthanide of interest. The CHN

protocol is based on analysis using the Dumas method,[4] where combustion and oxidation with a WO_3 catalyst converts carbon, hydrogen and nitrogen to CO_2, H_2O and NO_X, respectively. The NO_X is reduced to N_2 and the gases are separated using a packed column prior to detection via thermal conductivity. Metal prep involves acid digestion and detection via inductively coupled argon plasma atomic emission spectroscopy (ICAP-AES).

Mass spectrometry. Dried crystals were dissolved in methanol and the mass spectrum obtained using a LCQ Finnigan MAT electrospray ionization mass spectrometer (ESI-MS) in negative ion mode.

Results and Discussion

The same procedure developed for $Tb(DO2A)(DPA)^-$ was used to produce crystals of the samarium, europium, gadolinium and dysprosium ternary complexes as tetrabutylammonium salts. Detailed characterization of each batch of crystals is provided (vide infra). Low yields are due to the relatively low solubility of the complex in acetone, as evidenced by a significant percentage of precipitate remaining after centrifugation. As the focus of this crystallization was on quality as opposed to quantity, the yield was not optimized.

TBA·Sm(DO2A)(DPA). 0.474 g, yield: 44.8%. Anal. Calcd (found) in duplicate for $NC_{16}H_{36}\cdot SmC_{19}H_{25}N_5O_8\cdot 3.29H_2O\cdot 0.21C_{16}H_{36}NCl$ (fw = 960.8): C, 47.88 (47.80); H, 7.87 (7.40); N, 9.05 (9.32); Sm, 15.65 (15.65). ESI-MS (*m/z*): calcd (found) for $SmC_{19}H_{25}N_5O_8$ (M^-) 603.4 (603.1).

TBA·Eu(DO2A)(DPA). 0.269 g, yield: 38.9%. Anal. Calcd (found) in duplicate for $NC_{16}H_{36}\cdot EuC_{19}H_{25}N_5O_8\cdot 3.52H_2O\cdot 0.93C_{16}H_{36}NCl$ (fw = 1168.8): C, 51.32 (51.33); H, 8.77 (8.00); N, 8.31 (8.49); Eu, 13.00 (12.95). ESI-MS (*m/z*): calcd (found) for $EuC_{19}H_{25}N_5O_8$ (M^-) 604.4 (604.1).

TBA·Gd(DO2A)(DPA). 0.158 g, yield: 19.8%. Anal. Calcd (found) in duplicate for $NC_{16}H_{36}\cdot GdC_{19}H_{25}N_5O_8\cdot 3.3H_2O\cdot 1.8C_3H_6O\cdot 0.3HCl$ (fw = 1027.7): C, 47.36 (47.37); H, 7.74 (7.41); N, 8.18 (8.70); Gd, 15.30 (15.30); Cl, 0.95 (0.95). TOF-MS ES (*m/z*): calcd (found) for $Gd_1C_{19}H_{25}N_5O_8$ (M^-) 609.0944 (609.0947).

TBA·Tb(DO2A)(DPA). 0.301 g, yield: 42.3%. Anal. Calcd (found) in duplicate for $NC_{16}H_{36}\cdot TbC_{19}H_{25}N_5O_8\cdot 1.00C_3H_6O\cdot 4.00H_2O$ (fw = 982.97): C, 46.43 (46.63); H, 7.69 (8.17); N, 8.55 (8.71); Tb, 16.17 (15.65). ESI-MS (*m/z*): calcd (found) for $TbC_{19}H_{25}N_5O_8$ (M^-) 610.4 (610.1).

TBA·Dy(DO2A)(DPA). 0.102 g, yield: 45.4%. Anal. Calcd (found) in duplicate for $NC_{16}H_{36}\cdot DyC_{19}\ H_{25}N_5O_8\cdot 9.24H_2O\cdot 1.45C_{16}H_{36}NCl$ (fw = 1426.9): C, 49.04 (49.05); H, 9.31 (7.66); N, 7.32 (8.68); Dy, 11.39 (11.40). ESI-MS (*m/z*): calcd (found) for $Dy_1C_{19}H_{25}N_5O_8$ (M^-) 615.4 (615.1).

Even in acetone, the crystals were visibly luminescent under UV excitation with a handheld UVGL-25 multiband UV lamp (UVP, Upland, CA) in short wave (254 nm) and long wave (365 nm) modes. The terbium crystals displayed green luminescence, the europium crystals had red emission, dysprosium a faint yellow and samarium a dim pink (Figure 2.1). Once dry, the crystals became opaque and much more luminescent under UV irradiation, presumably due to loss of solvent from the unit cell.

2.2.2 X-ray Crystallography

All five TBA·Ln(DO2A)(DPA) complexes will be analyzed to determine ligand chelation motif and the corresponding bond lengths and angles. The DO2A ligand should coordinate in a hexadentate fashion, with the tridentate dipicolinate ligand occupying the remaining three coordination sites on the Ln^{3+} ion. We anticipate slight variations due to the lanthanide contraction as we go from the largest Sm^{3+} ion to the smallest Dy^{3+} ion in the series of five lanthanides investigated.

Experimental Section

Methods. Diffraction data for the Sm, Eu, Tb and Dy crystals were collected at 100 ± 2 K on a Bruker SMART 1000 CCD area detector diffractometer equipped with graphite monochromated MoKα radiation (λα = 0.71073 Å). A Bruker KAPPA APEX II diffractometer was utilized for the Gd crystals at the same temperature and wavelength. To reduce solvent loss, all crystals were coated in a layer of epoxy prior to mounting and data collection.

The structures were solved by direct methods for the Sm, Eu, and Gd complexes and isomorphous methods for the Dy complex using SHELXS-97.[5] The Tb structure was solved by direct methods using Bruker XS (version 6.12).[6] All complexes were refined by full-matrix least-squares calculations on F^2 against all reflections using the Direct Bruker XL (Tb)[7] or SHELXL-97 (Sm, Eu, Gd, Dy) program packages.[8, 9] Non-hydrogen atoms were refined anisotropically. The hydrogen atoms were introduced in calculated positions. CCDC reference numbers 655647 (Sm), 634507 (Eu), 746157 (Gd), 629354 (Tb) and 643596 (Dy). Crystal and refinement data are collected in Table 2.1. Complete

crystallographic data for all five complexes, including asymmetric unit contents, atomic coordinates, bond distances and angles, and anisotropic displacement parameters, is listed in Appendix D.

Results and Discussion

With the exception of europium, all Ln(DO2A)(DPA)$^{-}$ complexes crystallized in the monoclinic space group $P2_1/c$, indicating a primitive lattice with an inversion center. The unit cell has a 2_1 screw axis, meaning a two-fold rotation (180°) followed by a translation of ½ of the lattice vector in the direction of symmetry. This space group also has a glide plane along the c-axis, signifying a translation along half the lattice vector orthogonal to the direction of symmetry.[10] The Eu(DO2A)(DPA)$^{-}$ complex crystallized in the triclinic space group P1, indicating a primitive lattice with no symmetry. Though this is a different space group in Hermann-Mauguin notation,[11, 12] all five ternary complexes are crystallographically isostructural, with slight differences (< 0.05 Å) appearing to follow the trend of Ln^{3+} ionic radius (Figures 2.2, 2.3). The difference in space groups is attributed to the fact that the solvent region of the unit cell in all structures was disordered, containing acetone/isopropanol, ethanol and water.

As anticipated, in all five structures the lanthanide is complexed in a 9-coordinate fashion between the tridentate DPA and hexadentate DO2A ligands, and solvent is completely excluded from the Ln^{3+} coordination sphere. The coordination geometry of the lanthanide in each structure can be described as a slightly distorted capped staggered square bipyramidal conformation, with a pseudo-C2 axis passing through the DO2A core, the lanthanide and the DPA nitrogen (Figure 2.4). Although there are four possible

stereoisomers of the lanthanide-cyclen compound,[13, 14] only Δ(λλλλ) or Λ(δδδδ) is observed in the asymmetric unit. On average, the Ln--N interatomic distances for the DO2A ligand are slightly shorter than reported values for similar macrocyclic lanthanide complexes, whereas the Ln--O distances are slightly longer (Table 2.2).[15] This may indicate that the lanthanide ion is sitting more deeply in the DO2A macrocycle ring, which is supported by a slight decrease in the N-Ln-O bite angle for the coordinated carboxylate 'arms' from 66.4° in Eu(DOTA) to 65.9° in the $Eu(DO2A)(DPA)^-$ complex.[15] In contrast to the DOTA case, the Ln--N distances for the DO2A ligand are also no longer equivalent; the two substituted aza nitrogens are ~ 0.08 Å closer than the two nitrogens lacking coordinating arms. Similar distortions (0.04 – 0.05 Å) have been reported for DO3A derivatives coordinated to Tb^{3+} and Eu^{3+}.[16]

The crystal structure for calcium dipicolinate trihydrate contains the DPA ligand in a planar configuration.[17] However, all five crystal structures of the $Ln(DO2A)(DPA)^-$ complex show a slight torsion of the carboxylate oxygens coordinated to the lanthanide out of the plane of symmetry. Though this might indicate a steric interaction between the dipicolinate and macrocyclic ligands, this distortion does not appear to hinder dipicolinate coordination; Ln--O and Ln--N distances for DPA are within the range reported for the terbium tris(dipicolinate) complex (± 0.01 Å).[18]

2.2.3 Temperature Dependence

Crystals of TBA·Tb(DO2A)(DPA) and TBA·Eu(DO2A)(DPA) will be studied at temperatures of 100, 200 and 300 K to determine if any discernable temperature dependence exists in bond lengths and/or angles of the crystal structures.

Experimental Section

Methods. Crystals were mounted on a glass fiber using Paratone oil, coated in epoxy and placed on the diffractometer under a nitrogen stream at the designated temperature. Diffraction data were collected at 100 ± 2 K, 200 ± 2 K and 300 ± 2 K on a Bruker KAPPA APEX II diffractometer equipped with graphite monochromated MoKα radiation (λα = 0.71073 Å). For each complex, the same crystal was used for all three temperatures. The structures were solved by direct methods using SHELXS-97 and refined by full-matrix least-squares calculations on F^2 against all reflections using the SHELXL-97 program package. Non-hydrogen atoms were refined anisotropically.

For the Eu complex, the asymmetric unit contained acetone at one site that was disordered between two orientations; this site was refined as a rigid body starting with the coordinates from the 100 K structure. Hydrogen atoms on water were located in the electron density difference map and were constrained to ride the appropriate oxygen. All other hydrogens were placed at geometric positions and refined as riding atoms. No other restrains were placed on the model. CCDC reference numbers 761599 (100 K), 762705 (200 K) and 763335 (300 K). Crystal and refinement data are collected in Table 2.3. Complete crystallographic data for all three complexes, including asymmetric unit contents, atomic coordinates, bond distances and angles, and anisotropic displacement parameters, is listed in Appendix E.

Results and Discussion

As temperature increases from 100 K to 300 K, the Ln--DPA distance decreases slightly (0.01 Å) and the Ln--DO2A distance increases by approximately the same

margin for both the Tb and Eu complexes. This trend with temperature only appears to affect the Ln^{3+} coordination to the macrocyclic ring; the Ln--O distances of the carboxyl arms do not change. We attribute most of the observed shift to libration, and conclude that if there is a temperature dependence in the crystal structures of the TBA·Ln(DO2A)(DPA) complexes, it is negligible.

2.3 Photophysics

2.3.1 Spectroscopy

While absorption spectroscopy can provide some information about complexes involving dipicolinate, this technique does not tell us much about the lanthanides due to the forbidden nature of f–f transitions. Fluorescence spectrophotometry, in contrast, can reveal the symmetry of the lanthanide coordination sphere, the extent of sensitization by the chromophore and whether solvent deactivation is a significant source of quenching.

Experimental Section

Materials. The following chemicals were purchased and used as received: DPA (dipicolinic acid, pyridine-*2,6,*-dicarboxylic acid) (Aldrich), deuterium oxide 99.9% (Cambridge Isotope Laboratories, Inc.), dysprosium(III) chloride hydrate (Alfa Aesar), europium(III) chloride hexahydrate (Aldrich), nitric acid (EMD Chemicals, Inc.), samarium(III) chloride (Alfa Aesar), sodium acetate trihydrate (Mallinckrodt), sodium hydroxide (NaOH 50% in water) (Mallinckrodt), terbium(III) chloride hexahydrate (Alfa Aesar), tris buffer (tris-[hydroxymethyl]aminomethane) (MP Biomedicals, LLC) and L-tryptophan (Alfa Aesar). DO2A was prepared as previously described (Section 2.2.1).

Methods. Stock solutions of LnDPA and $Ln(DPA)_3$ were prepared gravimetrically by addition of the lanthanide chloride salt to 0.9 or 10 equivalents of dipicolinate, respectively, and dilution in nanopure water (18.2 MΩ-cm resistivity). Stock solutions of ternary complex were prepared gravimetrically from dried TBA·Ln(DO2A)(DPA) crystals of known molecular weight (Section 2.2.1). These stock solutions were diluted to 10.0 μM in 0.1 M Tris buffer (pH 7.9, adjusted with 50% NaOH added dropwise) or 0.2 M sodium acetate (pH 7.4, adjusted with 50% NaOH added dropwise). All solutions were allowed to equilibrate for at least 24 hours prior to analysis.

Absorbance measurements were made in quartz cuvettes (1 cm path length) using a Cary 50 Bio UV/Visible Spectrophotometer (Varian, Inc., Palo Alto, CA), and luminescence measurements, also in quartz, were performed using a Fluorolog-3 Fluorescence Spectrometer (Horiba Jobin-Yvon, Edison, NJ). To prevent the second-order diffraction of the source radiation, a 350-nm cutoff filter (03 FCG 055, Melles Griot, Covina, CA) was used in all luminescence measurements. All reported spectra were obtained as a ratio of corrected signal to corrected reference (S_c/R_c), where the reference is a separate photodiode detector, to eliminate the effect of varying background radiation in the sample chamber (Figure 2.5). Reported intensities are in units of counts per second per microampere (cps/μA).

Results and Discussion

Absorbance, luminescence excitation (λ_{Sm} = 600 nm, λ_{Eu} = 615 nm, λ_{Tb} = 544 nm, λ_{Dy} = 574 nm) and emission (λ_{ex} = 278 nm) spectra were obtained for each ternary

complex (excluding Gd). The UV absorption spectra of all four complexes (Figure 2.6) revealed peaks at 271 and 278 nm, attributable to the $\pi \rightarrow \pi^*$ transitions of bound DPA.[19] Luminescence excitation and emission spectra (Figures 2.7–2.10) are consistent with a DPA $\rightarrow Ln^{3+}$ energy transfer mechanism, where the most intense emission occurs at 601 nm ($^4G_{5/2} \rightarrow {}^6H_{7/2}$) for the Sm complex, 617 nm ($^5D_0 \rightarrow {}^7F_2$) for the Eu complex, 545 nm ($^5D_4 \rightarrow {}^7F_5$) for the Tb complex and 484 nm ($^4F_{9/2} \rightarrow {}^6H_{15/2}$) for the Dy complex.[20-23]

To confirm that the observed increase in luminescence upon dipicolinate coordination is due to an absorption-energy transfer-emission (AETE) mechanism and not simply exclusion of solvent molecules from the lanthanide coordination sphere, the emission spectra of the Tb aquo ion was recorded in H_2O and in D_2O. Deuterated water has a greater mass and therefore a lower O–D oscillator frequency, meaning it does not participate in nonradiative deactivation through vibronic quenching as normal O–H oscillators in water do. The $Tb^{3+}\cdot 9D_2O$ species therefore represents the unquenched lanthanide luminescence in solution, whereas $Tb^{3+}\cdot 9H_2O$, with O–H oscillators comprising the entire coordination sphere, represents the most severely quenched species. Though there is a marked increase (threefold) in luminescence of the Tb^{3+} cation when in deuterated solvent, this is almost negligible in comparison to the effect of one dipicolinate ligand (Figure 2.11). If the only function of tridentate DPA binding were to displace three water molecules from the Tb^{3+} coordination sphere, the intensity should be a factor of three lower than the $Tb^{3+}\cdot 9D_2O$ spectrum, which has displaced all nine waters. The nearly 3-orders-of-magnitude increase in luminescence is clear evidence of lanthanide sensitization via the AETE mechanism.

It is quite curious that the dipicolinate anion alone exhibits no detectable fluorescence.[24] Though the sodium and calcium salts of DPA emit very weak fluorescence in the 400–420 nm range when excited around 300 nm,[25] the DPA^{2-} anion has no detectable fluorescent signal, despite theoretical studies which suggest otherwise.[19] We have verified this same result in a variety of solvents (H_2O, acetonitrile, dichloromethane, toluene). Though the reasons why the dipicolinate anion is invisible are still unknown, this adds an advantage of reduced fluorescent background in terms of developing a luminescence-based assay for DPA.

The ternary complex emission spectra all display unique band splittings that are dependent on the site symmetry of the lanthanide coordination sphere, including those of Sm^{3+} ([Xe] $4f^5$) and Dy^{3+} ([Xe] $4f^9$), which exhibit Kramers' degeneracy in low symmetry cases such as this (see Section 2.4.1).[26] For all four lanthanides this splitting is present in all observable emission peaks, regardless of hypersensitivity (i.e., the $^5D_0 \rightarrow {}^7F_2$ transition of Eu^{3+}), degeneracy of the lanthanide ground state, or whether assigned as electric dipole or magnetic dipole transitions. For example, emission spectra of the mono $Tb(DPA)^+ \cdot 6H_2O$ complex, the homoleptic $Tb(DPA)_3^{3-}$ species, and ternary $Tb(DO2A)(DPA)^-$ all exhibit very different splittings, and these characteristic differences can be used to visually identify the major component in solution.

2.3.2 Quantum Yields

Using absorbance and fluorescence measurements in tandem, it is possible to quantitatively measure the efficiency of lanthanide sensitization in our complexes. For our purposes, 'quantum yield' refers to the luminescence quantum yield (Φ_L), defined as

the ratio of photons absorbed (by the chromophore) to photons emitted through luminescence (by the lanthanide). Therefore, Φ_L represents the probability of formation of the lanthanide the excited state via the absorption-energy transfer-emission (AETE) mechanism, coupled to the probability of the excited state being deactivated by luminescence as opposed to non-radiative deactivation pathways. Several deactivation pathways can cause this value to be significantly less than unity, such as inefficient coupling of the chromophore triplet energy level to the lanthanide excited state, or vibrational quenching from solvent molecules in or near the lanthanide coordination sphere. Typically, a compound with a quantum yield greater than 0.1 is considered to be quite luminescent.

Experimental Section

Methods. Five concentrations ranging from 5.0 to 15.0 μM were prepared for each lanthanide complex (excluding Gd) in 0.1 M Tris buffer (pH 7.9). Absorbance and luminescence measurements were made in quartz cuvettes (1 cm path length) using a Cary 50 Bio UV/Visible Spectrophotometer, and a Fluorolog-3 Fluorescence Spectrometer (λ_{ex} = 280 nm). Absorbance measurements were zeroed to an empty quartz cuvette in the sample chamber; quartz cuvettes containing solvent only were run in triplicate as a control, so no baseline correction was necessary. All recorded absorbances were under 0.1 and all luminescence intensities were below 5 x 10^5 cps (counts per second), well within the linear range of both instruments. Quartz cuvettes were cleaned using a nitric acid (50% in nanopure water) digest and rinsed thoroughly with nanopure water between samples. No background fluorescence was observed for the solvents used.

The quantum yield of each complex was calculated using the following equation:

$$\Phi_X = \Phi_{ST} \cdot \frac{Grad_X}{Grad_{St}} \cdot \frac{I_{ST}(\lambda_{ST})}{I_X(\lambda_X)} \cdot \frac{\eta_X^2}{\eta_{ST}^2} \quad [2.1]$$

where Φ is quantum yield, X is the sample, ST is the standard, I is the intensity of the excitation light at wavelength λ and η is the refractive index of the solvent. 'Grad' refers to the gradient relationship in equation 2.2 obtained by plotting data as integrated luminescence emission intensity (E) against absorbance (A).

$$Grad = \frac{E}{A} \quad [2.2]$$

Emission spectra were plotted as intensity against energy (cm^{-1}) and integrated using the FluorEssence software package. Quantum yield measurements were standardized to L-tryptophan in deionized water (18.2 MΩ-cm resistivity) at the same excitation wavelength, pH 5 (Φ_{ref} = 0.13 ± 0.01).[27] Corrections were made for the difference in refractive index between buffered H_2O (0.1 M Tris) and pure H_2O. Molar extinction coefficients were also calculated for the ternary complexes and the dipicolinate anion by plotting absorbance against concentration (Figure 2.12).

We attempted to use $Cs_3[Eu(DPA)_3]$ as our secondary standard, which was reported by Chauvin et al.[28, 29] to have a quantum yield of 24 ± 2.5% (λ_{ex} = 279 nm) at 75 μM in 0.1 M Tris buffer. $Cs_3[Eu(DPA)_3]$ was prepared as described by Brayshaw et al.[30] 9.73 g, yield: 96.2%. Anal. Calcd (found) in duplicate for $Cs_3Eu_1C_{21}N_3O_{12}H_9 \cdot 26.4H_2O \cdot Cs_2CO_3$ (fw = 1215.7): C, 22.29 (22.29); H, 5.13 (2.08); N, 3.46 (3.71); Eu, 12.50 (12.50). However, this concentration of $Cs_3[Eu(DPA)_3]$ has an absorbance around 1.0 with a 1 cm path length cell, not in the 0.2 range as was described. In order to obtain absorbances in the proper linear range, the concentration of the $Cs_3[Eu(DPA)_3]$ had to be

decreased to 5.0 μM. This was problematic, as the stability constant of $Eu(DPA)_3^{3-}$ is in this range (3.1 μM).[31] We believe that the authors must have used 0.2 cm path length cells, and that these should be used for any quantum yield experiments involving tris-DPA lanthanide complexes as secondary standards. Otherwise, the $Eu(DPA)_3^{3-}$ complex dissociates to $Eu(DPA)_2^-$ and DPA^{2-}, and emission intensity no longer tracks linearly with absorbance (Figure 2.13). As we were using 1 cm path length cells, we simply discarded this standard in favor of the more accepted L-tryptophan.

Results and Discussion

Molar extinction coefficients for the four luminescent ternary complexes and the dipicolinate anion are all in the same range of 10^3 $M^{-1}cm^{-1}$, which is expected as all contain the same amount of chromophore, the only strongly absorbing species (Table 2.4). The calculated molar extinction coefficient of the tryptophan standard (ε_{Exp} = 5277 $M^{-1}cm^{-1}$) was within 5% of the reported value (ε_{Exp} = 5502 $M^{-1}cm^{-1}$).[27]

The luminescence quantum yields for Tb complexes are greater than those of the Dy, Eu, and Sm complexes (Table 2.5). This is most likely due to (1) the small energy gap and corresponding strong coupling between the DPA triplet state and the terbium $^5D_4$ excited state[22, 32, 33] and (2) the absence of other terbium excited states lower in energy than the DPA triplet, which might quench emission via nonradiative decay.[34] Samarium and europium have larger energy gaps between accepting energy levels and the DPA triplet level,[35, 36] so intensity loss in these lanthanide complexes is probably due to poor coupling and lack of efficient energy transfer (Table 2.6). For the case of Dy, the quantum yield is lower despite an even smaller energy gap,[37] because the $^4I_{15/2}$ and $^4G_{11/2}$

excited states are also populated and each contributing to the loss of quantum yield via nonradiative decay.[35] The high efficiency and intensity of the Tb complex suggests that $Tb(DO2A)^+$ is the optimal choice as a dipicolinate receptor site.

2.3.3 Lifetime Measurements

Luminescence lifetimes of lanthanide complexes can provide information about the coordination environment and degree of quenching of the lanthanide in solution. According to the Judd-Ofelt theory of lanthanide photophysics, the radiative lifetimes of Laporte-forbidden f–f transitions should be on the order of milliseconds.[38-40] However, reported experimental decay lifetimes for lanthanide complexes are significantly faster (microseconds), suggesting that non-radiative transitions have considerable influence on radiative lifetimes in these complexes.[41]

As described in Chapter 1, non-radiative relaxation due to solvent interactions can severely reduce lanthanide luminescence due to energy dissipation by vibronic modes, with the O–H oscillator being the most common and efficient quencher. However, if these O–H oscillators are replaced with low-frequency O–D oscillators, the efficiency of the vibronic deactivation pathway decreases substantially. Therefore, the rate constants for luminescence lifetimes (τ_{H_2O}) of lanthanide excited states in water or alcoholic solvents are often much shorter than those in the analogous deuterated solvents (τ_{D_2O}). This property can be utilized to determine the degree of solvation for luminescent lanthanides with a fair amount of certainty.

The hydration number, or the number of bound water molecules in the lanthanide coordination sphere, can be calculated using a method derived by Horrocks and Sudnick for terbium and europium complexes.[42] The relationship between Tb or Eu excited-state lifetimes (τ) experimentally determined in H_2O and D_2O solvents, and the hydration number (q) is given in equation 2.3.

$$q = A_{Ln}\left(\frac{1}{\tau_{H_2O}} - \frac{1}{\tau_{D_2O}}\right) \qquad [2.3]$$

All lifetimes are in milliseconds, and the A_{Ln} constant is a proportionality factor specific to a given lanthanide which takes into account the energy gap between the ground and excited state manifolds. For example, A_{Tb} is 4.2 ± 0.5 ms while A_{Eu} is only 1.05 ± 0.5 ms. This equation was later modified by Parker et al. to produce equation 2.4, which takes into account quenching effects from coordinated N–H oscillators (where 'x' is the number of N–H oscillators) and outer sphere water molecules.[43]

$$\begin{aligned} q^{Eu} &= A_{Eu}\left[\left(\frac{1}{\tau_{H_2O}} - \frac{1}{\tau_{D_2O}}\right) - 0.25 - 0.075x\right] \\ q^{Tb} &= A_{Tb}\left[\left(\frac{1}{\tau_{H_2O}} - \frac{1}{\tau_{D_2O}}\right) - 0.06 - 0.0056x\right] \end{aligned} \qquad [2.4]$$

The effect of the DO2A ligand, which contains two N–H oscillators, results in a proportionality factor of 4.6 ± 0.5 ms when coordinated to Tb^{3+}, assuming slow exchange with D_2O.[44]

Experimental Section

Materials. Deuterium oxide 99.9% (Cambridge Isotope Laboratories, Inc.), DPA (dipicolinic acid, pyridine-*2,6,*-dicarboxylic acid) (Aldrich), sodium hydroxide (NaOH 50% in water) (Mallinckrodt), and terbium(III) chloride hexahydrate (Alfa Aesar) were purchased and used as received. DO2A was prepared as previously described (Section 2.2.1).

Methods. All samples were prepared in triplicate to a final volume of 4.00 mL with 1 mM NaOH (pH 7.5) in nanopure water (18.2 MΩ-cm resistivity) in disposable acrylate cuvettes (Spectrocell, Oreland, PA), 1 cm path length, and were allowed to equilibrate for at least 24 hours prior to analysis. Complex formation was verified using the characteristic profiles of the various emission spectra obtained on a Fluorolog-3 Fluorescence Spectrometer. Samples to be investigated in D_2O were prepared in the same manner and then dried in a dessicator with Drierite (W. A. Hammond Drierite Co., Ltd., Xenia, OH) under vacuum for at least 7 days. The solid precipitate in these cuvettes was redissolved in D_2O by gentle mixing immediately prior to analysis. The solution pH/pD was checked using a calibrated handheld pH/mV/temperature meter (Model IQ150, I. Q. Scientific Instruments, Loveland, CO) following data collection.

A modified Fluorolog 3-τ spectrofluorometer (Horiba Jobin-Yvon, Edison, NJ) was used for lifetime measurements at 25 °C (Figure 2.14.). The fourth harmonic generation (λ_{ex} = 266 nm) of a 10 nanosecond pulsed Quanta Ray Lab Series neodymium-doped yttrium aluminum garnet (Nd:YAG) laser (Newport Corp, Irvine, CA) was used as the excitation source, with output of the photomultiplier tube (PMT) detector digitized using an oscilloscope to obtain plots of voltage against time (Figure 2.15). The

laser power was adjusted to 1.0 mW to avoid heating the sample or destroying the acrylate cuvettes. Lifetime decay curves were fit to a monoexponential curve of the form in equation 2.5 using the Kaleidagraph software package.

$$I(t) = C + I_0 e^{-t/\tau} \qquad [2.5]$$

In this fit, I is the signal intensity (measured in volts), I_0 is the initial or maximum signal intensity, t is the time in seconds, τ is the lifetime in seconds and C is a constant to adjust for background intensity due to scatter in the sample chamber. The hydration number (q) for each terbium complex was then calculated using equation 2.3, with A_{Tb} = 4.6 or 4.2 ± 0.5 ms per bound water molecule for complexes with and without DO2A, respectively.

Results and Discussion

Luminescence lifetime measurements of the various terbium complexes indicate a significant increase in lifetime in D_2O compared to H_2O, as expected due to quenching from vibronic coupling (Table 2.7). The lifetime of the terbium dipicolinate complex in water (0.6 ms) is consistent with the values reported by Jones and Vullev at a similar pH (0.599 ms).[45] Further, the hydration number of each complex is within range of what was expected assuming Tb^{3+} is 9-coordinate, and indeed, a value of q = 8.8 was calculated for the terbium-aquo complex. The $Tb(DO2A)^+$ complex, containing the hexadentate DO2A ligand, had a hydration number of 2.4, which is consistent with reported values of q = 3.0 and 2.6 inner-sphere water molecules for $Eu(DO2A)(H_2O)_q^+$ and $Eu(DO2A)(OH)(H_2O)_{q-1}$, respectively.[46] The very low hydration number (q = 0.3) for the $Tb(DO2A)(DPA)^-$ ternary complex indicates exclusion of water from the terbium

coordination sphere, and is consistent with the high quantum yield of this complex, which no longer experiences quenching effects due to inner-sphere vibronic deactivation.

2.4 Theoretical Investigations

2.4.1 Crystal Field Theory: Europium as an Example

As described in Chapter 1, lanthanide emission profiles have complex character due to Stark sublevel splitting, which is largely dependent on the site symmetry of the central lanthanide ion. Thus, if the emission spectrum of a pure lanthanide complex (or the absorption spectrum for lanthanide-doped single crystals) is known, it is in principle possible to determine the point group of the lanthanide site, even in solution.[47] However, the group theory and resulting crystal-field parameterization of lanthanides is significantly more complex than transition metals, and complications such as low site symmetry or the additional degeneracy of odd-electron lanthanides make spectral assignment of crystal-field transitions even more difficult. Systems with an odd number of f-electrons (i.e., Sm^{3+}, Gd^{3+} and Dy^{3+}) are nearly impossible to use as probes for the site symmetry around the lanthanide ion due to Kramer's degeneracy.[26] For a complex with symmetry lower than cubic, every $^{2S+1}L_J$ level will be split into J + ½ crystal-field levels in the absence of an external magnetic field. A progressive lowering of the site symmetry will thus not result in a progressive removal of the 2J + 1 fold degeneracy of the $^{2S+1}L_J$ level. We therefore focus on lanthanides with an even number of f-electrons for our analysis of site symmetry in lanthanide complexes.

The europium ion has several characteristics that make it ideal for use as a probe of site symmetry. First, Eu^{3+} has an even number of electrons ([Xe] $4f^6$), so total

degeneracy is removed in low symmetry cases. Second, the $^7F_0$ ground state of Eu^{3+} is non-degenerate, meaning it will transform as the totally symmetric representation of the point group, which simplifies spectral interpretation significantly. Third, many of the $^{2S+1}L_J$ levels where J is small (and there is a straightforward relationship between crystal-field splitting and crystal-field parameters) are present in the optical region for europium, meaning crystal field parameters can be measured directly from experimental spectra. Finally, there is very little overlap between the crystal-field levels of different J states, so levels in the ground ^7F_J and excited ^5D_J terms can be easily distinguished in high-resolution spectra. We can therefore use our europium complexes to validate lanthanide site symmetries in solution against what is observed in the crystal structure.

For this exercise, we focus on the $Eu(DPA)_3^{3-}$ and $Eu(DO2A)(DPA)^-$ complexes, for which the point groups are known from the crystal structures. The $Eu(DO2A)(DPA)^-$ complex crystallized in a geometry best described by the C_2 point group (see Section 2.2.2) . Though no crystal structure of the $Eu(DPA)_3^{3-}$ complex has been reported, the analogous $Tb(DPA)_3^{3-}$ complex has been crystallized as the sodium salt; the three tridentate dipicolinate ligands arranged in a D_3 fashion around the terbium ion.[18] This symmetry is supported by absorption measurements of the $Eu(DPA)_3^{3-}$ complex in solution.[48] Using high-resolution emission spectra of these two complexes, we can qualitatively determine the point group of each in solution and compare to that found in the corresponding crystal structures.

The most interesting and informative transitions in the europium luminescence spectrum are: $^5D_0 \rightarrow {}^7F_0$ (580 nm), $^5D_0 \rightarrow {}^7F_1$ (595 nm), $^5D_0 \rightarrow {}^7F_2$ (615 nm) and $^5D_0 \rightarrow {}^7F_4$ (695 nm). All of these are electric dipole transitions with the exception of $^5D_0 \rightarrow {}^7F_1$,

which is a magnetic dipole transition.[26] The first peak in the emission spectrum allows for determination of sample purity and significantly narrows down the list of potential point groups. If the $^5D_0 \rightarrow {}^7F_0$ transition shows any splitting whatsoever, more than one non-equivalent site is present. This transition is also reported to shift with coordination number, most likely due to an increase in Eu^{3+}-ligand covalency via the nephelauxetic effect.[49, 50] Further, according to the selection rules for electric dipole transitions, this transition can only be present in cases of C_{nv}, C_n or C_s symmetry. Therefore, if this peak is absent, the symmetry around the Eu^{3+} ion is high.

The next peak, usually found around 595 nm, allows for further isolation of the correct point group of the complex. If the $^5D_0 \rightarrow {}^7F_1$ transition is split into three peaks, the symmetry must be either orthorhombic (D_2, C_{2v}), monoclinic (C_2, C_s) or triclinic (C_1). If the transition has only two peaks, we are left with hexagonal, trigonal or tetragonal symmetries.

If the symmetry is high, more transitions are forbidden by symmetry restrictions; therefore, lanthanides occupying sites of low symmetry will have more peaks within a spin-orbit coupling band than those in site of higher symmetry. This feature is well illustrated by the $^5D_0 \rightarrow {}^7F_2$ (615 nm) transition. If the symmetry is found to be orthorhombic, monoclinic or triclinic, the point group can be mostly ferreted out using this transition. If the band at 615 nm has only three peaks, the point group is D_2, four peaks indicate a point group of C_{2v}, and five peaks leave the remaining point groups (C_2, C_s and C_1) as possibilities. For the hexagonal, trigonal and tetragonal symmetries, further information is required. If polarized spectra can be obtained, distinctions can be made

using this and the $^5D_0 \rightarrow {}^7F_4$ transition to clearly identify the point group of the Eu^{3+} coordination sphere (Figure 2.16).

Each transition of the emission spectra for $Eu(DPA)_3^{3-}$ and $Eu(DO2A)(DPA)^-$ were deconvoluted into a sum of Gaussians to quantify the number of peaks in each band (Figure 2.17). For the europium tris(dipicolinate) complex, we find the $^5D_0 \rightarrow {}^7F_0$ transition is absent and the $^5D_0 \rightarrow {}^7F_1$ transition is split into two peaks, indicating a point group of higher symmetry (hexagonal, trigonal or tetragonal). We can also see that the intense $^5D_0 \rightarrow {}^7F_2$ transition is split into only two peaks which, despite the fact that we cannot identify polarizability in this spectrum, is strong evidence for the D_3 point group. The analysis of crystal field splitting of the $Eu(DPA)_3^{3-}$ emission spectrum therefore implies that the europium ion is in a similar configuration in both the crystal structure and in solution, and that this configuration is best described by the D_3 point group.

For the ternary complex, we clearly identify a single peak for the $^5D_0 \rightarrow {}^7F_0$ transition, meaning our sample has low symmetry and high purity. The position of this peak at 581 nm (17,215 cm^{-1}) indicates a 9-coordinate environment around the Eu^{3+} central ion.[49] The triply-split $^5D_0 \rightarrow {}^7F_1$ transition confirms orthorhombic, monoclinic or triclinic symmetry. Finally, the $^5D_0 \rightarrow {}^7F_2$ transition is split into 5 peaks, narrowing down the possibilities to C_1, C_2 or C_s. Cursory analysis of the $Eu(DO2A)(DPA)^-$ emission spectrum using selection rules of specific transitions is therefore in close agreement with the crystal structure, which purports a point group of C_1 or C_2 for this complex. Hence, the coordination sphere of the Eu^{3+} ion appears to remain consistent in terms of symmetry from solid state to solution.

Our theoretical investigation using europium as an example suggests that the symmetries observed in the crystal structures of $Eu(DPA)_3^{3-}$ and $Eu(DO2A)(DPA)^-$ are preserved when these complexes are in solution. Though systematic structural studies of various lanthanide complexes have shown that it can be rather difficult to satisfactorily extrapolate what is observed in the solid state to behavior in solution, in some cases the gross aspects such as symmetry are retained.[51-53] While not necessarily conclusive, this exercise serves to demonstrate the potential of crystal field theory to validate experimental data for lanthanide complexes that are well characterized.

2.4.2 Density Functional Theory

To better understand the energetics of the $Ln(DO2A)(DPA)^-$ ternary complex and dipicolinate binding to $Ln(DO2A)^+$, a collaboration was established with John A. Keith, Josef Anton and Timo Jacob at the University of Ulm, Germany, to perform density functional theory (DFT) calculations on this system.

Calculations were run with the PBE0 hybrid method (a variant of the PBE generalized-gradient exchange-correlation functional including exact Hartree exchange) with Tb^{3+} as the central lanthanide. The number of atoms within these complexes prevented practical simulation of the highest-accuracy basis sets. Instead, the CSDZ pseudopotential was used on the lanthanide while all other atoms used the double-zeta quality 6-31G** basis set. As these were relatively high-spin complexes, calculations used the restricted open-shell Hartree-Fock (ROHF) method; spin-polarized unrestricted Hartree-Fock (UHF) calculations found near-identical energies as minimal spin contamination was found at the minimum energy spin state. After pre-optimization in

vacuum, the geometric structures were then optimized under the constraints of a self-consistent reaction field (SCRF) continuum method to model a surrounding water solvent. Energy values (E_{SCF} and E_{solv}) were recalculated with more expansive triple-zeta basis sets to minimize basis set superposition errors (BSSEs). Density functional methods are known to poorly describe long- and medium-range vdW contributions, and to address the importance of these terms, they were explicitly calculated with a semiempirical approach[54] prior to computation of $\Delta\Delta E$ for all reactions.

Computational results indicated only two solvent molecules in the terbium coordination sphere for the $Tb(DO2A)^{+}$ complex, even after full optimization in solvent (Figure 2.18). This is consistent with reported hydration states of $Ln(DO2A)(H_2O)_n$ complexes, with $n = 3$ for Ce through Eu and $n = 2$ for Tb to Yb,[55] though our lifetime measurements suggest a slightly higher hydration number for this complex.

Further computational investigations found very similar relative binding energies for all Ln complexes, not in agreement with our experimental results. For a given binding constant k_n, the binding energy is given by equation 2.6.

$$k_n = \frac{kT}{h} \cdot e^{-\Delta G_n / kT} \qquad [2.6]$$

For detection of two binding constants (k_1 and k_2) within a factor of 100, we can determine the minimum allowable difference in ΔG for a given temperature by substituting and solving as shown in equation 2.7.

$$\frac{k_1}{k_2} = 100$$
$$\frac{\frac{kT}{h} \cdot e^{-\Delta G_1 / kT}}{\frac{kT}{h} \cdot e^{-\Delta G_2 / kT}} = 100 \qquad [2.7]$$
$$e^{(\Delta G_2 - \Delta G_1)/kT} = 100$$
$$(\Delta\Delta G) = \ln(100) \cdot kT$$

At 298 K, kT = 0.592 kcal/mol. Substituting in this value and solving for ΔΔG, we have equation 2.8.

$$\Delta\Delta G = 2.73 \text{ kcal/mol} \qquad [2.8]$$

We therefore must have computational accuracy within 3.0 kcal/mol to accurately detect two binding constants within a factor of 100. Since similar calculations are capable of errors from 2-5 kcal/mol for small organics, let alone for substantially more complicated lanthanide complexes, it would not be surprising if the standard computational approach could not successfully discern binding constants within this order, and a more advanced approach is necessary.

One likely possibility is the lack of rigorous treatment of relativistic effects and spin-orbit coupling; treatment of these effects was the motivation for the collaboration with the Ulm group. Unfortunately, the highly polarizable dipicolinate ligand was found to cause convergence errors in the Ulm code, and an accurate theoretical model of the ternary complex could not be obtained (energetics within 5 kcal/mol). Since these errors could not lead to an improvement over the previously used model, further understanding of these complexes from theory could not be obtained.

2.5 Conclusions

Five Ln(DO2A)(DPA)$^-$ ternary complexes, where Ln = Sm, Eu, Gd, Tb and Dy, were successfully crystallized as tetrabutylammonium salts by slow evaporation out of acetone. Crystallographic analysis revealed the structures were all isostructural and superimposable, with slight differences following the trend of lanthanide ionic radius. Variation of temperature from 100 to 300 K resulted in negligible differences in the crystal structures of the Tb and Eu complexes.

Excitation and absorption spectra of the four luminescent complexes (Sm, Eu, Tb and Dy) were very similar, with two $\pi \rightarrow \pi^*$ transitions at 271 and 278 nm. Emission spectra confirm sensitized luminescence via the AETE mechanism for all four complexes, with emission intensities in the order of Tb >> Eu >> Dy > Sm. Quantum yield measurements verify optimal energy transfer efficiency in the Tb^{3+} complex, most likely due to close coupling between the dipicolinate triplet energy level and the terbium $^5D_4$ excited state.

Lifetime measurements of various Tb^{3+} complexes indicate nine waters bound in the aquo complex, six in the Tb(DPA)$^+$ complex, and two to three in the Tb(DO2A)$^+$ complex. The fully formed Tb(DO2A)(DPA)$^-$ complex excludes solvent completely from the lanthanide coordination sphere.

Analysis of Stark splitting in the europium emission spectra using selection rules corroborates point group assignments of D_3 and C_1/C_2 for the $Eu(DPA)_3^{3-}$ and Eu(DO2A)(DPA)$^-$ complexes, respectively, suggesting symmetry is conserved when such complexes are in solution. Theoretical calculations using density functional theory (DFT) were found to be limited and inconsistent with experimental results.

With the ternary complexes fully characterized in terms of their structure and photophysics, we may begin to approach the $Ln(DO2A)^{+}$ series in terms of receptor site design. The complex that is most effective as a dipicolinate sensor will be validated with real bacterial spores both from laboratory and environmental samples.

REFERENCES

(1) Brunet, E.; Juanes, O.; Rodriguez-Ubis, J. C. *Current Chemical Biology* **2007**, *1*, 11-39.

(2) Cotton, S. *Lanthanide and Actinide Chemistry*; John Wiley & Sons Ltd.: West Sussex, England, 2006.

(3) Huskens, J. *Inorganic Chemistry* **1997**, *36*, 1495-1503.

(4) Sweeney, R. A.; Rexroad, P. R. *Journal of AOAC International* **1987**, *70*, 1028-1030.

(5) Sheldrick, G. M. *Acta Crystallographica* **1990**, *A46*, 467-473.

(6) 6.12 ed.; Bruker-AXS: Madison, WI, 2001.

(7) 6.12 ed.; Bruker-AXS: Madison, WI, 2001.

(8) Sheldrick, G. M.; University of Göttingen: Göttingen, Germany, 1997.

(9) Sheldrick, G. M. *Acta Crystallographica* **2008**, *A64*, 112-122.

(10) Sands, D. E. In *Introduction to Crystallography*; Dover Publications, Inc.: Mineola, New York, 1993, pp 47-165.

(11) Hermann, C., Ed. *Internationale Tabellen zur Bestimmung von Kristallstrukturen. I. Band*, 1 ed.: Borntrager, Berlin, 1935.

(12) Dewolff, P. M.; Billiet, Y.; Donnay, J. D. H.; Fischer, W.; Galiulin, R. B.; Glazer, A. M.; Hahn, T.; Senechal, M.; Shoemaker, D. P.; Wondratschek, H.; Wilson, A. J. C.; Abrahams, S. C. *Acta Crystallographica Section A* **1992**, *48*, 727-732.

(13) Thompson, M. K.; Lough, A. J.; White, A. J. P.; Williams, D. J.; Kahwa, I. A. *Inorganic Chemistry* **2003**, *42*, 4828-4841.

(14) Moreau, J.; Guillon, E.; Aplincourt, P.; Pierrard, J.-C.; Rimbault, J.; Port, M.; Aplincourt, M. *European Journal Of Inorganic Chemistry* **2003**, *2003*, 3007-3020.

(15) Chang, C. A.; Francesconi, L. C.; Malley, M. F.; Kumar, K.; Gougoutas, J. Z.; Tweedle, M. F. *Inorganic Chemistry* **1993**, *32*, 3501-3508.

(16) Gunnlaugsson, T.; Harte, A. J.; Leonard, J. P.; Nieuwenhuyzen, M. *Supramolecular Chemistry* **2003**, *15*, 505-519.

(17) Strahs, G.; Dickerson, R. E. *Acta Crystallographica Section B* **1968**, *24*, 571-578.

(18) Van Meervelt, L.; Binnemans, K.; Van Herck, K.; Görller-Walrand, C. *Bulletin des Sociétés Chimiques Belges* **1997**, *106*, 25-27.

(19) Hameka, H. F.; Jensen, J. O.; Jensen, J. L.; Merrow, C. N.; Vlahacos, C. P. *Journal of Molecular Structure (Theochem)* **1996**, *365*, 131-141.

(20) Sabbatini, N.; Guardigli, M.; Bolletta, F.; Manet, I.; Ziessel, R. *Angewandte Chemie-International Edition In English* **1994**, *33*, 1501-1503.

(21) Bünzli, J.-C. G. *Lanthanide probes in life, chemical and earth sciences: Theory and practice*; Elsevier: New York, 1989.

(22) Latva, M.; Takalo, H.; Mukkala, V.-M.; Matachescu, C.; Rodriguez-Ubis, J. C.; Kankare, J. *Journal Of Luminescence* **1997**, *75*, 149-169.

(23) Rudzinski, C. M.; Engebretson, D. S.; Hartmann, W. K.; Nocera, D. G. *Journal of Physical Chemistry A* **1998**, *102*, 7442-7446.

(24) Barela, T. D.; Sherry, A. D. *Analytical Biochemistry* **1976**, *71*, 351-352.

(25) Nudelman, R.; Bronk, B. V.; S., E. *Applied Spectroscopy* **2000**, *54*, 445-449.

(26) Görller-Walrand, C.; Binnemans, K. In *Handbook on the Physics and Chemistry of Rare Earths*; Gschneidner, J., K. A., Eyring, L., Eds.; Elsevier Science B. V.: New York, 1996; Vol. 23, pp 122-283.

(27) Chen, R. F. *Analytical Letters* **1967**, *1*, 35 - 42.

(28) Chauvin, A. S.; Gumy, F.; Imbert, D.; Bunzli, J. C. G. *Spectroscopy Letters* **2004**, *37*, 517-532.
(29) Chauvin, A. S.; Gumy, F.; Imbert, D.; Bunzli, J. C. G. *Spectroscopy Letters* **2007**, *40*, 193-193.
(30) Brayshaw, P. A.; Bunzli, J. C. G.; Froidevaux, P.; Harrowfield, J. M.; Kim, Y.; Sobolev, A. N. *Inorganic Chemistry* **1995**, *34*, 2068-2076.
(31) Grenthe, I. *Journal Of The American Chemical Society* **1961**, *83*, 360-364.
(32) Arnaud, N.; Vaquer, E.; Georges, J. *Analyst* **1998**, *123*, 261-265.
(33) Sharma, P. K.; Van Doorn, A. R.; Staring, A. G. J. *Journal of Luminescence* **1994**, *62*, 219-225.
(34) Carnall, W. T.; Fields, P. R.; Rajnak, K. *Journal Of Chemical Physics* **1968**, *49*, 4447-4449.
(35) Carnall, W. T.; Fields, P. R.; Rajnak, K. *Journal Of Chemical Physics* **1968**, *49*, 4424-4442.
(36) Carnall, W. T.; Fields, P. R.; Rajnak, K. *Journal Of Chemical Physics* **1968**, *49*, 4450-4455.
(37) Hemmila, I.; Laitala, V. *Journal Of Fluorescence* **2005**, *15*, 529-542.
(38) Judd, B. R. *Physical Review* **1962**, *127*, 750-761.
(39) Ofelt, G. S. *Journal Of Chemical Physics* **1962**, *37*, 511-520.
(40) Walsh, B. M. In *Advances in Spectroscopy for Lasers and Sensing*; Di Bartolo, B., Forte, O., Eds.; Springer: The Netherlands, 2006, pp 403-433.
(41) Sabbatini, N.; Guardigli, M.; Lehn, J. M. *Coordination Chemistry Reviews* **1993**, *123*, 201-228.
(42) Horrocks Jr., W. D.; Sudnick, D. R. *Journal Of The American Chemical Society* **1979**, *101*, 334-340.
(43) Beeby, A.; Clarkson, I. M.; Dickins, R. S.; Faulkner, S.; Parker, D.; Royle, L.; de Sousa, A. S.; Williams, J. A. G.; Woods, M. *Journal of the Chemical Society-Perkin Transactions 2* **1999**, 493-503.
(44) Parker, D.; Williams, J. A. G. *Journal Of The Chemical Society-Perkin Transactions 2* **1995**, 1305-1314.
(45) Jones, G.; Vullev, V. I. *Photochemical & Photobiological Sciences* **2002**, *1*, 925-933.
(46) Chang, C. A.; Chen, Y.-H.; Chen, H.-Y.; Shieh, F.-K. *Journal Of The Chemical Society-Dalton Transactions* **1998**, 3243-3248.
(47) Sinha, S. P.; Butter, E. *Molecular Physics* **1969**, *16*, 285-298.
(48) Binnemans, K.; Van Herck, K.; Görller-Walrand, C. *Chemical Physics Letters* **1997**, *266*, 297-302.
(49) Choppin, G. R.; Wang, Z. M. *Inorganic Chemistry* **1997**, *36*, 249-252.
(50) Frey, S. T.; Horrocks Jr., W. D. *Inorganica Chimica Acta* **1995**, *229*, 383-390.
(51) Shestakova, A. K.; Chertkov, V. A.; Schneider, H.-J.; Lysenko, K. A. *Organic Letters* **2001**, *3*, 325-327.
(52) Aime, S.; Barge, A.; Botta, M.; Fasano, M.; Ayala, J. D.; Bombieri, G. *Inorganica Chimica Acta* **1996**, *246*, 423-429.
(53) Harrowfield, J. M. In *Metal Ions in Biological Systems: The Lanthanides and Their Interrelations with Biosystems*; Sigel, A., Sigel, H., Eds.; Marcel Dekker, Inc.: New York, 2003; Vol. 40, pp 105-159.
(54) Grimme, S. *Journal of Computational Chemistry* **2006**, *27*, 1787-1799.
(55) Yerly, F.; Dunand, Frank A.; Tóth, É.; Figueirinha, A.; Kovács, Z.; Sherry, A. D.; Geraldes, C. F. G. C.; Merbach, André E. *European Journal Of Inorganic Chemistry* **2000**, *2000*, 1001-1006.

FIGURES

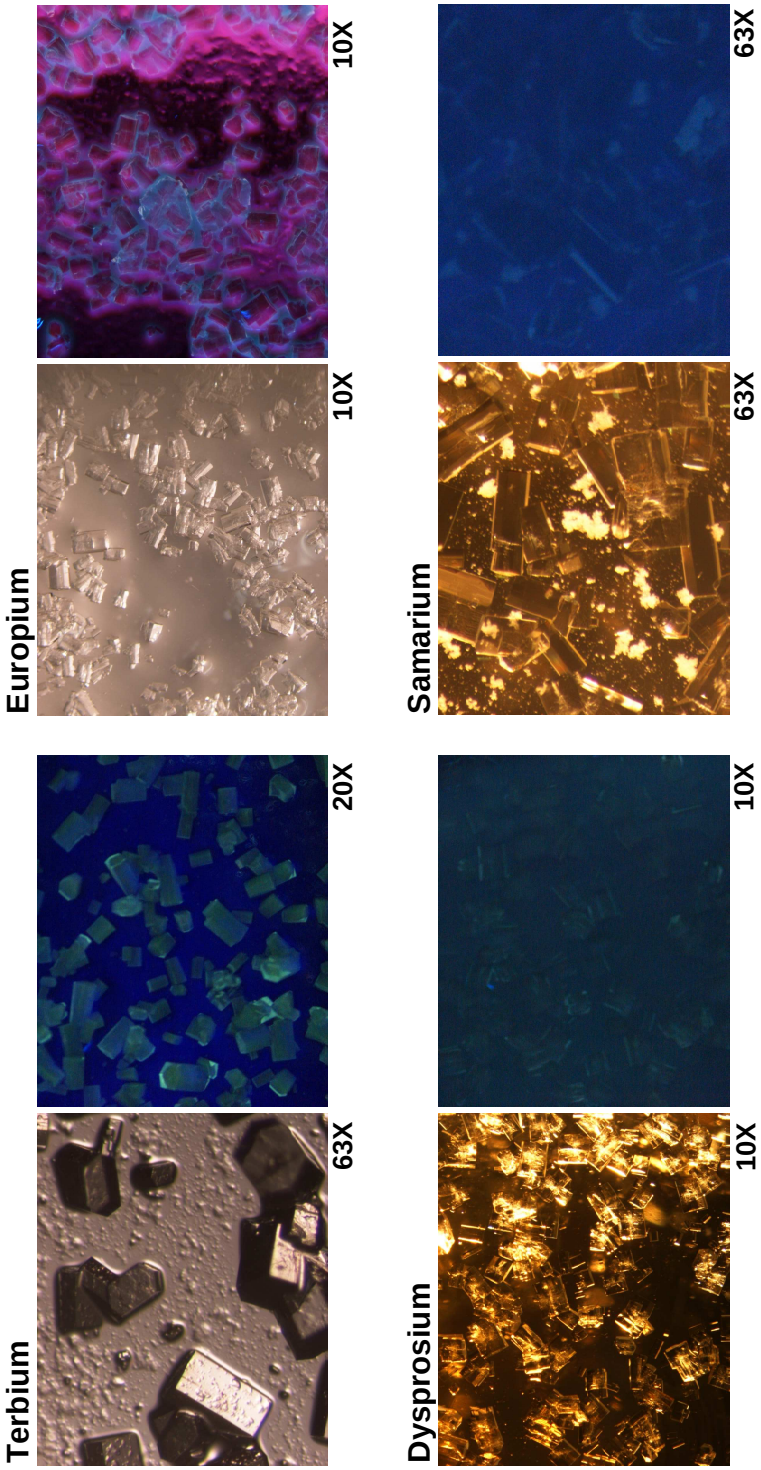

Figure 2.1. Photos of TBA·Ln(DO2A)(DPA) crystals (Ln = Tb, Eu, Dy and Sm). In each pair, image at left is under normal illumination, image at right under UV excitation at 365 nm. Images taken using a Nikon SMZ800 optical microscope. Magnifications indicated below each image.

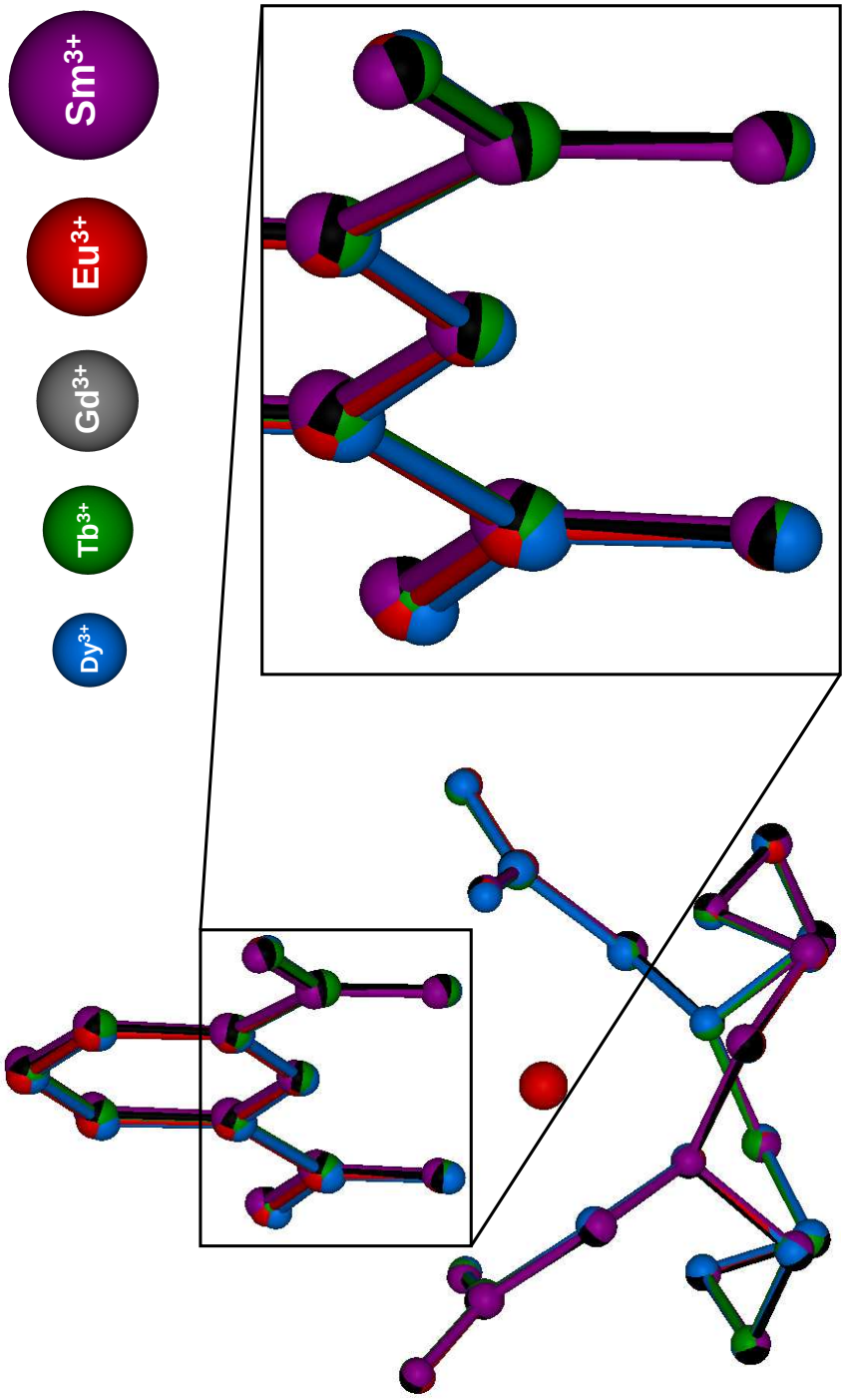

Figure 2.2. Comparison of Ln(DO2A)(DPA)$^-$ crystal structures, where Ln = Sm, Eu, Gd, Tb and Dy. All five ternary complexes are almost perfectly superimposable; in these views, structures have been tethered via the lanthanide and the four nitrogens of the DO2A ring. The slight trend of extension following lanthanide ionic radius is visible in the upward shift of the DPA ligand from Dy to Sm (inset). Legend of lanthanide ions (upper right) are exaggerated in size to illustrate the trend of ionic radius.

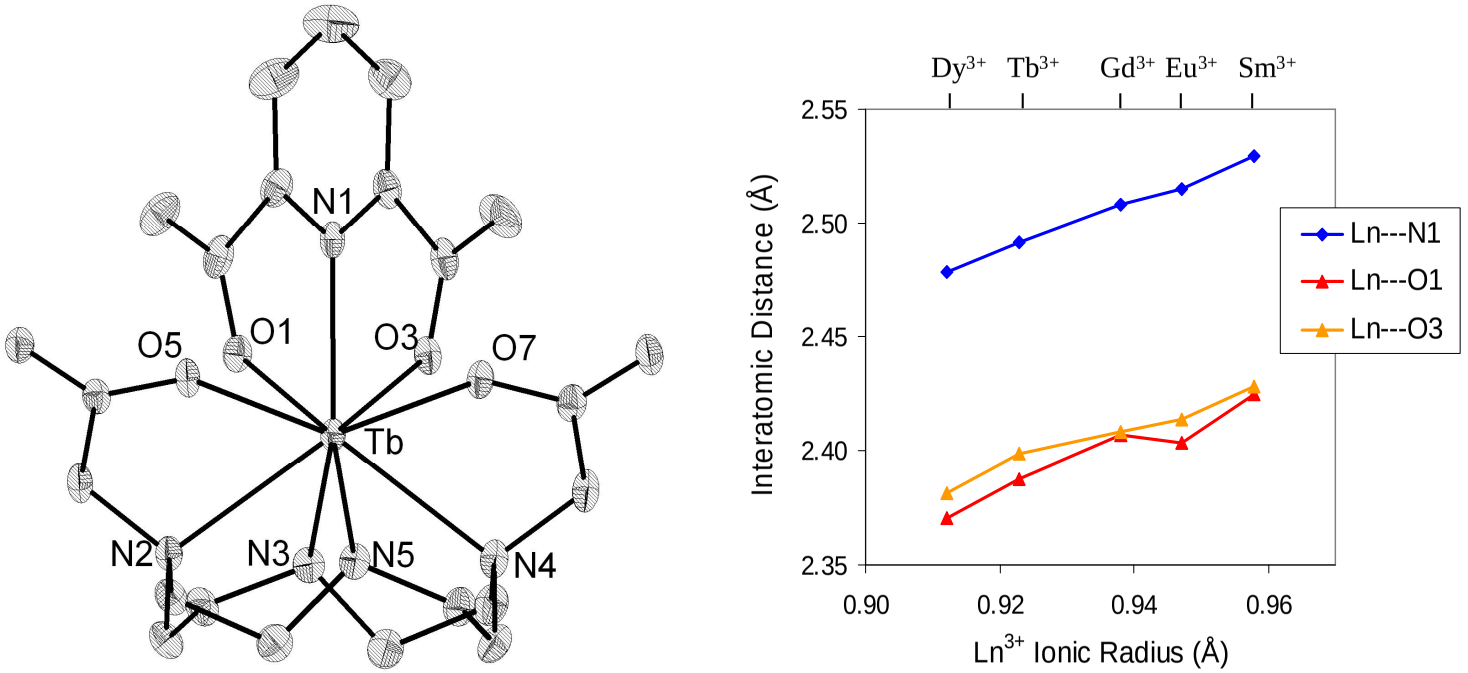

Figure 2.3. Ternary complex expansion due to lanthanide ionic radius. Left: Thermal ellipsoid plot of the Tb(DO2A)(DPA)$^{-}$ ternary complex with 50% probability. Hydrogens omitted for clarity. Right: Plot of Ln^{3+}--DPA interatomic distances for the five ternary complex crystal structures against Ln^{3+} ionic radius. Trivalent ionic radius values from S. Cotton, Lanthanide and Actinide Chemistry, John Wiley & Sons Ltd., 2006.

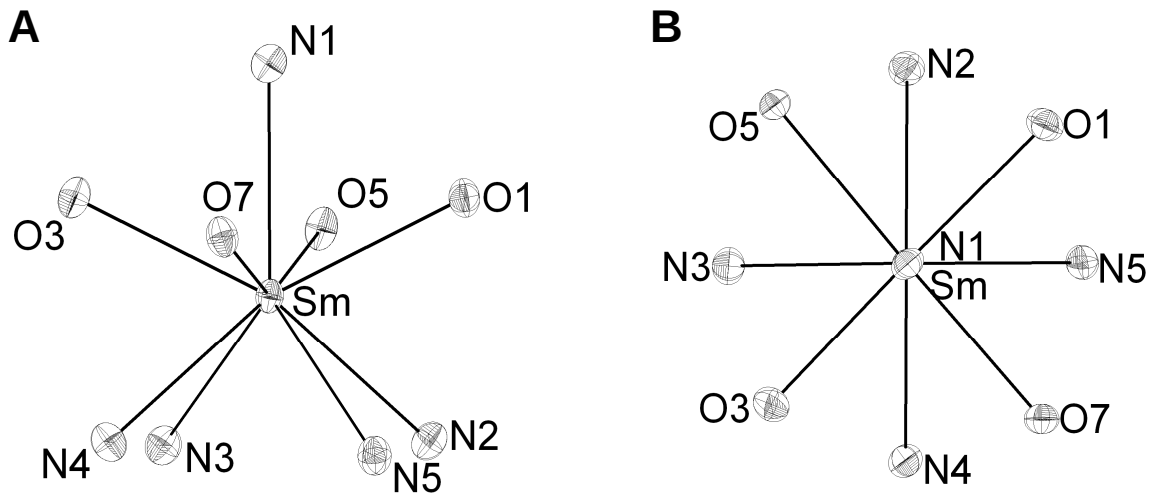

Figure 2.4. Geometry of the lanthanide coordination site in the Tb(DO2A)(DPA)$^{-}$ complex. Thermal ellipsoid plots (50% probability) of the samarium coordination sphere show the capped square bipyramidal geometry, with the four DO2A nitrogens in the lower plane and four oxygens (two from DPA, two from DO2A) in the upper plane. (A) Looking across the complex, with DO2A below and DPA above the Sm^{3+} central ion. (B) Looking down the DPA ligand (the N1 of the DPA is obstructing the view of the Sm).

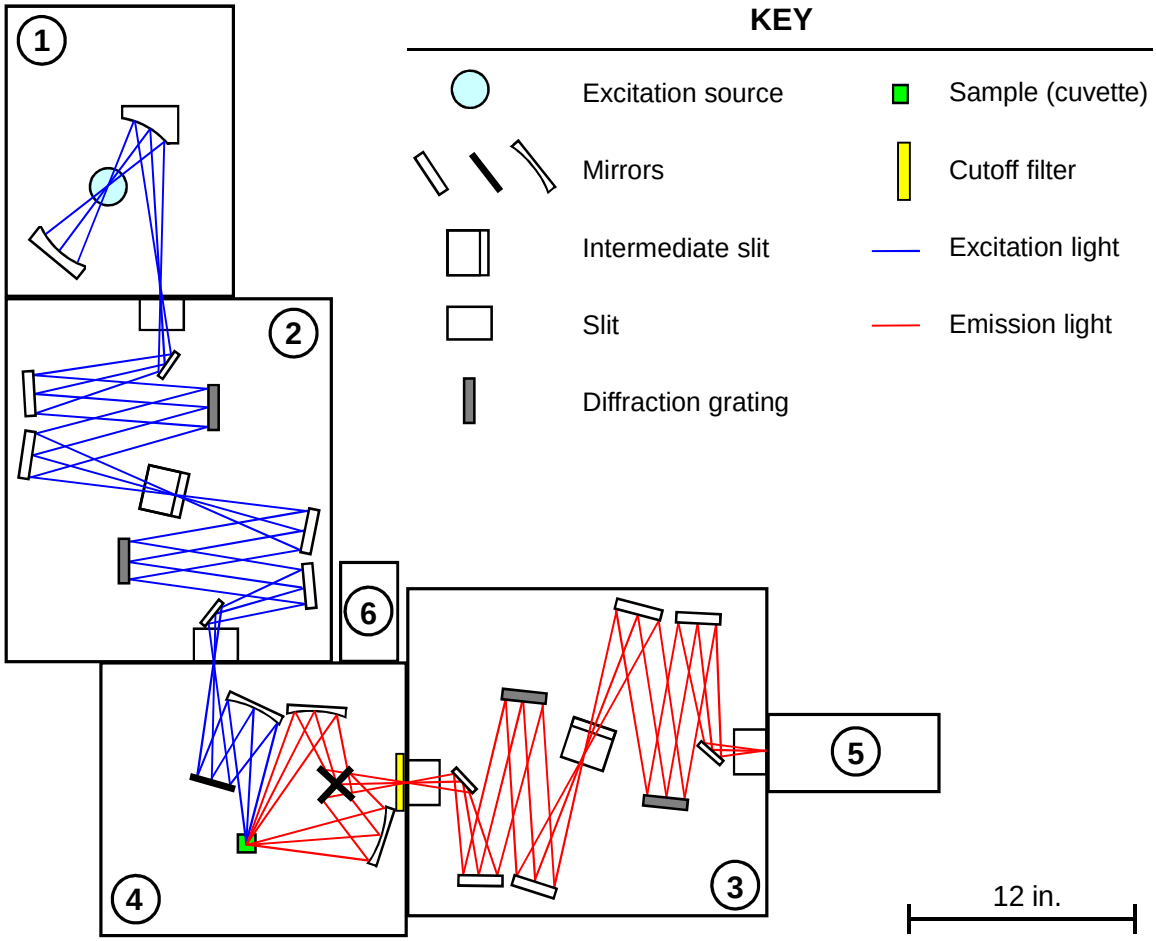

Figure 2.5. Schematic of the Fluorolog-3 Model FL3-22 spectrofluorometer. The instrument is comprised of interchangeable modules arranged in an 'L' configuration. The light source is a 450-W xenon short-arc lamp (1) mounted vertically in an air-cooled housing. Wavelength selection is accomplished using Czerny-Turner double-grating monochromators for excitation (2) and emission (3) light with all-reflective optics and 0.5-nm accuracy. The sample chamber (4) is temperature-controlled and adjustable for right-angle or front-face detection. This model has two detectors: the primary signal detector is a R928P photomultiplier tube (5) thermoelectrically cooled with a Peltier cooling unit, and the reference detector is a photodiode (6). The 350-nm cutoff filter (yellow) is positioned between the sample chamber and the emission double monochromator module. The hardware is directed by a SpectrAcq controller and the user interface is managed by the FluorEssence software package.

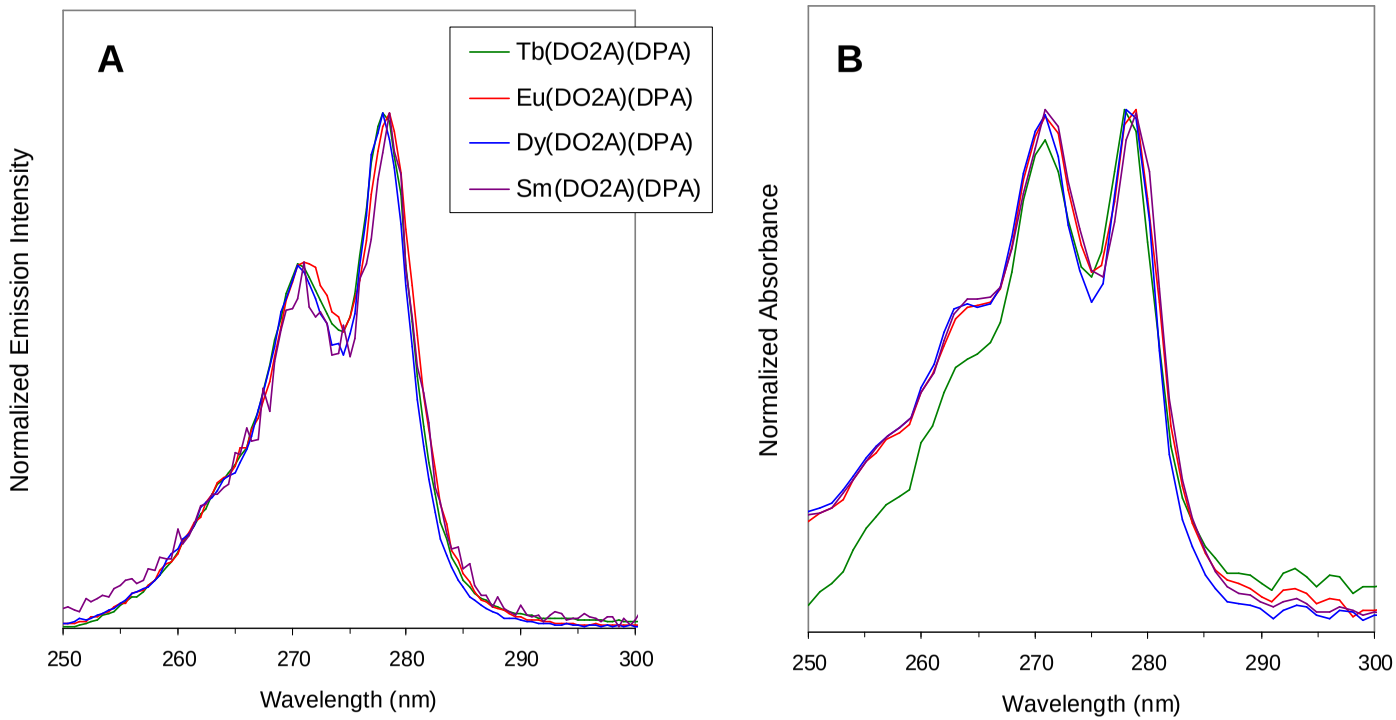

Figure 2.6. Normalized excitation (A) and absorption (B) spectra of Ln(DO2A)(DPA)$^{-}$ complexes, where Ln = Sm, Eu, Tb or Dy, at 10.0 μM in 0.1 M Tris, pH 7.9. Excitation wavelengths: λ_{Sm} = 600 nm, λ_{Eu} = 615 nm, λ_{Tb} = 544 nm, λ_{Dy} = 574 nm.

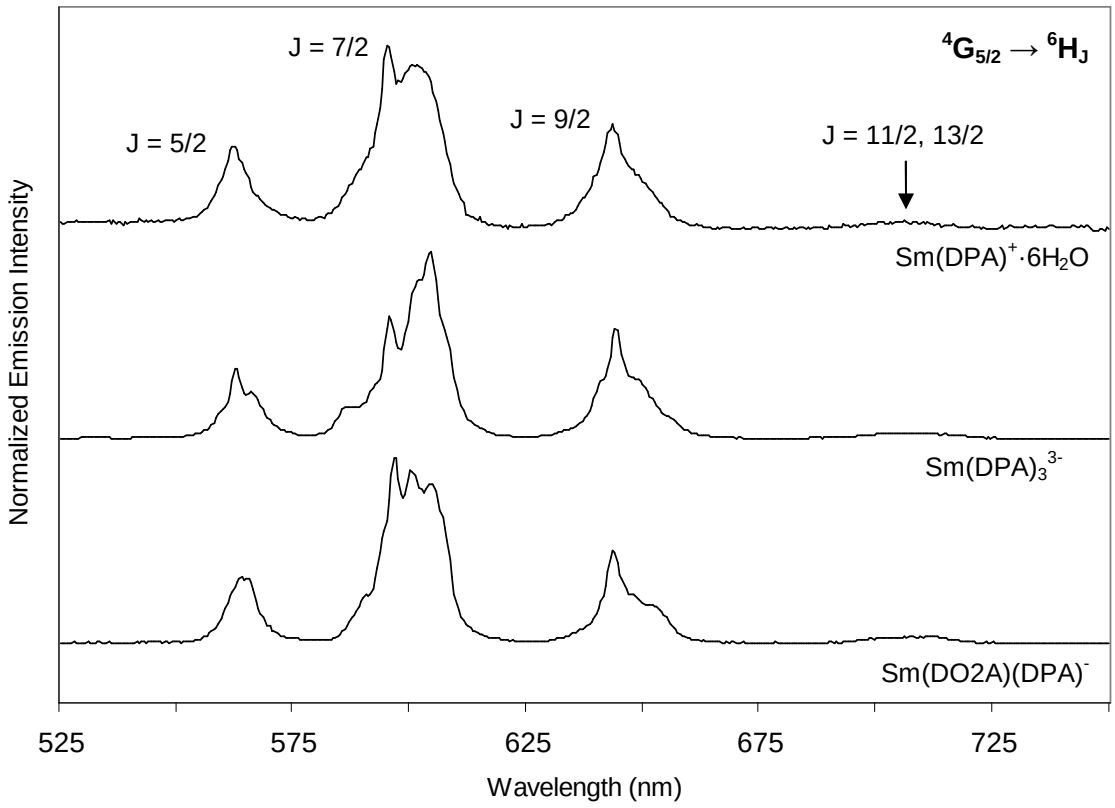

Figure 2.7. Emission spectra of samarium complexes, 10.0 μM in 0.2 M sodium acetate, pH 7.4 (λ_{ex} = 278 nm), showing characteristic splitting as a result of changes in the symmetry of the Sm^{3+} coordination sphere.

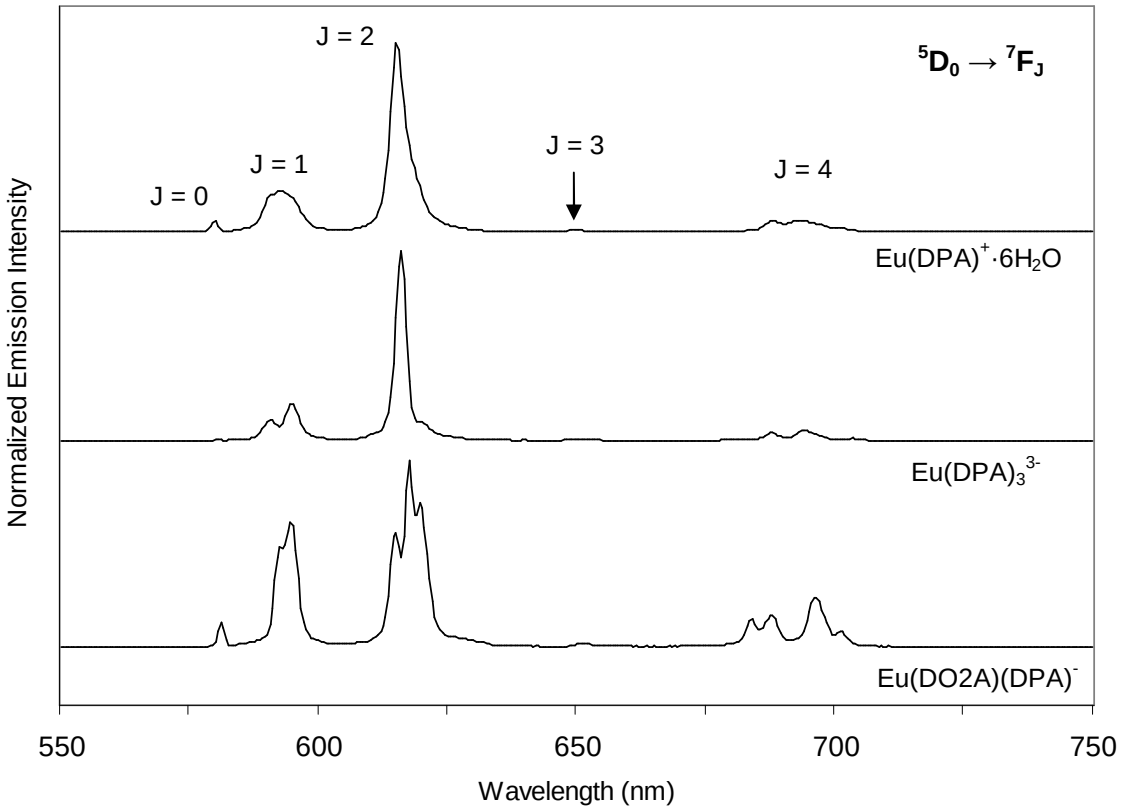

Figure 2.8. Emission spectra of europium complexes, 10.0 μM in 0.2 M sodium acetate, pH 7.4 (λ_{ex} = 278 nm).

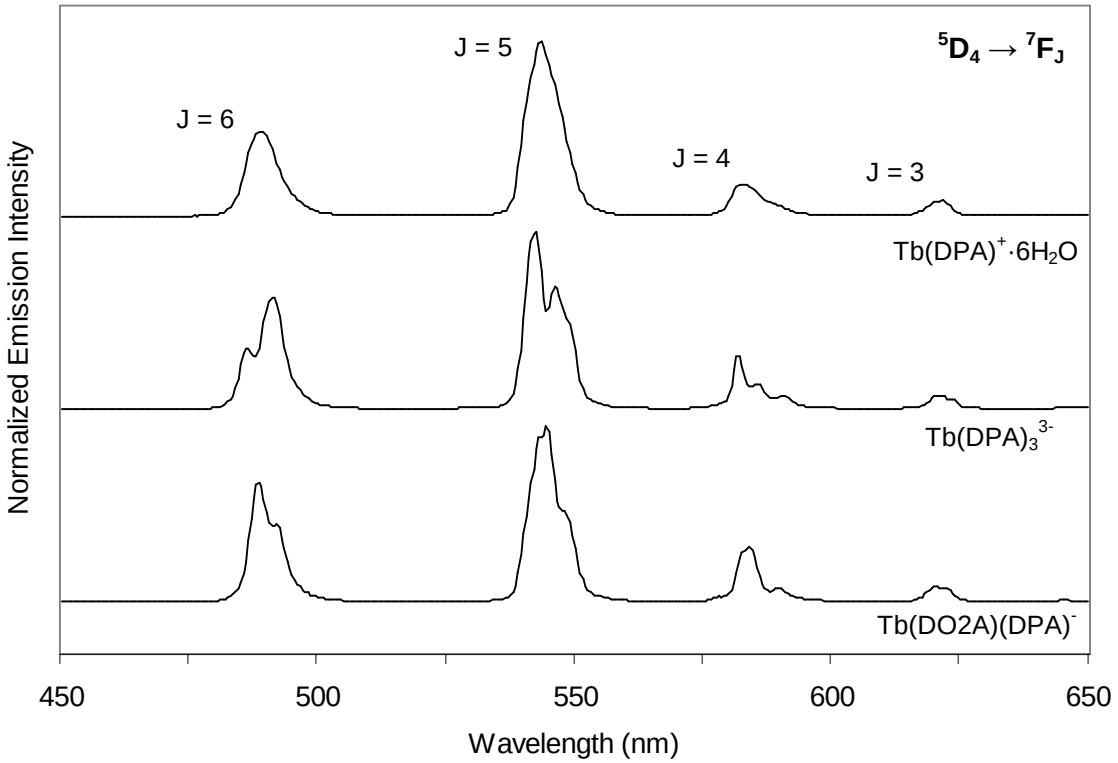

Figure 2.9. Emission spectra of terbium complexes, 10.0 μM in 0.2 M sodium acetate, pH 7.4 (λ_{ex} = 278 nm).

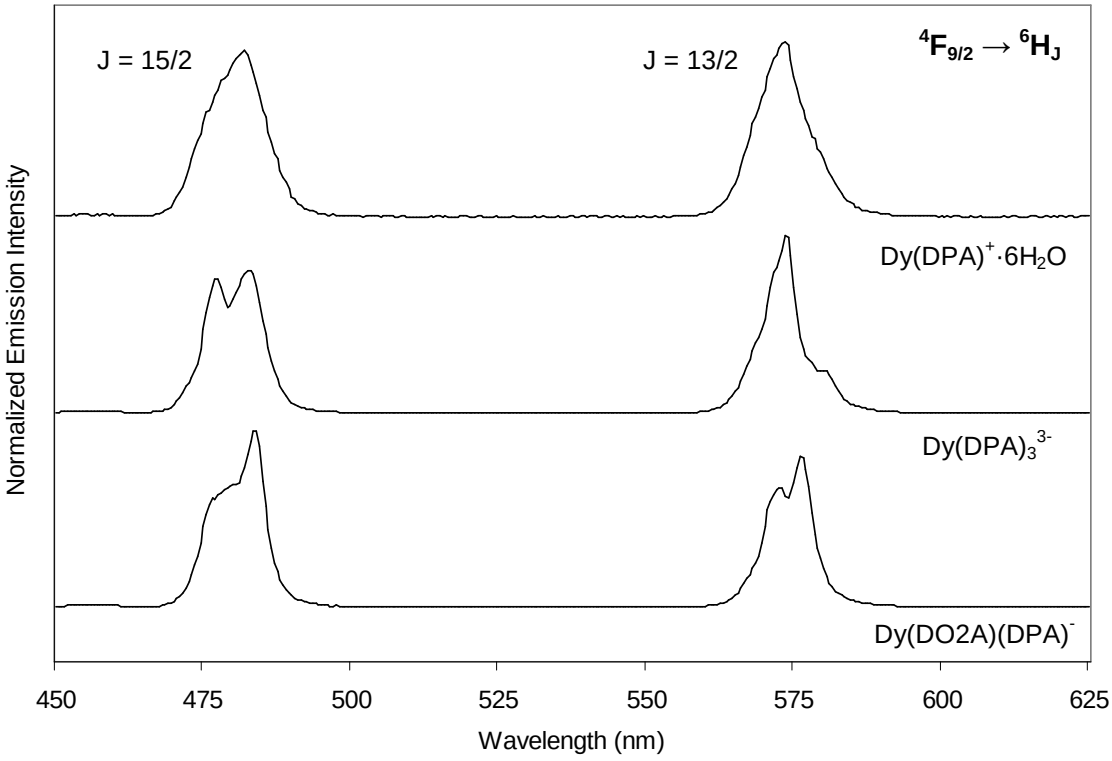

Figure 2.10. Emission spectra of dysprosium complexes, 10.0 μM in 0.2 M sodium acetate, pH 7.4 (λ_{ex} = 278 nm).

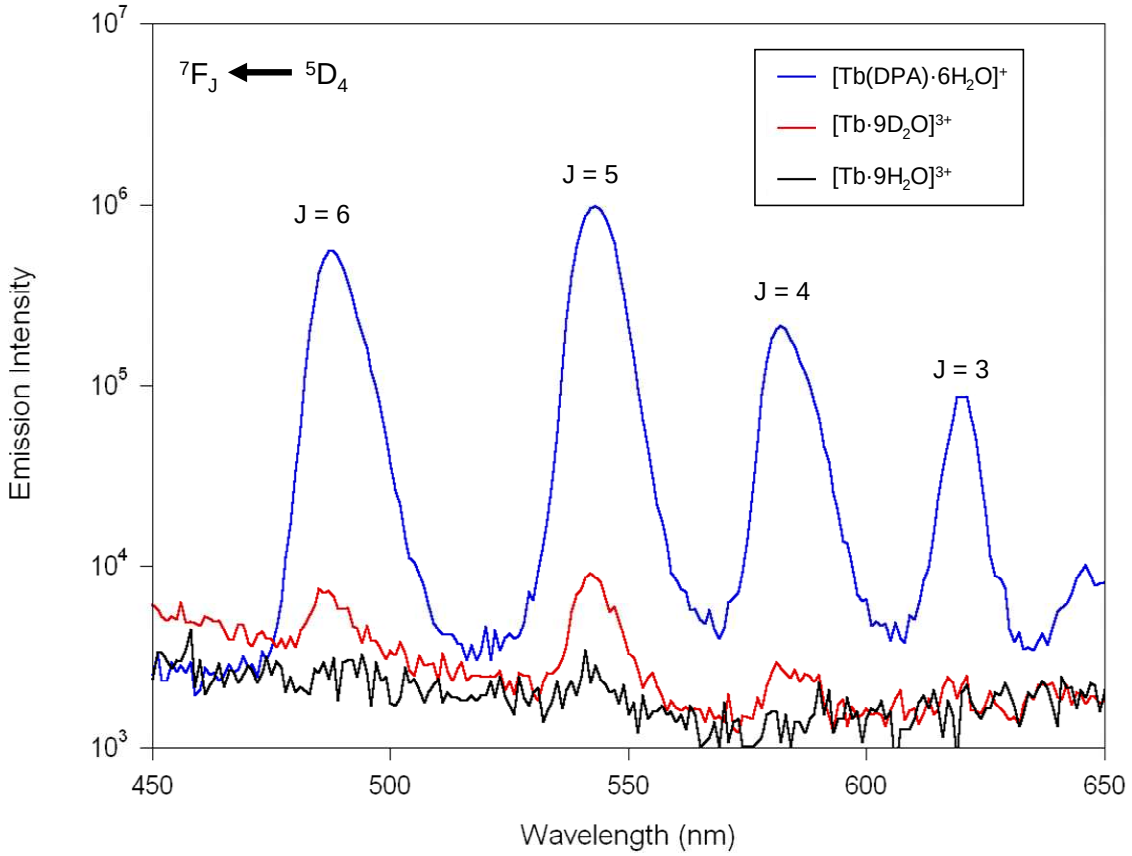

Figure 2.11. Effect of lanthanide sensitization compared to displacement of quenching solvent molecules. The emission spectrum of Tb^{3+} in D_2O shows a modest 3-fold increase in intensity (note Emission Intensity is a logarithmic scale), whereas the addition of one chromophore increases the terbium intensity by nearly three orders of magnitude.

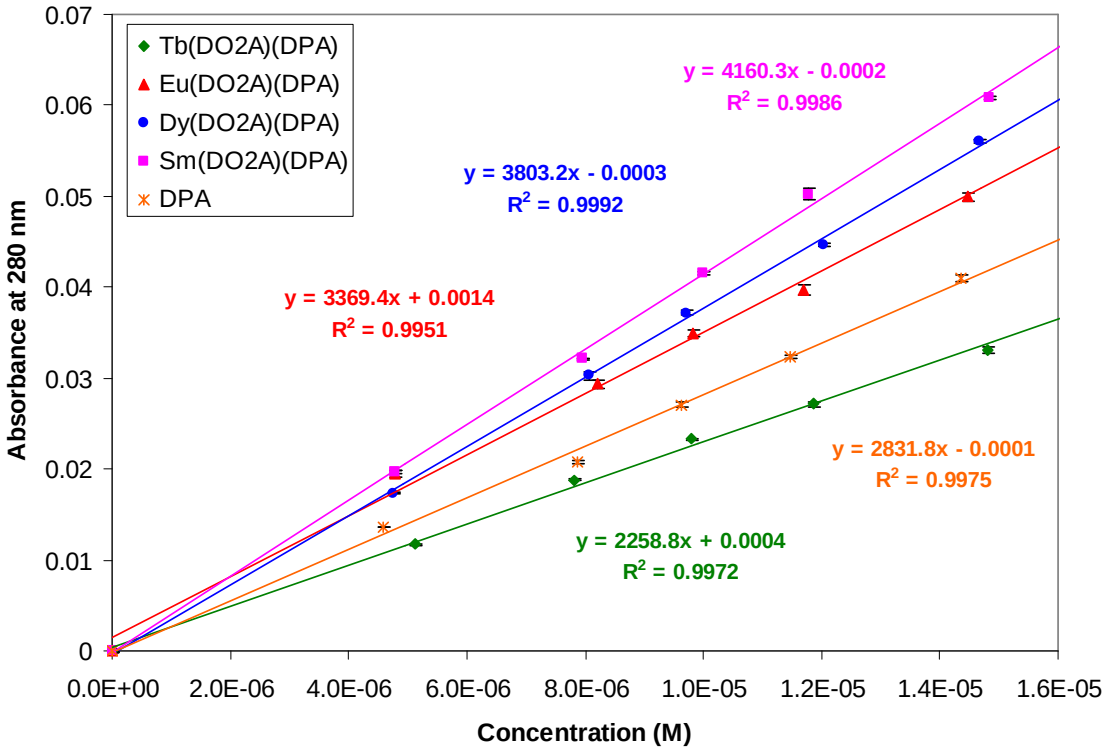

Figure 2.12. Linear fit of absorbance (λ_{abs} = 280 nm) versus concentration for the Ln(DO2A)(DPA)$^-$ complexes (Ln = Sm, Eu, Tb and Dy) in 0.1 M Tris buffer, pH 7.9.

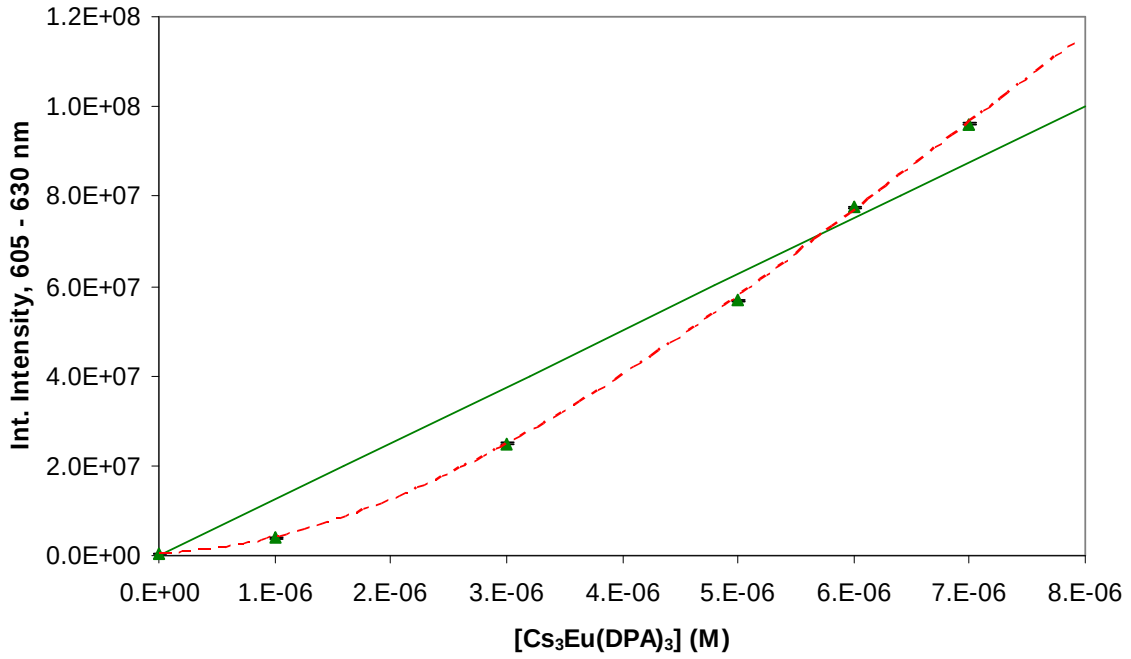

Figure 2.13. Fluorescence of $Cs_3Eu(DPA)_3$ in 0.1M Tris, pH 7.9, showing nonlinear behavior due to dissociation at low concentration.

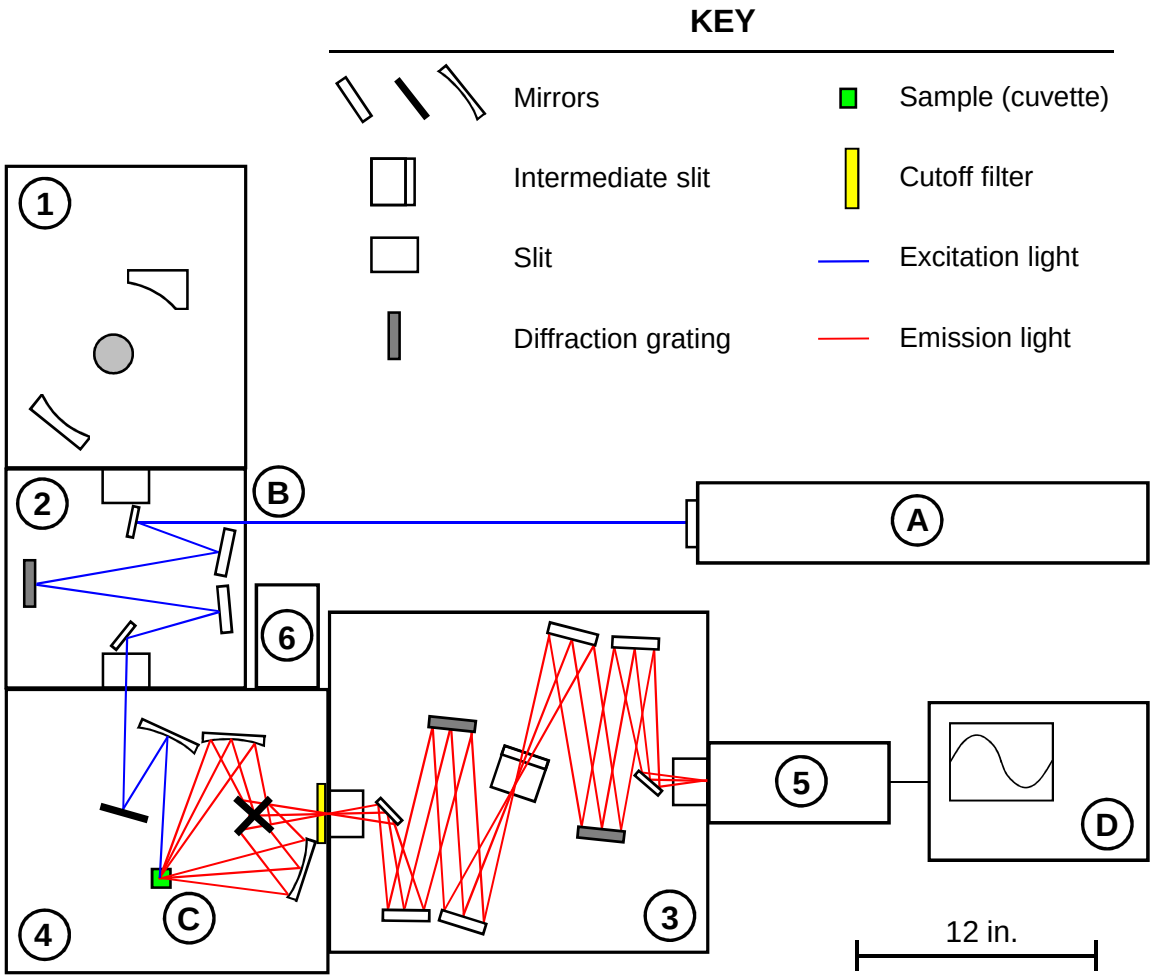

Figure 2.14. Schematic of the Fluorolog-3τ Model FL3-12 spectrofluorometer used for lifetime measurements. Instead of the xenon lamp (1), a Nd:YAG laser with fourth-harmonic generation (266 nm) is used as the excitation source (A), so the excitation single monochromator (2) is no longer necessary as a wavelength selector and serves only as an alignment tool for the laser. The laser beam enters the excitation monochromator via a port on the side of the module (B), and is aligned to strike the center of the cuvette (C). An oscilloscope (D) is attached to the R928P photomultiplier tube (5) to obtain measurements of intensity as a function of time.

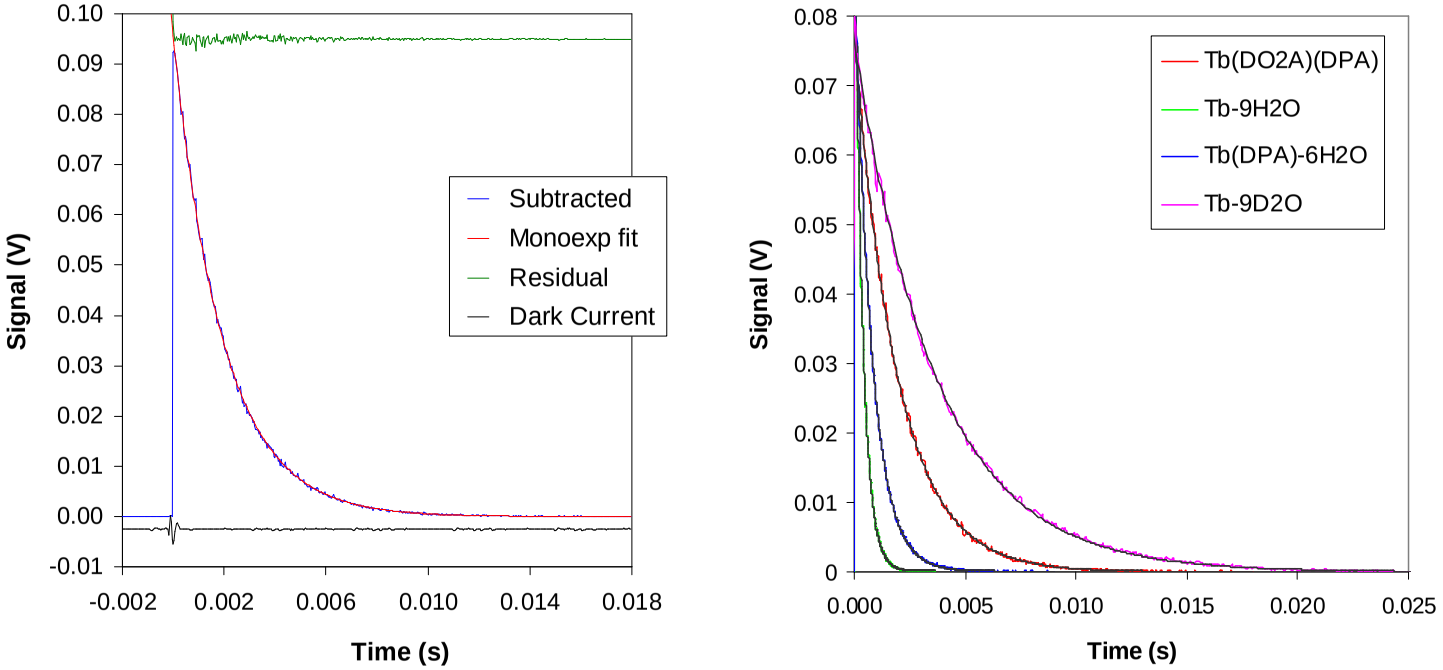

Figure 2.15. Exponential decay curves for lifetime measurements of various terbium complexes. Left: Example of raw data for 10 µM Tb(DO2A)(DPA), showing the adjusted decay curve (blue) following subtraction of the dark current (black) and the residual (green) resulting from subtraction. Right: Examples of final data and fits for several Tb complexes. Excitation at 266 nm (10 ns pulsed Nd:YAG laser), emission detected at 544 nm, sample concentrations 1 to 10 µM, pH 7.5 (adj with NaOH). These curves were fit to a monoexponential and used to determine the number of coordinated waters in the Tb^{3+} coordination sphere.

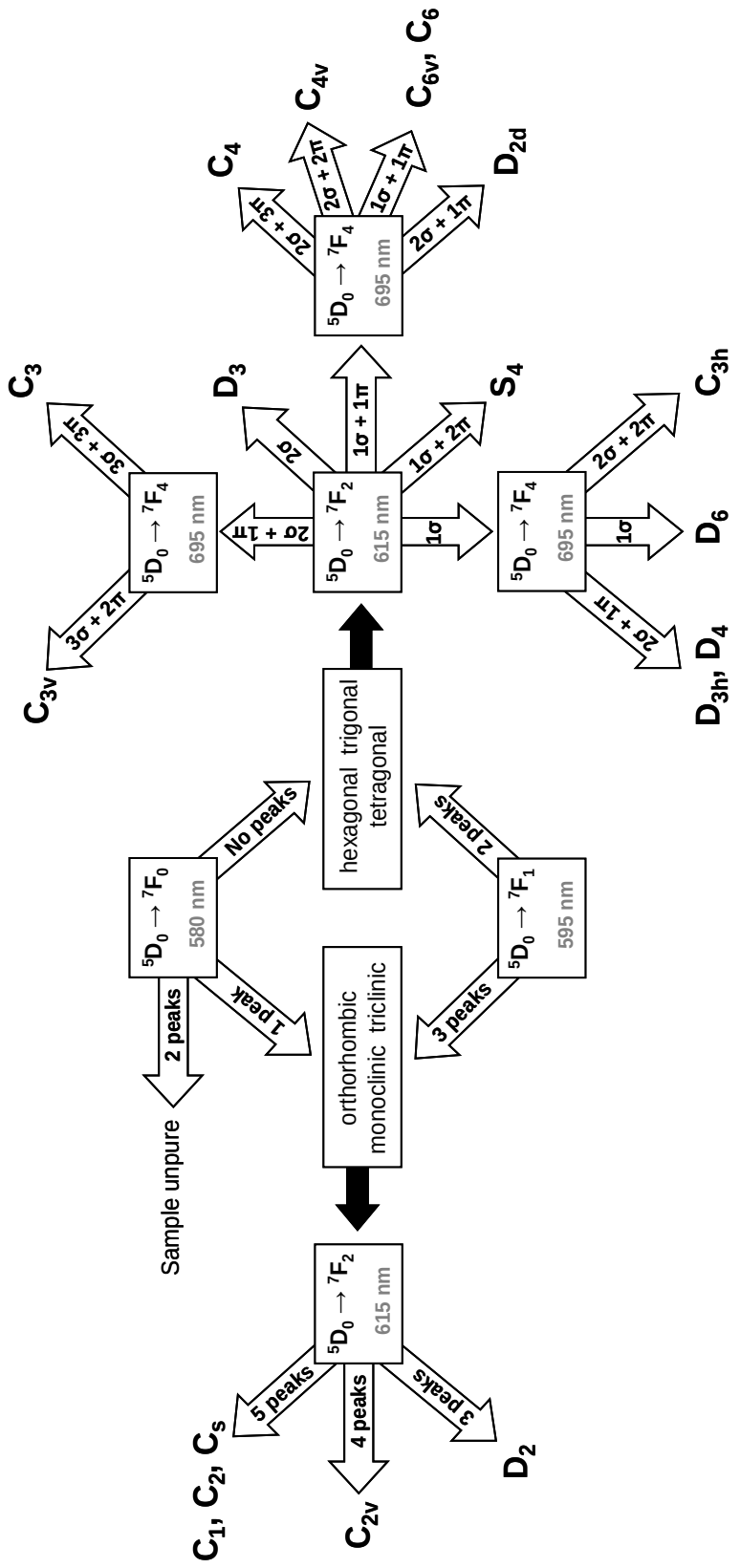

Figure 2.16. Scheme for point group determination based on selected transitions in the Eu^{3+} ion. Modified for luminescence spectra from reference 25.

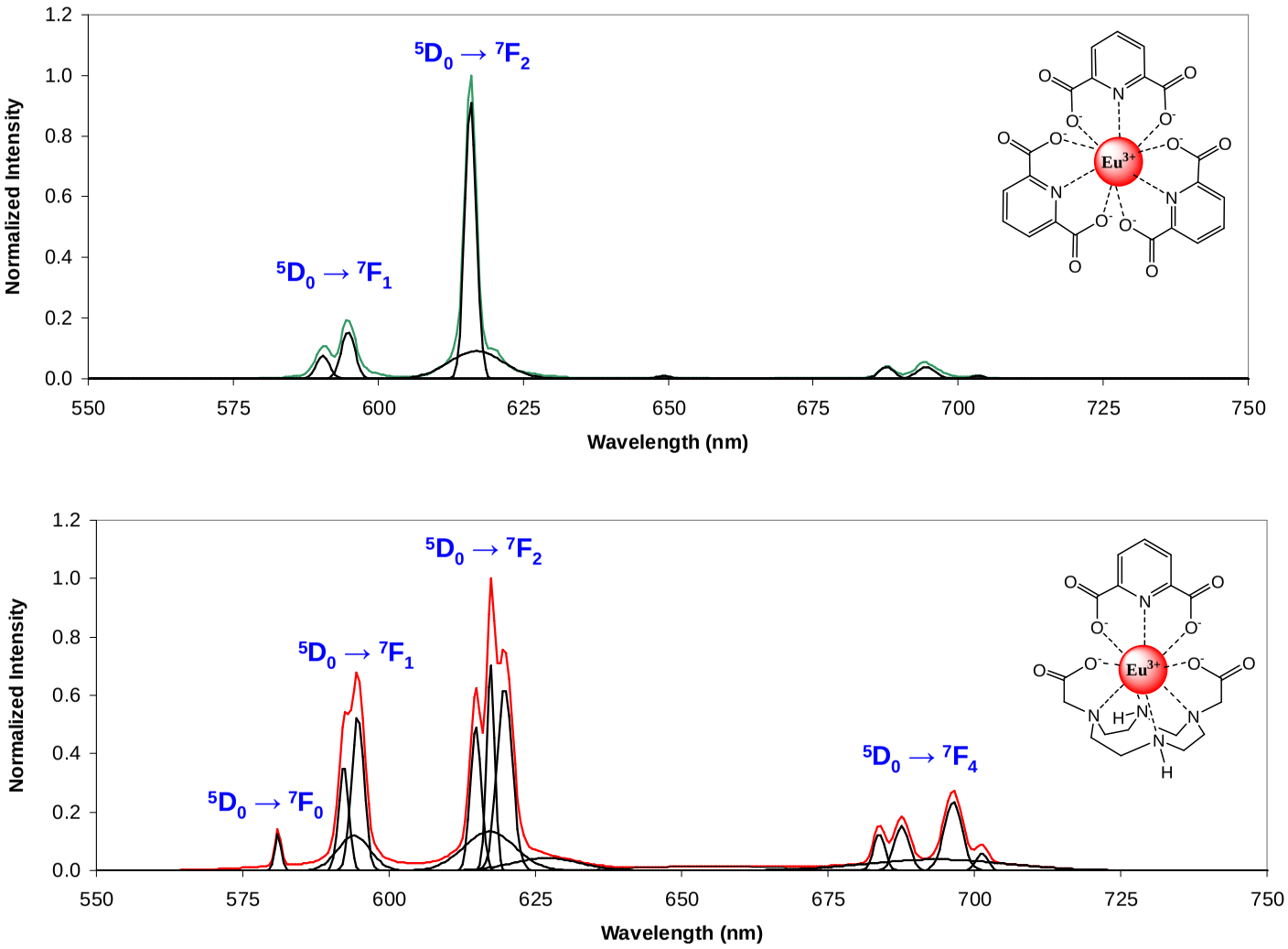

Figure 2.17. Emission spectra of $Eu(DPA)_3$ and Eu(DO2A)(DPA) complexes in green and red, respectively, with each transition deconvoluted into individual Stark sublevels via a sum of Gaussians program.

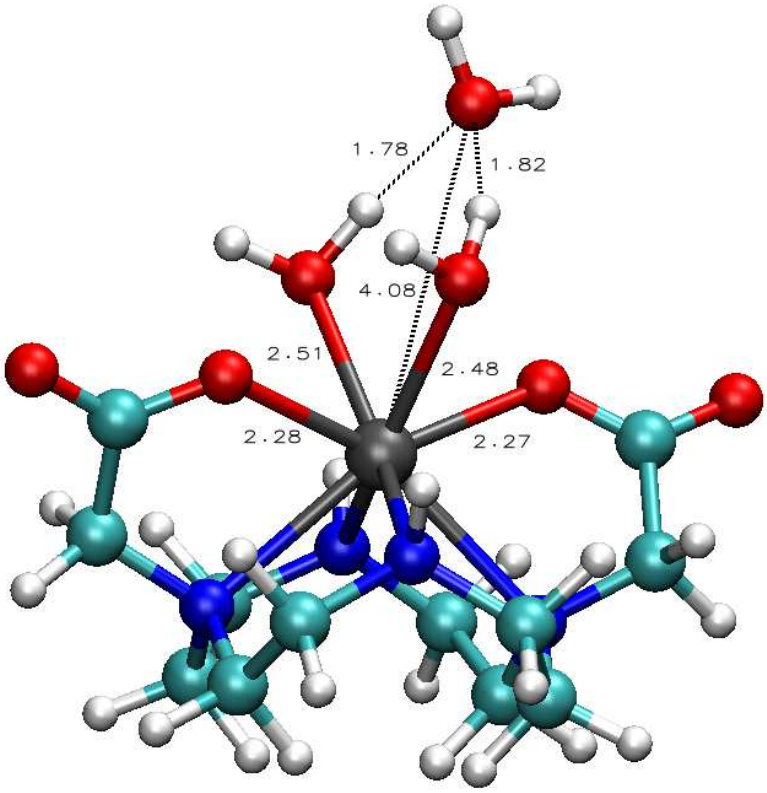

Figure 2.18. Theoretical model of $Tb(DO2A)^{+}$ complex, showing two solvent molecules in the terbium coordination sphere and one less strongly associated. Courtesy of J. Keith, Universität Ulm.

Table 2.1. Crystallographic data for the five TBA•Ln(DO2A)(DPA) structures.

Ln	Sm	Eu	Gd	Tb	Dy
Formula	$[C_{19}H_{25}N_5O_8Sm]^-$ $[C_{16}H_{36}N]^+$• 0.27(C_2H_6O•O) 0.73(C_3H_6O) 2(H_2O)	$[C_{19}H_{25}N_5O_8Eu]^-$ $[C_{16}H_{36}N]^+$• 0.68(C_3H_8O) 0.32(C_3H_6O) 3(H_2O)	$[C_{19}H_{25}N_5O_8Gd]^-$ $[C_{16}H_{36}N]^+$• 0.38(C_3H_6O•O) 0.62(C_3H_6O) 2(H_2O)	$[C_{19}H_{25}N_5O_8Tb]^-$ $[C_{16}H_{36}N]^+$• 0.47(C_3H_8O) 0.53(C_3H_6O) 3(H_2O)	$[C_{19}H_{25}N_5O_8Dy]^-$ $[C_{16}H_{36}N]^+$• 2(C_3H_8O) 3(H_2O)
M_w	939.36	957.23	946.79	964.94	966.51
Crystal system	Monoclinic	Triclinic	Monoclinic	Monoclinic	Monoclinic
Space group	$P2_1/c$	P1	$P2_1/c$	$P2_1/c$	$P2_1/c$
a (Å)	13.0658(4)	13.1473(4)	13.1910(5)	13.1047(5)	13.1742(4)
b (Å)	13.4504(4)	13.2269(4)	13.4544(5)	13.3397(5)	13.1860(4)
c (Å)	26.1778(7)	26.2248(8)	26.1712(9)	26.0901(9)	26.1130(8)
β (°)	90.3240(10)	90.0540(10)	90.368(2)	90.0130(10)	90.3720(10)
V ($Å^3$), Z	4600.4(2)	4560.4(2)	4644.7(3)	4560.9(3)	4536.1(2)
λ (Å)	0.71073	0.71073	0.71073	0.71073	0.71073
D_c (Mg/m^3)	1.356	1.394	1.354	1.405	1.415
μ,Mo-Kα (mm^{-1})	1.336	1.438	1.487	1.613	1.710
T (K)	100(2)	100(2)	100(2)	100(2)	100(2)
R_1, wR_2‡	0.0422, 0.0734	0.0437, 0.0750	0.0302, 0.0482	0.0384, 0.0639	0.0408, 0.0721

‡ Structure refined on F^2 using all reflections: $wR_2 = [\Sigma[w(F^2 - F_c^2)^2]/\Sigma w(F^2)^2]^{1/2}$, where $w^{-1} = [\Sigma(F^2) + (aP)^2 + bP]$ and $P = [\max(F^2,0) + 2F_c^2]/3$.

Table 2.2. Relevant bond distances for various gadolinium complexes.

	Gd(DO2A)(DPA)	**$[Gd(DO3A)]_3 \bullet Na_2CO_3$** †	**$Na[Gd(H_2O)(DOTA)]$** †
Gd--N1	2.6607(9)	2.63	2.656(3)
Gd--N2	2.5960(9)	2.60	2.688(3)
Gd--N3	2.6727(9)	2.59	2.645(3)
Gd--N4	2.5816(9)	2.56	2.661(4)
Gd--O1	2.3941(7)	2.35	2.379(3)
Gd--O3	2.3850(7)	2.34	2.362(3)
Gd--O7		2.35	2.359(3)
Gd--O9			2.370(3)

† Reference 14

Note: Numbering of O atoms was modified in the DO2A complex to be consistent with the reported DO3A and DOTA complexes.

Table 2.3. Crystallographic data for the three TBA•Eu(DO2A)(DPA) structures.

Temp	**100 K**	**200 K**	**300 K**
Formula	$[C_{19}H_{25}N_5O_8Eu]^-$ $[C_{16}H_{36}N]^+$• C_3H_6O • 3.68(H_2O)	$[C_{19}H_{25}N_5O_8Eu]^-$ $[C_{16}H_{36}N]^+$• C_3H_6O • 3.68(H_2O)	$[C_{19}H_{25}N_5O_8Eu]^-$ $[C_{16}H_{36}N]^+$• C_3H_6O • 3.68(H_2O)
M_w	970.23	970.23	949.07
Crystal system	Monoclinic	Monoclinic	Monoclinic
Space group	$P2_1/c$	$P2_1/c$	$P2_1/c$
a (Å)	13.0309(5)	13.1516(5)	13.3306(9)
b (Å)	13.4740(5)	13.5276(5)	13.4557(9)
c (Å)	26.1088(9)	26.1946(9)	26.3443(17)
β (°)	90.600(2)	90.701(2)	90.450(3)
V ($Å^3$), Z	4583.9(3)	4659.9(3)	4725.3(5)
λ (Å)	0.71073	0.71073	0.71073
D_c (Mg/m^3)	1.406	1.383	1.334
μ,Mo-Kα (mm^{-1})	1.432	1.409	1.386
T (K)	100(2)	200(2)	300(2)
R_1, wR_2[‡]	0.0341, 0.0624	0.0337, 0.0550	0.0469, 0.0623

[‡] Structure refined on F^2 using all reflections: $wR_2 = [\Sigma[w(F^2 - F_c^2)^2]/\Sigma w(F^2)^2]^{1/2}$, where $w^{-1} = [\Sigma(F^2) + (aP)^2 + bP]$ and $P = [\max(F^2,0) + 2F_c^2]/3$.

Table 2.4. Molar extinction coefficients of the Ln(DO2A)(DPA)$^{-}$ complexes (Ln = Sm, Eu, Tb, Dy) and the DPA^{2-} anion.

Complex	Buffer	λ_{abs} (nm)	Temp (℃)	pH	ε_{Exp} ($M^{-1}cm^{-1}$)
Sm(DO2A)(DPA)$^{-}$	0.1 M Tris	280	22.0	7.49	4160 ± 10
Eu(DO2A)(DPA)$^{-}$			22.1	7.46	3369 ± 24
Tb(DO2A)(DPA)$^{-}$			22.0	7.43	2259 ± 10
Dy(DO2A)(DPA)$^{-}$			22.1	7.49	3803 ± 2
DPA^{2-}			22.3	7.50	2832 ± 21

Table 2.5. Luminescence quantum yield data, 0.1 M Tris buffer, L-Trp standard.

Complex	Temp (℃)	pH	Φ_L (x 10^{-3})
Sm(DO2A)(DPA)$^-$	25.4 ± 0.3	7.93 ± 0.02	1.09 ± 0.03
Eu(DO2A)(DPA)$^-$	24.7 ± 0.1	7.92 ± 0.02	7.51 ± 0.03
Tb(DO2A)(DPA)$^-$	24.8 ± 0.2	7.93 ± 0.01	110 ± 2
Dy(DO2A)(DPA)$^-$	25.6 ± 0.3	7.87 ± 0.02	5.58 ± 0.07

Table 2.6. Ligand energy levels and lanthanide ion resonance levels in the absorbance-energy transfer-emission (AETE) mechanism of DPA-sensitized lanthanide luminescence.

Ligand Energy Level (cm^{-1})		Ln^{3+} Ion Resonance Level (cm^{-1})	
DPA Triplet	26,600 [32]	Sm^{3+} $^4G_{5/2}$	17,900 [35]
		Eu^{3+} $^5D_0$	17,264 [36]
		Tb^{3+} $^5D_4$	20,500 [34]
		Dy^{3+} $^4F_{9/2}$	21,100 [35]

Table 2.7. Luminescent lifetime measurements[a] of various terbium complexes.

complex[b]	τ_{H_2O} (ms)	τ_{D_2O} (ms)	q[c]
$[Tb(H_2O)_9]^{3+}$	0.4	3.4	8.8 ± 1.1
$[Tb(DPA)(H_2O)_6]^{+}$	0.6[d]	3.5	5.6 ± 0.7
$[Tb(DO2A)(H_2O)_3]^{+}$	1.1	2.6	2.4 ± 0.3
$[Tb(DO2A)(DPA)]^{-}$	1.9	2.2	0.3 ± 0.0

[a] Excitation at 266 nm (10 ns, pulsed Nd:YAG laser), emission detection at 544 nm, sample concentrations 1 to 10 μM, pH 7.5 (adjusted with NaOH).

[b] Waters included assuming that the Tb^{3+} ion is 9-coordinate.

[c] The number of water molecules, q, in the Tb^{3+} coordination sphere, where

$$q = A_{Ln} (\tau^{-1}_{H_2O} - \tau^{-1}_{D_2O})$$

and A_{Tb} = 4.6 or 4.2 ± 0.5 ms^{-1} per bound water molecule for complexes with and without DO2A, respectively.

[d] See reference 45.

CHAPTER 3

A First-Generation Receptor Site for the Detection of Bacterial Spores

3.1 Introduction

To design an effective receptor site for a given analyte, we consider certain basic criteria: (1) the receptor site must exhibit an obvious, measurable response upon analyte binding, meaning there must be a clear and distinguishable difference between the two states of analyte bound or unbound; (2) the receptor site should have a very high affinity for the analyte of interest, on the order of $K \sim 10^9$ or greater;[1] (3) binding kinetics should be proportional to the rate of analyte release and consistent with timescales for field work in situ; (4) the receptor site should be resistant to local changes in the environment, such as pH and temperature variations; and (5) the binding of receptor site to analyte should be highly selective, even in complex matrices containing common environmental interferents.

All four luminescent $Ln(DO2A)^+$ binary complexes (Ln = Sm, Eu, Tb and Dy) meet this first requirement in improving lanthanide-based detection of dipicolinate. Based on quantum yield measurements, the $Tb(DO2A)^+$ complex has the greatest sensitization efficiency (Section 2.3.2) and would produce the greatest signal-to-noise ratio as a sensor. We therefore gear our analysis around characterizing the binding properties and robust qualities of $Tb(DO2A)^+$ in order to validate this complex as an effective DPA receptor site. Where appropriate, studies of the entire series will be performed to determine if lanthanide ionic radius has a significant influence.

Binding and kinetics studies will unveil the $Ln(DO2A)^+$ complex with the greatest affinity for dipicolinate and establish dependence of binding rate on lanthanide ionic radius. The effects of modifications to the dipicolinate ligand can be assessed using structural isomers and targeted substitutions. Temperature and pH dependence

experiments will determine if the DO2A ligand can make dipicolinate detection more robust. The impact of both cationic and anionic interferents on DPA detection by the $Tb(DO2A)^{+}$ receptor site will be investigated. Finally, we will apply the $Tb(DO2A)^{+}$ complex to detection of bacterial spores, both in controlled conditions and environmental samples.

3.2 Binding Studies

Various studies will be performed to determine the binding affinities of the luminescent lanthanide complexes for the dipicolinate anion. Binding stoichiometry is established using the Jobs method of continuous variations. Association constants for both the Ln^{3+} and the $Ln(DO2A)^{+}$ complexes for DPA^{2-} will be calculated, the latter with a novel competition experiment. A brief kinetics investigation will also delve into the speed and selectivity of dipicolinate binding.

3.2.1 Jobs Plots

A method of continuous variations will be employed to determine the binding stoichiometries of various lanthanide complexes. The concentrations of two components are varied inversely to produce a range of ratios between the two, with the total concentration held constant. Following spectroscopic analysis, the resulting Jobs Plot reveals any correlation between the components as a function of mole fraction (Figure 3.1). As the maximum response occurs when the mole fraction of the reactants is closest to the actual stoichiometric mole ratio, the binding stoichiometry can be estimated using this approach.[2] In our case, the two components are the lanthanide ion and the

dipicolinate ligand, with the macrocyclic protecting ligand in excess to ensure lanthanide complexation under constant ionic strength. The Jobs method can be applied to a wide variety of measurements (temperature, absorbance, conductivity, etc.); we utilize emission intensity as our metric to qualify lanthanide-dipicolinate binding ratios. Partially hydrolyzed lanthanide species are known to adhere to glass surfaces,[3] so these studies will be performed in disposable acrylate cuvettes (transmission range: 280–900 nm, ~ 70% transmission at 278 nm, reported variation < 1% between cuvettes).

We will use the Jobs method to determine optimal binding stoichiometries for the $Ln(DO2A)^{+}$ complex (Ln = Eu, Tb and Dy) with dipicolinate. We will also investigate several macrocyclic ligands for the terbium case: DO2A, DO3A, DOTA and hexacyclen (Figure 3.2). We anticipate that the two hexadentate ligands (DO2A and hexacyclen) will allow for dipicolinate binding to the lanthanide, with a binding ratio of approximately 1:1 for Tb:DPA. The DO3A and DOTA ligands, which are hepta- and octadentate, respectively, should restrict dipicolinate association to the lanthanide as less than three coordination sites remain available for binding.

Experimental Section

Materials. The following chemicals were purchased and used as received: trichloromethane (chloroform) (Mallinckrodt), DOTA (*1,4,7,10*-tetraazacyclododecane-*1,4,7,10*-tetraacetate) (Macrocyclics), DPA (dipicolinic acid, pyridine-*2,6*,-dicarboxylic acid) (Aldrich), dysprosium(III) chloride hydrate (Alfa Aesar), ether anhydrous (Acros Organics), ethyl alcohol (200-proof) (Acros Organics), europium(III) chloride hexahydrate (Aldrich), hexacyclen (hexamine, 18-azacrown-6, *1,4,7,10,13,16*-hexaaza-

cyclooctadecane) trisulfate (Aldrich), hydrochloric acid (36.5–38.0% in water) (EMD Chemicals), sodium hydroxide pellets (Mallinckrodt), terbium(III) chloride hexahydrate (Alfa Aesar). All lanthanide salts were 99.9% pure or greater, all solvents were ACS certified or HPLC grade, and all other salts were 97% pure or greater. Water was deionized to a resistivity of 18.2 MΩ-cm using a Purelab® Ultra laboratory water purification system (Siemens Water Technologies, Warrendale, PA). DO2A was prepared as previously described (Section 2.2.1).

The *1,4,7,10*-tetraazacyclododecane-*1,4,7*-triacetate (DO3A) ligand was prepared by hydrolysis of *1,4,7,10*-tetraazacyclododecane-*1,4,7*-tri(*tert*-butyl acetate) (DO3A-tBu-ester) (Macrocyclics, Dallas, TX) following a method adapted from the DO2A protocol. The DO3A-tBu-ester (0.9757 g, 1.90 mmol), a slightly off-white powder, was dissolved in 20.0 mL of 20% hydrochloric acid in a roundbottom flask and refluxed for 24 hours with stirring in an oil bath (115 °C). The hydrochloric acid was removed by rotary evaporation under vacuum (~ 50 mbar) in a hot water bath (60 °C) to give an off-white solid. The deprotected ligand was then rinsed using a fine frit (Pyrex, 15 mL, ASTM 4-5.5F, No. 36060) and vacuum filtration with the following in sequence: 20 mL of absolute ethanol (200-proof), 4 mL of diethyl ether, 8 mL of an ethanol-ether (1:1) mixture, and three 8-mL aliquots of ether. The solid was dried in a dessicator under vacuum for 7 days to produce DO3A·1.7HCl·2.8H_2O (0.4632 g, 1.02 mmol) in 53.56% yield. Anal. Calcd (found) for $C_{12}H_{24}N_4O_4$·1.7HCl·2.8H_2O (fw = 456.20): C, 36.86 (36.86); H, 6.69 (6.69); N, 12.28 (12.10). Purity was confirmed with thin-layer chromatography (TLC) using ethanol and chloroform and analysis with a handheld UVGL-25 multiband UV lamp (UVP, Upland, CA) in short wave (254 nm) mode.

It should be noted that subsequent attempts to synthesize DO3A using this same procedure resulted in a brown, viscous substance, presumably decomposition products according to analysis with NMR and mass spectroscopy. It is hypothesized that the hot plate heating the oil bath from the first, successful attempt did not maintain a constant temperature of 115 °C through the 24-hour reflux period, and in fact the reaction might have taken place at a lower temperature. An alternative deprotection procedure with milder reaction conditions was used for later batches (see Section 5.2.2).

Methods. All samples were prepared in triplicate from stock solutions to a final volume of 4.00 mL in disposable acrylate cuvettes (Spectrocell, Oreland, PA) with a 1 cm path length and were allowed to equilibrate for at least 5 days prior to analysis. The concentrations of $LnCl_3$ (Dy, Eu or Tb) and DPA were varied inversely in 1.0-μM increments from 0 to 12.0 μM with 100 μM ligand (DO2A, DO3A, DOTA or EDTA). Solution pH was maintained either by 1.0 mM NaOH (pH 9.0) or 100 mM CHES buffer (pH 9.4) to ensure that the ligands were sufficiently deprotonated for optimum binding.[4-7]

Luminescence spectral analysis was performed by a Fluorolog Fluorescence Spectrometer (Horiba Jobin-Yvon, Edison, NJ). To prevent second-order diffraction of the source radiation, all measurements were taken with a 350-nm colorless sharp cutoff glass filter (03 FCG 055, Melles Griot, Covina, CA). The solution pH was measured using a calibrated handheld pH/mV/temperature meter (Model IQ150, I. Q. Scientific Instruments, Loveland, CO) following data collection. All reported spectra were obtained as a ratio of corrected signal to corrected reference (S_c/R_c) to eliminate the effect of varying background radiation in the sample chamber; intensities are in units of counts per second per microampere (cps/μA).

Results and Discussion

Dipicolinate exhibits no detectable fluorescence (Section 2.3.1), and the emission of the lanthanide without a chromophore is negligible (Section 1.2); we therefore can attribute any significant change in emission intensity to the formation of a lanthanide-dipicolinate complex. The binding affinity of the lanthanide for the macrocycle is very high (Table 3.1),[5, 8, 9] so we can assume that all Ln^{3+} is bound as the lanthanide-macrocycle binary complex when the concentration of macrocycle is in excess. As the lanthanide mole fraction is increased, the emission intensity increases as more of the free dipicolinate binds to the lanthanide, producing a positive slope. Following complete complexation of all lanthanide-macrocycle species with dipicolinate, an increased mole fraction of the lanthanide will result in a decreasing amount of total ternary complex (the dipicolinate concentration is decreasing to maintain a constant total concentration), producing a negative slope. The point at which the biphasic curve shifts from positive to negative slope represents the optimal binding stoichiometry of the lanthanide binary complex to the dipicolinate ligand.

For the DO2A complex, the optimal binding stoichiometry occurs at a terbium mole fraction of 0.5, as would be expected if the $Tb(DO2A)^{+}$ and DPA^{2-} species were binding in a one-to-one fashion (Figure 3.3). The hexacyclen ligand, in contrast, shows nonlinear behavior and the greatest intensity at a Tb mole fraction below 0.5. This implies that an increased concentration of dipicolinate is necessary to completely form the ternary complex, most likely due to steric effects or poor association between the lanthanide and the larger binding cavity of this ligand.[10] The curving behavior of this Jobs plot is also indicative of low to moderate stability.[11] As lanthanides tend to be

oxophilic in character (see Section 1.1), this may be evidence of reduced Tb-hexacyclen binding affinity due to the replacement of two O-donors with two N-donors in the hexacyclen ligand.

The DO3A and DOTA ligands, which should exclude dipicolinate from the lanthanide coordination sphere, both show a binding stoichiometry of approximately 1:3 for Tb:DPA. This suggests that dipicolinate has a strong affinity for the Tb^{3+} cation, and when in excess is able to overcome steric hindrance and partially displace the strongly bound macrocyclic ligand. The Jobs plots of these ligands also show flattening around the maxima, indicating the presence of multiple species in solution. These are most likely the Tb(macrocycle) complex and multiple Tb(macrocycle)(dipicolinate) complexes, with various conformations possible as the dipicolinate forces one or two of the macrocycle carboxyl arms to decouple from the lanthanide.

Jobs plots with various lanthanides and DO2A show a potential relationship between stability and lanthanide ionic radius (Figure 3.4). Europium and terbium have identical binding stoichiometries to DPA with the DO2A ligand in excess, but the dysprosium case indicates the formation of $Dy(DPA)_3$ at low Dy mole fraction. This may be due to the smaller ionic radius of this lanthanide compared to Eu^{3+} and Tb^{3+}, such that there is reduced interaction between the Dy^{3+} cation and the DO2A ligand cavity.

Binding stoichiometry studies using the Jobs method of continuous variations indicate that, as expected, the hexadentate DO2A ligand is the ideal candidate to protect the lanthanide ion from solvent and leave sufficient space available for the tridentate dipicolinate chromophore to bind. We now focus on further characterization of the $Ln(DO2A)^+$ species as sensing complexes for DPA.

3.2.2 Calculation of Dipicolinate Association Constants

The primary measure of receptor site efficacy is binding affinity for the target analyte. Ideal sensing complexes have nanomolar sensitivity or better.[1] However, most titrimetric techniques for experimentally determining association constants, such as the Benesi-Hildebrand method,[12] break down under conditions where (1) binding constants are large ($> 10^9\ M^{-1}$), (2) the system contains more than two components, or (3) changes in absorbance or luminescence are small.[13, 14] We therefore developed and tested a binding affinity by competition (BAC) assay to determine DPA to binary complex binding constants.

Ternary $Ln(DO2A)(DPA)^-$ complex solutions (of crystallographically characterized TBA·Ln(DO2A)(DPA)) are titrated with $LnCl_3$; increased Ln^{3+} concentration results in a shift in equilibrium population from $Ln(DO2A)(DPA)^-$ to $Ln(DO2A)^+$ and $Ln(DPA)^+$, which is monitored via a ligand field sensitive transition using fluorescence spectroscopy (see Figure 3.5). A best fit of luminescence intensity titration data to a two-state thermodynamic model yields the competition equilibrium constant (K_c), which in conjunction with independent measurement of the $Ln(DPA)^+$ formation constant (K_a) allows calculation of the ternary complex formation constant (K_a'). In general, the BAC assay can be employed to determine ligand binding constants in systems were the lanthanide platform (usually a binary complex) is stable and the ligand bound versus unbound states can be spectroscopically distinguished.

Experimental Section

Materials. Dysprosium(III) chloride hydrate (Alfa Aesar), europium(III) chloride hexahydrate (Aldrich), samarium(III) chloride (Alfa Aesar), sodium acetate trihydrate (Mallinckrodt) and terbium(III) chloride hexahydrate (Alfa Aesar) were purchased and used as received. All lanthanide salts were 99.9% pure or greater and all other salts were 97% pure or greater. DO2A was prepared as previously described (Section 2.2.1). Dried, fully characterized TBA·Ln(DO2A)(DPA) crystals (Section 2.2.1) were used to produce a 1:1:1 ratio of Ln:DO2A:DPA in solution. Water was deionized to a resistivity of 18.2 MΩ-cm using a Purelab® Ultra laboratory water purification system.

Methods. All samples were prepared to a final volume of 3.50 mL from stock solutions in disposable acrylate cuvettes (Spectrocell, Oreland, PA) with a 1 cm path length and were allowed to equilibrate for at least 7 days. Luminescence spectral analysis was performed by a Fluorolog Fluorescence Spectrometer with a 350-nm cutoff filter as previously described (Section 3.2.1). The solution pH was measured using a calibrated handheld IQ150 pH/mV/temperature meter (I. Q. Scientific Instruments) following data collection. Sample temperature was monitored using a handheld Fluke 62 Mini Infrared Thermometer (Fluke Corp, Everett, WA).

Calculation of K_a. Initially, a Microlab 500 Series Autotitrator (Hamilton Co., Reno, NV) with Instrument Control software was used to adjust the concentrations of terbium and dipicolinate in a single cuvette for in situ luminescence monitoring. However, results were inconsistent in all titrations involving DPA, most likely due to retention of this species within the titrator tubing. An alternative approach using disposable acrylate cuvettes, with one cuvette per concentration point prepared

individually in triplicate, yielded reproducible results and allowed for pH measurement of each data point. This method will be used for all future titrimetric assays.

Association constants for Ln^{3+} to DPA^{2-} (Ln = Sm, Eu, Tb and Dy) were determined via titration of Ln^{3+} against 10.0 nM DPA in 0.2 M sodium acetate (pH 7.4). A linear fit similar to that of the one-step equilibrium model of Jones and Vullev[15] was applied as $[Ln^{3+}] > [DPA^{2-}]$, and the binding affinity of the binary complex (K_a) was calculated using the following linear relationship:

$$\log\left(\frac{R}{C_{Ln}}\right) = \log(1-R) + \log K_a$$
$$R = \frac{[LnDPA]_{eq}}{[LnDPA]_{eq} + [DPA]_{eq}} \qquad [3.1]$$

where C_{Ln} is the total concentration of the lanthanide and R is the normalized integrated emission intensity (see Appendix A for derivation).

Calculation of K_a'. Samples were prepared using solvated $Ln(DO2A)(DPA)^-$ crystals and lanthanide chloride salts in 0.2 M sodium acetate (pH 7.4), such that the concentration of $Ln(DO2A)(DPA)^-$ was 1.0 μM and the concentration of free Ln^{3+} ranged from 1.0 nM to 1.0 mM. The use of X-ray quality, solvated TBA·Ln(DO2A)(DPA) crystals in this work demonstrates a major advantage, especially at low concentrations; the precise measure of the initial concentration of $Ln(DO2A)(DPA)^-$ could not be achieved without this important step. As Ln^{3+} was added, the shift in equilibrium $Ln(DO2A)(DPA)^-$ and $Ln(DPA)^+$ concentrations was monitored via a ligand field sensitive transition in the emission spectrum using luminescence spectroscopy. Emission spectra (λ_{ex} = 278 nm) were integrated over the most ligand-field-sensitive peak (Sm: $^4G_{5/2} \rightarrow {}^6H_{7/2}$, 580–625 nm; Eu: $^5D_0 \rightarrow {}^7F_4$, 675–710 nm;

Tb: $^5D_4 \rightarrow {}^7F_4$, 570–600 nm; Dy: $^4F_{9/2} \rightarrow {}^6H_{13/2}$, 555–595 nm) to produce curves of observed integrated intensity (I_{obs}) against the log of excess free lanthanide (log $[Ln^{3+}]_{xs}$). A best fit to a two-state thermodynamic model using the Curve Fitting Tool in Matlab® yielded the competition equilibrium constant (K_c) by equation 3.2.

$$I_{obs} = \left(1 - \frac{[Ln(DPA)^+]_{eq}}{[Ln(DO2A)(DPA)^-]_T}\right) I_{max} + \left(\frac{[Ln(DPA)^+]_{eq}}{[Ln(DO2A)(DPA)^-]_T}\right) I_{min}$$

where [3.2]

$$[Ln(DPA)^+]_{eq} = \frac{[Ln^{3+}]_T + \left(\begin{array}{l}\left\{[Ln^{3+}]_T - 2\left(1 - K_C^{-1}\right)[Ln(DO2A)(DPA)^-]_T\right\}^2 \\ + 4K_C^{-1}\left(1 - K_C^{-1}\right)\left([Ln(DO2A)(DPA)^-]_T\right)^2\end{array}\right)^{1/2}}{2\left(1 - K_C^{-1}\right)}$$

The total concentrations of free lanthanide ($[Ln^{3+}]_T$) and ternary complex ($[Tb(DO2A)(DPA)^-]_T$) are known from initial conditions. Following independent measurement of the $Ln(DPA)^+$ formation constant (K_a) at identical pH and temperature, the ternary complex formation constant K_a' was calculated using the relation in equation 3.3 (see Appendix B for derivation).

$$K_C = \frac{K_a}{K_a'} \qquad [3.3]$$

Results and Discussion

The serial dilution method used for calculation of K_a, though not as ubiquitous as that of Jones and Vullev, presents certain advantages. Both were derived from the same one-step Tb-DPA equilibration model, but Jones and Vullev made the assumption that

[Ln] >> [DPA] to cancel a term and arrive at the final equation used for the linear fit (see Supporting Information of reference 15). As the intrinsic luminescence of the Ln^{3+} species alone presents an upper bound (which usually occurs in the millimolar regime), this high lower bound limiting the lanthanide concentration means that there is a very small range where this fit can be applied. In contrast, our fit makes no such assumption, and only requires that [Tb] ≥ [DPA] to be valid. Therefore, a broader data set can be applied to this fit, allowing for more accurate binding constant measurement (see Figure 3.6).

Secondly, though the linear fit provided by the Jones and Vullev method produces a value *n* for the slope that can be used to approximate the number of DPA moieties bound to the lanthanide, i.e., $Tb(DPA)_n$, this allows for more possible error in terms of the fit when the coordination number is already known. In other words, a value of n = 0.93 would be considered close enough to 1, and one might assume that the y-intercept of such a fit would therefore be an accurate measure of the K_a for TbDPA. However, a difference of 7% in the slope of this fit can produce a y-intercept that is off by nearly 10%, and this error would not be included in the reported value of K_a. In our fitting technique, the slope is set to unity, so the only parameter that can be shifted to fit the data is that of the quantity of interest – the y-intercept, or the value of K_a. We therefore have more confidence in our calculated values of K_a than in those of other methods.

Using the solvated TBA·Ln(DO2A)(DPA) crystals to achieve an optimized 1:1:1 ratio of Ln/DO2A/DPA, we were able to perform titrations over 6 orders of magnitude, with added $[Ln^{3+}]_{xs}$ ranging from 1.0 nM to 1.0 mM. The shift from ternary to binary complex was easily observed via luminescence spectroscopy in this range. Titration of

free Ln^{3+} in buffer over the same concentration range resulted in negligible intensity increase, confirming that the intensity change observed is due to the transition from ternary to mono-DPA complex.

Our calculated values of K_a and K_a' for various lanthanide complexes (Ln = Sm, Eu, Tb and Dy) appear in Table 3.2. The association constant K_a for the terbium case is in agreement with the formation constant obtained by Jones and Vullev at a similar pH and ionic strength.[15] As seen in Figures 3.7 and 3.8, the addition of the DO2A ligand enhances the binding affinity of the Ln^{3+} ion for the DPA^{2-} analyte by at least an order of magnitude. This result is quite intriguing, as this trend does not follow predictions based on total charges of the binding species. Specifically, upon addition of the DO2A ligand, the dipicolinate receptor site decreases from a net +3 charge of the lanthanide alone to a binary complex with a total charge of only +1. As binding interactions with lanthanides tend to be electrostatic in character (Section 1.1), this should have resulted in a decrease in binding affinity. We postulate that the lanthanide-macrocycle platform increases the positive charge of the binding site through the electron-withdrawing N and O moieties of the macrocycle, which allows for greater compatibility with the negative surface of the dipicolinate moiety. This property of 'ligand enhancement' in analyte binding affinity will be further explored in the Conclusions section at the end of the chapter.

Another interesting discovery was that the binding affinity of the $Tb(DO2A)^+$ binary complex is even more effective and nearly an order of magnitude greater than the other three lanthanides. The calculated association constant for $Tb(DO2A)^+$ to DPA^{2-} is also several orders of magnitude greater than that of Tb(EDTA).[16] Both DO2A and EDTA are hexadentate and leave three remaining sites available for dipicolinate

binding,[17] but closer examination of the geometry of those sites may provide an explanation for the discrepancy in binding affinity. A crystal structure of the Tb(EDTA) complex reveals that the three coordination sites are adjacent, but arranged in a trigonal fashion (Figure 3.9). The dipicolinate ligand is a linear molecule, and requires three adjacent *linear* sites available on the lanthanide to bind properly. The DO2A ligand, with its more rigid azacrown backbone and two carboxyl arms, coordinates to the lanthanide with the appropriate geometry. The floppy EDTA ligand must undergo reorganization around the Tb^{3+} ion to accommodate the dipicolinate ligand, and therefore the binding affinity is lower for the Tb(EDTA) complex. This is supported by a study involving picolinic acid, dipicolinic acid and various terbium polycarboxylate ligands, where in many cases the ligand entered a forced conformational change to facilitate chromophore binding and form the ternary complex.[18]

The binding affinity by competition (BAC) assay can be employed to quantify ternary lanthanide complex formation under conditions where the lanthanide-macrocycle platform is stable and the concentrations of the two states of the receptor site – bound and vacant – can be measured. In our case, the binary and ternary complexes of interest are spectroscopically resolvable. The BAC assay is especially useful in high binding regimes, where direct measures of ligand binding, such as the Benesi-Hildebrand method, break down. A similar luminescence-based study has demonstrated calculation of europium-macrocycle stability constants based on lifetime measurements,[19] also in the high binding constant regime. However, this technique is only valid for two components and where lifetimes of the two species of interest are discernable, and cannot be applied to environmental samples. Our assay, in contrast, can be applied to equilibria with more

than two components and can be implemented in a variety of conditions such as those expected in environmental samples. As long as K_a and K_a' are measured in identical conditions, the change in binding affinity can be calculated quantitatively. The BAC assay allows for the unambiguous measure of relative stability, to guide us toward a superior sensor for bacterial spores via DPA-triggered Tb^{3+} luminescence.

3.2.3 Binding Rates and Kinetics

Another important quality of an effective receptor site is rapid binding to the analyte of interest. To determine the rate of dipicolinate binding by the $Ln(DO2A)^+$ complexes, time courses and a brief kinetics study will be performed. Various studies have shown that macrocyclic ligands can take hours to even days to completely coordinate the lanthanide.[5, 6, 20] The carboxylate groups coordinate first, followed by the lanthanide moving into the macrocycle cavity in a concerted rearrangement that may take several steps to produce the final thermodynamically stable complex.[21] However, once the lanthanide-macrocycle binary complex is formed, we believe dipicolinate binding will occur rapidly as little or no reorganization of the macrocycle is necessary.

Experimental Section

Materials. CAPS (*N*-cyclohexyl-*3*-aminopropanesulfonic acid) buffer (Alfa Aesar), DPA (dipicolinic acid, pyridine-*2,6,*-dicarboxylic acid) (Aldrich), dysprosium(III) chloride hydrate (Alfa Aesar), europium(III) chloride hexahydrate (Aldrich), MOPS (*3*-(*N*-morpholino)ethanesulfonic acid) buffer (Alfa Aesar), samarium(III) chloride (Alfa Aesar), sodium acetate trihydrate (Mallinckrodt) and terbium(III) chloride hexahydrate

(Alfa Aesar) were purchased and used as received. All lanthanide salts were 99.9% pure or greater and all other salts were 97% pure or greater. DO2A was prepared as previously described (Section 2.2.1). Water was deionized to a resistivity of 18.2 MΩ-cm using a Purelab® Ultra laboratory water purification system.

Methods. Unless otherwise specified, all experiments were performed at 25 °C in disposable acrylate cuvettes with a 1 cm path length. Sample injection during spectral acquisition was performed in the dark to prevent signal bleaching or damage to the photomultiplier tube of the fluorescence spectrometer.

Time courses. A 3.80 mL solution of 1.05 μM $Tb(DO2A)^+$ in 0.1 M buffer was placed in an acrylate cuvette in the spectrofluorometer sample chamber. A time course was initiated (λ_{ex} = 278 nm, λ_{em} = 544 nm), and after an appropriate baseline was obtained (~ 200 s) a 200-μL aliquot of 20.0 μM DPA was injected to produce a final concentration of 1.0 μM DPA in a 4.00 mL solution of 1.0 μM $Tb(DO2A)^+$. Ternary complex formation was confirmed with an analogous setup and emission scans every 5 minutes. This was performed in MOPS (pH 7.4) and CAPS (pH 10.4) to determine if OH^- is more difficult to displace from the Tb^{3+} coordination sphere than H_2O.

Kinetics study. Solutions of 1.0 and 10.0 μM Ln(DO2A)(DPA), where Ln = Sm, Eu, Tb and Dy, were injected with various aliquots of 4.0 mM $GdCl_3$ in 0.2 M NaOAc, pH 7.5, using the same time course method described above. Emission intensity at the λ_{max} for each lanthanide was monitored as a function of time (λ_{Sm} = 600 nm, λ_{Eu} = 614 nm, λ_{Tb} = 544 nm, λ_{Dy} = 575 nm).

Stability over time. The same series of cuvettes prepared for the calculation of K_a' (Section 3.2.2) were stored at room temperature and analyzed again after 5 and 11

months. Cuvettes that had lost an appreciable amount of solvent (> 0.5 mL) due to evaporation were refilled back to the 4.00 mL volume by mass using nanopure water (18.2 MΩ-cm resistivity). Sample pH was determined after collection of each data set.

Results and Discussion

Though others have noted that complex formation involving macrocyclic ligands can occur on the order of several hours to even days, we have found that DPA binding is rapid at neutral to high pH provided that the $Tb(DO2A)^+$ binary complex is already formed in solution, as would be the case for a receptor site (see Figure 3.10). The rate of DPA complexation is slightly longer at higher pH (~ 10 s as compared to 3 s); this is attributed to the negatively charged OH^- moieties being more difficult to displace from the Tb^{3+} coordination sphere than neutral H_2O molecules. However, as complete DPA binding occurs on the order of seconds in both cases, the applicability of the $Tb(DO2A)^+$ complex as a dipicolinate sensor in real-time is confirmed.

An initial experiment competing 10 μM $Tb(DO2A)(DPA)^-$ with 10 μM Eu^{3+} in 0.2 M NaOAc, pH 7.4, validated the hypothesis that the DO2A ligand is not labile over the course of the experiment, as only $Eu(DPA)^+$ is produced (see Figure 3.11), described in equilibrium 3.4.

$$Tb(DO2A)(DPA)^- + Eu^{3+} \rightleftharpoons Tb(DO2A)^+ + EuDPA^+ \qquad [3.4]$$

The DO2A ligand does not begin to dissociate from the Tb^{3+} ion and bind to the Eu^{3+} ion for several weeks, as evidenced by formation of the $Eu(DO2A)(DPA)^-$ complex from the characteristic emission spectrum.

The kinetics study involving competition of $Ln(DO2A)(DPA)^-$ against Gd^{3+} produced decay curves that were fit to a monoexponential model. Gadolinium does not luminesce under excitation at 278 nm, and therefore as the Gd^{3+} competes with the $Ln(DO2A)^+$ complex and removes the dipicolinate ligand to form $Gd(DPA)^+$, the luminescence intensity will decrease to zero. This is illustrated in equilibrium 3.5 with the observable rate described by equation 3.6.

$$Ln(DO2A)(DPA)^- + Gd^{3+} \underset{k_{-1}}{\overset{k_1}{\rightleftharpoons}} Ln(DO2A)^+ + GdDPA^+ \qquad [3.5]$$

$$k_{obs} = k_1 - k_{-1} \qquad [3.6]$$

Results indicate that the observed rate of DPA loss by the ternary complex (k_{obs}) is a function of lanthanide ionic radius, with the smallest lanthanide (dysprosium) exhibiting the slowest rate (see Figure 3.12). We postulate this is due to effective shielding of the smaller lanthanides by the DO2A and DPA ligands, reducing ligand exchange rates for these species. This is also substantiated by the higher dipicolinate binding affinities for the $Tb(DO2A)^+$ and $Dy(DO2A)^+$ binary complexes (log K_a' = 9.25 and 8.79, respectively) as compared to the Eu and Sm complexes (Section 3.2.2).

For the terbium and europium ternary complexes, kinetics experiments involving gadolinium were more thoroughly explored, and a relationship between the observed luminescence decay rate (k_{obs}) and gadolinium concentration was established. These decay curves were also fit to a monoexponential model, though we found it interesting that as the Gd^{3+} concentration increased, the rate of luminescence decay decreased in a logarithmic fashion (see Figure 3.13). It must be noted, however, that only in the limit of 1000-fold Gd^{3+} concentration versus ternary complex does the luminescence drop

completely to zero; for all cases where [Gd^{3+}] < 1 mM, a population of $Tb(DO2A)(DPA)^-$ or $Eu(DO2A)(DPA)^-$ persisted. This indicates that the rate of DPA abstraction by Gd^{3+} is limited by concentration, and that the affinity of Gd^{3+} for dipicolinate is significantly less than that of the $Tb(DO2A)^+$ and $Eu(DO2A)^+$ complexes, as expected.

Once formed, the $Tb(DO2A)(DPA)^-$ ternary complex remains stable in solution for extended periods of time, approaching a year or more, with negligible loss in dipicolinate binding affinity (Figure 3.14). The emission intensity of the complex also does not decrease over time or repeated spectral analysis, indicating substantial resistance to photobleaching.

3.3 DPA Derivatives

In order to better understand the binding behavior of dipicolinate, the coordination geometries of various DPA analogues with Tb^{3+} and $Tb(DO2A)^+$ will be explored. Structural isomers and related pyridines, in which one or more of the carboxyl arms of the dipicolinate are moved around the pyridine ring or removed altogether, and DPA species with targeted substitutions in the para-position, will all be investigated to determine what factors are most important for effective chelation to the lanthanide or lanthanide complex.

3.3.1 Structural Isomers and Related Pyridines

Three structural isomers will be utilized in this study: pyridine-*2,4*-dicarboxylic acid (2,4-DPA), pyridine-*3,5*-dicarboxylic acid (3,5-DPA) and dipicolinate itself (pyridine-*2,6*-dicarboxylic acid, DPA). Picolinic acid (Pic) and pyridine (Pyr), which

have one and both carboxyl arms removed, respectively, are also included. As DPA usually coordinates in a tridentate fashion with the two carboxyl arms and the pyridine amine involved, shifting one or both of the carboxyl moieties around the ring will result in multiple bidentate chelation possibilities (Figure 3.15).

Lanthanides tend to be oxophilic, but evidence from complexes with azacrown ligands suggests that neutral N donors may be slightly preferred to neutral O donors.[22] Though admittedly formal neutrality of ligands is not the most important factor governing complexation, this may still suggest that nitrogen can be an effective chelator and can compete with oxygen in some cases. By comparison of the relative stabilities of the various isomers and pyridine species, we can learn whether the carboxyl or the amine substituent is more important in lanthanide chelation.

Experimental Section

Materials. DPA (dipicolinic acid, pyridine-*2,6*,-dicarboxylic acid) (Aldrich), 2,4-DPA (pyridine-*2,4*-dicarboxylic acid) monohydrate (Aldrich), 3,5-DPA (pyridine-*3,5*-dicarboxylic acid) (Aldrich), EDTA (ethylenediaminetetraacetic acid) (Aldrich), MOPS (*3*-(*N*-morpholino)ethanesulfonic acid) buffer (Alfa Aesar), picolinic acid (pyridine-*2*-carboxylic acid, Pic) (Aldrich), pyridine (Pyr) (J.T. Baker), terbium(III) chloride hexahydrate (Alfa Aesar) and sodium acetate trihydrate (Mallinckrodt) were purchased and used as received. All lanthanide salts were 99.9% pure or greater, all DPA derivatives and pyridines were 98% pure or greater, and all other salts were 97% pure or greater. DO2A and DO3A were prepared as previously described (Sections 2.2.1 and

3.2.1). Water was deionized to a resistivity of 18.2 MΩ-cm using a Purelab® Ultra laboratory water purification system.

Methods. Unless otherwise specified, all samples were prepared to a final volume of 4.00 mL in disposable acrylate cuvettes with a 1 cm path length. Luminescence spectral analysis was performed by a Fluorolog Fluorescence Spectrometer with a 350-nm cutoff filter as previously described (Section 3.2.1).

Pyridines. Stock solutions of DPA, Pic and Pyr were prepared volumetrically in clean 100-mL volumetric flasks. Solutions of 10.0 μM Tb(ligand) were prepared in 0.2 M NaOAc buffer, pH 5.5, and allowed to equilibrate for one hour prior to analysis. For the picolinate study, 10.0 μM solutions of Tb(Pic), $Tb(Pic)_4$ (100.0 μM Pic; saturation number of 4 Pic ligands on the lanthanide assumes bidentate coordination), Tb(Pic)(DO2A) and Tb(Pic)(DO3A) were prepared in 0.1 M MOPS buffer, pH 7.2, and allowed to equilibrate for 24 hours before analysis.

Structural isomers. Solutions of 10.0 μM dipicolinate species (DPA, 2,4-DPA and 3,5-DPA) and picolinate in 1.0 mM Tb(ligand), where ligand is DO2A, DO3A, DOTA or EDTA, were prepared in 50 mM MOPS buffer, pH 7.5, and allowed to equilibrate for 5 days prior to analysis.

DFT calculations. The equilibrium geometry, orbitals and energies of the minimized pyridine, picolinate and dipicolinate derivatives were refined by the semi-empirical PM3 method using the Titan® software package (Wavefunction, Inc.; Schrödinger, Inc.). Electron density maps were generated for the highest occupied molecular orbital (HOMO) of each species.

Results and Discussion

Pyridine has no detectable emission when in solution with terbium (Figure 3.16), indicating either very low binding affinity or little to no energy transfer. This is expected, as relatively few lanthanide complexes with monodentate nitrogen donors exist (Section 1.1), and without any carboxyl moieties to donate to binding, pyridine has little appeal to the oxophilic lanthanide. Picolinate has some coordination to Tb^{3+} as evidenced by excitation spectra, but dipicolinate exhibits the greatest intensity by a significant margin. This indicates that lanthanide sensitization is directly proportional to chromophore denticity, as anticipated, at least in the mono- to tridentate regime.

The excitation of terbium picolinate exhibits two peaks similar to the terbium dipicolinate spectrum, attributed to $\pi \rightarrow \pi^*$ transitions. However, the terbium picolinate maxima (268 and 273 nm) are blue-shifted by approximately 5 nm compared to the dipicolinate case. This may indicate reduced terbium sensitization efficiency as greater energy is required to produce lanthanide emission, possibly due to a shift in electron density back onto the pyridine ring. This is supported by simulations using the Titan® software package, which depict more of the electron density localized around the ring in the Pic structure than DPA (Figure 3.15).

Emission intensities of picolinate with $Tb(DO2A)^+$ and Tb(DO3A) are nearly identical (Figure 3.17), indicating that the Pic anion has a similar affinity for the binary complex in both cases. This suggests that picolinate coordinates to the Tb^{3+} ion in a bidentate fashion, most likely via a carboxyl oxygen and the pyridine nitrogen, which would not be hindered by the heptadentate DO3A ligand as the lanthanide is nine-coordinate. Coordination in an η-fashion through both oxygens of the single carboxyl

moiety is possible, though increased distance from the pyridine ring would severely reduce energy transfer efficiency (Section 1.2).[23] Further, a published crystal structure of hydrated dysprosium picolinate reports chelation via the nitrogen atom and one carboxyl oxygen of the picolinate ion.[24] The dipicolinate anion, in contrast, suffers a large decrease in emission intensity for the Tb(DO3A) case, as tridentate chelation is not possible without disruption of one of the DO3A carboxylate arms. High resolution emission spectra of the Tb(DO2A)(Pic) and Tb(DO3A)(Pic)$^-$ complexes also display different Stark splittings (Figure 3.18), consistent with a change in the composition and/or symmetry of the lanthanide coordination sphere (Section 2.4.1).

The emission spectra of the 2,4-DPA and DPA ternary complexes with Tb(DO2A)$^+$ and Tb(DO3A) have similar intensities, suggesting these two species coordinate with similar affinity (Figure 3.17). Loss of intensity by approximately half with the DO3A complex in both cases indicates steric hindrance when only two coordination sites are available on the terbium; as the 2,4-DPA derivative has only two possible coordination modes, both of them bidentate, this implies that the option with the greater 'bite' is favored. We therefore postulate that the 2,4-DPA species is coordinating via the two carboxyl arms to the terbium, with the pyridine amine not directly involved in binding. This is also supported by the difference in emission intensity between the 2,4-DPA and Pic ternary complexes with Tb(DO2A)$^+$; if the 2,4-DPA species was coordinating through the pyridine amine and one carboxyl arm as the Pic ligand does, these intensities should be much more similar.

In contrast, the 3,5-DPA emission spectra are about an order of magnitude lower in intensity than the 2,6- and 2,4-dipicolinate derivatives, indicating weak coordination

and/or lanthanide sensitization. Further, the DO3A complex has the greatest intensity for this isomer. This suggests bidentate coordination in a manner of low surface area with respect to the lanthanide. Most likely, the 3,5-DPA is coordinating via one of the carboxyl groups and the pyridine nitrogen. Such coordination is unusual, considering the potential for bidentate binding with the two carboxyl groups on the opposite side of the pyridine ring. Perhaps the pyridine nitrogen is more significant than supposed when it comes to lanthanide coordination.

All attempts at crystallization of these species were unsuccessful, and the only reported crystal structures of lanthanides with these dipicolinate derivatives are of polymeric species obtained under hydrothermal conditions,[25] which cannot be directly related to solution studies. Obviously more thorough analysis is required before accurate binding models can be proposed, but we have established through our brief investigation that the chelation properties of dipicolinate and related pyridines to lanthanides are not trivial, and that the pyridine nitrogen may play a significant part in dictating both binding motif and lanthanide sensitization.

3.3.2 Targeted Substitution

To determine the effect of electrostatics on dipicolinate binding interactions with the lanthanide, various spectroscopic and stability experiments were performed with a 4-substituted dipicolinate analogue, specifically *4*-fluoro-pyridine-*2,6*-dicarboxylic acid (F-DPA). With a highly electron-withdrawing group in the 4-position on the dipicolinate ligand, we anticipate decreased electron density on the chelating side of the DPA. Assuming the interaction between the lanthanide cation and the dipicolinate anion is

electrostatic in nature, this should manifest in decreased binding affinity and changes in intramolecular bond distances for complexes involving the F-DPA ligand.

A previous study[26] reported a trend of energy transfer efficiency to the Tb^{3+} ion with 4-substituted dipicolinate ligands as follows:

$$NH_2 > OH > NHAc > Cl > H \sim Br$$

We assume that the 4-fluoro-substituted DPA ligand will behave similarly to the 4-chloro-substituted species, and should therefore have a greater energy transfer efficiency than the unmodified DPA chelator.

Experimental Section

Materials. Acetone (J. T. Baker), DPA (dipicolinic acid, pyridine-*2,6*-dicarboxylic acid) (Aldrich), MOPS (*3*-(*N*-morpholino)ethanesulfonic acid) buffer (Alfa Aesar), sodium hydroxide (NaOH 50% in water) (Mallinckrodt), sodium hydroxide pellets (Mallinckrodt), terbium(III) chloride hexahydrate (Alfa Aesar) and tetrabutylammonium hydroxide (TBAOH 10% in *2*-propanol) (TCI America) were purchased and used as received. The terbium salt was 99.9% pure, DPA was 98% pure, all solvents were ACS certified or HPLC grade, and all other salts were 97% pure or greater. DO2A was prepared as previously described (Section 2.2.1). F-DPA (*4*-fluoro-pyridine-*2,6*-dicarboxylic acid) was synthesized by CB Research & Development, Inc., from the *4*-oxo-dipicolinate in five steps (Project code CIT-1000CB-b, Lots KW-5-133 and KW-5-155) (Figure 3.19) with a reported purity of > 95% and melting point of > 250 °C. Water was deionized to a resistivity of 18.2 MΩ-cm using a Purelab® Ultra laboratory water purification system.

Methods. Unless otherwise specified, all samples were prepared in triplicate to a final volume of 3.50 mL in disposable acrylate cuvettes with a 1 cm path length. Luminescence spectral analysis was performed by a Fluorolog Fluorescence Spectrometer with a 350-nm cutoff filter as previously described (Section 3.2.1).

Spectroscopy. Solutions of 10.0 μM terbium mono-dipicolinate (with Tb in 10% excess) and tris-dipicolinate (with 1:10 Tb:dipicolinate), where dipicolinate is DPA or F-DPA, were prepared in nanopure H_2O (18.2 MΩ-cm resistivity). The Tb(DO2A)(DPA)$^-$ and Tb(DO2A)(F-DPA)$^-$ ternary complexes were prepared to 10.0 μM in 1.0 mM NaOH, pH 9. All solutions were allowed to equilibrate for 90 hours prior to analysis. Absorbance measurements were made in quartz cuvettes (1 cm path length) using a Cary 50 Bio UV/Visible Spectrophotometer (Varian, Inc., Palo Alto, CA).

Binding studies. A Jobs method of continuous variations was performed as previously described (Section 3.2.1) with the concentrations of F-DPA and Tb(DO2A)$^+$ inversely varied from 0 to 12 μM in 1.0 mM NaOH, pH 9.0. Samples were allowed to equilibrate for 2 days prior to analysis. The binding affinity of F-DPA for Tb^{3+} was calculated using the one-step equilibration model previously described (equation 3.1), with 10.0 nM F-DPA and the concentration of $TbCl_3$ ranging from 10.0 nM to 1.0 μM in 0.2 M NaOAc, pH 7.6 at 25 °C. Each trial was fit separately and the three values of log K_a averaged to produce the final result.

pH dependence. Samples of 10.0 μM Tb(DO2A)(DPA)$^-$ or Tb(DO2A)(F-DPA) were prepared in 0.1 M buffer. Five buffers were used: MES (pK_a = 6.1), MOPS (pK_a = 7.2), TAPS (pK_a = 8.4), CHES (pK_a = 9.3) and CAPS (pK_a = 10.4), with pH adjustment

to within 0.1 of the pK_a value using 50% NaOH added dropwise. Emission spectra were obtained after an equilibration time of 21 hours.

Crystallization. Crystals of TBA·Tb(DO2A)(F-DPA) were obtained after several attempts following the same procedure as the normal ternary complex crystallization (Section 2.2.1) using similar reactant masses and solvent volumes and a new frit. Crystal formation was observed after sitting at room temperature for 3 days. Suitable crystals were utilized for X-ray diffraction studies at the Beckman Institute X-ray Crystallography Facility (Caltech).

X-ray crystallography. Crystals were mounted on a glass fiber using Paratone oil and then placed on the diffractometer under a nitrogen stream. Diffraction data were collected at 100 ± 2 K on a Bruker KAPPA APEX II diffractometer equipped with graphite monochromated MoKα radiation (λα = 0.71073 Å). The structure was solved by direct methods using SHELXS-97[27] and refined by full-matrix least-squares calculations on F^2 against all reflections using the SHELXL-97 program package.[28, 29] Non-hydrogen atoms were refined anisotropically. Due to disorder at the halogen site, the fluorine was refined isotropically, and fluorine and chlorine were restrained to a total occupancy of unity. The hydrogen atoms were introduced in calculated positions. CCDC reference number 761002. Crystal and refinement data are collected in Table 3.3. Complete crystallographic data, including asymmetric unit contents, atomic coordinates, bond distances and angles, and anisotropic displacement parameters, are listed in Appendix F.

Results and Discussion

Excitation spectra of the F-DPA and DPA ternary complexes reveal a blue-shift with respect to the fluorinated dipicolinate species of approximately 5–6 nm, similar to the picolinate complex (Figure 3.20). This could be due to reduced coupling of the substituted dipicolinate and the lanthanide as a result of shifted electron density towards the fluorine moiety, away from the chelating face of the ligand. Though we do see more pronounced Stark splitting in the F-DPA ternary complex (Figure 3.21), there is no evidence of a heavy-atom effect in terms of enhancement of luminescence intensity or spin-orbit coupling.[30] The Jobs plot (Figure 3.22) indicates a clear 1:1 binding stoichiometry of the $Tb(DO2A)^{+}$ binary complex and F-DPA.

The binding affinity of F-DPA^{2-} for Tb^{3+} was calculated using the same procedure as the dipicolinate ligand (Section 3.2.2) in identical conditions. The binding constant for the 4-fluoro-substituted ligand ($\log K_a = 7.10 \pm 0.04$) is less than that of the normal dipicolinate ligand ($\log K_a = 7.41 \pm 0.03$). This is consistent with the hypothesis that the electron density in the F-DPA ligand is shifted away from the chelating side of the ligand, thereby reducing electrostatic attraction between the F-DPA and the lanthanide. The $Tb(DO2A)(F\text{-}DPA)^{-}$ complex also exhibits a slight pH dependence (Figure 3.23), with the emission intensity decreasing by more than 10% below pH 7. This could also support reduced electron density near the carboxyl moieties, making them more easily protonated as pH decreases.

Crystallographic analysis indicates that the crystal structure is composed of approximately 63% $Tb(DO2A)(Cl\text{-}DPA)^{-}$ and 37% $Tb(DO2A)(F\text{-}DPA)^{-}$, where Cl-DPA is *4*-chloro-pyridine-*2,6*-dicarboxylic acid. Given that the F-DPA starting material is

approximately 10% Cl-DPA by elemental analysis (meaning the initial F-DPA purity was not 95% as reported) and the likelihood of halogen exchange on the dipicolinate is very low in this temperature and pressure regime,[31] this result indicates a preference for the chloro-substituted dipicolinate ligand in the crystallization protocol. Most likely, the larger chlorine atom is more thermodynamically favored in the unit cell. Contrary to expectations, no significant deviation is observed in the dipicolinate-lanthanide intramolecular distances; instead, certain C-C and C-O bonds within the F-DPA ligand appear to have lengthened or shortened to accommodate the halogen in the 4-position (Figure 3.24). However, as the crystal structure is not purely F-DPA, little conclusions can be drawn from such an analysis.

Due to the F/Cl discrepancy between solution studies and crystallographic analysis, calculation of K_a' using the BAC assay with solvated crystals was not attempted. Pure crystals of either Tb(DO2A)(F-DPA)$^-$ or Tb(DO2A)(Cl-DPA)$^-$ are necessary for binding constant calculation, and require a 4-substituted dipicolinate starting material with purity greater than 90%.

Overall, spectroscopic and binding studies of the 4-fluoro-subsituted dipicolinate chromophore indicate that electrostatic effects play a significant role in lanthanide chelation and stability. Introduction of an electron-withdrawing group in a position opposite of the tridentate binding site results in an observable decrease in binding affinity and an increased susceptibility to protonation.

3.4 Effects of pH and Temperature

Ideal sensing complexes should be highly resistant to pH and temperature variations in the local environment. Temperature studies can also provide information regarding the thermodynamics of our system through isolation of enthalpic and entropic effects. The protonation constants of dipicolinate are known (Table 3.4); we are interested in the pH regime where the DPA is fully deprotonated (pH > 5.2)[15] and binding affinity is dictated by pH effects on the $Tb(DO2A)^+$ complex alone. Potential factors that may affect dipicolinate binding include protonation/deprotonation of the DO2A macrocycle, the hydration state of the lanthanide, the difference in exchange rates between H_2O and OH^- in the binary complex binding site, and the propensity for lanthanides to form hydroxide precipitates at high pH.[32, 33]

3.4.1 pH Dependence Studies

Various pH dependence studies will be conducted over a range from 6.1 to 10.4 to determine the extent of ternary complex stability. This will be performed both with Jobs plots and deconvolution of emission spectra to determine the dominant species in solution. The change in dipicolinate binding affinity for the europium binary complex (K_a') can also be monitored over a smaller pH regime (6.1 to 8.0) where high concentrations of free europium can be maintained in solution. Previous work indicates that macrocyclic ligands, due to their high binding affinities with lanthanides, can hinder bridging interactions with hydroxyl species that might lead to insoluble oligomers and thus stabilize these metals in basic conditions, at least temporarily.[34] We therefore anticipate that the DO2A ligand should impart some degree of resistance to changes in

pH, as evidenced by minimal intensity variation and reduced precipitation compared to the analogous Ln^{3+} species.

Experimental Section

Materials. The following chemicals were purchased and used as received: CAPS (*N*-cyclohexyl-*3*-aminopropanesulfonic acid) buffer (Alfa Aesar), CHES (*N*-cyclohexyl-*2*-aminoethanesulfonic acid) buffer (Alfa Aesar), DPA (dipicolinic acid, pyridine-*2,6,*-dicarboxylic acid) (Aldrich), dysprosium(III) chloride hydrate (Alfa Aesar), europium(III) chloride hexahydrate (Aldrich), MES monohydrate (*2*-(*N*-morpholino)ethanesulfonic acid monohydrate) buffer (Alfa Aesar), MOPS (*3*-(*N*-morpholino)-propanesulfonic acid) buffer (Alfa Aesar), samarium(III) chloride (Alfa Aesar), sodium acetate trihydrate (Mallinckrodt), sodium hydroxide (NaOH 50% in water) (Mallinckrodt), TAPS (*N*-tris(hydroxymethyl)methyl-*3*-aminopropanesulfonic acid) buffer (TCI America) and terbium(III) chloride hexahydrate (Alfa Aesar). All lanthanide salts were 99.9% pure or greater, all other salts were 99% pure or greater, and all buffers were at least 98% pure. DO2A was prepared as previously described (Section 2.2.1). Water was deionized to a resistivity of 18.2 MΩ-cm using a Purelab® Ultra laboratory water purification system.

Methods. Unless otherwise specified, all samples were prepared in triplicate to a final volume of 3.50 mL in disposable acrylate cuvettes with a 1 cm path length. Luminescence spectral analysis was performed by a Fluorolog Fluorescence Spectrometer with a 350-nm cutoff filter as previously described (Section 3.2.1). The

solution pH was measured using a calibrated handheld IQ150 pH/mV/temperature meter (I. Q. Scientific Instruments) following data collection.

Jobs plots. The concentrations of $LnCl_3$ (Ln = Tb, Eu) and DPA were varied inversely from 0 to 12.0 μM in 1.0-μM increments with 100 μM DO2A in 0.1 M buffer. Five buffers were used: MES (pK_a = 6.1), MOPS (pK_a = 7.2), TAPS (pK_a = 8.4), CHES (pK_a = 9.3) and CAPS (pK_a = 10.4), with pH adjustment to within 0.1 of the pK_a value using 50% NaOH added dropwise. Solutions were allowed to equilibrate for 7 days prior to analysis.

Speciation study. For each lanthanide, samples were prepared from 4.00 mM stock solutions of $LnCl_3$, DPA and DO2A to contain 10.0 μM $Ln(DO2A)(DPA)^-$ or $Ln(DPA)^+$ in 0.1 M buffer (MES, MOPS, TAPS, CHES and CAPS). Emission spectra were obtained after an equilibration time of 7 days. Normalized spectra were deconvoluted into a linear combination of the three standard emission profiles for $Ln(DPA)^+$, $Ln(DPA)_3^{3-}$ and $Ln(DO2A)(DPA)^-$ using the Solver function in Excel® based on the most ligand field sensitive peak in each spectrum. Transitions used in calculation: Sm ($^4G_{5/2} \rightarrow {}^6H_{7/2}$, 580–625 nm), Eu ($^5D_0 \rightarrow {}^7F_4$, 675–710 nm), Tb ($^5D_4 \rightarrow {}^7F_4$, 570–600 nm), Dy ($^4F_{9/2} \rightarrow {}^6H_{13/2}$, 555–595 nm). The resulting percentage of mono, tris or ternary complex in each emission spectrum was then used to determine the average number of DPA molecules bound per lanthanide.

pH dependence of K_c. Samples were prepared using solvated $Eu(DO2A)(DPA)^-$ crystals ($TBA{\cdot}Eu(DO2A)(DPA){\cdot}4.0H_2O{\cdot}3.0C_3H_8O$, FW = 1098.2 g/mol) and $EuCl_3$ in 0.1 M buffer such that the concentration of $Eu(DO2A)(DPA)^-$ was 1.0 μM and the concentration of free Eu^{3+} ranged from 1.0 nM to 1.0 mM. Four buffers were used: MES

(pH 6.1), NaOAc (pH 7.4), MOPS (pH = 7.5) and TAPS (pH = 8.0). Higher pH buffers were attempted, but precipitate was observed in cuvettes containing high concentrations of $EuCl_3$, assumed to be $Eu(OH)_3$. With the concentration of europium in solution not accurately known, the data could not be appropriately fit and was therefore discarded.

As Eu^{3+} was added, the shift in equilibrium $Eu(DO2A)(DPA)^-$ and $Eu(DPA)^+$ concentrations was monitored via the ligand field sensitive $^5D_0 \rightarrow {}^7F_4$ transition (675–710 nm) in the emission spectrum using luminescence spectroscopy. Emission spectra (λ_{ex} = 278 nm) were integrated to produce curves of observed integrated intensity (I_{obs}) against the log of excess free europium (log $[Eu^{3+}]_{xs}$). These were then fit to the two-state thermodynamic model derived previously (Section 3.2.2) using the Curve Fitting Tool in Matlab® to yield the competition equilibrium constant (K_c) for each pH value.

Results and Discussion

Jobs plots of the $Tb(DO2A)(DPA)^-$ and $Eu(DO2A)(DPA)^-$ complexes indicate formation of the $Ln(DPA)_3^{3-}$ species at low Ln mole fraction when the pH reaches 7.2 or below (Figures 3.25 and 3.26). This indicates that the DO2A ligand may be easier to displace in acidic conditions, as would be expected considering the protonation constants of this and the dipicolinate species.[6, 15] However, this only occurs when DPA is in excess to $Ln(DO2A)^+$, which would be unlikely in any situation where this complex might be applied to detect bacterial spores. When the $Ln(DO2A)^+$ receptor site complex is equal to or greater than the concentration of DPA, we see near perfect linearity over the entire pH range (pH 6.1 to 10.4).

In the speciation study, the number of DPA molecules bound per lanthanide was calculated using the luminescence transition with the most obvious change in band splitting (i.e., the 'ligand field sensitive' peak) for the three complexes, $Ln(DPA)^{+}$, $Ln(DPA)_3^{3-}$ and $Ln(DO2A)(DPA)^{-}$, and solving each pH dependence emission spectrum as a best fit of a linear combination of these three profiles. With the DO2A ligand bound, a ratio of one DPA molecule per lanthanide is maintained over the entire pH range, meaning all four lanthanide ternary complexes remained stable (Figure 3.27). In contrast, the $Ln(DPA)^{+}$ complexes began to form the tris $Ln(DPA)_3^{3-}$ species at high pH as evidenced by the Ln:DPA ratio approaching 1:3, indicating precipitation of some of the lanthanide as $Ln(OH)_3$. This suggests that the addition of the DO2A ligand prevents precipitation of the trivalent lanthanide cation and confers additional stability to the complex.

A clear pH dependence of the binding affinity for dipicolinate was observed over the range 6.1 to 8.0 for the europium complex (Figure 3.28). As no analogous K_a values for the association of Eu^{3+} to DPA^{2-} were derived (except at pH 7.5 as shown in Section 3.2.2), we did not calculate K_a' values and instead focus our analysis on the competition constant K_c. The competition constant, which is proportional to K_a and inversely proportional to K_a' (equation 3.3), decreases as the pH becomes more basic. This indicates that the binding affinity of the Eu^{3+} ion for dipicolinate is decreasing and/or the binding affinity of the $Eu(DO2A)^{+}$ complex for dipicolinate is increasing. In either case, the DO2A ligand stabilizes the complex in more basic conditions, and allows for greater relative dipicolinate binding in comparison to the Eu^{3+} ion alone.

These pH dependence studies have also demonstrated an important point in terms of using lanthanides and lanthanide complexes as sensors for bacterial spores. In every lanthanide studied, the luminescence intensity of the $Ln(DPA)^+$ complex varies significantly with pH, due largely to the precipitation of $Ln(OH)_3$ and the resulting formation of the more strongly luminescent $Ln(DPA)_n$ species, where n = 2 or 3. This means that unless the solution pH is known, there is no longer a direct correlation between luminescence intensity and dipicolinate concentration, and the number of bacterial spores cannot be quantified. With the $Ln(DO2A)^+$ complex, fortunately, the change in luminescence intensity over the pH range from 6.1 to 9.4 is no more than 5%, and therefore bacterial spore concentration can be determined directly from emission intensity with a high degree of confidence.

3.4.2 Temperature Dependence Study

The stabilities of complexes are governed by enthalpic (H) and entropic (S) changes as described in equation 3.7.

$$\Delta G = \Delta H - T\Delta S \qquad [3.7]$$

The changes in Gibbs free energy (ΔG) are related to temperature and stability constants (K) by equation 3.8,

$$\Delta G = -RT(\ln K) \qquad [3.8]$$

where R is the universal gas constant (8.314 $J \cdot K^{-1} \cdot mol^{-1}$). We can therefore use the change in stability constant with temperature to calculate the changes in enthalpy (ΔH) and entropy (ΔS) using the Van ‘t Hoff equation (see equation 3.9).

$$\ln K = -\frac{\Delta H}{R}\left(\frac{1}{T}\right) + \frac{\Delta S}{R} \qquad [3.9]$$

A plot of the natural logarithm of the association constant (K_a or K_a') against the reciprocal of absolute temperature will therefore produce a linear relationship with slope equal to -ΔH/R and a y-intercept of ΔS/R.

Lanthanide ions are net structure promoters, and the enthalpy and entropy terms in complex formation will reflect the disruption of solvent structure as well as the combination of the ions.[35, 36] For both the $Ln(DPA)^+$ and the $Ln(DO2A)(DPA)^-$ complexes, ionic combination should outweigh disruption of the hydration structure and result in an exothermic enthalpic parameter (-ΔH). For entropy, displacement of three water molecules to allow one dipicolinate molecule to bind to the lanthanide should produce a positive entropy contribution (+ΔS).

Temperature has been shown to influence the water exchange dynamics of the $Eu(DO2A)^+$ complex in aqueous solution, resulting in a decrease in hydration number from 3 to 2 with increasing temperature.[20] As this will most likely decrease the positive surface area of the Ln^{3+} binding site, we anticipate a decrease in the binding affinity for dipicolinate with increasing temperature for $Ln(DO2A)^+$ complexes (Ln = Eu and Tb). The change in hydration structure may also cause variations in enthalpy and entropy for these systems.

Methods. The previously prepared sets of $Ln(DO2A)(DPA)^-$ and $Ln(DPA)^+$ cuvettes (Ln = Tb and Eu) used to calculate K_a and K_a' (Section 3.2.2) were heated or cooled to a specified temperature (equilibration time of ~ 24 hrs for each temperature point) in the range of 10–50 °C using a refrigerator (Marvel Scientific, Greenville, MI),

incubator (VWR International, West Chester, PA), or AccuBlock™ Digital Dry Bath (Labnet International, Edison, NJ). The sample chamber of the Fluorolog-3, which has a cuvette-holder that can be temperature-controlled, was connected to a Neslab RTE 7 Digital Plus water heater/chiller (Thermo Scientific, Waltham, MA) to maintain the desired temperature of the cuvette during scans. Sample temperature was monitored using a handheld Fluke 62 Mini Infrared Thermometer. The temperature of each cuvette was checked prior to and following each measurement, and these values were averaged over the set of cuvettes to produce the reported temperature. The solution pH was measured using a calibrated handheld IQ150 pH/mV/temperature meter following data collection. Association constants K_a and K_a' were calculated as described previously (Section 3.2.2) and plotted as ln K against 1/T in Kaleidagraph®. Enthalpic and entropic parameters were calculated using equation 3.6 from the slope and y-intercept, respectively, of a linear fit.

Results and Discussion

The temperature dependence study reveals a decrease in luminescence intensity for both Tb(DO2A)(DPA)$^-$ and Eu(DO2A)(DPA)$^-$ as temperature increases from 10 °C to 50 °C. This is consistent with previous temperature dependence studies of europium complexes,[20] and is most likely due to increased nonradiative deactivation through thermal population of vibrational modes.

The binding affinities of both Tb^{3+} and Eu^{3+} for dipicolinate, determined using the one-step equilibration model derived previously (equation 3.1), display a similar temperature dependence. In both cases, the value of K_a decreases by 0.7 logarithmic

units (Table 3.5), indicating a decrease in dipicolinate binding affinity. An Eyring-Polanyi plot of 1/T against ln K_a (Figure 3.29) yields an enthalpy of activation of -30.8 kJ/mol for the $Tb(DPA)^+$ association constant and -34.7 kJ/mol for the $Eu(DPA)^+$ system (Table 3.6). The negative value of enthalpy for both Tb^{3+} and Eu^{3+} suggests that the hydration sphere is only partially disrupted in the formation of $Ln(DPA)^+$ from the Ln^{3+} aquo species, and that the ionic combination to produce a net +1 complex is the dominant contributor, causing the net enthalpy to be exothermic. The increase in enthalpic destabilization for terbium over europium observed here is consistent with observed trends in lanthanide dipicolinate complexes, and may be due to secondary interactions involving the carboxyl arms of the dipicolinate ligand.[37]

The net entropy change in both the Tb and Eu cases is positive, consistent with the elimination of water molecules from the inner coordination sphere, with a slightly greater entropy value for the terbium case. Studies have shown variation in thermodynamics for the solvation steric effect of lanthanides based ionic radius,[38] so the observed differences in entropy are probably due to variation in ionic radius and/or charge density between the Tb^{3+} and Eu^{3+} cations.

Results of the equilibrium model fits (Figure 3.30) indicate a nonlinear temperature dependence on the stability of the $Tb(DO2A)(DPA)^-$ complex over the range from 10–50 °C and a slight trend for the Eu complex. Though a previous study involving $Eu(EDTA)^-$ reported an increase in binding affinity for citrate from 25 °C to 60 °C,[39] we see the opposite effect for the dipicolinate anion, with binding affinity decreasing more than half an order of magnitude as temperature increases (Table 3.5). This effect is most likely due to the reported decrease in hydration number of the $Eu(DO2A)^+$ complex from

3 to 2, possibly from expansion of the DO2A ligand reducing solvent exposure of the lanthanide. Calculations of enthalpy and entropy for each complex from plots of ln K_a' versus 1/T (Figure 3.31) are given in Table 3.6. Binding of dipicolinate generates less entropy for the europium case than for the terbium complex, supporting the theory of decreased hydration number at higher temperature for the $Eu(DO2A)^+$ complex. If only two waters must be displaced for dipicolinate to bind to $Eu(DO2A)^+$ compared to three for $Tb(DO2A)^+$, the entropy for the terbium case should be greater. The relative difference between these two entropy values and those of the corresponding $Ln(DPA)^+$ complexes are attributed to the elimination of water molecules from the inner hydration zone for the $Ln(DO2A)(DPA)^-$ complexes.[35]

As with the $Ln(DPA)^+$ case, the change in enthalpy for dipicolinate binding is more negative for the $Eu(DO2A)^+$ complex than the $Tb(DO2A)^+$ complex by approximately 5 kJ/mol, most likely due to differences in lanthanide ionic radius. Overall, the net change in enthalpy for the complexes involving DO2A is less than those without the ligand. We attribute this more endothermic enthalpy value to the change in ionic combination. In the $Ln(DPA)^+$ case, the binding of dipicolinate results in the net charge decreasing from +3 for the lanthanide aquo ion to +1 for the mono-dipicolinate complex. With DO2A bound, dipicolinate binds to the lanthanide macrocycle binary complex and reduces the net charge from +1 to –1. This should cause reorganization of polar solvent in the outer sphere to account for the change from positive to negative, so the change in enthalpy is less favorable.

We have established the dependence of dipicolinate binding affinity and emission intensity on temperature for europium and terbium complexes. While both $Ln(DPA)^+$

complexes present a clear temperature dependence, the addition of the DO2A ligand appears to disrupt this effect for the terbium case. Differences between the europium and terbium complexes are attributed to variations in lanthanide ionic radius and charge density, as well as evidence that the $Eu(DO2A)^+$ complex loses a solvent molecule at higher temperature. Our data indicate that this is not the case for the $Tb(DO2A)^+$ complex, which maintains a dipicolinate binding affinity near the nanomolar regime even at temperatures of 50 °C. We can therefore qualify the $Tb(DO2A)^+$ complex as robust to temperature variation, with the note that emission intensity is temperature dependent and appropriate adjustments should be made for in situ measurement of environmental samples to obtain an accurate dipicolinate concentration.

3.5 Interferent Studies

A primary concern when applying tailored receptor sites to in situ detection is the potential for undesired chelation of environmental interferents. For lanthanide-based sensors such as $Tb(DO2A)^+$ which rely on ionic interactions for analyte binding, the greatest threat is from charged species. Anions, particularly those containing oxygen and/or the ability to complex metal ions, could compete with dipicolinate for the oxophilic lanthanide receptor site and produce a false negative result. If these anionic interferents are aromatic and capable of transferring energy to the terbium, we might also encounter false positives. Alternatively, cationic interferents such as calcium or metal ions could bind to dipicolinate and prevent coordination to the lanthanide complex, producing a false negative result. We will investigate a plethora of cations and anions commonly found in environmental samples which may adversely affect dipicolinate

detection, including species that are known to quench Tb-DPA luminescence such as phosphate and carbonate.[40] We will also compare the efficacy of DO2A to other proposed interferent mitigation techniques.

3.5.1 Ion Screen

A screen was performed to test the robustness of the $Tb(DO2A)^{+}$ receptor site in the presence of common environmental interferents. The lanthanide complex and dipicolinate were kept at very low concentration, with the interferent concentration varied from three to six orders of magnitude in excess. To avoid any complexities introduced by the concomitant presence of buffer ions, solutions were unbuffered and instead the pH was adjusted to neutral using sodium hydroxide or hydrochloric acid. Any change in emission intensity, whether due to displacement of dipicolinate or some other mechanism such as precipitation of the lanthanide, would represent a vulnerability of the lanthanide complex to that interferent.

Experimental Section

Materials. The following chemicals were purchased and used as received: ammonium chloride (J.T. Baker), calcium chloride trihydrate (Aldrich), cesium chloride (MP Biomedicals), DPA (dipicolinic acid, pyridine-*2,6,*-dicarboxylic acid) (Aldrich), lithium chloride (Aldrich), magnesium chloride hexahydrate (Mallinckrodt), potassium chloride (Mallinckrodt), samarium(III) chloride (Alfa Aesar), sodium acetate trihydrate (Mallinckrodt), sodium bromide (J.T. Baker), sodium carbonate (Mallinckrodt), sodium chloride (EM Science), sodium citrate dihydrate (Mallinckrodt), sodium fluoride

(Aldrich), sodium hydroxide (NaOH 50% in water) (Mallinckrodt), sodium iodide hydrate (Alfa Aesar), sodium nitrate (Mallinckrodt), sodium phosphate tribasic dodecahydrate (BDH), anhydrous sodium sulfate (Mallinckrodt) and terbium(III) chloride hexahydrate (Alfa Aesar). All lanthanide salts were 99.9% pure or greater, all other salts were 99% pure or greater, and all buffers were at least 98% pure. DO2A was prepared as previously described (Section 2.2.1). Water was deionized to a resistance of 18.2 MΩ-cm using a Siemens Purelab® Ultra laboratory water purification system.

Methods. Unless otherwise specified, all samples were prepared in triplicate to a final volume of 3.50 mL in disposable acrylate cuvettes with a 1 cm path length. Luminescence spectral analysis was performed by a Fluorolog Fluorescence Spectrometer with a 350-nm cutoff filter as previously described (Section 3.2.1).

Cuvettes were prepared from 400 μM stock solutions to contain 0.10 μM $Tb(DO2A)(DPA)^-$ or $Tb(DPA)^+$ and an excess (100, 10, 1.0 or 0.10 mM) of one of the following ions: magnesium, calcium, lithium, sodium, potassium, ammonium, cesium, acetate, nitrate, fluoride, chloride, bromide, iodide, carbonate, sulfate, phosphate and citrate. All cations were chloride salts, and all anions were sodium salts. Solution pH was adjusted to ~ 7 with NaOH or HCl added dropwise. Solutions were allowed to equilibrate for 2 days prior to spectral analysis. The solution pH was measured using a calibrated handheld IQ150 pH/mV/temperature meter following data collection. Emission intensities were normalized to $Tb(DO2A)(DPA)^-$ or $Tb(DPA)^+$ control solutions of identical concentrations.

Results and Discussion

Addition of common cations and anions in large excess (10^3 to 10^6-fold) to submicromolar Tb(DO2A)$(DPA)^-$ at near neutral pH resulted in minimal emission intensity change for most ions in comparison to the $Tb(DPA)^+$ complex (Figures 3.32 and 3.33). For most potential ionic interferents, the inclusion of DO2A improved luminescence intensity to some degree ($\leq 10^2$-fold) when the ion concentration was up to six orders of magnitude greater than the Tb-DPA concentration (Figure 3.34). Carbonate interference was only observed at concentrations five orders of magnitude or greater than that of Tb-DPA; in this regime, DO2A improves dipicolinate sensing efficiency tenfold. Citrate interferes significantly with Tb-DPA complexation; this is reduced with the use of DO2A for concentrations up to five orders of magnitude greater than Tb-DPA. Further, as the resting concentration of citrate in extracellular fluid is around 130 μM,[41] where interference is almost completely mitigated by DO2A, we do not anticipate significant luminescence quenching from this interferent in environmental samples. DO2A complexation successfully eliminates phosphate interference for concentrations up to five orders of magnitude greater than Tb and DPA.

The inclusion of DO2A successfully improves Tb-DPA binding in the presence of a wide array of interfering ions, most up to concentrations five orders of magnitude greater than that of DPA. This indicates that the $Tb(DO2A)^+$ complex is able to selectively bind dipicolinate, even in the presence of similar oxygen-containing ligands such as acetate, carbonate and citrate.

3.5.2 Cation/Anion Competition Experiments

Cations and anions of particular interest from the ion screen were further explored via competition experiments. These included carbonate, sulfate, phosphate, calcium and potassium. Phosphate in particular has been shown to severely inhibit DPA^{2-} binding to Tb^{3+} in previous studies, completely quenching Tb luminescence via an unknown mechanism even when DPA is in excess.[15, 42] L-alanine was also investigated, as this amino acid is a commonly used germinant of *Bacillus* bacterial spores and is often present in high concentrations in various endospore viability assays.[43-45]

Experimental Section

Materials. Aluminum chloride hexahydrate (Aldrich), calcium chloride trihydrate (Aldrich), DPA (dipicolinic acid, pyridine-*2,6,*-dicarboxylic acid) (Aldrich), MOPS (*3*-(*N*-morpholino)ethanesulfonic acid) buffer (Alfa Aesar), potassium chloride (Mallinckrodt), sodium acetate trihydrate (Mallinckrodt), sodium carbonate (Mallinckrodt), sodium phosphate tribasic dodecahydrate (BDH), anhydrous sodium sulfate (Mallinckrodt) and terbium(III) chloride hexahydrate (Alfa Aesar) were purchased and used as received. All lanthanide salts were 99.9% pure or greater, all other salts were 99% pure or greater, and all buffers were at least 98% pure. DO2A was prepared as previously described (Section 2.2.1). Water was deionized to a resistance of 18.2 MΩ-cm using a Siemens Purelab® Ultra laboratory water purification system.

Methods. Carbonate, sulfate, phosphate, calcium and potassium were used in competition experiments against 0.1 μM $Tb(DO2A)(DPA)^-$ in 0.1 M MOPS (pH 7.5), where the concentration of the ion was varied from 1.0 nM to 0.1 M. For ions where

significant competition was observed, the data was fit using the Curve Fitting Tool in Matlab® with a chemical equilibrium model similar to that used for the BAC Assay (see Appendix C for derivation). For phosphate, an additional competition experiment was performed for 0.10 μM $Tb(DPA)^{+}$ with 0.10 mM aluminum chloride in 0.2 M NaOAc, pH 7.3, to compare the efficacy of DO2A in phosphate mitigation to a compound established in the literature.

Results and Discussion

Competition experiments were performed for selected ions (Figure 3.35); of those, only calcium demonstrated any significant competition with $Tb(DO2A)^{+}$ for dipicolinate, and only at ~ 10^4 excess (Figure 3.36). This was expected, as CaDPA is a stable neutral salt (log K_{CaDPA} = 4.05 [46]), and the mode by which most bacterial spores store the high concentrations of dipicolinic acid present in the spore cortex.[47] The data were fit to a two-state chemical equilibrium model similar to that used in the BAC assay, and competition constants were calculated for Ca^{2+} competing with the $Tb(DO2A)^{+}$ binary complex (log K_{cation} = 4.36 ± 0.23) and the Tb^{3+} ion alone (log K_{cation} = 3.68 ± 0.17) for DPA^{2-}. The addition of the DO2A ligand improves the stability of Tb-DPA binding by a factor of 4.7 compared to Tb^{3+} alone, increasing the range over which this receptor site can be used in environmental conditions.

Phosphate has been reported to severely quench Tb-DPA luminescence via an unknown mechanism even when DPA is in excess. This was supported in the competition experiment for phosphate with $Tb(DPA)^{+}$; however, application of DO2A successfully mitigated phosphate interference in the binding of DPA^{2-} to Tb^{3+} by more

than three orders of magnitude compared to Tb^{3+} alone (Figure 3.37). Aluminum chloride is reported to mitigate phosphate interference of Tb-DPA luminescence via precipitation of $AlPO_4$.[42, 48] Though the addition of aluminum chloride in micromolar concentrations does appear to improve Tb-DPA stability in the presence of phosphate, the effect is minor in comparison to that of nanomolar concentrations of DO2A.

L-alanine appears to detrimentally affect Tb-DPA luminescence, though the effect is not concentration-dependent. Emission intensity of the $Tb(DPA)^+$ complex varied by a margin of more than 11%, compared to less than 3% for the $Tb(DO2A)(DPA)^-$ complex (Figure 3.38). We therefore recommend the use of $Tb(DO2A)^+$ instead of Tb^{3+} in any endospore assays where the L-alanine germinant is used, regardless of germinant concentration.

The application of DO2A improves the resistance of the Tb-DPA luminescence assay to calcium interference nearly five-fold. The concentration of calcium must be at least 1000 times greater than that of DPA for the ion to affect luminescence intensity. The DO2A ligand also successfully mitigates phosphate interference of Tb-DPA luminescence, and exhibits great improvement over other compounds cited in the literature such as aluminum chloride. Further, DO2A reduces variation in luminescence intensity from germinants like L-alanine that are often used to trigger dipicolinate release from bacterial spores. We can therefore recommend the use of the $Tb(DO2A)^+$ binary complex over the Tb^{3+} ion in the sensitive, robust detection of endospores over a wide pH and temperature range, as well as in the presence of environmental interferents.

3.6 Applications

3.6.1 Bacterial Spore Study

With the superior stability and performance of the $Tb(DO2A)^{+}$ binary complex over Tb^{3+} alone verified experimentally, we have applied this novel DPA receptor site to the detection of bacterial spore samples. *Bacillus atrophaeus* spores have been well characterized in the literature[49-51] and represent spores found in typical environmental samples in their relative size and DPA content.[52, 53] We will compare the emission intensity and signal-to-noise ratios of dipicolinate detection using Tb^{3+} or $Tb(DO2A)^{+}$ for these spores, which will be physically lysed to release DPA into solution. We anticipate an improvement with the use of DO2A, as this ligand should reduce or eliminate any interfering effects from various other biomolecules (amino acids, proteins, nucleic acids, fatty acids, etc.) released from the lysed spores.

Experimental Section

Materials. Ethyl alcohol (Acros Organics), sodium acetate trihydrate (Mallinckrodt) and terbium(III) chloride hexahydrate (Alfa Aesar) were purchased and used as received. All lanthanide salts were 99.9% pure or greater and all other salts were at least 99% pure. DO2A was prepared as previously described (Section 2.2.1). *Bacillus atrophaeus* bacterial spores were purchased from Raven Biological Laboratories (Mesa Laboratories, Inc., Omaha, NE) and stored at 4 °C until use. Water was deionized to a resistance of 18.2 MΩ-cm using a Siemens Purelab® Ultra laboratory water purification system, and filter-sterilized using a Nalgene® MF75 sterile disposable filter unit containing a polyethersulfone (PES) membrane (0.2 μm pore size).

Methods. Sterile technique was used throughout the bacterial spore study, and controls were treated identically to samples containing spores. Samples were prepared in a SterilGARD III Advance Class II Biological Safety Cabinet (Model SG-403A, Baker Co., Sanford, ME) to minimize contamination.

Preparation of the spore suspension. Approximately 100 μL of a *Bacillus atrophaeus* spore stock suspension (approx. concentration 10^9 spores/mL) was diluted to 500 μL in a sterile microcentrifuge tube with cold filter-sterilized deionized water (18.2 MΩ-cm resistivity). The spores were washed twice via centrifugation (16,100 rcf for 20 min at 4 °C), decanting the supernatant and resuspending the pellet in 500 μL of cold filter-sterilized deionized water. The washed spores were diluted 1:50 using cold filter-sterilized deionized water to produce a suspension in the 10^7 spores/mL range (just visibly turbid). These suspensions were kept in ice until use.

Determination of spore concentration. Bacterial spore concentration was determined using a haemocytometer (Hausser Scientific Partnership, Horsham, PA), a glass microscope slide with a chamber of precisely known volume containing a laser-etched grid. The coverslip was cleaned with 70% ethanol and anchored to the haemocytometer using two 3.5-μL drops of deionized water. A 7-μL aliquot of the diluted spore suspension was slowly injected between the haeomocytometer grid and coverslip, ensuring no bubble formation. Enumeration was performed with phase-contrast microscopy using a Nikon Eclipse 80i microscope (Nikon Instruments, Inc., Melville, NY) with a Hamamatsu ORCA-ER Digital Camera (Model C4742-80, Hamamatsu Corporation, Bridgewater, NJ) under 40X magnification and a phase range setting of 2. The phase rings were aligned prior to counting. Once in focus, the number

of spores in a 16-square block was counted; this was repeated 8 times with different 16-square units. The enumeration procedure was repeated for three separate aliquots of the diluted spore suspension and the results averaged. The spore concentration (C_{spore}) was then calculated using the conversion in equation 3.10, to produce a result in units of spores per milliliter.

$$C_{spore} = \left(\frac{\text{Avg spores in}}{\text{16 squares}} \right) \times 25 \times 50{,}000 \qquad [3.10]$$

The calculation produced a concentration of 3.11 x 10^7 (± 6.11 x 10^6) spores/mL. The suspension was then diluted using cold filter-sterilized deionized water to a final concentration of 1.00 x 10^5 spores/mL.

Bacterial spore experiment. Samples were prepared in quintuplicate as follows: two 2.97 mL aliquots of the spore suspension were transferred to two microwave tubes and sealed using a crimper. Ten microwave tubes, along with two sets of controls containing filter-sterilized deionized water, were autoclaved at 134 ºC for 45 min using a Tuttnauer 3870 EA autoclave (Tuttnauer USA Co, Ltd., Hauppauge, NY) to lyse the spores and effect DPA release. The solution from each tube was transferred to a cuvette, to which either 30 μL of 100 μM $TbCl_3$ or $Tb(DO2A)^+$ was added to the lysed spore suspensions and the control solutions. The excitation and emission spectra were obtained following ~ 30 seconds of thorough mixing. The signal-to-noise (S/N) ratio was calculated by dividing the sample amplitude of the most intense peak (544 nm) by the control amplitude using equation 3.11. Signal amplitude was calculated by subtracting the maximum observed intensity in the range of 530–560 nm from the minimum observed intensity in that range.

$$S/N = \frac{Max_{Sample} - Min_{Sample}}{Max_{Control} - Min_{Control}} \quad [3.11]$$

The calculated S/N ratios for each of the five trials were averaged to produce the final values for Tb^{3+} and $Tb(DO2A)^{+}$.

Results and Discussion

The use of DO2A in the detection of dipicolinate from *B. atrophaeus* bacterial spores not only doubles the luminescence intensity, but also improves the signal-to-noise ratio threefold (Figure 3.39). As the concentration of terbium in this experiment was always in excess to the predicted DPA concentration released from the bacterial spores, meaning no multimeric $Tb(DPA)_n$ species ($n > 1$) could be formed, the observed increase in intensity is most likely the result of two mechanisms. First, we anticipated a minor improvement due to exclusion of water from the Tb^{3+} coordination sphere. This is confirmed by the slight intensity increase in the $Tb(DO2A)^{+}$ control compared to the Tb^{3+} control. However, the increase in luminescence intensity coupled to the significant enhancement of the signal-to-noise ratio is attributed largely to the improved binding affinity of the $Tb(DO2A)^{+}$ complex for dipicolinate.

It is important to note that this result was achieved for low concentrations of bacterial spores without any sample purification (filtration to remove cell debris, extraction, pH adjustment, etc.), minimizing sample preparation and enabling facile automation of this technique. We can therefore conclude that the $Tb(DO2A)^{+}$ complex is superior to the Tb^{3+} ion in rapid, reliable detection of bacterial spores via sensitized lanthanide luminescence.

3.6.2 Ice Core Experiments

With the successful application of the $Tb(DO2A)^+$ complex to the detection of bacterial spores in a laboratory setting, we will now apply this novel receptor site to the quantitation of bacterial spores in environmental samples. We will focus on ice core samples, as these tend to have a low spore concentration in a clean matrix. We will compare the efficacy of Tb^{3+} to $Tb(DO2A)^+$ to determine if the DO2A ligand can improve the limit of detection of bacterial spores in environmental samples.

The Greenland Ice Sheet Project 2 (GISP2) was an international study administered by the Office of Polar Programs (OPP) of the U.S. National Science Foundation (NSF) under the Arctic System Science (ARCSS) program. Under this project, an ice core was drilled over a five-year period starting in 1993 from the surface to the bedrock more than 3000 meters down, making it the deepest continuous ice core recovered in the world at the time.[54] The GISP2 ice core contains information of approximately the last 110,000 years, which includes the Holocene and part of the Pleistocene epochs.[55] We will investigate the bacterial spore content of four sections of this ice core in the hopes of understanding the viability and diversity of microorganisms over time.

Experimental Section

Materials. D-alanine (Aldrich), L-alanine (Aldrich), ethyl alcohol (Acros Organics), nitric acid 68–70% (EMD Chemicals, Inc.) and terbium(III) chloride hexahydrate (Alfa Aesar) were purchased and used as received. All lanthanide salts were 99.9% pure or greater, and all other salts were 98% pure or greater. DO2A was prepared

as previously described (Section 2.2.1). All solutions of lanthanide complex and/or germinant were filter-sterilized using sterile Acrodisc® 25 mm syringe filters with a 0.2 μm Supor® membrane (Pall Corporation, Ann Arbor, MI) prior to use. Ice cores from the Greenland Ice Sheet Project 2 (GISP2) were obtained from the National Ice Core Laboratory and stored at -80 °C until use. Specific ice cores used in study:

- Core GISP2D, Tube 158. Top depth 157.45 m, bottom depth 157.70 m. Cut MCA02. Length 0.25 m. Date 5 Jan 2007. Age 600 years.
- Core GISP2D, Tube 270. Top depth 269.43 m, bottom depth 269.68 m. Cut MCA02. Length 0.25 m. Date not specified. Age unknown.
- Core GISP2D, Tube 480. Top depth 480.15 m, bottom depth 480.40 m. Cut MCA02. Length 0.25 m. Date 5 Jan 2007. Age 2,000 years.
- Core GISP2D, Tube 835. Top depth 834.10 m, bottom depth 834.35 m. Cut MCA02. Length 0.25 m. Date 4 Jan 2007. Age 4,000 years.

Note that the reported date on the ice core sample is not the date of collection (1993–1998) but instead the date of cutting each section from the larger core.

Methods. Sterile technique was used in all protocols. All glassware was sterilized in a Cress™ C100-6B Electric Kiln (Cress MFG Co., Carson City, NV) at 500 °C for 4 hours prior to use. Water was deionized to a resistance of 18.2 MΩ-cm using a Siemens Purelab® Ultra laboratory water purification system, and filter-sterilized using a Nalgene® MF75 sterile disposable filter unit containing a polyethersulfone (PES) membrane (0.2 μm pore size).

Decontamination. To slowly increase the temperature, each ice core was removed from -80 °C storage and placed in a -25 °C freezer for 8 hours, followed by a transition to 0 °C for 2 hours. This prevented the decontamination solutions from simply freezing to the exterior of the core. Each ice core was then cut in half on a sterilized aluminum block kept at -80 °C until use. The shallower portion of the core was placed back in the -80 °C freezer. The deeper half of the ice core was dipped in a solution of bleach (6.15% sodium hypochlorite, 4 °C) for 10 seconds, and then three separate aliquots of filter-sterilized deionized water (4 °C) for 10 seconds each.

Melting and filtration. The decontaminated ice core was placed in a sterile 1-L beaker in a SterilGARD III Advance Class II Biological Safety Cabinet to melt. Melting was timed. Immediately following complete melting, the solution was filtered using a 0.1-μm 47 mm polycarbonate nucleopore track-etch filter membrane and vacuum filtration.

Resuspension. The filter was transferred to a sterile 15-mL polypropylene centrifuge tube containing 4.40 mL of filter-sterilized nanopure water (4 °C). The tube was vortexed for 1 min and then chilled on ice for 1 min. This was repeated four times. Twelve 225-μL aliquots of the solution were placed into sterile microcentrifuge tubes.

Germination. For each batch of 4 tubes, a 25-μL aliquot of one of the following was added:

- 10.0 μM $TbCl_3$ with 1.0 M L-alanine
- 10.0 μM $Tb(DO2A)^+$ with 1.0 M L-alanine
- 10.0 μM $TbCl_3$ with 1.0 M D-alanine
- 10.0 μM $Tb(DO2A)^+$ with 1.0 M D-alanine

The 12 tubes were then placed in an AccuBlock™ Digital Dry Bath (Labnet International) at 37 °C for 48 hours to induce germination. The solutions were then transferred to 0.6-mL quartz microcuvettes with a 1 cm path length. Quartz cells were washed with 50% nitric acid and rinsed ten times with filter-sterilized nanopure water (18.2 MΩ-cm resistivity) prior to each use. Luminescence spectral analysis was performed at 37 °C by a Fluorolog Fluorescence Spectrometer with a 350-nm cutoff filter as previously described (Section 3.2.1). Emission spectra were normalized to a 10.0 μM $Tb(DPA)^+$ standard solution, also in quartz.

DPA release. Following germination and spectral analysis, the solutions were transferred back into their respective microcentrifuge tubes and autoclaved at 134 °C for 45 minutes to lyse any remaining spores and effect complete DPA release. These solutions were transferred into quartz microcuvettes for luminescence spectral analysis.

Results and Discussion

Due to issues involving contamination of the L-alanine germinant with DPA (from the vendor Aldrich) and lack of sufficiently concentrated sample, no detectable signal for dipicolinate was observed either in excitation or emission spectra that could be attributed to bacterial spores in the ice core sample. Though the use of DO2A would most likely have reduced intensity variations from the high L-alanine concentration (Section 3.5.2) and produced an improved signal-to-noise ratio, we appear to be below the limit of detection for both the Tb^{3+} and $Tb(DO2A)^+$ species. Given the high binding affinity of the $Tb(DO2A)^+$ complex in these conditions (log K_a' = 9.25) and the assumption of an average dipicolinate content of 10^8 DPA molecules per spore, this

indicates that, if any bacterial spores are present in these ice core samples, they are most likely below a concentration of 100 spores/mL. Hence, though the $Tb(DO2A)^{+}$ complex demonstrates significant improvement over Tb^{3+} in the detection of bacterial spores, further optimization of dipicolinate binding affinity by this receptor site is necessary to reach the desired limit of detection to apply to environmental samples such as ice cores.

3.7 Conclusions

An investigation of $Ln(DO2A)^{+}$, where Ln = Sm, Eu, Tb and Dy, was performed to determine the efficacy of these binary complexes in sensitive, selective detection of bacterial spores via DPA-triggered Ln^{3+} luminescence. We based our analysis on five basic qualities of an effective receptor site: (1) the receptor site must present an obvious, measurable response upon analyte binding; (2) the binding affinity for the analyte of interest should be high, in the nanomolar regime or better; (3) binding should be rapid and compatible with the rate of analyte release in situ; (4) the receptor site should be resistant to pH and temperature changes; and (5) the binding affinity and selectivity should not be susceptible to environmental interferents. Of the lanthanide(macrocycle) complexes studied, the $Tb(DO2A)^{+}$ complex was the best match according to our criteria for the optimal dipicolinate receptor site.

One of the commonly exploited features of macrocyclic ligands is that of rendering several coordination sites inert to substitution and consequently limiting both the number and geometry of available binding sites.[56] The $Ln(DO2A)^{+}$ complex leaves exactly three adjacent, linearly-arranged coordination sites open for binding, ideal for the dipicolinate ligand. Work with pyridines and DPA derivatives suggests that the nitrogen

is integral to the strong binding observed, despite the usual preference of lanthanides for oxygen moieties. In comparison to other ligands such as hexacyclen, EDTA, DO3A and DOTA, which either coordinate to the lanthanide with less affinity or present a binding site with unfavorable size and/or geometry, the DO2A ligand produces the most effective lanthanide binary complex in terms of dipicolinate binding.

Binding affinity studies reveal an increase in dipicolinate complexation for the $Ln(DO2A)^{+}$ complex compared to the Ln^{3+} ion alone. This increase in binding affinity for the binary complex goes contrary to predictions based purely on net complex electrostatics, in that the DPA^{2-} analyte should be more strongly attracted to the tripositive Ln^{3+} species than the $Ln(DO2A)^{+}$ complex. Apparently, binding of the DO2A ligand affords an enhancement in DPA affinity that is substantial enough to counteract this loss of charge and still improve dipicolinate binding by an order of magnitude. Evidence of this 'ligand enhancement' can be found for various other lanthanide/ligand/analyte systems in the literature, and are tabulated in Table 3.7.[57-61] In each case, application of a chelating ligand improves binding affinity of the oxyanion analyte (picolinate, acetate and lactate) by around an order of magnitude, regardless of the type (cyclic or linear), denticity or charge of the ligand. We attribute this 'ligand enhancement' to a shift in electron density of the lanthanide upon ligand chelation, generating a binding site with a greater positive character due to the electron-withdrawing O and N moieties of the ligand. Though the net charge of the complex may have decreased, the *local* charge in the binding site may be even greater than the Ln^{3+} aquo case, where the nine solvent molecules are evenly distributed in the lanthanide coordination sphere and the electron density is still uniform. Though further

experimentation is required to support this theory, the existence of ligand enhancement is nevertheless a powerful tool in receptor site design. Any chemist seeking to improve the binding affinity of an oxyanion with a lanthanide cation *should utilize a helper ligand*, preferably one rich in nitrogen and oxygen.

The difference in binding affinity between the $Tb(DO2A)^{+}$ and $Dy(DO2A)^{+}$ complexes and the $Eu(DO2A)^{+}$ and $Sm(DO2A)^{+}$ species is most likely due to a phenomenon known as the "gadolinium break." Various studies of stability constants across the lanthanide series, such as those with acetate and anthranilate, indicate a change in stability constant around gadolinium.[62] Suggestions as to why this occurs include solvent exchange or the possibility of a mechanistic change occurring in the middle of the series. Evidence of the gadolinium break can also be seen in enzymatic inhibition studies,[63] and in a shift in hydration number from 9 for the larger lanthanides to 8 for the smaller lanthanides.[36, 64] An expansion of the Dy^{3+} coordination sphere from 8- to 9-coordinate is known to occur when two or more negatively charged ligands are coordinated,[6, 65] which may explain why the potentially 8-coordinate Dy^{3+} was able to accommodate the $DO2A^{2-}$ and DPA^{-2} ligands in a 9-coordinate motif.

The interesting aspect of the gadolinium break observed in our binding studies is that it appears to be *induced by ligation of DO2A*. The dipicolinate affinity for the Ln^{3+} ions exhibits little variation, but the analogous $Ln(DO2A)^{+}$ complexes show an obvious divide between those to the left of gadolinium (Sm, Eu) and those to the right (Tb, Dy). Another study concerning lanthanide(macrocycle) binary complexes also noted a similar trend, in this case using a chiral heptadentate DO3A derivative. The authors noticed an increase in the binding affinity of the terbium complex for certain oxy-anions (acetate,

bicarbonate and phosphate) in comparison to the analogous europium complex by about the same margin as we have observed for dipicolinate (Table 3.8).[60] As with our system, lifetime measurements of these complexes indicated no differences in hydration state that might explain the discrepancy. They attribute the affinity trend to a divergence of pK_a for the two complexes. If the pK_a of the europium complex were lower than that of the terbium complex, the presence of a population of hydroxylated species for the europium case would reduce the overall binding affinity due to a decrease in electrostatic attraction for this population of dipositive complex. Differences in pK_a values for Eu and Gd macrocyclic complexes with DOTA derivatives have been noted in the literature,[66] though it is not clear if this trend is extended to include Tb, or if these ligands can be directly compared to DO2A or others. We see no evidence of such a hydroxylated species in our pH dependence studies, which should have manifested in a change in stability of the $Eu(DO2A)(DPA)^-$ complex compared to the $Tb(DO2A)(DPA)^-$ complex at lower pH. We therefore cannot accept this hypothesis, and instead turn to ionization energy for a possible explanation.

The ability of a chelating ligand to perturb the electron density of a Ln^{3+} cation is dependent on (1) the number and arrangement of electron-withdrawing groups in the ligand and (2) the susceptibility of the lanthanide to polarization. The former property can be tuned by judicial choice of ligand; the latter is defined by how easily the electron density of the lanthanide can be externally influenced, one measure of which is ionization energy. A lanthanide with a low $Ln^{3+} \rightarrow Ln^{4+}$ ionization energy requires less energy to remove an electron, and is arguably more susceptible to perturbation by ligating species than a lanthanide with a high ionization energy. As shown in Figure 3.40, the Tb^{3+} ion

has the lowest 3+ → 4+ ionization energy of all the lanthanides investigated,[67] due primarily to the fact that the Tb^{4+} ion has an electronic configuration with an *exactly half-filled 4f-shell*. This lanthanide is therefore particularly susceptible to perturbation by an electronegative chelating ligand, as Tb^{3+} has the lowest energy barrier to losing an electron. Thus, the observed phenomenon of the ligand-induced gadolinium break is simply a manifestation of the half-shell effect, where lanthanides with the lowest ionization energies are the most significantly affected by electron density perturbations from a chelating helper ligand. In terms of receptor site design, this ligand-induced effect presents a strong case for using terbium as the lanthanide of choice in a sensing complex, as the Tb^{3+} ion will yield the greatest binding affinity increase when paired with a helper ligand.

The detection of bacterial spores via dipicolinate-triggered lanthanide luminescence has been improved in terms of detection limit, stability, and susceptibility to interferents by use of lanthanide-macrocycle binary complexes. The $Ln(DO2A)^{+}$ binary complexes bind dipicolinic acid, a major constituent of bacterial spores, with greater affinity and demonstrate significant improvement in bacterial spore detection. Of the four luminescent lanthanides studied (Sm, Eu, Tb and Dy), the terbium complex exhibits the greatest dipicolinate binding affinity (100-fold greater than Tb^{3+} alone, and 10-fold greater than other $Ln(DO2A)^{+}$ complexes) and highest quantum yield. Moreover, the inclusion of DO2A extends the pH range over which Tb-DPA coordination is stable, reduces the interference of calcium ions nearly five-fold, and mitigates phosphate interference 1000-fold compared to free terbium alone. In addition, detection of *Bacillus atrophaeus* bacterial spores was improved by the use of $Tb(DO2A)^{+}$, yielding a three-

fold increase in the signal-to-noise ratio over Tb^{3+}. However, initial experiments with Greenland ice core samples suggests further optimization is necessary to reach target limits of detection for very low concentrations of bacterial spores.

As a first-generation receptor site, the $Tb(DO2A)^{+}$ binary complex demonstrates improved dipicolinate binding affinity and enhanced resistance to pH, temperature and environmental interferents. We therefore conclude that the $Tb(DO2A)^{+}$ complex represents an excellent first step towards development of a rapid, robust DPA receptor for the detection of bacterial spores.

REFERENCES

(1) Nogrady, T.; Weaver, D. F. In *Medicinal Chemistry: A Molecular and Biochemical Approach*; Oxford University Press, 2005, pp 67-105.
(2) Job, P. *Comptes redus de l'Academie des sciences* **1925**, *180*, 928-930.
(3) Samuel, A. P. S.; Moore, E. G.; Melchior, M.; Xu, J.; Raymond, K. N. In *Lawrence Berkeley National Laboratory*; Lawrence Berkeley National Laboratory, 2009.
(4) Choppin, G. R.; Schaab, K. M. *Inorganica Chimica Acta* **1996**, *252*, 299-310.
(5) Chang, C. A.; Chen, Y.-H.; Chen, H.-Y.; Shieh, F.-K. *Journal Of The Chemical Society-Dalton Transactions* **1998**, 3243-3248.
(6) Huskens, J. *Inorganic Chemistry* **1997**, *36*, 1495-1503.
(7) Kimura, E.; Sakonaka, A.; Yatsunami, T.; Kodama, M. *Journal Of The American Chemical Society* **1981**, *103*, 3041-3045.
(8) Kim, W. D.; Hrncir, D. C.; Kiefer, G. E.; Sherry, A. D. *Inorganic Chemistry* **1995**, *34*, 2225-2232.
(9) Loncin, M. F.; Desreux, J. F.; Merciny, E. *Inorganic Chemistry* **1986**, *25*, 2646-2648.
(10) Mitewa, M.; Bontchev, P. R. *Coordination Chemistry Reviews* **1994**, *135/136*, 129-163.
(11) Gil, V. M. S.; Oliveira, N. C. *Journal of Chemical Education* **1990**, *67*, 473-478.
(12) Benesi, H. A.; Hildebrand, J. H. *Journal Of The American Chemical Society* **1949**, *71*, 2703-2707.
(13) Wang, R.; Yu, Z. W. *Acta Physico-Chimica Sinica* **2007**, *23*, 1353-1359.
(14) Yang, C.; Liu, L.; Mu, T. W.; Guo, Q. X. *Analytical Sciences* **2000**, *16*, 537-539.
(15) Jones, G.; Vullev, V. I. *Journal of Physical Chemistry A* **2002**, *106*, 8213-8222.
(16) Sanny, C. G.; Price, J. A. *Bioconjugate Chemistry* **1999**, *10*, 141-145.
(17) Horrocks Jr., W. D.; Sudnick, D. R. *Journal Of The American Chemical Society* **1979**, *101*, 334-340.
(18) Spaulding, L.; Brittain, H. G.; O'Connor, L. H.; Pearson, K. H. *Inorganic Chemistry* **1986**, *25*, 188-193.
(19) Wu, S. L.; Horrocks, W. D. *Analytical Chemistry* **1996**, *68*, 394-401.
(20) Yerly, F.; Dunand, Frank A.; Tóth, É.; Figueirinha, A.; Kovács, Z.; Sherry, A. D.; Geraldes, C. F. G. C.; Merbach, André E. *European Journal Of Inorganic Chemistry* **2000**, *2000*, 1001-1006.
(21) Moreau, J.; Guillon, E.; Pierrard, J.-C.; Rimbault, J.; Port, M.; Aplincourt, M. *Chemistry: A European Journal* **2004**, *10*, 5218-5232.
(22) Shestakova, A. K.; Chertkov, V. A.; Schneider, H.-J.; Lysenko, K. A. *Organic Letters* **2001**, *3*, 325-327.
(23) Abusaleh, A.; Meares, C. F. *Photochemistry and Photobiology* **1984**, *39*, 763-769.
(24) Jian-Fang, M.; Ning-Hai, H.; Jia-Zuan, N. *Polyhedron* **1996**, *15*, 1797-1799.
(25) Min, D.; Lee, S. W. *Inorganic Chemistry Communications* **2002**, *5*, 978-983.
(26) Lamture, J. B.; Hong Zhou, Z.; Kumar, S.; Wensel, T. G. *Inorganic Chemistry* **1995**, *34*, 864-869.
(27) Sheldrick, G. M. *Acta Crystallographica* **1990**, *A46*, 467-473.
(28) Sheldrick, G. M.; University of Göttingen: Göttingen, Germany, 1997.
(29) Sheldrick, G. M. *Acta Crystallographica* **2008**, *A64*, 112-122.
(30) McNaught, A. D.; Wilkinson, A., Eds. *IUPAC Compendium of Chemical Terminology*, 2nd ed.; Royal Society of Chemistry: Cambridge, UK, 1997.

(31) Werner, J. A.; Office, U. S. P. a. T., Ed.; The Dow Chemical Company (Midland, MI): United States, 1985.
(32) Moeller, T.; Kremers, H. E. *Journal Of Physical Chemistry* **1944**, *48*, 395-406.
(33) Arnaud, N.; Georges, J. *Analyst* **1999**, *124*, 1075-1078.
(34) Voss, D. A.; Buttrey-Thomas, L. A.; Janik, T. S.; Churchill, M. R.; Morrow, J. R. *Inorganica Chimica Acta* **2001**, *317*, 149-156.
(35) Choppin, G. R.; Strazik, W. F. *Inorganic Chemistry* **1965**, *4*, 1250-1254.
(36) Choppin, G. R.; Graffeo, A. J. *Inorganic Chemistry* **1965**, *4*, 1254-1257.
(37) Piguet, C.; Bunzli, J. C. G. *Chemical Society Reviews* **1999**, *28*, 347-358.
(38) Ishiguro, S.; Umebayashi, Y.; Komiya, M. *Coordination Chemistry Reviews* **2002**, *226*, 103-111.
(39) Mathur, J. N.; Cernochova, K.; Choppin, G. R. *Inorganica Chimica Acta* **2007**, *360*, 1785-1791.
(40) Barela, T. D.; Sherry, A. D. *Analytical Biochemistry* **1976**, *71*, 351-352.
(41) Parker, D.; Williams, J. A. G. In *Metal Ions in Biological Systems: The Lanthanides and Their Interrelations with Biosystems*; Sigel, A., Sigel, H., Eds.; Marcel Dekker, Inc.: New York, 2003; Vol. 40, pp 233-280.
(42) Pellegrino, P. M.; Fell, N. F.; Rosen, D. L.; Gillespie, J. B. *Analytical Chemistry* **1998**, *70*, 1755-1760.
(43) Akoachere, M.; Squires, R. C.; Nour, A. M.; Angelov, L.; Brojatsch, J.; Abel-Santos, E. *The Journal of Biological Chemistry* **2007**, *282*, 12112-12118.
(44) Gounina-Allouane, R.; Broussolle, V.; Carlin, F. *Food Microbiology* **2008**, *25*, 202-206.
(45) Titball, R. W.; Manchee, R. J. *Journal Of Applied Microbiology* **1987**, *62*, 269-273.
(46) Chung, L.; Rajan, K. S.; Merdinge.E; Grecz, N. *Biophysical Journal* **1971**, *11*, 469-482.
(47) Murrell, W. G. *The Bacterial Spore*; Academic Press: New York, 1969.
(48) Rosen, D. L. *Applied Optics* **2006**, *45*, 3152-3157.
(49) Fritze, D.; Pukall, R. *Int. J. Syst. Evol. Microbiol.* **2001**, *51*, 35-37.
(50) Setlow, P. *Journal Of Applied Microbiology* **2006**, *101*, 514-525.
(51) Kunst, F.; Ogasawara, N.; Moszer, I.; Albertini, A. M.; Alloni, G.; Azevedo, V.; Bertero, M. G.; Bessières, P.; Bolotin, A.; Borchert, S.; Borriss, R.; Boursier, L.; Brans, A.; Braun, M.; Brignell, S. C.; Bron, S.; Brouillet, S.; Bruschi, C. V.; Caldwell, B.; Capuano, V.; Carter, N. M.; Choi, S. K.; Codani, J. J.; Connerton, I. F.; Cummings, N. J.; Daniel, R. A.; Denizot, F.; Devine, K. M.; Düsterhöft, A.; Ehrlich, S. D.; Emmerson, P. T.; Entian, K. D.; Errington, J.; Fabret, C.; Ferrari, E.; Foulger, D.; Fritz, C.; Fujita, M.; Fujita, Y.; Fuma, S.; Galizzi, A.; Galleron, N.; Ghim, S.-Y.; Glaser, P.; Goffeau, A.; Golightly, E. J.; Grandi, G.; Guiseppi, G.; Guy, B. J.; Haga, K.; Haiech, J.; Harwood, C. R.; Hénaut, A.; Hilbert, H.; Holsappel, S.; Hosono, S.; Hullo, M.-F.; Itaya, M.; Jones, L.; Joris, B.; Karamata, D.; Kasahara, Y.; Klaerr-Blanchard, M.; Klein, C.; Kobayashi, Y.; Koetter, P.; Koningstein, G.; Krogh, S.; Kumano, M.; Kurita, K.; Lapidus, A.; Lardinois, S.; Lauber, J.; Lazarevic, V.; Lee, S.-M.; Levine, A.; Liu, H.; Masuda, S.; Mauël, C.; Médigue, C.; Medina, N.; Mellado, R. P.; Mizuno, M.; Moestl, D.; Nakai, S.; Noback, M.; Noone, D.; O'Reilly, M.; Ogawa, K.; Ogiwara, A.; Oudega, B.; Park, S.-H.; Parro, V.; Pohl, T. M.; Portetelle, D.; Porwollik, S.; Prescott, A. M.; Presecan, E.; Pujic, P.; Purnelle, B.; Rapoport, G.; Rey, M.; Reynolds, S.; Rieger, M.; Rivolta, C.; Rocha, E.; Roche, B.; Rose, M.; Sadaie, Y.; Sato, T.; Scanlan, E.; Schleich, S.; Schroeter, R.; Scoffone, F.; Sekiguchi, J.; Sekowska, A.; Seror, S. J.; Serror, P.; Shin, B.-S.; Soldo, B.; Sorokin, A.; Tacconi, E.; Takagi, T.; Takahashi, H.; Takemaru, K.; Takeuchi, M.; Tamakoshi, A.; Tanaka, T.; Terpstra, P.; Tognoni, A.; Tosato, V.; Uchiyama, S.; Vandenbol,

M.; Vannier, F.; Vassarotti, A.; Viari, A.; Wambutt, R.; Wedler, E.; Wedler, H.; Weitzenegger, T.; Winters, P.; Wipat, A.; Yamamoto, H.; Yamane, K.; Yasumoto, K.; Yata, K.; Yoshida, K.; Yoshikawa, H.-F.; Zumstein, E.; Yoshikawa, H.; Danchin, A. *Nature* **1997**, *390*, 249-256.

(52) Shafaat, H. S.; Ponce, A. *Applied and Environmental Microbiology* **2006**, *72*, 6808-6814.

(53) Sojka, B.; Ludwig, H. *Pharm. Ind.* **1997**, *59*, 355-359.

(54) Mayewski, P.; Bender, M. *Reviews of Geophysics* **1995**, *33*, 1287-1296.

(55) Stratigraphy, I. C. o.; International Union of Geological Sciences, 2009.

(56) Harrowfield, J. M. In *Metal Ions in Biological Systems: The Lanthanides and Their Interrelations with Biosystems*; Sigel, A., Sigel, H., Eds.; Marcel Dekker, Inc.: New York, 2003; Vol. 40, pp 105-159.

(57) Powell, J. E.; Ingemanson, J. W. *Inorganic Chemistry* **1968**, *7*, 2459-2461.

(58) Elkström, C.-G.; Nilsson, L.; Duncan, I. A.; Grenthe, I. *Inorganica Chimica Acta* **1980**, *40*, 91-98.

(59) Moeller, T.; Martin, D. F.; Thompson, L. C.; Ferrus, R.; Feistel, G. R.; Randall, W. J. *Chemical Reviews* **1965**, *65*, 1-50.

(60) Bruce, J. I.; Dickins, R. S.; Govenlock, L. J.; Gunnlaugsson, T.; Lopinski, S.; Lowe, M. P.; Parker, D.; Peacock, R. D.; B., P. J. J.; Aime, S.; Botta, M. *Journal Of The American Chemical Society* **2000**, *122*, 9674-9684.

(61) Kolat, R. S.; Powell, J. E. *Inorganic Chemistry* **1962**, *1*, 293-296.

(62) Silber, H. B.; Paquette, S. J. In *Metal Ions in Biological Systems: The Lanthanides and Their Interrelations with Biosystems*; Sigel, A., Sigel, H., Eds.; Marcel Dekker, Inc.: New York, 2003; Vol. 40, pp 69-104.

(63) Yang, Z.; Batra, R.; Floyd, D. L.; Hung, H.-C.; Chang, G.-G.; Tong, L. *Biochemical and Biophysical Research Communications* **2000**, *274*, 440-444.

(64) Kimura, T.; Kato, Y. *Journal Of Alloys And Compounds* **1998**, *278*, 92-97.

(65) Huskens, J.; Kennedy, A. D.; Van Bekkum, H.; Peters, J. A. *Journal Of The American Chemical Society* **1995**, *117*, 375-382.

(66) Aime, S.; Barge, A.; Bruce, J. I.; Botta, M.; Howard, J. A. K.; Moloney, J. M.; Parker, D.; De Sousa, A. S.; Woods, M. *Journal Of The American Chemical Society* **1999**, *121*, 5762-5771.

(67) Cotton, S. *Lanthanide and Actinide Chemistry*; John Wiley & Sons Ltd.: West Sussex, England, 2006.

Tb (μM)	DPA (μM)	Mole Fraction Tb	Ratio Tb:DPA
0	12	0.000	0:12
1	11	0.083	1:11
2	10	0.167	1:5
3	**9**	**0.250**	**1:3**
4	8	0.333	1:2
5	7	0.417	1:1.4
6	**6**	**0.500**	**1:1**
7	5	0.583	1.4:1
8	**4**	**0.667**	**2:1**
9	3	0.750	3:1
10	2	0.833	5:1
11	1	0.917	11:1
12	0	1.000	12:0

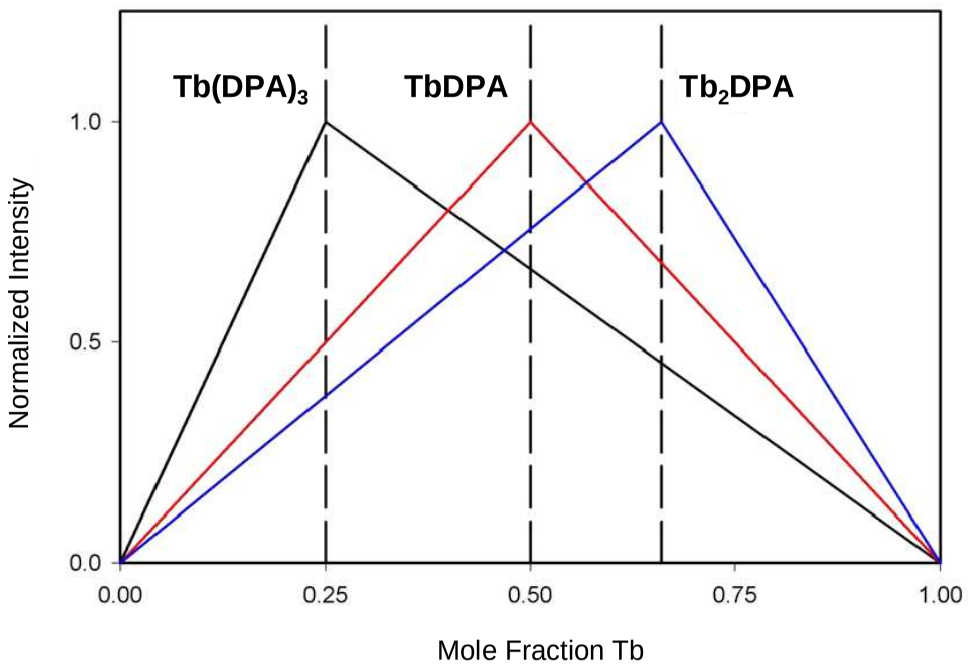

Figure 3.1. Method of continuous variations to determine optimal binding stoichiometry. The two components, in this case Tb and DPA, are varied inversely to produce various mole fractions (left). The best response (in this case, luminescence intensity) will be produced for the optimal ratio of the two (right).

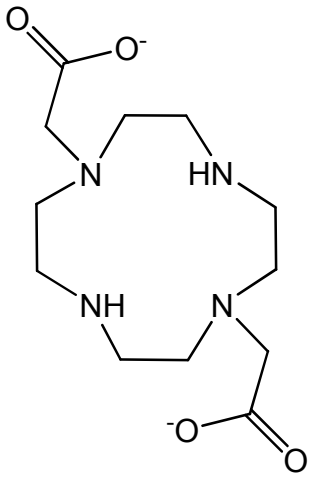

DO2A

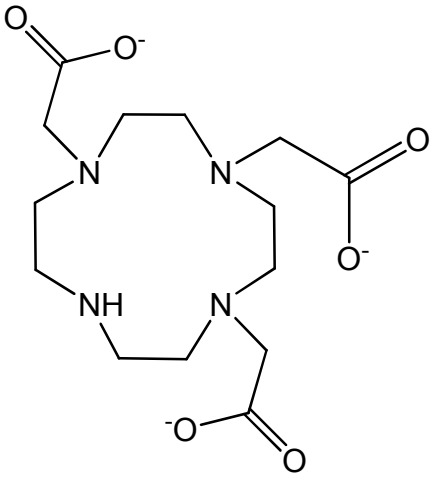

DO3A

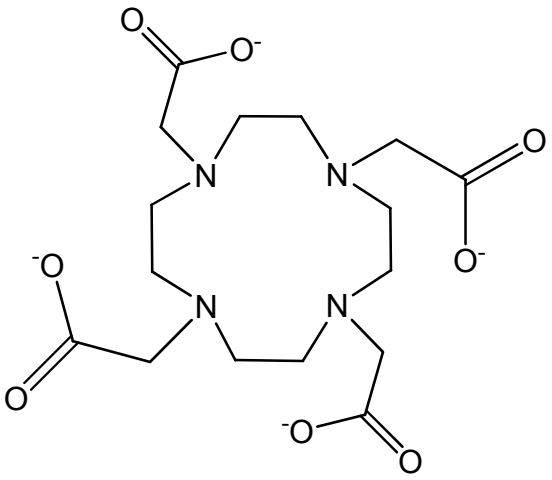

DOTA

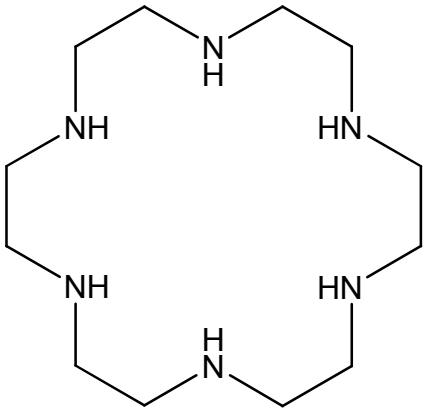

Hexacyclen

Figure 3.2. Macrocyclic ligands utilized for determining binding stoichiometries.

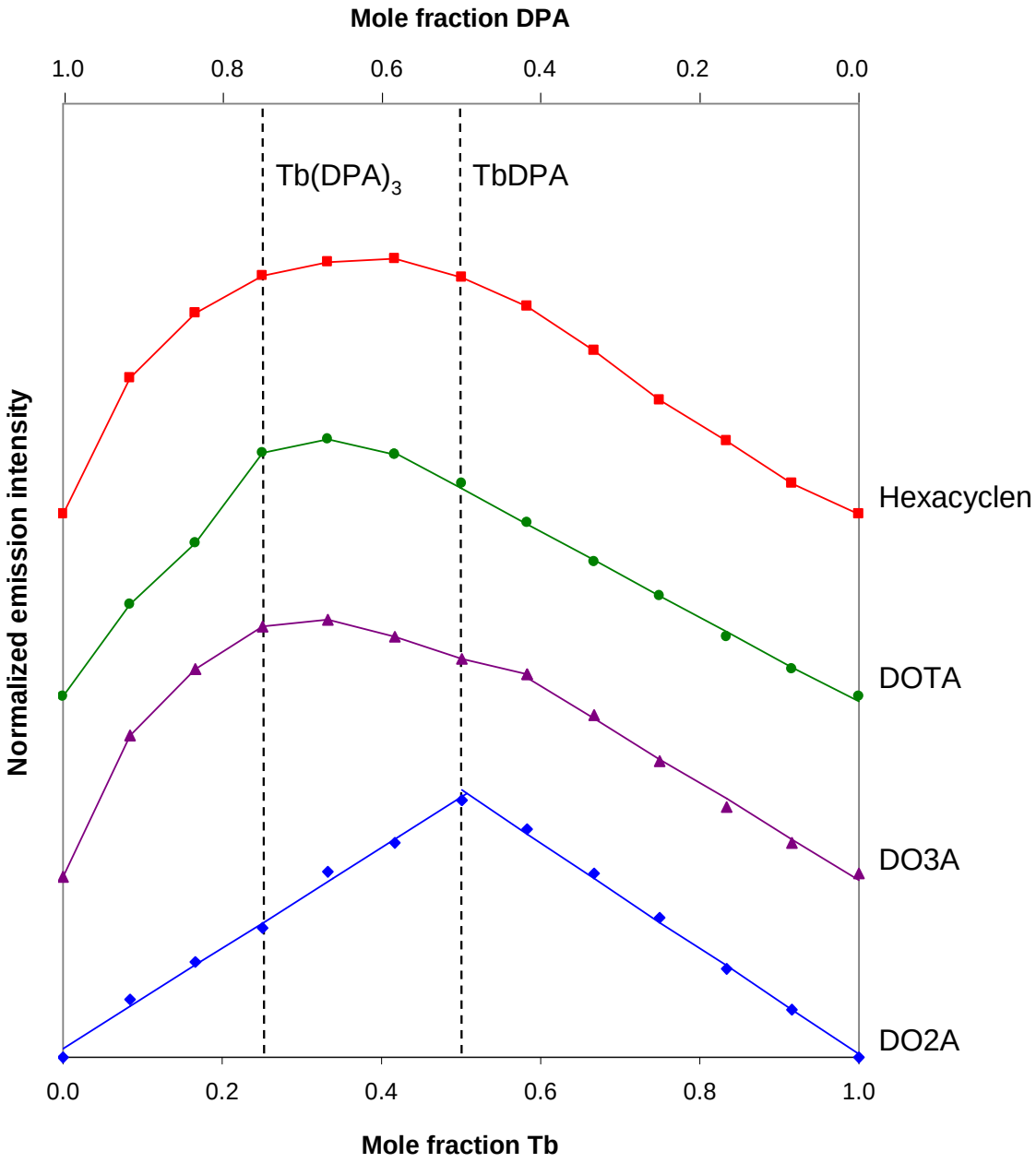

Figure 3.3. Jobs plots of various macrocyclic ligands in 1.0 mM NaOH, pH 8.1. The concentrations of Tb and DPA are varied inversely from 0 to 12 μM in 1 μM increments, with the macrocyclic ligand in excess (100 μM). Linear regions are fitted with trendlines, and significant Tb:DPA ratios are noted by dashed lines.

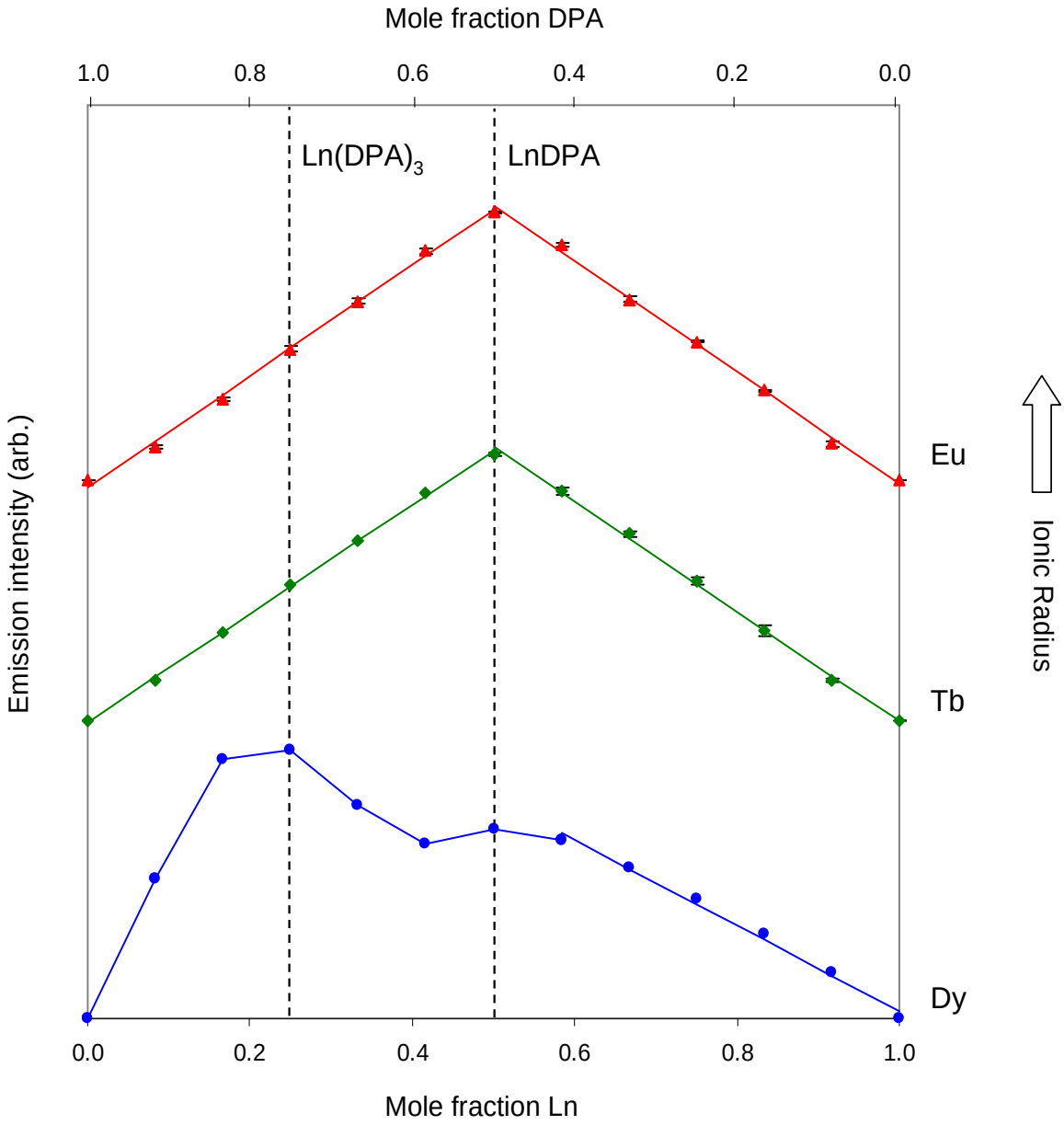

Figure 3.4. Jobs plots of various lanthanides in 100 mM CHES, pH 9.4. The concentrations of lanthanide and DPA are varied inversely from 0 to 12 μM in 1 μM increments, with DO2A in excess (100 μM).

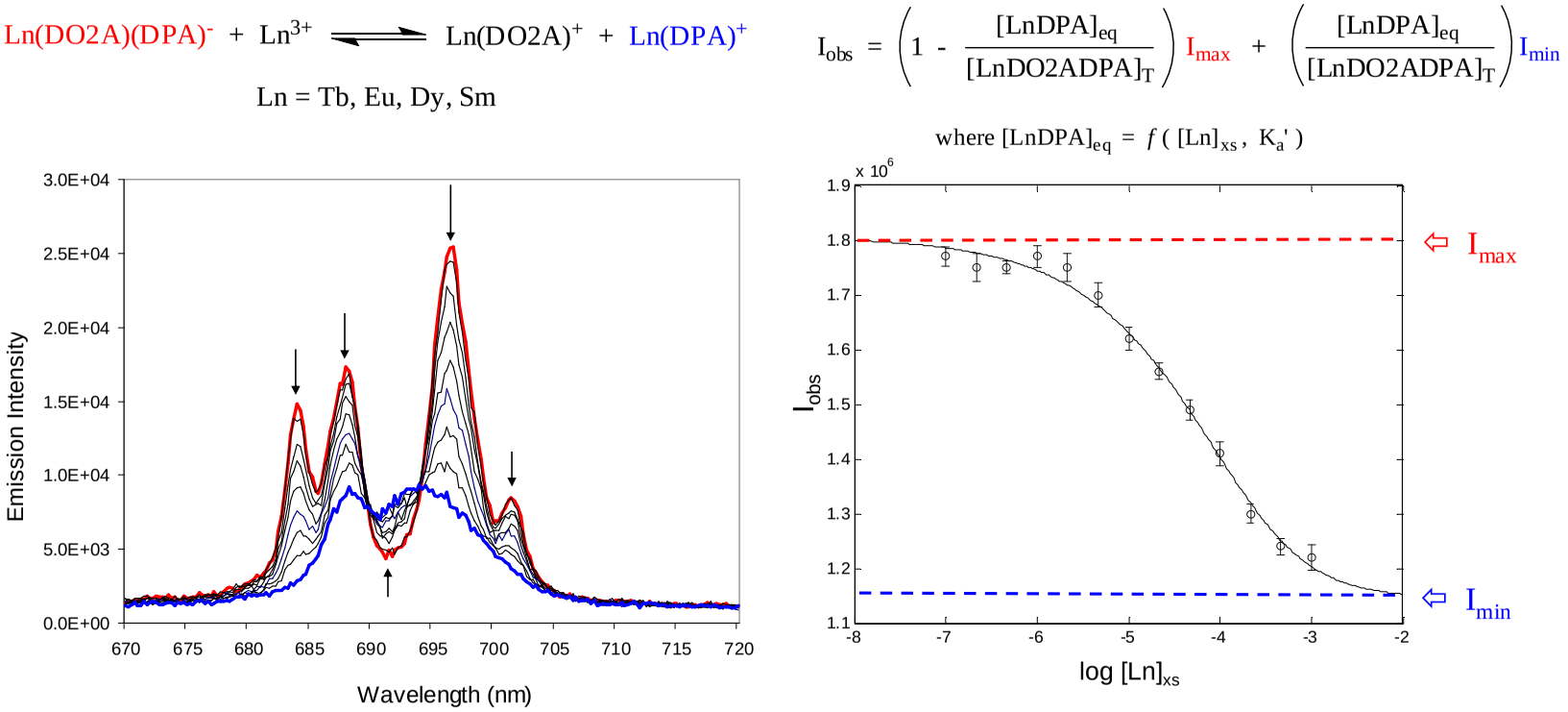

Figure 3.5. Binding affinity by competition (BAC) assay. The ternary complex (red) with the greatest luminescence is competed against free Ln^{3+}, which eventually strips the dipicolinate and forms the $Ln(DPA)^{+}$ complex (blue), whose luminescence is diminished due to solvent quenching (left). The luminescence of the Ln^{3+} and $Ln(DO2A)^{+}$ species is negligible, as these lack the DPA chromophore. The resulting curve (right) is then fitted to a model to produce an association constant (K_a') for $Ln(DO2A)^{+}$ to DPA^{2-}.

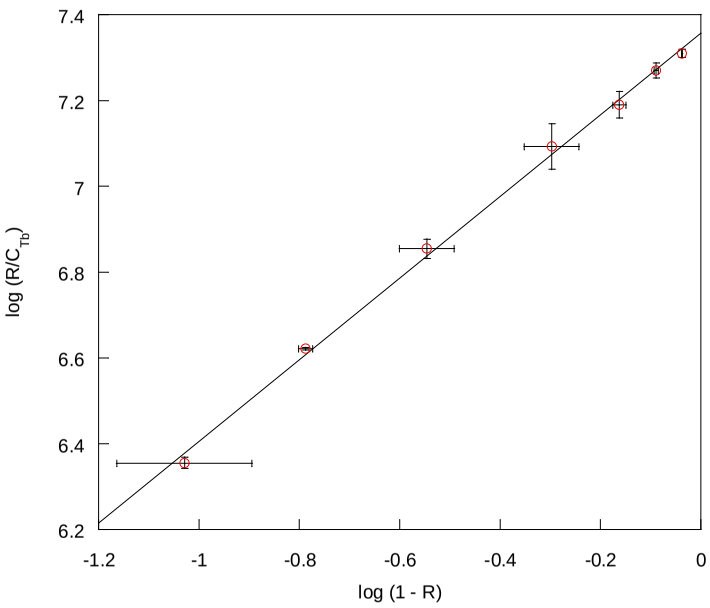

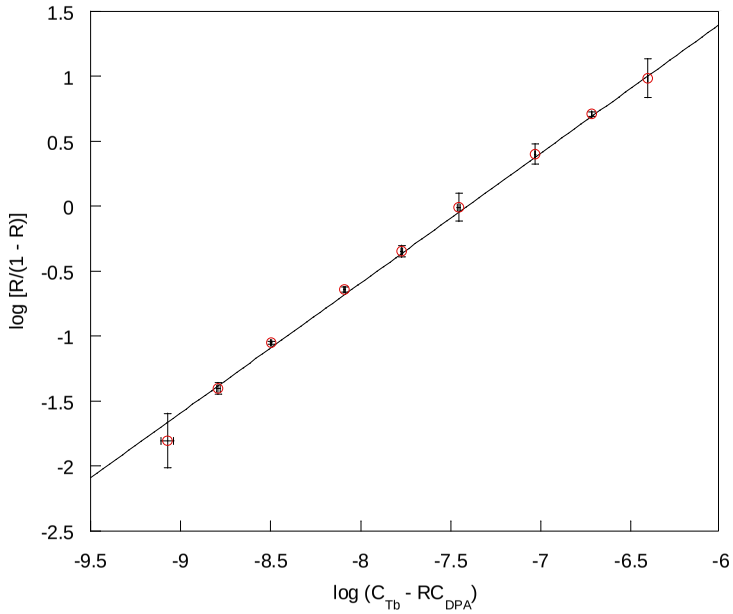

$\log (R/C_{Tb}) = n \log (1 - R) + \log K_a$

$\log [R/(1 - R)] = \log (C_{Tb} - RC_{DPA}) + \log K_a$

n = 0.932 (No. of DPA's per Tb)

No additional parameters used

$\log K_a = 7.35 \pm 0.03$

$\log K_a = 7.41 \pm 0.03$

Figure 3.6. Methods to calculate K_a. (A) Linear fit using the Jones and Vullev method to determine Tb^{3+}/DPA^{2-} binding affinity, 0.2 M NaOAc, pH 7.4, 25℃. (B) The exact same data set treated with our fitting model. Fewer constraints mean more data points can be used, producing a more accurate fit.

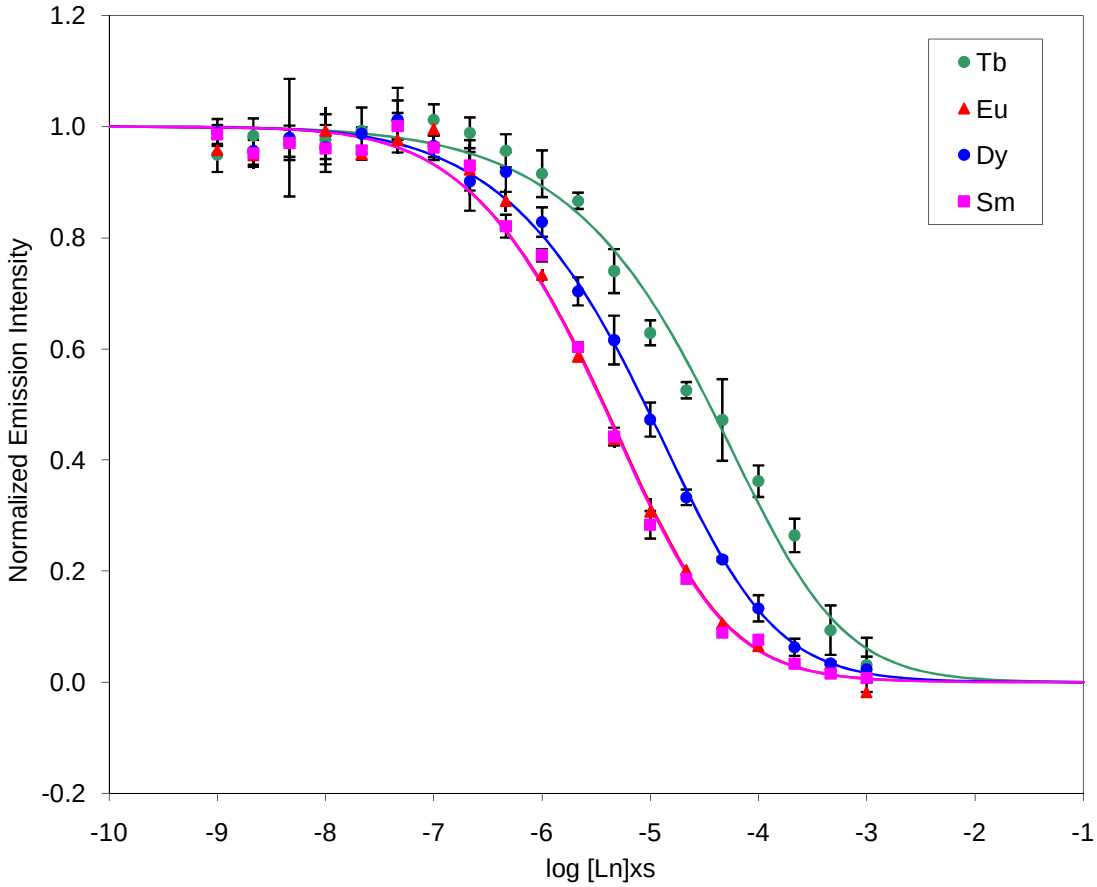

Figure 3.7. Lanthanide competition experiment. Binding affinity by competition (BAC) assay titration curves for Sm, Eu, Tb and Dy, 0.2 M NaOAc, pH 7.5.

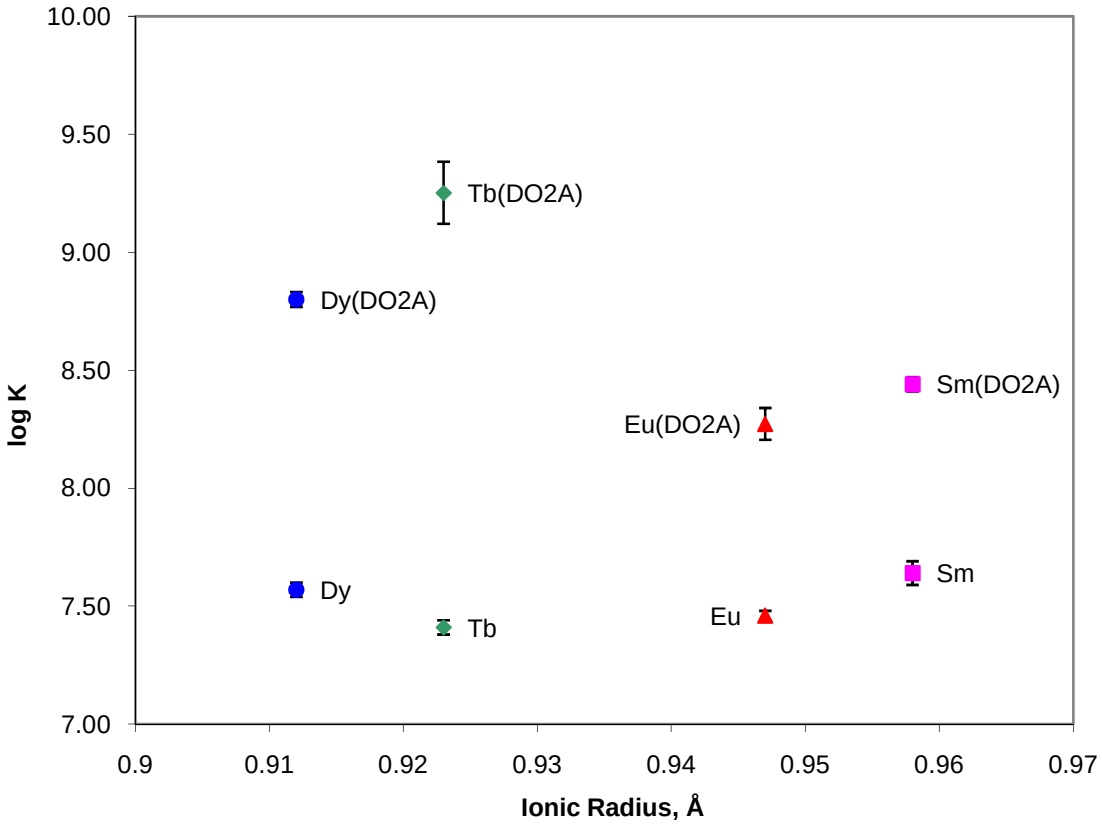

Figure 3.8. Plot of association constants for Ln^{3+} and $Ln(DO2A)^{+}$ to DPA^{2-} against lanthanide ionic radius, 0.2 M NaOAc, pH 7.5. The addition of DO2A enhances dipicolinate binding affinity by an order of magnitude for most lanthanides, and by nearly two orders of magnitude for terbium (green).

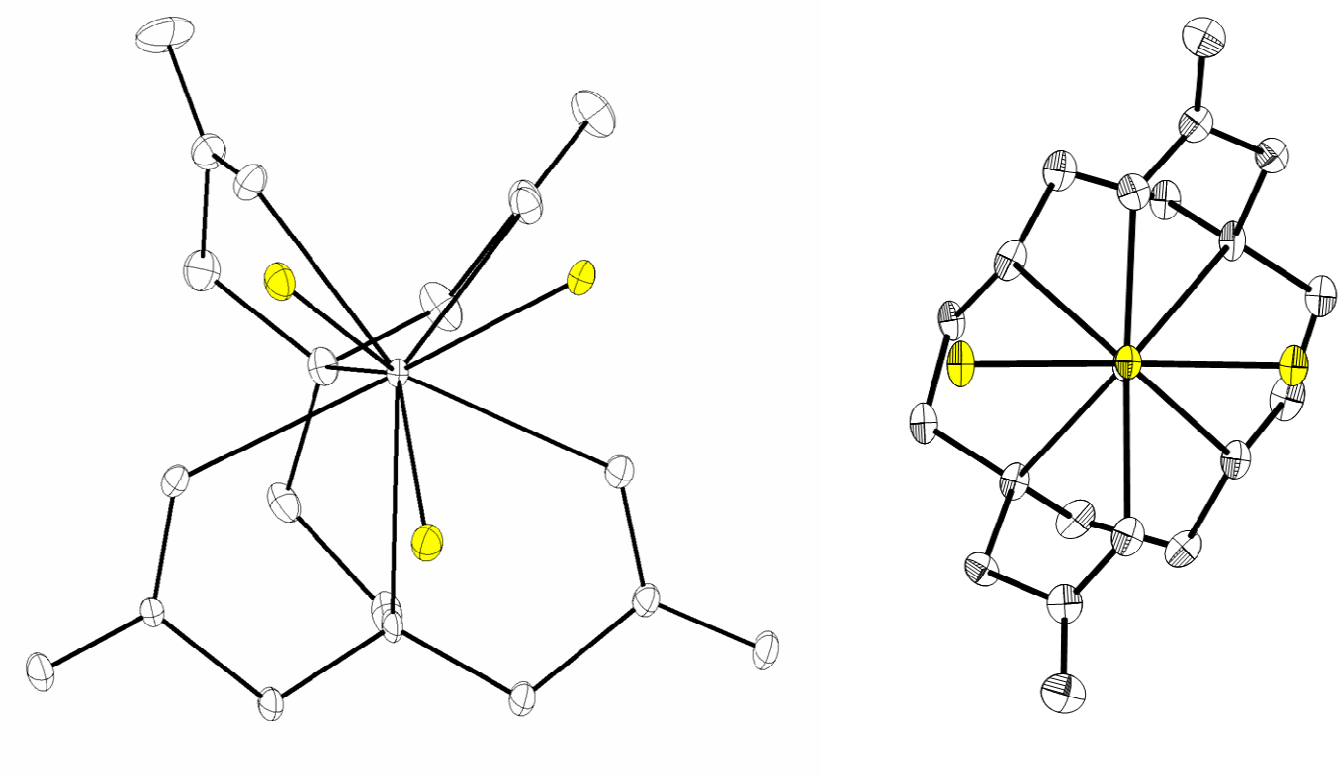

Figure 3.9. Crystal structures of Tb(EDTA)·NaOH·2H_2O and TBA·Tb(DO2A)(DPA), showing trigonal and linear coordination sites, respectively, available for dipicolinate binding (yellow). Thermal ellipsoids are at 50% probability; hydrogens and extraneous atoms omitted for clarity. Tb(EDTA)·NaOH·2H_2O crystallized out of deionized water (18.2 MΩ-cm resistivity) at 4℃.

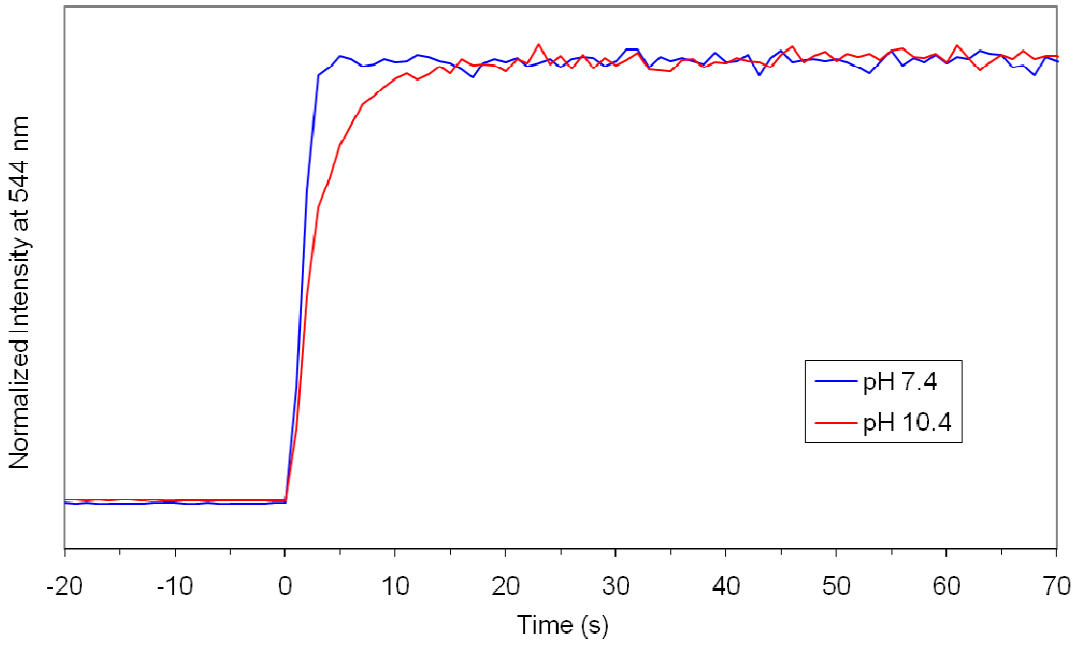

Figure 3.10. Time courses for binding of $Tb(DO2A)^{+}$ to DPA^{2-} at neutral and high pH. Both reach completion in seconds; the longer time required for the time course at high pH is attributed to displacement of hydroxyl groups from the terbium coordination sphere.

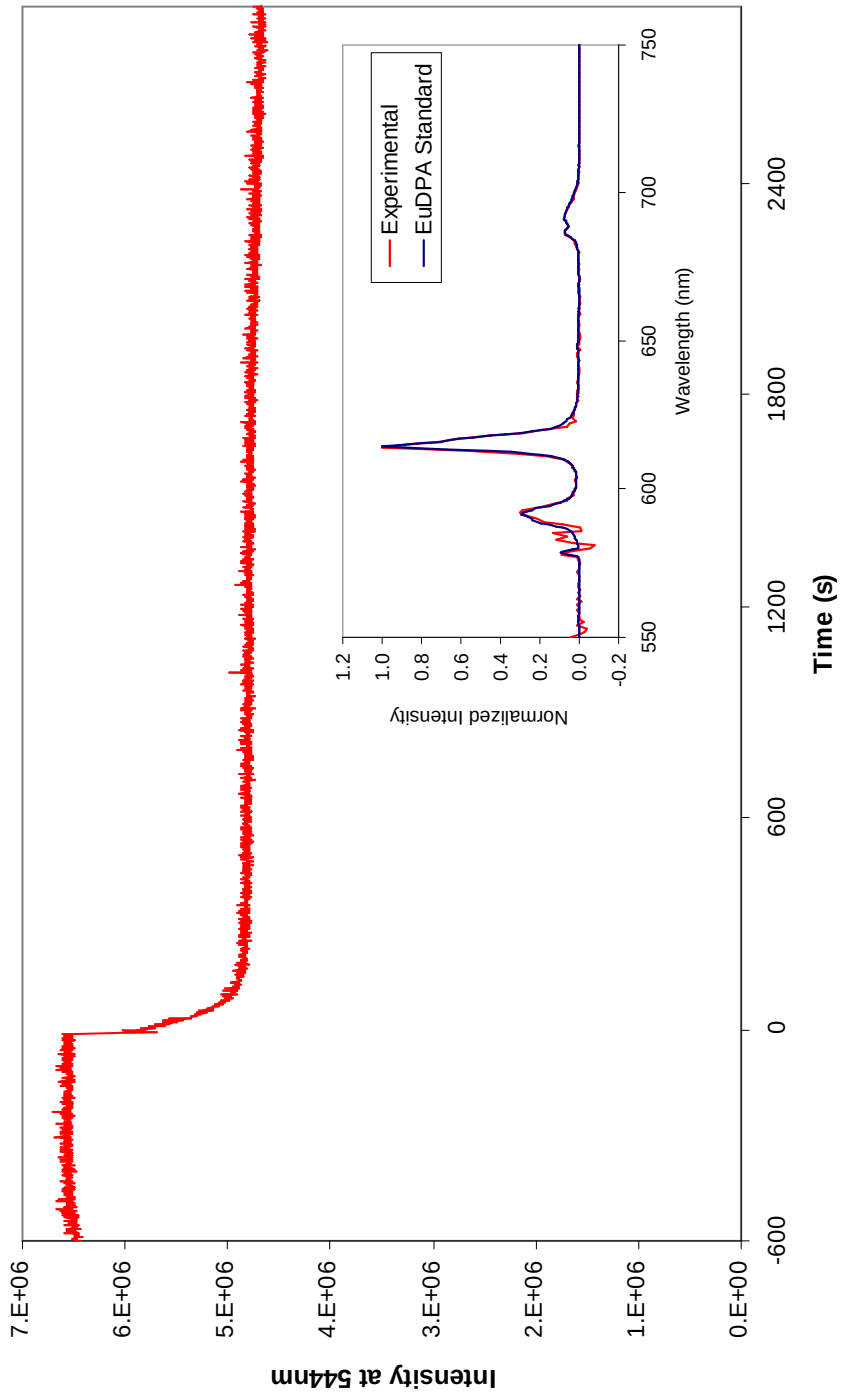

Figure 3.11. Kinetics experiment competing equimolar Tb(DO2A)(DPA)$^{-}$ against Eu^{3+}, 0.2 M NaOAc, pH 7.5, 25℃. $EuDPA^{+}$ is the only europium species produced (inset), supporting the assumption that DO2A remains bound to the terbium for the duration of the experiment.

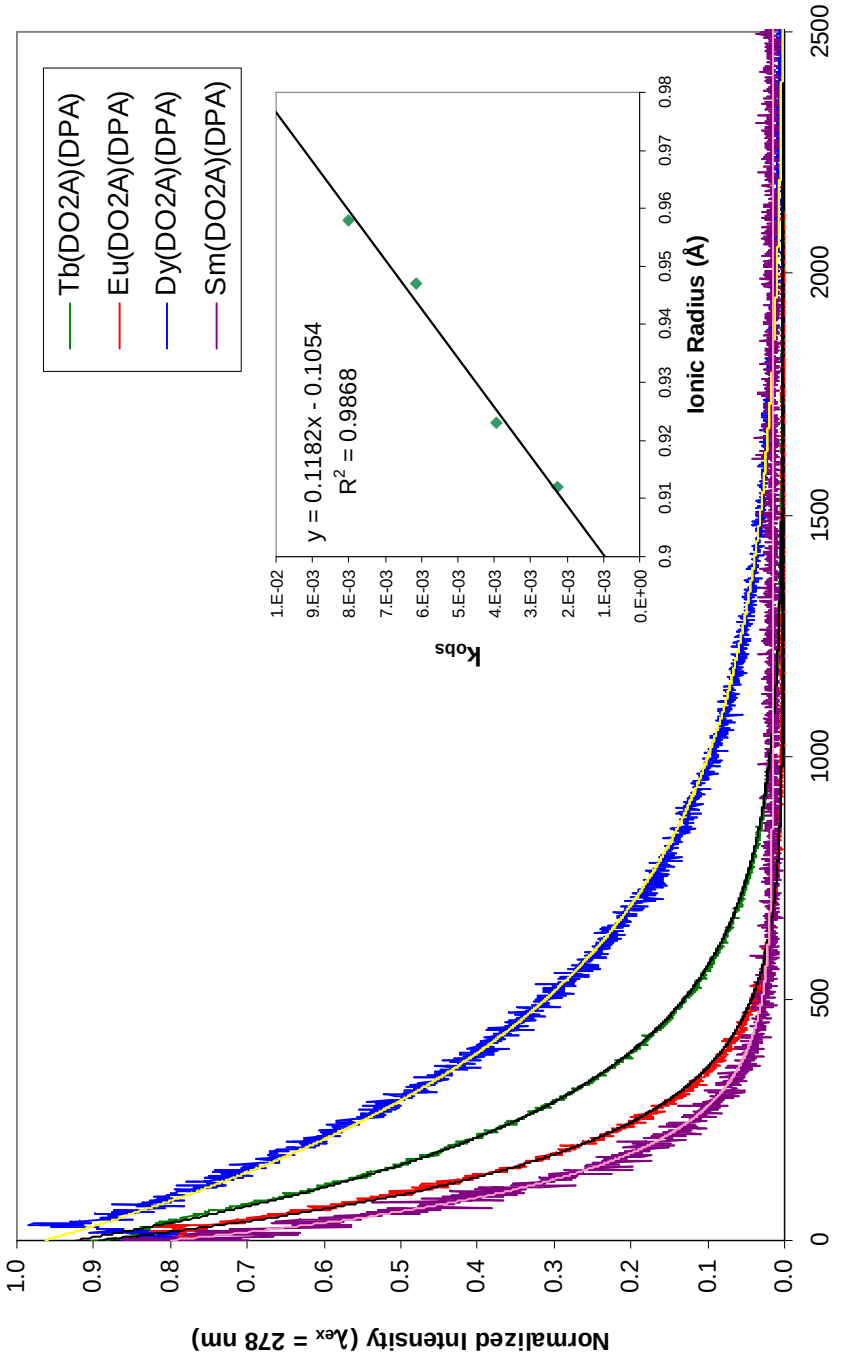

Figure 3.12. Kinetics decay curves of 1.0 μM Ln(DO2A)(DPA)$^{-}$ with 1.0 mM Gd^{3+} in 0.2 M NaOAc, pH 7.5, 25 ℃ (Ln = Sm, Eu, Tb and Dy). The rate of luminescence decay, fitted to a monoexponential model, tracks linearly with lanthanide ionic radius (inset).

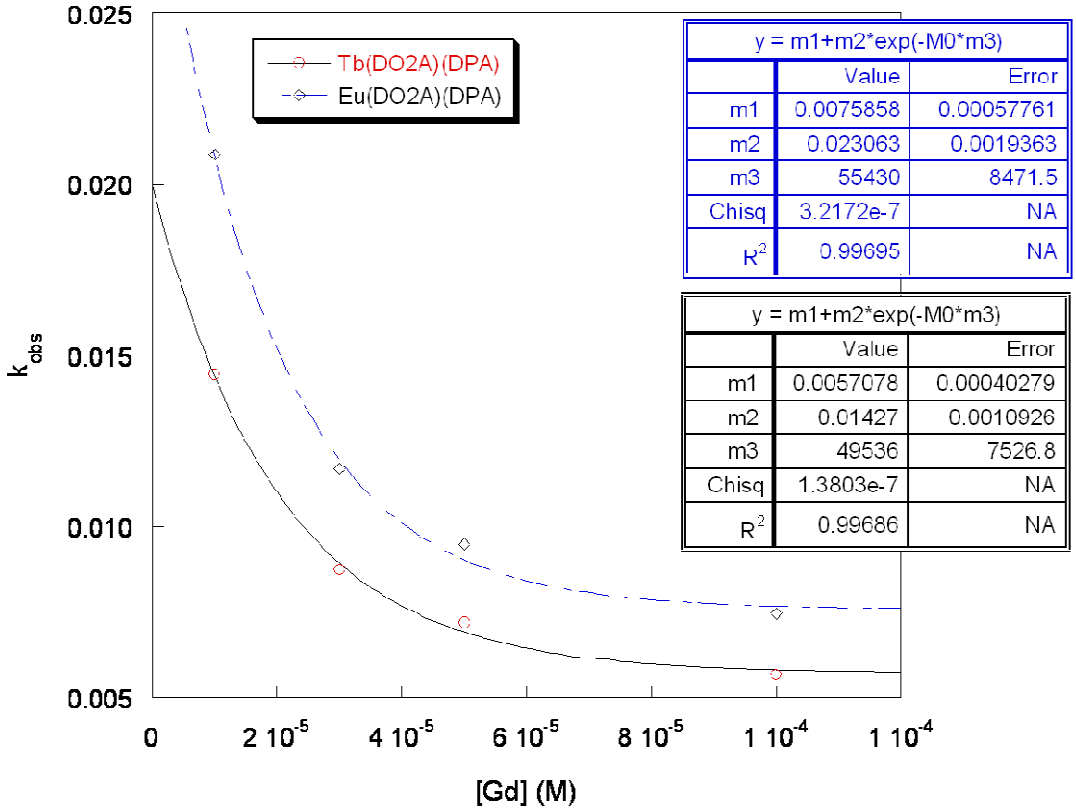

y = m1+m2*exp(-M0*m3)		
	Value	Error
m1	0.0075858	0.00057761
m2	0.023063	0.0019363
m3	55430	8471.5
Chisq	3.2172e-7	NA
R^2	0.99695	NA

y = m1+m2*exp(-M0*m3)		
	Value	Error
m1	0.0057078	0.00040279
m2	0.01427	0.0010926
m3	49536	7526.8
Chisq	1.3803e-7	NA
R^2	0.99686	NA

Figure 3.13. Kinetics experiments with $Tb(DO2A)(DPA)^-$ and $Eu(DO2A)(DPA)^-$ competed with Gd^{3+}, showing a decrease in the rate with increasing [Gd].

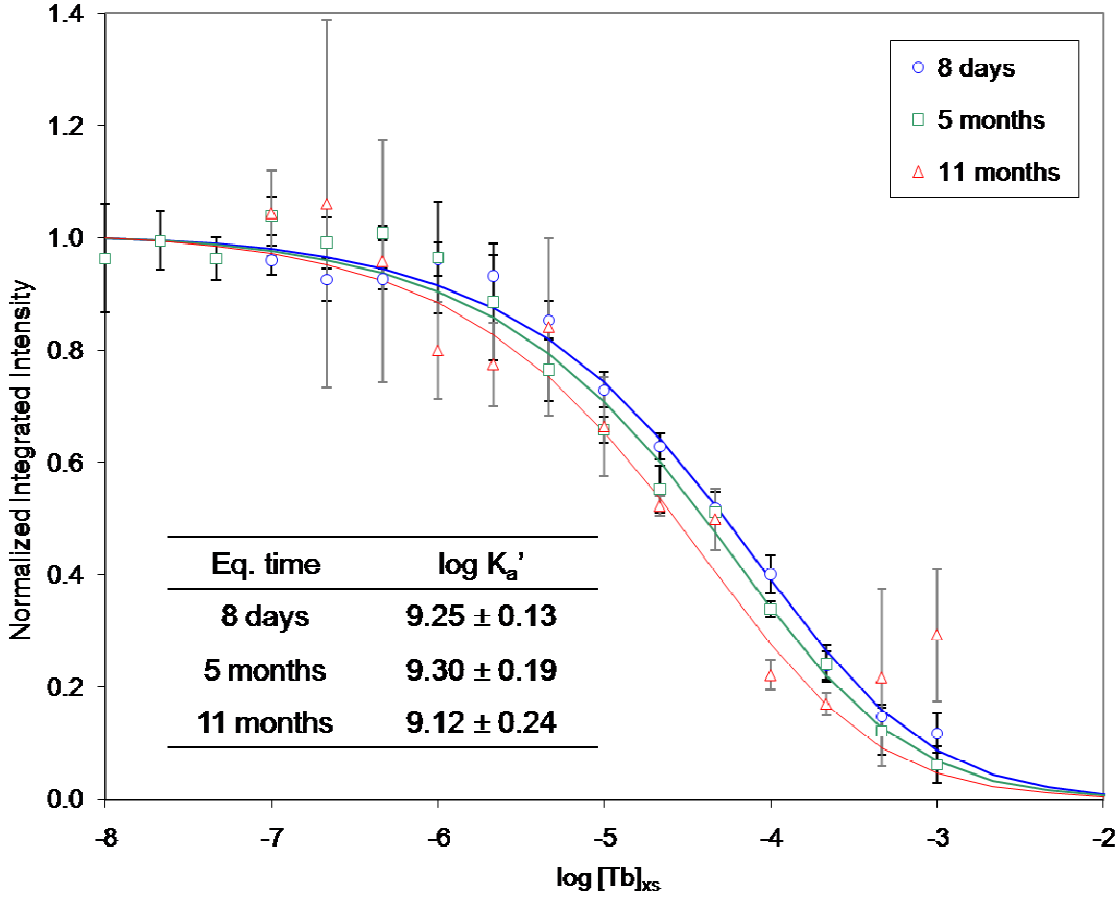

Figure 3.14. Stability of Tb(DO2A)(DPA)$^{-}$ over time, 0.2 M NaOAc, pH 7.5, 25 ℃. λ_{ex} = 278 nm, emission spectra integrated from 570–600 nm. Large error bars in 11 months data set (gray) are due to loss of solvent through evaporation.

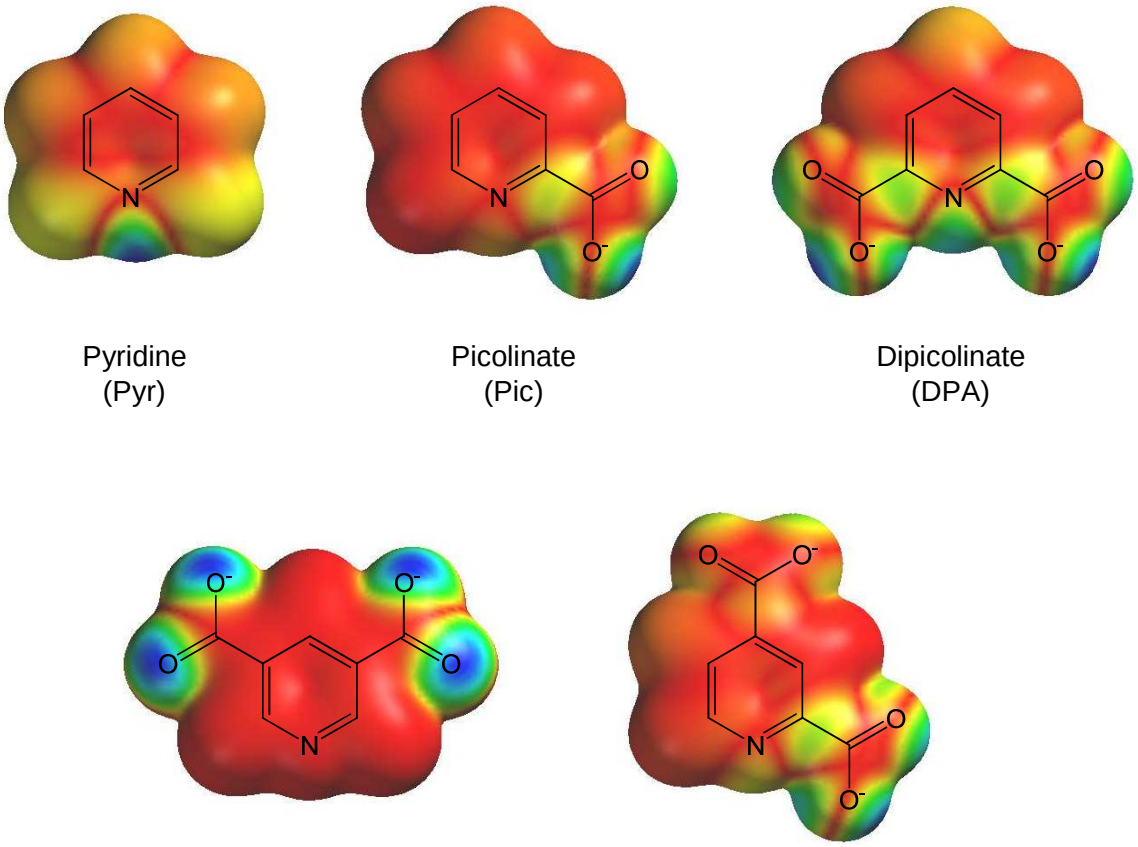

Figure 3.15. Structures of pyridine, picolinate, and three structural isomers of dipicolinate, overlaid with an electron density map of the highest occupied molecular orbital (HOMO) for each ligand. These chromophores were explored to better understand the binding properties of DPA. Electron density maps generated using Titan®; higher electron density is in blue, lower in red.

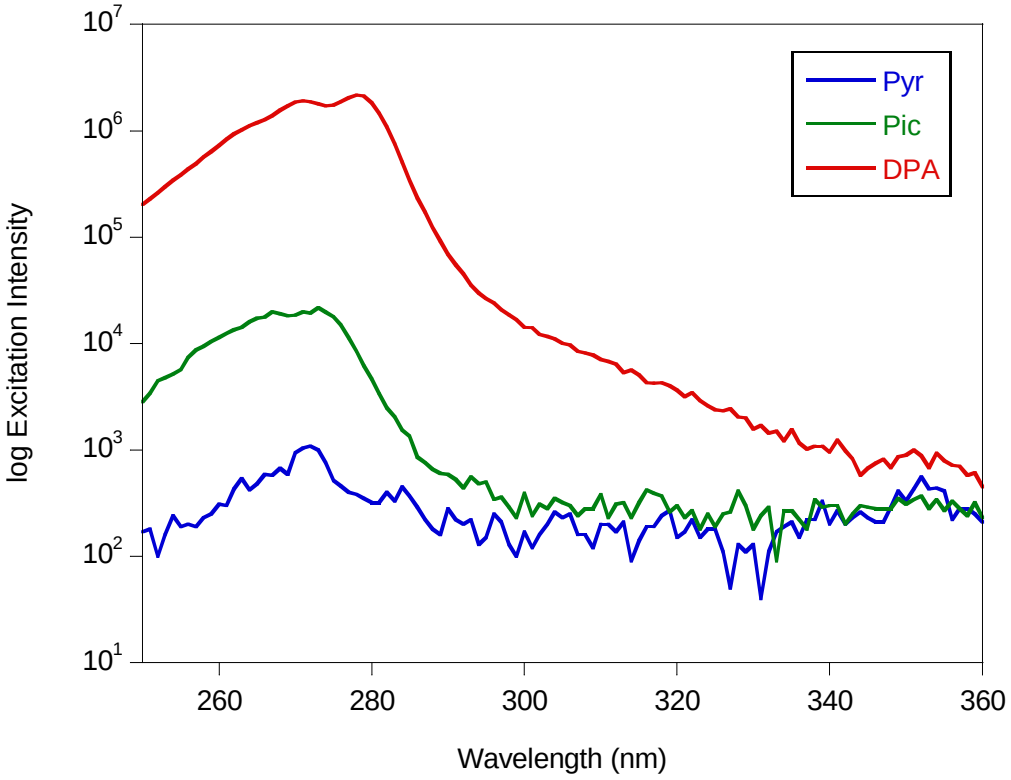

Figure 3.16. Excitation spectra (λ_{em} = 544 nm) of various terbium complexes, 10 μM in 0.2 M NaOAc, pH 5.5. Note the logarithmic y-axis. Pyridine (Pyr) has little detectable terbium sensitization, picolinate (Pic) is moderately effective, and dipicolinate (DPA) is most effective.

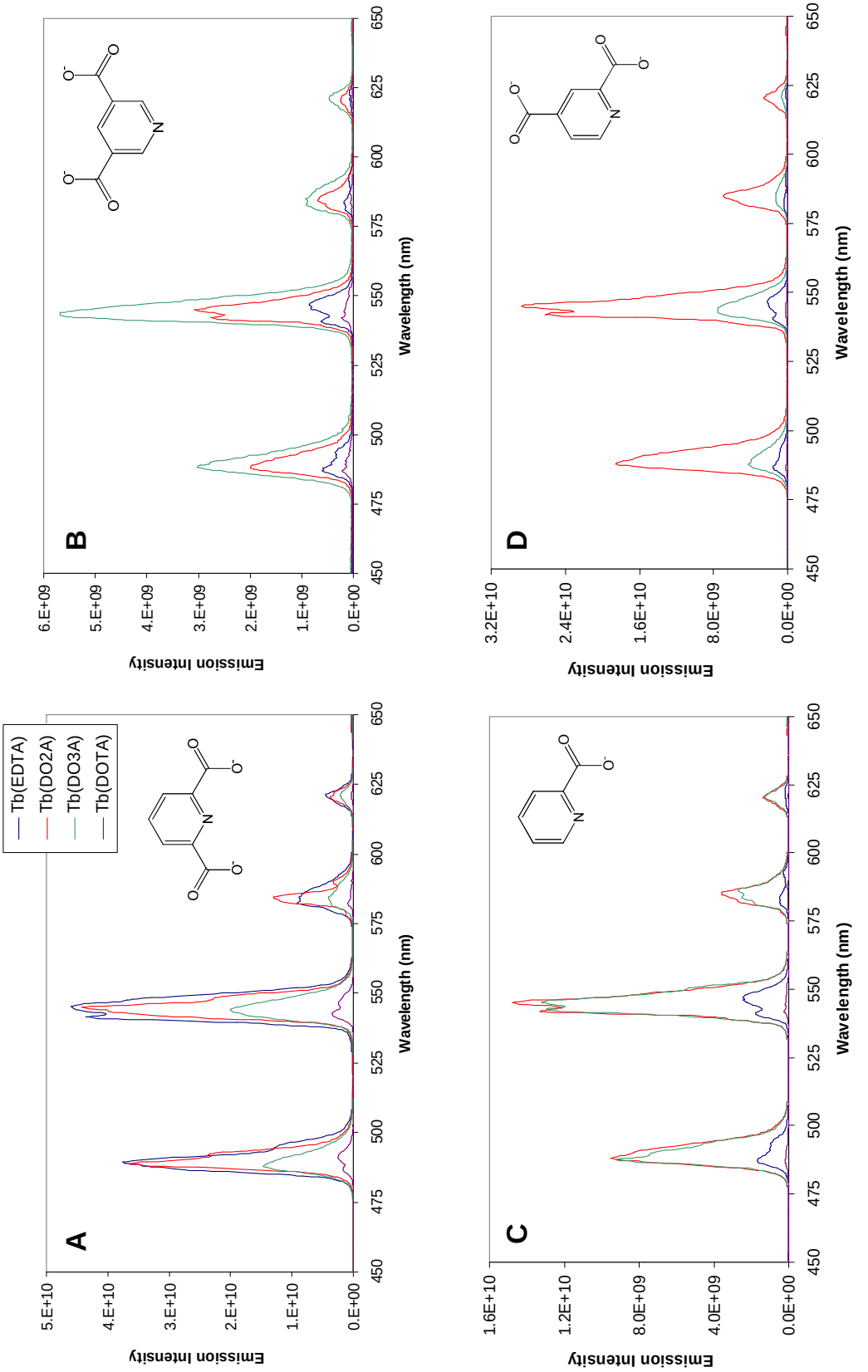

Figure 3.17. Emission spectra (λ_{ex} = 278 nm) of various terbium complexes in 50 mM MOPS buffer, pH 7.5. (A) DPA; (B) 3,5-DPA; (C) Pic; (D) 2,4-DPA.

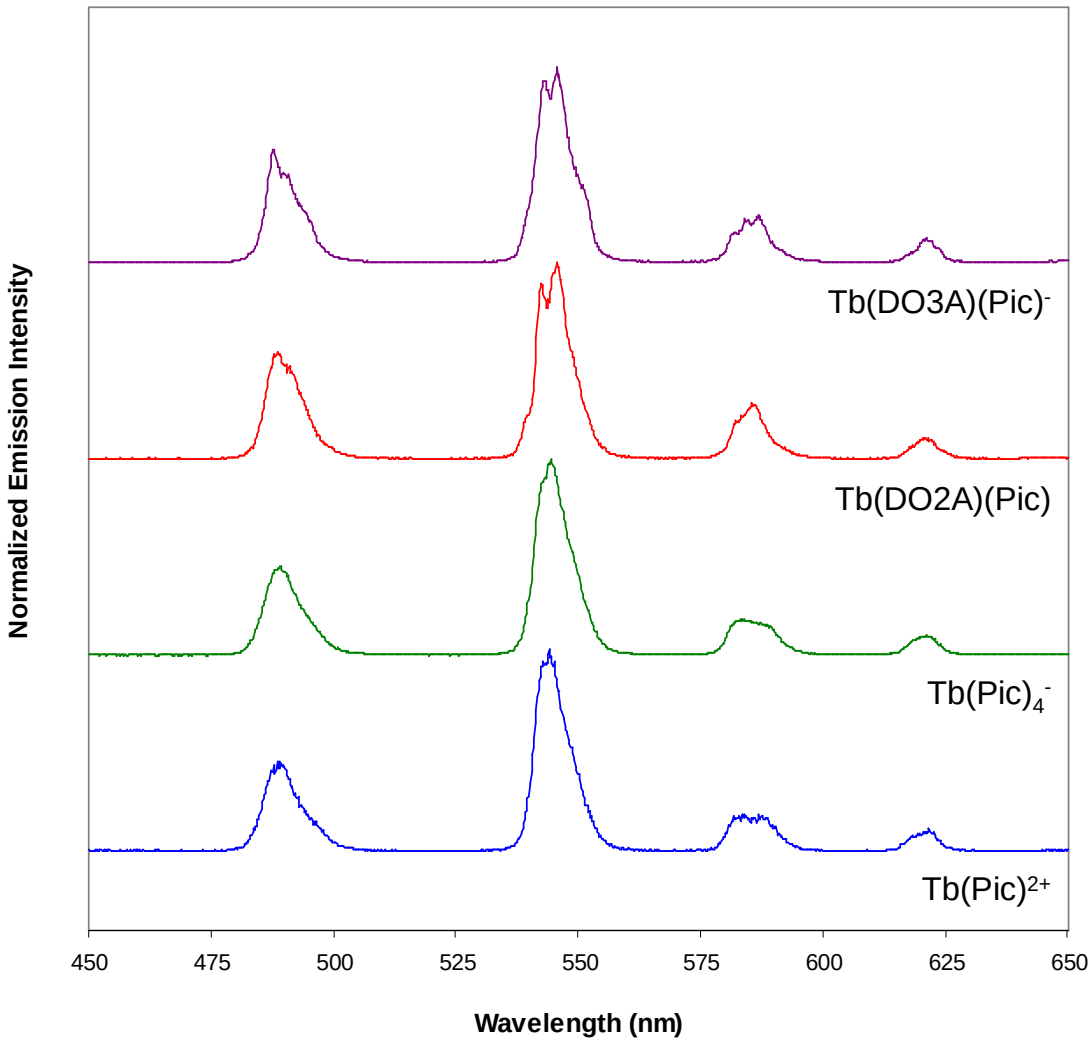

Figure 3.18. Emission spectra (λ_{em} = 274 nm) of various terbium picolinate complexes in 0.1 M MOPS buffer, pH 7.2. Charges and coordination numbers of Pic ligand assume deprotonation of carboxyl group (i.e., charge of -1) and bidentate coordination to Tb^{3+}.

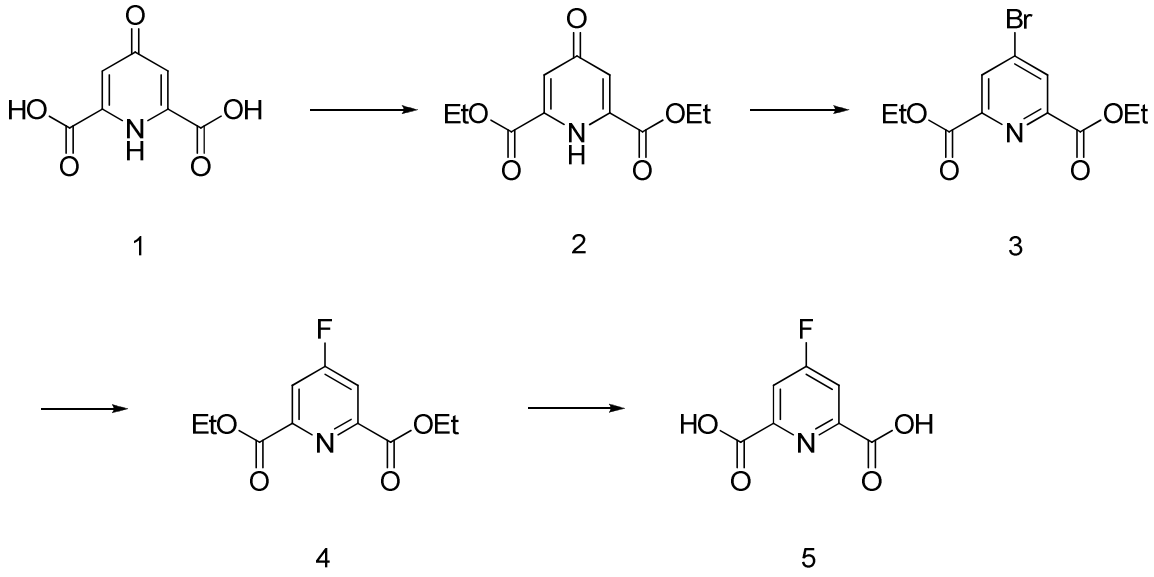

Figure 3.19. Protocol for synthesis of 4-fluoro-pyridine-2,6-dicarboxylic acid (F-DPA). Reproduced from CB Research & Development, Inc., personal communication.

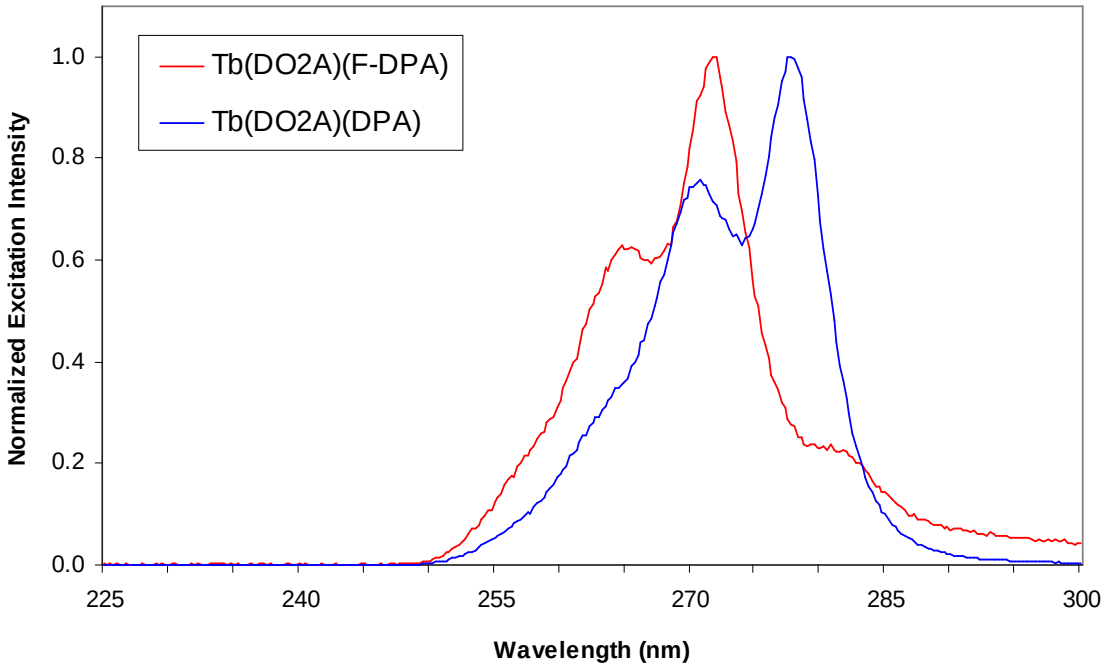

Figure 3.20. Normalized excitation spectra (λ_{em} = 544 nm) for $Tb(DO2A)(DPA)^-$ and $Tb(DO2A)(F\text{-}DPA)^-$, 10.0 μM in 1.0 mM NaOH, pH 9. The fluorinated dipicolinate complex is blue-shifted by approximately 5 nm, indicative of a shift of electron density away from the lanthanide.

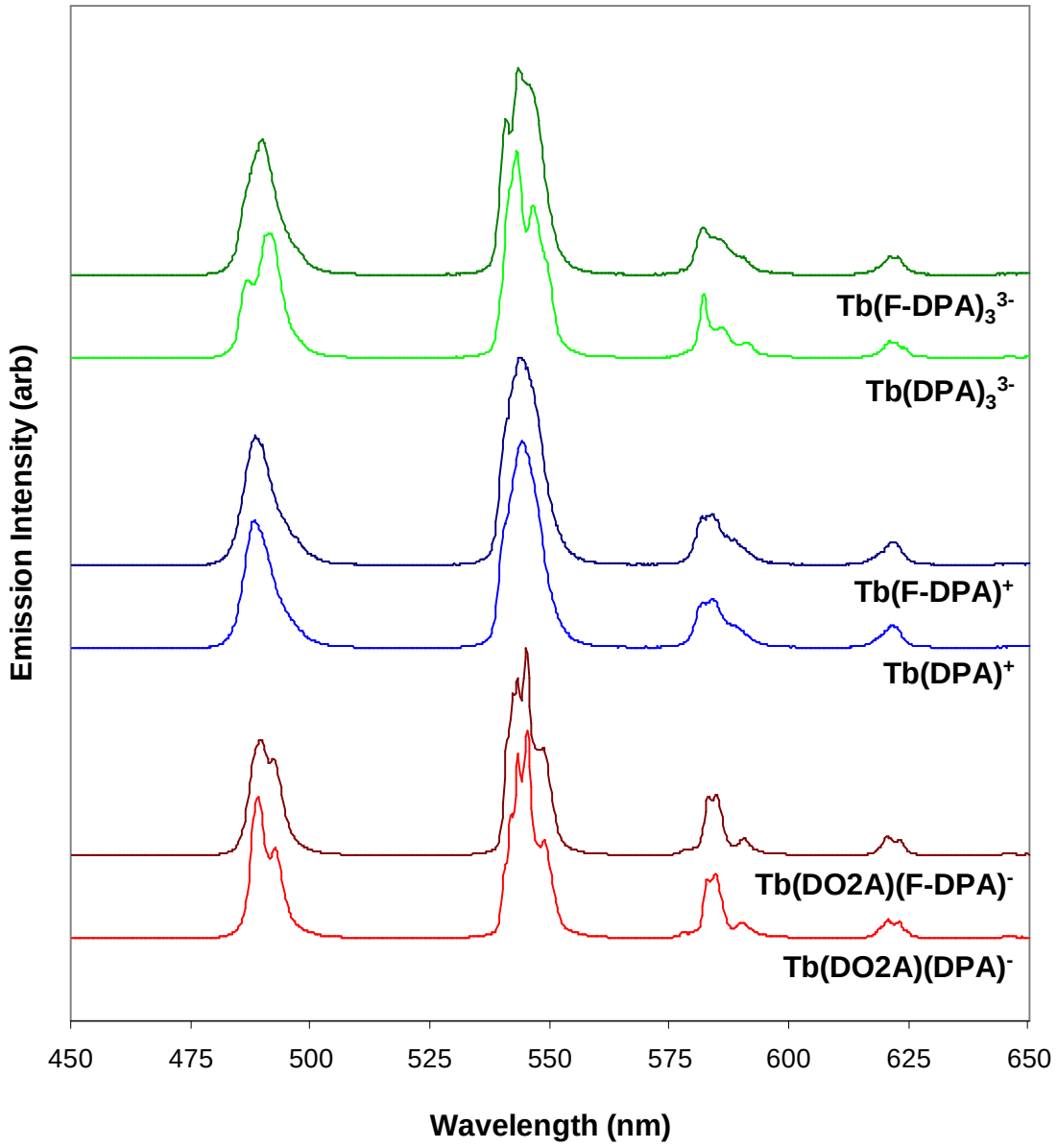

Figure 3.21. Normalized emission spectra (λ_{ex} = 278 nm) for various DPA and F-DPA complexes, 1.0 mM NaOH, pH 9. The F-DPA ternary complex (dark red) shows finer Stark splitting than its DPA counterpart (red), while the situation is reversed for the tris-dipicolinate species (light and dark green).

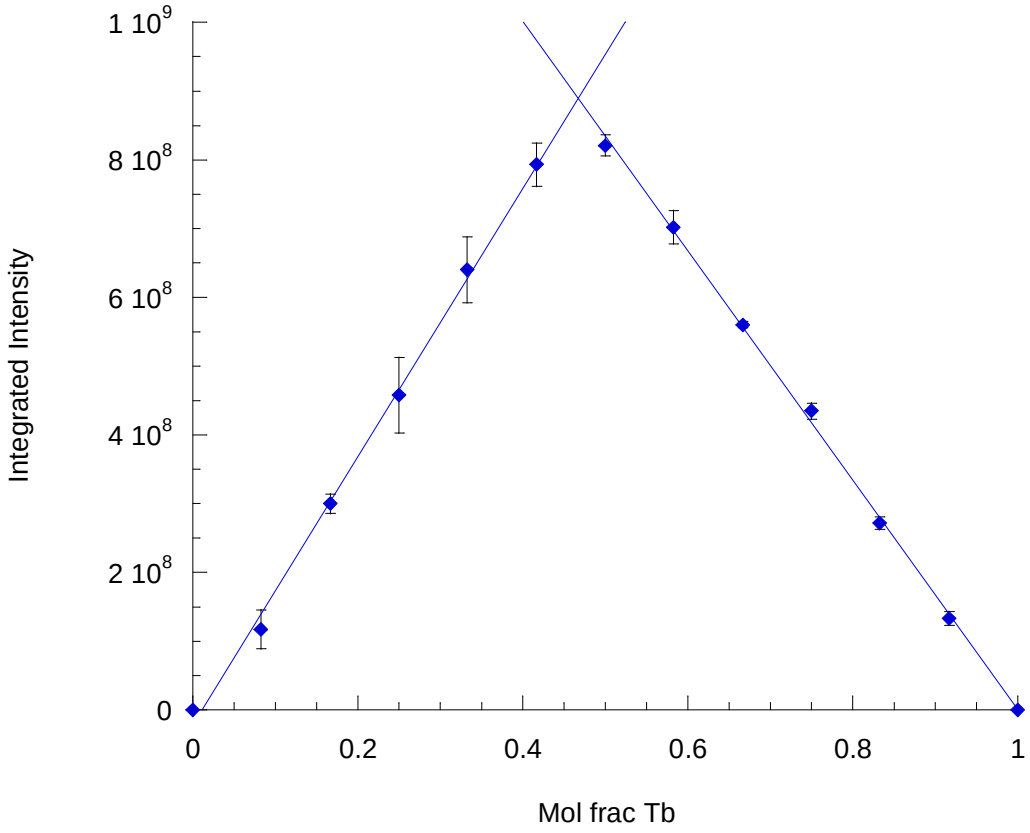

Figure 3.22. Jobs plot of $Tb(DO2A)^{+}$ with F-DPA in 1.0 mM NaOH, pH 9.0, indicating an optimal Tb mole fraction of 0.47 for complete binding of F-DPA.

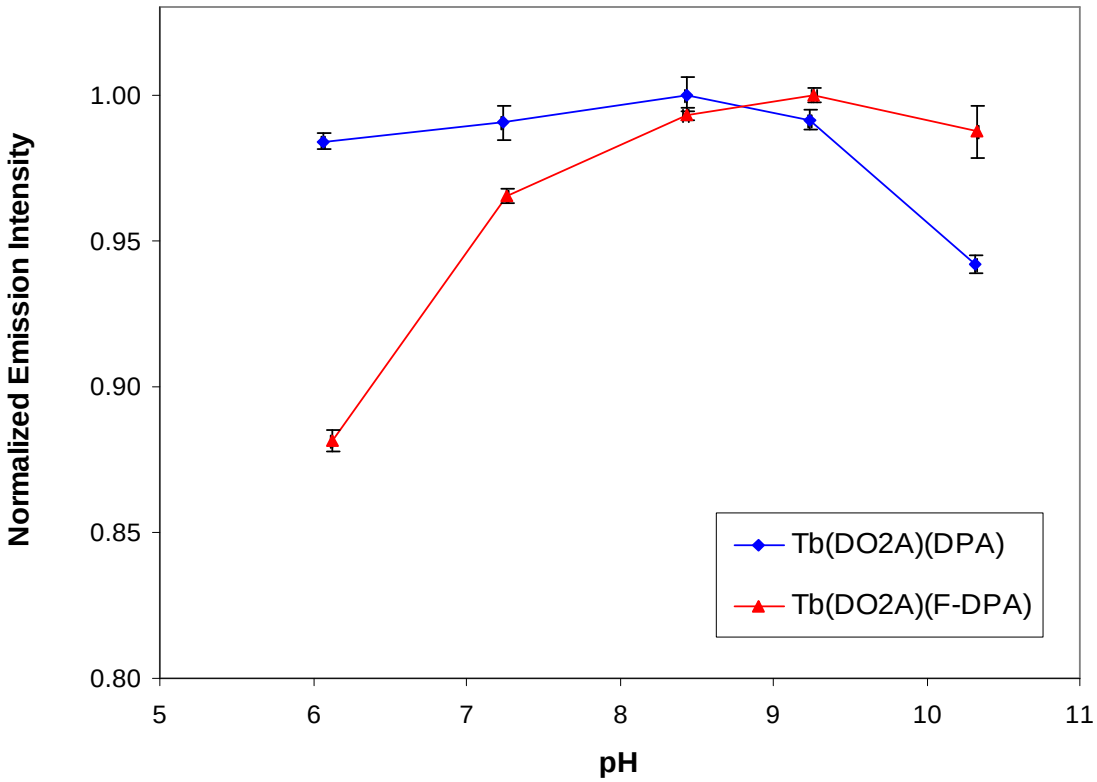

Figure 3.23. pH dependence of $Tb(DO2A)(DPA)^-$ and $Tb(DO2A)(F\text{-}DPA)^-$, 10.0 μM in 0.1 M buffer. Normalized emission spectra (λ_{ex} = 278 nm) are integrated from 530–560 nm.

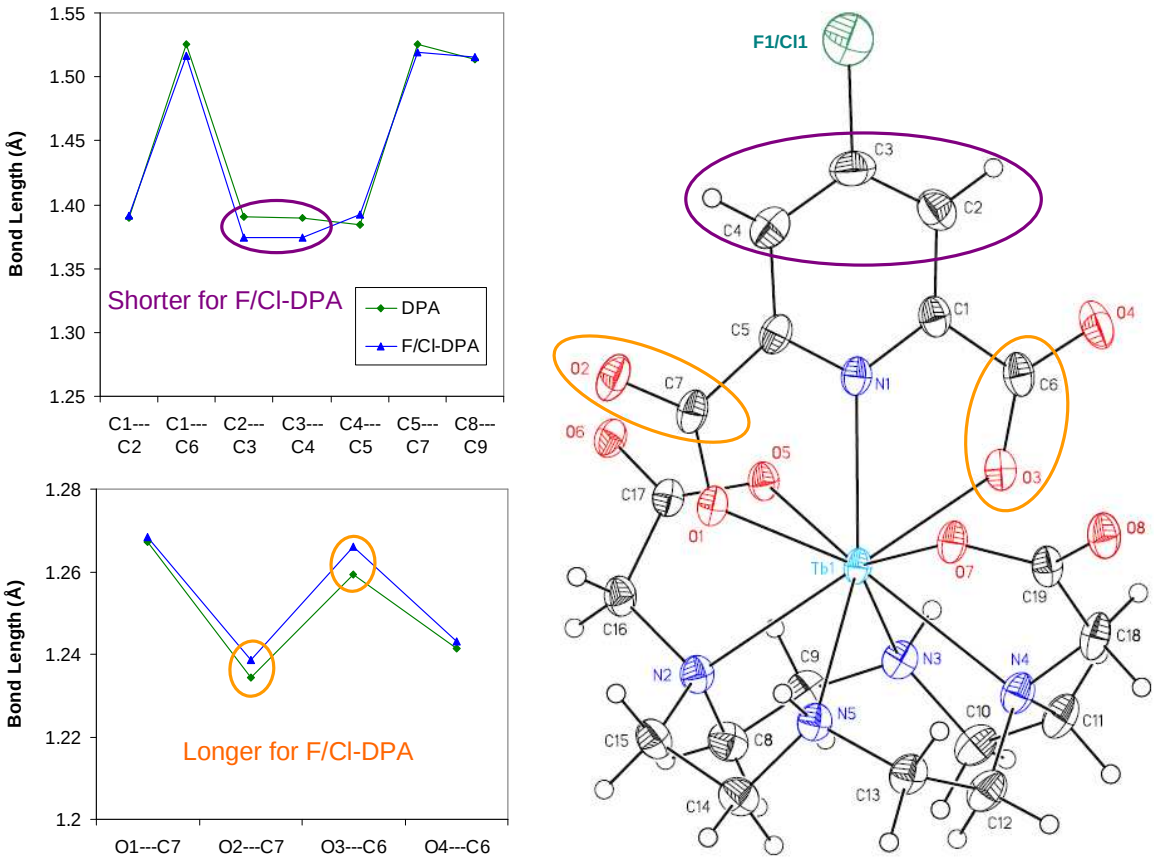

Figure 3.24. Various bond lengths (Å) for the dipicolinate of the TBA·Tb(DO2A)(F/Cl-DPA) crystal structure, where the 4-substituted dipicolinate species is 37% F-DPA and 63% Cl-DPA.

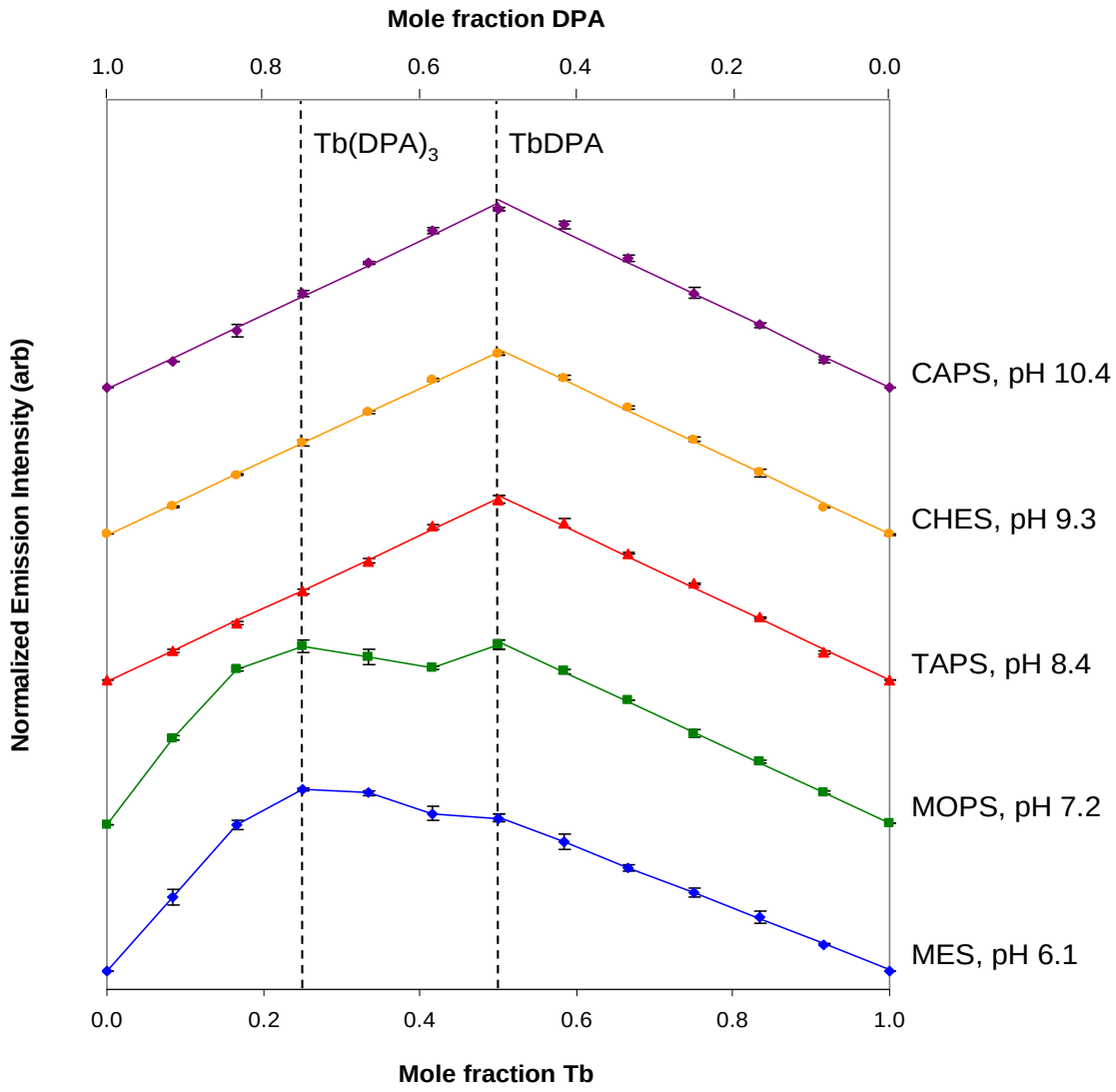

Figure 3.25. Jobs plots of Tb(DO2A)(DPA)$^-$ in 0.1 M buffer at various pH values. The concentrations of Tb and DPA are varied inversely from 0 to 12 μM in 1 μM increments, with the DO2A in excess (100 μM). Emission spectra (λ_{ex} = 278 nm) are integrated over 530–560 nm. Linear regions are fitted with trendlines, and significant Tb:DPA ratios are noted by dashed lines.

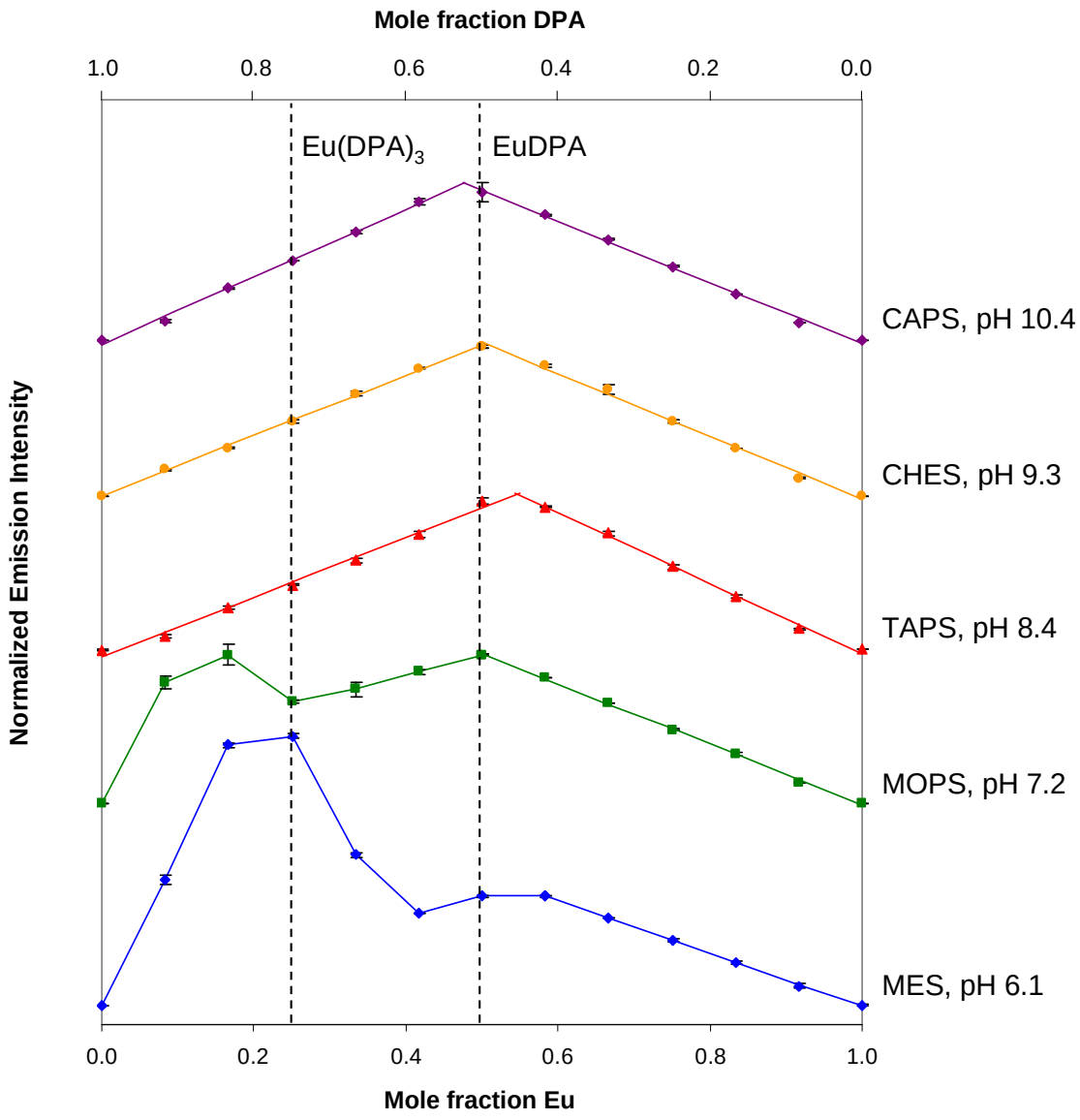

Figure 3.26. Jobs plots of Eu(DO2A)(DPA)$^{-}$ in 0.1 M buffer at various pH values. The concentrations of Eu and DPA are varied inversely from 0 to 12 μM in 1 μM increments, with the DO2A in excess (100 μM). Emission spectra (λ_{ex} = 278 nm) are integrated over 680–710 nm. Linear regions are fitted with trendlines, and significant Eu:DPA ratios are noted by dashed lines.

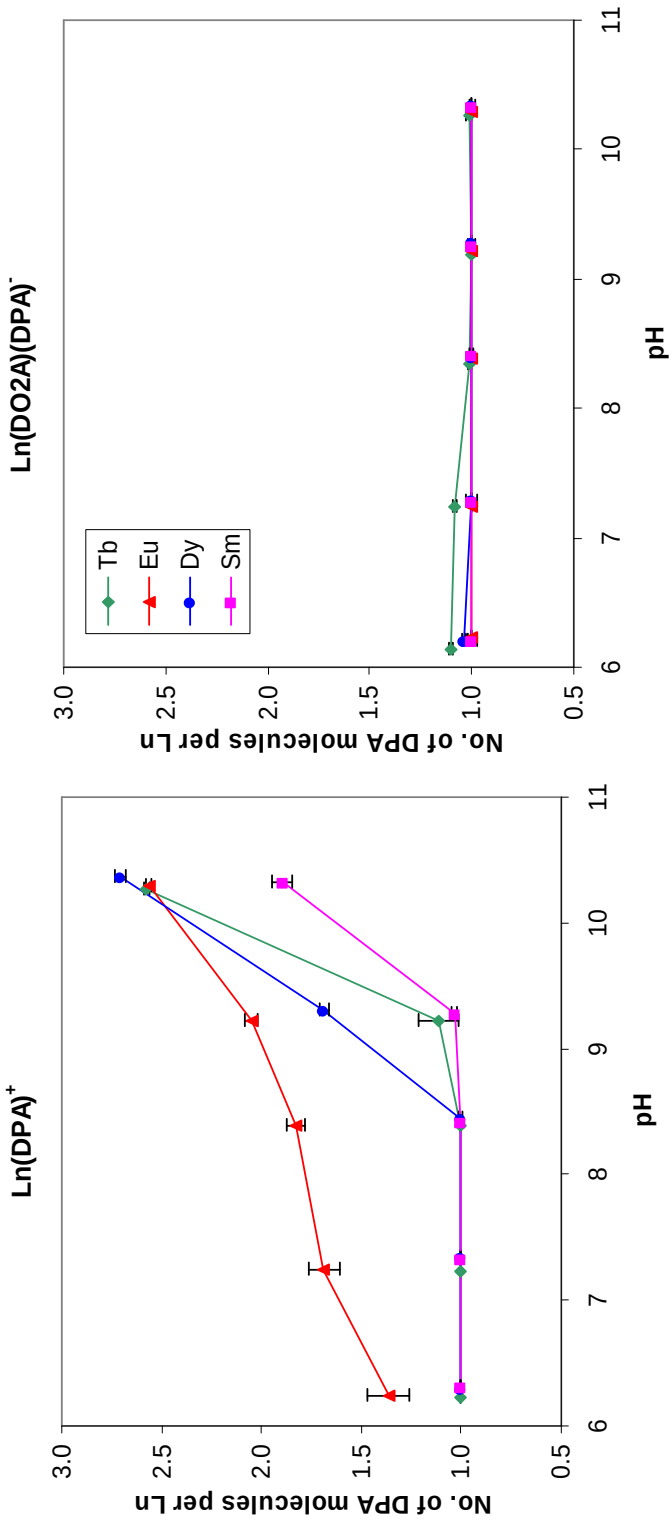

Figure 3.27. Number of DPA molecules bound per Ln^{3+} as a function of pH for $Ln(DPA)^{+}$ and $Ln(DO2A)(DPA)^{-}$ complexes (Ln = Sm, Eu, Tb and Dy), 10.0 µM in 0.1 M buffer (λ_{ex} = 278 nm).

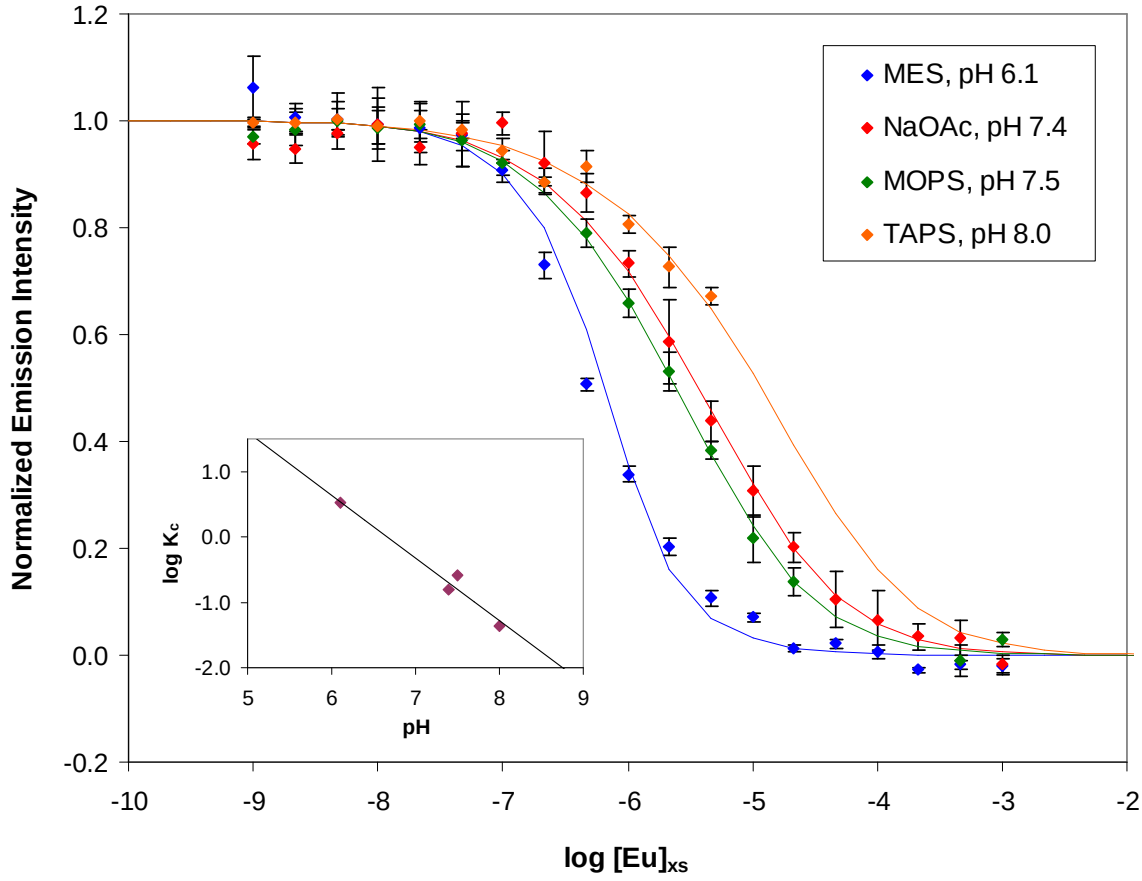

Figure 3.28. Binding affinity by competition (BAC) assay titration curves for Eu(DO2A)(DPA)$^{-}$ in 0.1 M buffer at various pH values. Emission spectra (λ_{ex} = 278 nm) integrated from 675–710 nm. Inset: Logarithm of competition constant (K_c) against pH.0

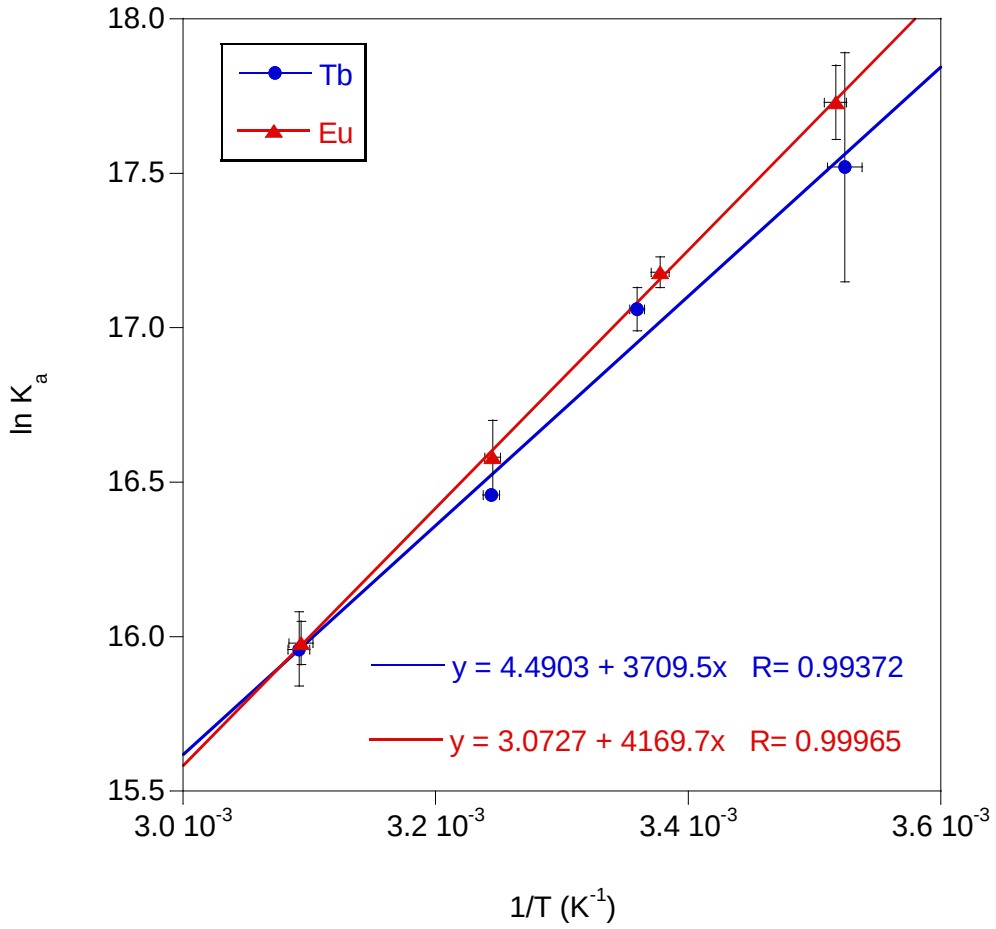

Figure 3.29. Plot of ln K_a against 1/T for $Tb(DPA)^+$ and $Eu(DPA)^+$ in 0.2 M NaOAc, pH 7.4. Slopes, y-intercepts and correlation coefficients (R) are shown for each linear fit.

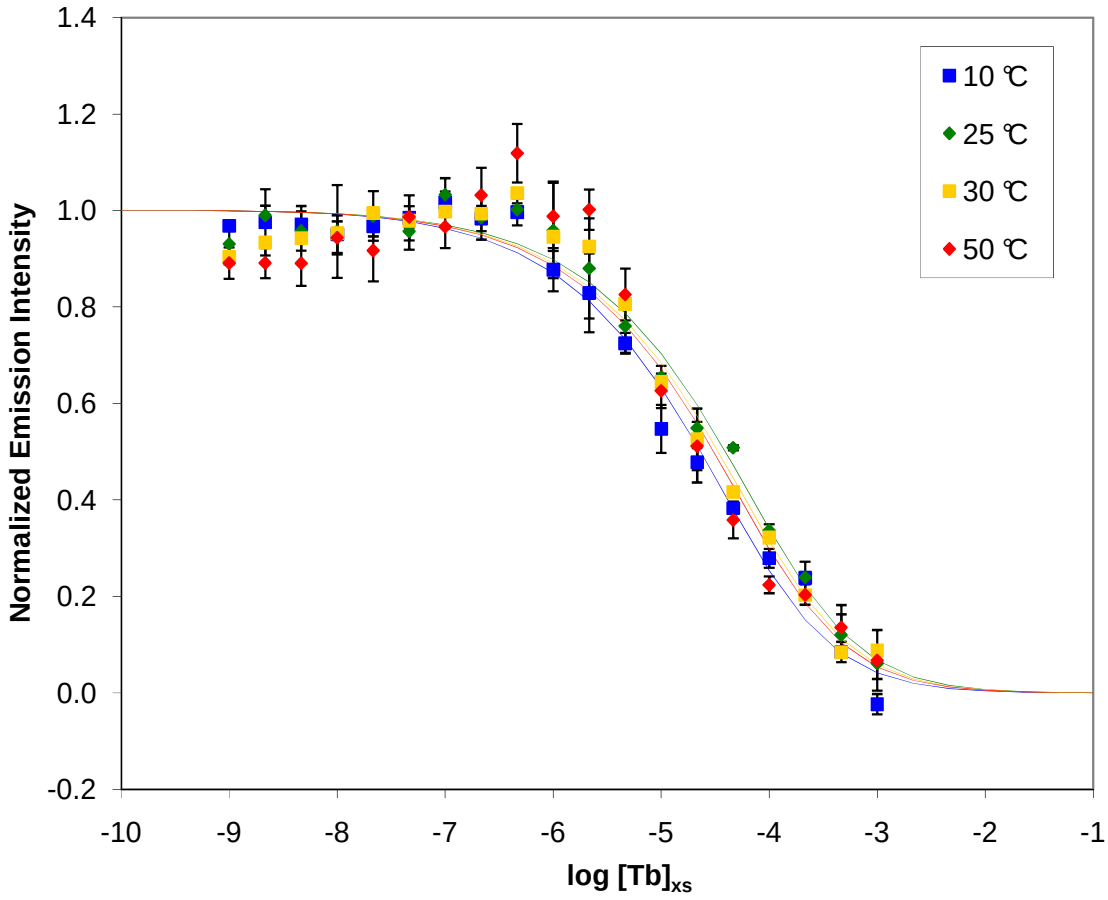

Figure 3.30. Binding affinity by competition (BAC) assay titration curves for Tb(DO2A)(DPA)$^{-}$ in 0.1 M buffer at various temperatures. Emission spectra (λ_{ex} = 278 nm) integrated from 570–600 nm.

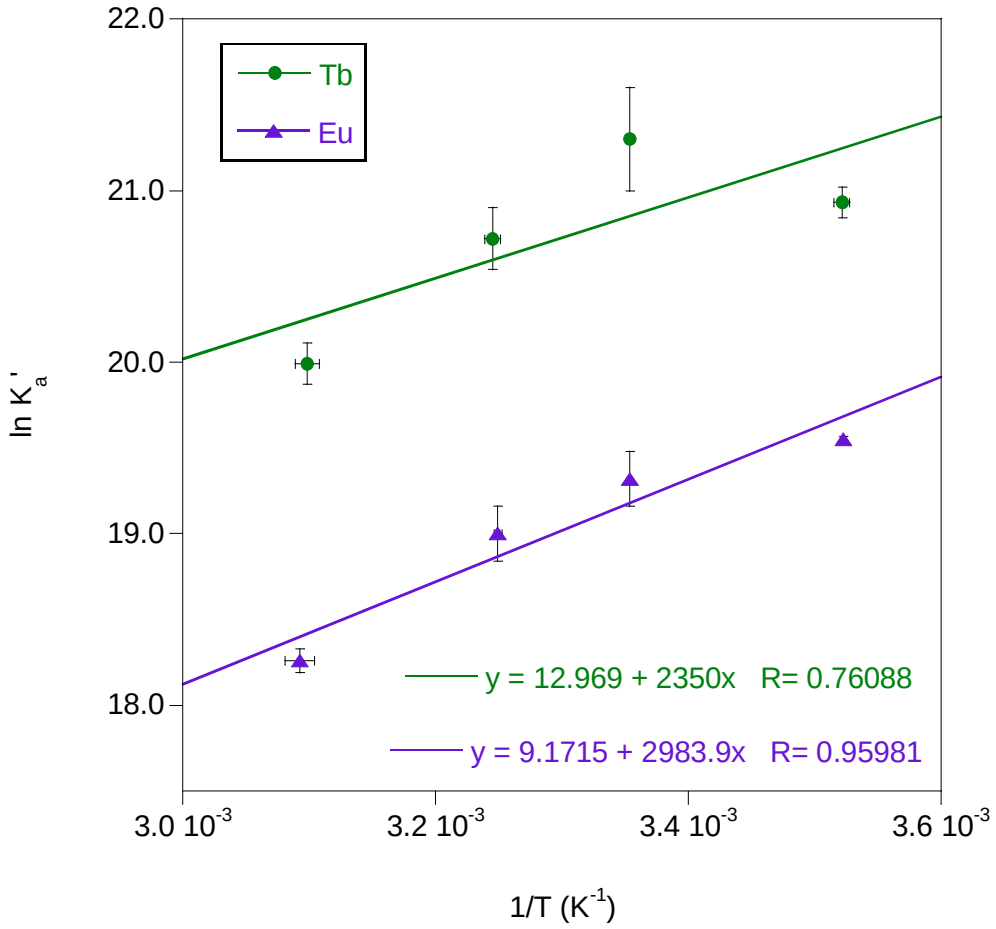

Figure 3.31. Plot of ln K_a' against 1/T for $Tb(DO2A)(DPA)^-$ and $Eu(DO2A)(DPA)^-$ in 0.2 M NaOAc, pH 7.4.

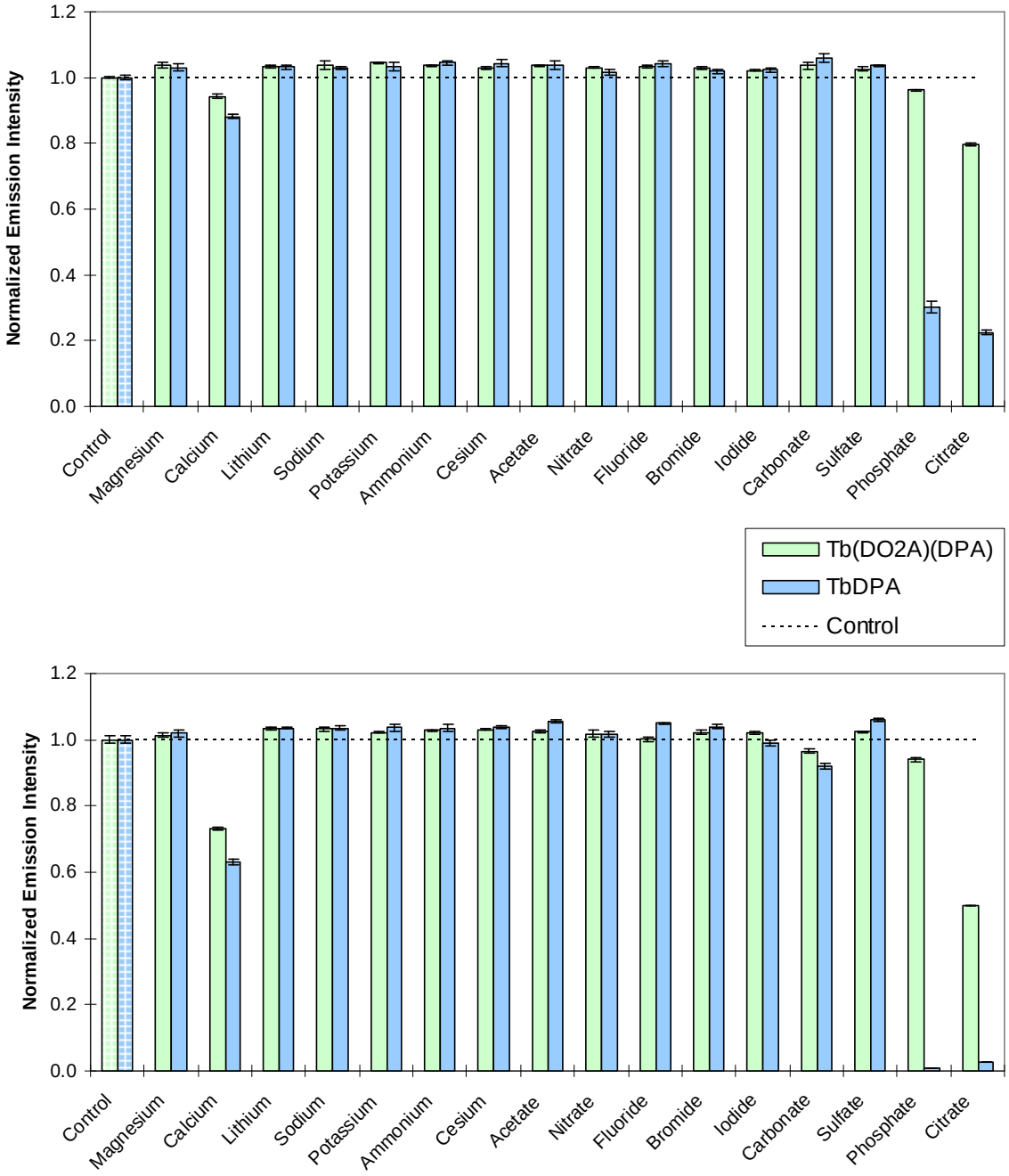

Figure 3.32. Emission intensity variation of 0.10 μM $Tb(DO2A)(DPA)^-$ or $Tb(DPA)^+$ complex with the addition of 100 μM (top) or 1.0 mM (bottom) of interfering ion, pH 5.2. Normalized integrated emission intensity, 530–560 nm; λ_{ex} = 278 nm.

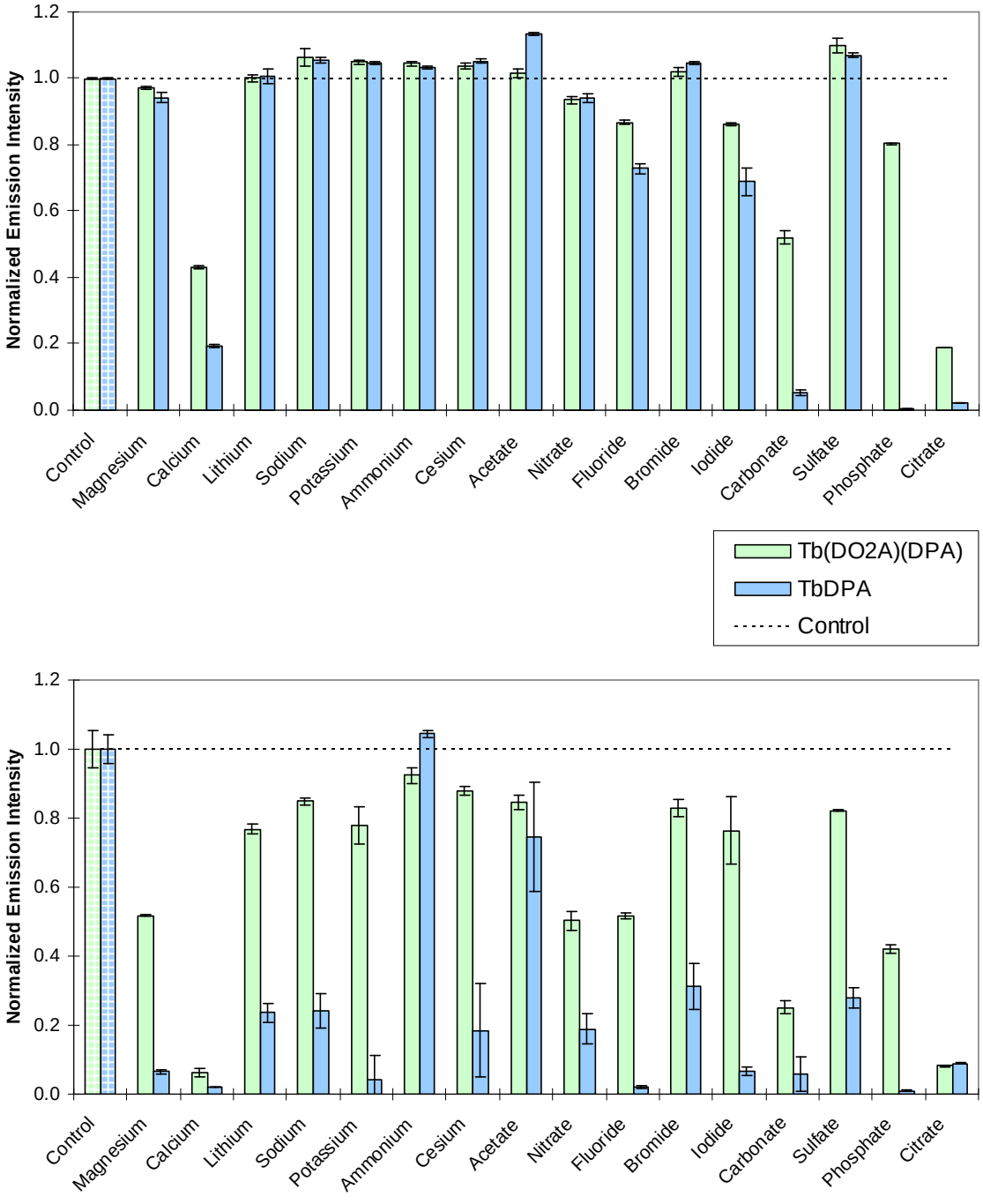

Figure 3.33. Emission intensity variation of 0.10 μM $Tb(DO2A)(DPA)^-$ or $Tb(DPA)^+$ complex with the addition of 10.0 mM (top) or 0.10 M (bottom) of interfering ion, pH 6. Normalized integrated emission intensity, 530–560 nm; λ_{ex} = 278 nm.

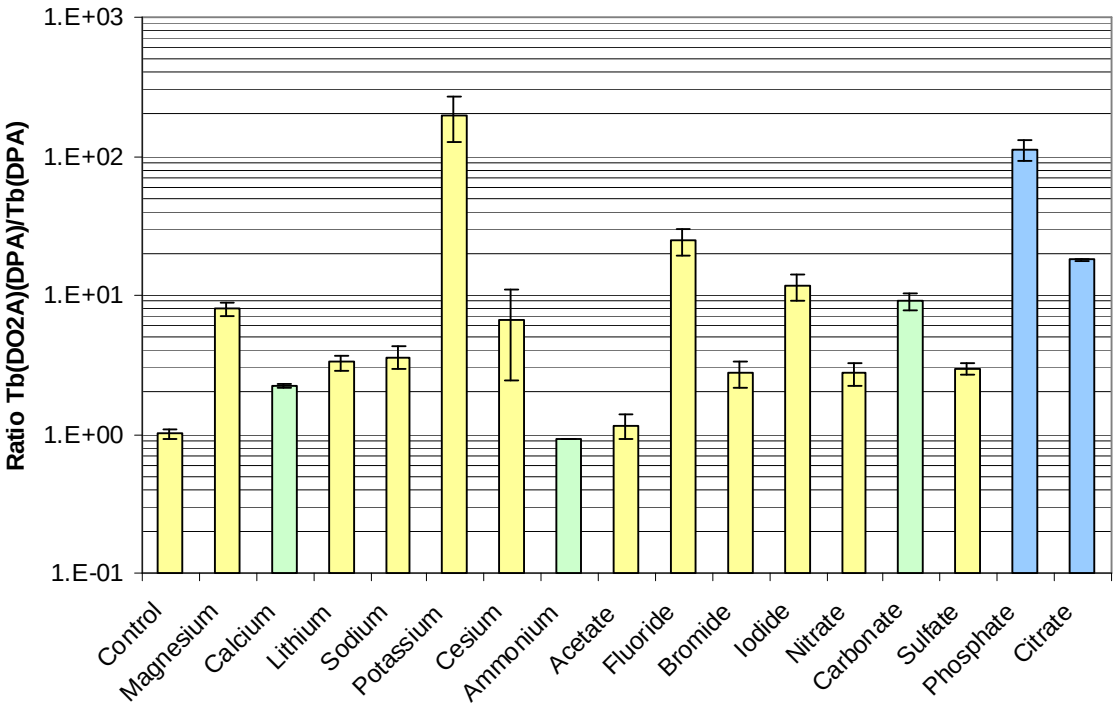

Figure 3.34. Ratio of 100 nM Tb(DO2A)(DPA)$^{-}$ to Tb(DPA)$^{+}$ emission intensity in 0.1 M (yellow), 10 mM (green) or 1 mM (blue) competing ion, pH 6.6. Ions are listed in order of charge from positive (left) to negative (right). Normalized integrated emission intensity, 530–560 nm; λ_{ex} = 278 nm.

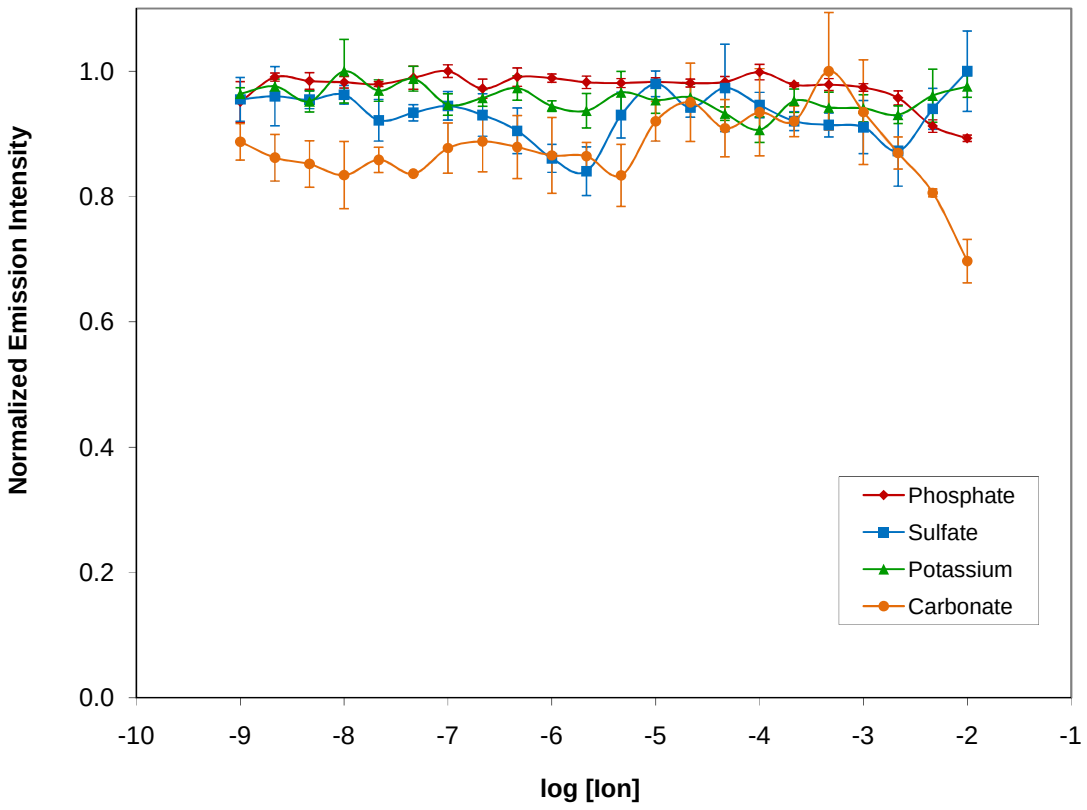

Figure 3.35. Ion competition experiment of 0.1 μM Tb(DO2A)(DPA)$^{-}$ titrated with phosphate (red), sulfate (blue), potassium (green) or carbonate (orange) over a concentration range from 1.0 nM to 100 mM, pH 7.5 (0.1 M MOPS). Carbonate appears to be the only ion that competes, and only at very high concentrations (1:10^5 [Tb(DO2A)(DPA)$^{-}$] : [CO_3^{2-}]).

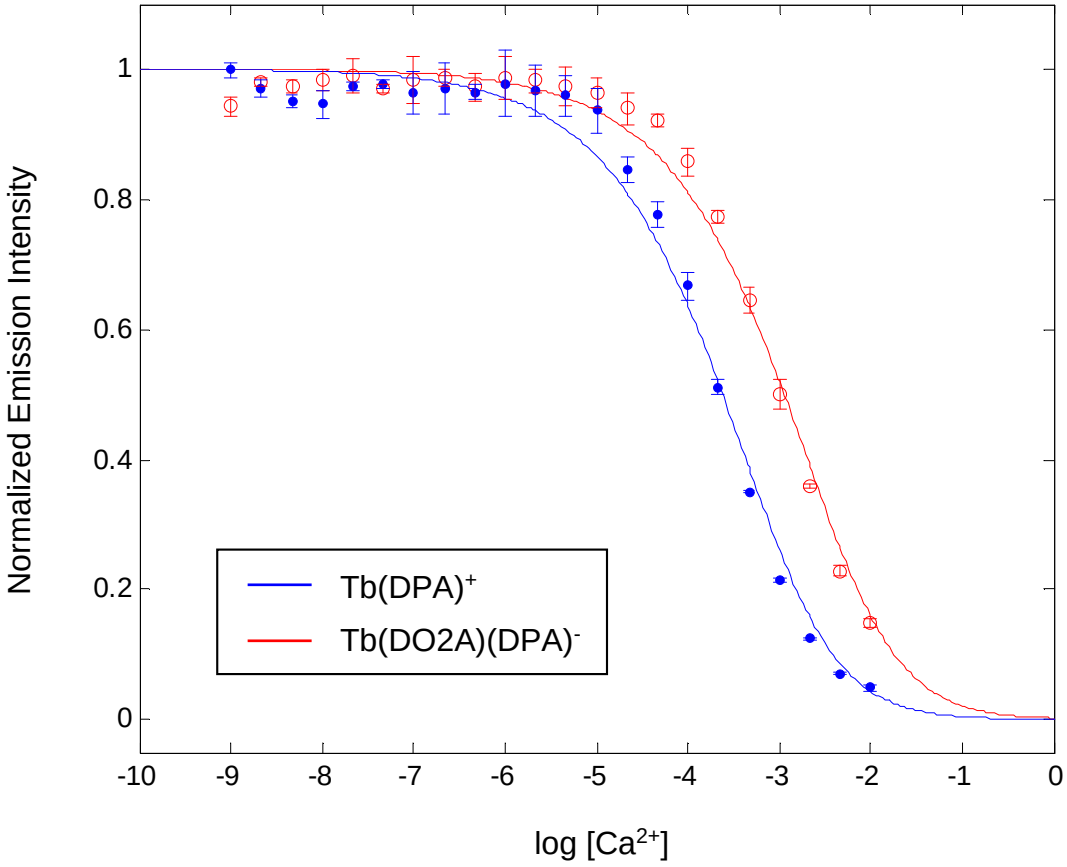

Figure 3.36. Cation competition experiment of 0.1μM $Tb(DO2A)(DPA)^-$ or $Tb(DPA)^+$ titrated with Ca^{2+} over a concentration range from 1.0 nM to 0.1 M, pH 7.5 (0.1 M MOPS). Emission intensity integrated from 530–560 nm, λ_{ex} = 278 nm.

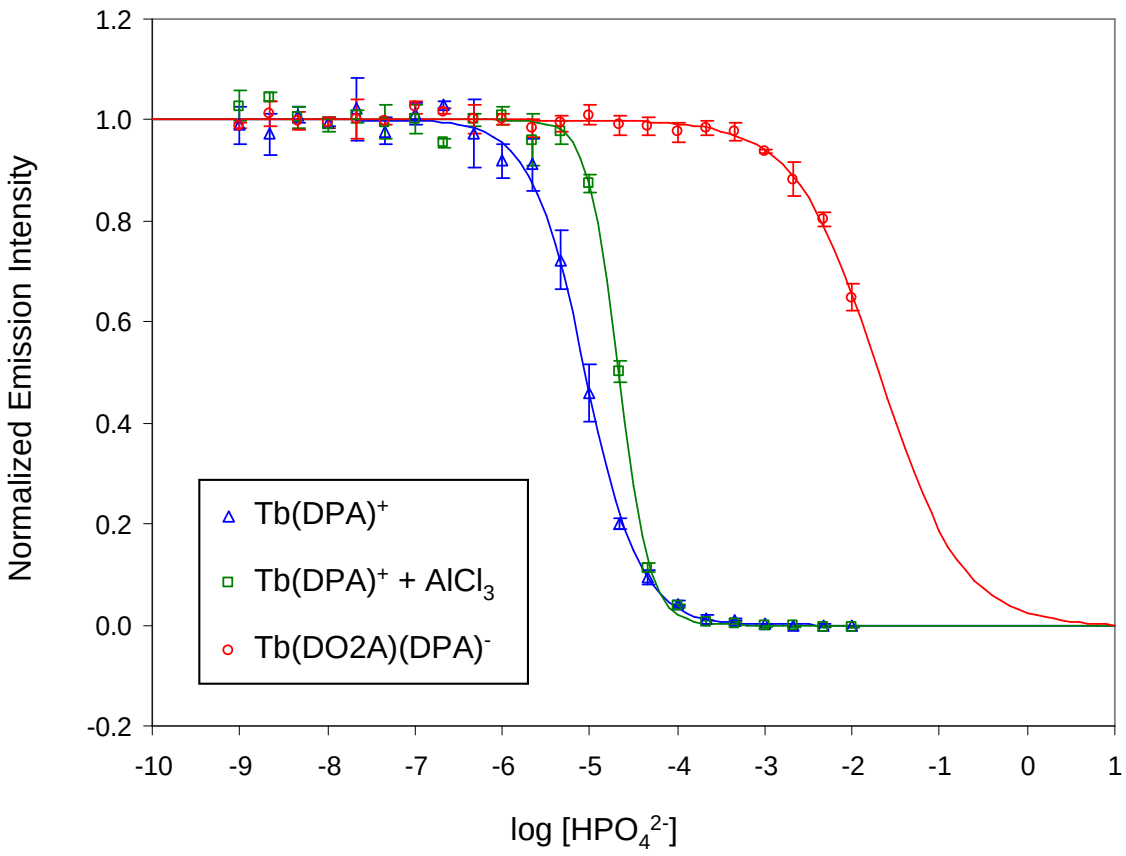

Figure 3.37. Anion competition experiment of 0.1μM Tb(DO2A)(DPA)$^{-}$, 0.1 μM Tb(DPA)$^{+}$ or 0.1 μM Tb(DPA)$^{+}$ with 100 μM aluminum chloride. Each was titrated with phosphate over a concentration range from 1.0 nM to 0.1 M, pH 7.3 (0.2 M NaOAc). Emission intensity integrated from 530–560 nm, λ_{ex} = 278 nm.

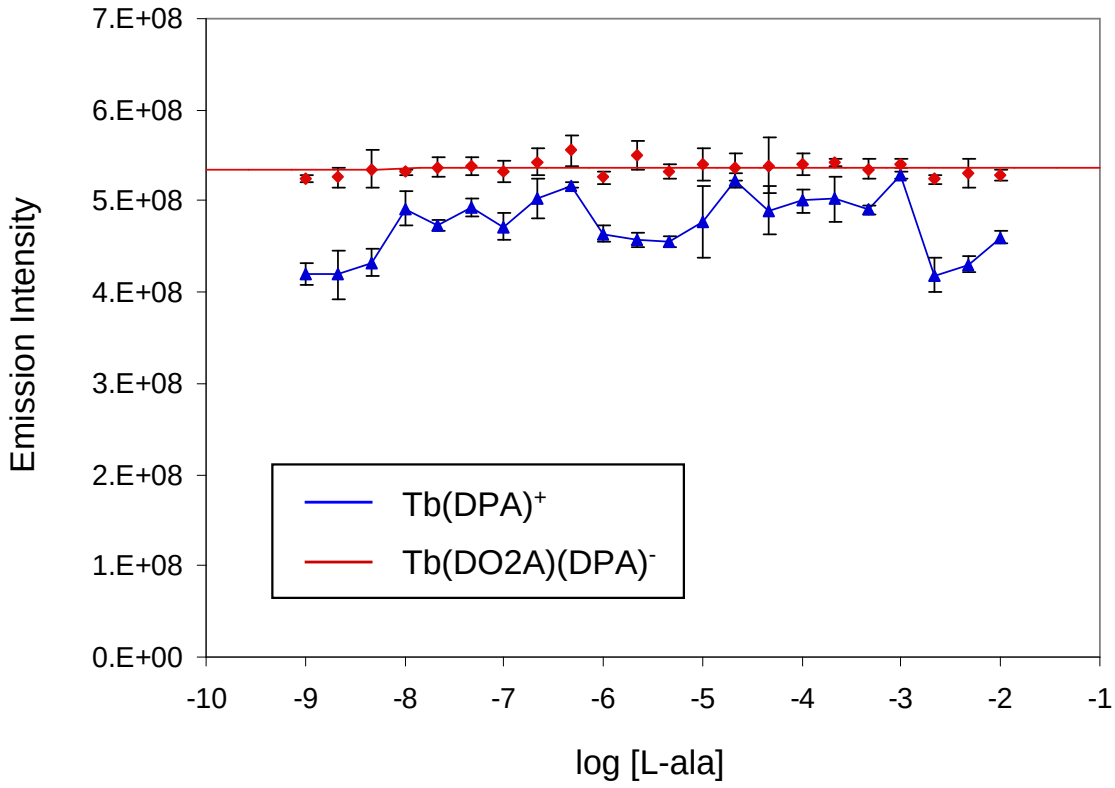

Figure 3.38. Germinant competition experiment of 0.1μM $Tb(DO2A)(DPA)^-$ or $Tb(DPA)^+$ titrated with L-alanine over a concentration range from 1.0 nM to 0.1 M, pH 7.5 (0.1 M MOPS). Emission intensity integrated from 530–560 nm, λ_{ex} = 278 nm.

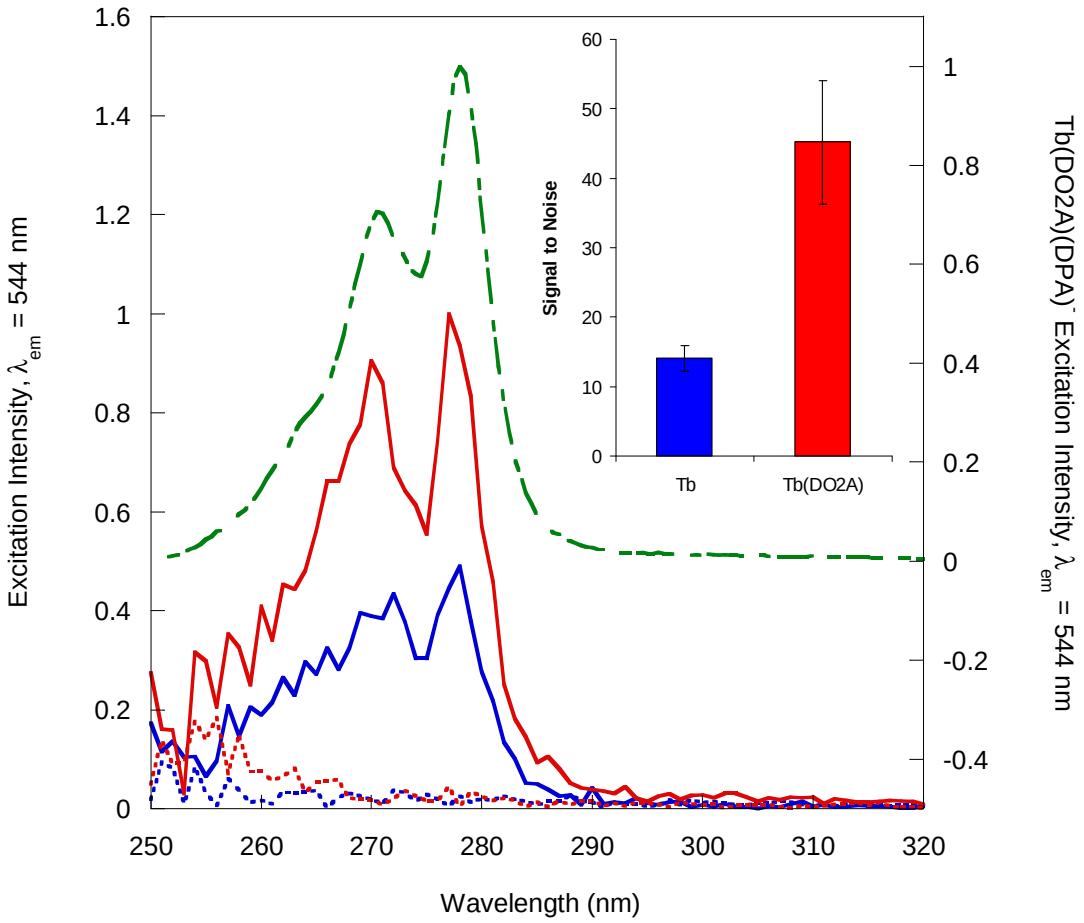

Figure 3.39. Excitation spectra of unfiltered samples of autoclaved *Bacillus atrophaeus* spores containing 10.0 μM of Tb^{3+} (blue) or the $Tb(DO2A)^{+}$ binary complex (red) in filter-sterilized nanopure H_2O. Dashed offset excitation spectrum (green) of 10 μM Tb(DO2A)(DPA) in 0.2 M sodium acetate, pH 7.4, confirms excitation profile as DPA. Concentration of bacterial spores approx. 10^5 spores/mL. Controls of Tb^{3+} or $Tb(DO2A)^{+}$ are shown in dotted blue and red, respectively. Inset: Signal-to-noise ratio of emission intensity, 530–560 nm, for Tb^{3+} (blue) and $Tb(DO2A)^{+}$ (red), showing a three-fold improvement in S/N with the use of DO2A.

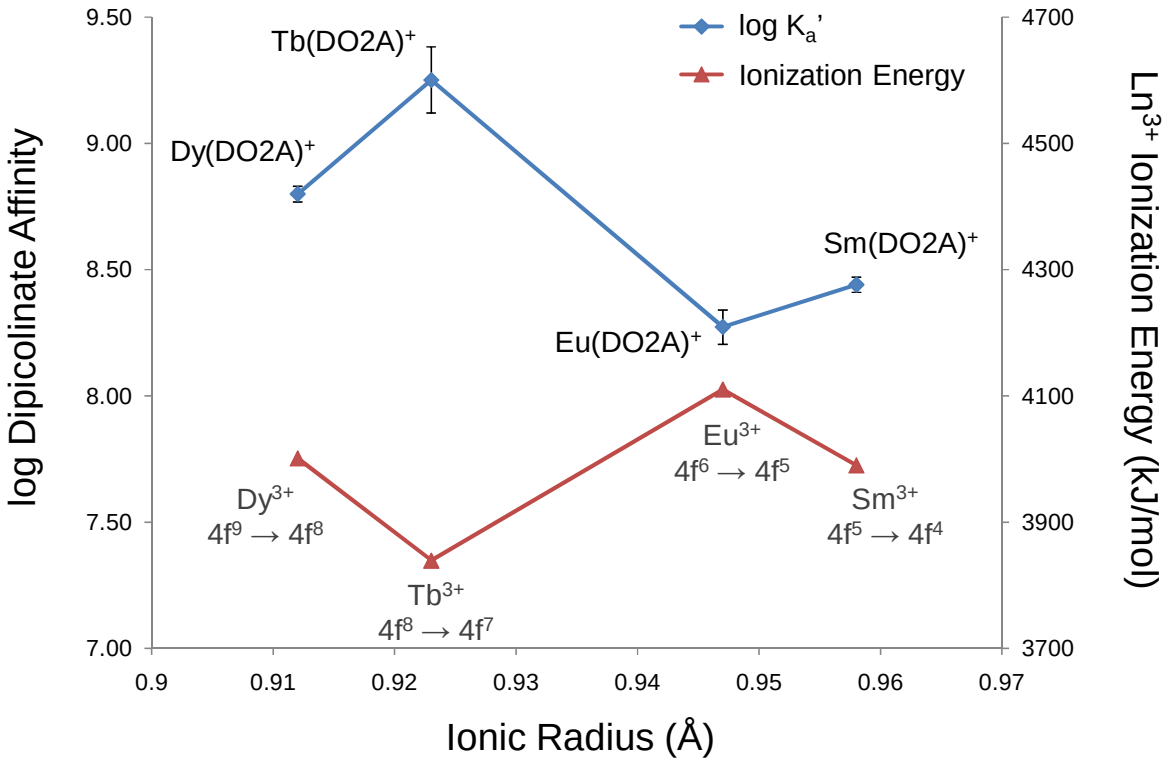

Figure 3.40. Relationship between Ln(DO2A)$^+$ dipicolinate binding affinity and $Ln^{3+} \rightarrow Ln^{4+}$ ionization energy with lanthanide ionic radius. The Tb(DO2A)$^+$ complex has the greatest affinity for DPA^{2-} because the low ionization energy of the Tb^{3+} ion makes it the most susceptible to perturbation by the DO2A ligand, shifting the electron density of the lanthanide and thereby generating the most positive binding site for the DPA^{2-} analyte. Ionization energies from reference 67.

TABLES

Table 3.1. Association constants of various lanthanide-macrocycle complexes.

Ln^{3+}	Macrocycle	log K	Ref
Gd	DO2A	19.42	8
	DO3A	21.0	▪
	DOTA	24.7	8
Sm	DOTA	23.0	5
Eu	DOTA	28.2	9
Tb	DOTA	28.6	9
Dy	DOTA	24.2	5

Table 3.2. Association constants of Ln^{3+} and $Ln(DO2A)^{+}$ with DPA^{2-}, calculated using a one-step equilibration model and the BAC assay, respectively, 0.2 M NaOAc, pH 7.5.

Ln	log K_a	log K_a'
Sm	7.64 ± 0.05	8.44 ± 0.03
Eu	7.46 ± 0.02	8.39 ± 0.07
Tb	7.41 ± 0.03	9.25 ± 0.13
Dy	7.57 ± 0.03	8.79 ± 0.03

Table 3.3. Crystallographic data for the TBA•Tb(DO2A)(F-DPA) structure.

Dipicolinate	**DPA**	**F-DPA**
Formula	$[C_{19}H_{25}N_5O_8Tb]^-[C_{16}H_{36}N]^+$• 0.47($C_3H_8O$) 0.53($C_3H_6O$) 3($H_2O$)	$[C_{19}H_{25}N_5O_8Tb]^-[C_{16}H_{36}N]^+$• ($C_3H_8O$) 2($H_2O$)
M_w	964.94	975.45
Crystal system	Monoclinic	Monoclinic
Space group	$P2_1/c$	$P2_1/c$
a (Å)	13.1047(5)	13.2324(6)
b (Å)	13.3397(5)	12.9812(6)
c (Å)	26.0901(9)	26.2126(11)
β (°)	90.0130(10)	90.528(2)
V ($Å^3$), Z	4560.9(3)	4502.4(3)
λ (Å)	0.71073	0.71073
D_c (Mg/m^3)	1.405	1.439
μ,Mo-Kα (mm^{-1})	1.613	1.671
T (K)	100(2)	100(2)
R_1, wR_2‡	0.0384, 0.0639	0.0285, 0.0499

‡ Structure refined on F^2 using all reflections: $wR_2 = [\Sigma[w(F^2 - F_c^2)^2]/\Sigma w(F^2)^2]^{1/2}$, where $w^{-1} = [\Sigma(F^2) + (aP)^2 + bP]$ and $P = [max(F^2,0) + 2F_c^2]/3$.

Table 3.4. Protonation constants of relevant ligands.

Ligand	pK_{a1}	pK_{a2}	pK_{a3}	pK_{a4}	pK_{a5}	pK_{a6}	Ref
DPA	-1.05	2.22	5.22	---------	---------	---------	15
DO2A	3.18	4.09	9.45	10.91	---------	---------	6
	2.55	3.85	9.55	10.94	---------	---------	5
DO3A	3.48	4.43	9.24	11.59	---------	---------	4
	3.39	4.40	9.51	10.72	---------	---------	5
DOTA	4.30	4.61	9.50	11.14	---------	---------	6
	4.00	4.60	9.90	11.34	---------	---------	5
Hexacyclen	~1	~2	4.09	8.73	9.23	10.19	7

Table 3.5. Calculated association constants for Ln^{3+} (K_a) and $Ln(DO2A)^{+}$ (K_a') for DPA^{2-} at various temperatures in 0.2 M NaOAc, pH 7.4 (Ln = Tb, Eu).

Temp (℃)	Tb		Eu	
	log K_a	log K_a'	log K_a	log K_a'
10.8	7.61 ± 0.16	9.09 ± 0.04	7.70 ± 0.05	8.49 ± 0.01
25.0	7.41 ± 0.03	9.25 ± 0.13	7.46 ± 0.02	8.39 ± 0.07
34.8	7.15 ± 0.01	9.00 ± 0.08	7.20 ± 0.05	8.25 ± 0.07
50.0	6.93 ± 0.05	8.68 ± 0.05	6.94 ± 0.03	7.93 ± 0.03

Table 3.6. Thermodynamic parameters calculated from the temperature dependence of K_a and K_a' for Tb and Eu in 0.2 M NaOAc, pH 7.4.

Reaction	ΔH (kJ/mol)	ΔS (J/mol·K)
$Tb^{3+} + DPA^{2-} \rightarrow Tb(DPA)^{+}$	-30.8	37.3
$Tb(DO2A)^{+} + DPA^{2-} \rightarrow Tb(DO2A)(DPA)^{+}$	-19.5	108
$Eu^{3+} + DPA^{2-} \rightarrow Eu(DPA)^{+}$	-34.7	25.5
$Eu(DO2A)^{+} + DPA^{2-} \rightarrow Eu(DO2A)(DPA)^{+}$	-24.8	76.3

Table 3.7. 'Ligand enhancement' in various lanthanide/analyte systems. Change in the analyte binding affinity (Δ log K)* due to the ligand in comparison to the lanthanide alone.

Ligand	Analyte	Δ log K	Ref
$DO2A^{2-}$	Dipicolinate	0.8 – 1.8	This work
$EDTA^{2-}$	Picolinate	0.2 – 1.5[†]	57, 58
L_1	Lactate	0.8 – 1.5[‡]	59, 60
L_2	Acetate	0.1 – 1.4[¥]	60, 61

*Δ log K = log K_a' – log K_a

[†] log K_a: 0.1 M KNO_3, 25 ℃; log K_a': 0.5 M $NaClO_4$, 25 ℃

[‡] log K_a: 0.1 M $NaClO_4$, 20 ℃; log K_a': 0.1 M collidine/HCl, 21.8 ℃, pH 7.4

[¥] log K_a: 0.1 M $NaClO_4$, 20 ℃; log K_a': 0.1 M collidine/HCl, 21.8 ℃, pH 7.4

L_1 = (*SSS*)-*1,4,7*-Tris[*1*-(*1*-phenyl)ethylcarbamoylmethyl]-*1,4,7,10*-tetraazacyclododecane, L_2 = (*SSS*)-*1,4,7*-Tris[*1*-(*1*-phenyl)ethylcarbamoylmethyl]-*10*-methyl-*1,4,7,10*-tetraazacyclo-dodecane

Table 3.8. Binding affinities for various Tb and Eu complexes for oxy-anions, pH 7.4–7.5, 295–298 K, showing the difference between the Tb and Eu species, Δ(Ln).

Ligand	Analyte	log K[†]		Δ(Ln)
		Tb	Eu	
DO2A	DPA	9.25	8.39	0.86
L_1	HCO_3^-	3.8	2.6	1.2
	$CH_3CO_2^-$	2.3	< 1.0	> 1.3
	HPO_4^{2-}	≥ 4.7	4.15	≥ 0.55
L_2	HCO_3^-	≥ 4.7	3.75	≥ 0.95
	$CH_3CO_2^-$	3.5	2.4	1.1
	HPO_4^{2-}	> 4.7	> 4.7	unknwn

[†] DPA values from this work, all others from reference 60 with errors ± 0.2

L_1 = (*SSS*)-*1,4,7*-Tris[*1*-(*1*-phenyl)ethylcarbamoylmethyl]-*1,4,7,10*-tetraazacyclododecane,
L_2 = (*SSS*)-*1,4,7*-Tris[*1*-(*1*-phenyl)ethylcarbamoylmethyl]-*10*-methyl-*1,4,7,10*-tetraazacyclo-dodecane

CHAPTER 4

Towards a Second-Generation Receptor Site for Bacterial Spore Detection

4.1 Introduction

To improve upon our first-generation receptor site, we have two general directions to pursue: (1) alter the architecture of the macrocyclic ligand to improve binding affinity for dipicolinate, at the risk of losing some of the advantages of the current ligand, or (2) modify the ligand slightly to append the complex to a solid substrate and improve the limit of detection for dipicolinate as opposed to the binding affinity. The first method, though seemingly straightforward, can be quite difficult to implement. We could predict through structural simulations, for example, that attaching phenyl moieties on the carboxyl arms of the DO2A ligand might enhance dipicolinate binding affinity through stabilization due to pi-stacking. However, such modifications to the DO2A ligand would most likely severely limit solubility of the complex and have a variety of other unexpected effects on properties. We therefore aim to retain the demonstrated advantages of the DO2A ligand and improve upon bacterial spore detection through attaching the dipicolinate sensing complex to a solid matrix. This strategy could resolve multiple issues regarding bacterial spore imaging and current limits of detection in environmental samples.

Appending the $Tb(DO2A)^{+}$ complex to polydimethylsiloxane (PDMS) could significantly improve our microscopic endospore viability assay (μEVA) developed to image bacterial spores. In this assay, endospores are inoculated onto wells of agarose doped with $TbCl_3$ and induced to germinate via the addition of either L- or D-alanine for aerobic or anaerobic spores, respectively. As the bacterial spores germinate and return to the normal vegetative cycle, their DPA is released and binds to the Tb^{3+} ions in the agarose. The resulting 'halos' of $Tb(DPA)_n$ complexes (n = 1–3) around each endospore

are visible using time-gated fluorescence microscopy.[1-3] In the current protocol, certain species of endospore are more easily observed than others. This is due to the fact that μEVA only images bacterial spores that are capable of germination, and the rate of germination varies significantly between spore species. Germination occurs when endospores are triggered to reenter the normal vegetative cell cycle, during which they release DPA into the environment. *Bacillus* spores germinate relatively quickly, on the order of minutes. *Clostridium* spores, however, exhibit germination profiles on the order of hours to even days.[4] For these slow germinating species, the rate of DPA diffusion begins to outcompete the rate of germination, and little or no signal results in μEVA. PDMS is used as a 'coverslip' in μEVA to slow drying of the agarose, limit DPA diffusion and improve image quality. However, we have yet to explore its potential to serve as a synthon upon which DPA binding receptor sites can be covalently bound. By appending the Tb-macrocycle complex to the PDMS, we may be able to significantly lengthen the residence time of DPA proximal to the endospore that released it, elongating our imaging window. Additionally, another problem encountered with μEVA involves the microscopy. The agarose surface on which the spores sit is often uneven due to multiple variables in its preparation, meaning that not all spores are present on the same focal plane, rendering an accurate enumeration in any single microscopic view impossible. But, if the DPA released from the germinating spores is effectively bound to a Tb-macrocycle complex that is itself covalently attached to the PDMS coverslip, the PDMS is the only surface necessary to image. The PDMS could be peeled off of the agarose following germination, placed on a flat surface and imaged separately, eliminating the problem of multiple focal planes.

Another mode of improvement via construction of a solid-state bacterial spore sensor lies in sample concentration to enhance the current limit of detection. If the terbium-macrocycle complex were covalently bound to the stationary phase of a column, such as silica or alumina, a dilute DPA solution could be readily concentrated. When applied to environmental samples this protocol would involve sample collection, DPA release via physical (heating, pressure) or chemical (germinant or lysozyme) means, and filtration to remove any cell debris or other material. The dilute DPA solution, buffered to pH 7–10, could then be passed through the column containing $Tb(DO2A)^{+}$ bound to the solid substrate. The high binding affinity of the terbium-macrocycle binary complex for DPA at this pH would cause the dipicolinate to be retained in the column. After saturation, the addition of a small aliquot of acidic solution (pH ~ 2) will protonate the macrocyclic ligand and release the $Tb(DPA)^{+}$ complex, which could then be quantified using fluorescence spectroscopy and correlated to the original filtrate volume to yield a value of spores per mL of solution. The column could then be treated with a $TbCl_3$ solution at neutral pH to reform the terbium-macrocycle complex in the solid phase for reuse. Current limits of detection of bacterial spores in environmental samples for spectroscopic techniques are in the 10^3–10^4 spores/mL range.[5-7] This technology could improve the current limit of detection of bacterial spores by several orders of magnitude.

We therefore explore a novel macrocyclic ligand DOAAM (*1,4,7,10*-tetraazacyclododecane-*1*-acetate-*7*-amide) bound to terbium as the next step in achieving this goal. We have chosen to replace one of the acetate pendant arms with an amide functional group, because the primary amide can be easily functionalized to append the ligand to a solid substrate without perturbing the hexadentate chelation motif to the

lanthanide (Figure 4.1). The neutral tetraamide derivative DOTAM (*1,4,7,10*-tetraazacyclododecane-*1,4,7,10*-tetraamide) is known to strongly bind lanthanides in the same configuration as DOTA, with coordination through the four ring nitrogen atoms and four amide oxygen atoms.[8, 9] However, binding affinity is approximately 10–15 orders of magnitude less than the DOTA ligand (Table 4.1),[10-13] presumably due to the lower basicity of the ring N-atoms and the loss of electrostatic attraction for the neutral amide ligands compared to the acetate groups. The absence of protonated intermediates in the complexation of lanthanides also distinguishes the DOTAM ligand from DOTA.[14] However, with modification of only one pendant arm, any loss in lanthanide chelation should be minimal and electrostatics should dominate the observed binding interactions.

We will fully characterize our second-generation $Tb(DOAAM)^{2+}$ dipicolinate receptor site in terms of photophysics, binding affinity and pH dependence. We will also discuss future techniques to anchor this complex in the process of constructing a solid-state sensor.

4.2 Photophysics and Structure

With the substitution of an amide for one of the DO2A acetate groups, the DOAAM ligand should still coordinate the lanthanide in a hexadentate fashion. Due to the oxophilic character of lanthanide binding and reported work with the DOTAM ligand, we anticipate binding via the oxygen of the amide with negligible change in symmetry of the lanthanide coordination sphere. The replacement of an OH with an NH-oscillator may increase the quantum yield of the Tb(DOAAM)(DPA) complex compared to its DO2A analogue.

4.2.1 Structural Characterization

We will attempt to crystallize the Tb(DOAAM)(DPA) ternary complex for complete characterization. If high quality crystals cannot be obtained, the complex will be characterized using elemental analysis and mass spectrometry.

Experimental Section

Materials. The following chemicals were purchased and used as received: acetone (J. T. Baker), acetonitrile (Fluka Biochemika), ammonium hydroxide (28.0–30.0% in water) (J. T. Baker), DPA (dipicolinic acid, pyridine-*2,6*-dicarboxylic acid) (Aldrich), ethyl alcohol (200-proof) (Acros Organics), hydrochloric acid (36.5–38.0% in water) (EMD Chemicals), isopropyl alcohol (*2*-propanol) (J. T. Baker), methanol (J. T. Baker), potassium carbonate anhydrous (Alfa Aesar), sodium carbonate anhydrous (Mallinckrodt), sodium hydroxide (NaOH 50% in water) (Mallinckrodt), terbium (III) chloride hexahydrate (Alfa Aesar) and tetrahydrofuran (THF) (EM Science). All lanthanide salts were 99.9% pure or greater, all solvents were ACS certified or HPLC grade, and all other salts were 99% pure or greater. The DOAAM ligand (*1,4,7,10*-tetraazacyclododecane-*1*-acetate-*7*-amide) was synthesized under contract by Macrocyclics (Ref. GKRD02-38-080121). See Appendix G for characterization. Water was deionized to a resistivity of 18.2 MΩ-cm using a Purelab® Ultra laboratory water purification system (Siemens Water Technologies, Warrendale, PA).

Methods. Crystallization attempts included use of various solvent systems (water, methanol, ethanol, isopropanol and THF), with different bases for pH adjustment (NaOH, NH_4OH). Extraction with hot solvent (water or isopropanol), freezing saturated

solvents, and various double-boiler combinations (acetone/ethanol, acetone/isopropanol) were also attempted. In the double-boiler method, a saturated solution containing the complex was placed in an open vial in a sealed container with another miscible solvent of high vapor pressure in which the complex is less soluble (acetone in this case). Slow diffusion of this solvent into the saturated solution should reduce the solubility of the complex and induce crystallization. However, this only led to precipitation for the Tb(DOAAM)(DPA) complex.

We also attempted phase separation with isopropanol and a saturated aqueous solution of Na_2CO_3, which causes the normally miscible solvents to separate and produced a solution of Tb(DOAAM)(DPA) in the isopropanol layer. This solution, when placed in a double-boiler with acetone, formed small filamentous crystals after three days that were luminescent under UV illumination. However, these were not of crystallographic quality and the method did not produce sufficient sample for characterization using elemental analysis or mass spectrometry. This was repeated with K_2CO_3 instead of Na_2CO_3, but only produced precipitation.

In a clean, kilned 30-mL beaker, 0.30791 g (0.830 mmol) of $TbCl_3 \cdot 6$and 0.24218 g (0.843 mmol) of DOAAM were combined in 2.0 mL of nanopure water (18.2 MΩ-cm resistivity) and sonicated to dissolve. The clear yellow solution was already near neutral (pH 6.5), so 0.13130 g (0.786 mmol) of DPA was added, along with 4.0 mL of nanopure water. The pH of the opaque white solution was adjusted to ~ 7 with a saturated Na_2CO_3 solution, added dropwise, while stirring with gentle heating (40 °C). Solution clarification was not observed. Following positive identification of the ternary complex via fluorescence spectroscopy (equilibration time of 2 days), the solution was lyophilized

using a MicroModulyo Freeze Dryer (Thermo Electron Corporation, Waltham, MA) to dryness (2 days). The solid was redissolved in ~ 7 mL of pure (200-proof) ethanol and filtered using a fine frit (Pyrex, 15mL, ASTM 4-5.5F) into a new scintillation vial (rinsed 2 times with ethanol and 2 times with filtered ethanol to remove any particulates). This vial, with cap cracked open slightly, was placed in a double-boiler with acetone in the outer container. Precipitation of a white solid from the clear, colorless solution was observed after 1.5 hours. The ethanol was decanted and the solid lyophilized to dryness. The resulting white powdery precipitate was characterized using elemental analysis and mass spectrometry.

Elemental analysis and mass spectrometry were performed by Desert Analytics Transwest Geochem and the Caltech mass spectrometer facility, respectively, as previously described (Section 2.2.1).

Results and Discussion

Despite many attempts to crystallize the ternary complex using a plethora of solvent systems and techniques, no high quality crystals could be obtained, possibly due to the lack of a counterion for the neutral Tb(DOAAM)(DPA) complex. Regardless, the pure compound was obtained as a precipitate (0.15661 g, yield: 21.3%), and positively identified via elemental analysis and mass spectrometry. Anal. Calcd (found) in duplicate for $TbC_{19}H_{27}N_6O_7 \cdot 2.8NH_4 \cdot 1.0CO_3 \cdot 3.2C_2H_6O \cdot 1.6Cl \cdot 0.5OH$ (fw = 934.65): C, 33.90 (33.90); H, 6.27 (5.07); N, 13.25 (13.30); Tb, 17.00 (16.97); Cl, 6.20 (6.20). ESI-MS (*m/z*): calcd (found) for $TbC_{19}H_{28}N_6O_7$ (M + H) 611.4 (611.1).

4.2.2 Spectroscopy

We will explore the absorbance, excitation and emission spectra of the Tb(DOAAM)(DPA) complex to determine if the structural modification has altered binding geometry or spectroscopic response. If the DOAAM ligand is coordinating to the lanthanide in a different fashion than the DO2A ligand, such as via the amide nitrogen as opposed to the oxygen, this will significantly alter the symmetry of the lanthanide coordination sphere and should therefore result in unique fine structure in the emission spectrum (Section 2.3.1). Similarly, any changes in the chelation mode or distance of the dipicolinate ligand should be evident in a shift of the excitation spectrum, as previously seen for the F-DPA and Pic ligands (Section 3.3).

Experimental Section

Materials. MOPS (*3*-(*N*-morpholino)ethanesulfonic acid) buffer (Alfa Aesar) was purchased and used as received. Dried, fully characterized TBA·Tb(DO2A)(DPA) crystals (Section 2.2.1) or Tb(DOAAM)(DPA) precipitate were used to generate a 1:1:1 ratio of Tb/macrocycle/dipicolinate in solution. Water was deionized to a resistivity of 18.2 MΩ-cm using a Purelab® Ultra laboratory water purification system.

Methods. Solutions of 10.0 μM Tb(DO2A)(DPA)$^-$ and Tb(DOAAM)(DPA) were prepared in 0.1 M MOPS buffer (pH 7.3) in triplicate in disposable acrylate cuvettes (Specrocell, Oreland, PA) with a 1 cm path length and allowed to equilibrate for 24 hours. Luminescence spectral analysis was performed by a Fluorolog Fluorescence Spectrometer (Horiba Jobin-Yvon, Edison, NJ) at 25 °C. To prevent second-order diffraction of the source radiation, all measurements were taken with a 350-nm colorless

sharp cutoff glass filter (03 FCG 055, Melles Griot, Covina, CA). The solution pH was measured using a calibrated handheld pH/mV/temperature meter (Model IQ150, I. Q. Scientific Instruments, Loveland, CO) following data collection. All reported spectra were obtained as a ratio of corrected signal to corrected reference (S_c/R_c) to eliminate the effect of varying background radiation in the sample chamber; intensities are in units of counts per second per microampere (cps/μA).

Results and Discussion

The normalized excitation and emission spectra of the Tb(DOAAM)(DPA) complex are identical to that of the Tb(DO2A)(DPA)$^-$ complex (Figures 4.2 and 4.3), indicating that the symmetry and composition of the lanthanide coordination sphere is unaffected by the acetate/amide substitution. This strongly suggests that the amide moiety is coordinating via the oxygen as opposed to the nitrogen, and that the arrangement around the terbium cation remains in a slightly distorted capped staggered square bipyramidal conformation (Section 2.2.2). The intensity of the emission spectrum for the Tb(DOAAM)(DPA) complex is also nearly twofold greater than that of the Tb(DO2A)(DPA)$^-$ complex; this will be addressed in the next section (vide infra).

4.2.3 Quantum Yield

As described in Section 2.3.2, we define luminescence quantum yield (Φ_L) as the ratio of photons absorbed by the chromophore to photons emitted through luminescence from the lanthanide following energy transfer. We will measure the luminescence quantum yield of Tb(DOAAM)(DPA) with respect to the L-tryptophan standard used

previously, and compare this value to that of the DO2A complex. As mentioned in Chapter 1, OH oscillators are the greatest quenchers of lanthanide luminescence; replacement of an OH oscillator with an NH group should therefore reduce quenching and result in enhanced quantum yield for the DOAAM complex.

Experimental Section

Materials. Tris buffer (tris-[hydroxymethyl]aminomethane) (MP Biomedicals, LLC) and L-tryptophan (Alfa Aesar) were purchased and used as received. Dried, fully characterized Tb(DOAAM)(DPA) precipitate was used to generate a 1:1:1 ratio of Tb/macrocycle/dipicolinate in solution. Water was deionized to a resistivity of 18.2 MΩ-cm using a Purelab® Ultra laboratory water purification system.

Methods. Five concentrations ranging from 5.0 to 15.0 μM were prepared for the Tb(DOAAM)(DPA) complex in 0.1 M Tris buffer (pH 7.9) and the L-Trp standard in nanopure water (pH 4.5). Absorbance and luminescence measurements were made in quartz cuvettes (1 cm path length) using a Cary 50 Bio UV/Visible Spectrophotometer (Varian, Inc., Palo Alto, CA), and a Fluorolog-3 Fluorescence Spectrometer (λ_{ex} = 280 nm). Absorbance measurements were zeroed to an empty quartz cuvette in the sample chamber; quartz cuvettes containing solvent only were run in triplicate as a control, so no baseline correction was performed. All recorded absorbances were under 0.1 and all luminescence intensities were below 5 x 10^5 cps, well within the linear range of both instruments. Quartz cuvettes were cleaned using a nitric acid (50% in nanopure water) digest and rinsed thoroughly with nanopure water between samples. No background fluorescence was observed for the solvents used. The quantum yield was calculated

using equation 2.1 as described previously (Section 2.3.2) with L-tryptophan in nanopure water as the standard (Φ_{ref} = 0.13 ± 0.01).[15] The molar extinction coefficient was calculated by plotting absorbance against concentration (Figure 4.4).

Results and Discussion

The molar extinction coefficient for the Tb(DOAAM)(DPA) complex is 2902 ± 94 $M^{-1}cm^{-1}$, in the same range of the Tb(DO2A)$(DPA)^-$ complex (2259 ± 10 $M^{-1}cm^{-1}$) and the dipicolinate ligand (2832 ± 21 $M^{-1}cm^{-1}$) as would be expected. The calculated molar extinction coefficient of the tryptophan standard (ε_{Exp} = 5494 $M^{-1}cm^{-1}$) was within 1% of the reported value (ε_{Exp} = 5502 $M^{-1}cm^{-1}$).

The luminescent quantum yield of the Tb(DOAAM)(DPA) complex is nearly twice as large as that of the Tb(DO2A)$(DPA)^-$ complex (Table 4.2). As these complexes have the same chromophore and lanthanide, and therefore the energy gap between the chromophore triplet and the lanthanide excited state is unchanged, we attribute this increase to a reduction in quenching. According to the superimposable emission spectra, the terbium coordination sphere is identical in terms of symmetry and composition; the quenching must therefore be an outer-sphere effect, most likely due to the acetate/amide substitution. Even though the change from OH to NH in this substitution is not in the inner-coordination sphere, the reduction in quenching is still substantial, confirming the strong influence of outer-sphere effects on lanthanide photophysics.[16, 17]

4.3 Binding Studies

The replacement of a negatively charged acetate by a neutral amide in the DOAAM ligand increases the overall charge of the binary complex from $Tb(DO2A)^{+}$ to $Tb(DOAAM)^{2+}$ at neutral pH. Due to the increase in electropositive charge for the receptor site, we might anticipate a greater electrostatic attraction for the DPA^{2-} analyte and therefore an increase in dipicolinate binding affinity. However, previous investigations have shown that 'ligand enhancement' of lanthanide-analyte binding affinity can often be independent of the net electrostatics of the system, and may depend more on changes in the local environment of the binding site in the lanthanide coordination sphere (Section 3.7). Spectroscopic studies suggest that the DOAAM ligand chelates to the lanthanide in the same fashion as DO2A, with presumably the same 'footprint' and leaving a binding cavity of similar size and shape. If these assumptions are valid, the local electrostatics in the binding site should be similar in both cases, and if this is indeed the dominant factor in dipicolinate coordination, the binding affinity may not change significantly.

4.3.1 Jobs Plots

A method of continuous variations was applied to determine the binding stoichiometry of dipicolinate to the $Tb(DOAAM)^{2+}$ binary complex. The replacement of an acetate arm by an amide may destabilize the $Tb(DOAAM)^{2+}$ binary complex, but as the ligand is hexadentate we still anticipate a 1:1 binding ratio of binary complex to dipicolinate.

Experimental Section

Materials. The following chemicals were purchased and used as received: DPA (dipicolinic acid, pyridine-*2,6,*-dicarboxylic acid) (Aldrich), sodium acetate trihydrate (Mallinckrodt) and terbium(III) chloride hexahydrate (Alfa Aesar). All lanthanide salts were 99.9% pure or greater and all other salts were 98% pure or greater. The DOAAM ligand was synthesized by Macrocyclics (Section 4.2.1). Water was deionized to a resistivity of 18.2 MΩ-cm using a Purelab® Ultra laboratory water purification system.

Methods. All samples were prepared in triplicate from stock solutions to a final volume of 3.50 mL in disposable acrylate cuvettes (Spectrocell, Oreland, PA) with a 1 cm path length and were allowed to equilibrate for at least 6 days prior to analysis. The concentrations of $TbCl_3$ and DPA were varied inversely in 1.0-μM increments from 0 to 12.0 μM with 100 μM DOAAM in 0.2 M NaOAc, pH 7.4.

Luminescence spectral analysis was performed by a Fluorolog Fluorescence Spectrometer with a 350-nm cutoff filter as previously described (Section 4.2.2). The solution pH was measured using a calibrated handheld IQ150 pH/mV/temperature meter (I. Q. Scientific Instruments) following data collection.

Results and Discussion

According to the Jobs plot (Figure 4.5), the optimal binding stoichiometry for DPA to $Tb(DOAAM)^{2+}$ occurs at a terbium mole fraction of approximately 0.5, meaning a one-to-one correlation. However, the flattened appearance of the plot indicates low to moderate stability of the complex,[18] especially at high DPA concentrations. This is consistent with reports of lower stability constants for amide-substituted macrocylic

ligands compared to their acetate analogs.[10, 11] Though the stability of the complex appears to have diminished, we still see linearity in the range of high terbium mole fraction, meaning the $Tb(DOAAM)^{2+}$ complex can bind dipicolinate effectively when in excess.

4.3.2 Calculation of Dipicolinate Association Constant

Though the Tb(DOAAM)(DPA) complex could not be successfully crystallized, we were able to fully characterize a solid precipitate of this complex. As this solid is consistent in terms of its Tb/DOAAM/DPA ratio, we can still perform the binding affinity by competition (BAC) assay to determine the DPA to binary complex binding constant.

Experimental Section

Materials. Terbium(III) chloride hexahydrate (Alfa Aesar) was purchased and used as received. All lanthanide salts were 99.9% pure or greater and all other salts were 97% pure or greater. Dried, fully characterized Tb(DOAAM)(DPA) precipitate was used to produce a 1:1:1 ratio of Ln:DO2A:DPA in solution. Water was deionized to a resistivity of 18.2 MΩ-cm using a Purelab® Ultra laboratory water purification system.

Methods. All samples were prepared to a final volume of 3.50 mL from stock solutions in disposable acrylate cuvettes (Spectrocell) with a 1 cm path length and were allowed to equilibrate for 5 days. Luminescence spectral analysis was performed by a Fluorolog Fluorescence Spectrometer with a 350-nm cutoff filter as previously described (Section 4.2.2). The solution pH was measured using a calibrated handheld IQ150

pH/mV/temperature meter (I. Q. Scientific Instruments) following data collection. Sample temperature was monitored using a handheld Fluke 62 Mini Infrared Thermometer (Fluke Corp, Everett, WA).

Samples were prepared using solvated Tb(DOAAM)(DPA) precipitate and terbium chloride in 0.2 M sodium acetate (pH 7.4), such that the concentration of Tb(DOAAM)(DPA) was 1.0 μM and the concentration of free Tb^{3+} ranged from 1.0 nM to 1.0 mM. As Tb^{3+} was added, the shift in equilibrium Tb(DOAAM)(DPA) and $Tb(DPA)^{+}$ concentrations was monitored via a ligand field sensitive transition in the emission spectrum using luminescence spectroscopy. Emission spectra (λ_{ex} = 278 nm) were integrated over the most ligand-field sensitive peak ($^5D_4 \rightarrow {}^7F_4$, 570–600 nm) to produce a curve of observed integrated intensity (I_{obs}) against the log of excess free lanthanide (log $[Ln^{3+}]_{xs}$). A best fit to a two-state thermodynamic model using the Curve Fitting Tool in Matlab® yielded the competition equilibrium constant (K_c) and dipicolinate affinity constant (K_a') as described previously (Section 3.2.2).

Results and Discussion

Despite the fact that no crystals could be obtained for the Tb(DOAAM)(DPA) complex, the competition assay using the characterized precipitate still produced a curve that could be fit using the two-state thermodynamic model (Figure 4.6). The use of the precipitate as opposed to crystals for the Tb(DOAAM)(DPA) complex demonstrates the power and versatility of the BAC assay. As long as a 1:1:1 ratio of the three components can be obtained, whether via high quality crystals or a fully characterized precipitate, the method can be applied and will produce a binding constant with acceptable error.

The binding affinity for dipicolinate decreases slightly from the $Tb(DO2A)^{+}$ complex to the $Tb(DOAAM)^{2+}$ complex (Table 4.3), despite the increase in electrostatic attraction between the complex and the DPA^{2-} dianion. This is most likely due to (1) the replacement of the acetate arm with an amide group, which is not as electronegative and not as capable of perturbing the electron density of the Tb^{3+} ion, and (2) decreased stability of the complex, as evidenced by the nonlinear Jobs plot and previous studies with similar amide-substituted macrocyclic ligands. The negligible change in dipicolinate binding affinity despite an increase in binary complex charge is consistent with our hypothesis that net electrostatics do not dominate in these systems involving 'ligand enhancement'. Instead, the ability of the ligand to shift the electron density of the lanthanide cation, thereby generating a binding cavity with more local electropositive charge, might be a better explanation. We see an improvement in dipicolinate binding affinity over the Tb^{3+} ion alone, but the less-electronegative amide group of the DOAAM ligand is not as effective at perturbing the electron density of the lanthanide as the dual-acetate arms of the DO2A ligand. Hence, binding studies with the DOAAM ligand support the theory of 'ligand enhancement' due to ligand-induced perturbation of lanthanide electron density, and confirm that the correct choice of helper ligand is significant in order to maximize analyte binding affinity.

4.4 pH Dependence

The stability of the Tb(DOAAM)(DPA) complex in terms of pH variations will be determined and compared to the $Tb(DO2A)(DPA)^{-}$ complex. The acetate/amide substitution of the macrocyclic ligand will invariably shift the pK_a of that chelating arm

substantially. However, as primary amides tend to resist deprotonation and only form weak conjugate acids, this substituent will most likely remain neutral over the pH range of interest and therefore the relative stability of the complex should remain constant.

Experimental Section

Materials. The following chemicals were purchased and used as received: CAPS (I-cyclohexyl-*3*-aminopropanesulfonic acid) buffer (Alfa Aesar), CHES (*N*-cyclohexyl-*2*-aminoethanesulfonic acid) buffer (Alfa Aesar), MES monohydrate (*2*-(*N*-morpholino)ethanesulfonic acid monohydrate) buffer (Alfa Aesar), MOPS (*3*-(*N*-morpholino)-propanesulfonic acid) buffer (Alfa Aesar), sodium hydroxide (NaOH 50% in water) (Mallinckrodt) and TAPS (*N*-tris(hydroxymethyl)methyl-*3*-aminopropane-sulfonic acid) buffer (TCI America). All salts were 99% pure or greater, and all buffers were at least 98% pure. Dried, fully characterized TBA·Tb(DO2A)(DPA) crystals (Section 2.2.1) or Tb(DOAAM)(DPA) precipitate were used to generate a 1:1:1 ratio of Tb/macrocycle/dipicolinate in solution. Water was deionized to a resistivity of 18.2 MΩ-cm using a Purelab® Ultra laboratory water purification system.

Methods. Samples of 10.0 μM pre-equilibrated $Tb(DO2A)(DPA)^-$ or Tb(DOAAM)(DPA) were prepared in 0.1 M buffer. Five buffers were used: MES (pK_a = 6.1), MOPS (pK_a = 7.2), TAPS (pK_a = 8.4), CHES (pK_a = 9.3) and CAPS (pK_a = 10.4), with pH adjustment to within 0.1 of the pK_a value using 50% NaOH added dropwise. Emission spectra were obtained after an equilibration time of 21 hours.

Results and Discussion

The pH dependence study suggests that the DOAAM ligand behaves in a similar manner to the DO2A ligand in terms of retaining the lanthanide in solution and preventing precipitation of the hydroxide species in alkaline conditions. This is interesting, as previous studies indicate a severe loss in lanthanide chelation when the acetate arms of the macrocycle are substituted for amide moieties. Apparently the stability of the complex is still great enough to resist changes in pH over a range from 6.1 to 10.4, meaning the correlation between luminescence intensity and dipicolinate concentration is maintained.

4.5 Conclusions

Binding studies of the $Tb(DOAAM)^{2+}$ and $Tb(DO2A)^{+}$ complexes indicate that substitution of an amide group for an acetate arm in the macrocyclic ligand destabilizes the binary complex and reduces affinity slightly for dipicolinate, despite the increase in electropositive charge of the complex. However, this decrease in stability is not evident in the pH dependence of the Tb(DOAAM)(DPA) complex, most likely due to the ternary complex maintaining a constant neutral state over the pH range studied.

The minor change in dipicolinate binding constant despite a difference in charge for the two terbium(macrocycle) complexes studied supports the interesting theory that net electrostatic attractions do not dominate in systems involving ‘ligand enhancement’. Instead, the localized electrostatic charge of the binding site, generated by the ability of the helper ligand to perturb the electron density of the lanthanide, may play the defining role. Electron withdrawing effects of the helper ligand generate an increased positive

charge at the dipicolinate binding site, the magnitude of which is governed by the polarizability of the lanthanide and the number and arrangement of O and N moieties on the ligand. By replacement of an acetate with a less electronegative amide group, we have decreased the ability of the ligand to perturb the electron density of the lanthanide, resulting in a decrease in analyte binding affinity. However, further work involving binding affinities of lanthanide(macrocycle) complexes for other aromatic anions (picolinate, isophthalate, *2,2'*-bipyridine, etc.) using various macrocyclic ligands of different charge and denticity should be explored.

With the replacement of an acetate arm on the macrocyclic ligand with an amide, we have maintained a nanomolar detection sensitivity for dipicolinate while nearly doubling the luminescence quantum yield. Studies also indicate that amide-substituted macrocyclic ligands, when bound to lanthanides, produce kinetically inert complexes with respect to acid-catalyzed dissocation,[13] meaning this complex could function as a robust in situ sensor. Though the DOAAM ligand appears to produce a less stable complex than DO2A, the increased quantum yield coupled to functionality of tethering this complex to a solid substrate makes $Tb(DOAAM)^{2+}$ a suitable second-generation dipicolinate receptor and puts us one step closer to reaching the ideal receptor site for bacterial spore detection (Figure 4.8).

The next step in the enhancement of bacterial spore detection is to covalently attach the $Tb(DOAAM)^{2+}$ complex to a solid substrate. As previously discussed, if this substrate is flexible and UV light-permeable, such as PDMS, we could use the Tb(DOAAM)-functionalized surface to improve the microscopic endospore viability assay. Appending the $Tb(DOAAM)^{2+}$ complex to silica or alumina could also improve

the limit of detection of bacterial spores through concentration of environmental samples. In both cases, attachment to the substrate surface would most likely involve click chemistry or similar techniques, such as a Michael addition of a thiol-functionalized macrocycle to a vinyl-sulfone derivatized surface.[19-22] Macrocyclic ligands such as DOTA and DO2A have been conjugated to various target vectors and supramolecular architectures such as lipids, dendrimers and amino acids via similar methods.[23-26] With the high stability and robust quality of these lanthanide-macrocycle binary complexes, we believe the resulting dipicolinate-binding surfaces will significantly improve bacterial spore detection technologies.

REFERENCES

(1) Yung, P. T.; Ponce, A. *Applied and Environmental Microbiology* **2008**, *74*, 7669-7674.
(2) Yung, P. T.; Kempf, M. J.; Ponce, A. *IEEE Aerospace Conference* **2006**, 1-13.
(3) Yang, W.-W.; Ponce, A. *International Journal of Food Microbiology* **2009**, *133*, 213-216.
(4) Yang, W.-W., California Institute of Technology, Pasadena, 2009.
(5) Hindle, A. A.; Hall, E. A. H. *Analyst* **1999**, *124*, 1599-1604.
(6) Pellegrino, P. M.; Fell, N. F.; Rosen, D. L.; Gillespie, J. B. *Analytical Chemistry* **1998**, *70*, 1755-1760.
(7) Cable, M. L.; Kirby, J. P.; Sorasaenee, K.; Gray, H. B.; Ponce, A. *J. Am. Chem. Soc.* **2007**, *129*, 1474-1475.
(8) Amin, S.; Morrow, J. R.; Lake, C. H.; Churchill, M. R. *Angewandte Chemie-International Edition* **1994**, *33*, 773-775.
(9) Amin, S.; Voss, D. A.; Horrocks Jr., W. D.; Lake, C. H.; Churchill, M. R.; Morrow, J. R. *Inorganic Chemistry* **1995**, *34*, 3294-3300.
(10) Voss, D. A.; Farquhar, E. R.; Horrocks Jr., W. D.; Morrow, J. R. *Inorganica Chimica Acta* **2004**, *357*, 859-863.
(11) Baranyai, Z.; Brücher, E.; Iványi, T.; Király, R.; Lázár, I.; Zékány, L. *Helvetica Chimica Acta* **2005**, *88*, 604-617.
(12) Chang, C. A.; Chen, Y.-H.; Chen, H.-Y.; Shieh, F.-K. *Journal Of The Chemical Society-Dalton Transactions* **1998**, 3243-3248.
(13) Pasha, A.; Tircsó, G.; Benyó, E. T.; Brücher, E.; Sherry, A. D. *European Journal Of Inorganic Chemistry* **2007**, *27*, 4340-4349.
(14) Baranyai, Z.; Bányai, I.; Brücher, E.; Király, R.; Terreno, E. *European Journal Of Inorganic Chemistry* **2007**, *2007*, 3639-3645.
(15) Chen, R. F. *Analytical Letters* **1967**, *1*, 35 - 42.
(16) Breen, P. J.; Horrocks Jr., W. D. *Inorganic Chemistry* **1983**, *22*, 536-540.
(17) Kimura, T.; Kato, Y. *Journal Of Alloys And Compounds* **1998**, *278*, 92-97.
(18) Gil, V. M. S.; Oliveira, N. C. *Journal of Chemical Education* **1990**, *67*, 473-478.
(19) Voivodov, K. I.; Ching, J.; Hutchens, T. W. *Tetrahedron Letters* **1996**, *37*, 5669-5672.
(20) Strother, T.; Hamers, R. J.; Smith, L. M. *Nucleic Acids Research* **2000**, *28*, 3535-3541.
(21) Wang, H.; Fang, Y.; Cui, Y.; Hu, D.; Gao, G. *Materials Chemistry and Physics* **2002**, *77*, 185-191.
(22) Nandivada, H.; Jiang, X.; Lahann, J. *Advanced Materials* **2007**, *19*, 2197-2208.
(23) Parker, D. *Chemical Society Reviews* **1990**, *19*, 271-291.
(24) Bottrill, M.; Kwok, L.; Long, N. J. *Chemical Society Reviews* **2006**, *35*, 557-571.
(25) Burchardt, C.; Riss, P. J.; Zoller, F.; Maschauer, S.; Prante, O.; Kuwert, T.; Roesch, F. *Bioorganic & Medicinal Chemistry Letters* **2009**, *19*, 3498-3501.
(26) Caravan, P. *Chemical Society Reviews* **2006**, *35*, 512-523.

FIGURES

DO2A

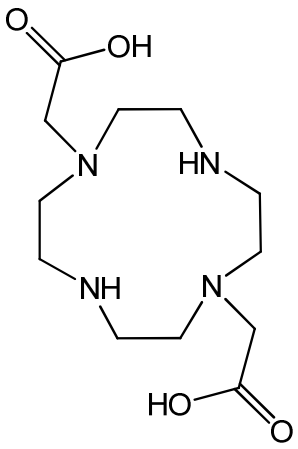

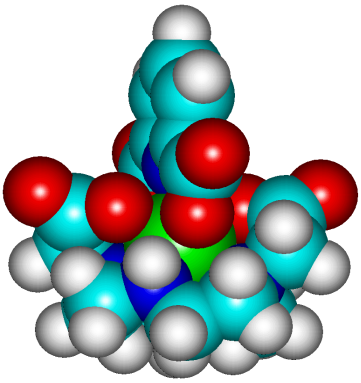

DOAAM

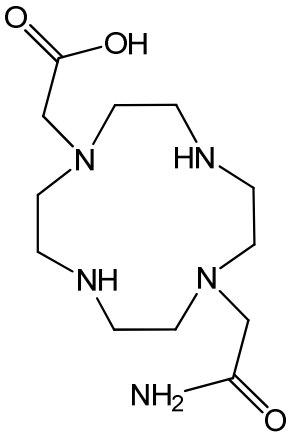

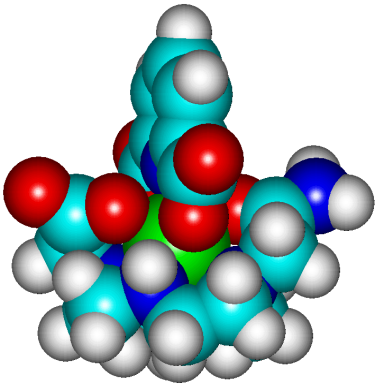

Figure 4.1. Structures of the DO2A and DOAAM macrocyclic ligands, with space-filling models of the Tb(ligand)(dipicolinate) ternary complexes.

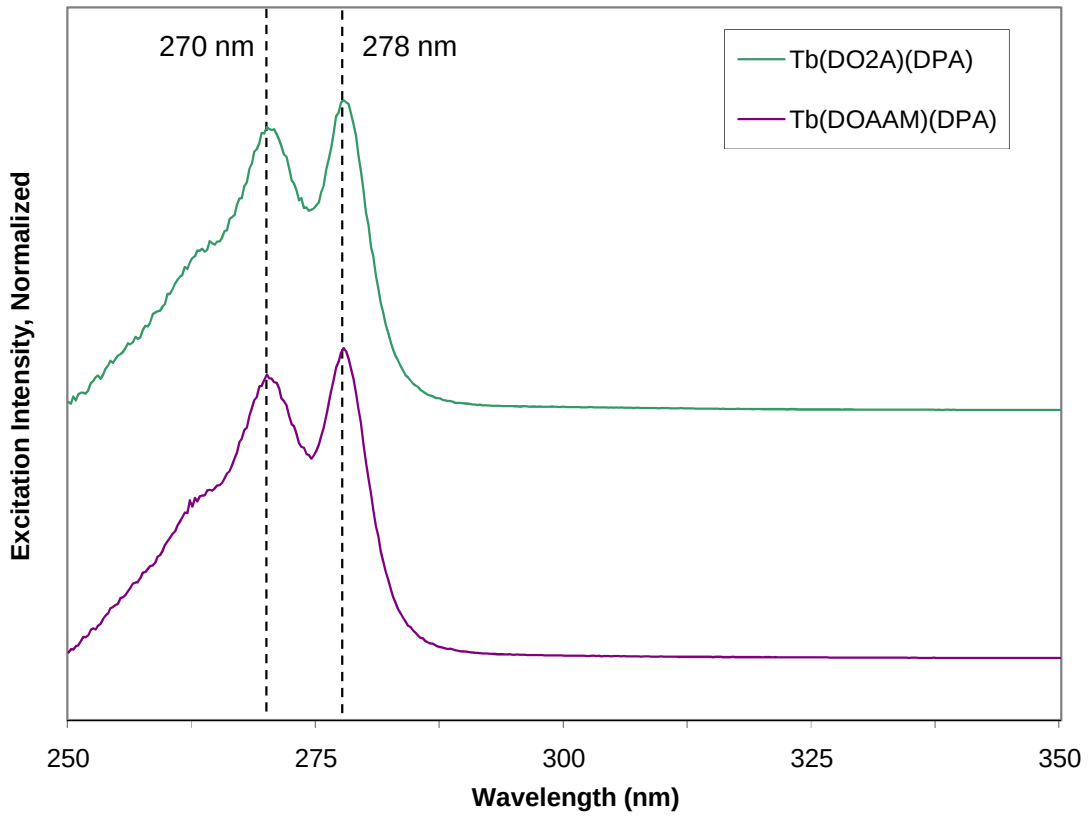

Figure 4.2. Excitation spectra of terbium dipicolinate ternary complexes with DO2A (green) and DOAAM (purple), 10.0 μM in 0.1 M MOPS buffer (pH 7.3). The normalized spectra are perfectly superimposable. Relevant transitions are identified with vertical dotted lines (black).

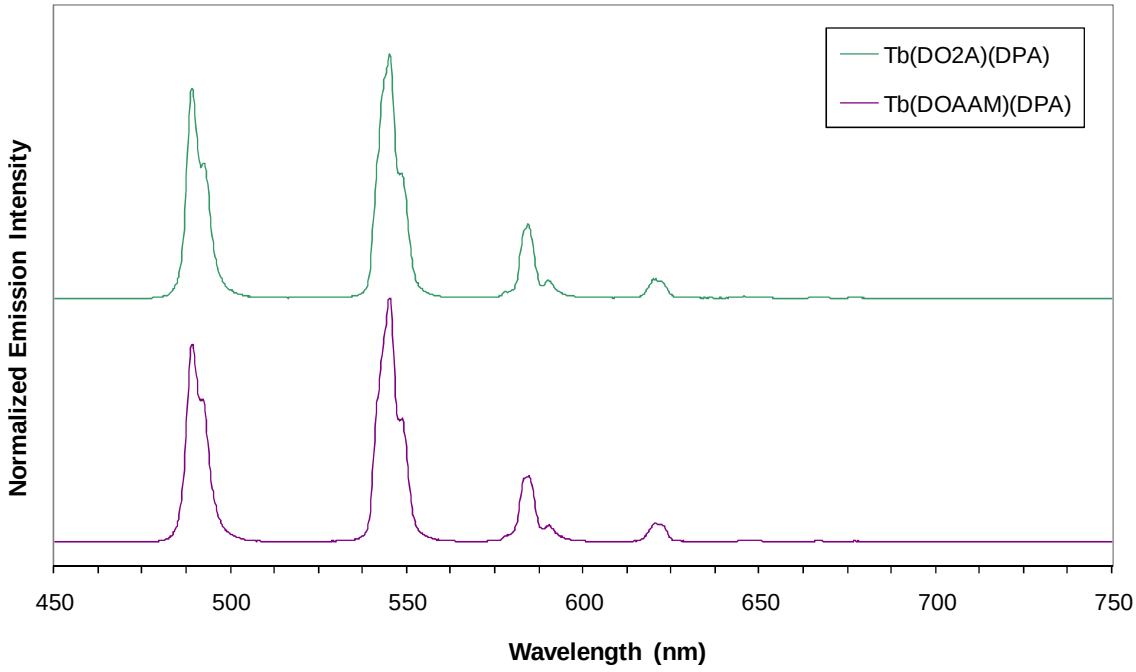

Figure 4.3. Emission spectra of terbium dipicolinate ternary complexes with DO2A (green) and DOAAM (purple), 10.0 μM in 0.1 M MOPS buffer (pH 7.3). The identical splitting indicates that the Tb^{3+} is in a similar coordination environment in both complexes.

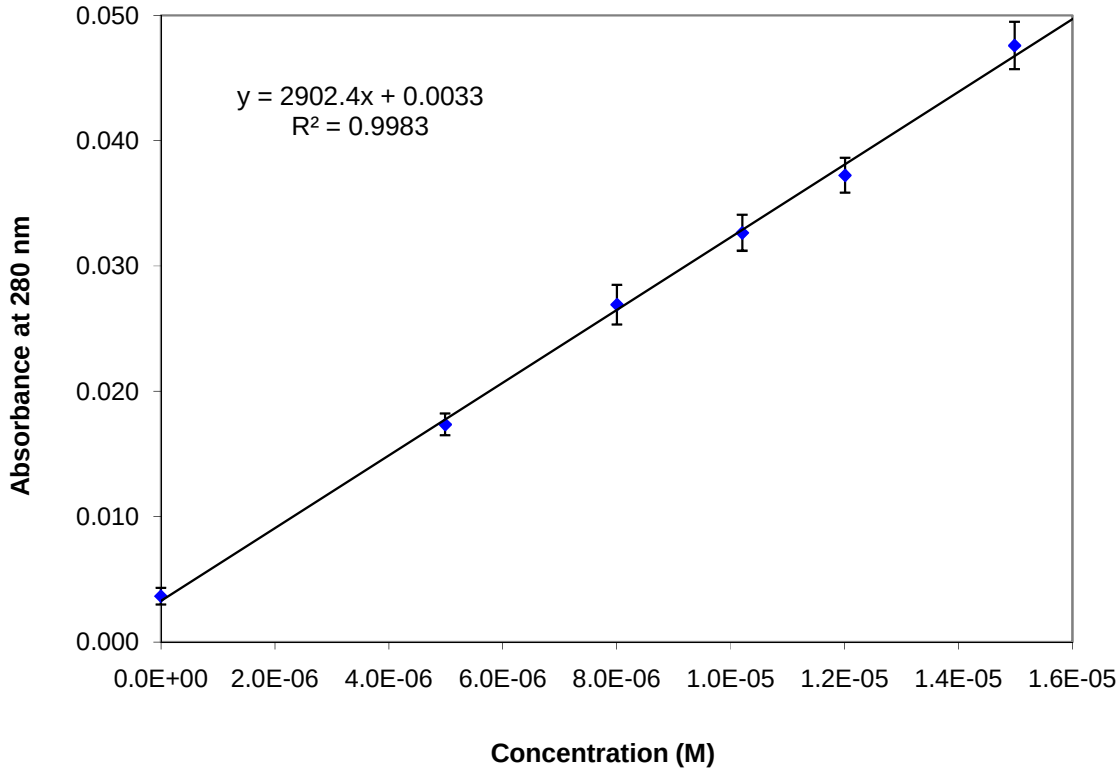

Figure 4.4. Linear fit of absorbance (λ_{abs} = 280 nm) versus concentration for the Tb(DOAAM)(DPA) complex in 0.1 M Tris buffer, pH 7.9, 25 ℃.

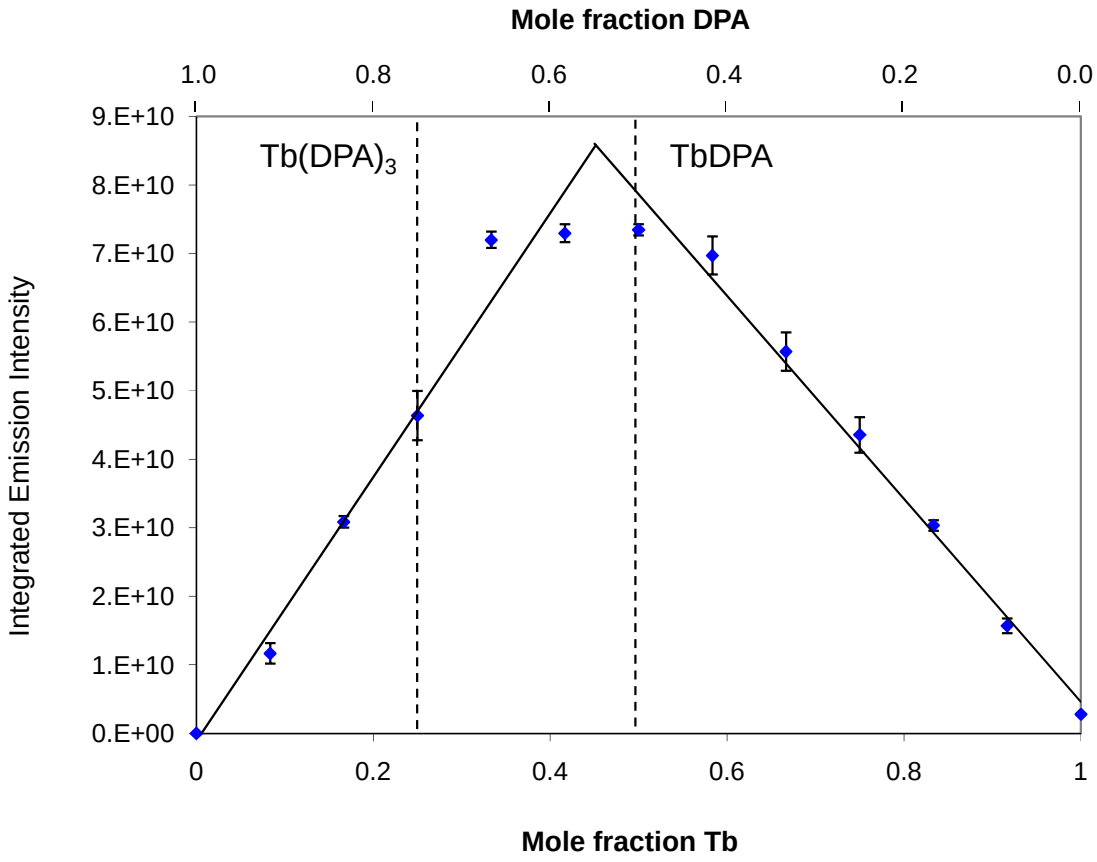

Figure 4.5. Jobs plot of Tb(DOAAM)(DPA) in 0.2 M NaOAc, pH 7.4. The concentrations of Tb and DPA are varied inversely from 0 to 12 μM in 1 μM increments, with the macrocyclic ligand in excess (100 μM). λ_{ex} = 278 nm, emission integrated from 570–600 nm. Linear regions are fitted with trendlines, and significant Tb:DPA ratios are noted by dashed lines.

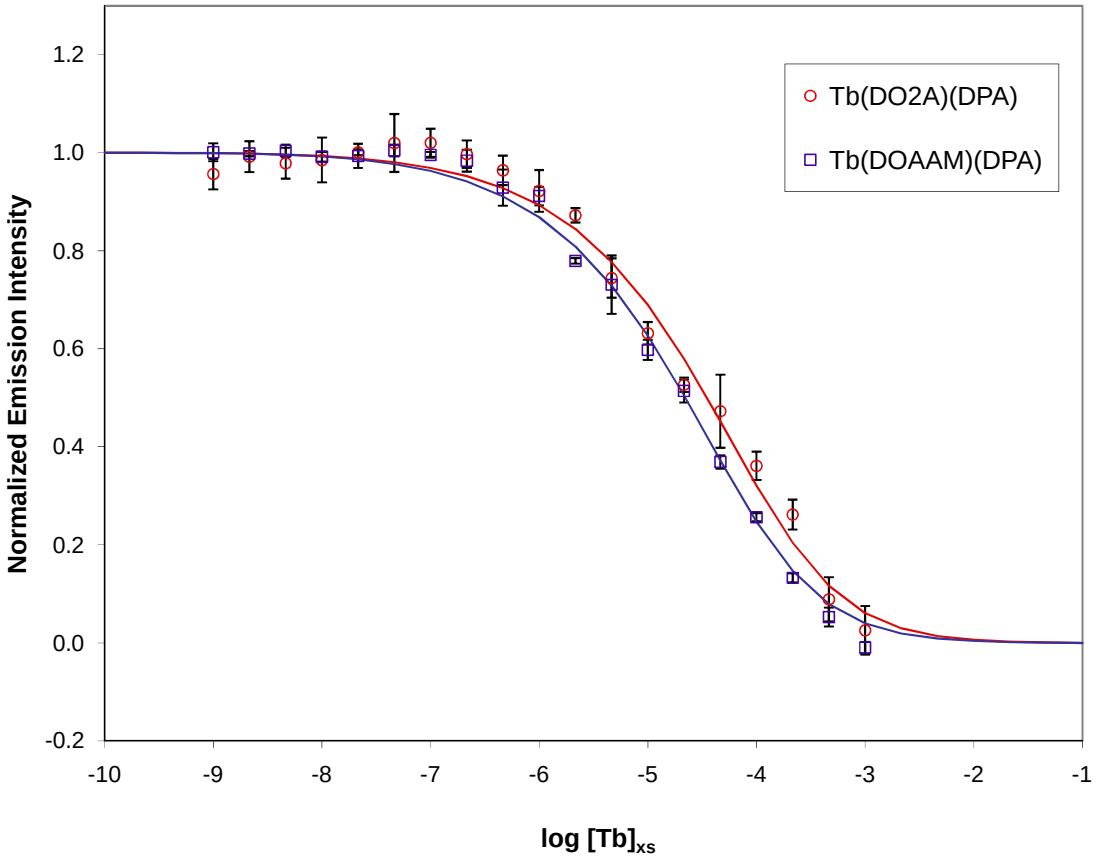

Figure 4.6. Lanthanide competition experiment for Tb(DO2A)(DPA)$^{-}$ and Tb(DOAAM)(DPA). Binding affinity by competition (BAC) assay titration curves in 0.2 M NaOAc, pH 7.5, 25 ℃. λ_{ex} = 278 nm, emission intensity integrated over 570–600 nm.

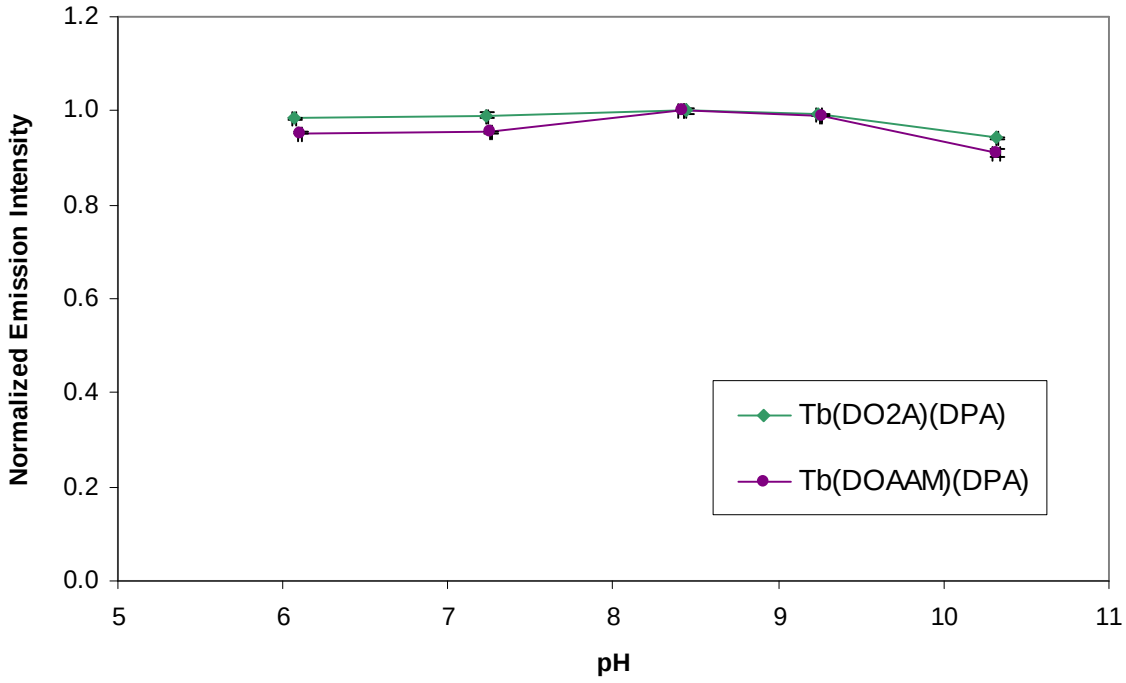

Figure 4.7. pH dependence study of Tb(DO2A)(DPA)$^{-}$ and Tb(DOAAM)(DPA) in 0.1 M buffer, 25 ℃. Emission integrated from 530–560 nm and nor malized to maximum value. (λ_{ex} = 278 nm)

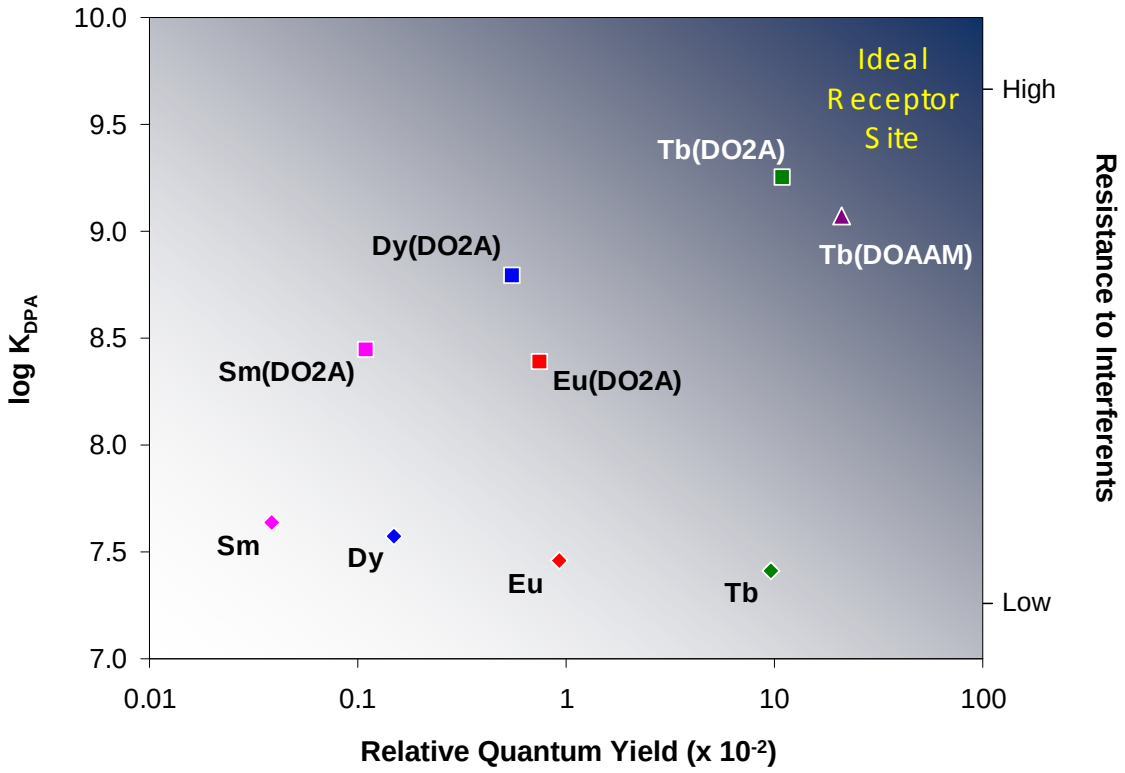

Figure 4.8. Graphic depicting our current improvements of a DPA receptor site in terms of DPA binding affinity (log K_{DPA}), relative quantum yield, and resistance to interferents. The use of Tb along with the DO2A and DOAAM ligands has allowed us to move closer towards development of an ideal receptor site.

TABLES

Table 4.1. Stability constants of various lanthanide macrocycle complexes.

Ln^{3+}	DOTA[†]	DOTAM[‡]
Eu	23.5	13.8
Gd	24.7	13.1
Dy	24.2	13.6

[†] Reference 12; [‡] Reference 13

Table 4.2. Luminescence quantum yield data, 0.1 M Tris buffer, L-Trp standard.

Complex	Temp (℃)	pH	Φ_L (x 10^{-3})
Tb(DO2A)(DPA)$^-$	24.8 ± 0.2	7.93 ± 0.01	110 ± 2
Tb(DOAAM)(DPA)	24.5 ± 0.3	7.92 ± 0.20	210 ± 7

Table 4.3. Calculated association constants (K_a') for terbium macrocycle complexes with dipicolinate in 0.2 M NaOAc.

Ligand	Temp (℃)	pH	log K_a'
DO2A	25.0 ± 0.2	7.36 ± 0.09	9.25 ± 0.13
DOAAM	24.8 ± 0.4	7.52 ± 0.06	9.07 ± 0.02

CHAPTER 5

Lanthanide-Macrocycle Complexes and the Targeted Detection of Other Analytes

5.1 Introduction

Now that we have effectively demonstrated the advantages of using tailored lanthanide(macrocycle) binary complexes as highly specific, robust receptor sites, we plan to expand this receptor site design technology and apply it to the detection of other aromatic analytes. As described in Chapter 1, virtually any aromatic anion can be detected using sensitized lanthanide luminescence, provided that (1) the aryl anion can coordinate the lanthanide cation, and (2) the triplet state of the anion is well coupled to the excited state manifold of the lanthanide, though not too close as to be vulnerable to thermal deactivation. Fortunately, several flavors of aromatic ligands meet this criteria, many of which are of medical relevance. We will investigate two types in particular: salicylates and catecholamines (Figure 5.1).

Salicylates, specifically salicylurate (SU) and salicylic acid (SA), are metabolites of acetylsalicylic acid (ASA), generally known as aspirin. These metabolites are comprised of a benzene ring with a hydroxyl group adjacent to either a carboxyl group (SA) or a glycine-conjugated amide group (SU). Upon deprotonation, both form mono- or dianions that can chelate a lanthanide in a bidentate (or potentially tridentate for SU) fashion. Detection of SA using a terbium-EDTA binary complex has been previously reported,[1-3] though no methods involving lanthanides or lanthanide complexes have yet been proposed for SU.

Catecholamines, such as epinephrine (Epi), norepinephrine (NE) and dopamine (DA), are neurotransmitters involved in the 'fight-or-flight' response of the sympathetic nervous system. These hormones all contain the same *1,2*-dihydroxybenzene or catechol group, coupled to a primary or secondary ethylamine group on the opposite side of the

aryl ring. The protonation constants of the two phenol hydrogens tend to have a large gap, with the first pK_a starting around 8.5 and the other approaching 13 or greater.[4, 5] We will therefore explore chelation of these species to lanthanide-macrocycle complexes in extremely basic conditions to allow for bidentate coordination to the lanthanide.

Due to time constraints or difficulties with certain analytes (extreme pH conditions, light-sensitivity, solubility problems, etc.) most of these investigations are incomplete. We consequently present this work not as a comprehensive study, but rather as a collection of 'first-steps' in the endeavor to engineer selective, robust lanthanide receptor sites for the targeted detection of aryl analytes of interest.

5.2 Salicyluric Acid

5.2.1 Introduction

Acetylsalicylic acid, commonly known as aspirin, is one of the most widely used therapeutic substances. Aspirin is effective as an anti-inflammatory agent, an analgesic to relieve minor aches and pains, and an antipyretic to reduce fever.[6] It is also the primary medication used to treat chronic rheumatic fever, rheumatoid arthritis and osteoarthritis.[7] Further, recent studies have shown the anti-thrombotic benefits of an aspirin regimen in stroke prevention.[8, 9] The widespread use of aspirin mandates a complete and thorough understanding of the pharmacodynamics and pharmacokinetics of this medication in the human body. In addition, salicylates are used as markers to assess free radical damage *in vivo* due to hydroxyl radicals.[10] As a result, a detection method to monitor acetylsalicylate and its metabolites in blood plasma and urine – with high sensitivity at low cost – is in high demand.

In the body, acetylsalicylic acid (ASA) is hydrolyzed to salicylic acid (SA) by carboxylesterases in the gut walls and liver, with an elimination half-life of 15–20 minutes.[11] Salicylic acid is then metabolically converted primarily to salicyluric acid (SU) and other metabolites, which are excreted in the urine.[12, 13] Due to the high elimination rate constant for SU in comparison to SA,[14] and the fact that endogenous SU formation only occurs in a limited capacity,[15, 16] it is possible to use SU urinary excretion data to establish a relationship between SU formation and the amount of SA in the body. We can therefore use SU as an indicator of SA in vivo, and hence detection of SU in urine can be utilized as a noninvasive means of monitoring aspirin dosage and residence in the body. Further, unusually high or low concentrations of SU in the urine have been correlated to a variety of diseases and conditions, such as appendicitis, anemia, abdominal trauma, liver diseases, uremia and Down's Syndrome.[17] Hence, detection of SU in urine has a variety of applications, including a facile way to monitor aspirin dosage and corroborating the presence of certain medical conditions.

Current detection methods of salicylates in blood and urine involve significant sample preparation prior to analysis and are time- and/or labor-intensive. High performance liquid chromatography (HPLC) can be used to detect ASA, SA and SU simultaneously with a sensitivity of 0.1 mg/L,[18] but this requires solvent extraction and the addition of internal standards. Other HPLC techniques report sensitivities of 0.2 mg/L SA in urine[12] or 0.5 mg/L SA in plasma.[19] A liquid chromatographic method with UV detection has a sensitivity of 0.5 mg/L with a precision of 8.6 mg/L, but takes 25 minutes and requires purification steps.[20] Capillary electrophoresis coupled to laser-induced fluorescence has also been described to detect SA, SU and other metabolites in

urine following sample filtration and dilution.[21] A spectrophotometric method using absorption spectra and multicomponent analysis can distinguish between SA and SU, but not in blood or urine.[22] We therefore seek a method with similar sensitivity but greater efficiency that is cost-effective.

Salicylurate has been shown to bind metal cations such as divalent copper,[23] trivalent cobalt,[24] VO(IV)[25] and dimethyltin(IV).[26] In such complexes SU is either bidentate or tridentate, coordinating through the carbonyl, carboxyl and phenolate oxygens of the ligand. Lanthanides as hard ions make excellent chelators for oxygen-containing ligands. However, no lanthanide complexes containing ligated SU have been reported in the literature. Europium-macrocycle complexes have previously been applied to the detection of oxyanions in urine such as lactate and citrate.[27, 28] Here, we report the first lanthanide-macrocycle receptor to detect salicylurate in urine.

We have selected the $Tb(DO2A)^{+}$ binary complex, where DO2A is the macrocyclic ligand *1,4,7,10*-tetraazacyclododecane-*1,7*-bisacetate, as our first-generation salicylurate receptor site. Terbium is the only luminescent lanthanide with a solitary excited state ($^5D_4$, 20,500 cm^{-1})[29] lying below the triplet excited state of salicylate (23,000 cm^{-1}),[30] which is responsible for sensitization via energy transfer to the lanthanide.[31] Europium, dysprosium and samarium all have at least two excited state energy levels below the chromophore triplet, which results in multiple nonradiative deactivation pathways and decreased luminescence intensity.[32-34] Terbium also has a large energy gap between the lowest lying excited state and the ^7F_n ground state manifold, allowing for intense emission in the visible region (λ_{max} = 544 nm).[29] The DO2A ligand binds Tb^{3+} with high affinity (log K_{GdDO2A} = 19.4 [35]), conferring thermo-

dynamic stability and reducing vibrational quenching of luminescence by excluding solvent molecules from the lanthanide coordination sphere. Further, our work with the dipicolinate system indicates that terbium exhibits the greatest perturbation of electron density due to the electron-withdrawing effects of a chelating ligand (Section 3.7), and therefore the $Tb(DO2A)^+$ complex presents a binding site with the greatest attraction to an anionic analyte. We consequently expect coordination of the salicylurate anion to produce a strongly luminescent $Tb(DO2A)(SU)^-$ ternary complex. This work demonstrates a proof-of-concept in terms of designing a lanthanide-based receptor site to monitor medication dosage in a manner that is rapid and cost-effective.

5.2.2 Spectroscopy and Characterization

Experimental Section

Materials. The following chemicals were purchased and used as received: ammonium hydroxide (NH_4OH 28–30% in water) (Mallinckrodt Baker), ether anhydrous (Acros Organics), sodium hydroxide (NaOH 50% in water) (Mallinckrodt Baker), TAPS (*N*-tris(hydroxymethyl)methyl-*3*-aminopropanesulfonic acid) buffer (TCI America), trifluoroacetic acid (*2,2,2*-trifluoroacetic acid, TFA) (J. T. Baker), terbium(III) chloride hexahydrate (Alfa Aesar), and SU (salicyluric acid, *2*-hydroxyhippuric acid) (Acros Organics). The $TbCl_3$ salt was 99% pure, all solvents were ACS certified or HPLC grade, all buffers were at least 98% pure, and SU was 97% pure. Water was deionized to a resistivity of 18.2 MΩ-cm using a Purelab® Ultra laboratory water purification system (Siemens Water Technologies, Warrendale, PA). The *1,4,7,10*-tetraazacyclododecane-*1,7*-diacetate (DO2A) ligand was prepared by hydrolysis of *1,4,7,10*-tetraazacyclo-

dodecane-*1,7*-di(tert-butyl acetate) (Macrocyclics, Dallas, TX), as described previously (Section 2.2.1) resulting in a white solid in 79.9% yield. DO2A·0.6H_2O·2.1HCl. Anal. Calcd. (found) for $C_{12}H_{24}N_4O_4$ ·2.80HCl · 0.85H_2O (fw = 378.18): C, 38.32 (38.32); H, 7.31 (7.19); N, 14.89 (14.54); Cl, 20.0 (20.0).

The *1,4,7,10*-tetraazacyclododecane-*1,4,7*-triacetate (DO3A) ligand was prepared by hydrolysis of *1,4,7,10*-tetraazacyclododecane-*1,4,7*-tri(*t*-butyl-acetate)·HBr (DO3A-tBu-ester) (Macrocyclics) with trifluoroacetic acid (TFA).[36] All glassware used in this procedure was washed, placed in a nitric acid digest (50% HNO_3 in nanopure water), rinsed 10 times with nanopure water and kilned at 500 °C for 2 hours prior to use. The DO3A-tBu-ester HBr salt (2.50060 g, 4.198 mmol), a white powder, was placed in a 100-mL cylindrical flask with a side inlet and top opening fitted with a glass stopper. Neat TFA (10.0 mL, 134.6 mmol) was added at room temperature to produce a clear yellow solution. This solution was left stirring at room temperature open to air (side inlet cracked slightly) for 22 hours. The TFA was removed by rotary evaporation under vacuum (~ 50 mbar) in a hot water bath (55 °C) leaving a yellow oil. White crystals were obtained after 8 days at room temperature. The product was rinsed with two 10-mL aliquots of ether using a new fine frit (Pyrex, 15 mL, ASTM 4-5.5F, No. 36060) and dried by pulling air through the sample for 15 minutes to produce a white powder of DO3A·1.9H_2O·3.0TFA (2.50298 g, 3.486 mmol) in 83.05% yield. Anal. Calcd (found) in duplicate for $C_{14}H_{27}N_4O_6$·1.9H_2O·3.0$C_2HF_3O_2$ (fw = 717.96): C, 33.42 (33.43); H, 4.18 (4.27); N, 7.80 (7.93). ESI-MS (*m/z*): calcd (found) for $C_{14}H_{27}N_4O_6$ (M + H): 347.1931 (347.1939). ^{13}C NMR: δ 42.18, δ 47.62, δ 49.07, δ 51.83, δ 52.97, δ 55.02, δ 115.08, δ 163.02, δ 168.96, δ 174.32.

The Tb(DO2A)(SU)$^-$ ternary complex was prepared in aqueous solution by addition of 0.464 mL of 0.032318 M $TbCl_3$ (15.00 μmol) to 0.269 mL of 0.5593 M DO2A (15.05 μmol), followed by 1.650 mL of 9.0717 mM SU (14.97 μmol). pH was adjusted to 8.0 with ammonium hydroxide (28–30% in H_2O), added dropwise. TOF-MS ES$^-$ (*m/z*): calcd (found) for $TbC_{21}H_{29}N_5O_8$ (M^-): 638.41 (638.13).

Methods. All samples were prepared in triplicate to a final volume of 3.50 mL in disposable acrylate cuvettes (Spectrocell, Oreland, PA) with a 1 cm path length. Luminescence spectral analysis was performed by a Fluorolog Fluorescence Spectrometer (Horiba Jobin-Yvon, Edison, NJ). To prevent second-order diffraction of the source radiation, all measurements were taken with a 350-nm colorless sharp cutoff glass filter (03 FCG 055, Melles Griot, Covina, CA). All reported spectra were obtained as a ratio of corrected signal to corrected reference (S_c/R_c) to eliminate the effect of varying background radiation in the sample chamber; emission intensities are in units of counts per second per microampere (cps/μA).

Luminescence excitation (λ_{ex} = 316 nm) and emission (λ_{em} = 544 nm) spectra were obtained for the Tb(macrocycle)(SU) ternary complexes, where the macrocycle was DO2A or DO3A, at a concentration of 100 μM in 0.1 M TAPS buffer, pH 8.4. Absorption spectra were obtained using a Cary 50 Bio UV/visible spectrophotometer (Varian, Inc., Palo Alto, CA) in quartz cuvettes.

Several attempts were made to crystallize the Tb(DO2A)(SU)$^-$ ternary complex out of acetone with a tetrabutylammonium counterion. However, the only crystals obtained were of a trimer containing terbium and the macrocycle, but no salicylurate. We believe this is due to the low to moderate stability of the ternary complex.

Results and Discussion

The excitation spectrum of the Tb(DO2A)(SU)$^{-}$ complex shows a broad band at 316 nm, attributed to the $\pi \rightarrow \pi^*$ transition of the SU chromophore.[37] The emission spectrum presents a large, broad band with a λ_{max} of 419 nm, presumably due to excited state intramolecular proton transfer (ESIPT) from the hydroxyl moiety to the nearby carbonyl group of the SU ligand. This type of ESIPT is known to occur in salicylic acid and para-methoxy substituted salicylates, with similar excitation and emission wavelengths.[38, 39] The unusually large Stokes shifts in these compounds are due to a significant geometry change as the proton-transfer tautomer is formed and then relaxes to a relatively unstable isomer of the ground state.[40-42] This band at 419 nm can be used as an internal standard to validate SU concentration in solution (Figure 5.2).

The sharp bands at 488, 545, 585 and 621 nm are the $^5D_4 \rightarrow {}^7F_n$ transitions for sensitized terbium emission, where n = 6,5,4 and 3, respectively (Figure 5.3). The intensities of these transitions are consistent with the luminescence turn-on associated with an aromatic anion binding to the terbium cation and yielding efficient intersystem crossing via the absorption-energy transfer-emission (AETE) mechanism following UV excitation. This effect results in an increase in terbium luminescence by several orders of magnitude, and cannot be accounted for simply by the exclusion of water – which quenches luminescence via nonradiative decay pathways – from the Tb^{3+} coordination sphere.[43, 44]

The ESIPT band at 419 nm can also provide information concerning the coordination behavior of the salicylurate ligand. Though our luminescence measurements were made at pH 8.4, above the two pK_a values of SU (Table 5.1),[23] we

still see strong evidence of intramolecular proton transfer, indicating that the phenol moiety of the SU is still protonated. If this is the case, then the terbium would interfere with proton transfer if it were coordinating to the carbonyl and phenolate groups as expected. Most likely, the SU is binding to the lanthanide in a bidentate fashion via the carbonyl and the carboxyl group (Figure 5.4). However, a tridentate motif involving the amine group is also a possibility. The excitation and emission spectra of the $Tb(DO3A)(SU)^{2-}$ complex are more than an order of magnitude lower in intensity than the corresponding DO2A spectra (Figure 5.5), indicating that the SU ligand does not bind with much affinity to the Tb(DO3A) complex. This may corroborate either the tridentate chelation motif or a bidentate mode with a significant amount of steric bulk around the binding site, as apparently two adjacent binding sites on the lanthanide are not sufficient for SU ligation. Only the $Tb(DO2A)^{+}$ complex, which has three linear adjacent binding sites available on the Tb^{3+} cation, is able to accommodate the SU ligand.

5.2.3 Binding Studies and Stability

Experimental Section

Materials. The following chemicals were purchased and used as received: CAPS (*N*-cyclohexyl-3-aminopropanesulfonic acid) buffer (Alfa Aesar), CHES (*N*-cyclohexyl-*2*-aminoethanesulfonic acid) buffer (Alfa Aesar), MES monohydrate (*2*-(*N*-morpholino) ethanesulfonic acid monohydrate) buffer (Alfa Aesar), sodium acetate trihydrate (Mallinckrodt), sodium hydroxide (NaOH 50% in water) (Mallinckrodt Baker), TAPS (*N*-tris(hydroxymethyl)methyl-*3*-aminopropanesulfonic acid) buffer (TCI America), terbium(III) chloride hexahydrate (Alfa Aesar) and SU (salicyluric acid, *2*-

hydroxyhippuric acid) (Acros Organics). The $TbCl_3$ salt was 99% pure, all buffers were at least 98% pure and SU was 97% pure. DO2A was prepared as previously described (Section 2.2.1). Water was deionized to a resistivity of 18.2 MΩ-cm using a Purelab® Ultra laboratory water purification system.

Methods. All samples were prepared in triplicate to a final volume of 3.50 mL in disposable acrylate cuvettes (Spectrocell) with a 1 cm path length. Luminescence spectral analysis was performed by a Fluorolog Fluorescence Spectrometer with a 350-nm colorless sharp cutoff glass filter as previously described (Section 5.2.2). Integrated intensities are evaluated over 534–554 nm. The solution pH was measured using a calibrated handheld IQ150 pH/mV/temperature meter (I. Q. Scientific Instruments, Loveland, CO) following data collection. Because of SU intrinsic luminescence, all integration values are reported after emission spectra are fit and then subtracted to a SU aqueous solution to isolate the bound Tb-SU signal.

Binding studies. A method of continuous variations was used to determine the binding stoichiometry for the Tb/DO2A/SU system. Samples were prepared in 0.1 M TAPS buffer (pH 8.4) with the concentrations of Tb and SU varying inversely from 0 to 120 μM in 10 μM increments, and the concentration of DO2A maintained at 500 μM. Emission spectra were obtained following 1–3 hours of equilibration time.

pH dependence study. Solutions of 100 μM $Tb(DO2A)(SU)^-$ were prepared in 0.1 M buffer with five-fold excess DO2A to ensure full Tb complexation. Four buffers were used: MES (pK_a = 6.1), TAPS (pK_a = 8.4), CHES (pK_a = 9.3) and CAPS (pK_a = 10.4), with pH adjustment to within 0.1 of the pK_a value using 50% NaOH added dropwise.

Sodium acetate trihydrate, 0.2 M, was also used to maintain a pH of 7.5. Emission spectra were obtained after 15 min, 18 hrs and 5 days.

Results and Discussion

A method of continuous variations indicates an optimal binding stoichiometry of about 1:1 for Tb and SU with DO2A in excess (Figure 5.6). We can therefore conclude that SU^{2-} binds to $Tb(DO2A)^{+}$ to form the $Tb(DO2A)(SU)^{-}$ complex. However, the curvature of the Jobs plot may indicate lower stability than anticipated of the ternary complex. This can be mitigated by working in a higher concentration regime.

To optimize conditions for detection of SU in complex matrices, a pH dependence study was performed from pH 6.1 to 10.6. Results indicate that the $Tb(DO2A)(SU)^{-}$ complex is most stable in neutral to slightly basic conditions, with pH 8.4 optimal (Figure 5.7). This is consistent with the pK_a values reported for SU (3.34 and 7.91)[23] suggesting that the SU ligand must be at least partially deprotonated for effective terbium binding and efficient energy transfer. Experiments indicate that the $Tb(DO2A)(SU)^{-}$ complex is unstable after 24 hours, as evidenced by a significant loss of signal. Reproducibility is conserved if samples are analyzed within 5–6 hours of solution preparation.

5.2.4 Calibration Curve and Limit of Detection

Experimental Section

Materials. The following chemicals were purchased and used as received: TAPS (*N*-tris(hydroxymethyl) methyl-*3*-aminopropanesulfonic acid) buffer (TCI America), terbium(III) chloride hexahydrate (Alfa Aesar) and SU (salicyluric acid, *2*-

hydroxyhippuric acid) (Acros Organics). DO2A was prepared as previously described (Section 2.2.1). Water was deionized to a resistivity of 18.2 MΩ-cm using a Purelab® Ultra laboratory water purification system. Urine was collected from healthy volunteers, with unmarked samples chosen at random from a larger sample set for analysis within 24 hours of donation. Samples were kept refrigerated at 4 °C until use.

Methods. All samples were prepared in triplicate to a final volume of 3.50 mL in disposable acrylate cuvettes (Spectrocell) with a 1 cm path length. Luminescence spectral analysis was performed by a Fluorolog Fluorescence Spectrometer with a 350-nm colorless sharp cutoff glass filter as previously described (Section 5.2.2).

Urine samples were spiked with SU over a range from 0–150 μM. An aliquot from each spiked sample was diluted into a pre-equilibrated solution containing 5 mM $Tb(DO2A)^+$ in 0.1 M TAPS buffer (pH 8.4) in various volumes, and the emission spectra obtained within 1 hour of dilution. Intrinsic SU fluorescence was eliminated from the emission spectra using a fitting algorithm, and the largest terbium emission peak at 544 nm was integrated and normalized to an external standard. A linear regression model was used to determine the endogenous SU concentration in each donated sample by setting the y-intercept to the integrated intensity of 5 mM $Tb(DO2A)^+$ alone (I_0), and solving for an endogenous SU concentration $[SU]_{end}$ such that the correlation coefficient (R^2) is optimized to near unity (equation 5.1).

$$I_{obs} = C \cdot \left([SU]_{spike} + [SU]_{end} \right) + I_0 \qquad [5.1]$$

In this model, I_{obs} is the observed integrated intensity of the spiked sample in 5 mM $Tb(DO2A)^+$, $[SU]_{spike}$ is the concentration of SU added to the sample, and *C* is the calibration constant, in units of cps/(M·μA). It was empirically determined from these

experiments that a sample dilution factor of 1:350 produces a linear, reproducible correlation between SU concentration and emission intensity that is independent of donor. A calibration curve was generated from this data set, and can be applied to any urine sample to determine SU concentration.

The limit of detection (LOD) for SU in urine was identified for a signal to noise ratio of 3:1. An average noise value was obtained from an emission spectrum used in the calibration curve (λ_{em} = 544 nm); this was multiplied by the S/N ratio and added to the background intensity (λ_{em} = 542 nm) for a 5 mM $Tb(DO2A)^{+}$ control solution. Integration of the Tb(DO2A)(SU) emission spectrum adjusted to this value resulted in an SU concentration obtained from the constructed calibration curve that corresponds to the limit of detection for this assay.

Results and Discussion

To determine the efficacy of SU detection using the $Tb(DO2A)^{+}$ receptor site in body fluids, urine samples provided by healthy donors were used to generate a calibration curve and calculated a limit of detection. Signal quenching was observed with high concentrations of urine, probably due to competition with other ions or loss of emission signal due to the high absorptivity of the samples. Dilution of the sample while maintaining a high concentration of $Tb(DO2A)^{+}$ (4–5 mM) eliminated this problem and produced results similar to those obtained in aqueous solution (Figure 5.8). A dilution factor of 1:350 allows for reproducibility over the entire sample set tested. Using this dilution factor, a calibration curve was constructed using spiked SU urine samples from three separate donors, with a correlation coefficient near unity (Figure 5.9). Assuming a

signal-to-noise ratio of 3:1, a limit of detection (LOD) for this assay was determined to be 0.027 μM SU in the diluted samples, which corresponds to an SU concentration of 9.4 μM in urine or approximately 1.8 mg/L. For a first iteration of an SU receptor site, this value is already in the range of highly specialized detection methods such as HPLC or capillary electrophoresis, and can be performed in a fraction of the time.

5.2.5 Aspirin Study

Experimental Section

Materials. TAPS (*N*-tris(hydroxymethyl) methyl-*3*-aminopropanesulfonic acid) buffer (TCI America, Portland, OR) and terbium(III) chloride hexahydrate (Alfa Aesar) were purchased and used as received. DO2A was prepared as previously described (Section 2.2.1). Water was deionized to a resistivity of 18.2 MΩ-cm using a Purelab® Ultra laboratory water purification system. Urine collected from a healthy anonymous volunteer was kept refrigerated at 4 °C until use.

Methods. All samples were prepared in triplicate to a final volume of 3.50 mL in disposable acrylate cuvettes (Spectrocell) with a 1 cm path length. Luminescence spectral analysis was performed by a Fluorolog Fluorescence Spectrometer with a 350-nm colorless sharp cutoff glass filter as previously described (Section 5.2.2).

Samples were collected from a healthy anonymous volunteer before and following two self-medicated aspirin regimens. The subject took 81 mg of aspirin every 6 hours for a total of 24 hours, and provided a urine sample 4 hours after the final dose. The process was repeated again with a 325-mg regimen. Both regimens were within recommended low-dose ranges for stroke and myocardial infarction prevention.[8] A 10-

μL aliquot of each sample was diluted 1:350 into pre-equilibrated 5.0 mM $Tb(DO2A)^+$ in 0.1 M TAPS (pH 8.4). Emission spectra (λ_{ex} = 316 nm) were obtained following 1 minute of thorough mixing.

Results and Discussion

As a proof-of-concept, we obtained urine samples from a healthy anonymous volunteer on a low-dose aspirin regimen. We successfully detected an increase in luminescence intensity that tracked with the two aspirin dosage aliquots of 81 mg or 325 mg, indicating an increase in SU elimination in the urine (Figure 5.10). The intensity of the intrinsic SU luminescence band (419 nm) is much lower relative to the terbium emission peaks for this experiment. We attribute the decrease to absorption by other species in solution in this region. The unpredictable change in intensity of this band, which varies significantly between donors, emphasizes the problems associated with using SU luminescence alone for concentration determination and reinforces our technique of using sensitized lanthanide luminescence that is specific for SU.

5.2.6 Conclusion

We have demonstrated a first-generation SU receptor site composed of a lanthanide reporter chelated to a selective macrocyclic ligand. Preliminary results suggest a high degree of selectivity for SU, even in a matrix as complex as urine. Complete sample preparation and analysis can be performed within 5 minutes. This SU detection assay represents a proof-of-concept for the design and implementation of lanthanide-macrocycle receptor sites with high sensitivity and selectivity for a target

biomolecule. Further optimization of the macrocycle by adding or substituting functional groups to modify the electrostatics and sterics of the Tb receptor site should enhance SU binding and improve the limit of detection by at least an order of magnitude.[45] Such an improvement would make this type of SU detection more sensitive than all other reported techniques, in addition to being more rapid and cost-effective.

Spectroscopic determination of salicylurate by terbium-macrocycle complexes has three advantages: (1) rapid detection and quantification, (2) low cost and (3) capability of automation. We anticipate application of such a straightforward method for in-line monitoring of SU, possibly via an automated cathaderized system. Salicylurate levels in the bloodstream could also be determined using sufficiently selective terbium complexes, though further experimentation is required.

5.3 Salicylic Acid

5.3.1 Introduction

Salicylic acid, named after the willow tree (*Salix* genus) from whose leaves and bark it was originally obtained, is the primary metabolite of aspirin. As stated in Section 5.2.1, acetylsalicylic acid (ASA) of aspirin is rapidly hydrolyzed upon ingestion to salicylic acid (SA), which is later converted to salicylurate (SU) and other compounds. Salicylic acid itself also has many applications due to its keratinolytic effects and ability to affect metabolic processes;[46] common uses include food preservation, acne medication and topical treatment of fungal skin infections.[47, 48] Further, SA sensitivity can cause ototoxicity (hearing loss) and metabolic acidosis in some individuals.[49, 50]

Salicylic acid can be toxic when taken in large doses.[51] The recommended therapeutic level in plasma is around 150–300 mg/L. SA intoxication symptoms can start to appear at 300 mg/L plasma concentration, and severe intoxication, including acidosis and tetany (involuntary muscle contraction) can occur at levels above 500 mg/L.[52] Many methods for the detection of salicylic acid have been reported, including colorimetric,[53] fluorimetric,[54, 55] chromatographic[20, 56-58] and voltametric[59] assays. The simplest and most cost-effective method is the Trinder test, in which salicylate binds to Fe^{3+} to produce a purple complex which can be quantified by optical density (530 nm).[60] However, this technique suffers from poor selectivity and false positives.[61]

As described in Section 5.2.1, current methods of detection for salicylates are too slow, too expensive, or have poor detection limits. Additionally, most involve sample pretreatment, such as extraction, derivatization or preconcentration steps prior to analysis. Salicylate can form chelate compounds with metal ions, with most stability constants in the micromolar range (log K = 5.5 to 7.0) in near-neutral conditions; the notable exceptions are Cu^{2+} (log K = 10.6) and Fe^{3+} (log K = 16.4).[62] This propensity to effectively bind divalent and trivalent ions makes salicylic acid an ideal candidate for detection methods involving complexation to lanthanides. The triplet excited state of salicylic acid (23,041 cm^{-1})[30] lies in the optimal energy transfer region to effectively sensitize the terbium cation (20,500 cm^{-1}).[29] As a result, assays involving SA detection in serum using the Tb(EDTA) binary complex have been proposed, with limits of detection in the micromolar range at high pH.[2, 3] These involve second derivative scanning fluorescence spectrometry or purification using capillary electrophoresis. Another

method involving micelles claims a subnanomolar detection limit, although this was for pure salicylic acid in buffered aqueous solution.[1]

Due to the kinetic and thermodynamic stability of macrocyclic ligands and our previous success in receptor site design involving lanthanide-macrocycle complexes, we plan to explore cyclic chelating ligands in the detection of SA and compare these to results obtained with EDTA. A neutral terbium complex of a DO3A derivative with a pendant 15-aza-crown-5 substituent has also been found to chelate salicylic acid with a binding affinity in the millimolar range (log K_a' = 3.9 ± 0.2) in 0.1 M Tris buffer, pH 7.4.[63] We believe we can substantially enhance the binding affinity for salicylate with judicial choice of chelating macrocycle and shifting the pH to more basic conditions where the salicylate is fully deprotonated (Table 5.1).[64, 65] We will use a screening protocol to determine the optimal chelating ligand, whether cyclic or acyclic, that when combined with terbium produces the most effective receptor site for salicylate.

5.3.2 Photophysics and Ligand Screen

As with the salicylurate system (Section 5.2) the photophysics of salicylate are more complex, owing to the phenomenon of excited-state intramolecular proton transfer (ESIPT) from the phenol to the proximal carboxyl moiety during tautomerization of the photoexcited SA structure.[38-40, 42] We will explore the effect of lanthanide chelation on the intrinsic luminescence of salicylic acid.

Several macrocyclic ligands of varying denticity (hexa- to octadentate) will be used to generate Tb(ligand)(SA) ternary complexes in highly basic conditions. The screening protocol will involve obtaining excitation and emission spectra; the optimal SA

receptor site complex should produce the greatest luminescence intensity for a given concentration. Salicylic acid is also light-sensitive, so a photodegradation study will be performed as well.

Experimental Section

Materials. The following chemicals were purchased and used as received: CAPS (*N*-cyclohexyl-*3*-aminopropanesulfonic acid) buffer (Alfa Aesar), CHES (*N*-cyclohexyl-*2*-aminoethanesulfonic acid) buffer (Alfa Aesar), DOTA (*1*,*4*,*7*,*10*-tetraazacyclododecane-*1*,*4*,*7*,*10*-tetraacetate) (Macrocyclics), EDTA (ethylenediaminetetraacetic acid) (Aldrich), sodium hydroxide (NaOH 50% in water) (Mallinckrodt Baker), sodium salicylate (NaSA, sodium *2*-hydroxybenzoic acid) (Fisher) and terbium(III) chloride hexahydrate (Alfa Aesar). All lanthanide salts were 99.9% pure and all other salts were 97% pure or greater. Water was deionized to a resistivity of 18.2 MΩ-cm using a Purelab® Ultra laboratory water purification system. DO2A was prepared as previously described (Section 2.2.1). DO3A was prepared as previously described (Section 5.2.2).

Methods. All samples were prepared in triplicate *under a red light* from stock solutions to a final volume of 4.00 mL in disposable acrylate cuvettes (Spectrocell) with a 1 cm path length and *stored in the dark* at room temperature prior to analysis. Luminescence spectral analysis was performed by a Fluorolog Fluorescence Spectrometer with a 350-nm cutoff filter as previously described (Section 5.2.2). The solution pH was measured using a calibrated handheld IQ150 pH/mV/temperature meter (I. Q. Scientific Instruments).

Spectroscopy. Cuvettes of 10.0 μM SA, Tb(SA) and Tb(ligand)(SA), where ligand is EDTA, DO3A or DOTA, were prepared in 0.1 M MOPS buffer (pH 7.5) and 0.1 M CAPS buffer (pH 10.0). All Tb(ligand) complexes were pre-equilibrated for at least 2 weeks prior to use. Absorbance measurements were made using a Cary 50 Bio UV/Visible Spectrophotometer (Varian, Inc., Palo Alto, CA) following 1 hour equilibration time. Excitation (λ_{em} = 544 nm) and emission (λ_{ex} = 314 nm) spectra were also obtained following 1 hour of equlibration.

Ligand screen study. Cuvettes of 1.0 μM SA and either 100 μM or 1.0 mM of Tb(ligand), where ligand is EDTA, DO2A, DO3A or DOTA, were prepared in 50 mM CAPS or CHES (DO2A only) buffer, pH 12.5. All Tb(ligand) complexes were pre-equilibrated for at least 2 weeks prior to use. Excitation (λ_{em} = 544 nm) and emission (λ_{ex} = 326 nm) spectra were obtained following 1, 2, 3, 4, 8, 24, 48 and 72 hours equilibration time.

Photodegradation study. A cuvette containing 1.0 μM SA and 1.0 mM Tb(EDTA) at pH 12.5 (adj. with 50% NaOH added dropwise), was prepared and stored in the dark at room temperature for 5 days. Luminescence emission spectra were obtained after this storage period for time points of 0, 15, 17, 19, 21, 23, 25 and 27 minutes. Spectra were integrated from 530–560 nm, and the percentage of intensity lost was calculated from an initial scan of the cuvette after 1 hour equilibration time.

Results and Discussion

Absorption spectra at pH 7.5 and pH 10.0 do not show any shift upon addition of Tb^{3+} or any Tb(ligand) complex, where ligand is EDTA, DO3A or DOTA (Figure 5.11).

This supports previous reports that pH conditions must be near or above the second pK_a value of SA (13.62) in order for the lanthanide to displace the phenolic hydrogen and provide for bidentate chelation. At pH 12.5, excitation spectra (Figure 5.12) show two populations in solution, one with a broad band at 419 nm (λ_{ex} = 296 nm) and the other with the characteristic terbium emission profile (λ_{ex} = 318 nm). The 419-nm band is assigned as the excited-state intramolecular proton transfer (ESIPT) transition. The red shift of approximately 20 nm upon complexation of deprotonated SA with the terbium binary complex is consistent with that reported for previous studies.[1]

Emission spectra indicate that the $Tb(EDTA)(SA)^{3-}$ complex exhibits the greatest luminescence intensity compared to the analogous DO2A, DO3A and DOTA complexes (Figure 5.13). This is intriguing, as we anticipated the macrocyclic ligands to perform better than the acyclic EDTA ligand. The macrocylic ligands have greater binding affinities for terbium than EDTA (Table 5.2),[35, 66, 67] and should therefore stabilize Tb^{3+} in highly basic conditions to a greater degree, reducing precipitation of the terbium hydroxide species. Secondly, in this high pH regime, the EDTA ligand should have a -4 charge (Table 5.3),[68] meaning the $Tb(EDTA)^-$ binary complex is *negatively charged*. The doubly-deprotonated SA^{2-} ligand is therefore binding to a binary complex irrespective of electrostatic attraction or repulsion. Perhaps the geometry of the open coordination sites on the lanthanide are not in the correct orientation for the hexadentate DO2A and the heptadentate DO3A. Maybe with the flexible nature of the EDTA ligand, it is more able to accomodate the sterics of the SA analyte. It has been noted by previous authors that it is impossible to explain spectroscopic behavior of Eu and Tb salicylates by position of the triplet levels alone.[69] There could be a more complex mechanism at work here.

Regardless, the $Tb(EDTA)^-$ binary complex appears to be the optimal receptor site for the detection of salicylic acid.

The photodegradation study revealed that the $Tb(EDTA)(SA)^{3-}$ complex shows no loss of signal over a period of 5 days if the sample is prepared under a red lamp and kept in the dark. However, emission intensity dropped by 24% following 30 minutes of nearly constant UV exposure in the fluorescence spectrometer (7 emission scans, approximately 3 minutes of exposure per scan). We will therefore continue to prepare all samples under minimal light exposure and store them in the dark.

5.3.3 Binding Studies and Stability

With the $Tb(EDTA)^-$ complex established as the optimal SA receptor site, we will explore the stability of the ternary $Tb(EDTA)(SA)^{3-}$ complex via Jobs method of continuous variations and a pH dependence study. Due to the high pH regime, the BAC assay will not be attempted due to the high proclivity of terbium hydroxide formation and precipitation.

Experimental Section

Materials. The following chemicals were purchased and used as received: CAPS (*N*-cyclohexyl-*3*-aminopropanesulfonic acid) buffer (Alfa Aesar), CHES (*N*-cyclohexyl-*2*-aminoethanesulfonic acid) buffer (Alfa Aesar), EDTA (ethylenediamine-tetraacetic acid) (Aldrich), MOPS (*3*-(*N*-morpholino)ethanesulfonic acid) buffer (Alfa Aesar), sodium hydroxide (NaOH 50% in water) (Mallinckrodt Baker), sodium salicylate (NaSA, sodium *2*-hydroxybenzoic acid) (Fisher), TAPS (*N*-tris(hydroxymethyl) methyl-

3-aminopropanesulfonic acid) buffer (TCI America), terbium(III) chloride hexahydrate (Alfa Aesar) and Tris (tris(hydroxymethyl)aminomethane) hydrochloride buffer (J. T. Baker). The $TbCl_3$ salt, EDTA and NaSA were all 99% pure or greater, and all buffers were at least 97% pure. Water was deionized to a resistivity of 18.2 MΩ-cm using a Purelab® Ultra laboratory water purification system.

Methods. All samples were prepared in triplicate to a final volume of 4.00 mL in disposable acrylate cuvettes (Spectrocell) with a 1 cm path length. Luminescence spectral analysis was performed by a Fluorolog Fluorescence Spectrometer with a 350-nm colorless sharp cutoff glass filter as previously described (Section 5.2.2). The solution pH was measured using a calibrated handheld IQ150 pH/mV/temperature meter (I. Q. Scientific Instruments) following data collection.

Binding studies. A method of continuous variations was used to determine the binding stoichiometry for the Tb/EDTA/SA system. Samples were prepared in 50.0 mM CAPS buffer (pH 13.5) with the concentrations of Tb and SA varied inversely from 0 to 120 μM in 10 μM increments, and the concentration of EDTA maintained at 1.00 mM. Emission spectra (λ_{ex} = 314 nm) were obtained following an equilibration time of 24 hours.

pH dependence study. Solutions of 1.00 μM Tb(EDTA)(SA) were prepared in 50.0 mM buffer with 1.00 μM SA and 500 μM $Tb(EDTA)^-$ to ensure complete SA complexation. Five buffers were used: MOPS (pK_a = 7.2), TAPS (pK_a = 8.4), Tris (pK_a = 8.1), CHES (pK_a = 9.3) and CAPS (pK_a = 10.4), with pH adjustment to 0.5 increments from 7.0 to 14.0 using 50% NaOH added dropwise. Emission spectra (λ_{ex} = 314 nm) were obtained after 1 hour equilibration time.

Results and Discussion

Many attempts were made to crystallize the $Tb(EDTA)(SA)^{3-}$ ternary complex, using various counterions (TBA^+, Na^+, NH_4^+) and solvents (nanopure water, methanol, ethanol, *2*-propanol, acetone, acetonitrile, ammonium hydroxide and diethyl ether). However, the only crystals obtained were of $Tb(EDTA)\cdot NaOH\cdot 2H_2O$ (Section 3.2.2). This is most likely due to either the low stability of the ternary complex or the photodegradation of the SA ligand over the crystallization period.

Binding studies indicate that the SA^{2-} ligand binds in a 1:1 ratio to the $Tb(EDTA)^-$ binary complex at high pH (13.5), confirming formation of the $Tb(EDTA)(SA)^{3-}$ ternary complex (Figure 5.14). As with the SU case (Section 5.2.3), the nonlinearity of the Jobs plot may indicate lower stability of the ternary complex. Due to the high pH regime and the high pK_{a2} of salicylate, this may be due to (1) competing equilibria of the formation of $Tb(OH)_3$, and (2) the presence of a population of SA^- species that is not fully deprotonated and unable to chelate Tb^{3+}. The intrinsic SA luminescence band at 419 nm can be used as an internal standard of protonated SA^- concentration (Figure 5.15).

As expected, the pH dependence study reveals very little sensitized terbium luminescence until the SA ligand is fully deprotonated (Figure 5.16). Further, as the luminescence of the $Tb(EDTA)(SA)^{3-}$ increases with pH, the intrinsic SA^- luminescence due to ESIPT decreases (Figure 5.17). This confirms that lanthanide chelation occurs following deprotonation of the phenol hydrogen on the SA ligand, and therefore the SA^{2-} species must be binding to the $Tb(EDTA)^-$ complex in a bidentate fashion with the carboxylate and phenolate oxygens.

5.3.4 Conclusion

Our investigation into the detection of salicylate using lanthanide binary complexes validated the results of other studies, in that the $Tb(EDTA)^-$ complex proved to have the greatest binding affinity for the SA^{2-} ligand at high pH. The fully deprotonated salicylate analyte chelates to the lanthanide ion via the phenolate and carboxylate oxygens in a bidentate manner, allowing for energy transfer to the Tb^{3+} under UV excitation at 314 nm through the AETE mechanism. It is interesting that the macrocyclic ligands did not perform nearly as well as the acyclic EDTA ligand in this case, despite their greater binding affinities for the Tb^{3+} ion and higher thermodynamic stabilities. It is possible that the rigidity of these macrocycles may impede SA binding due to steric effects, or perhaps the EDTA and SA ligands are in the proper orientation around the terbium cation to allow for intramolecular interactions that are not accessible using DO2A or DO3A. Further exploration of this system, including targeted substitutions, molecular modeling and DFT calculations, may provide insight into the unexpected binding preferences of this biologically relevant aspirin metabolite.

5.4 Catecholamines

5.4.1 Introduction

We now shift our focus to another interesting group of aromatic anions, the catecholamines (CAs). These ‘fight-or-flight’ hormones are part of the sympathetic nervous system, and are released by the adrenal glands in response to stress.[70] Catecholamines are produced from the amino acids phenylalanine and tyrosine, and

contain the *1,2*-dihydroxybenzene (catechol) group and either a primary or secondary amine group. Biosynthesis of catecholamines starts with the production of dopamine from L-tyrosine, which involves conversion to L-dihydroxyphenylalanine (L-DOPA) by tyrosine hydroxylase and conversion to dopamine using DOPA decarboxylase. Epinephrine and norepinephrine require further conversion steps using dopamine β-hydroxylase, a copper cofactor and phenylethanolamine *N*-methyltransferase.[71]

Catecholamines are water-soluble and circulate in the bloodstream with a half-life of approximately 3 minutes.[72] Overstimulation and/or damage of the brainstem nuclei can lead to catecholamine toxicity. This can also be caused by pheochromocytoma, neuroendocrine tumors in the adrenal medulla, and carcinoid syndrome (carcinoid tumors in the gastrointestinal tract and/or lungs). CA toxicity can also be caused by a deficiency in monoamine oxidase A, which is normally responsible for the degradation of CAs. High levels of CAs have been associated with various functional and degenerative cardiovascular disorders, such as angina pectoris, arterial hypertension and atherogenesis.[73] Decreased dopamine levels have been linked to Parkinson's disease and ADHD, while elevated levels can cause mood swing, psychosis and other neurotic disorders.[74-76] Increased levels of epinephrine (when controlled properly) can help the body reduce negative allergenic responses and regenerate lost liver cell functions.[77, 78] Thus, rapid detection of catecholamines in blood and urine can provide vital information regarding various medical conditions that might aid in more efficient diagnosis or more effective treatment.

Current methods of detection for catecholamines in biological fluids (urine, plasma and serum) involve chromatographic separation coupled to either electro-

chemical[79, 80] or fluorescence-based[81] techniques. However, most fluorescence-based methods rely purely on the native fluorescence of catecholamines (λ_{ex} ~ 280 nm, λ_{em} ~ 310 nm),[82] which has a short Stokes shift and makes it difficult to distinguish between different CAs. Others involve pre- or post-column derivatization with various fluorophores, such as naphthalene-*2,3*-dicarboxaldehyde,[83] *1,2*-diphenylethylene-diamine[84, 85] or fluorescamine.[86] These all require time for separation using expensive instrumentation, and are not feasible for CA detection in situ on the necessary time scale of 3 minutes.

Catecholamines coordinate to Cu(II), Co(II), Ni(II), Mn(II) and Zn(II) via the two phenolic hydroxyl groups.[87, 88] CAs have also been reported to complex Al^{3+} with submicromolar affinity (Table 5.4), though citrate and ATP can interfere.[5] When bound to Y^{3+}, Ca^{2+} or La^{3+}, the catecholamine still coordinates through the two phenolic groups at neutral pH, but one of the two groups remains protonated.[89-91] We therefore anticipate chelation to lanthanides at high pH where both of the phenol groups are deprotonated, allowing for bidentate coordination to the Ln^{3+} cation.

We will investigate the potential of lanthanide complexes to detect catecholamines, specifically dopamine (DA), epinephrine (Epi) and norepinephrine (NE) (Figure 5.1). The triplet energy levels of the catecholamines (23,800 to 24,000 cm^{-1})[82] lie in the appropriate range for efficient energy transfer to the $^5D_4$ energy level of Tb^{3+} (20,500 cm^{-1}).[29] Previous work using the $Tb(EDTA)^-$ complex following capillary electrophoresis has reported detection limits on the order of 0.1 μM for catecholamines (DA, NE, Epi and others).[92] However, the EDTA ligand in this case was only used to reduce terbium precipitation in basic conditions (pH 11), and not as a helper ligand with a

tailored binding site specific for the catecholamine of interest. We hope to use lanthanide(macrocycle) complexes to this aim, avoiding capillary electrophoresis or other purification/separation techniques, and attaining better limits of detection in a much shorter time period for these biologically relevant analytes.

5.4.2 Spectroscopy

Due to the high pK_as of the phenol hydrogens for catecholamines (Table 5.1),[93, 94] we will be working in very basic conditions to ensure deprotonation of these hydroxyl groups and promote lanthanide complexation. In addition to dopamine, epinephrine and norepinephrine, we will also use catechol (Cat) alone as a control species, to ensure deprotonation of the two hydroxyl species and bidentate chelation to the lanthanide.[95] We will perform a ligand screen using various Tb(ligand) complexes, where the ligand is EDTA, DO2A, DO3A or DOTA, to determine the optimal binary complex for CA chelation. The ligand should prevent precipitation of the terbium as $Tb(OH)_3$ in this high pH regime and allow effective binding of the CA analyte. We anticipate that DO3A, which binds in a heptadentate fashion and leaves space for one bidentate chelator on the Tb^{3+} ion, should be the best ligand for CA complexation.

Experimental Section

Materials. The following chemicals were purchased and used as received: CAPS (*N*-cyclohexyl-3-aminopropanesulfonic acid) buffer (Alfa Aesar), catechol (bis-benzenediol, *1,2*-dihydroxybenzene) (TCI America), dopamine hydrochloride (*2*-(*3,4*-dihydroxyphenyl)ethylamine hydrochloride) (Alfa Aesar), DOTA (*1,4,7,10*-tetraaza-

cyclododecane-*1,4,7,10*-tetraacetate) (Macrocyclics), EDTA (ethylenediaminetetraacetic acid) (Aldrich), L-epinephrine (L-adrenaline) (Alfa Aesar), norepinephrine (L-noradrenaline) (Alfa Aesar), sodium hydroxide (NaOH 50% in water) (Mallinckrodt Baker) and terbium(III) chloride hexahydrate (Alfa Aesar). The $TbCl_3$ salt and CAPS buffer were 99.99% pure and all CAs were at least 98% pure. DO2A was prepared as previously described (Section 2.2.1). DO3A was prepared as previously described (Section 5.2.2). Water was deionized to a resistivity of 18.2 MΩ-cm using a Purelab® Ultra laboratory water purification system.

Methods. All samples were prepared to a final volume of 4.00 mL in disposable acrylate cuvettes (Spectrocell) with a 1 cm path length. Catecholamine stock solutions (4.0 mM) were kept refrigerated (4 °C) in the dark until use. Tb(ligand) stock solutions (4.0 mM, pH 7.5) were allowed to equilibrate for 1 week before use to ensure complete lanthanide complexation. Luminescence spectral analysis was performed by a Fluorolog Fluorescence Spectrometer with a 350-nm colorless sharp cutoff glass filter as previously described (Section 5.2.2). The solution pH was measured using ColorpHast™ pH indicator strips (EMD Chemicals) following data collection.

It should be noted that many catecholamines are light-sensitive, and must be prepared and stored carefully to prevent degradation. Norepinephrine is the most sensitive to light. Fresh NE solutions will have a brownish color (depending on concentration), and should be refrigerated or preferably frozen for storage. Epinephrine solutions should be clear; upon degradation, which for refrigerated samples can take a few weeks, the solution will turn pink and then brown. Dopamine is less soluble, and

makes clear solutions. As with NE, there is no visual indication when DA solutions have started to degrade, so it is recommended they are prepared fresh for each experiment.

Cuvettes of 10.0 μM CA (Cat, DA, Epi or NE) and 1.0 mM of Tb(ligand), where ligand is EDTA, DO2A, DO3A or DOTA, were prepared in 50 mM CAPS buffer, pH 13.5 (adj. with 50% NaOH added dropwise). Excitation (λ_{em} = 544 nm) and emission (λ_{ex} = 255 nm, 290 nm) spectra were obtained following 1 hour equilibration time.

Results and Discussion

Excitation spectra of the Tb(ligand)(CA) complexes (Figure 5.18) illustrate one band near 255 nm and another centered around 290–295 nm. The former is assigned as the singlet $\pi \rightarrow \pi^*$ transition L_a (in the notation of Platt[96]) of the catechol dianion (256 nm),[97] while the latter is consistent with the L_b transition of the catechol dianion, which is red-shifted from 308 nm to 290 nm when bound to a metal.[98] The Tb(DOTA)(CA) spectra all exhibit the sharp bands of the Tb^{3+} excitation spectrum, as expected considering the high concentration of terbium (1.0 mM) and the exclusion of all but one water from the lanthanide coordination sphere. For all of the catecholamines (DA, Epi and NE), the excitation intensity of the Tb(ligand)(CA) complexes was of the order DO2A > EDTA > DO3A ~ DOTA. For catechol (Cat), the order was slightly different: DO2A > DO3A ~ DOTA > EDTA. It should be noted that for all four analytes, precipitation was observed in the DO3A and DOTA cuvettes, so we will focus on the EDTA and DO2A ligands for our analysis.

Emission spectra were obtained at both λ_{max} values (255 and 290 nm) seen in the excitation spectra, but as the intensities obtained for excitation at 255 nm were about an

order of magnitude greater, we will focus on these spectra (Figure 5.19). In all cases except dopamine, the Tb(DO2A)(CA) complex had the greatest luminescence intensity. Due to the intense excitation spectrum for the Tb(DO2A)$(DA)^-$ complex, we believe the extremely low intensity of the emission spectrum for this complex is in error, possibly due to the slits of the fluorescence spectrometer opening improperly. As these measurements were not performed in triplicate, these spectra should be collected again under the same conditions before conclusions can be drawn for dopamine.

For the other three analytes studied (catechol, epinephrine and norepinephrine), the emission spectral profiles for the Tb(DO2A)(CA) complexes are all very similar, as are the splittings of all four Tb(EDTA)(CA) emission spectra. Since the Stark splitting of the emission bands is indicative of the composition and geometry of the lanthanide coordination sphere, this suggests that these three ligands chelate to the Tb^{3+} cation in the same fashion for a given Tb(ligand) binary complex. The excitation spectra indicate that these are all the catechol dianion species, and therefore bidentate coordination via the deprotonated hydroxyl moieties is the most likely mode of binding. The relative intensities of the Tb(DO2A)(CA) spectra indicate that epinephrine and norepinephrine coordinate with slightly greater affinity than catechol. We attribute this to the electron-withdrawing effects of the substituents on the opposite side of the ring from the dihydroxy binding site.

It is interesting that only the binary complexes with hexadentate ligands (EDTA and DO2A) showed any significant binding for all bidentate catecholamines examined. Although this may be simply a result of poor solubility of the Tb(DO3A) complex in this pH regime, there may be steric factors involved as well. Perhaps the two remaining

coordination sites available on the Tb(DO3A) complex are not in the correct configuration to accommodate the dihydroxy catechol face of the analyte. A steric argument could also explain why the DO2A ligand is preferred over EDTA; though both have three adjacent binding sites available for CA chelation, they are arranged in a linear pattern for $Tb(DO2A)^{+}$ and in a triangular pattern for $Tb(EDTA)^{-}$. This preliminary analysis implies that further experimentation is necessary to understand the complex relationship between ligand denticity, binding site geometry and catecholamine binding affinity.

5.4.3 Conclusion

Though we have only begun to explore the potential of lanthanide(macrocycle) complexes in the detection of catecholamines, we have established through simple spectroscopic analysis that DO2A is superior to the previously proposed EDTA in forming a luminescent Tb(ligand)(CA) complex at high pH. Future work such as evaluation of catecholamine binding affinities and lifetime measurements to determine the hydration numbers of the Tb(ligand)(CA) complexes would help significantly in our understanding of this system. Luminescence intensities would be further improved by degassing these samples and working under inert atmosphere to avoid oxidation of the catecholamines and related compounds.

5.5 Concluding Remarks

We have demonstrated the versatility of Tb(ligand) binary complexes in the detection of various salicylates and catecholamines using sensitized lanthanide luminescence. Both cyclic (DO2A) and linear (EDTA) chelators can be utilized to generate a receptor site with increased stability and greater affinity for the analyte of interest. In each case, finding the optimal match between lanthanide complex and target analyte is not always intuitive; indeed, all bidentate analytes explored here were most compatible with hexadentate ligands, which leave not two but three sites available on the nine-coordinate lanthanide ion (Table 5.5). The mechanisms that govern optimization of effective ligand-analyte pairings remain to be elucidated, though binding site geometry, interligand interactions and electron density perturbations on the central lanthanide are likely contributing factors.

The use of a helper ligand for analyte detection affords several advantages over lanthanide ions alone. The ligand stabilizes the complex over a wider pH range, allowing for detection even in very basic conditions, which is often required for analytes that must be fully deprotonated to bind effectively (i.e., SA and CAs). The chelating ligand also prevents the coordination of multiple analyte molecules to the same lanthanide, and therefore establishes a linear correlation between luminescence intensity and analyte concentration. In addition, use of these ligands provides greater options for sensor specificity and design, in that modifications can be incorporated for enhanced interligand interactions or tethering the complex to a solid substrate.

We anticipate further development of lanthanide binary complexes as receptor sites for aromatic anions, with the ultimate goal of generating highly specific sensors

capable of sensitive detection in matrices such as environmental samples or biological fluids. The possibility of using several lanthanide-based receptor sites simultaneously then becomes possible. For instance, as salicylic acid is broken down into salicylurate in the liver, the ratio of SA to SU could be an efficient method to monitor liver health and function. A dual assay could be envisioned using $Tb(DO2A)^{+}$ at pH 8.4 to detect SU and $Tb(EDTA)^{-}$ at pH 13.5 to detect SA in aliquots taken from the same plasma or urine sample. Though we are only in the initial stages of meeting such goals, the work presented here represents the first step in the application of tailored lanthanide-based receptor sites in the detection of aromatic analytes.

Through the investigations reported in this dissertation, we have learned some important lessons regarding sensor design that have applications in a multitude of fields. We have discovered that the property of 'ligand enhanced' binding affinity is not unique to the dipicolinate system, and that ligand chelation can significantly improve the lanthanide-based detection of a variety of oxyanions. We have also learned that net electrostatic interaction is not the dominant factor governing coordination to lanthanide binary complexes, and in fact variations in the local charge density may be much more important. Even neutral lanthanide complexes can attract anionic ligands better than the corresponding tripositive Ln^{3+} ion alone, with improvements in binding affinity by an order of magnitude or more. This ligand enhancement is most likely due to perturbations in the electron density of the lanthanide by the electron-withdrawing moieties of the ligand, generating a more electropositive binding site for the complex than the aquo ion alone is capable. This theory could be verified by modifying a ligand like DO2A to contain strongly electronegative species (such as fluorine) on the opposite side as the

dipicolinate binding site. If indeed the lanthanide electron density is affected, this should result in an even more positive binding site, and hence a greater dipicolinate binding affinity. Further experiments with photoelectron or Raman spectroscopy are expected to ascertain the degree of perturbation of the lanthanide by the helper ligand.

Our work also indicates that ligand interactions with lanthanide complexes cannot be predicted based on the number of available binding sites or their geometry. Bidentate ligands sometimes prefer a lanthanide complex with three remaining coordination sites instead of two, and monodentate ligands in some cases can bind more strongly to a lanthanide ion encapsulated by a heptadentate ligand as opposed to an octadentate one. We have also found that both cyclic and acyclic ligands can produce lanthanide complexes that are effective receptor sites for analytes. We therefore recommend that, to determine the optimal partnering between lanthanide complex and analyte, ligand screens should always be performed to enhance receptor site performance and specificity. This could be best accomplished with binding studies to quantify analyte binding affinity, such as the binding affinity by competition (BAC) assay proposed here.

The advantages of ligand enhancement can be implemented in current detection schemes where lanthanide ions alone are used to chelate other molecules of interest. As mentioned in Chapter 1, there are various areas of research involving sensitized lanthanide luminescence, ranging from PCR and gene detection techniques which monitor disease and toxins, to drug discovery applications and high-throughput screening assays. The application of lanthanide(ligand) complexes instead of lanthanide ions alone could significantly enhance the efficacy of these methods. For instance, detection of tyrosine kinase activity by terbium luminescence could be improved markedly with the

addition of a chelating ligand such as DO2A or DO3A. The terbium cation binds to phosphorylated tyrosine, which is used to mitigate diseases involving tyrosine kinase-mediated signaling.[99] With the binding enhancement of a chelating ligand, the limit of detection of phosphorylated tyrosine is expected to be improved by an order of magnitude or more. One can envision taking further advantage of this effect by addition of electronegative groups such as fluorine to the helper ligand to generate an even more electropositive binding cavity. Such binary complexes could also find use in time-resolved Förster resonance energy transfer (FRET) systems, where improved lanthanide luminescence lifetime as a result of ligand coordination could manifest in enhanced limits of detection.

Further, evidence of a ligand-induced 'gadolinium break' effect can have implications in various studies involving lanthanide chelation. One cannot assume that a given trend in a physical or chemical property for the lanthanide series will remain constant in the presence of a chelating ligand, especially one containing nitrogen and oxygen donor atoms. In the work described here, the unique susceptibility of Tb^{3+} to electron density perturbation by a chelating ligand worked to our advantage, producing a more electropositive binding site in the $Tb(DO2A)^{+}$ complex than any other lanthanide complex. However, this gadolinium break effect is only one of many phenomena governing the stability and photophysics of lanthanide complexes. Those exploring lanthanide complexes for targeted detection should keep in mind that choice of lanthanide can significantly influence binding affinity and related properties, especially near gadolinium in the lanthanide series (i.e., terbium and europium).

Lanthanide chemistry is a rich and often enigmatic field; in many ways we are still only scratching the surface of applications and possibilities. We hope that the lessons learned in the course of this dissertation will promote the development of more sensitive and selective receptor sites in the sensor design pursuits of the future.

REFERENCES

(1) Arnaud, N.; Georges, J. *Analyst* **1999**, *124*, 1075-1078.
(2) Bailey, M. P.; Rocks, B. F.; Riley, C. *Analytica Chimica Acta* **1987**, *201*, 335-338.
(3) Lianidou, E. S.; Ioannou, P. C.; Polydorou, C. K.; Efstathiou, C. E. *Analytica Chimica Acta* **1996**, *320*, 107-114.
(4) Tuckerman, M. M.; Mayer, J. R.; Nachod, F. C. *Journal Of The American Chemical Society* **1959**, *81*, 92-94.
(5) Kiss, T.; Sóvágó, I.; Martin, R. B. *Journal Of The American Chemical Society* **1989**, *111*, 3611-3614.
(6) Services, D. o. H. a. H., Ed.; Food and Drug Administration, 1998; Vol. 63, pp 56802-56819.
(7) Bayer, A. *Clinicians' Guide to Aspirin*; Chapman & Hall Medical: London, 1998.
(8) Taylor, D. W.; Barnett, H. J. M.; Haynes, R. B.; Ferguson, G. G.; Sackett, D. L.; Thorpe, K. E.; Simard, D.; Silver, F. L.; Hachinski, V.; Clagett, G. P.; Bames, R.; Spence, J. D. *The Lancet* **1999**, *353*, 2179-2184.
(9) Group, T. C. C. S. *New England Journal of Medicine* **1978**, *299*, 53-59.
(10) Coolen, S. A. J.; Huf, F. A.; Reijenga, J. C. *Journal of Chromatography B* **1998**, *717*, 119-124.
(11) Williams, F. M. *Clinical Pharmacokinetics* **1985**, *10*, 392-403.
(12) Liu, J.-H.; Smith, P. C. *Journal of Chromatography B* **1996**, *675*, 61-70.
(13) Miners, J. O. *Clinical Pharmacokinetics* **1989**, *17*, 327-344.
(14) Levy, G.; Amsel, L. P.; Elliott, H. C. *Journal of Pharmaceutical Sciences* **1969**, *58*, 827-829.
(15) Levy, G. *Journal of Pharmaceutical Sciences* **1965**, *54*, 959-967.
(16) Paterson, J. R.; Baxter, G. J.; Dreyer, J. S.; Halket, J. M.; Flynn, R.; Lawrence, J. R. *Journal of Agricultural and Food Chemistry* **2008**, *56*, 11648-11652.
(17) Bar-Or, D.; Office, U. S. P. a. T., Ed.; Appenditech, Inc.: United States, 1995, pp 1-16.
(18) Buskin, J. N.; Upton, R. A.; Williams, R. L. *Clinical Chemistry* **1982**, *28*, 1200-1203.
(19) Peng, G. W.; Gadalla, M. A. F.; Smith, V.; Peng, A.; Chiou, W. L. *Journal of Pharmaceutical Sciences* **1977**, *67*, 710-712.
(20) Cham, B. E.; Bochner, F.; Imhoff, D. M.; Johns, D.; Rowland, M. *Clinical Chemistry* **1980**, *26*, 111-114.
(21) Zaugg, S.; Zhang, X.; Sweedler, J.; Thormann, W. *Journal of Chromatography B* **2001**, *752*, 17-31.
(22) Salinas, F.; Berzas Nevado, J. J.; Espinosa Mansilla, A. *Talanta* **1990**, *37*, 347-351.
(23) Bavoso, A.; Menabue, L.; Saladini, M.; Sola, M. *Inorganic Chemica Acta* **1996**, *244*, 207-212.
(24) Ferrer, E. G.; Gonzalez Baro, A. C.; Castellano, E. E.; Piro, O. E.; Williams, P. A. M. *Journal of Inorganic Biochemistry* **2004**, *98*, 413-421.
(25) Kiss, T.; Jakusch, T.; Kilyen, M.; Kiss, E.; Lakatos, A. *Polyhedron* **2000**, *19*, 2389-2401.
(26) Jancso, A.; Gajda, T.; Szorcsik, A.; Kiss, T.; Henry, B.; Vanko, G.; Rubini, P. *Journal of Inorganic Biochemistry* **2001**, *83*, 187-192.
(27) Parker, D. *Chemical Communications* **2005**, 3141-3143.
(28) Pal, R.; Parker, D.; Costello, L. C. *Organic and Biomolecular Chemistry* **2009**, *7*, 1525-1528.
(29) Carnall, W. T.; Fields, P. R.; Rajnak, K. *Journal Of Chemical Physics* **1968**, *49*, 4447-4449.
(30) Wang, Q.-M. *Journal of Organometallic Chemistry* **2006**, *691*, 545-550.

(31) Arnaud, N.; Vaquer, E.; Georges, J. *Analyst* **1998**, *123*, 261-265.
(32) Carnall, W. T.; Fields, P. R.; Rajnak, K. *Journal Of Chemical Physics* **1968**, *49*, 4424-4442.
(33) Carnall, W. T.; Fields, P. R.; Rajnak, K. *Journal Of Chemical Physics* **1968**, *49*, 4450-4455.
(34) Hemmila, I.; Laitala, V. *Journal Of Fluorescence* **2005**, *15*, 529-542.
(35) Kim, W. D.; Hrncir, D. C.; Kiefer, G. E.; Sherry, A. D. *Inorganic Chemistry* **1995**, *34*, 2225-2232.
(36) Mishra, A., 2008.
(37) Maheshwari, S.; Chowdhury, A.; Sathyamurthy, N. *Journal of Physical Chemistry A* **1999**, *103*, 6257-6262.
(38) Lahmani, F.; Zehnacker-Rentien, A. *Journal of Physical Chemistry A* **1997**, *101*, 6141-6147.
(39) Ainsworth, C. C.; Friedrich, D. M.; Gassman, P. L.; Wang, Z.; Joly, A. G. *Geochimica et Cosmochimica Acta* **1998**, *62*, 595-612.
(40) Weller, A. *Progress in Reaction Kinetics and Mechanisms* **1961**, *1*, 188-214.
(41) Heimbrook, L.; Kenny, J. E.; Kohler, B. E.; Scott, G. W. *Journal of Physical Chemistry* **1983**, *87*, 280-289.
(42) Barbara, P. F.; Walsh, P. K.; Brus, L. E. *Journal of Physical Chemistry* **1989**, *93*, 29-34.
(43) Horrocks Jr., W. D.; Sudnick, D. R. *Journal Of The American Chemical Society* **1979**, *101*, 334-340.
(44) Beeby, A.; Clarkson, I. M.; Dickins, R. S.; Faulkner, S.; Parker, D.; Royle, L.; de Sousa, A. S.; Williams, J. A. G.; Woods, M. *Journal of the Chemical Society-Perkin Transactions 2* **1999**, 493-503.
(45) Cable, M. L.; Kirby, J. P.; Levine, D. J.; Manary, M. J.; Gray, H. B.; Ponce, A. *Journal Of The American Chemical Society* **2009**, *131*, 9562-9570.
(46) Bosund, L. *Advances in Food Research* **1962**, *11*, 331-353.
(47) Gollnick, H.; Schramm, M. *Dermatology* **1998**, *196*, 119-125.
(48) Russell, A. D. In *Principles and Practice of Disinfection, Preservation and Sterilization,* Third ed.; Russell, A. D., Hugo, W. B., Ayliffe, G. A. J., Eds.; Blackwell Science Ltd.: Oxford, 1999, pp 95-123.
(49) Davies, M. G.; Briffa, D. V.; Greaves, M. W. *British Journal of Medicine* **1979**, *1*, 661.
(50) Bernstein, J. M.; Weiss, A. D. *Journal of Laryngology & Otology* **1967**, *81*, 915-926.
(51) Chaniotakis, N. A.; Park, S. B.; Meyerhoff, M. E. *Analytical Chemistry* **1989**, *61*, 566-570.
(52) Goto, Y.; Makino, K.; Kataoka, Y.; Shuto, H. *Journal of Chromatography B* **1998**, *706*, 329-335.
(53) Brodie, B. B.; Udenfriend, S.; Coburn, A. F. *Journal of Pharmacology And Experimental Therapeutics* **1944**, *80*, 114-117.
(54) Lange, W. E.; Bell, S. A. *Journal of Pharmaceutical Sciences* **1966**, *55*, 386-389.
(55) Saltzman, A. *Journal of Biological Chemistry* **1948**, *174*, 399-404.
(56) Bae, S. K.; Seo, K. A.; Jung, E. J.; Kim, H.-S.; Yeo, C.-W.; Shon, J.-H.; Park, K.-M.; Liu, K.-H.; Shin, J.-G. *Biomedical Chromatography* **2008**, *22*, 590-595.
(57) Kees, F.; Jehnich, D.; Grobecker, H. *Journal of Chromatography B* **1996**, *677*, 172-177.
(58) Cham, B. E.; Johns, D.; Bochner, F.; Imhoff, D. M.; Rowland, M. *Clinical Chemistry* **1979**, *25*, 1420-1425.
(59) Torriero, A. A. J.; Luco, J. M.; Sereno, L.; Raba, J. *Talanta* **2004**, *62*, 247-254.
(60) Trinder, P. *Biochemical Journal* **1954**, *57*, 301-303.
(61) Silva, T. R.; Valdman, E.; Valdman, B.; Leite, S. G. F. *Brazilian Journal of Microbiology* **2007**, *38*, 39-44.

(62) Perrin, D. D. *Nature* **1958**, *182*, 741-742.
(63) Li, C.; Wong, W.-T. *Tetrahedron Letters* **2004**, *45*, 6055-6058.
(64) Minnick, L. J.; Kilpatrick, M. *Journal Of Physical Chemistry* **1939**, *43*, 259-274.
(65) Porto, R.; De Tommaso, G.; Furia, E. *Annali di Chimica* **2005**, *95*, 551-558.
(66) Martell, A. E.; Smith, R. M. *Critical Stability Constants*; Plenum Press: New York, 1974.
(67) Chang, C. A.; Chen, Y.-H.; Chen, H.-Y.; Shieh, F.-K. *Journal Of The Chemical Society-Dalton Transactions* **1998**, 3243-3248.
(68) Schwarzenbach, G.; Freitag, E. *Helvetica Chimica Acta* **1951**, *34*, 1503-1508.
(69) Tsaryuk, V. I.; Zhuravlev, K.; Zolin, V. F.; Gawryszewska, P.; Legendziewicz, J.; Kudryashova, V. A.; Pekareva, I. *journal Of Photochemistry And Photobiology A-Chemistry* **2006**, *177*, 314-323.
(70) Hockenbury, D. H.; Hockenbury, S. E. *Psychology*, Fourth Edition ed.; Worth Publishers: New York, 2006.
(71) Goldstein, D. S.; Eisenhofer, G.; McCarty, R. *Catecholamines: Bridging Basic Science with Clinical Medicine*; Academic Press: San Diego, 1998.
(72) Whitby, L.; Axelrod, J.; Weil-Malherbe, H. *Journal of Pharmacology And Experimental Therapeutics* **1961**, *132*, 191-201.
(73) Raab, W. *The American Journal of Cardiology* **1960**, *5*, 571-578.
(74) Madras, B. K.; Miller, G. M.; Fischman, A. J. *Behavioural Brain Research* **2002**, *130*, 57-63.
(75) Greer, M.; Williams, C. M. *Neurology* **1963**, *13*, 73-76.
(76) Barbeau, A. *Canadian Medical Association Journal* **1962**, *87*, 802-807.
(77) Middleton, E.; Finke, S. R. *Journal of Allergy* **1968**, *42*, 288-299.
(78) Lockey, S. D.; Glennon, J. A.; Reed, C. E. *Journal of Allergy* **1967**, *40*, 349-354.
(79) Riggin, R. M.; Kissinger, P. T. *Analytical Chemistry* **1977**, *49*, 2109-2111.
(80) Hallman, H.; Farnebo, L.-O.; Hamberger, B.; Jonsson, G. *Life Sciences* **1978**, *23*, 1049-1052.
(81) van der Hoorn, F. A. J.; Boomsma, F.; Man In't Veld, A. J.; Schalekamp, M. A. D. H. *Journal of Chromatography B: Biomedical Sciences and Applications* **1989**, *487*, 17-28.
(82) Yamaguchi, M.; Yutani, Y.; Kohashi, K.; Ohkura, Y. *Analytica Chimica Acta* **1979**, *108*, 297-308.
(83) Robert, F.; Bert, L.; Denoroy, L.; Renaud, B. *Analytical Chemistry* **1995**, *67*, 1838-1844.
(84) Nohta, H.; Mitsui, A.; Ohkura, Y. *Analytica Chimica Acta* **1984**, *165*, 171-176.
(85) Nohta, H.; Mitsui, A.; Umegae, Y.; Ohkura, Y. *Biomedical Chromatography* **1986**, *2*, 9-12.
(86) Imai, K.; Tsukamoto, M.; Tamura, Z. *Journal of Chromatography A* **1977**, *137*, 357-362.
(87) Jameson, R. F.; Neillie, W. F. S. *Journal of Inorganic and Nuclear Chemistry* **1965**, *27*, 2623-2634.
(88) Jameson, R. F.; Neillie, W. F. S. *Journal of Inorganic and Nuclear Chemistry* **1966**, *28*, 2667-2675.
(89) Aydin, R. *Journal of Chemical and Engineering Data* **2007**, *52*, 2400-2404.
(90) Wu, Z. J.; Gao, F.; Wang, J. P.; Niu, C. J.; Niu, V. J. *Journal Of Coordination Chemistry* **2005**, *58*, 473-478.
(91) Chakrawarti, P. B.; Vijayvargiya, B. L.; Sharma, H. N. *Journal of the Indian Chemical Society* **1983**, *60*, 89-91.
(92) Zhu, R. H.; Kok, W. T. *Analytical Chemistry* **1997**, *69*, 4010-4016.
(93) Kiss, T.; Gergely, A. *Inorganica Chimica Acta* **1979**, *36*, 31-36.
(94) Gergely, A.; Kiss, T.; Deák, G.; Sóvágó, I. *Inorganica Chimica Acta* **1981**, *56*, 35-40.

(95) Borraccino, R.; Kharoune, M.; Giot, R.; Agathos, S. N.; Nyns, E.-J.; Naveau, H. P.; Pauss, A. *Water Research* **2001**, *35*, 3729-3737.
(96) Platt, J. R. *Journal Of Chemical Physics* **1949**, *17*, 484-495.
(97) Vaillancourt, F. H.; Barbosa, C. J.; Spiro, T. G.; Bolin, J. T.; Blades, M. W.; Turner, R. F. B.; Eltis, L. D. *Journal Of The American Chemical Society* **2002**, *124*, 2485-2496.
(98) Horsman, G. P.; Jirasek, A.; Vaillancourt, F. H.; Barbosa, C. J.; Jarzecki, A. A.; Xu, C.; Mekmouche, Y.; Spiro, T. G.; Lipscomb, J. D.; Blades, M. W.; Turner, R. F. B.; Eltis, L. D. *Journal Of The American Chemical Society* **2005**, *127*, 16882-16891.
(99) Zondlo, S. C.; Gao, F.; Zondlo, N. J. *Journal Of The American Chemical Society* **2010**, *ASAP*.

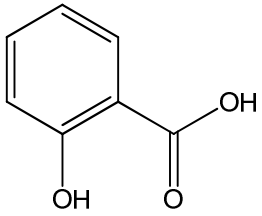

Salicylic acid (SA)

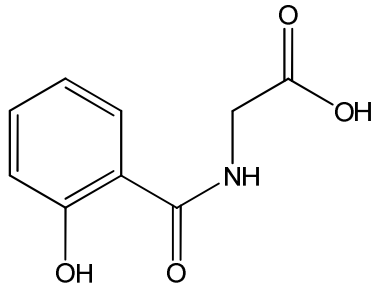

Salicyluric acid (SU)

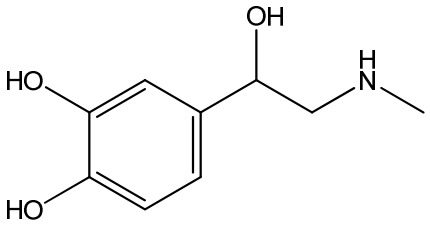

Epinephrine (Epi)

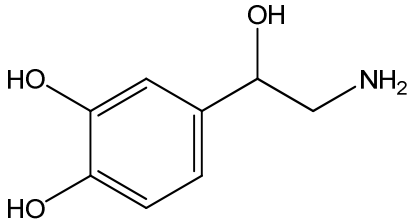

Norepinephrine (NE)

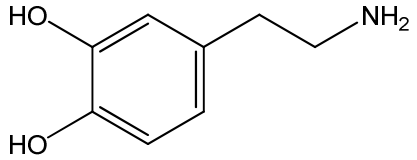

Dopamine (DA)

Figure 5.1. Various aromatic analytes to be investigated in terms of detection using a tailored terbium-macrocycle binary complex. Top row: salicylates. Bottom row: catecholamines.

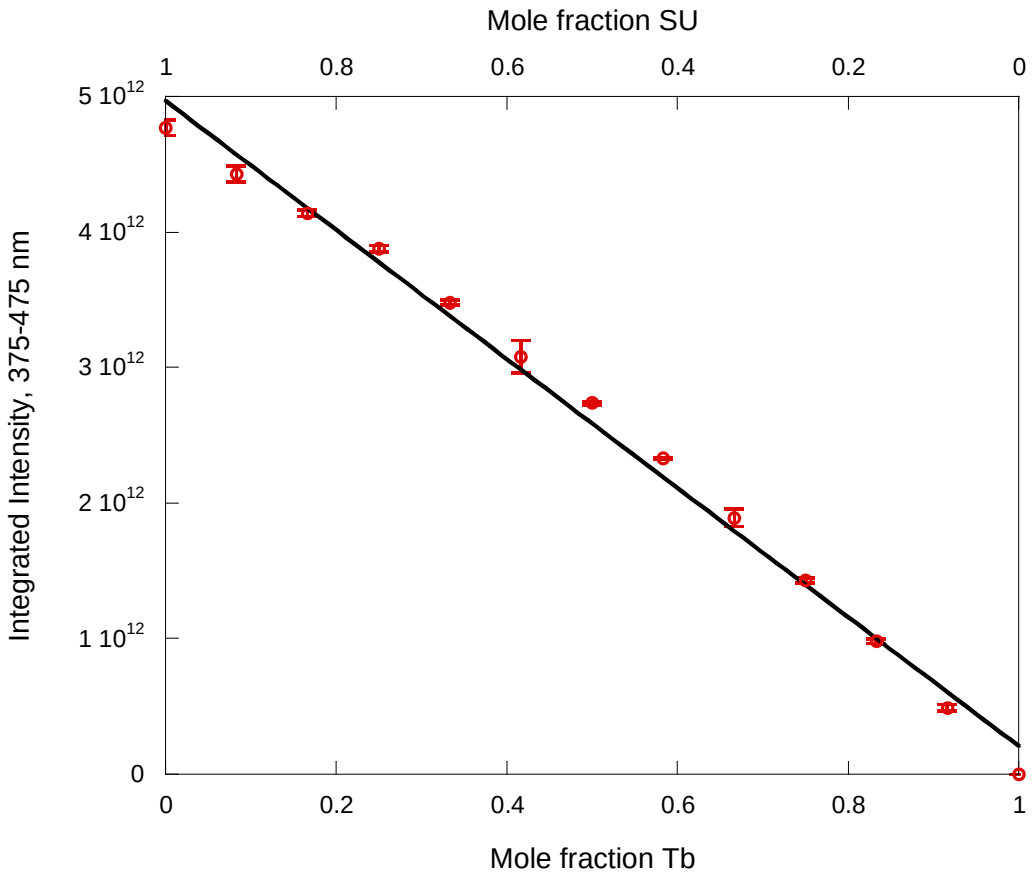

Figure 5.2. Method of continuous variations, showing linear correlation of intrinsic salicylurate (SU) luminescence (419 nm) that can be used as an internal standard. Concentrations of Tb and SU were varied inversely from 0 to 120 μM in 10 μM increments, with 500 μM DO2A in 0.1 M TAPS buffer, pH 8.4.

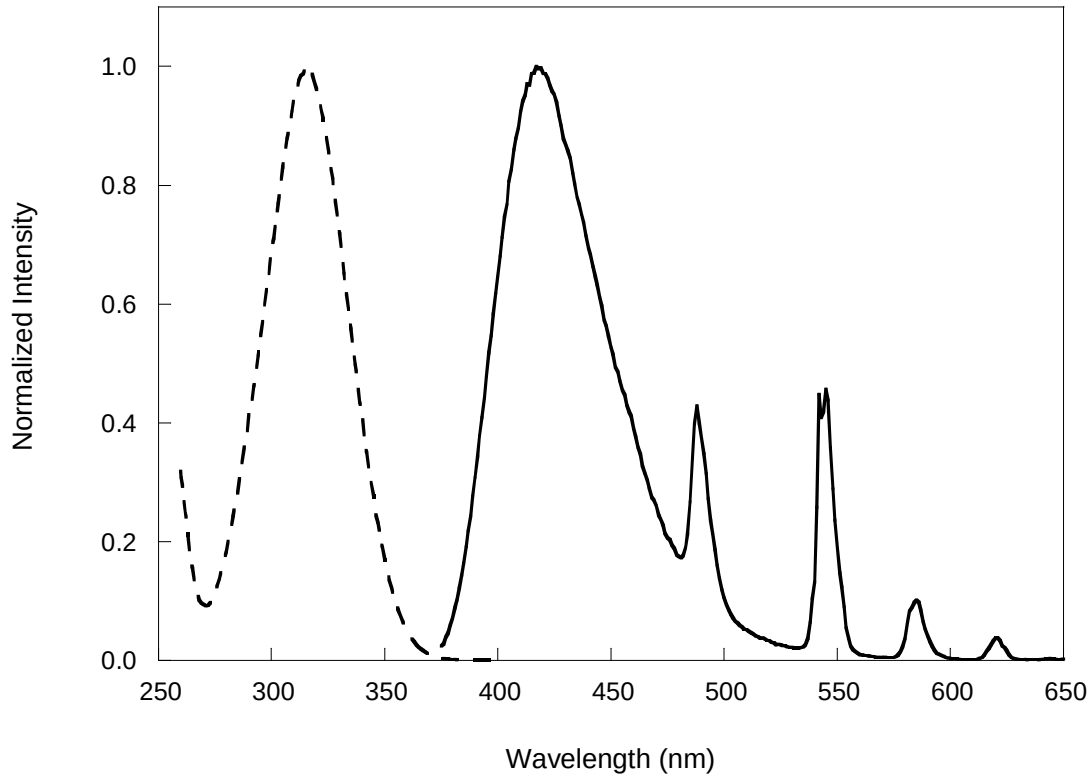

Figure 5.3. Excitation (dashed) and emission (solid) spectra of Tb(DO2A)(SU)$^{-}$ complex, 100 μM in 0.1 M TAPS buffer, pH 8.4 (λ_{ex} = 316 nm, λ_{em} = 544 nm).

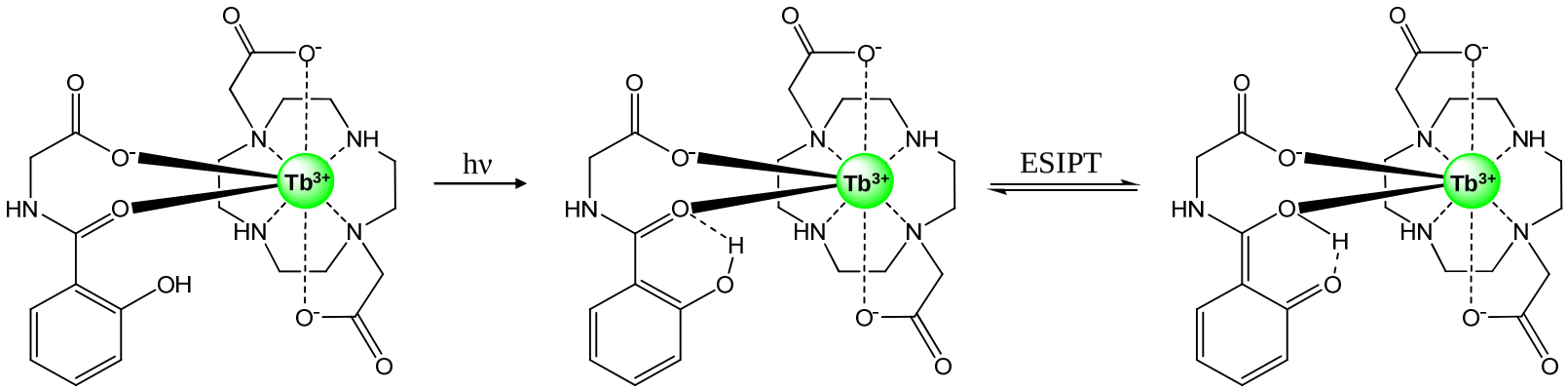

Figure 5.4. Most likely chelation mode of the salicylurate (SU) ligand to the $Tb(DO2A)^{+}$ complex. As shown, excited-state intramolecular proton transfer (ESIPT) can still occur on the SU ligand with this binding motif.

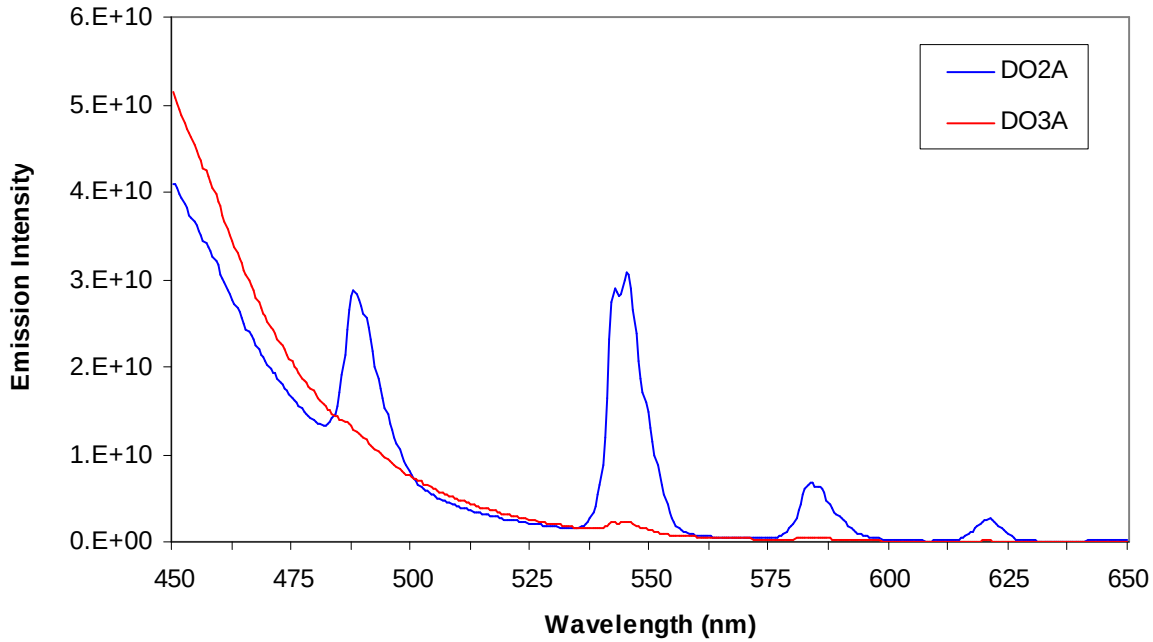

Figure 5.5. Emission spectra of Tb(DO2A)(SU)$^{-}$ and Tb(DO3A)(SU)$^{2-}$, 100 μM in 0.1 M TAPS, pH 8.4 (λ_{ex} = 316 nm).

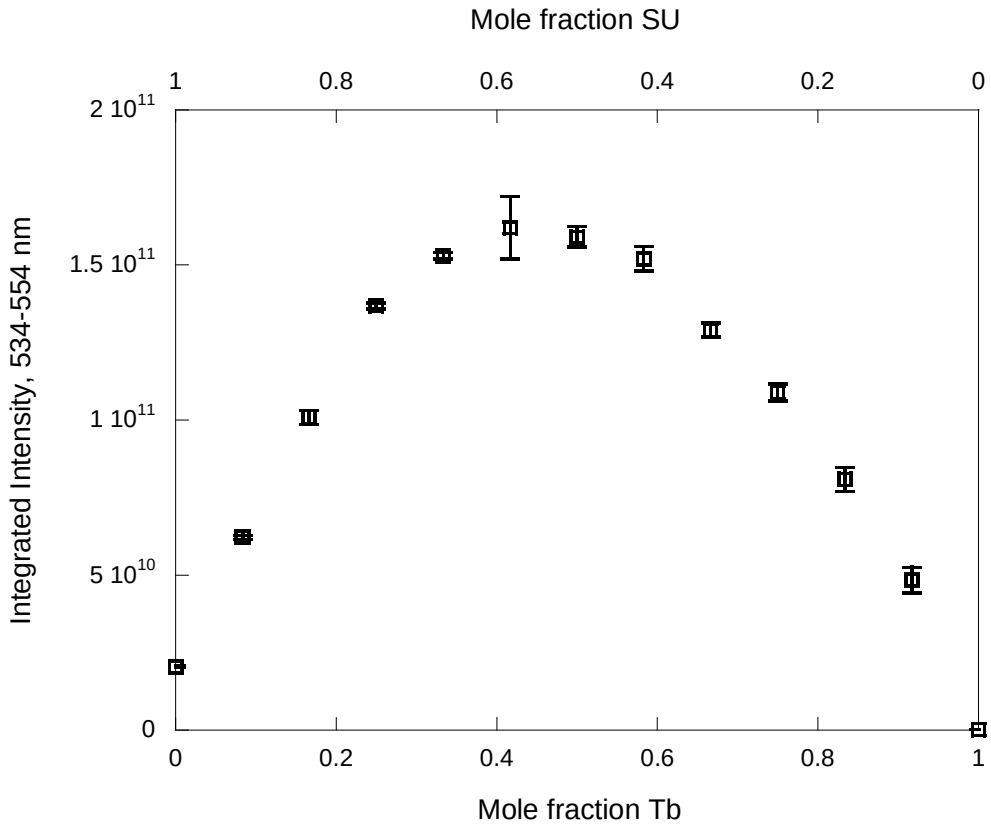

Figure 5.6. Method of continuous variations to determine binding stoichiometry of SU to $Tb(DO2A)^{+}$. [Tb] and [SU] varied inversely from 0–120 μM in 10 μM increments with 500 μM DO2A in 0.1 M TAPS buffer, pH 8.4 (λ_{ex} = 316 nm).

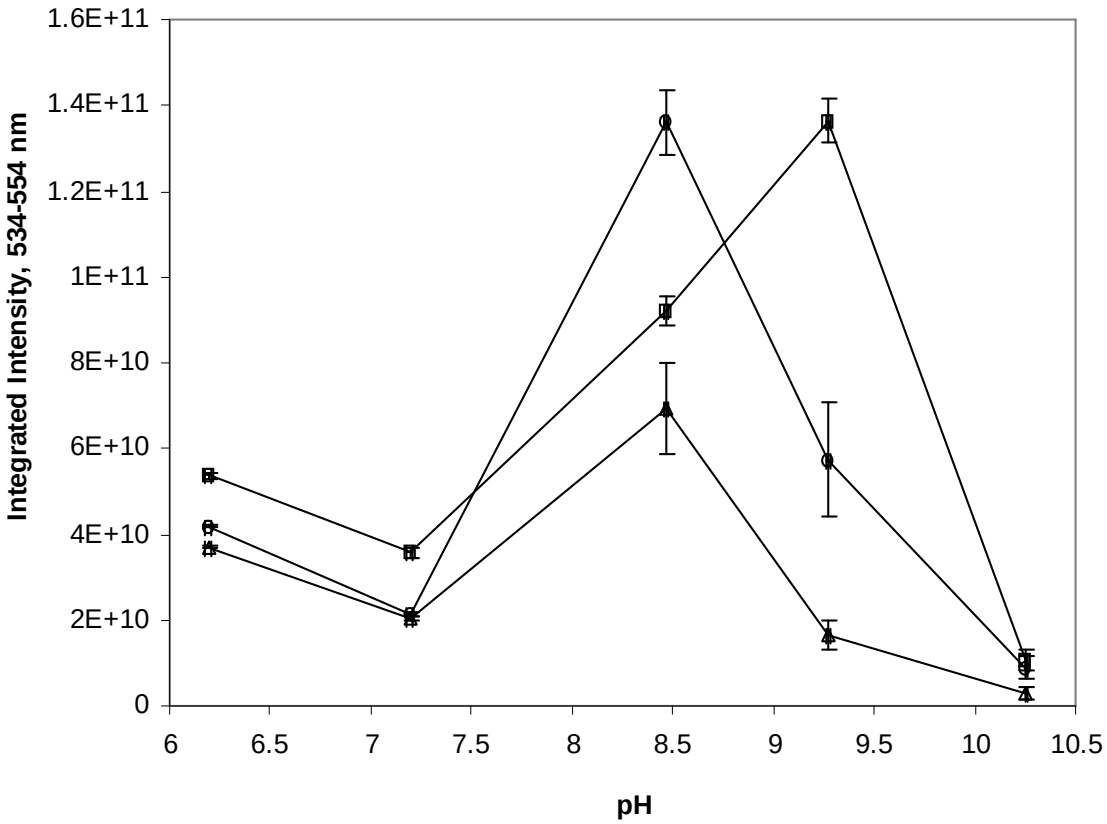

Figure 5.7. pH dependence study of Tb(DO2A)(SU)$^{-}$ complex, 100 μM with 5X excess DO2A. Emission spectra (λ_{ex} = 316 nm) obtained following 15 min (□), 18 hr (○) or 5 days (Δ) equilibration time.

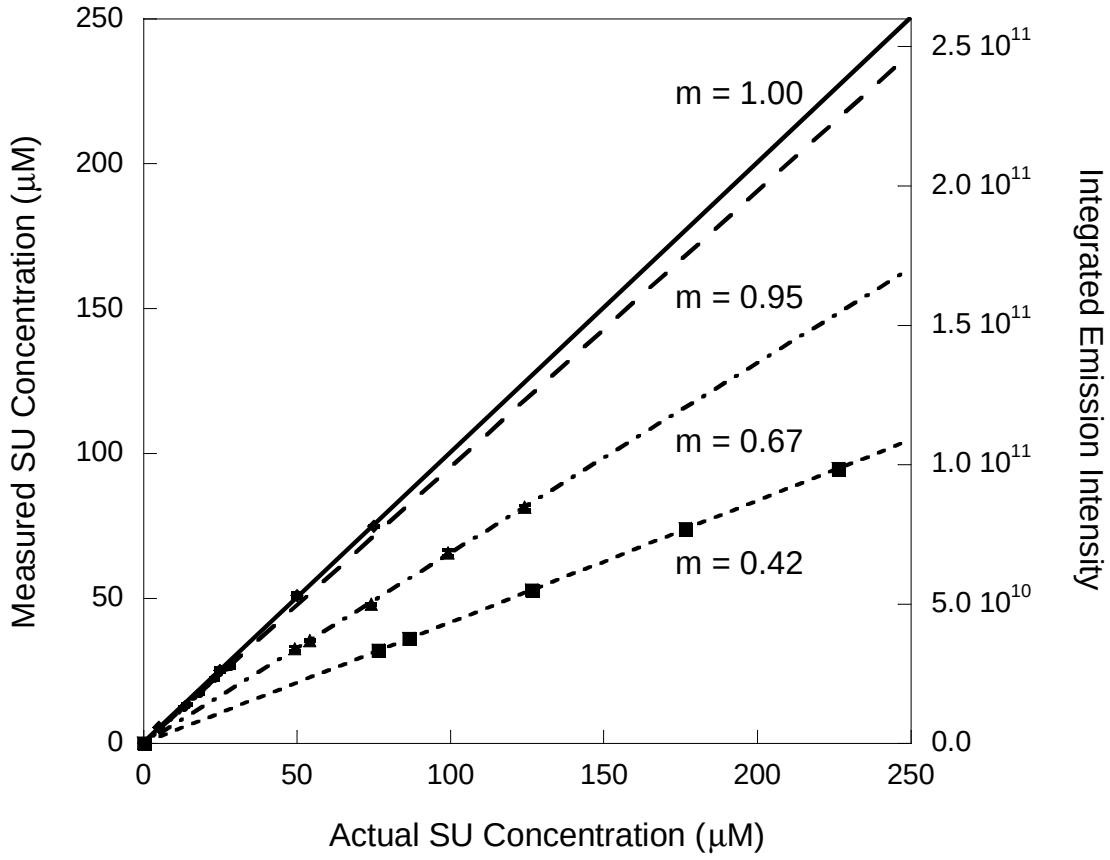

Figure 5.8. Dilution study of an SU-spiked urine sample for dilution factors of 1:3.5 (dotted), 1:7 (dashed-dotted), and 1:35 (dashed) into 5 mM $Tb(DO2A)^{+}$ in 0.1 M TAPS buffer, pH 8.4 (λ_{ex} = 316 nm). As the dilution factor is increased, the slope (m) approaches unity, equivalent to an aqueous solution spiked with SU (solid).

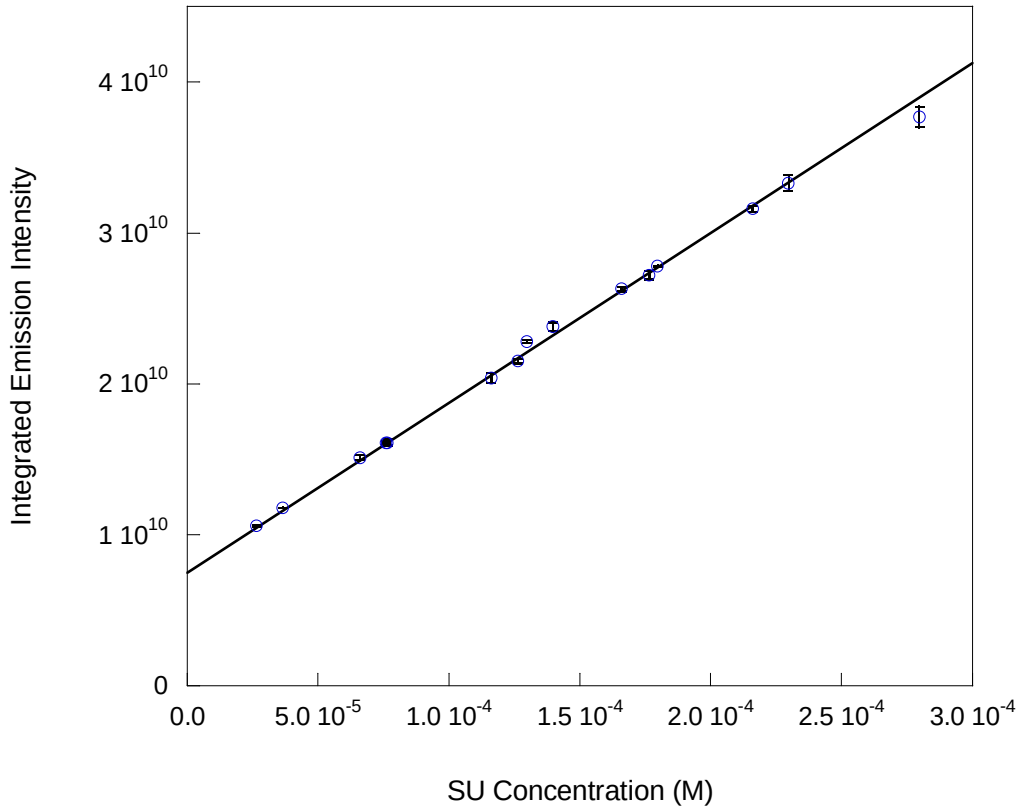

Figure 5.9. Calibration curve of SU spiked into urine samples (dilution factor 1:350) from three individual healthy donors, relating luminescence intensity to SU concentration. Samples diluted into 5 mM $Tb(DO2A)^{+}$ in 0.1 M TAPS buffer, pH 8.4 (λ_{ex} = 316 nm).

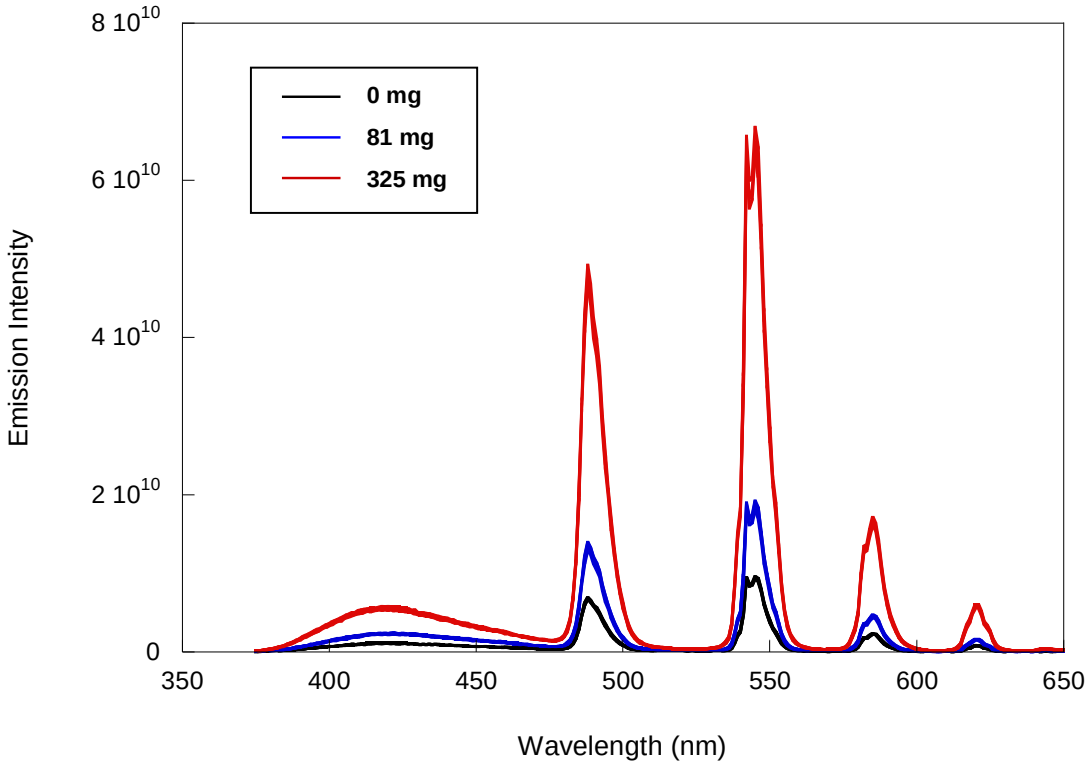

Figure 5.10. Aspirin study showing an increase in luminescence due to increased ASA dosage. Samples diluted 1:350 into 5 mM $Tb(DO2A)^{+}$ in 0.1 M TAPS buffer, pH 8.4 (λ_{ex} = 316 nm). Emission spectra, taken for three separate samples, are nearly superimposable for each aspirin dosage.

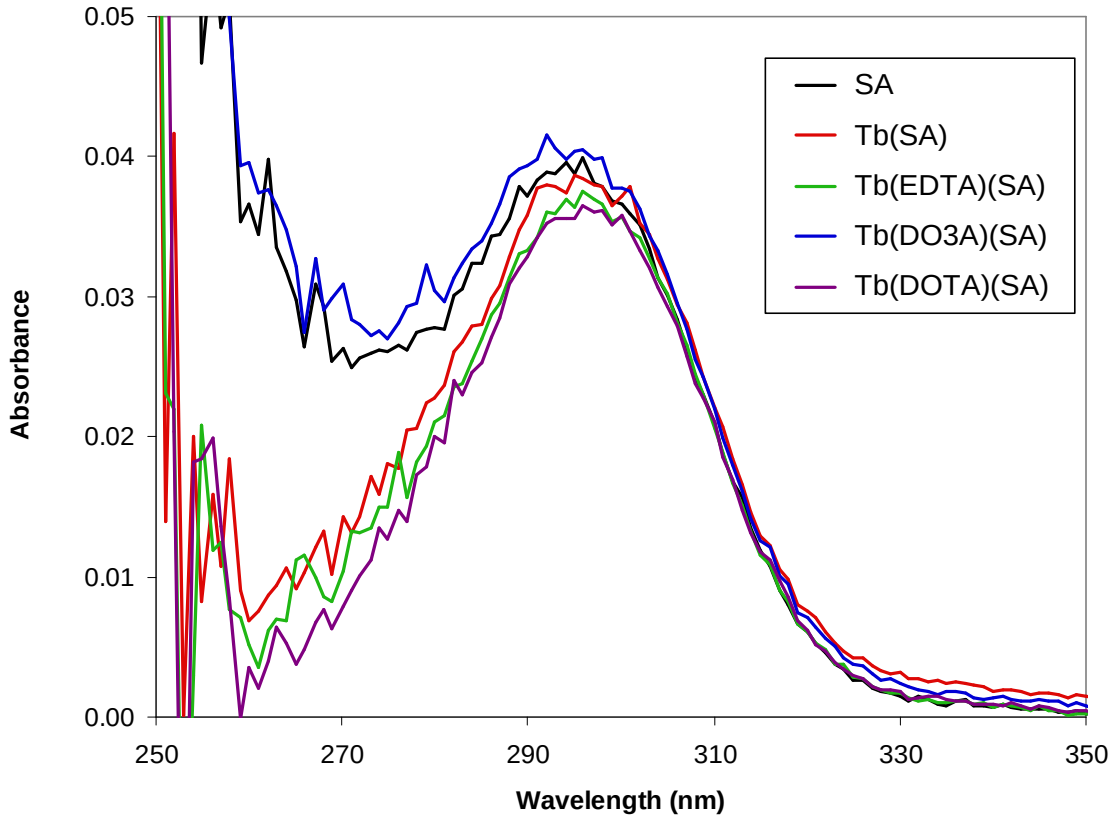

Figure 5.11. Absorption spectra for 10.0 μM SA, Tb(SA), Tb(EDTA(SA), Tb(DO3A)(SA) and Tb(DOTA)(SA) in 0.1 M CAPS (pH 10.0).

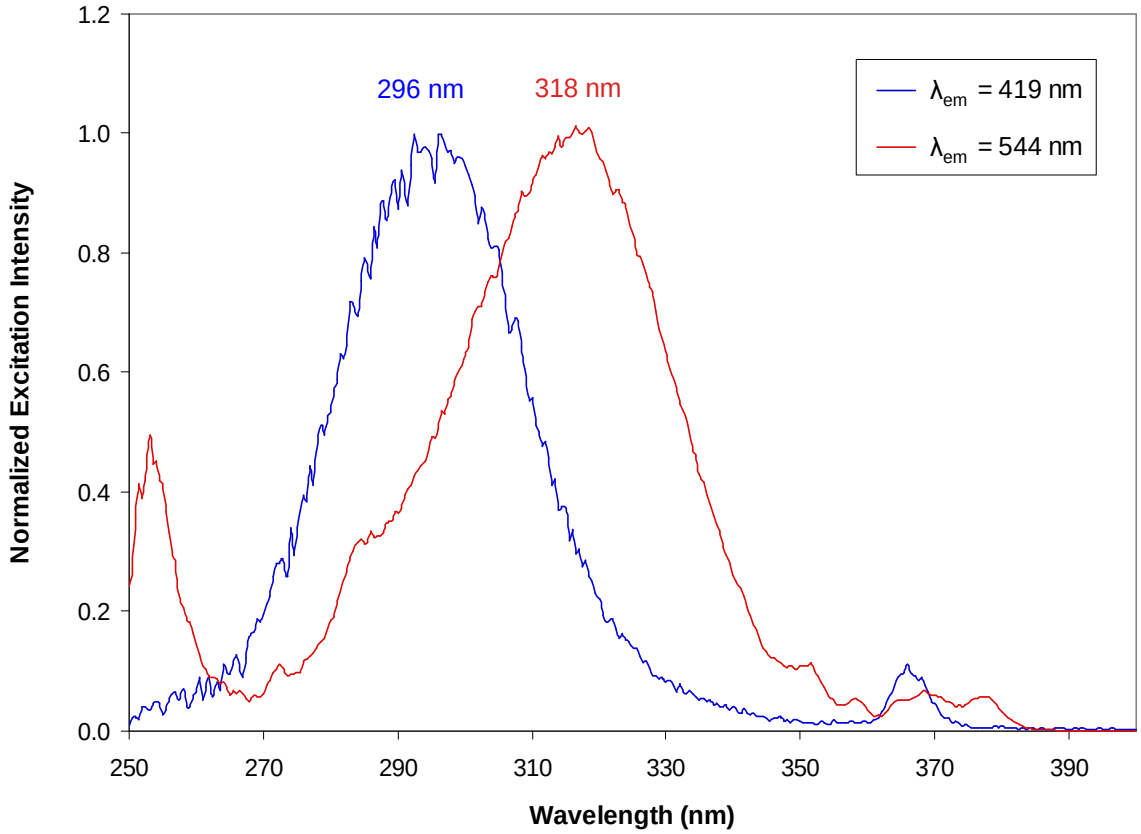

Figure 5.12. Normalized excitation spectra of Tb(EDTA)(SA) complex in 50 mM CAPS buffer (pH 12.5) at two emission wavelengths. The two populations are unchelated SA (blue) and the Tb(EDTA)(SA) complex (red) according to the emission spectra at 296 nm and 318 nm, respectively, which show ESIPT from SA alone or the characteristic terbium emission bands from the Tb(EDTA)(SA) complex.

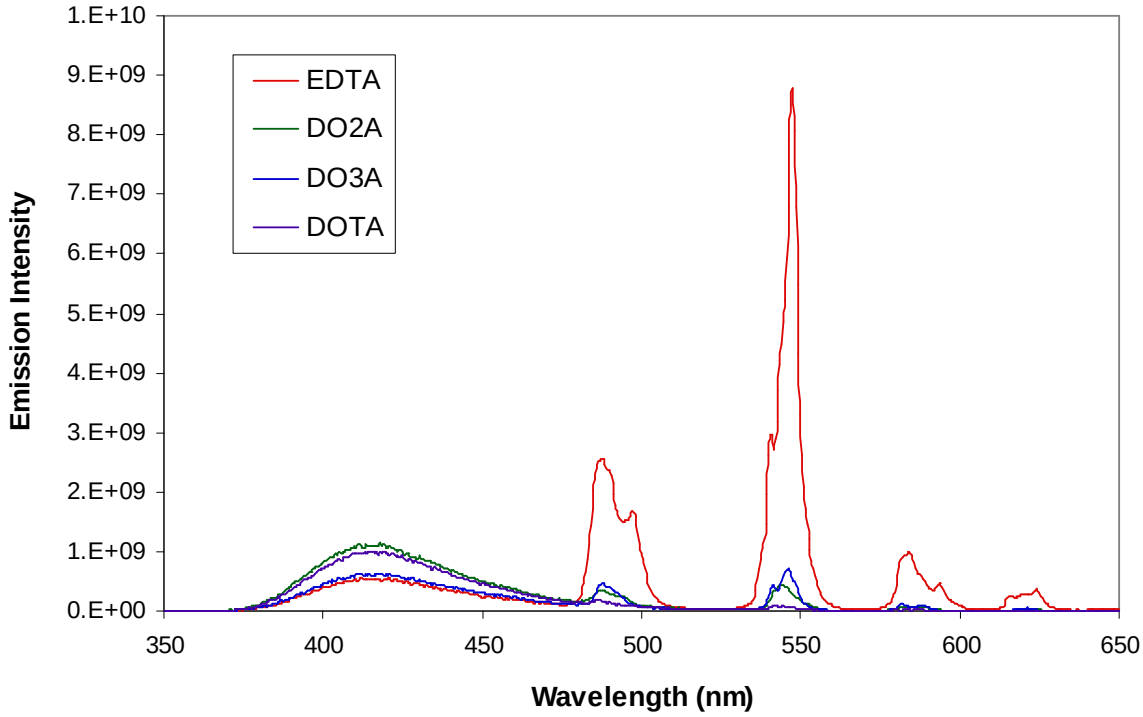

Figure 5.13. Emission spectra (λ_{ex} = 326 nm) of various Tb(ligand)(SA) complexes in 50 mM CAPS buffer, pH 12.5 (DO2A complex in CHES buffer, same concentration and pH). 10 μM SA, 1.0 mM Tb(ligand) complex. The Tb(EDTA)(SA) complex has the greatest emission intensity.

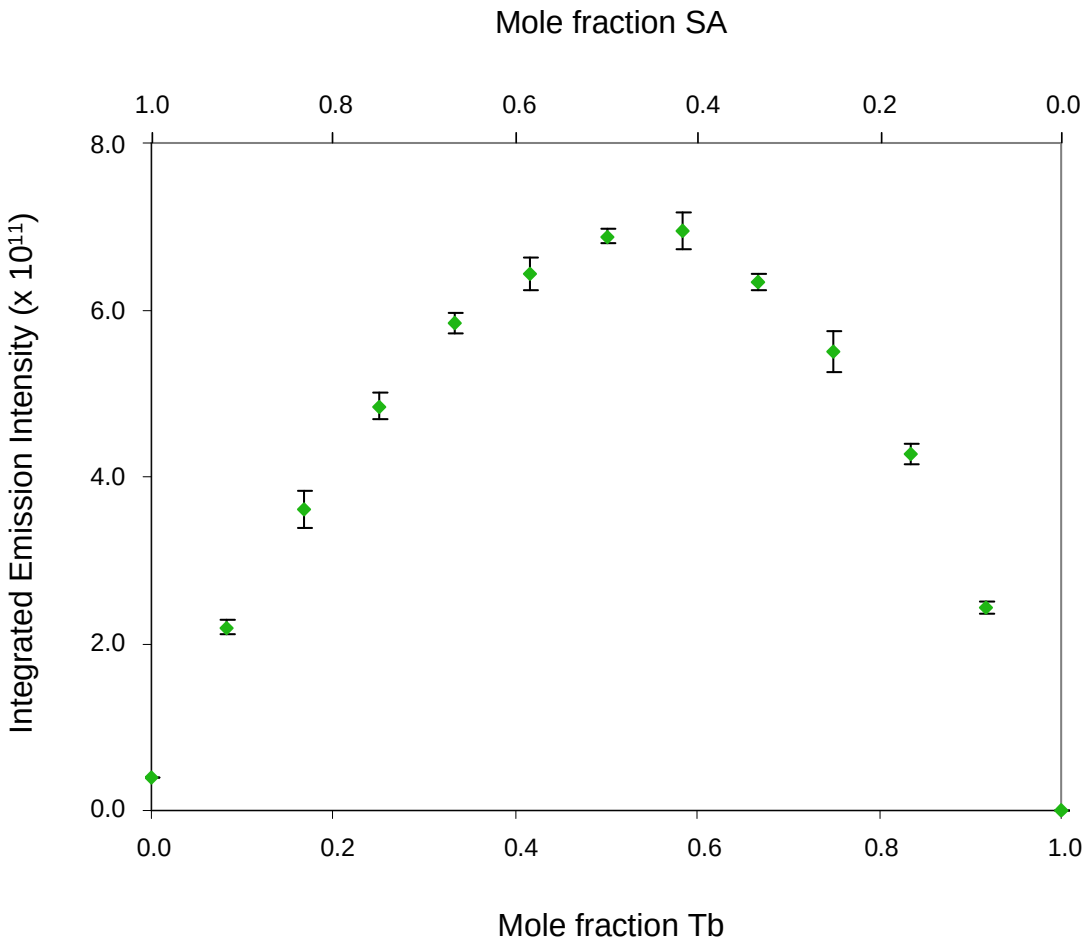

Figure 5.14. Method of continuous variations to determine binding stoichiometry of SA^{2-} to $Tb(EDTA)^{-}$. [Tb] and [SA] varied inversely from 0-120 μM in 10 μM increments with 1.00 mM EDTA in 50.0 mM CAPS buffer, pH 13.5 (λ_{ex} = 314 nm). Emission intensity integrated from 530–560 nm. Equilibration time of 24 hours.

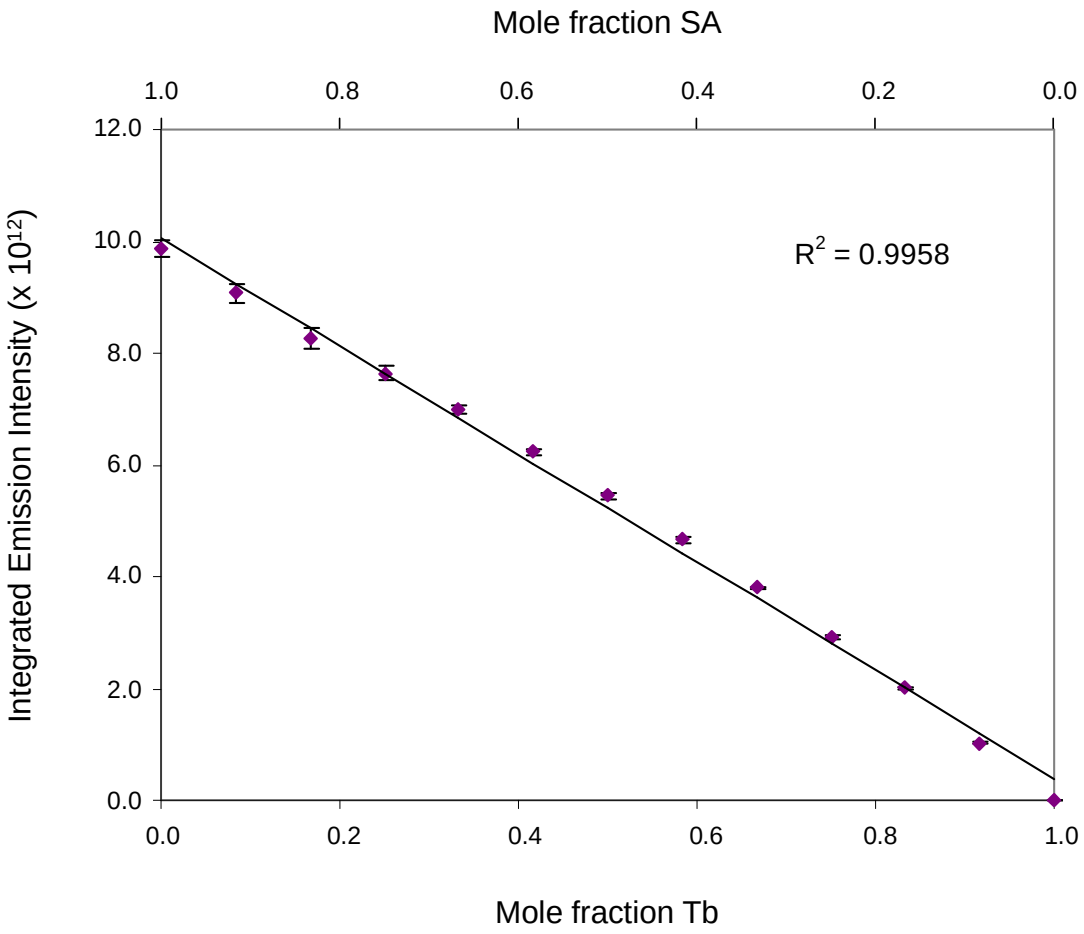

Figure 5.15. Method of continuous variations, showing linear correlation of intrinsic salicylate (SA) luminescence (419 nm) that can be used as an internal standard. Concentrations of Tb and SA were varied inversely from 0 to 120 μM in 10 μM increments, with 1.00 mM EDTA in 50 mM CAPS buffer, pH 13.5 (λ_{ex} = 314 nm). Emission intensity integrated from 375–470 nm.

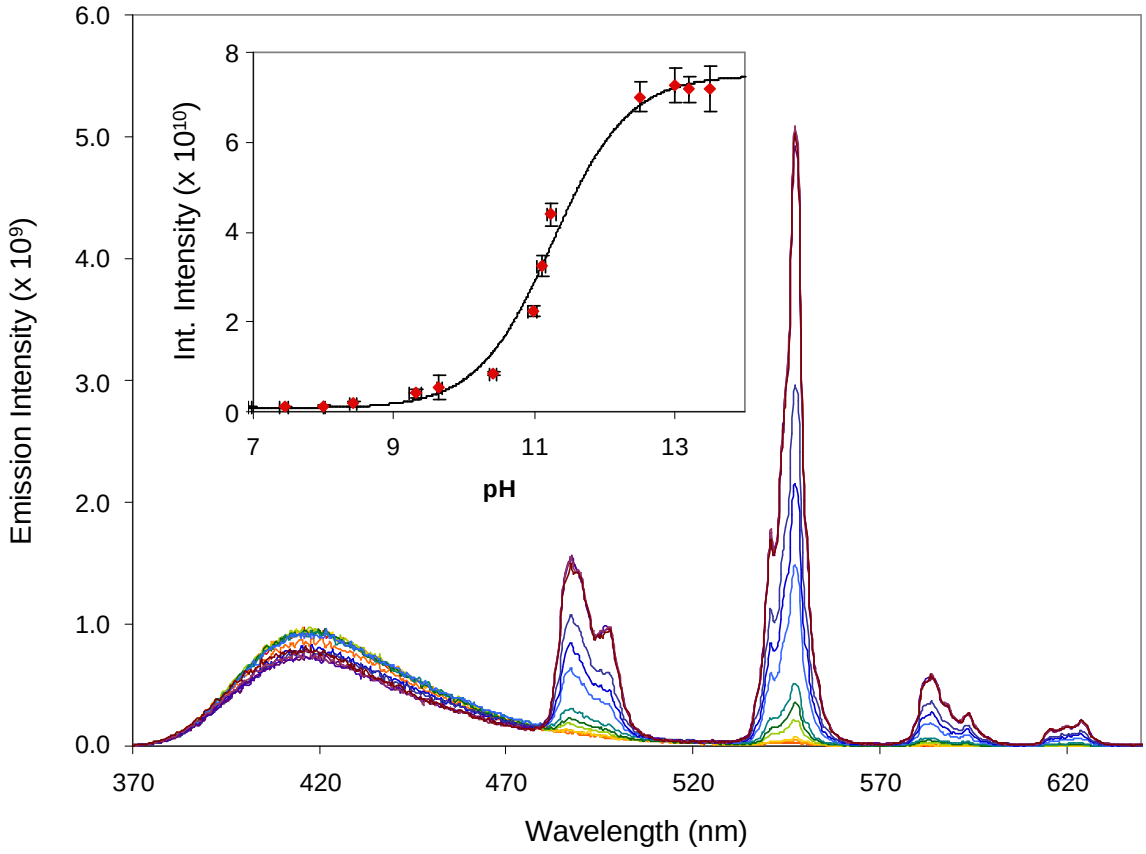

Figure 5.16. pH dependence study of 1.00 μM Tb(EDTA)(SA)$^{3-}$ in 50 mM buffer (λ_{ex} = 314 nm). [Tb(EDTA)$^{-}$] = 500 μM, 1 hour equilibration time. Inset: Plot of integrated emission intensity (530–560 nm) against pH.

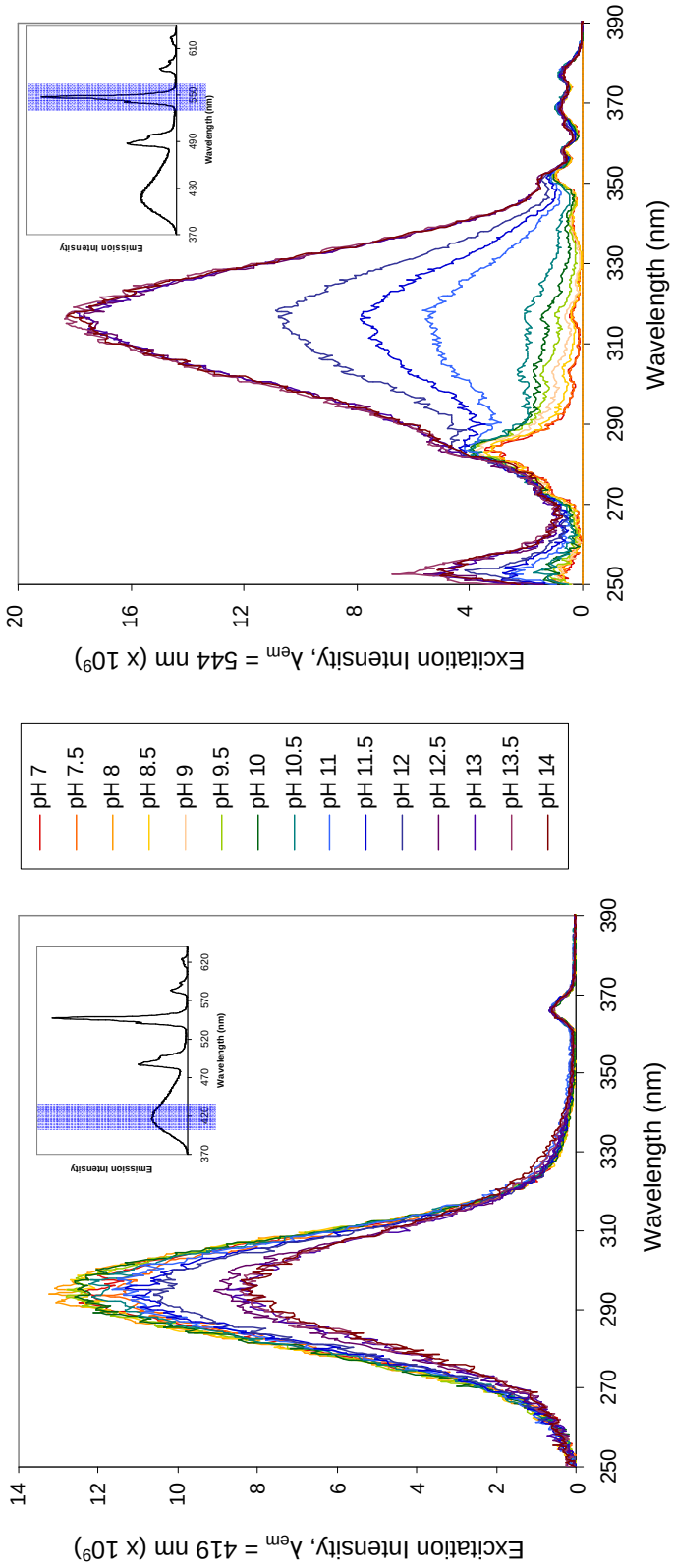

Figure 5.17. Two populations in pH dependence study of 1.00 µM Tb(EDTA)$(SA)^{3-}$ in 50 mM buffer. [Tb(EDTA)] = 500 µM, 1 hour equilibration time. Left: Decrease in SA^- population, monitored by intrinsic luminescence (λ_{em} = 419 nm) with increasing pH. Right: Increase in Tb(EDTA)$(SA)^{3-}$ population, monitored by Tb^{3+}-sensitized luminescence (λ_{em} = 544 nm).

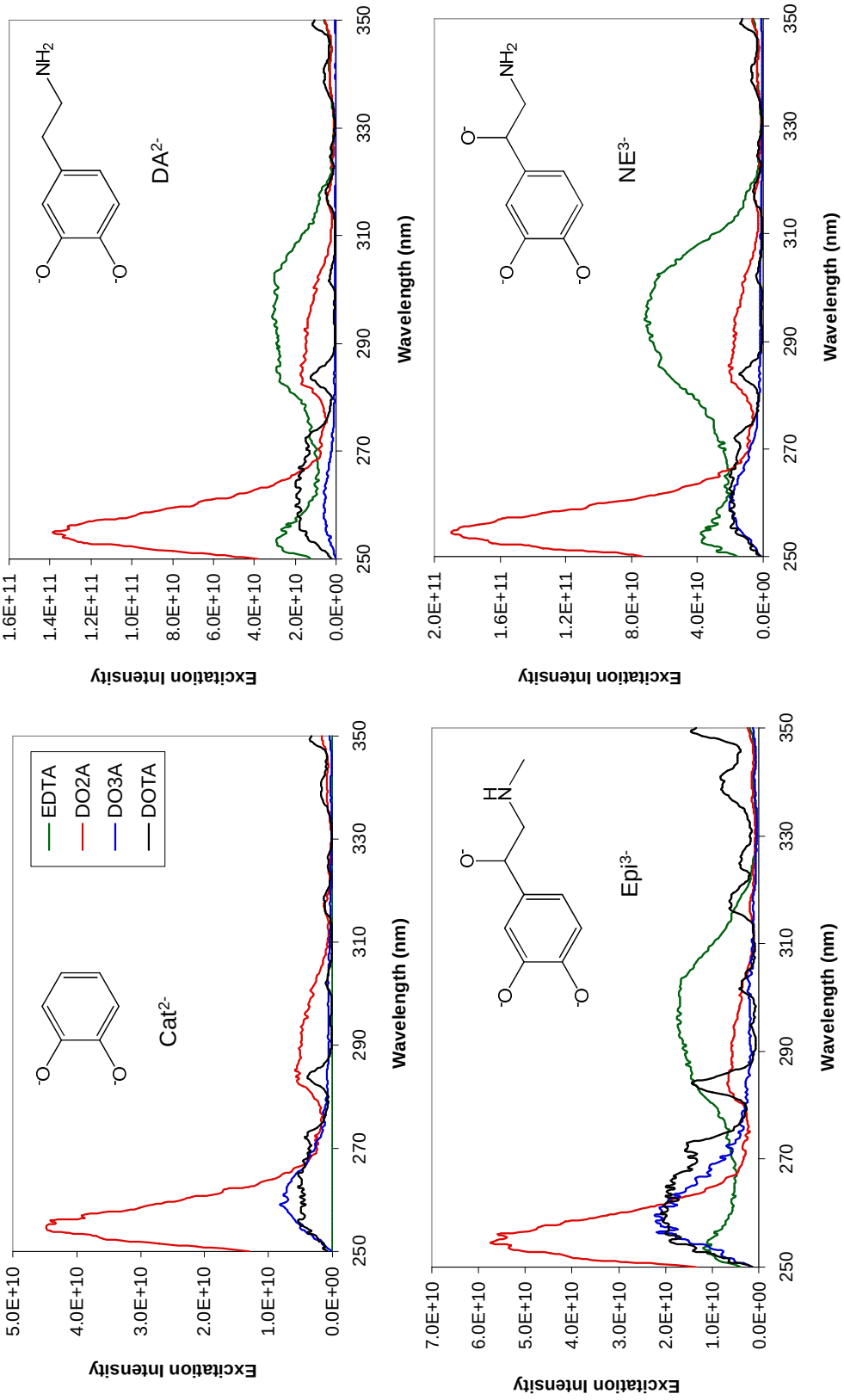

Figure 5.18. Excitation spectra (λ_{em} = 544 nm) of various Tb(ligand)(CA) complexes in 50 mM CAPS buffer, pH 13.5. 10 µM CA, 1.0 mM Tb(ligand) complex. CA abbreviations: catechol (Cat), dopamine (DA), epinephrine (Epi), norepinephrine (NE).

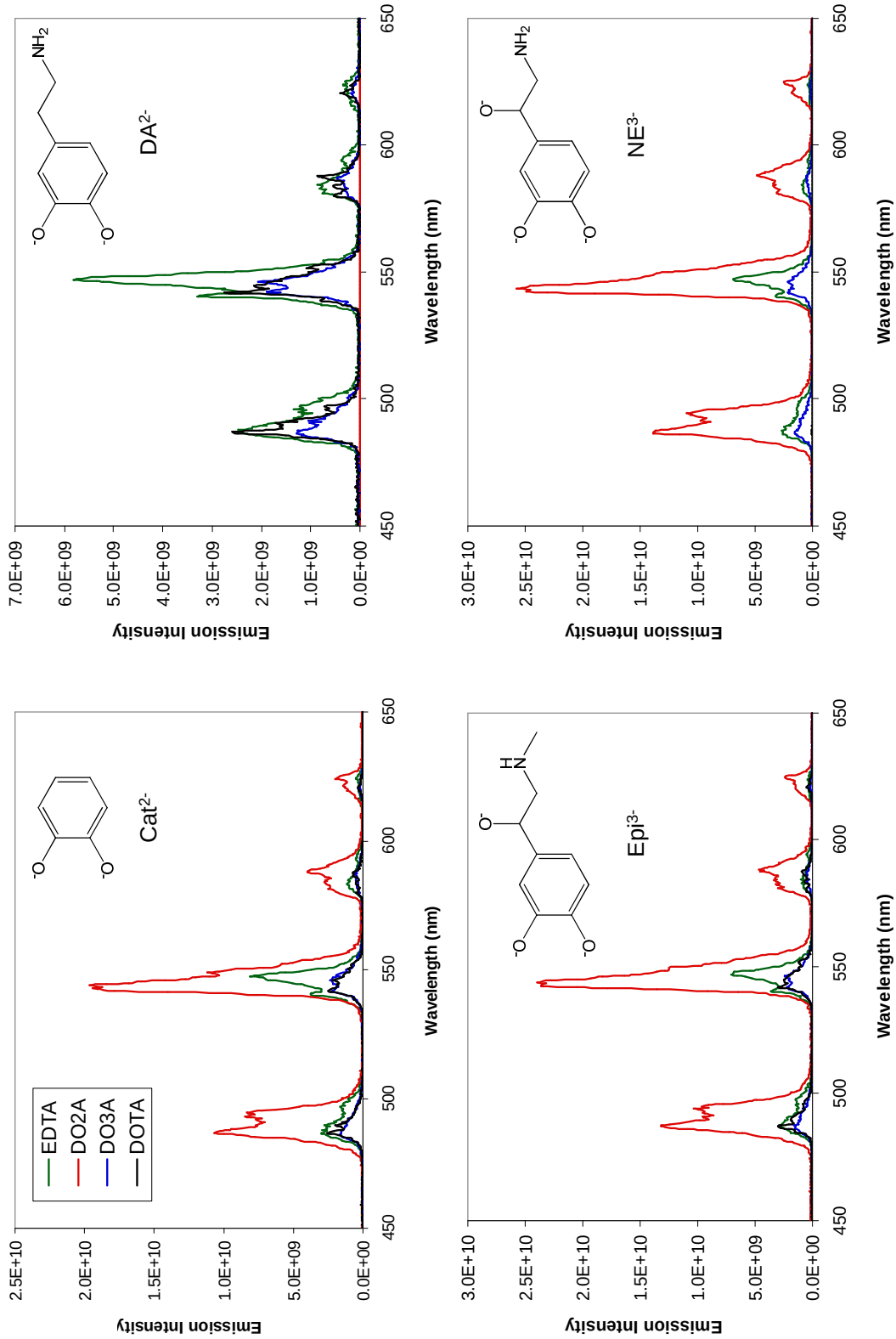

Figure 5.19. Emission spectra (λ_{ex} = 255 nm) of various Tb(ligand)(CA) complexes in 50 mM CAPS buffer, pH 13.5. 10 µM CA, 1.0 mM Tb(ligand) complex. CA abbreviations: catechol (Cat), dopamine (DA), epinephrine (Epi), norepinephrine (NE).

TABLES

Table 5.1. Protonation constants for various aromatic analytes.

Analyte	pK_{a1}	pK_{a2}	pK_{a3}	Ref
SU	3.34	7.91	----------	23
SA	2.98	13.62	----------	64, 65
Cat	9.48	12.08	----------	95
Epi	8.64	9.84	13.1	94
NE	8.58	9.53	12.9	94
DA	8.89	10.41	13.1	93

SU = salicyluric acid; SA = salicylic acid; Cat = catechol;
Epi = epinephrine; NE = norepinephrine; DA = dopamine

Table 5.2. Stability constants for Tb^{3+} and Gd^{3+} with various ligands.

Type	Ligand	Coord. No.	log K_{Tb}	log K_{Gd}	Ref
Linear	EDTA	6	17.92	17.35	66
	DTPA	8	22.71	22.46	66
Cyclic	DO2A	6	---------	19.42	35
	DO3A	7	---------	21.0	67
	DOTA	8	24.8	24.6	67, 35

Table 5.3. Protonation constants of various ligands.

Ligand	pK_{a1}	pK_{a2}	pK_{a3}	pK_{a4}	pK_{a5}	Ref
EDTA	2.00	2.67	6.13	10.26	---------	68
DTPA	2.08	2.41	4.26	8.60	10.55	66
DO2A	2.55	3.85	9.55	10.94	---------	67
DO3A	3.39	4.40	9.51	10.72	---------	67
DOTA	4.00	4.60	9.90	11.34	---------	67

Table 5.4. Stability constants (log K) of catecholamines with various metals (25 ℃, 0.2 M ionic strength).

Metal	DA	Epi	NE	Ref
Ca^{2+}	-------	5.96	5.67	91
La^{3+}	-------	5.91	-------	90
Y^{3+}	7.95	7.40	7.07	89
Al^{3+}	8.01	8.22	8.31	5

DA = dopamine; Epi = epinephrine;
NE = norepinephrine

Table 5.5. Summary of lanthanide(ligand) complexes optimized in this chapter for the detection of various analytes of biological relevance. SU = salicylurate; SA = salicylate; CA = catecholamine

Analyte	Ln^{3+}	Ligand	Conditions
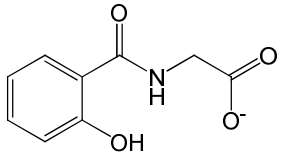 SU	Tb^{3+}	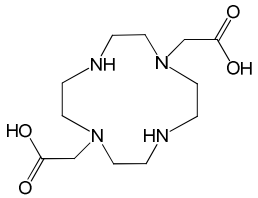 DO2A	0.1 M TAPS pH 8.4 λ_{ex} = 316 nm
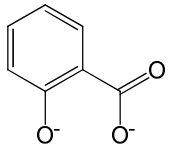 SA	Tb^{3+}	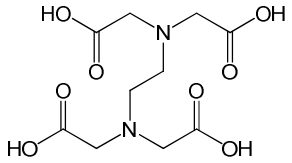 EDTA	50 mM CAPS pH 13.5 λ_{ex} = 314 nm
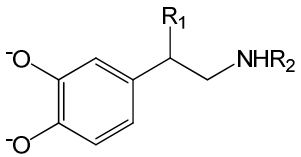 CA	Tb^{3+}	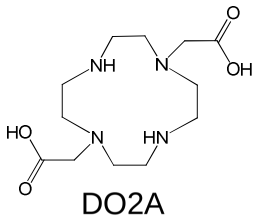 DO2A	50 mM CAPS pH 13.5 λ_{ex} = 255 nm

APPENDIX A

Derivation of Model for Ln(DPA) Binding Affinity

We start with the equilibrium described in [1], where Ln^{3+} is any lanthanide, and which has the corresponding equilibrium expression written in [2].

$$Ln^{3+} + DPA^{2-} \underset{}{\overset{K_a}{\rightleftharpoons}} Ln(DPA)^{+} \quad [1]$$

$$K_a = \frac{[Ln(DPA)^{+}]_{eq}}{[Ln^{3+}]_{eq}[DPA^{2-}]_{eq}} \quad [2]$$

We can write the total concentrations of lanthanide and DPA, or C_{Ln} and C_{DPA}, as follows in equations [3] and [4].

$$C_{Ln} = [Ln^{3+}]_{eq} + [Ln(DPA)^{+}]_{eq} \quad [3]$$

$$C_{DPA} = [DPA^{2-}]_{eq} + [Ln(DPA)^{+}]_{eq} \quad [4]$$

These can be rearranged to produce equations [5] and [6].

$$[Ln^{3+}]_{eq} = C_{Ln} - [Ln(DPA)^{+}]_{eq} \quad [5]$$

$$[DPA^{2-}]_{eq} = C_{DPA} - [Ln(DPA)^{+}]_{eq} \quad [6]$$

Substituting equations [5] and [6] into equation [2], we have equation [7].

$$K_a = \frac{[Ln(DPA)^{+}]_{eq}}{(C_{Ln} - [Ln(DPA)^{+}]_{eq})(C_{DPA} - [Ln(DPA)^{+}]_{eq})} \quad [7]$$

Rearranging, we have equation [8].

$$K_a = \frac{[Ln(DPA)^+]_{eq}}{C_{Ln}C_{DPA} - [Ln(DPA)^+]_{eq}C_{DPA} - [Ln(DPA)^+]_{eq}C_{Ln} + ([Ln(DPA)^+]_{eq})^2} \quad [8]$$

Let us introduce a normalization factor, R, given in equation [9].

$$R = \frac{[Ln(DPA)^+]_{eq}}{[Ln(DPA)^+]_{eq} + [(DPA)^{2-}]_{eq}} \quad [9]$$

Substituting equation [6] into equation [9], we have equation [10].

$$R = \frac{[Ln(DPA)^+]_{eq}}{C_{DPA}} \quad [10]$$

Substituting equation [10] into equation [8] and simplifying, we have equation [11].

$$K_a = \frac{R}{C_{Ln} - RC_{DPA} - RC_{Ln} + R^2C_{DPA}} \quad [11]$$

Rearranging, we end with equation [12], which has a linear relationship between two components dependent on $[Ln(DPA)^+]_{eq}$, C_{Ln} and C_{DPA}.

$$\log\left(\frac{R}{1-R}\right) = \log(C_{Ln} - RC_{DPA}) + \log(K_a) \quad [12]$$

Thus, a plot of $\log(C_{Ln} - RC_{DPA})$ vs $\log (R/(1 - R))$ will produce a linear fit with a slope of unity and a y-intercept equal to the logarithm of K_a.

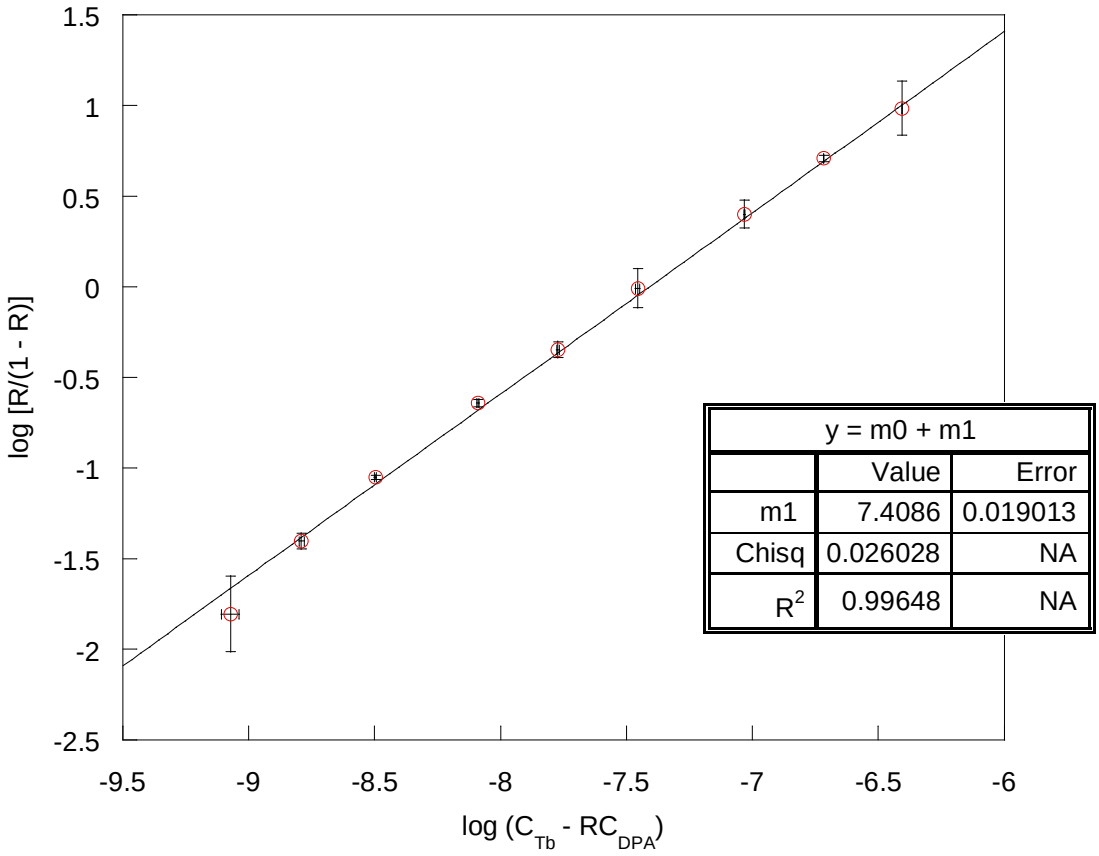

Figure A1. Linear fit of log(C_{Tb} – RC_{DPA}) vs log (R/(1 – R)) with slope set to unity and y-intercept corresponding to log K_a. 10.0 nM DPA titrated with $TbCl_3$ in 0.2 M sodium acetate, pH 7.4, 24.5℃ (λ_{ex} = 278 nm).

APPENDIX B

Derivation of Model for Ln(DO2A)(DPA) Binding Affinity by Competition

Here we report details of the Binding Affinity by Competition (BAC) assay applied to determine the binding constant, K_a', for DPA binding to the binary complex of Ln-(*1,4,7,10*-tetraazacyclododecane-*1,7*-diacetate) (i.e., $Ln(DO2A)^+$), as shown in equilibrium [1] and depicted in the corresponding equilibrium expression [2].[a]

$$Ln(DO2A)^+ + DPA^{2-} \overset{K_a'}{\rightleftharpoons} Ln(DO2A)(DPA)^- \qquad [1]$$

$$K_a' = \frac{[Ln(DO2A)(DPA)^-]_{eq}}{[Ln(DO2A)^+]_{eq}[DPA^{2-}]_{eq}} \qquad [2]$$

In order to determine K_a', we performed a competitive binding experiment described by equilibrium [3] with equation [4], where the addition of excess Ln^{3+} to $Ln(DO2A)(DPA)^-$ results in the equimolar formation of the two species $Ln(DO2A)^+$ and $Ln(DPA)^+$.

$$Ln(DO2A)(DPA)^- + Ln^{3+} \overset{K_c}{\rightleftharpoons} Ln(DO2A)^+ + Ln(DPA)^+ \qquad [3]$$

$$K_c = \frac{[Ln(DO2A)^+]_{eq}[Ln(DPA)^+]_{eq}}{[Ln(DO2A)(DPA)^-]_{eq}[Ln^{3+}]_{eq}} \qquad [4]$$

As Ln^{3+} is added, the shift in equilibrium concentrations of $Ln(DO2A)(DPA)^-$ and $Ln(DPA)^+$ are monitored *via* a specific ligand field-sensitive transition using luminescence spectroscopy. A best fit of luminescence intensity titration data to a two-state thermodynamic model yields the competition equilibrium constant (K_c), which in

[a] Based on lifetime measurements of analogous Tb complexes, we assume that the remaining coordination sites of $Ln(DPA)^+$ and $Ln(DO2A)^+$ are occupied by water molecules.

conjunction with independent measurement of the $Ln(DPA)^+$ formation constant (K_a) allows calculation of the ternary complex formation constant (K_a').

We measure the luminescence intensity (I_{obs}) as a function of excess Ln^{3+} added ($[Ln^{3+}]_{xs}$). The titration data are fit using a two state model [5], assuming that only the two DPA-bound species contribute to the observed luminescence intensities (*i.e.*, $I_{Ln(DO2A)(DPA)}$ and $I_{Ln(DPA)} >> I_{Ln(DO2A)}$ and I_{Ln} [1]), and where I_{max} and I_{min} are the maximum and minimum observed intensities, and c_1 and c_2 are the respective fractions of $Ln(DO2A)(DPA)^-$ and $Ln(DPA)^+$ at equilibrium (*i.e.*, $c_1 = [Ln(DO2A)(DPA)^-]_{eq}/[Ln(DO2A)(DPA)^-]_T$, $c_2 = [Ln(DPA)^+]_{eq}/[Ln(DO2A)(DPA)^-]_T$, and $c_1 + c_2 = 1$).

$$\begin{aligned} I_{obs} &= c_1 I_{max} + c_2 I_{min} \\ &= \left(1 - \frac{[Ln(DPA)^+]_{eq}}{[Ln(DO2A)(DPA)^-]_T}\right) I_{max} + \left(\frac{[Ln(DPA)^+]_{eq}}{[Ln(DO2A)(DPA)^-]_T}\right) I_{min} \end{aligned} \quad [5]$$

To fit the data for I_{obs} versus $[Ln^{3+}]_{xs}$, we derive an expression for $[Ln(DPA)^+]_{eq}$ in terms of $[Ln^{3+}]_{xs}$ and K_a' from [2]. Towards this end, we consider the equilibrium of Ln^{3+} and DPA^{2-} expressed in [6] and depicted in [7].

$$Ln^{3+} + DPA^{2-} \overset{K_a}{\rightleftharpoons} Ln(DPA)^+ \quad [6]$$

$$K_a = \frac{[Ln(DPA)^+]_{eq}}{[Ln^{3+}]_{eq}[DPA^{2-}]_{eq}} \quad [7]$$

The value of K_a has been previously determined through a dilution study at pH 7.5 (see Appendix A). Since K_c is related to K_a' by equation [8], and $[Ln(DO2A)(DPA)^-]_{eq}$ and $[Ln^{3+}]_{eq}$ can be expressed in terms of mass balance equations [9] and [10], respectively, we obtain an expression for $[Ln(DPA)^+]_{eq}$ in terms of K_a', K_a, $[Ln(DO2A)(DPA)^-]_T$, and $[Ln^{3+}]_T$.

$$K_c = \frac{K_a}{K_a'} = \frac{[Ln(DPA)^+]_{eq}^2}{[Ln(DO2A)(DPA)^-]_{eq}[Ln^{3+}]_{eq}}$$
$$= \frac{[Ln(DPA)^+]_{eq}^2}{\left([Ln(DO2A)(DPA)^-]_T - [Ln(DPA)^+]_{eq}\right)\left([Ln^{3+}]_T - [Ln(DO2A)(DPA)^-]_T - [Ln(DPA)^+]_{eq}\right)} \quad [8]$$

In equation [8], we assume that the $DO2A^{2-}$ ligand stays bound to Ln^{3+}, given that log K_{GdDO2A} =19.4. [2] As a result, the total ternary complex concentration $[Ln(DO2A)(DPA)^-]_T$ at equilibrium can be expressed as the sum of all $Ln(DO2A)^+$-containing species in equation [9]:

$$[Ln(DO2A)(DPA)^-]_T = [Ln(DO2A)(DPA)^-]_{eq} + [Ln(DO2A)^+]_{eq}$$
$$= [Ln(DO2A)(DPA)^-]_{eq} + [Ln(DPA)^+]_{eq} \quad [9]$$

The total Ln^{3+} concentration ($[Ln^{3+}]_T$) at equilibrium is defined as the sum of all Ln^{3+} containing equilibrated species as shown in equation [10]:

$$[Ln^{3+}]_T = [Ln^{3+}]_{eq} + [Ln(DO2A)(DPA)^-]_{eq} + [Ln(DO2A)^+]_{eq} + [Ln(DPA)^+]_{eq}$$
$$= [Ln^{3+}]_{eq} + [Ln(DO2A)(DPA)^-]_{eq} + 2[Ln(DPA)^+]_{eq} \quad [10]$$

Solving equation [8] for $[Ln(DPA)^+]_{eq}$, we obtain equation [11]:

$$[Ln(DPA)^+]_{eq} = \frac{[Ln^{3+}]_T + \left(\left\{[Ln^{3+}]_T - 2\left(1 - K_a' \cdot K_a^{-1}\right)[Ln(DO2A)(DPA)^-]_T\right\}^2 + 4K_a' \cdot K_a^{-1}\left(1 - K_a' \cdot K_a^{-1}\right)[Ln(DO2A)(DPA)^-]_T^2\right)^{1/2}}{2\left(1 - K_a' \cdot K_a^{-1}\right)} \quad [11]$$

The total concentration of the ternary complex, $[Ln(DO2A)(DPA)^-]_T$, is experimentally fixed (in this case 1.0 μM), and the total Ln^{3+} concentration ($[Ln^{3+}]_T$) is the sum of this

initial ternary complex concentration and any excess Ln^{3+} added ($[Ln]_{XS}$) as shown in equation [12].

$$[Ln^{3+}]_T = [Ln(DO2A)(DPA)^-]_T + [Ln^{3+}]_{XS} \quad [12]$$

Substituting the expression for $[Ln(DPA)^+]_{eq}$ from equation [11] into equation [5], we obtain equation [13], the BAC assay two-state model expression used to calculate K_a'.

$$I_{obs} = \left(1-(2AB)^{-1}\left\{A+[Ln^{3+}]_{XS}+\left(\left\{A+[Ln^{3+}]_{XS}-2AB\right\}^2+4A(1-A)B^2\right)^{1/2}\right\}\right)I_{max} + \left((2AB)^{-1}\left\{A+[Ln^{3+}]_{XS}+\left(\left\{A+[Ln^{3+}]_{XS}-2AB\right\}^2+4A(1-A)B^2\right)^{1/2}\right\}\right)I_{min} \quad [13]$$

where $A = [Ln(DO2A)(DPA)^-]_T$

$B = 1 - K_a' \cdot K_a^{-1}$

This model is used to calculate K_a' from the data with the Curve Fitting Toolbox in Matlab® in the following format:

f(x) = (1 - (1e-06 + 10^x - ((1e-06 + 10^x - (2e-06)*(1 - (1/c)))^2 + (4/c)*(1 - (1/c))*(1e-06)^2)^0.5)/((2e-06)*(1 - (1/c))))*a + ((1e-06 + 10^x - ((1e-06 + 10^x - (2e-06)*(1 - (1/c)))^2 + (4/c)*(1 - (1/c))*(1e-06)^2)^0.5)/((2e-06)*(1 - (1/c))))*b

where x = $[Ln^{3+}]_{XS}$ in M

a = I_{max}

b = I_{min}

c = K_a/K_a'

Each trial is fit independently to produce values for all three coefficients (a, b, and c). Assuming reasonable fits, K_a' is calculated from c using the K_a value from identical pH and temperature conditions, and the three values are averaged to produce the final reported value of K_a' with standard deviation.

References

1. Jones, G.; Vullev, V. I., Medium effects on the stability of terbium(III) complexes with pyridine-2,6-dicarboxylate. *Journal of Physical Chemistry A* **2002,** 106, (35), 8213-8222.
2. Kim, W. D.; Hrncir, D. C.; Kiefer, G. E.; Sherry, A. D., Synthesis, Crystal-Structure, And Potentiometry Of Pridine-Containing Tetraaza Macrocyclic Ligands With Acetate Pendant Arms. *Inorganic Chemistry* **1995,** 34, (8), 2225-2232.

APPENDIX C

Derivation of Model for Cationic Interferent Study

We consider calcium as our example to derive this model. We start with the equilibrium described in [1], which has the corresponding equilibrium expression written in [2].

$$Tb(DO2A)(DPA)^{-} + Ca^{2+} \underset{}{\overset{K_{cation}}{\rightleftharpoons}} Tb(DO2A)^{+} + CaDPA \qquad [1]$$

$$K_{cation} = \frac{[Tb(DO2A)^{+}]_{eq}[CaDPA]_{eq}}{[Tb(DO2A)(DPA)^{-}]_{eq}[Ca^{2+}]_{eq}} \qquad [2]$$

Since $K_{Tb(DO2A)} >> K_{Ca(DO2A)}$,[1] we assume negligible formation of Ca(DO2A) or $TbDPA^{+}$. As $Tb(DO2A)^{+}$ and CaDPA form in a ratio of 1:1 from the dissociation of one $Tb(DO2A)(DPA)^{-}$, we obtain equation [3].

$$[Tb(DO2A)^{+}]_{eq} = [CaDPA]_{eq} \qquad [3]$$

The total concentration of Tb^{3+} is expressed in [4], and similarly the total concentration of Ca^{2+} is given in [5].

$$[Tb^{3+}]_{Tot} = [Tb(DO2A)(DPA)^{-}]_{eq} + [Tb(DO2A)^{+}]_{eq} \qquad [4]$$

$$[Ca^{2+}]_{Tot} = [Ca^{2+}]_{eq} + [CaDPA]_{eq} \qquad [5]$$

Rearranging, we have [6] and [7]:

$$[Tb(DO2A)^{+}]_{eq} = [Tb^{3+}]_{Tot} - [Tb(DO2A)(DPA)^{-}]_{eq} \qquad [6]$$

$$[Ca^{2+}]_{eq} = [Ca^{2+}]_{Tot} - [CaDPA]_{eq} = [Ca^{2+}]_{Tot} - [Tb(DO2A)^{+}]_{eq} \qquad [7]$$

Substituting [3], [6] and [7] into [2], we have expression [8].

$$K_{cation} = \frac{\left\{[Tb]_{Tot} - [Tb(DO2A)(DPA)^{-}]_{eq}\right\}^2}{[Tb(DO2A)(DPA)^{-}]_{eq}\left([Ca^{2+}]_{Tot} - [Tb]_{Tot} + [Tb(DO2A)(DPA)^{-}]_{eq}\right)} \quad [8]$$

After some rearranging, we have:

$$(1 - K_{cation})\left\{[Tb(DO2A)(DPA)^{-}]_{eq}\right\}^2 + \begin{pmatrix} K_{cation}[Tb^{3+}]_{Tot} \\ -K_{cation}[Ca^{2+}]_{Tot} \\ -2[Tb^{3+}]_{Tot} \end{pmatrix}[Tb(DO2A)(DPA)^{-}]_{eq} + \left\{[Tb^{3+}]_{Tot}\right\}^2 = 0 \quad [9]$$

Solving for $[Tb(DO2A)(DPA)^{-}]_{eq}$, we have equation [10].

$$[Tb(DO2A)(DPA)^{-}]_{eq} = \frac{-A + \sqrt{A^2 - 4B\left\{[Tb^{3+}]_{Tot}\right\}^2}}{2B} \quad [10]$$

where $A = (K_{cation} - 2)[Tb^{3+}]_{Tot} - K_{cation}[Ca^{2+}]_{Tot}$

$B = 1 - K_{cation}$

In terms of intensity, we need an expression in the form of [11], as only the terbium-containing species will be observable via luminescence measurements.

$$I_{obs} = c_1 I_1 + c_2 I_2 \quad [11]$$

where $I_1 = \text{intensity of } [Tb(DO2A)(DPA)^{-}]_{eq}$

$I_2 = \text{intensity of } [Tb(DO2A)^{+}]_{eq}$

$$c_1 = \frac{[Tb(DO2A)(DPA)^{-}]_{eq}}{[Tb(DO2A)(DPA)^{-}]_{Tot}}$$

$$c_2 = \frac{[Tb(DO2A)^{+}]_{eq}}{[Tb(DO2A)(DPA)^{-}]_{Tot}} = 1 - c_1$$

Substituting in eq [10], we finally end with eq [12].

$$I_{obs} = \left(\frac{[Tb(DO2A)(DPA)^{-}]_{eq}}{[Tb(DO2A)(DPA)^{-}]_{Tot}}\right)I_1 + \left(1 - \frac{[Tb(DO2A)(DPA)^{-}]_{eq}}{[Tb(DO2A)(DPA)^{-}]_{Tot}}\right)I_2 \quad [12]$$

where

$$[\mathrm{Tb(DO2A)(DPA)^-}]_{eq} = \frac{-\left\{\left(10^{-7} - [\mathrm{Ca^{2+}}]_{Tot}\right)K_{cation} - 2\left(10^{-7}\right)\right\} + \sqrt{\left\{\left(10^{-7} - [\mathrm{Ca^{2+}}]_{Tot}\right)K_{cation} - 2\left(10^{-7}\right)\right\}^2 - 4\left(1 - K_{cation}\right)\left\{[\mathrm{Tb^{3+}}]_{Tot}\right\}^2}}{2\left(1 - K_{cation}\right)}$$

This equation was used in the Matlab® Curve-Fit Toolbox to fit the calcium competition experiment data and calculate the competition constants.

References

1. Chang, C. A.; Chen, Y.-H.; Chen, H.-Y.; Shieh, F.-K., Capillary electrophoresis, potentiometric and laser excited luminescence studies of lanthanide(III) complexes of 1,7-dicarboxymethyl-1,4,7,10-tetraazacyclododecane (DO2A). *Journal Of The Chemical Society-Dalton Transactions* **1998**, (19), 3243-3248.

APPENDIX D

Crystallographic Data for TBA·Ln(DO2A)(DPA) Structures

CALIFORNIA INSTITUTE OF TECHNOLOGY

BECKMAN INSTITUTE

X-RAY CRYSTALLOGRAPHY LABORATORY

Date 26 July 2007

Crystal Structure Analysis of:

MLC07

(shown below)

For Investigator: Morgan Cable ext. (818) 354-4345

Advisor: A. Ponce/H. B. Gray ext. 6500

Account Number: API.HSARPA-1-DOI.000002

By Michael W. Day 116 Beckman ext. 2734

e-mail: mikeday@caltech.edu

Contents

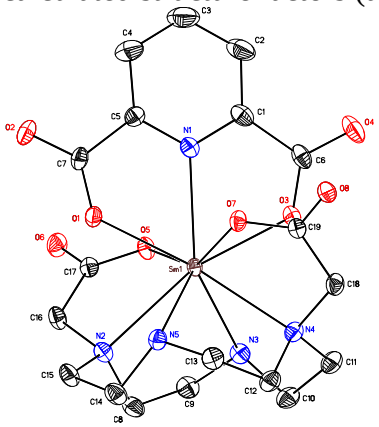

MLC07

Note: The crystallographic data have been deposited in the Cambridge Database (CCDC) and has been placed on hold pending further instructions from me. The deposition number is 655647. Ideally the CCDC would like the publication to contain a footnote of the type: "Crystallographic data have been deposited at the CCDC, 12 Union Road, Cambridge CB2 1EZ, UK and copies can be obtained on request, free of charge, by quoting the publication citation and the deposition number 655647."

Table 1. Crystal data and structure refinement for MLC07 (CCDC 655647).

Empirical formula	$[C_{19}H_{25}N_5O_8Sm]^-$ $[C_{16}H_{36}N]^+$ $2(H_2O)$, $0.73(C_3H_6O)$, $0.27(C_2H_6O \cdot O)$
Formula weight	939.36
Crystallization Solvent	Acetone/ethanol/isopropanol
Crystal Habit	Plate
Crystal size	0.33 x 0.24 x 0.11 mm^3
Crystal color	Yellow

Data Collection

Type of diffractometer	Bruker SMART 1000
Wavelength	0.71073 Å MoKα
Data Collection Temperature	100(2) K
θ range for 33380 reflections used in lattice determination	2.17 to 39.91°
Unit cell dimensions	a = 13.0658(4) Å b = 13.4504(4) Å β= 90.3240(10)° c = 26.1778(7) Å
Volume	4600.4(2) $Å^3$
Z	4
Crystal system	Monoclinic
Space group	$P2_1/c$
Density (calculated)	1.356 Mg/m^3
F(000)	1966
θ range for data collection	1.70 to 40.79°
Completeness to θ = 40.79°	94.6 %
Index ranges	$-23 \le h \le 23$, $-22 \le k \le 24$, $-47 \le l \le 44$
Data collection scan type	ω scans at 7 ϕ settings
Reflections collected	150100
Independent reflections	28270 [R_{int}= 0.1100]
Absorption coefficient	1.336 mm^{-1}
Absorption correction	None
Max. and min. transmission	0.8670 and 0.6669

Table 1 (cont.)

Structure solution and Refinement

Structure solution program	SHELXS-97 (Sheldrick, 1990)
Primary solution method	Direct methods
Secondary solution method	Difference Fourier map
Hydrogen placement	Geometric positions
Structure refinement program	SHELXL-97 (Sheldrick, 1997)
Refinement method	Full matrix least-squares on F^2
Data / restraints / parameters	28270 / 6 / 560
Treatment of hydrogen atoms	Riding
Goodness-of-fit on F^2	1.124
Final R indices [$I>2\sigma(I)$, 14923 reflections]	R1 = 0.0422, *w*R2 = 0.0734
R indices (all data)	R1 = 0.0997, *w*R2 = 0.0821
Type of weighting scheme used	Sigma
Weighting scheme used	$w=1/\sigma^2(Fo^2)$
Max shift/error	0.009
Average shift/error	0.000
Largest diff. peak and hole	3.079 and -2.442 e.Å^{-3}

Special Refinement Details

The solvent region is disordered, containing acetone (73%) and ethanol/water (27%). These were refined without restraint. Additionally, the solvent region contains two ordered water molecules which were refined with hydrogen geometry restrained.

Refinement of F^2 against ALL reflections. The weighted R-factor (*w*R) and goodness of fit (S) are based on F^2, conventional R-factors (R) are based on F, with F set to zero for negative F^2. The threshold expression of $F^2 > 2\sigma(F^2)$ is used only for calculating R-factors(gt) etc. and is not relevant to the choice of reflections for refinement. R-factors based on F^2 are statistically about twice as large as those based on F, and R-factors based on ALL data will be even larger.

All esds (except the esd in the dihedral angle between two l.s. planes) are estimated using the full covariance matrix. The cell esds are taken into account individually in the estimation of esds in distances, angles and torsion angles; correlations between esds in cell parameters are only used when they are defined by crystal symmetry. An approximate (isotropic) treatment of cell esds is used for estimating esds involving l.s. planes.

D5

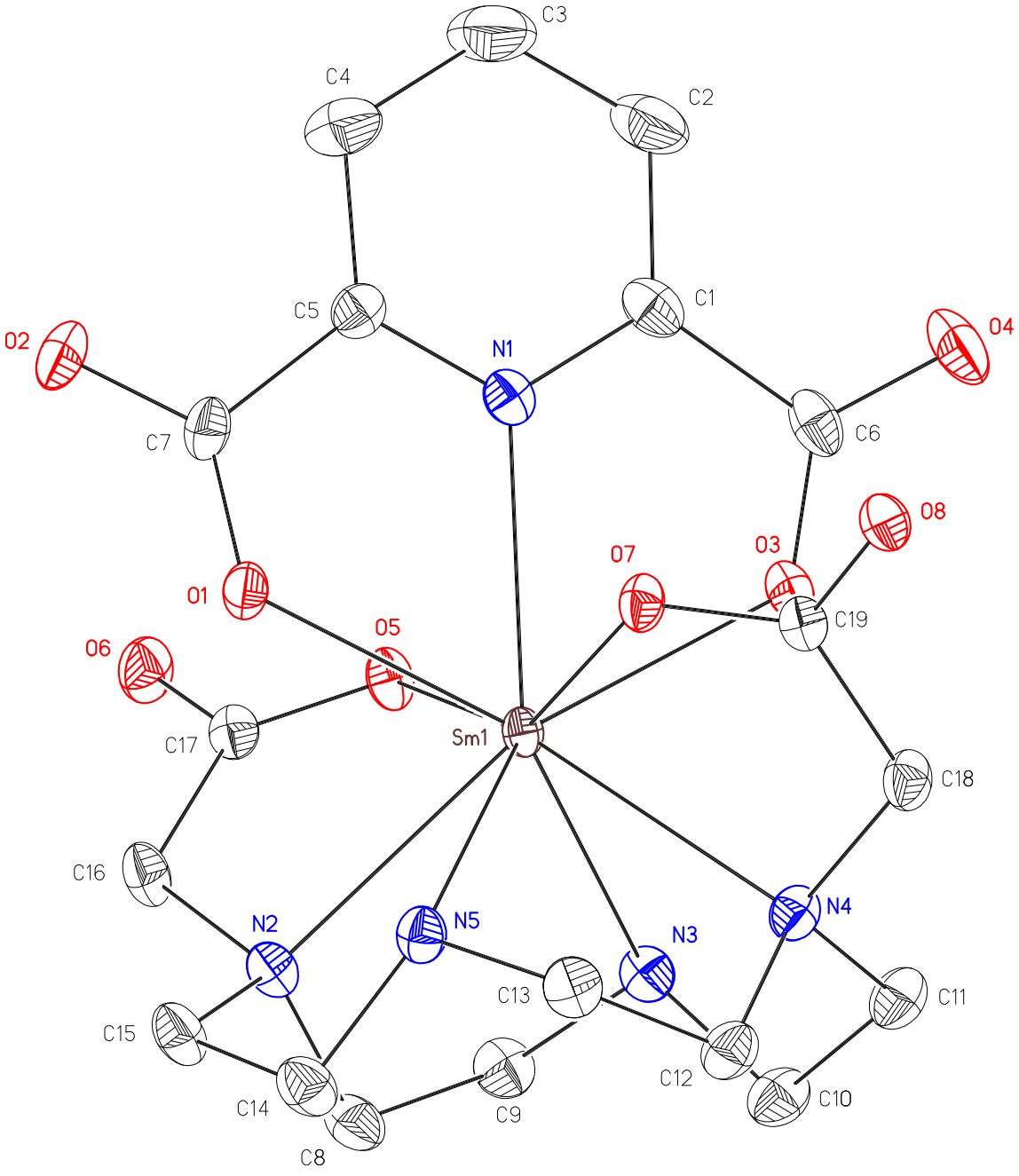
C3
C4
C2
C5
C1
O2
O4
N1
C7
C6
O8
O7
O3
O1
C19
O5
O6
Sm1
C17
C18
C16
N2
N5
N3
N4
C13
C11
C15
C12
C14
C10
C9
C8

D6

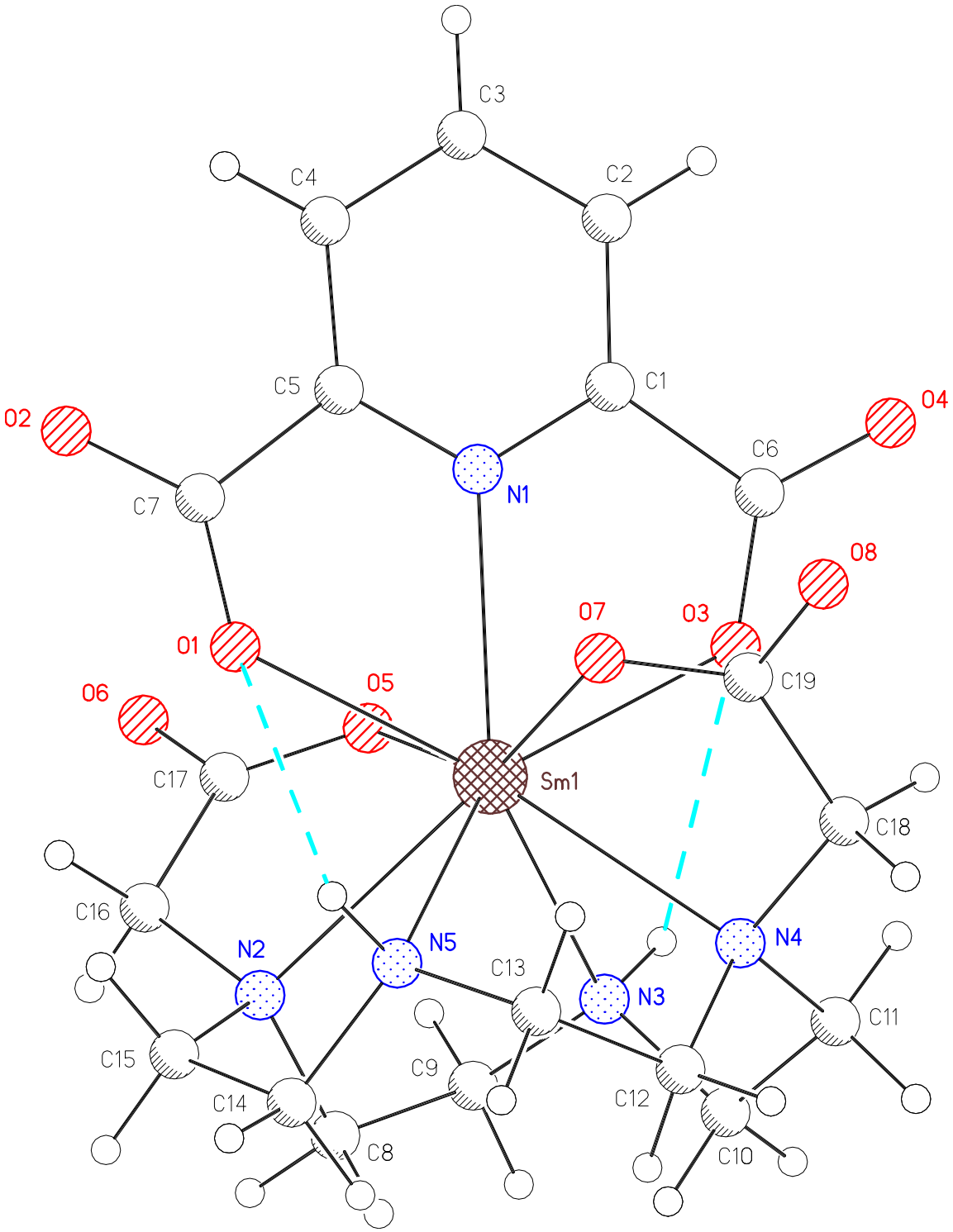
C3
C4
C2
C5
C1
O2
O4
C6
N1
C7
O8
O7
O3
O1
O5
C19
O6
C17
Sm1
C18
C16
N2
N5
C13
N4
N3
C11
C15
C9
C12
C14
C8
C10

D7

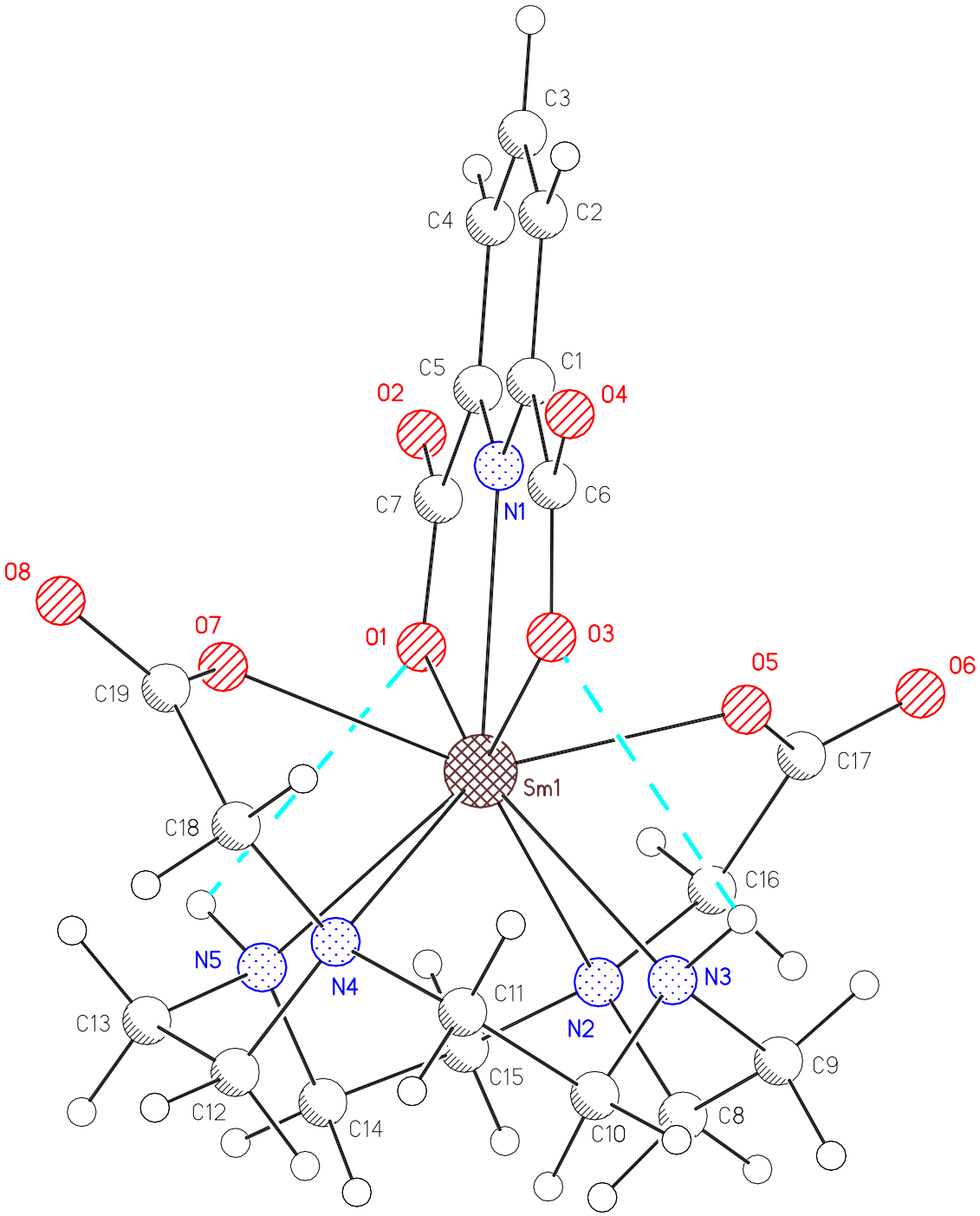
C3
C4
C2
C5
C1
O2
O4
C7
N1
C6
O8
O7
O1
O3
O5
O6
C19
Sm1
C17
C18
C16
N5
N4
N3
C11
N2
C13
C9
C15
C12
C14
C10
C8

Table 2. Atomic coordinates (x 10^4) and equivalent isotropic displacement parameters ($Å^2$x 10^3) for MLC07 (CCDC 655647). U(eq) is defined as the trace of the orthogonalized U^{ij} tensor.

	x	y	z	U_{eq}	Occ
Sm(1)	7494(1)	4931(1)	5001(1)	12(1)	1
O(1)	8313(1)	5490(1)	5785(1)	17(1)	1
O(2)	8658(2)	6668(1)	6366(1)	33(1)	1
O(3)	6717(1)	5941(1)	4337(1)	18(1)	1
O(4)	6445(1)	7418(1)	3952(1)	30(1)	1
O(5)	6038(1)	5292(1)	5515(1)	16(1)	1
O(6)	5302(1)	5278(1)	6280(1)	22(1)	1
O(7)	8982(1)	5576(1)	4585(1)	16(1)	1
O(8)	9678(1)	6092(1)	3855(1)	17(1)	1
N(1)	7516(1)	6789(1)	5149(1)	15(1)	1
N(2)	7032(1)	3512(1)	5682(1)	17(1)	1
N(3)	6029(1)	3789(1)	4676(1)	17(1)	1
N(4)	7949(1)	4027(1)	4121(1)	16(1)	1
N(5)	8939(1)	3607(1)	5116(1)	16(1)	1
C(1)	7140(2)	7403(2)	4792(1)	20(1)	1
C(2)	7132(2)	8426(2)	4863(1)	31(1)	1
C(3)	7519(2)	8808(2)	5318(1)	38(1)	1
C(4)	7901(2)	8169(2)	5686(1)	28(1)	1
C(5)	7893(2)	7152(2)	5583(1)	17(1)	1
C(6)	6733(2)	6888(2)	4315(1)	19(1)	1
C(7)	8319(2)	6373(2)	5948(1)	18(1)	1
C(8)	6332(2)	2770(2)	5449(1)	22(1)	1
C(9)	5538(2)	3231(2)	5096(1)	20(1)	1
C(10)	6284(2)	3149(2)	4236(1)	21(1)	1
C(11)	6975(2)	3701(2)	3870(1)	20(1)	1
C(12)	8624(2)	3161(2)	4212(1)	20(1)	1
C(13)	9426(2)	3352(2)	4624(1)	19(1)	1
C(14)	8670(2)	2724(2)	5418(1)	21(1)	1
C(15)	7985(2)	3011(2)	5856(1)	21(1)	1
C(16)	6535(2)	4022(2)	6114(1)	19(1)	1
C(17)	5899(1)	4923(2)	5959(1)	15(1)	1
C(18)	8457(2)	4782(2)	3800(1)	18(1)	1
C(19)	9099(1)	5537(1)	4103(1)	14(1)	1
N(6)	8625(1)	7115(1)	7812(1)	18(1)	1
C(21)	9621(2)	6949(2)	7523(1)	20(1)	1
C(22)	10552(2)	7499(2)	7733(1)	24(1)	1
C(23)	11416(2)	7497(2)	7342(1)	25(1)	1
C(24)	12372(2)	8025(2)	7542(1)	34(1)	1
C(25)	8744(2)	6830(2)	8371(1)	20(1)	1
C(26)	9016(2)	5745(2)	8471(1)	31(1)	1
C(27)	9270(3)	5576(2)	9024(1)	42(1)	1
C(28)	9436(3)	4504(2)	9174(2)	57(1)	1
C(29)	7815(2)	6478(2)	7547(1)	22(1)	1
C(30)	6729(2)	6619(2)	7742(1)	26(1)	1
C(31)	6007(2)	5924(3)	7458(1)	48(1)	1
C(32)	4887(2)	6117(3)	7596(1)	55(1)	1

C(33)	8325(2)	8203(2)	7802(1)	20(1)	1
C(34)	8166(2)	8649(2)	7271(1)	26(1)	1
C(35)	7925(2)	9747(2)	7314(1)	27(1)	1
C(36)	7715(2)	10218(2)	6793(1)	35(1)	1
O(21)	4163(1)	3901(1)	6866(1)	37(1)	1
O(22)	746(1)	5096(1)	3092(1)	26(1)	1
O(51)	3632(3)	9306(2)	5430(2)	69(1)	0.731(3)
C(51)	5010(4)	10204(4)	5845(2)	67(2)	0.731(3)
C(52)	4046(5)	9525(3)	5821(2)	54(1)	0.731(3)
C(53)	3596(5)	9324(4)	6253(3)	83(2)	0.731(3)
O(61)	5133(6)	8689(5)	7101(3)	40(2)	0.269(3)
C(62)	4947(11)	8807(10)	6546(6)	62(4)	0.269(3)
C(64)	4410(11)	9466(11)	6164(9)	91(8)	0.269(3)
O(71)	6114(5)	7249(5)	6485(2)	29(2)	0.269(3)

Table 3. Bond lengths [Å] and angles [°] for MLC07 (CCDC 655647).

Sm(1)-O(5)	2.3858(14)	C(27)-C(28)	1.510(4)
Sm(1)-O(7)	2.3964(14)	C(29)-C(30)	1.522(3)
Sm(1)-O(3)	2.4246(14)	C(30)-C(31)	1.519(3)
Sm(1)-O(1)	2.4283(14)	C(31)-C(32)	1.532(4)
Sm(1)-N(1)	2.5295(17)	C(33)-C(34)	1.527(3)
Sm(1)-N(3)	2.5940(17)	C(34)-C(35)	1.514(3)
Sm(1)-N(5)	2.6115(16)	C(35)-C(36)	1.528(3)
Sm(1)-N(4)	2.6740(16)	O(51)-C(52)	1.191(6)
Sm(1)-N(2)	2.6824(16)	C(51)-C(52)	1.556(8)
O(1)-C(7)	1.263(2)	C(52)-C(53)	1.306(8)
O(2)-C(7)	1.243(2)	O(61)-C(62)	1.481(17)
O(3)-C(6)	1.274(3)	C(62)-C(64)	1.51(2)
O(4)-C(6)	1.245(2)		
O(5)-C(17)	1.278(2)	O(5)-Sm(1)-O(7)	146.52(6)
O(6)-C(17)	1.245(2)	O(5)-Sm(1)-O(3)	87.60(5)
O(7)-C(19)	1.272(2)	O(7)-Sm(1)-O(3)	78.96(5)
O(8)-C(19)	1.247(2)	O(5)-Sm(1)-O(1)	79.02(5)
N(1)-C(5)	1.330(3)	O(7)-Sm(1)-O(1)	85.28(5)
N(1)-C(1)	1.339(3)	O(3)-Sm(1)-O(1)	127.82(5)
N(2)-C(16)	1.477(3)	O(5)-Sm(1)-N(1)	73.79(5)
N(2)-C(8)	1.482(3)	O(7)-Sm(1)-N(1)	72.75(5)
N(2)-C(15)	1.484(3)	O(3)-Sm(1)-N(1)	63.90(5)
N(3)-C(10)	1.478(3)	O(1)-Sm(1)-N(1)	63.92(5)
N(3)-C(9)	1.480(3)	O(5)-Sm(1)-N(3)	73.50(5)
N(4)-C(18)	1.478(2)	O(7)-Sm(1)-N(3)	131.63(5)
N(4)-C(12)	1.479(3)	O(3)-Sm(1)-N(3)	77.99(5)
N(4)-C(11)	1.496(2)	O(1)-Sm(1)-N(3)	141.36(5)
N(5)-C(14)	1.471(3)	N(1)-Sm(1)-N(3)	130.02(5)
N(5)-C(13)	1.479(3)	O(5)-Sm(1)-N(5)	130.71(5)
C(1)-C(2)	1.388(3)	O(7)-Sm(1)-N(5)	73.21(5)
C(1)-C(6)	1.520(3)	O(3)-Sm(1)-N(5)	139.83(5)
C(2)-C(3)	1.390(4)	O(1)-Sm(1)-N(5)	78.41(5)
C(3)-C(4)	1.383(4)	N(1)-Sm(1)-N(5)	130.45(5)
C(4)-C(5)	1.394(3)	N(3)-Sm(1)-N(5)	99.53(6)
C(5)-C(7)	1.521(3)	O(5)-Sm(1)-N(4)	139.46(5)
C(8)-C(9)	1.518(3)	O(7)-Sm(1)-N(4)	65.67(5)
C(10)-C(11)	1.514(3)	O(3)-Sm(1)-N(4)	74.43(5)
C(12)-C(13)	1.520(3)	O(1)-Sm(1)-N(4)	140.31(5)
C(14)-C(15)	1.510(3)	N(1)-Sm(1)-N(4)	125.36(5)
C(16)-C(17)	1.524(3)	N(3)-Sm(1)-N(4)	67.40(5)
C(18)-C(19)	1.535(3)	N(5)-Sm(1)-N(4)	67.97(5)
N(6)-C(33)	1.515(3)	O(5)-Sm(1)-N(2)	65.63(5)
N(6)-C(25)	1.520(3)	O(7)-Sm(1)-N(2)	138.22(5)
N(6)-C(29)	1.525(2)	O(3)-Sm(1)-N(2)	141.29(5)
N(6)-C(21)	1.526(3)	O(1)-Sm(1)-N(2)	76.02(5)
C(21)-C(22)	1.525(3)	N(1)-Sm(1)-N(2)	127.15(5)
C(22)-C(23)	1.528(3)	N(3)-Sm(1)-N(2)	68.16(5)
C(23)-C(24)	1.527(3)	N(5)-Sm(1)-N(2)	66.65(5)
C(25)-C(26)	1.525(3)	N(4)-Sm(1)-N(2)	107.50(5)
C(26)-C(27)	1.500(4)	C(7)-O(1)-Sm(1)	125.37(12)

C(6)-O(3)-Sm(1)	125.80(13)	O(8)-C(19)-O(7)	124.58(18)
C(17)-O(5)-Sm(1)	123.51(12)	O(8)-C(19)-C(18)	117.34(17)
C(19)-O(7)-Sm(1)	122.58(12)	O(7)-C(19)-C(18)	118.04(16)
C(5)-N(1)-C(1)	120.23(18)	C(33)-N(6)-C(25)	106.57(15)
C(5)-N(1)-Sm(1)	119.83(13)	C(33)-N(6)-C(29)	110.88(16)
C(1)-N(1)-Sm(1)	119.94(14)	C(25)-N(6)-C(29)	111.22(17)
C(16)-N(2)-C(8)	110.79(16)	C(33)-N(6)-C(21)	110.78(16)
C(16)-N(2)-C(15)	110.31(16)	C(25)-N(6)-C(21)	110.93(15)
C(8)-N(2)-C(15)	109.60(16)	C(29)-N(6)-C(21)	106.52(15)
C(16)-N(2)-Sm(1)	106.24(11)	C(22)-C(21)-N(6)	115.50(16)
C(8)-N(2)-Sm(1)	110.25(12)	C(21)-C(22)-C(23)	110.31(17)
C(15)-N(2)-Sm(1)	109.61(12)	C(24)-C(23)-C(22)	112.01(19)
C(10)-N(3)-C(9)	112.65(16)	N(6)-C(25)-C(26)	115.47(17)
C(10)-N(3)-Sm(1)	115.52(12)	C(27)-C(26)-C(25)	111.2(2)
C(9)-N(3)-Sm(1)	112.28(12)	C(26)-C(27)-C(28)	115.2(3)
C(18)-N(4)-C(12)	111.29(15)	C(30)-C(29)-N(6)	115.09(16)
C(18)-N(4)-C(11)	109.58(16)	C(31)-C(30)-C(29)	109.71(19)
C(12)-N(4)-C(11)	110.19(16)	C(30)-C(31)-C(32)	111.8(2)
C(18)-N(4)-Sm(1)	106.28(11)	N(6)-C(33)-C(34)	115.39(16)
C(12)-N(4)-Sm(1)	110.77(11)	C(35)-C(34)-C(33)	110.02(19)
C(11)-N(4)-Sm(1)	108.61(11)	C(34)-C(35)-C(36)	112.0(2)
C(14)-N(5)-C(13)	112.67(16)	O(51)-C(52)-C(53)	119.1(7)
C(14)-N(5)-Sm(1)	115.96(12)	O(51)-C(52)-C(51)	122.9(6)
C(13)-N(5)-Sm(1)	111.86(12)	C(53)-C(52)-C(51)	117.1(5)
N(1)-C(1)-C(2)	121.4(2)	O(61)-C(62)-C(64)	141.9(12)
N(1)-C(1)-C(6)	114.61(18)		
C(2)-C(1)-C(6)	124.01(19)		
C(1)-C(2)-C(3)	118.6(2)		
C(4)-C(3)-C(2)	119.7(2)		
C(3)-C(4)-C(5)	118.2(2)		
N(1)-C(5)-C(4)	121.9(2)		
N(1)-C(5)-C(7)	114.61(17)		
C(4)-C(5)-C(7)	123.52(19)		
O(4)-C(6)-O(3)	126.9(2)		
O(4)-C(6)-C(1)	117.9(2)		
O(3)-C(6)-C(1)	115.16(17)		
O(2)-C(7)-O(1)	126.8(2)		
O(2)-C(7)-C(5)	117.38(19)		
O(1)-C(7)-C(5)	115.76(17)		
N(2)-C(8)-C(9)	113.21(16)		
N(3)-C(9)-C(8)	111.14(16)		
N(3)-C(10)-C(11)	110.27(17)		
N(4)-C(11)-C(10)	112.00(17)		
N(4)-C(12)-C(13)	112.89(16)		
N(5)-C(13)-C(12)	111.03(16)		
N(5)-C(14)-C(15)	110.27(16)		
N(2)-C(15)-C(14)	112.50(17)		
N(2)-C(16)-C(17)	114.02(15)		
O(6)-C(17)-O(5)	123.96(18)		
O(6)-C(17)-C(16)	117.90(16)		
O(5)-C(17)-C(16)	118.09(16)		
N(4)-C(18)-C(19)	113.99(15)		

Table 4. Anisotropic displacement parameters ($Å^2 x 10^4$) for MLC07 (CCDC 655647). The anisotropic displacement factor exponent takes the form: $-2\pi^2 [h^2 a^{*2} U^{11} + ... + 2 h k a^* b^* U^{12}]$

	U^{11}	U^{22}	U^{33}	U^{23}	U^{13}	U^{12}
Sm(1)	103(1)	144(1)	102(1)	13(1)	7(1)	10(1)
O(1)	192(7)	191(7)	118(6)	-5(5)	-8(5)	27(5)
O(2)	562(12)	283(9)	148(7)	-69(6)	-67(7)	32(8)
O(3)	183(7)	195(7)	153(6)	48(5)	-15(5)	-1(5)
O(4)	324(9)	308(9)	274(9)	157(7)	-61(7)	-12(7)
O(5)	119(6)	222(7)	136(6)	36(5)	23(4)	20(5)
O(6)	234(7)	254(8)	157(6)	-9(5)	51(5)	31(5)
O(7)	159(6)	207(7)	115(6)	2(5)	12(5)	-22(5)
O(8)	175(6)	190(7)	153(6)	28(5)	21(5)	-7(5)
N(1)	122(6)	178(8)	155(6)	21(5)	33(5)	7(5)
N(2)	170(7)	169(8)	163(7)	32(6)	14(6)	15(5)
N(3)	139(7)	184(8)	184(8)	14(6)	-8(6)	-1(5)
N(4)	144(7)	190(8)	144(7)	-17(5)	17(5)	-25(5)
N(5)	147(7)	190(8)	147(7)	-1(6)	-5(5)	23(5)
C(1)	159(8)	196(10)	244(10)	61(7)	-2(7)	3(7)
C(2)	335(13)	191(11)	410(14)	79(9)	-75(11)	7(9)
C(3)	450(16)	181(12)	507(17)	-26(10)	-113(13)	23(10)
C(4)	274(11)	208(11)	352(12)	-73(9)	-24(9)	19(8)
C(5)	158(8)	183(9)	168(9)	-21(6)	25(6)	6(6)
C(6)	130(8)	254(10)	199(9)	88(7)	-13(7)	-7(7)
C(7)	199(9)	238(10)	115(8)	-22(6)	20(6)	19(7)
C(8)	233(10)	182(10)	229(10)	53(7)	11(7)	-29(7)
C(9)	155(8)	220(10)	225(10)	14(7)	15(7)	-26(7)
C(10)	174(9)	224(10)	224(10)	-37(7)	7(7)	-48(7)
C(11)	173(9)	243(10)	192(9)	-42(7)	-7(7)	-27(7)
C(12)	197(9)	204(10)	184(9)	-41(7)	14(7)	25(7)
C(13)	159(8)	212(10)	203(9)	-1(7)	28(7)	44(6)
C(14)	213(9)	192(10)	223(10)	38(7)	27(7)	55(7)
C(15)	213(9)	212(10)	191(9)	64(7)	5(7)	54(7)
C(16)	200(9)	229(10)	141(8)	48(7)	30(7)	31(7)
C(17)	119(7)	182(9)	153(7)	7(6)	-10(5)	-18(6)
C(18)	187(8)	231(10)	133(8)	5(6)	22(6)	-33(6)
C(19)	118(7)	172(9)	143(8)	14(6)	6(6)	17(6)
N(6)	155(7)	205(8)	176(8)	-71(6)	-12(6)	14(6)
C(21)	163(8)	248(10)	199(9)	-90(7)	0(7)	18(7)
C(22)	175(9)	343(12)	214(10)	-116(8)	28(7)	-27(8)
C(23)	231(10)	283(11)	246(11)	-49(8)	45(8)	-25(8)
C(24)	255(12)	362(14)	408(15)	-76(11)	93(10)	-52(9)
C(25)	191(9)	222(10)	189(9)	-54(7)	-16(7)	-13(7)
C(26)	378(13)	252(12)	289(12)	-35(9)	-3(10)	59(9)
C(27)	640(20)	279(14)	323(14)	14(10)	-125(13)	-28(12)
C(28)	670(20)	417(19)	620(20)	169(16)	-109(19)	81(16)
C(29)	173(9)	257(10)	220(9)	-133(7)	-38(7)	8(7)
C(30)	161(9)	328(13)	302(12)	-164(9)	-10(8)	-7(8)
C(31)	179(11)	640(20)	610(20)	-414(16)	10(11)	-63(11)

C(32)	197(12)	760(20)	690(20)	-361(19)	6(13)	-73(13)
C(33)	197(9)	192(9)	195(9)	-81(7)	-22(7)	40(7)
C(34)	302(12)	277(12)	212(10)	-50(8)	-23(8)	41(9)
C(35)	298(11)	265(11)	255(11)	-22(8)	-14(8)	64(8)
C(36)	428(15)	309(13)	323(13)	14(9)	-17(11)	55(10)
O(21)	424(11)	434(11)	248(9)	42(7)	74(7)	-159(8)
O(22)	377(9)	219(8)	187(7)	-4(6)	71(6)	62(6)
O(51)	870(30)	210(15)	980(30)	113(16)	-310(20)	-21(15)
C(51)	450(30)	820(40)	730(40)	150(30)	-100(20)	-140(30)
C(52)	810(40)	138(17)	680(30)	6(17)	-250(30)	154(19)
C(53)	720(40)	550(30)	1230(60)	-480(40)	340(40)	-190(30)
O(61)	510(50)	440(40)	240(30)	-60(30)	-80(30)	220(30)
C(62)	580(90)	440(80)	860(110)	-220(70)	160(70)	-170(60)
C(64)	390(70)	560(90)	1800(200)	-830(120)	-310(100)	240(70)
O(71)	250(30)	350(40)	280(30)	-120(30)	50(20)	-40(20)

Table 5. Hydrogen bonds for MLC07 (CCDC 655647) [Å and °].

D-H...A	d(D-H)	d(H...A)	d(D...A)	<(DHA)
N(3)-H(3)...O(5)#1	0.93	2.15	3.010(2)	152.5
N(3)-H(3)...O(6)#1	0.93	2.53	3.288(2)	139.4
N(5)-H(5)...O(7)#2	0.93	2.18	3.030(2)	152.0
N(5)-H(5)...O(8)#2	0.93	2.47	3.261(2)	142.4
O(21)-H(21C)...O(4)#1	0.96	1.931(3)	2.889(2)	175.4(14)
O(21)-H(21D)...O(6)	0.96	1.884(4)	2.832(2)	169.0(18)
O(22)-H(22C)...O(2)#1	0.96	1.912(2)	2.870(2)	174.7(7)
O(22)-H(22D)...O(8)#3	0.96	1.834(4)	2.7858(18)	170.7(17)
O(61)-H(61)...O(71)	0.84	2.30	2.831(9)	121.5

Symmetry transformations used to generate equivalent atoms:
#1 -x+1,-y+1,-z+1
#2 -x+2,-y+1,-z+1
#3 x-1,y,z

CALIFORNIA INSTITUTE OF TECHNOLOGY

BECKMAN INSTITUTE

X-RAY CRYSTALLOGRAPHY LABORATORY

Date 23 January 2007

Crystal Structure Analysis of:

MLC05

(shown below)

For Investigator: Morgan Cable (818) 354-4348

Advisor: Adrian Ponce/H. B. Gray (818) 354-8196

Account Number: NASA.00002-1-JPL.000174

By Michael W. Day 116 Beckman ext. 2734

e-mail: mikeday@caltech.edu

Contents

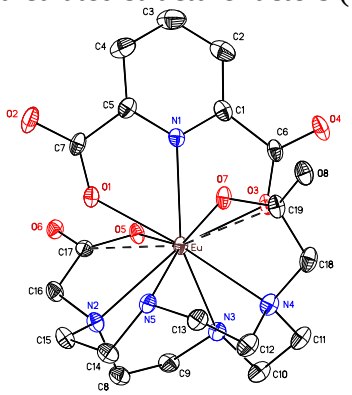

MLC05

Note: The crystallographic data have been deposited in the Cambridge Database (CCDC) and has been placed on hold pending further instructions from me. The deposition number is 634507. Ideally the CCDC would like the publication to contain a footnote of the type: "Crystallographic data have been deposited at the CCDC, 12 Union Road, Cambridge CB2 1EZ, UK and copies can be obtained on request, free of charge, by quoting the publication citation and the deposition number 634507."

Table 1. Crystal data and structure refinement for MLC05 (CCDC 634507).

Empirical formula	$[C_{19}H_{25}N_5O_8Eu]^-[C_{16}H_{36}N]^+ \cdot 3(H_2O) \cdot 0.32(C_3H_6O) \cdot 0.68(C_3H_8O)$
Formula weight	957.23
Crystallization Solvent	Acetone/isopropanol/water
Crystal Habit	Prism
Crystal size	0.34 x 0.13 x 0.11 mm^3
Crystal color	Colorless

Data Collection

Type of diffractometer	Bruker SMART 1000
Wavelength	0.71073 Å MoKα
Data Collection Temperature	100(2) K
θ range for 25559 reflections used in lattice determination	2.18 to 37.61°
Unit cell dimensions	a = 13.1473(4) Å b = 13.2269(4) Å β= 90.0540(10)° c = 26.2248(8) Å
Volume	4560.4(2) $Å^3$
Z	4
Crystal system	Triclinic
Space group	P1
Density (calculated)	1.394 Mg/m^3
F(000)	2005
θ range for data collection	1.55 to 40.67°
Completeness to θ = 40.67°	93.9 %
Index ranges	$-23 \le h \le 23, -24 \le k \le 23, -47 \le l \le 43$
Data collection scan type	ω scans at 7 ϕ settings
Reflections collected	126185
Independent reflections	27668 [R_{int}= 0.1140]
Absorption coefficient	1.438 mm^{-1}
Absorption correction	None
Max. and min. transmission	0.8579 and 0.6407

Table 1 (cont.)

Structure solution and Refinement

Structure solution program	SHELXS-97 (Sheldrick, 1990)
Primary solution method	Direct methods
Secondary solution method	Difference Fourier map
Hydrogen placement	Geometric positions
Structure refinement program	SHELXL-97 (Sheldrick, 1997)
Refinement method	Full matrix least-squares on F^2
Data / restraints / parameters	27668 / 0 / 560
Treatment of hydrogen atoms	Riding
Goodness-of-fit on F^2	1.004
Final R indices [$I>2\sigma(I)$, 12878 reflections]	R1 = 0.0437, *w*R2 = 0.0750
R indices (all data)	R1 = 0.1187, *w*R2 = 0.0854
Type of weighting scheme used	Sigma
Weighting scheme used	$w=1/\sigma^2(Fo^2)$
Max shift/error	0.004
Average shift/error	0.000
Largest diff. peak and hole	4.742 and -2.402 e.Å^{-3}

Special Refinement Details

Refinement of F^2 against ALL reflections. The weighted R-factor (*w*R) and goodness of fit (S) are based on F^2, conventional R-factors (R) are based on F, with F set to zero for negative F^2. The threshold expression of $F^2 > 2\sigma(F^2)$ is used only for calculating R-factors(gt) etc. and is not relevant to the choice of reflections for refinement. R-factors based on F^2 are statistically about twice as large as those based on F, and R-factors based on ALL data will be even larger.

All esds (except the esd in the dihedral angle between two l.s. planes) are estimated using the full covariance matrix. The cell esds are taken into account individually in the estimation of esds in distances, angles and torsion angles; correlations between esds in cell parameters are only used when they are defined by crystal symmetry. An approximate (isotropic) treatment of cell esds is used for estimating esds involving l.s. planes.

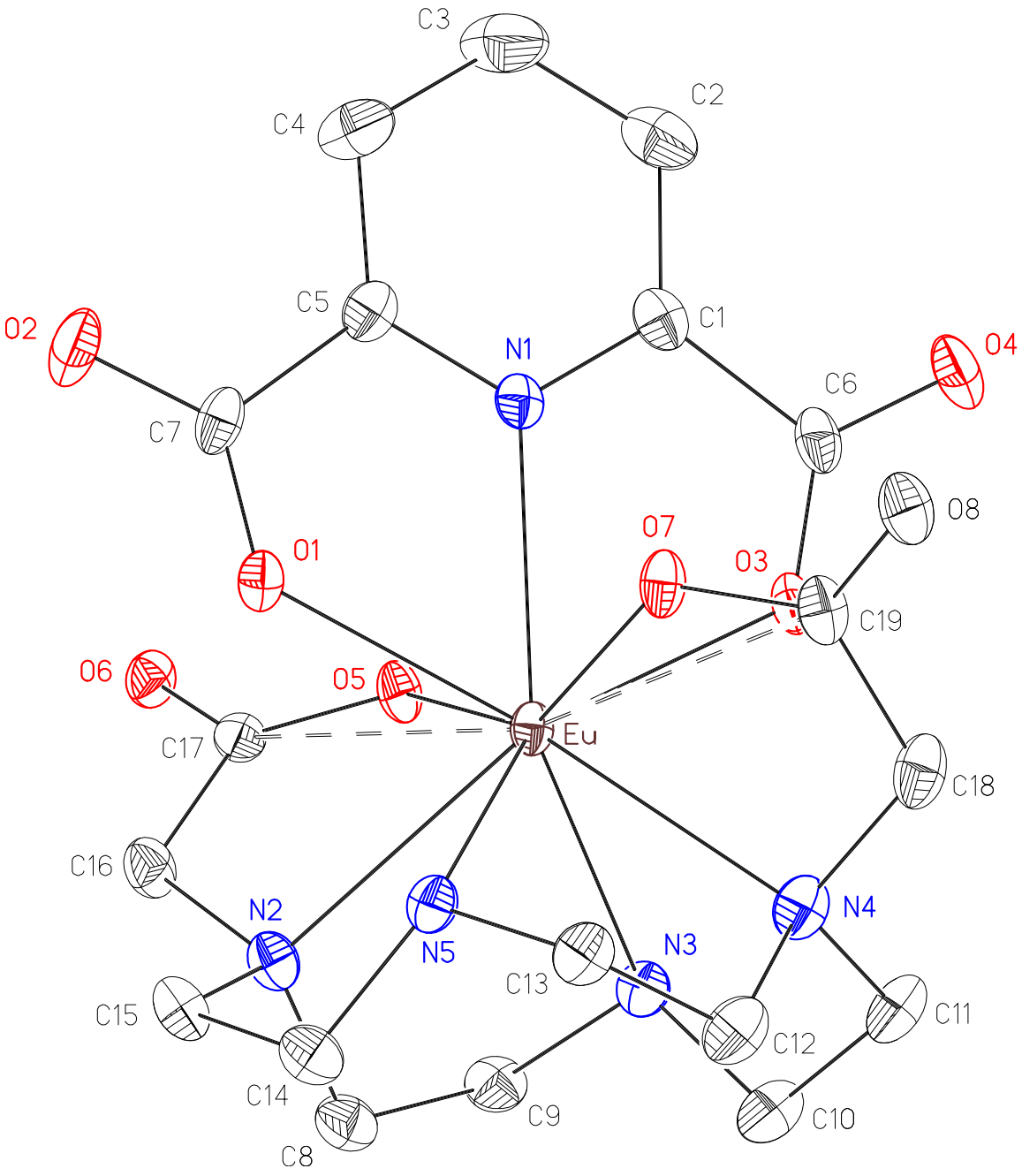
C3
C4
C2
C5
C1
O2
N1
O4
C7
C6
O8
O7
O1
O3
C19
O6
O5
Eu
C17
C18
C16
N2
N5
N4
C13
N3
C15
C12
C11
C14
C9
C10
C8

D19

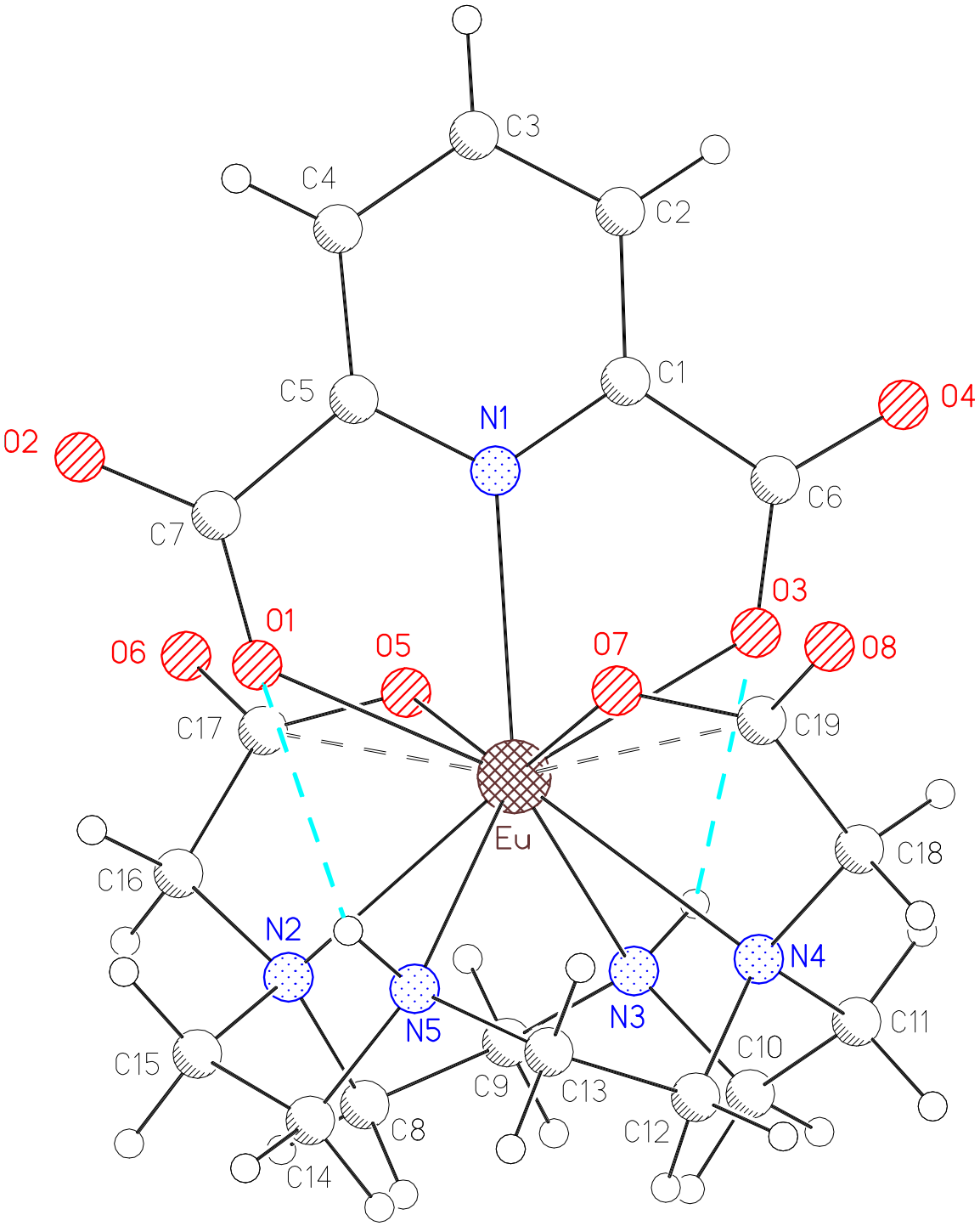
C3
C4
C2
C5
C1
O4
O2
N1
C6
C7
O3
O1
O6
O5
O7
O8
C17
C19
Eu
C18
C16
N2
N4
N5
N3
C11
C15
C10
C9
C13
C8
C12
C14

D20

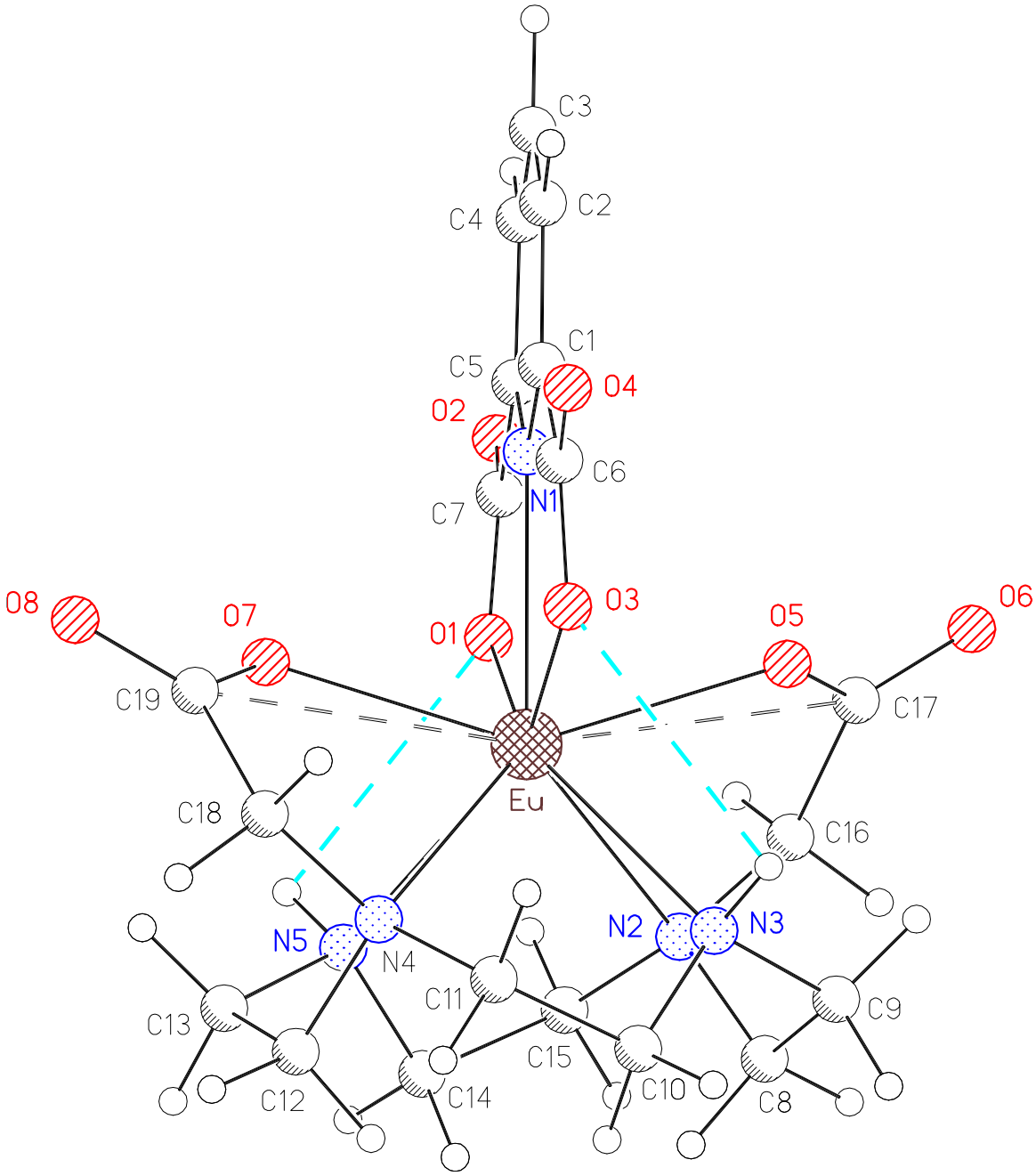
C3
C4
C2
C1
C5
O4
O2
C6
N1
C7
O8
O7
O1
O3
O5
O6
C19
C17
Eu
C18
C16
N5
N4
N2
N3
C13
C11
C15
C9
C12
C14
C10
C8

Table 2. Atomic coordinates (x 10^4) and equivalent isotropic displacement parameters ($Å^2$x 10^3) for MLC05 (CCDC 634507). U(eq) is defined as the trace of the orthogonalized U^{ij} tensor.

	x	y	z	U_{eq}	Occ
Eu	2482(1)	42(1)	4988(1)	13(1)	1
O(1)	1700(1)	-916(1)	5660(1)	17(1)	1
O(2)	1405(1)	-2377(1)	6074(1)	29(1)	1
O(3)	3302(1)	-577(1)	4226(1)	18(1)	1
O(4)	3666(2)	-1811(2)	3671(1)	33(1)	1
O(5)	3952(1)	-588(1)	5414(1)	16(1)	1
O(6)	4674(1)	-1048(1)	6147(1)	17(1)	1
O(7)	1036(1)	-372(1)	4488(1)	18(1)	1
O(8)	273(1)	-413(1)	3728(1)	24(1)	1
N(1)	2504(1)	-1847(1)	4880(1)	14(1)	1
N(2)	2944(1)	1026(2)	5847(1)	17(1)	1
N(3)	3919(1)	1359(1)	4850(1)	17(1)	1
N(4)	2024(1)	1421(2)	4281(1)	19(1)	1
N(5)	1041(1)	1232(1)	5286(1)	17(1)	1
C(1)	2899(2)	-2254(2)	4459(1)	18(1)	1
C(2)	2928(2)	-3296(2)	4384(1)	29(1)	1
C(3)	2559(2)	-3920(2)	4766(1)	35(1)	1
C(4)	2161(2)	-3496(2)	5208(1)	29(1)	1
C(5)	2135(2)	-2437(2)	5250(1)	18(1)	1
C(6)	3319(2)	-1489(2)	4083(1)	18(1)	1
C(7)	1713(2)	-1876(2)	5707(1)	18(1)	1
C(8)	3637(2)	1886(2)	5742(1)	21(1)	1
C(9)	4419(2)	1659(2)	5333(1)	20(1)	1
C(10)	3657(2)	2237(2)	4530(1)	24(1)	1
C(11)	2969(2)	1910(2)	4095(1)	23(1)	1
C(12)	1323(2)	2197(2)	4492(1)	24(1)	1
C(13)	549(2)	1762(2)	4856(1)	21(1)	1
C(14)	1299(2)	1924(2)	5709(1)	21(1)	1
C(15)	1988(2)	1395(2)	6088(1)	20(1)	1
C(16)	3443(2)	272(2)	6180(1)	19(1)	1
C(17)	4078(2)	-509(2)	5893(1)	15(1)	1
C(18)	1527(2)	858(2)	3860(1)	23(1)	1
C(19)	887(1)	-34(2)	4037(1)	18(1)	1
N(6)	6382(1)	2794(1)	2785(1)	17(1)	1
C(20)	7191(2)	3434(2)	2522(1)	21(1)	1
C(21)	8262(2)	3295(2)	2731(1)	26(1)	1
C(22)	8999(2)	4001(3)	2463(1)	43(1)	1
C(23)	10103(2)	3786(3)	2615(1)	50(1)	1
C(24)	6676(2)	1685(2)	2785(1)	20(1)	1
C(25)	6818(2)	1216(2)	2260(1)	27(1)	1
C(26)	7080(2)	113(2)	2307(1)	29(1)	1
C(27)	7262(2)	-389(2)	1791(1)	38(1)	1
C(28)	5397(2)	2956(2)	2488(1)	20(1)	1
C(29)	4473(2)	2393(2)	2688(1)	24(1)	1
C(30)	3638(2)	2365(2)	2286(1)	27(1)	1
C(31)	2678(2)	1825(2)	2470(1)	37(1)	1

C(32)	6253(2)	3105(2)	3340(1)	18(1)	1
C(33)	6042(2)	4216(2)	3431(1)	26(1)	1
C(34)	5672(2)	4384(2)	3972(1)	30(1)	1
C(35)	5627(3)	5483(2)	4128(1)	51(1)	1
O(11)	5766(1)	4998(1)	1879(1)	27(1)	1
O(12)	9151(2)	977(2)	3130(1)	34(1)	1
O(51A)	1461(4)	4404(3)	6187(2)	56(2)	0.685(4)
C(52A)	546(4)	4383(4)	6230(2)	51(2)	0.685(4)
C(53A)	16(4)	3724(4)	6593(2)	51(1)	0.685(4)
C(54A)	-150(10)	4899(10)	5837(5)	137(6)	0.685(4)
O(50A)	-1088(18)	2273(18)	6469(9)	617(15)	0.685(4)
O(51B)	1254(8)	4293(6)	5372(4)	82(4)	0.315(4)
C(52B)	844(12)	4542(8)	5759(5)	61(4)	0.315(4)
C(53B)	-37(16)	5278(11)	5958(7)	39(3)	0.315(4)
C(54B)	1210(20)	4450(30)	6257(9)	240(20)	0.315(4)
O(50B)	-141(9)	3709(9)	7102(5)	101(4)	0.315(4)

Table 3. Selected bond lengths [Å] and angles [°] for MLC05 (CCDC 634507).

Eu-O(7)	2.3740(15)	O(5)-Eu-N(4)	138.38(6)
Eu-O(5)	2.3801(14)	O(1)-Eu-N(4)	140.64(5)
Eu-O(1)	2.4038(15)	O(3)-Eu-N(4)	75.97(6)
Eu-O(3)	2.4140(15)	N(1)-Eu-N(4)	127.07(6)
Eu-N(1)	2.5146(18)	N(5)-Eu-N(4)	68.22(6)
Eu-N(5)	2.5848(18)	N(3)-Eu-N(4)	66.98(6)
Eu-N(3)	2.5947(18)	O(7)-Eu-N(2)	139.46(6)
Eu-N(4)	2.6692(18)	O(5)-Eu-N(2)	65.89(5)
Eu-N(2)	2.6711(18)	O(1)-Eu-N(2)	74.65(6)
Eu-C(17)	3.249(2)	O(3)-Eu-N(2)	139.65(5)
Eu-C(19)	3.2578(18)	N(1)-Eu-N(2)	125.21(5)
		N(5)-Eu-N(2)	67.34(6)
O(7)-Eu-O(5)	145.85(6)	N(3)-Eu-N(2)	68.04(6)
O(7)-Eu-O(1)	86.57(5)	N(4)-Eu-N(2)	107.73(7)
O(5)-Eu-O(1)	79.59(5)	O(7)-Eu-C(17)	150.24(5)
O(7)-Eu-O(3)	79.77(5)	O(5)-Eu-C(17)	19.27(5)
O(5)-Eu-O(3)	84.64(5)	O(1)-Eu-C(17)	67.79(5)
O(1)-Eu-O(3)	128.30(6)	O(3)-Eu-C(17)	103.91(5)
O(7)-Eu-N(1)	73.56(5)	N(1)-Eu-C(17)	81.50(5)
O(5)-Eu-N(1)	72.30(5)	N(5)-Eu-C(17)	112.87(5)
O(1)-Eu-N(1)	64.12(5)	N(3)-Eu-C(17)	77.48(5)
O(3)-Eu-N(1)	64.18(5)	N(4)-Eu-C(17)	143.74(6)
O(7)-Eu-N(5)	73.75(6)	N(2)-Eu-C(17)	49.23(5)
O(5)-Eu-N(5)	131.78(5)	O(7)-Eu-C(19)	19.10(5)
O(1)-Eu-N(5)	77.57(6)	O(5)-Eu-C(19)	150.37(5)
O(3)-Eu-N(5)	141.69(5)	O(1)-Eu-C(19)	105.62(5)
N(1)-Eu-N(5)	130.32(6)	O(3)-Eu-C(19)	69.12(5)
O(7)-Eu-N(3)	131.38(6)	N(1)-Eu-C(19)	83.68(6)
O(5)-Eu-N(3)	73.13(6)	N(5)-Eu-C(19)	77.21(5)
O(1)-Eu-N(3)	140.21(5)	N(3)-Eu-C(19)	112.48(6)
O(3)-Eu-N(3)	77.68(6)	N(4)-Eu-C(19)	49.06(6)
N(1)-Eu-N(3)	130.00(6)	N(2)-Eu-C(19)	143.73(6)
N(5)-Eu-N(3)	99.67(6)	C(17)-Eu-C(19)	165.18(6)
O(7)-Eu-N(4)	66.01(6)		

Table 4. Bond lengths [Å] and angles [°] for MLC05 (CCDC 634507).

Eu-O(7)	2.3740(15)	C(24)-C(25)	1.521(3)
Eu-O(5)	2.3801(14)	C(25)-C(26)	1.504(3)
Eu-O(1)	2.4038(15)	C(26)-C(27)	1.528(4)
Eu-O(3)	2.4140(15)	C(28)-C(29)	1.520(3)
Eu-N(1)	2.5146(18)	C(29)-C(30)	1.523(3)
Eu-N(5)	2.5848(18)	C(30)-C(31)	1.529(4)
Eu-N(3)	2.5947(18)	C(32)-C(33)	1.514(3)
Eu-N(4)	2.6692(18)	C(33)-C(34)	1.518(3)
Eu-N(2)	2.6711(18)	C(34)-C(35)	1.511(4)
Eu-C(17)	3.249(2)	O(51A)-C(52A)	1.209(7)
Eu-C(19)	3.2578(18)	C(52A)-C(53A)	1.467(8)
O(1)-C(7)	1.275(3)	C(52A)-C(54A)	1.538(13)
O(2)-C(7)	1.238(3)	O(51B)-C(52B)	1.194(14)
O(3)-C(6)	1.264(3)	C(52B)-C(54B)	1.40(3)
O(4)-C(6)	1.247(3)	C(52B)-C(53B)	1.60(2)
O(5)-C(17)	1.273(2)		
O(6)-C(17)	1.251(2)	O(7)-Eu-O(5)	145.85(6)
O(7)-C(19)	1.278(2)	O(7)-Eu-O(1)	86.57(5)
O(8)-C(19)	1.249(2)	O(5)-Eu-O(1)	79.59(5)
N(1)-C(1)	1.334(3)	O(7)-Eu-O(3)	79.77(5)
N(1)-C(5)	1.337(3)	O(5)-Eu-O(3)	84.64(5)
N(2)-C(16)	1.477(3)	O(1)-Eu-O(3)	128.30(6)
N(2)-C(8)	1.484(3)	O(7)-Eu-N(1)	73.56(5)
N(2)-C(15)	1.490(3)	O(5)-Eu-N(1)	72.30(5)
N(3)-C(10)	1.473(3)	O(1)-Eu-N(1)	64.12(5)
N(3)-C(9)	1.481(3)	O(3)-Eu-N(1)	64.18(5)
N(4)-C(18)	1.482(3)	O(7)-Eu-N(5)	73.75(6)
N(4)-C(11)	1.484(3)	O(5)-Eu-N(5)	131.78(5)
N(4)-C(12)	1.486(3)	O(1)-Eu-N(5)	77.57(6)
N(5)-C(13)	1.477(3)	O(3)-Eu-N(5)	141.69(5)
N(5)-C(14)	1.477(3)	N(1)-Eu-N(5)	130.32(6)
C(1)-C(2)	1.393(3)	O(7)-Eu-N(3)	131.38(6)
C(1)-C(6)	1.518(3)	O(5)-Eu-N(3)	73.13(6)
C(2)-C(3)	1.388(4)	O(1)-Eu-N(3)	140.21(5)
C(3)-C(4)	1.391(4)	O(3)-Eu-N(3)	77.68(6)
C(4)-C(5)	1.405(3)	N(1)-Eu-N(3)	130.00(6)
C(5)-C(7)	1.515(3)	N(5)-Eu-N(3)	99.67(6)
C(8)-C(9)	1.516(3)	O(7)-Eu-N(4)	66.01(6)
C(10)-C(11)	1.518(3)	O(5)-Eu-N(4)	138.38(6)
C(12)-C(13)	1.511(3)	O(1)-Eu-N(4)	140.64(5)
C(14)-C(15)	1.516(3)	O(3)-Eu-N(4)	75.97(6)
C(16)-C(17)	1.526(3)	N(1)-Eu-N(4)	127.07(6)
C(18)-C(19)	1.521(3)	N(5)-Eu-N(4)	68.22(6)
N(6)-C(24)	1.517(3)	N(3)-Eu-N(4)	66.98(6)
N(6)-C(32)	1.522(3)	O(7)-Eu-N(2)	139.46(6)
N(6)-C(20)	1.524(3)	O(5)-Eu-N(2)	65.89(5)
N(6)-C(28)	1.525(3)	O(1)-Eu-N(2)	74.65(6)
C(20)-C(21)	1.522(3)	O(3)-Eu-N(2)	139.65(5)
C(21)-C(22)	1.519(3)	N(1)-Eu-N(2)	125.21(5)
C(22)-C(23)	1.531(4)	N(5)-Eu-N(2)	67.34(6)

N(3)-Eu-N(2)	68.04(6)	N(1)-C(5)-C(4)	121.1(2)
N(4)-Eu-N(2)	107.73(7)	N(1)-C(5)-C(7)	114.95(19)
O(7)-Eu-C(17)	150.24(5)	C(4)-C(5)-C(7)	123.9(2)
O(5)-Eu-C(17)	19.27(5)	O(4)-C(6)-O(3)	126.2(2)
O(1)-Eu-C(17)	67.79(5)	O(4)-C(6)-C(1)	117.9(2)
O(3)-Eu-C(17)	103.91(5)	O(3)-C(6)-C(1)	115.84(19)
N(1)-Eu-C(17)	81.50(5)	O(2)-C(7)-O(1)	127.1(2)
N(5)-Eu-C(17)	112.87(5)	O(2)-C(7)-C(5)	118.3(2)
N(3)-Eu-C(17)	77.48(5)	O(1)-C(7)-C(5)	114.62(19)
N(4)-Eu-C(17)	143.74(6)	N(2)-C(8)-C(9)	113.37(18)
N(2)-Eu-C(17)	49.23(5)	N(3)-C(9)-C(8)	110.88(17)
O(7)-Eu-C(19)	19.10(5)	N(3)-C(10)-C(11)	110.02(19)
O(5)-Eu-C(19)	150.37(5)	N(4)-C(11)-C(10)	112.06(19)
O(1)-Eu-C(19)	105.62(5)	N(4)-C(12)-C(13)	112.99(19)
O(3)-Eu-C(19)	69.12(5)	N(5)-C(13)-C(12)	111.68(18)
N(1)-Eu-C(19)	83.68(6)	N(5)-C(14)-C(15)	110.13(18)
N(5)-Eu-C(19)	77.21(5)	N(2)-C(15)-C(14)	112.10(18)
N(3)-Eu-C(19)	112.48(6)	N(2)-C(16)-C(17)	114.17(17)
N(4)-Eu-C(19)	49.06(6)	O(6)-C(17)-O(5)	124.1(2)
N(2)-Eu-C(19)	143.73(6)	O(6)-C(17)-C(16)	117.79(18)
C(17)-Eu-C(19)	165.18(6)	O(5)-C(17)-C(16)	118.07(18)
C(7)-O(1)-Eu	126.12(14)	O(6)-C(17)-Eu	157.04(15)
C(6)-O(3)-Eu	125.35(14)	O(5)-C(17)-Eu	38.08(10)
C(17)-O(5)-Eu	122.65(14)	C(16)-C(17)-Eu	81.64(11)
C(19)-O(7)-Eu	123.46(14)	N(4)-C(18)-C(19)	113.93(17)
C(1)-N(1)-C(5)	120.5(2)	O(8)-C(19)-O(7)	123.9(2)
C(1)-N(1)-Eu	119.92(14)	O(8)-C(19)-C(18)	117.99(18)
C(5)-N(1)-Eu	119.60(14)	O(7)-C(19)-C(18)	118.03(18)
C(16)-N(2)-C(8)	110.82(17)	O(8)-C(19)-Eu	157.66(18)
C(16)-N(2)-C(15)	110.20(17)	O(7)-C(19)-Eu	37.44(10)
C(8)-N(2)-C(15)	110.22(18)	C(18)-C(19)-Eu	81.62(11)
C(16)-N(2)-Eu	105.65(12)	C(24)-N(6)-C(32)	106.84(16)
C(8)-N(2)-Eu	110.79(13)	C(24)-N(6)-C(20)	111.10(17)
C(15)-N(2)-Eu	109.06(12)	C(32)-N(6)-C(20)	111.13(17)
C(10)-N(3)-C(9)	112.29(18)	C(24)-N(6)-C(28)	110.59(17)
C(10)-N(3)-Eu	115.98(13)	C(32)-N(6)-C(28)	110.74(17)
C(9)-N(3)-Eu	112.52(13)	C(20)-N(6)-C(28)	106.50(16)
C(18)-N(4)-C(11)	110.08(18)	C(21)-C(20)-N(6)	114.57(18)
C(18)-N(4)-C(12)	110.54(17)	C(22)-C(21)-C(20)	110.45(19)
C(11)-N(4)-C(12)	109.94(19)	C(21)-C(22)-C(23)	111.8(2)
C(18)-N(4)-Eu	105.84(14)	N(6)-C(24)-C(25)	115.20(18)
C(11)-N(4)-Eu	109.68(13)	C(26)-C(25)-C(24)	110.46(19)
C(12)-N(4)-Eu	110.70(13)	C(25)-C(26)-C(27)	112.6(2)
C(13)-N(5)-C(14)	112.27(18)	C(29)-C(28)-N(6)	115.72(17)
C(13)-N(5)-Eu	112.26(13)	C(28)-C(29)-C(30)	110.40(19)
C(14)-N(5)-Eu	115.85(13)	C(29)-C(30)-C(31)	112.7(2)
N(1)-C(1)-C(2)	121.8(2)	C(33)-C(32)-N(6)	115.71(18)
N(1)-C(1)-C(6)	114.27(19)	C(32)-C(33)-C(34)	110.40(19)
C(2)-C(1)-C(6)	123.9(2)	C(35)-C(34)-C(33)	114.0(2)
C(3)-C(2)-C(1)	118.5(2)	O(51A)-C(52A)-C(53A)	123.2(6)
C(2)-C(3)-C(4)	119.7(2)	O(51A)-C(52A)-C(54A)	121.2(8)
C(3)-C(4)-C(5)	118.4(2)	C(53A)-C(52A)-C(54A)	114.6(7)

O(51B)-C(52B)-C(54B)	128.0(19)
O(51B)-C(52B)-C(53B)	140.5(15)
C(54B)-C(52B)-C(53B)	89.6(15)

Table 5. Anisotropic displacement parameters ($Å^2 x\ 10^4$) for MLC05 (CCDC 634507). The anisotropic displacement factor exponent takes the form: $-2\pi^2[h^2 a^{*2} U^{11} + ... + 2\ h\ k\ a^*\ b^*\ U^{12}]$

	U^{11}	U^{22}	U^{33}	U^{23}	U^{13}	U^{12}
Eu	106(1)	172(1)	111(1)	15(1)	-13(1)	1(1)
O(1)	175(7)	210(8)	129(7)	22(6)	18(5)	22(6)
O(2)	349(10)	306(10)	199(8)	116(7)	59(7)	42(8)
O(3)	198(8)	238(8)	101(7)	-8(6)	-5(5)	-16(6)
O(4)	485(12)	372(11)	142(8)	-82(8)	61(8)	-60(9)
O(5)	156(7)	230(8)	104(7)	-5(6)	-43(5)	24(6)
O(6)	167(7)	196(8)	143(7)	25(6)	-46(5)	-7(5)
O(7)	136(7)	265(8)	123(7)	43(6)	-36(5)	20(6)
O(8)	232(9)	323(9)	158(7)	-6(7)	-74(6)	18(7)
N(1)	113(7)	186(8)	128(8)	3(6)	-45(6)	-3(6)
N(2)	162(9)	210(9)	151(8)	-18(7)	-11(6)	16(7)
N(3)	148(8)	183(9)	174(9)	8(7)	8(7)	1(6)
N(4)	152(9)	230(10)	197(9)	45(8)	-15(7)	10(7)
N(5)	156(9)	187(9)	163(9)	27(7)	3(6)	12(6)
C(1)	119(9)	250(11)	165(10)	-29(8)	-31(7)	-1(8)
C(2)	267(13)	269(13)	325(14)	-106(11)	28(10)	-6(10)
C(3)	378(16)	209(12)	476(17)	-49(12)	75(13)	-13(11)
C(4)	281(13)	197(11)	381(15)	41(11)	48(11)	-12(9)
C(5)	143(10)	203(10)	191(10)	44(8)	-22(7)	19(7)
C(6)	149(10)	285(12)	115(9)	-14(8)	-26(7)	-26(8)
C(7)	129(10)	250(11)	163(10)	78(9)	-6(8)	10(8)
C(8)	210(11)	207(11)	214(11)	-34(9)	-33(8)	-10(8)
C(9)	153(10)	210(11)	226(11)	-8(9)	-41(8)	-50(8)
C(10)	209(11)	219(11)	282(13)	71(10)	-24(9)	-24(8)
C(11)	200(11)	250(12)	250(12)	107(10)	4(9)	-21(9)
C(12)	204(11)	243(12)	279(12)	76(10)	-23(9)	37(9)
C(13)	173(10)	216(11)	232(11)	30(9)	-20(8)	41(8)
C(14)	179(11)	220(11)	234(11)	-45(9)	-5(9)	30(8)
C(15)	170(10)	263(12)	172(10)	-56(9)	-6(8)	15(8)
C(16)	199(10)	221(11)	146(9)	-10(8)	-46(7)	24(7)
C(17)	130(9)	158(10)	158(9)	-4(8)	-18(7)	-24(7)
C(18)	177(11)	327(13)	179(10)	77(9)	-35(8)	-5(9)
C(19)	127(8)	276(11)	142(8)	2(10)	-29(6)	58(10)
N(6)	146(9)	216(9)	161(9)	64(7)	1(6)	1(7)
C(20)	160(10)	274(12)	209(11)	130(9)	19(8)	5(8)
C(21)	171(11)	323(13)	281(12)	135(10)	-15(9)	-8(9)
C(22)	203(13)	549(19)	524(19)	324(16)	-9(12)	-61(12)
C(23)	242(15)	640(20)	630(20)	269(18)	-3(14)	-85(14)
C(24)	167(10)	213(11)	207(11)	67(8)	3(8)	31(8)
C(25)	306(13)	302(14)	212(12)	36(10)	26(9)	49(10)
C(26)	301(12)	280(13)	290(11)	-3(11)	-28(9)	55(10)
C(27)	374(16)	411(16)	340(15)	-59(13)	4(12)	76(12)
C(28)	168(10)	265(12)	160(10)	81(9)	-24(8)	28(8)
C(29)	176(11)	348(13)	194(11)	90(10)	-23(8)	-19(9)
C(30)	268(13)	292(13)	257(13)	45(10)	-74(10)	-22(10)
C(31)	248(14)	390(16)	466(18)	69(13)	-109(12)	-69(11)

C(32)	180(10)	196(10)	158(9)	57(8)	9(7)	2(7)
C(33)	290(13)	201(11)	286(13)	65(10)	6(10)	-8(9)
C(34)	381(15)	237(13)	282(14)	-21(10)	34(11)	-6(10)
C(35)	610(20)	358(18)	560(20)	-86(16)	160(18)	-3(16)
O(11)	364(9)	263(9)	192(7)	30(8)	-82(6)	65(9)
O(12)	371(11)	419(12)	223(9)	24(8)	-77(8)	153(9)
O(51A)	224(18)	490(20)	960(40)	-60(20)	30(20)	-8(15)
C(52A)	280(20)	560(30)	700(40)	-270(30)	30(20)	60(20)
C(53A)	400(30)	540(30)	600(30)	-110(30)	20(20)	0(20)
C(54A)	560(60)	2450(180)	1110(100)	250(100)	110(70)	440(100)
O(51B)	1270(90)	350(50)	830(70)	-30(40)	480(60)	-110(50)
C(52B)	1050(120)	210(50)	570(80)	40(50)	360(80)	-120(50)
C(53B)	370(70)	420(60)	380(60)	80(50)	30(50)	80(40)
C(54B)	1400(300)	5200(600)	640(130)	-1500(200)	-210(160)	1100(300)

Table 6. Hydrogen bonds for MLC05 (CCDC 634507) [Å and °].

D-H...A	d(D-H)	d(H...A)	d(D...A)	<(DHA)
N(3)-H(3)...O(5)#1	0.93	2.23	3.059(2)	148.5
N(3)-H(3)...O(6)#1	0.93	2.45	3.232(2)	141.6
N(5)-H(5)...O(7)#2	0.93	2.17	3.016(2)	151.4
N(5)-H(5)...O(8)#2	0.93	2.54	3.294(3)	138.3
O(11)-H(11A)...O(4)#3	1.00	1.90	2.892(3)	175.7
O(11)-H(11B)...O(6)#4	1.00	1.80	2.769(2)	162.2
O(12)-H(12A)...O(2)#1	1.00	1.91	2.886(3)	164.7
O(12)-H(12B)...O(8)#5	1.00	1.88	2.830(2)	158.3
N(3)-H(3)...O(3)	0.93	2.82	3.144(2)	102.1
N(5)-H(5)...O(1)	0.93	2.81	3.128(2)	101.1

Symmetry transformations used to generate equivalent atoms:
#1 -x+1,-y,-z+1
#2 -x,-y,-z+1
#3 -x+1,y+1/2,-z+1/2
#4 x,-y+1/2,z-1/2
#5 x+1,y,z

CALIFORNIA INSTITUTE OF TECHNOLOGY

BECKMAN INSTITUTE

X-RAY CRYSTALLOGRAPHY LABORATORY

Date 1 September 2009

Crystal Structure Analysis of:

MLC13

(shown below)

For Investigator: Morgan Cable (818) 354-2539

Advisor: H. B. Gray ext. 6500

Account Number: AP1.HSARPA3-1-HSARPA.PONCE

By Michael W. Day 116 Beckman ext. 2734

e-mail: mikeday@caltech.edu

Contents

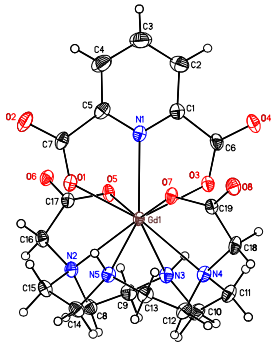

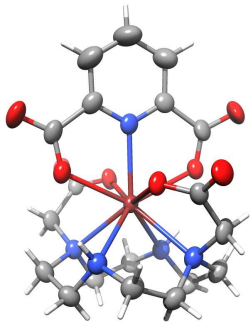

MLC13

Note: The crystallographic data have been deposited in the Cambridge Database (CCDC) and has been placed on hold pending further instructions from me. The deposition number is 746157. Ideally the CCDC would like the publication to contain a footnote of the type: "Crystallographic data have been deposited at the CCDC, 12 Union Road, Cambridge CB2 1EZ, UK and copies can be obtained on request, free of charge, by quoting the publication citation and the deposition number 746157."

Table 1. Crystal data and structure refinement for MLC13 (CCDC 746175).

Empirical formula	$[C_{19}H_{25}N_5O_8Gd]^-$ $[C_{16}H_{36}N]+ \bullet 2(H_2O)$ $0.62(C_3H_6O)$ $0.38(C_2H_6O \bullet O)$
Formula weight	946.79
Crystallization Solvent	Ethanol/
Crystal Habit	Block
Crystal size	0.22 x 0.16 x 0.13 mm^3
Crystal color	Colorless

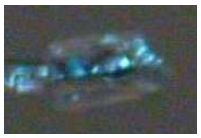

Data Collection

Type of diffractometer	Bruker KAPPA APEX II
Wavelength	0.71073 Å MoKα
Data Collection Temperature	100(2) K
θ range for 9360 reflections used in lattice determination	2.18 to 47.36°
Unit cell dimensions	a = 13.1910(5) Å b = 13.4544(5) Å β= 90.368(2)° c = 26.1712(9) Å
Volume	4644.7(3) $Å^3$
Z	4
Crystal system	Monoclinic
Space group	$P2_1/c$
Density (calculated)	1.354 Mg/m^3
F(000)	1975
θ range for data collection	2.16 to 47.72°
Completeness to θ = 47.72°	90.4 %
Index ranges	$-20 \le h \le 27$, $-27 \le k \le 27$, $-53 \le l \le 54$
Data collection scan type	ω scans; 19 settings
Reflections collected	245931
Independent reflections	39658 [R_{int}= 0.0563]
Absorption coefficient	1.487 mm^{-1}
Absorption correction	None
Max. and min. transmission	0.8302 and 0.7356

Table 1 (cont.)

Structure solution and Refinement

Structure solution program	SHELXS-97 (Sheldrick, 2008)
Primary solution method	Direct methods
Secondary solution method	Difference Fourier map
Hydrogen placement	Difference Fourier map
Structure refinement program	SHELXL-97 (Sheldrick, 2008)
Refinement method	Full matrix least-squares on F^2
Data / restraints / parameters	39658 / 0 / 664
Treatment of hydrogen atoms	Mixed
Goodness-of-fit on F^2	1.384
Final R indices [$I>2\sigma(I)$, 22019 reflections]	R1 = 0.0302, *w*R2 = 0.0482
R indices (all data)	R1 = 0.0805, *w*R2 = 0.0509
Type of weighting scheme used	Sigma
Weighting scheme used	$w=1/\sigma^2(Fo^2)$
Max shift/error	0.005
Average shift/error	0.000
Largest diff. peak and hole	3.917 and -2.616 e.Å^{-3}

Special Refinement Details

Crystals were mounted on a glass fiber using Paratone oil then placed on the diffractometer under a nitrogen stream at 100K.

Hydrogen atoms in the Gadolinium dipicolinate macrocycle were refined without restraint. Hydrogen atoms of the tetramethyammonium counterion were restrained. The solvent region is disordered, containing acetone (62%) and ethanol/water (38%). These were refined without restraint (except for riding hydrogens). Additionally, the solvent region contains two ordered water molecules which were refined with no restraint on corresponding hydrogens.

Refinement of F^2 against ALL reflections. The weighted R-factor (*w*R) and goodness of fit (S) are based on F^2, conventional R-factors (R) are based on F, with F set to zero for negative F^2. The threshold expression of $F^2 > 2\sigma(F^2)$ is used only for calculating R-factors(gt) etc. and is not relevant to the choice of reflections for refinement. R-factors based on F^2 are statistically about twice as large as those based on F, and R-factors based on ALL data will be even larger.

All esds (except the esd in the dihedral angle between two l.s. planes) are estimated using the full covariance matrix. The cell esds are taken into account individually in the estimation of esds in distances, angles and torsion angles; correlations between esds in cell parameters are only used when they are defined by crystal symmetry. An approximate (isotropic) treatment of cell esds is used for estimating esds involving l.s. planes.

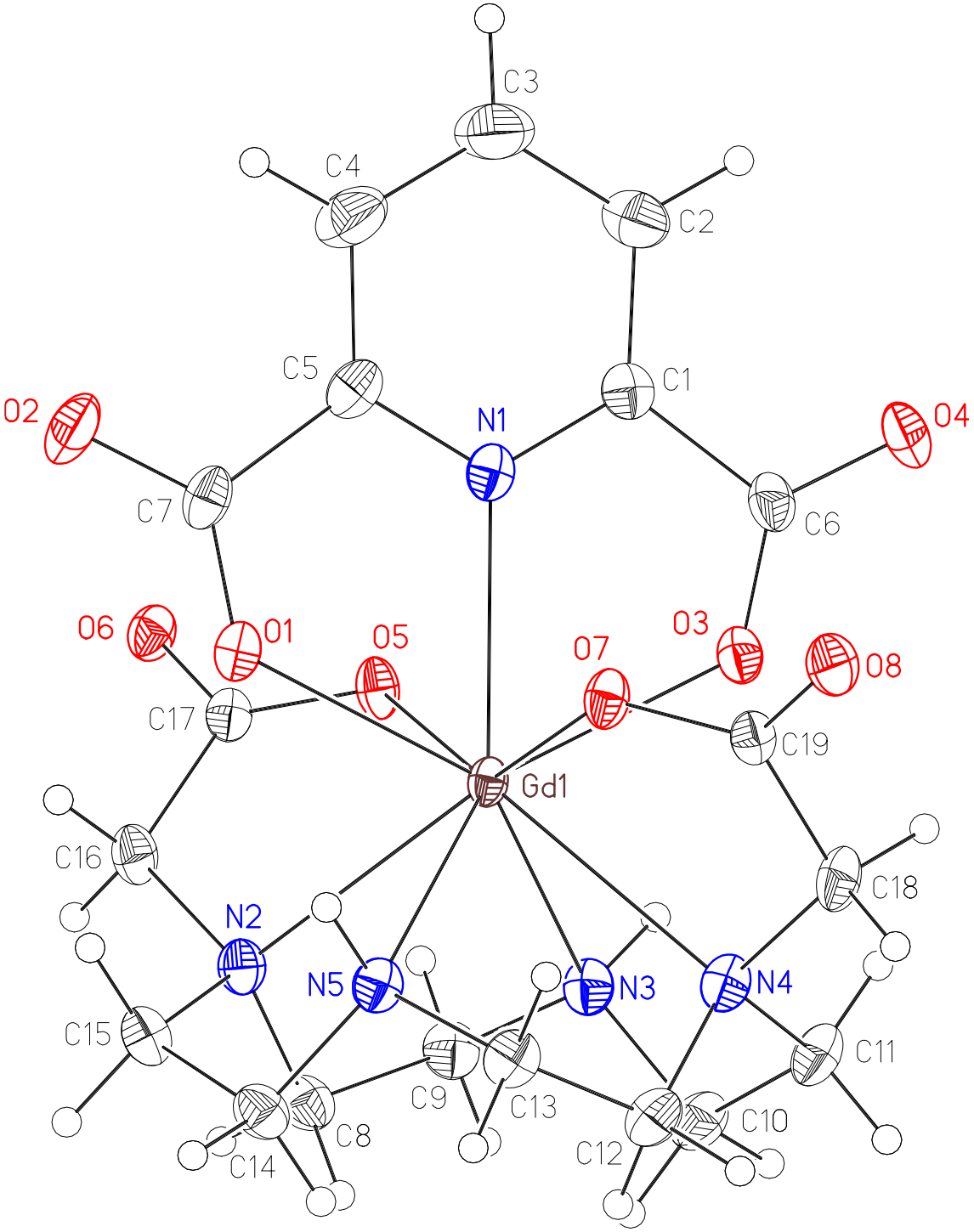
C3
C4
C2
C5
C1
O2
N1
O4
C7
C6
O6
O1
O5
O7
O3
O8
C17
C19
Gd1
C16
C18
N2
N5
N3
N4
C15
C11
C9
C13
C8
C10
C14
C12

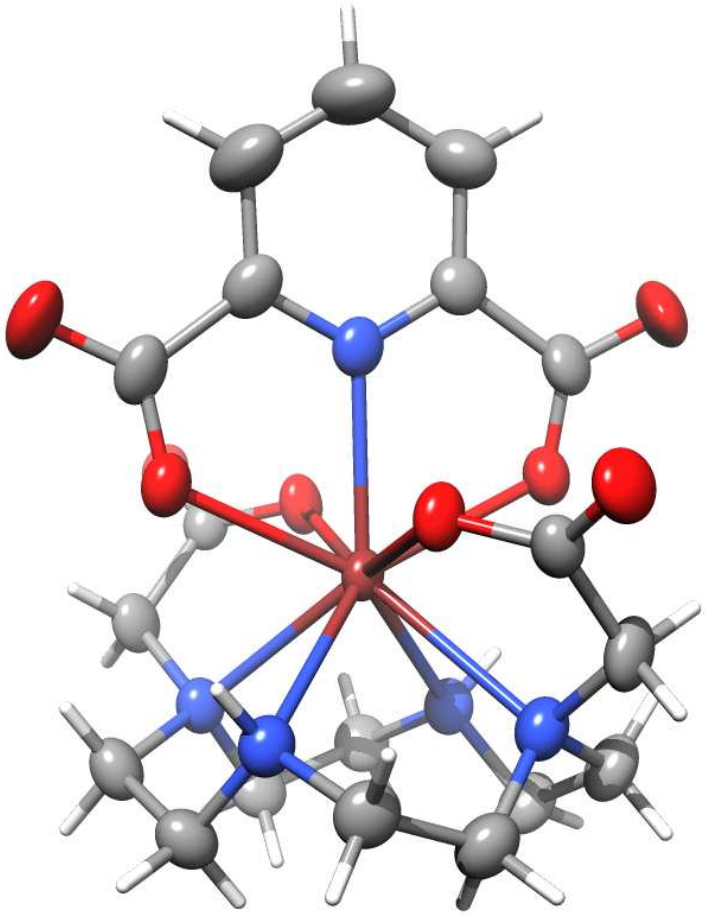

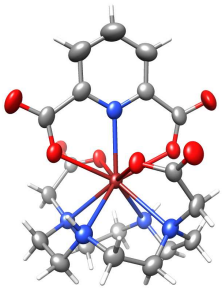

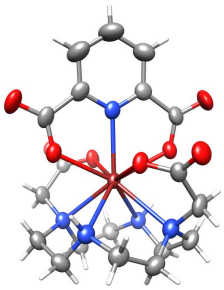

D35

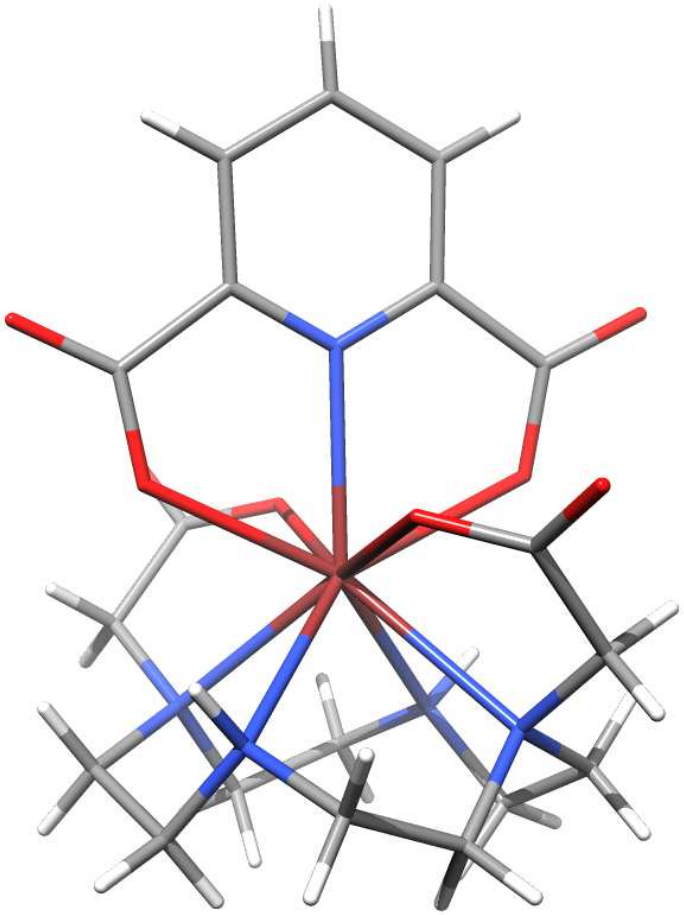

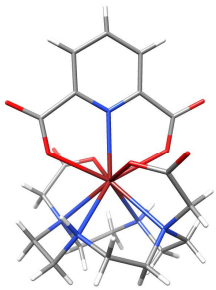

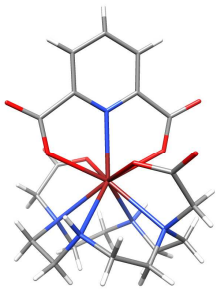

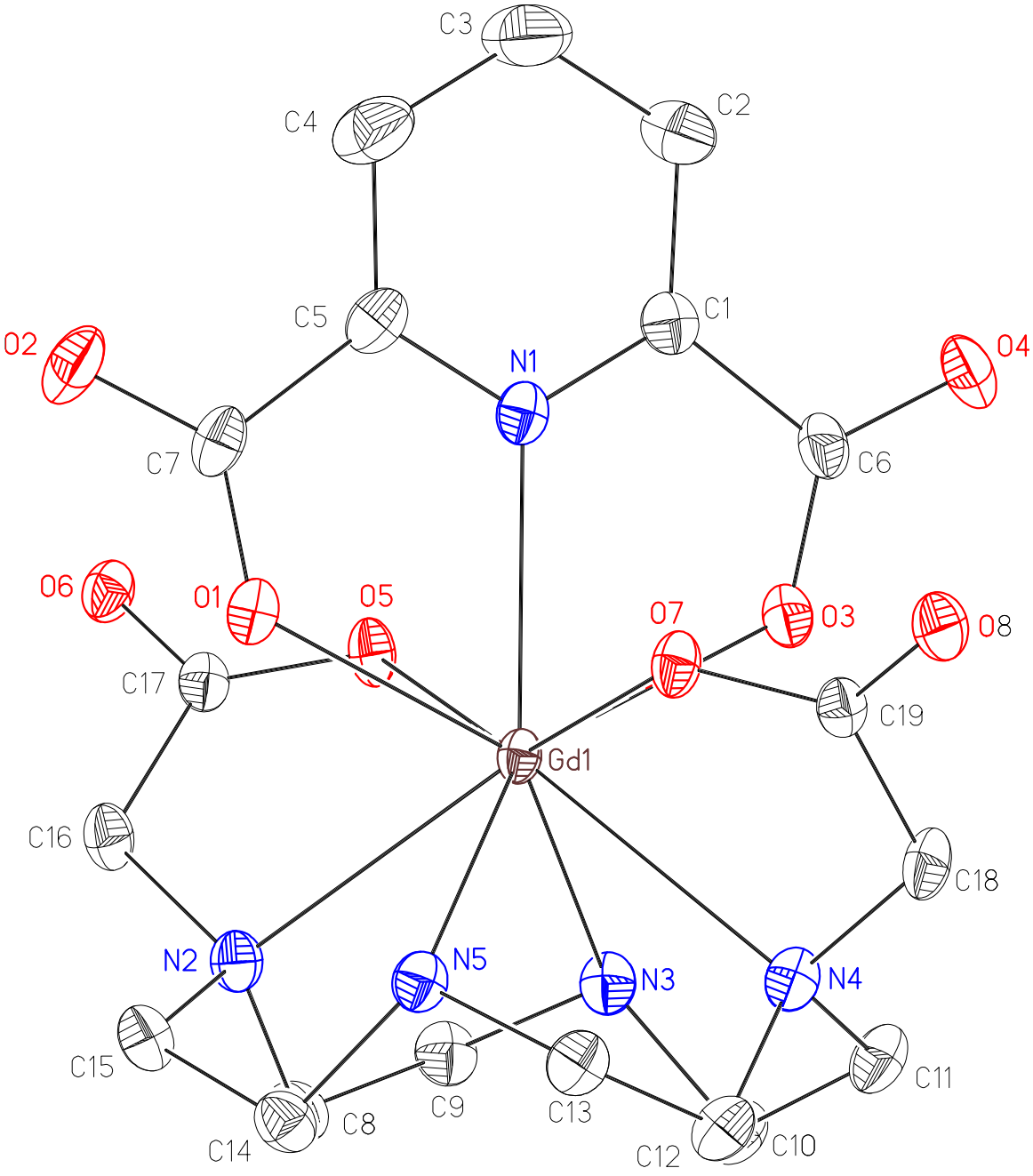
C3
C4
C2
C5
C1
O2
N1
O4
C7
C6
O6
O1
O5
O7
O3
O8
C17
C19
Gd1
C16
C18
N2
N5
N3
N4
C15
C11
C9
C13
C14
C8
C12
C10

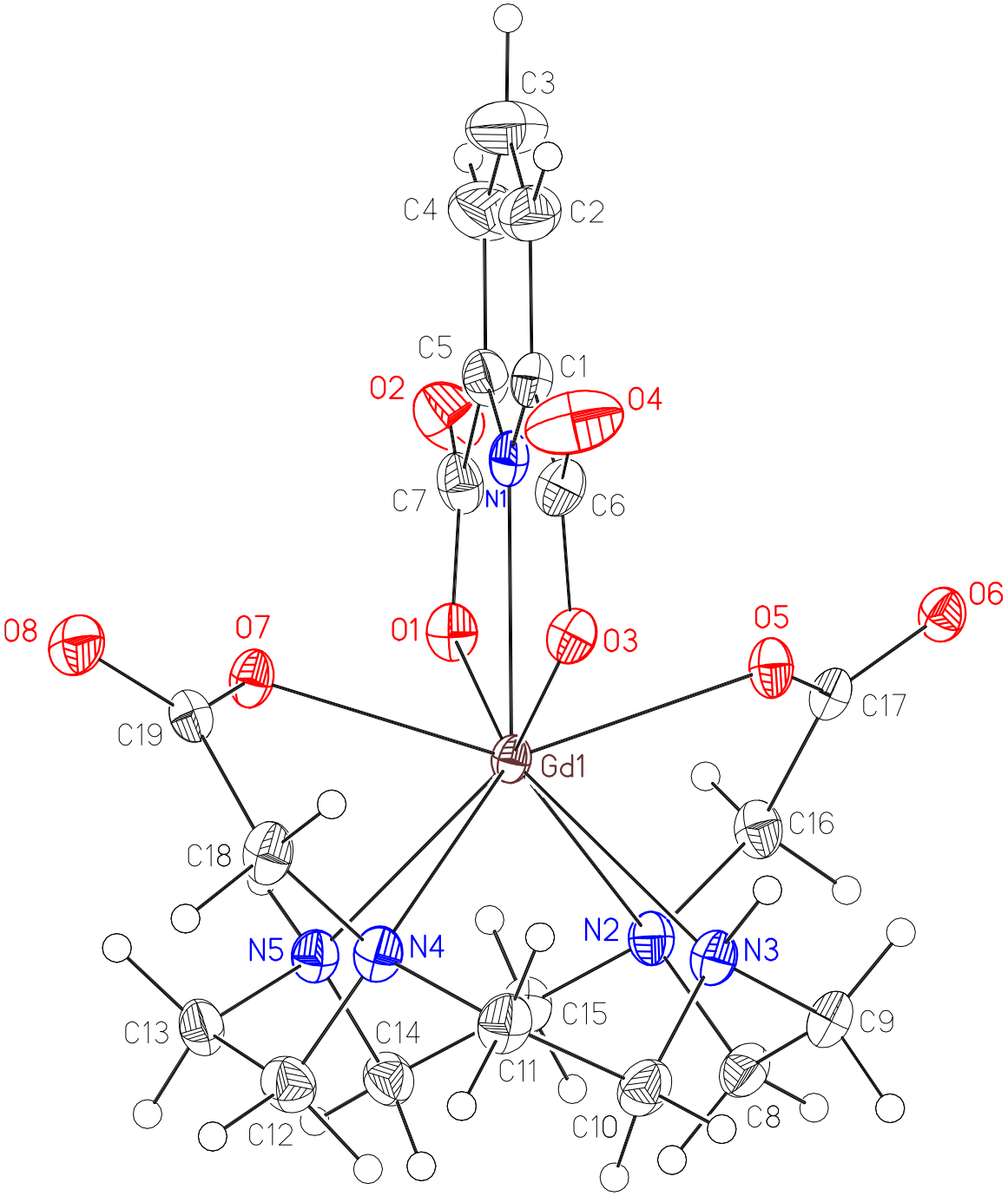
C3
C4
C2
C5
C1
O2
O4
C7
N1
C6
O8
O7
O1
O3
O5
O6
C19
C17
Gd1
C18
C16
N5
N4
N2
N3
C13
C14
C15
C9
C12
C11
C10
C8

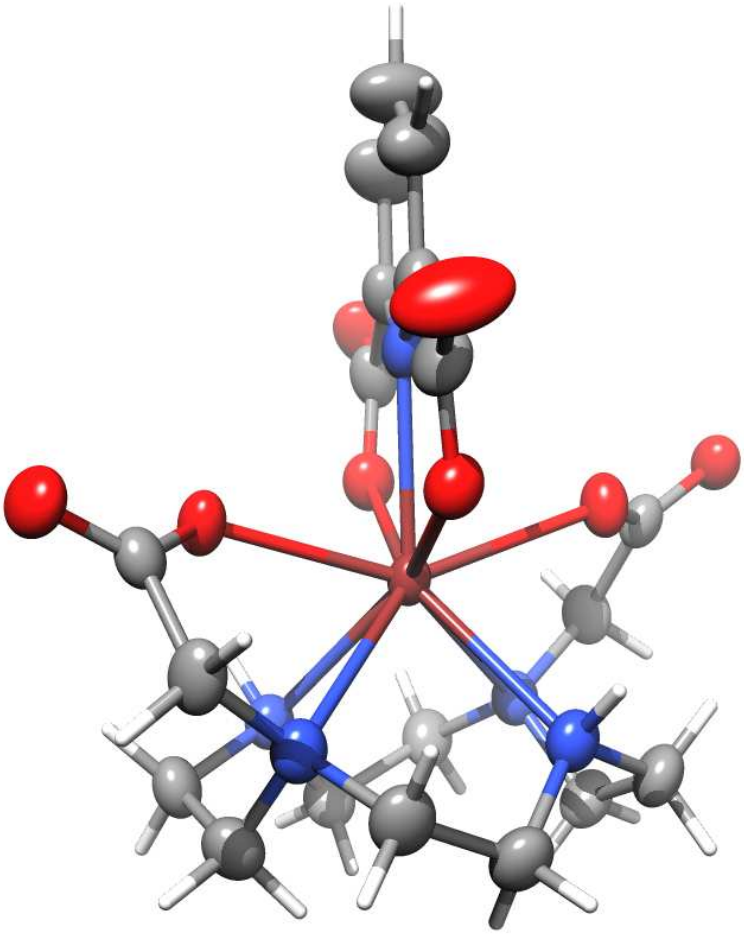

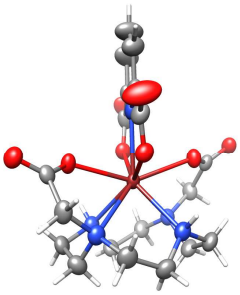

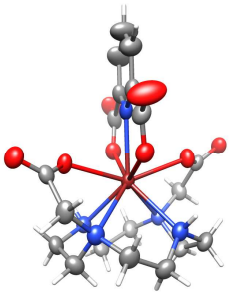

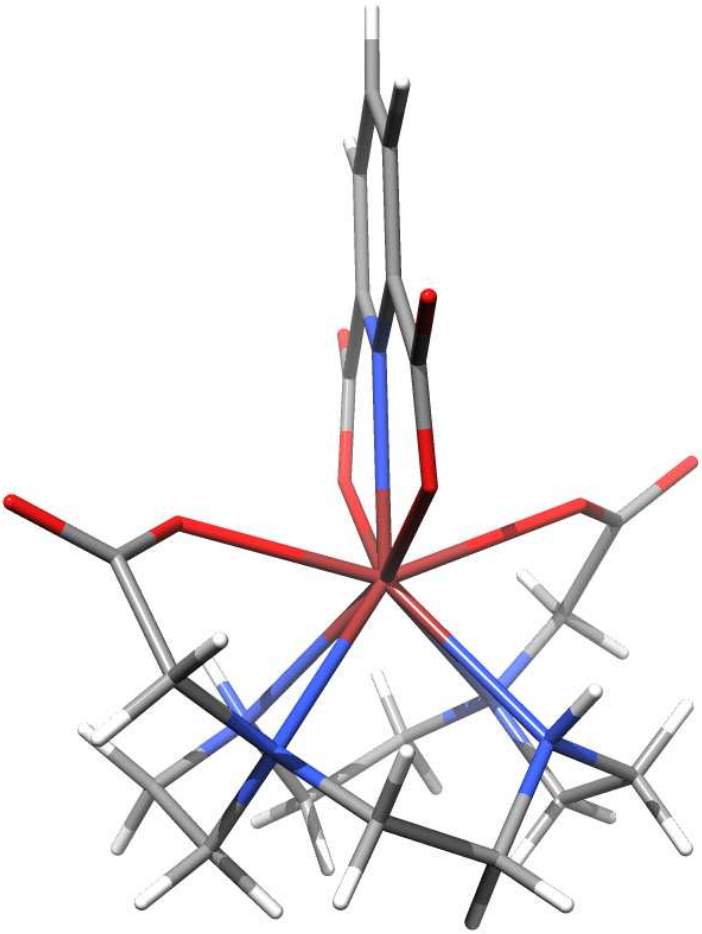

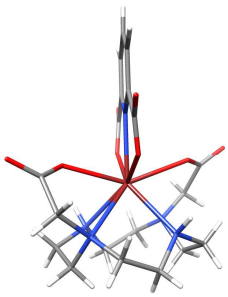

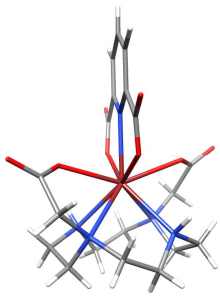

D40

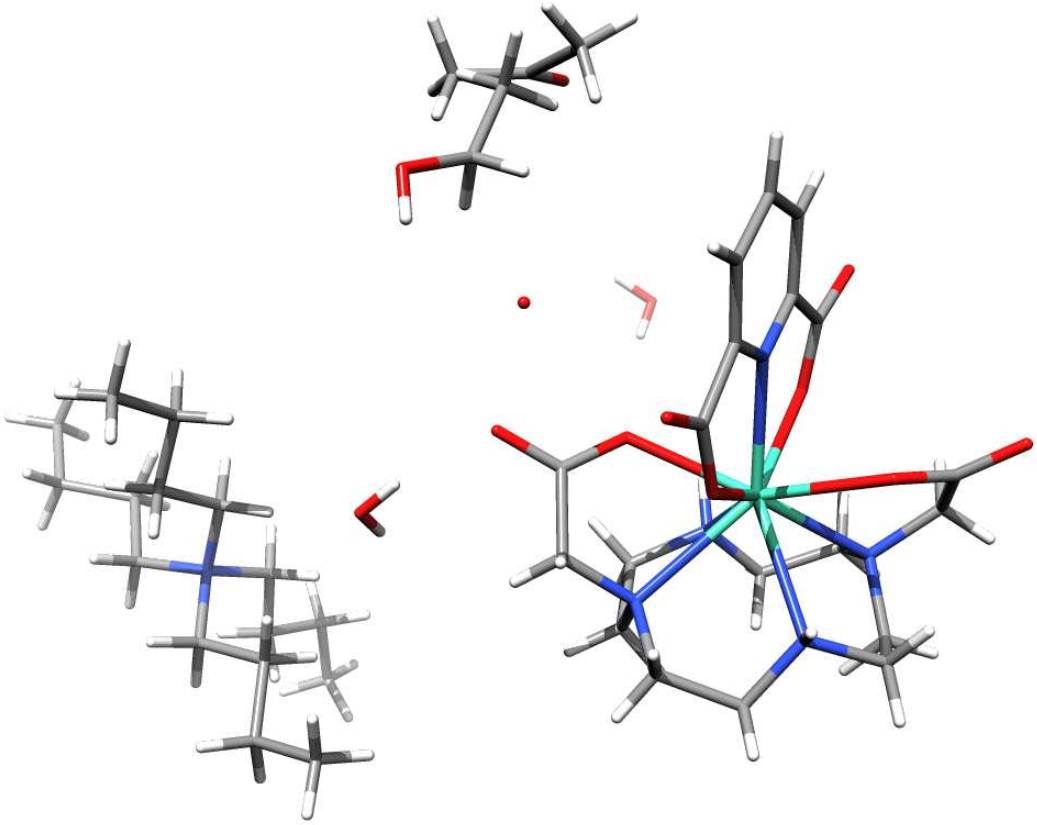

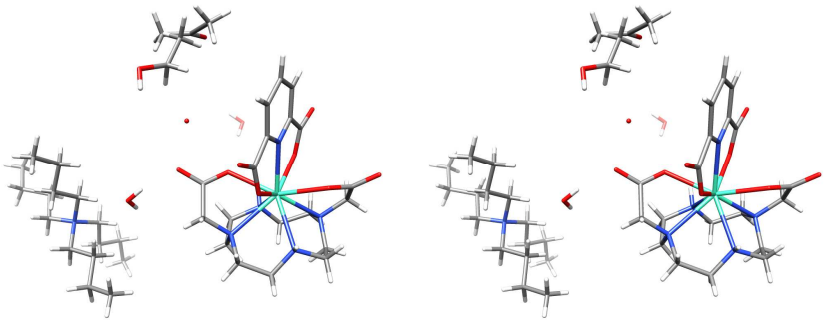

Table 2. Atomic coordinates (x 10^4) and equivalent isotropic displacement parameters ($Å^2$x 10^3) for MLC13 (CCDC 746175). U(eq) is defined as the trace of the orthogonalized U^{ij} tensor.

	x	y	z	U_{eq}	Occ
Gd(1)	7490(1)	4917(1)	5001(1)	13(1)	1
O(1)	6703(1)	5881(1)	4333(1)	19(1)	1
O(2)	6426(1)	7336(1)	3928(1)	30(1)	1
O(3)	8308(1)	5488(1)	5772(1)	19(1)	1
O(4)	8622(1)	6681(1)	6351(1)	39(1)	1
O(5)	8963(1)	5567(1)	4588(1)	18(1)	1
O(6)	9675(1)	6070(1)	3858(1)	18(1)	1
O(7)	6048(1)	5315(1)	5506(1)	18(1)	1
O(8)	5318(1)	5347(1)	6272(1)	24(1)	1
N(1)	7506(1)	6765(1)	5128(1)	17(1)	1
N(2)	7951(1)	3999(1)	4132(1)	17(1)	1
N(3)	8929(1)	3623(1)	5129(1)	18(1)	1
N(4)	7027(1)	3534(1)	5694(1)	19(1)	1
N(5)	6042(1)	3778(1)	4685(1)	18(1)	1
C(1)	7888(1)	7148(1)	5558(1)	18(1)	1
C(2)	7904(1)	8170(1)	5648(1)	28(1)	1
C(3)	7526(1)	8799(1)	5271(1)	38(1)	1
C(4)	7138(1)	8394(1)	4823(1)	33(1)	1
C(5)	7135(1)	7365(1)	4765(1)	21(1)	1
C(6)	8304(1)	6379(1)	5931(1)	20(1)	1
C(7)	6719(1)	6823(1)	4297(1)	20(1)	1
C(8)	8640(1)	3142(1)	4229(1)	21(1)	1
C(9)	9428(1)	3350(1)	4642(1)	21(1)	1
C(10)	8664(1)	2739(1)	5438(1)	23(1)	1
C(11)	7978(1)	3041(1)	5879(1)	23(1)	1
C(12)	6325(1)	2782(1)	5468(1)	23(1)	1
C(13)	5541(1)	3237(1)	5108(1)	21(1)	1
C(14)	6303(1)	3111(1)	4256(1)	21(1)	1
C(15)	6993(1)	3653(1)	3879(1)	20(1)	1
C(16)	8461(1)	4754(1)	3807(1)	20(1)	1
C(17)	9089(1)	5519(1)	4108(1)	16(1)	1
C(18)	6526(1)	4068(1)	6121(1)	21(1)	1
C(19)	5905(1)	4973(1)	5955(1)	17(1)	1
N(6)	1372(1)	2141(1)	7192(1)	20(1)	1
C(21)	1673(1)	3238(1)	7202(1)	22(1)	1
C(22)	1837(1)	3680(1)	7729(1)	29(1)	1
C(23)	2069(1)	4787(1)	7687(1)	29(1)	1
C(24)	2293(1)	5256(1)	8209(1)	40(1)	1
C(25)	2189(1)	1507(1)	7452(1)	25(1)	1
C(26)	3270(1)	1652(1)	7251(1)	30(1)	1
C(27)	3999(1)	924(1)	7509(1)	58(1)	1
C(28)	5108(1)	1149(2)	7379(1)	59(1)	1
C(29)	1242(1)	1851(1)	6635(1)	22(1)	1
C(30)	972(1)	767(1)	6537(1)	34(1)	1
C(31)	695(1)	590(1)	5986(1)	41(1)	1

C(32)	537(2)	-481(1)	5839(1)	61(1)	1
C(33)	383(1)	1976(1)	7488(1)	23(1)	1
C(34)	-548(1)	2528(1)	7282(1)	27(1)	1
C(35)	-1407(1)	2536(1)	7676(1)	28(1)	1
C(36)	-2365(1)	3059(1)	7484(1)	37(1)	1
O(21)	755(1)	5071(1)	3099(1)	27(1)	1
O(22)	4180(1)	3991(1)	6880(1)	37(1)	1
O(51)	3644(2)	9315(1)	5378(1)	71(1)	0.617(2)
C(51)	5077(2)	10064(4)	5838(2)	103(2)	0.617(2)
C(52)	3994(3)	9518(2)	5800(1)	70(1)	0.617(2)
C(53)	3504(2)	9414(2)	6205(1)	45(1)	0.617(2)
O(61)	5123(2)	8723(2)	7094(1)	45(1)	0.383(2)
C(62)	4987(4)	8771(4)	6547(2)	75(2)	0.383(2)
C(64)	4438(4)	9473(4)	6157(3)	72(2)	0.383(2)
O(71)	6124(2)	7291(2)	6479(1)	25(1)	0.383(2)

Table 3. Selected bond lengths [Å] and angles [°] for MLC13 (CCDC 746175).

Gd(1)-O(7)	2.3850(7)	O(3)-Gd(1)-N(5)	141.62(3)
Gd(1)-O(5)	2.3941(7)	N(1)-Gd(1)-N(5)	129.53(3)
Gd(1)-O(1)	2.4069(7)	O(7)-Gd(1)-N(3)	131.59(3)
Gd(1)-O(3)	2.4080(8)	O(5)-Gd(1)-N(3)	73.05(3)
Gd(1)-N(1)	2.5081(8)	O(1)-Gd(1)-N(3)	140.09(3)
Gd(1)-N(5)	2.5816(9)	O(3)-Gd(1)-N(3)	77.43(3)
Gd(1)-N(3)	2.5960(9)	N(1)-Gd(1)-N(3)	129.98(3)
Gd(1)-N(2)	2.6607(9)	N(5)-Gd(1)-N(3)	100.48(3)
Gd(1)-N(4)	2.6727(9)	O(7)-Gd(1)-N(2)	139.96(3)
		O(5)-Gd(1)-N(2)	66.05(3)
O(7)-Gd(1)-O(5)	145.15(3)	O(1)-Gd(1)-N(2)	74.30(3)
O(7)-Gd(1)-O(1)	86.56(3)	O(3)-Gd(1)-N(2)	139.52(2)
O(5)-Gd(1)-O(1)	79.85(3)	N(1)-Gd(1)-N(2)	124.89(3)
O(7)-Gd(1)-O(3)	79.50(3)	N(5)-Gd(1)-N(2)	67.89(3)
O(5)-Gd(1)-O(3)	84.32(3)	N(3)-Gd(1)-N(2)	68.18(3)
O(1)-Gd(1)-O(3)	128.75(3)	O(7)-Gd(1)-N(4)	65.99(3)
O(7)-Gd(1)-N(1)	73.11(3)	O(5)-Gd(1)-N(4)	138.60(3)
O(5)-Gd(1)-N(1)	72.07(3)	O(1)-Gd(1)-N(4)	140.23(3)
O(1)-Gd(1)-N(1)	64.25(3)	O(3)-Gd(1)-N(4)	75.90(3)
O(3)-Gd(1)-N(1)	64.50(3)	N(1)-Gd(1)-N(4)	127.00(3)
O(7)-Gd(1)-N(5)	73.71(3)	N(5)-Gd(1)-N(4)	68.35(3)
O(5)-Gd(1)-N(5)	132.39(3)	N(3)-Gd(1)-N(4)	67.37(3)
O(1)-Gd(1)-N(5)	76.86(3)	N(2)-Gd(1)-N(4)	108.11(3)

Table 4. Bond lengths [Å] and angles [°] for MLC13 (CCDC 746175).

Gd(1)-O(7)	2.3850(7)	C(12)-C(13)	1.5229(16)
Gd(1)-O(5)	2.3941(7)	C(12)-H(12A)	1.004(14)
Gd(1)-O(1)	2.4069(7)	C(12)-H(12B)	1.000(13)
Gd(1)-O(3)	2.4080(8)	C(13)-H(13A)	0.921(15)
Gd(1)-N(1)	2.5081(8)	C(13)-H(13B)	0.989(13)
Gd(1)-N(5)	2.5816(9)	C(14)-C(15)	1.5308(16)
Gd(1)-N(3)	2.5960(9)	C(14)-H(14A)	0.966(13)
Gd(1)-N(2)	2.6607(9)	C(14)-H(14B)	0.951(13)
Gd(1)-N(4)	2.6727(9)	C(15)-H(15A)	1.004(14)
O(1)-C(7)	1.2711(13)	C(15)-H(15B)	0.928(13)
O(2)-C(7)	1.2473(13)	C(16)-C(17)	1.5346(15)
O(3)-C(6)	1.2698(13)	C(16)-H(16A)	0.927(14)
O(4)-C(6)	1.2435(14)	C(16)-H(16B)	0.981(13)
O(5)-C(17)	1.2710(12)	C(18)-C(19)	1.5296(14)
O(6)-C(17)	1.2572(12)	C(18)-H(18A)	1.012(15)
O(7)-C(19)	1.2768(12)	C(18)-H(18B)	0.962(15)
O(8)-C(19)	1.2452(12)	N(6)-C(29)	1.5182(15)
N(1)-C(1)	1.3345(14)	N(6)-C(21)	1.5282(14)
N(1)-C(5)	1.3360(13)	N(6)-C(25)	1.5307(13)
N(2)-C(16)	1.4874(13)	N(6)-C(33)	1.5370(13)
N(2)-C(8)	1.4893(14)	C(21)-C(22)	1.5161(17)
N(2)-C(15)	1.4965(14)	C(22)-C(23)	1.5233(17)
N(3)-C(10)	1.4822(14)	C(23)-C(24)	1.532(2)
N(3)-C(9)	1.4851(14)	C(25)-C(26)	1.5362(16)
N(3)-H(3)	0.956(15)	C(26)-C(27)	1.5265(17)
N(4)-C(18)	1.4878(14)	C(27)-C(28)	1.535(2)
N(4)-C(12)	1.4905(15)	C(29)-C(30)	1.5234(16)
N(4)-C(11)	1.4974(14)	C(30)-C(31)	1.504(2)
N(5)-C(14)	1.4805(14)	C(31)-C(32)	1.506(2)
N(5)-C(13)	1.4842(14)	C(33)-C(34)	1.5312(16)
N(5)-H(5)	0.911(14)	C(34)-C(35)	1.5366(16)
C(1)-C(2)	1.3940(15)	C(35)-C(36)	1.5282(17)
C(1)-C(6)	1.5218(15)	O(21)-H(21D)	0.846(18)
C(2)-C(3)	1.3895(19)	O(21)-H(21C)	0.793(18)
C(2)-H(2)	0.973(15)	O(22)-H(22C)	0.825(17)
C(3)-C(4)	1.389(2)	O(22)-H(22D)	0.836(19)
C(3)-H(3A)	0.921(16)	O(51)-C(52)	1.227(4)
C(4)-C(5)	1.3934(16)	C(51)-C(52)	1.609(5)
C(4)-H(4)	0.937(16)	C(52)-C(53)	1.252(5)
C(5)-C(7)	1.5245(17)	O(61)-C(62)	1.445(7)
C(8)-C(9)	1.5191(17)	C(62)-C(64)	1.566(9)
C(8)-H(8A)	0.912(14)		
C(8)-H(8B)	0.989(14)	O(7)-Gd(1)-O(5)	145.15(3)
C(9)-H(9A)	0.976(13)	O(7)-Gd(1)-O(1)	86.56(3)
C(9)-H(9B)	0.965(13)	O(5)-Gd(1)-O(1)	79.85(3)
C(10)-C(11)	1.5270(16)	O(7)-Gd(1)-O(3)	79.50(3)
C(10)-H(10A)	0.971(14)	O(5)-Gd(1)-O(3)	84.32(3)
C(10)-H(10B)	0.979(13)	O(1)-Gd(1)-O(3)	128.75(3)
C(11)-H(11A)	0.955(13)	O(7)-Gd(1)-N(1)	73.11(3)
C(11)-H(11B)	0.948(12)	O(5)-Gd(1)-N(1)	72.07(3)

O(1)-Gd(1)-N(1)	64.25(3)	C(11)-N(4)-Gd(1)	109.53(6)
O(3)-Gd(1)-N(1)	64.50(3)	C(14)-N(5)-C(13)	112.16(8)
O(7)-Gd(1)-N(5)	73.71(3)	C(14)-N(5)-Gd(1)	115.28(6)
O(5)-Gd(1)-N(5)	132.39(3)	C(13)-N(5)-Gd(1)	112.63(7)
O(1)-Gd(1)-N(5)	76.86(3)	C(14)-N(5)-H(5)	112.6(9)
O(3)-Gd(1)-N(5)	141.62(3)	C(13)-N(5)-H(5)	107.9(9)
N(1)-Gd(1)-N(5)	129.53(3)	Gd(1)-N(5)-H(5)	94.9(9)
O(7)-Gd(1)-N(3)	131.59(3)	N(1)-C(1)-C(2)	121.92(10)
O(5)-Gd(1)-N(3)	73.05(3)	N(1)-C(1)-C(6)	114.23(9)
O(1)-Gd(1)-N(3)	140.09(3)	C(2)-C(1)-C(6)	123.85(10)
O(3)-Gd(1)-N(3)	77.43(3)	C(3)-C(2)-C(1)	118.41(12)
N(1)-Gd(1)-N(3)	129.98(3)	C(3)-C(2)-H(2)	120.6(9)
N(5)-Gd(1)-N(3)	100.48(3)	C(1)-C(2)-H(2)	121.0(9)
O(7)-Gd(1)-N(2)	139.96(3)	C(4)-C(3)-C(2)	119.31(11)
O(5)-Gd(1)-N(2)	66.05(3)	C(4)-C(3)-H(3A)	117.3(10)
O(1)-Gd(1)-N(2)	74.30(3)	C(2)-C(3)-H(3A)	123.3(10)
O(3)-Gd(1)-N(2)	139.52(2)	C(3)-C(4)-C(5)	118.78(12)
N(1)-Gd(1)-N(2)	124.89(3)	C(3)-C(4)-H(4)	122.2(10)
N(5)-Gd(1)-N(2)	67.89(3)	C(5)-C(4)-H(4)	119.0(10)
N(3)-Gd(1)-N(2)	68.18(3)	N(1)-C(5)-C(4)	121.54(11)
O(7)-Gd(1)-N(4)	65.99(3)	N(1)-C(5)-C(7)	114.25(9)
O(5)-Gd(1)-N(4)	138.60(3)	C(4)-C(5)-C(7)	124.21(11)
O(1)-Gd(1)-N(4)	140.23(3)	O(4)-C(6)-O(3)	126.56(10)
O(3)-Gd(1)-N(4)	75.90(3)	O(4)-C(6)-C(1)	117.65(9)
N(1)-Gd(1)-N(4)	127.00(3)	O(3)-C(6)-C(1)	115.77(9)
N(5)-Gd(1)-N(4)	68.35(3)	O(2)-C(7)-O(1)	127.06(11)
N(3)-Gd(1)-N(4)	67.37(3)	O(2)-C(7)-C(5)	117.88(10)
N(2)-Gd(1)-N(4)	108.11(3)	O(1)-C(7)-C(5)	115.06(9)
C(7)-O(1)-Gd(1)	125.67(7)	N(2)-C(8)-C(9)	113.16(8)
C(6)-O(3)-Gd(1)	124.95(7)	N(2)-C(8)-H(8A)	108.6(9)
C(17)-O(5)-Gd(1)	122.58(6)	C(9)-C(8)-H(8A)	110.5(8)
C(19)-O(7)-Gd(1)	123.58(6)	N(2)-C(8)-H(8B)	108.0(8)
C(1)-N(1)-C(5)	120.03(9)	C(9)-C(8)-H(8B)	109.7(8)
C(1)-N(1)-Gd(1)	119.87(7)	H(8A)-C(8)-H(8B)	106.7(11)
C(5)-N(1)-Gd(1)	120.10(7)	N(3)-C(9)-C(8)	110.49(8)
C(16)-N(2)-C(8)	110.35(8)	N(3)-C(9)-H(9A)	111.5(8)
C(16)-N(2)-C(15)	110.09(8)	C(8)-C(9)-H(9A)	109.5(8)
C(8)-N(2)-C(15)	110.33(8)	N(3)-C(9)-H(9B)	105.7(8)
C(16)-N(2)-Gd(1)	106.12(6)	C(8)-C(9)-H(9B)	110.8(8)
C(8)-N(2)-Gd(1)	110.83(6)	H(9A)-C(9)-H(9B)	108.7(10)
C(15)-N(2)-Gd(1)	109.02(6)	N(3)-C(10)-C(11)	110.04(9)
C(10)-N(3)-C(9)	112.22(8)	N(3)-C(10)-H(10A)	111.7(8)
C(10)-N(3)-Gd(1)	115.73(6)	C(11)-C(10)-H(10A)	106.3(8)
C(9)-N(3)-Gd(1)	112.49(6)	N(3)-C(10)-H(10B)	109.1(8)
C(10)-N(3)-H(3)	105.8(9)	C(11)-C(10)-H(10B)	112.2(7)
C(9)-N(3)-H(3)	108.7(9)	H(10A)-C(10)-H(10B)	107.5(11)
Gd(1)-N(3)-H(3)	100.9(9)	N(4)-C(11)-C(10)	111.80(9)
C(18)-N(4)-C(12)	110.36(8)	N(4)-C(11)-H(11A)	110.3(7)
C(18)-N(4)-C(11)	110.15(9)	C(10)-C(11)-H(11A)	109.3(8)
C(12)-N(4)-C(11)	110.16(8)	N(4)-C(11)-H(11B)	105.6(7)
C(18)-N(4)-Gd(1)	106.16(6)	C(10)-C(11)-H(11B)	108.4(7)
C(12)-N(4)-Gd(1)	110.41(6)	H(11A)-C(11)-H(11B)	111.3(11)

N(4)-C(12)-C(13)	112.92(9)
N(4)-C(12)-H(12A)	111.1(8)
C(13)-C(12)-H(12A)	109.8(8)
N(4)-C(12)-H(12B)	106.8(7)
C(13)-C(12)-H(12B)	111.4(8)
H(12A)-C(12)-H(12B)	104.5(11)
N(5)-C(13)-C(12)	110.78(9)
N(5)-C(13)-H(13A)	111.4(9)
C(12)-C(13)-H(13A)	108.3(9)
N(5)-C(13)-H(13B)	108.3(8)
C(12)-C(13)-H(13B)	113.2(8)
H(13A)-C(13)-H(13B)	104.8(11)
N(5)-C(14)-C(15)	110.07(8)
N(5)-C(14)-H(14A)	111.7(8)
C(15)-C(14)-H(14A)	107.6(8)
N(5)-C(14)-H(14B)	109.4(8)
C(15)-C(14)-H(14B)	111.6(8)
H(14A)-C(14)-H(14B)	106.4(11)
N(2)-C(15)-C(14)	111.56(9)
N(2)-C(15)-H(15A)	111.1(7)
C(14)-C(15)-H(15A)	109.0(8)
N(2)-C(15)-H(15B)	106.4(8)
C(14)-C(15)-H(15B)	109.0(8)
H(15A)-C(15)-H(15B)	109.8(11)
N(2)-C(16)-C(17)	114.22(9)
N(2)-C(16)-H(16A)	111.7(9)
C(17)-C(16)-H(16A)	103.9(9)
N(2)-C(16)-H(16B)	110.4(8)
C(17)-C(16)-H(16B)	107.5(8)
H(16A)-C(16)-H(16B)	108.8(12)
O(6)-C(17)-O(5)	124.68(10)
O(6)-C(17)-C(16)	117.42(9)
O(5)-C(17)-C(16)	117.88(9)
N(4)-C(18)-C(19)	114.25(9)
N(4)-C(18)-H(18A)	107.5(8)
C(19)-C(18)-H(18A)	107.9(8)
N(4)-C(18)-H(18B)	109.8(9)
C(19)-C(18)-H(18B)	108.2(9)
H(18A)-C(18)-H(18B)	109.1(12)
O(8)-C(19)-O(7)	124.37(9)
O(8)-C(19)-C(18)	117.81(9)
O(7)-C(19)-C(18)	117.77(8)
C(29)-N(6)-C(21)	106.92(8)
C(29)-N(6)-C(25)	110.97(9)
C(21)-N(6)-C(25)	110.39(8)
C(29)-N(6)-C(33)	110.84(8)
C(21)-N(6)-C(33)	110.70(8)
C(25)-N(6)-C(33)	107.05(8)
C(22)-C(21)-N(6)	115.44(9)
C(21)-C(22)-C(23)	110.31(10)
C(22)-C(23)-C(24)	112.18(11)
N(6)-C(25)-C(26)	115.42(9)
C(27)-C(26)-C(25)	110.50(10)
C(26)-C(27)-C(28)	111.96(11)
N(6)-C(29)-C(30)	115.63(9)
C(31)-C(30)-C(29)	111.61(11)
C(30)-C(31)-C(32)	115.48(13)
C(34)-C(33)-N(6)	115.70(8)
C(33)-C(34)-C(35)	111.05(9)
C(36)-C(35)-C(34)	113.25(10)
H(21D)-O(21)-H(21C)	99.8(17)
H(22C)-O(22)-H(22D)	107.2(17)
O(51)-C(52)-C(53)	123.0(4)
O(51)-C(52)-C(51)	119.1(4)
C(53)-C(52)-C(51)	117.6(3)
O(61)-C(62)-C(64)	136.7(4)

Table 5. Anisotropic displacement parameters ($Å^2 x\ 10^4$) for MLC13 (CCDC 746175). The anisotropic displacement factor exponent takes the form: $-2\pi^2[h^2 a^{*2} U^{11} + ... + 2\ h\ k\ a^*\ b^*\ U^{12}]$

	U^{11}	U^{22}	U^{33}	U^{23}	U^{13}	U^{12}
Gd(1)	125(1)	166(1)	111(1)	15(1)	12(1)	13(1)
O(1)	192(3)	237(3)	155(4)	33(3)	-3(3)	5(3)
O(2)	346(5)	310(4)	256(5)	142(3)	-71(4)	-35(3)
O(3)	194(3)	226(3)	136(4)	-7(3)	0(3)	23(3)
O(4)	708(7)	316(4)	158(4)	-72(3)	-88(4)	90(4)
O(5)	160(3)	269(4)	119(4)	-3(3)	20(3)	-11(3)
O(6)	189(3)	208(3)	156(4)	31(2)	36(3)	17(3)
O(7)	165(3)	243(3)	138(4)	29(3)	31(3)	25(3)
O(8)	278(4)	270(4)	164(4)	-11(3)	78(3)	15(3)
N(1)	130(3)	220(4)	154(4)	21(3)	34(3)	9(3)
N(2)	161(4)	212(4)	149(4)	4(3)	11(3)	-3(3)
N(3)	162(4)	220(4)	172(4)	9(3)	1(3)	23(3)
N(4)	181(4)	222(4)	174(4)	31(3)	11(3)	21(3)
N(5)	169(4)	203(4)	176(4)	13(3)	12(3)	7(3)
C(1)	147(4)	224(4)	184(5)	-8(3)	37(4)	14(3)
C(2)	276(6)	240(5)	313(7)	-54(4)	-25(5)	15(4)
C(3)	449(8)	216(5)	469(9)	-17(5)	-101(6)	22(5)
C(4)	342(6)	237(5)	408(8)	77(5)	-93(6)	10(5)
C(5)	161(4)	226(4)	233(6)	62(4)	11(4)	-4(3)
C(6)	213(5)	252(5)	135(5)	-20(3)	31(4)	28(4)
C(7)	163(4)	264(5)	187(5)	74(4)	4(4)	-16(4)
C(8)	197(5)	225(4)	209(5)	-41(4)	20(4)	37(4)
C(9)	172(5)	237(5)	211(6)	-14(4)	31(4)	49(4)
C(10)	223(5)	222(5)	248(6)	49(4)	14(4)	63(4)
C(11)	218(5)	250(5)	210(6)	76(4)	-4(4)	46(4)
C(12)	236(5)	222(5)	239(6)	59(4)	14(4)	-15(4)
C(13)	161(4)	233(5)	227(6)	23(4)	26(4)	-24(4)
C(14)	197(5)	222(4)	207(5)	-34(4)	6(4)	-32(4)
C(15)	185(5)	253(5)	168(5)	-33(4)	-5(4)	-10(4)
C(16)	194(5)	258(5)	135(5)	-5(3)	29(4)	-21(4)
C(17)	140(4)	199(4)	144(4)	4(3)	14(3)	40(3)
C(18)	215(5)	284(5)	141(5)	58(4)	42(4)	26(4)
C(19)	149(4)	206(4)	142(4)	1(3)	5(3)	-31(3)
N(6)	158(4)	254(4)	193(5)	98(3)	-12(3)	-19(3)
C(21)	191(5)	253(5)	203(5)	92(4)	-24(4)	-35(4)
C(22)	314(6)	342(6)	213(6)	61(5)	-39(5)	-66(5)
C(23)	298(6)	324(6)	262(6)	31(4)	2(5)	-61(5)
C(24)	447(8)	429(7)	333(8)	-29(6)	-16(6)	-93(6)
C(25)	174(5)	312(5)	269(6)	165(4)	-27(4)	-10(4)
C(26)	176(5)	405(7)	325(7)	198(5)	-7(5)	-2(5)
C(27)	193(6)	742(11)	809(14)	569(10)	-6(7)	53(6)
C(28)	191(6)	761(12)	825(15)	432(10)	6(7)	76(7)
C(29)	209(5)	241(5)	197(5)	69(4)	-7(4)	2(4)
C(30)	397(7)	290(6)	344(8)	50(5)	-16(6)	-92(5)
C(31)	560(9)	289(6)	379(9)	-10(5)	-107(7)	51(6)

C(32)	705(12)	419(9)	708(14)	-159(8)	-102(10)	-110(8)
C(33)	184(5)	301(5)	195(5)	99(4)	2(4)	-38(4)
C(34)	194(5)	391(6)	219(6)	115(4)	19(4)	18(4)
C(35)	262(6)	324(6)	248(6)	67(4)	57(5)	7(4)
C(36)	250(6)	419(7)	434(9)	83(6)	98(6)	53(5)
O(21)	377(5)	260(4)	174(4)	-7(3)	66(3)	70(3)
O(22)	446(6)	442(5)	223(5)	46(4)	66(4)	-175(4)
O(51)	1028(17)	250(8)	839(18)	80(9)	-287(14)	41(9)
C(51)	427(17)	2080(50)	580(20)	650(30)	-221(15)	-510(20)
C(52)	1170(30)	184(9)	740(20)	-39(11)	-640(20)	169(13)
C(53)	216(10)	577(15)	556(19)	-171(12)	-51(10)	59(9)
O(61)	565(17)	560(16)	236(14)	-88(11)	-133(12)	369(13)
C(62)	580(30)	600(30)	1060(50)	-340(30)	240(30)	-270(20)
C(64)	570(30)	650(30)	950(50)	-480(30)	-140(30)	40(20)
O(71)	253(11)	270(10)	238(12)	-85(8)	60(8)	-11(8)

Table 6. Hydrogen coordinates (x 10^4) and isotropic displacement parameters ($Å^2$x 10^3) for MLC13 (CCDC 746175) (refined hydrogens only).

	x	y	z	U_{iso}
H(3)	9397(11)	3996(11)	5332(6)	31(4)
H(5)	5627(10)	4286(11)	4588(5)	26(4)
H(2)	8179(10)	8438(11)	5965(6)	32(4)
H(3A)	7548(11)	9482(12)	5295(6)	35(4)
H(4)	6863(11)	8790(12)	4562(6)	41(4)
H(8A)	8947(10)	2974(10)	3930(6)	25(3)
H(8B)	8220(10)	2567(10)	4330(5)	24(3)
H(9A)	9866(9)	2771(9)	4683(5)	19(3)
H(9B)	9841(9)	3915(10)	4551(5)	17(3)
H(10A)	9260(10)	2436(11)	5592(5)	27(4)
H(10B)	8347(9)	2240(10)	5216(5)	19(3)
H(11A)	7818(9)	2467(10)	6078(5)	19(3)
H(11B)	8321(8)	3526(9)	6078(5)	9(3)
H(12A)	5975(10)	2392(10)	5742(5)	25(3)
H(12B)	6756(9)	2282(10)	5288(5)	22(3)
H(13A)	5131(10)	2734(12)	4987(5)	31(4)
H(13B)	5073(10)	3701(10)	5282(5)	23(3)
H(14A)	5706(10)	2898(10)	4069(5)	23(3)
H(14B)	6614(9)	2525(10)	4386(5)	21(3)
H(15A)	7143(10)	3199(10)	3585(5)	25(3)
H(15B)	6665(9)	4219(9)	3761(5)	16(3)
H(16A)	7997(11)	5136(10)	3627(6)	27(4)
H(16B)	8917(10)	4429(10)	3564(5)	21(3)
H(18A)	7078(11)	4306(11)	6362(6)	35(4)
H(18B)	6086(11)	3621(11)	6301(6)	34(4)
H(21D)	410(13)	5370(14)	3322(7)	45(5)
H(21C)	956(12)	4616(14)	3264(7)	42(5)
H(22C)	4487(12)	4446(13)	6737(6)	36(4)
H(22D)	3998(13)	3590(15)	6653(7)	54(5)

Table 7. Hydrogen bonds for MLC13 (CCDC 746175) [Å and °].

D-H...A	d(D-H)	d(H...A)	d(D...A)	<(DHA)
N(3)-H(3)...O(5)#1	0.956(15)	2.249(14)	3.0722(12)	143.7(12)
N(3)-H(3)...O(6)#1	0.956(15)	2.442(15)	3.2454(13)	141.5(12)
N(5)-H(5)...O(7)#2	0.911(14)	2.286(14)	3.0535(12)	141.7(11)
N(5)-H(5)...O(8)#2	0.911(14)	2.614(14)	3.2907(13)	131.6(11)
O(21)-H(21D)...O(6)#3	0.846(18)	1.952(19)	2.7966(11)	177.2(17)
O(21)-H(21C)...O(4)#2	0.793(18)	2.089(19)	2.8783(13)	173.6(17)
O(22)-H(22C)...O(8)	0.825(17)	2.042(17)	2.8533(12)	167.8(16)
O(22)-H(22D)...O(2)#2	0.836(19)	2.04(2)	2.8755(15)	177.1(19)
O(61)-H(61)...O(71)	0.84	2.36	2.841(3)	116.7

Symmetry transformations used to generate equivalent atoms:
#1 -x+2,-y+1,-z+1
#2 -x+1,-y+1,-z+1
#3 x-1,y,z

CALIFORNIA INSTITUTE OF TECHNOLOGY

BECKMAN INSTITUTE

X-RAY CRYSTALLOGRAPHY LABORATORY

Date 4 December 2004

Crystal Structure Analysis of:

MLC03

(shown below)

For Investigator: Morgan Cable ext. (818) 354-4348

Advisor: Adrian Ponce/ H. B. Gray ext. (818) 354-8196

Account Number: API.00002-1-NASA.000174

By Michael W. Day 116 Beckman ext. 2734

e-mail: mikeday@caltech.edu

Contents

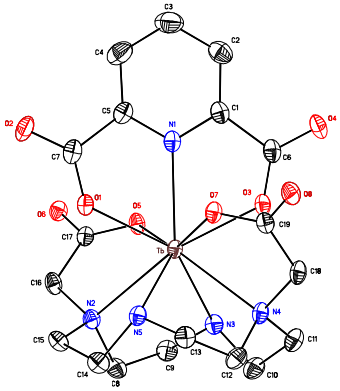

MLC03

Note: The crystallographic data have been deposited in the Cambridge Database (CCDC) and has been placed on hold pending further instructions from me. The deposition number is 629534. Ideally the CCDC would like the publication to contain a footnote of the type: "Crystallographic data have been deposited at the CCDC, 12 Union Road, Cambridge CB2 1EZ, UK and copies can be obtained on request, free of charge, by quoting the publication citation and the deposition number 629354."

Table 1. Crystal data and structure refinement for MLC03 (CCDC 629534).

Empirical formula	$[C_{19}H_{25}N_5O_8Tb]^-[C_{16}H_{36}N]^+ \bullet 0.47(C_3H_8O)$
$0.53(C_3H_6O)\ 3(H_2O)$	
Formula weight	964.94
Crystallization Solvent	Acetone/isopropanol/water
Crystal Habit	Square
Crystal size	0.35 x 0.31 x 0.11 mm^3
Crystal color	Colorless

Data Collection

Type of diffractometer	Bruker SMART 1000
Wavelength	0.71073 Å MoKα
Data Collection Temperature	100(2) K
θ range for 24638 reflections used in lattice determination	2.18 to 37.67°
Unit cell dimensions	a = 13.1047(5) Å b = 13.3397(5) Å β= 90.0130(10)° c = 26.0901(9) Å
Volume	4560.9(3) $Å^3$
Z	4
Crystal system	Monoclinic
Space group	$P2_1/c$
Density (calculated)	1.405 Mg/m^3
F(000)	2016
θ range for data collection	1.56 to 37.67°
Completeness to θ = 37.67°	83.6 %
Index ranges	$-22 \le h \le 22, -17 \le k \le 20, -40 \le l \le 44$
Data collection scan type	ω scans at 5 ϕ settings
Reflections collected	78733
Independent reflections	20316 [R_{int}= 0.0879]
Absorption coefficient	1.613 mm^{-1}
Absorption correction	None
Max. and min. transmission	0.8425 and 0.6022

Table 1 (cont.)

Structure solution and Refinement

Structure solution program	Bruker XS v6.12
Primary solution method	Direct methods
Secondary solution method	Difference Fourier map
Hydrogen placement	Geometric positions
Structure refinement program	Bruker XL v6.12
Refinement method	Full matrix least-squares on F^2
Data / restraints / parameters	20316 / 0 / 577
Treatment of hydrogen atoms	Riding
Goodness-of-fit on F^2	1.077
Final R indices [$I>2\sigma(I)$, 11252 reflections]	R1 = 0.0384, *w*R2 = 0.0639
R indices (all data)	R1 = 0.0900, *w*R2 = 0.0717
Type of weighting scheme used	Sigma
Weighting scheme used	$w=1/\sigma^2(Fo^2)$
Max shift/error	0.005
Average shift/error	0.000
Largest diff. peak and hole	3.035 and -2.004 e.Å^{-3}

Special Refinement Details

The crystals contain a disordered solvent. The site contains acetone and water or isopropanol and water, modeled as a combination of both with a total occupancy = 1.0.

Refinement of F^2 against ALL reflections. The weighted R-factor (*w*R) and goodness of fit (S) are based on F^2, conventional R-factors (R) are based on F, with F set to zero for negative F^2. The threshold expression of $F^2 > 2\sigma(F^2)$ is used only for calculating R-factors(gt) etc. and is not relevant to the choice of reflections for refinement. R-factors based on F^2 are statistically about twice as large as those based on F, and R-factors based on ALL data will be even larger.

All esds (except the esd in the dihedral angle between two l.s. planes) are estimated using the full covariance matrix. The cell esds are taken into account individually in the estimation of esds in distances, angles and torsion angles; correlations between esds in cell parameters are only used when they are defined by crystal symmetry. An approximate (isotropic) treatment of cell esds is used for estimating esds involving l.s. planes.

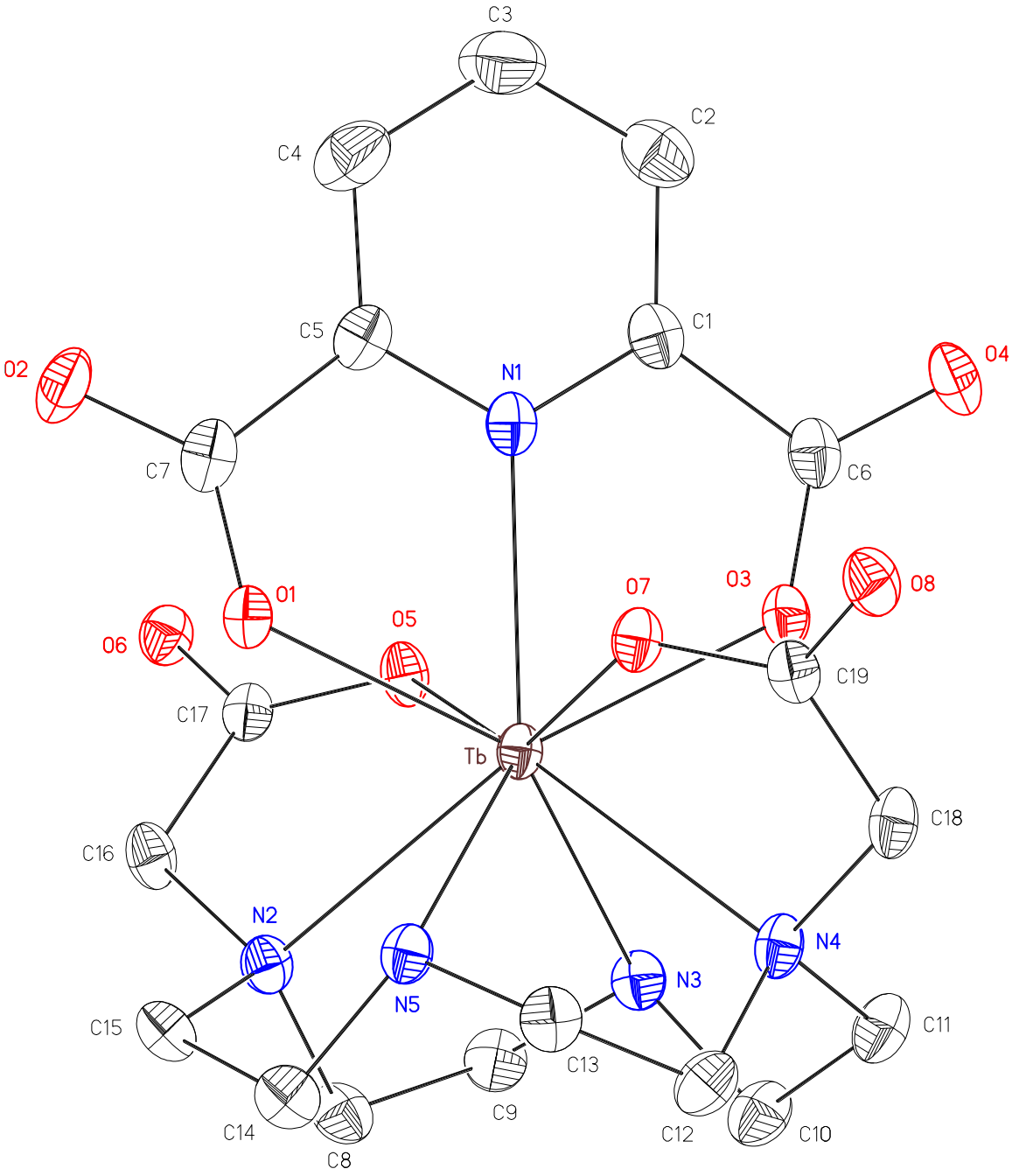
C3
C2
C4
C5
C1
O2
N1
O4
C7
C6
O1
O7
O3
O8
O6
O5
C19
C17
Tb
C18
C16
N2
N4
N5
N3
C15
C11
C13
C9
C14
C12
C10
C8

D55

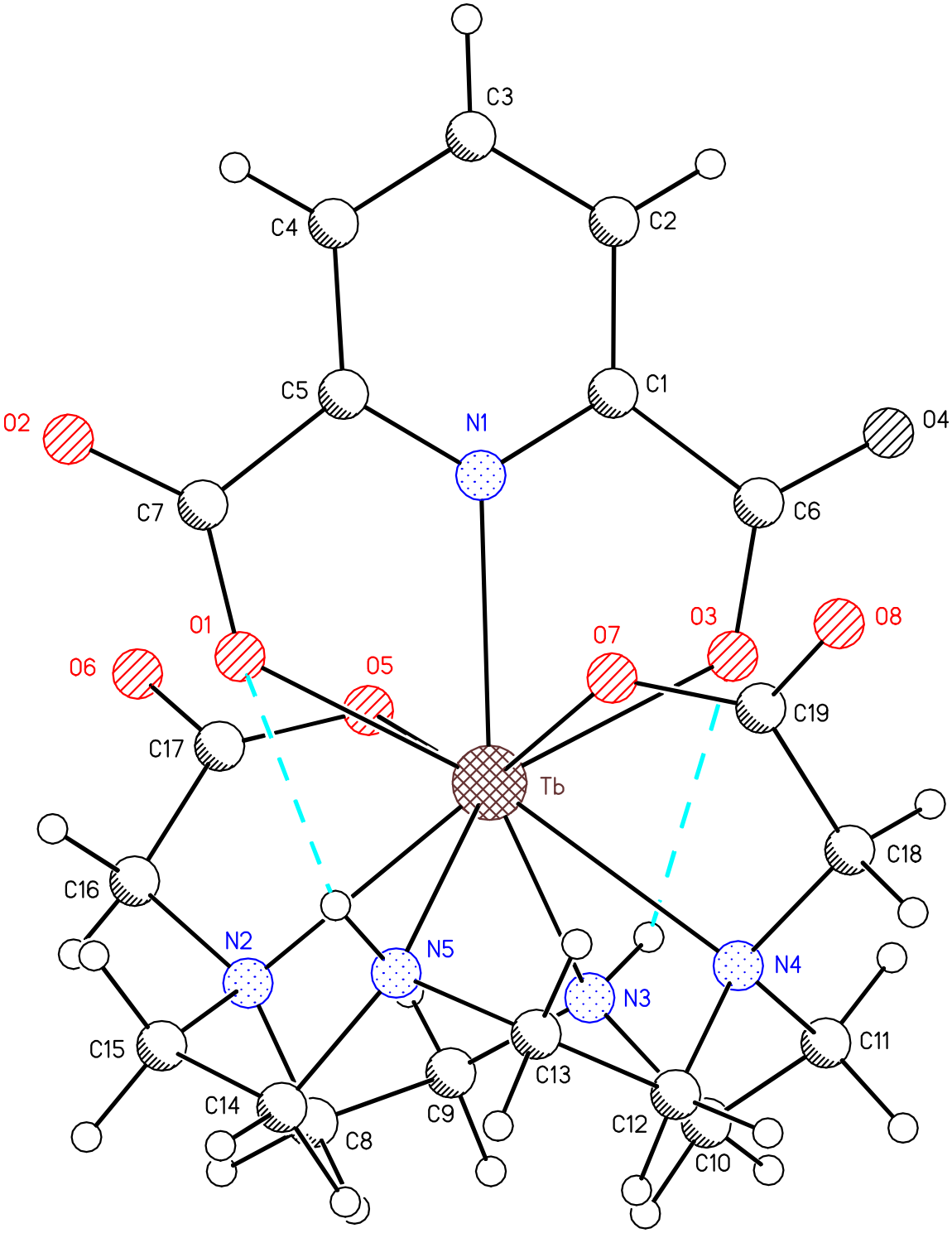
C3
C4
C2
C5
C1
O2
N1
O4
C7
C6
O1
O3
O8
O6
O5
O7
C19
C17
Tb
C18
C16
N2
N5
N3
N4
C15
C11
C13
C14
C9
C12
C8
C10

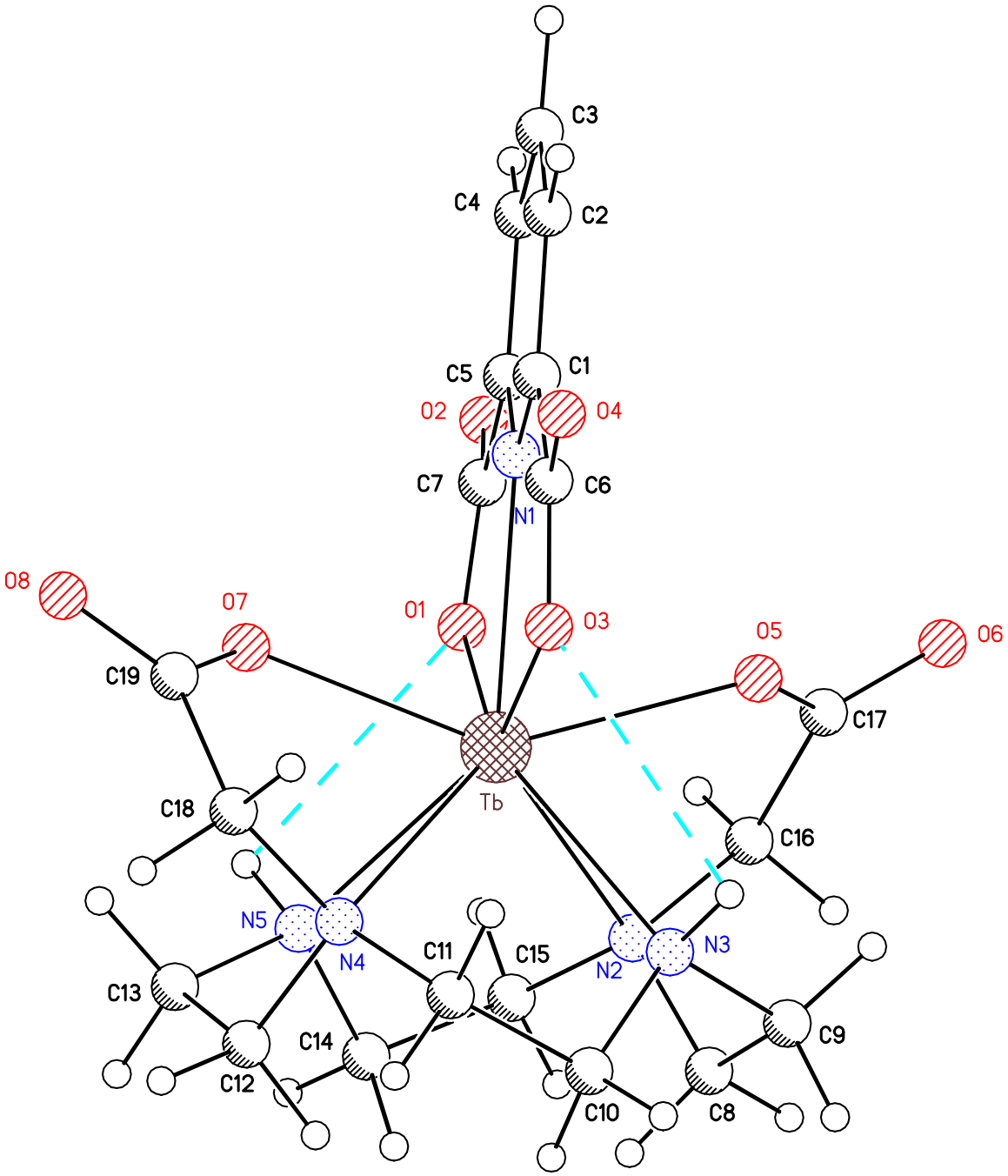
C3
C4
C2
C5
C1
O2
O4
C7
C6
N1
O8
O7
O1
O3
O5
O6
C19
C17
Tb
C18
C16
N5
N4
C11
C15
N2
N3
C13
C9
C14
C12
C10
C8

Table 2. Atomic coordinates (x 10^4) and equivalent isotropic displacement parameters ($Å^2$x 10^3) for MLC03 (CCDC 629534). U(eq) is defined as the trace of the orthogonalized U^{ij} tensor.

	x	y	z	U_{eq}	Occ
Tb	2488(1)	77(1)	4995(1)	14(1)	1
O(1)	1702(1)	-870(1)	5664(1)	19(1)	1
O(2)	1420(1)	-2322(1)	6074(1)	29(1)	1
O(3)	3304(1)	-500(1)	4227(1)	19(1)	1
O(4)	3642(2)	-1709(1)	3658(1)	36(1)	1
O(5)	3947(1)	-573(1)	5407(1)	18(1)	1
O(6)	4672(1)	-1065(1)	6137(1)	19(1)	1
O(7)	1058(1)	-336(1)	4497(1)	18(1)	1
O(8)	303(1)	-391(1)	3733(1)	24(1)	1
N(1)	2504(1)	-1777(1)	4876(1)	16(1)	1
N(2)	2951(1)	1011(1)	5858(1)	17(1)	1
N(3)	3914(1)	1368(1)	4861(1)	18(1)	1
N(4)	2027(1)	1446(2)	4294(1)	18(1)	1
N(5)	1048(1)	1222(1)	5302(1)	18(1)	1
C(1)	2893(2)	-2167(2)	4449(1)	19(1)	1
C(2)	2910(2)	-3195(2)	4365(1)	28(1)	1
C(3)	2534(2)	-3821(2)	4746(1)	38(1)	1
C(4)	2134(2)	-3404(2)	5191(1)	33(1)	1
C(5)	2135(2)	-2372(2)	5242(1)	20(1)	1
C(6)	3313(2)	-1395(2)	4073(1)	21(1)	1
C(7)	1713(2)	-1817(2)	5707(1)	21(1)	1
C(8)	3637(2)	1866(2)	5759(1)	21(1)	1
C(9)	4425(2)	1648(2)	5351(1)	22(1)	1
C(10)	3663(2)	2248(2)	4549(1)	24(1)	1
C(11)	2970(2)	1931(2)	4108(1)	23(1)	1
C(12)	1324(2)	2205(2)	4513(1)	24(1)	1
C(13)	542(2)	1760(2)	4874(1)	21(1)	1
C(14)	1301(2)	1900(2)	5731(1)	22(1)	1
C(15)	1991(2)	1367(2)	6106(1)	20(1)	1
C(16)	3455(2)	255(2)	6184(1)	20(1)	1
C(17)	4081(2)	-512(2)	5889(1)	16(1)	1
C(18)	1525(2)	894(2)	3870(1)	22(1)	1
C(19)	904(2)	-2(2)	4045(1)	18(1)	1
N(6)	6377(1)	2839(1)	2800(1)	20(1)	1
C(20)	7192(2)	3471(2)	2542(1)	24(1)	1
C(21)	8271(2)	3325(2)	2746(1)	29(1)	1
C(22)	8999(2)	4044(3)	2481(1)	55(1)	1
C(23)	10110(2)	3815(3)	2629(1)	57(1)	1
C(24)	6673(2)	1733(2)	2794(1)	22(1)	1
C(25)	6831(2)	1282(2)	2265(1)	30(1)	1
C(26)	7071(2)	176(2)	2308(1)	31(1)	1
C(27)	7281(2)	-300(2)	1788(1)	39(1)	1
C(28)	5383(2)	3004(2)	2504(1)	24(1)	1
C(29)	4458(2)	2451(2)	2707(1)	27(1)	1
C(30)	3606(2)	2431(2)	2311(1)	28(1)	1
C(31)	2648(2)	1905(2)	2501(1)	37(1)	1

C(32)	6243(2)	3133(2)	3359(1)	21(1)	1
C(33)	5990(2)	4229(2)	3451(1)	32(1)	1
C(34)	5677(2)	4402(2)	3999(1)	37(1)	1
C(35)	5560(3)	5486(3)	4151(1)	58(1)	1
O(11)	5754(1)	5055(1)	1892(1)	27(1)	1
O(12)	9175(2)	975(2)	3123(1)	35(1)	1
O(51A)	1484(7)	4416(5)	6143(5)	65(3)	0.476(4)
C(52A)	544(6)	4415(7)	6202(4)	64(3)	0.476(4)
C(53A)	2(6)	3743(6)	6551(3)	58(2)	0.476(4)
C(54A)	-223(9)	4727(10)	5781(5)	92(4)	0.476(4)
O(50A)	8868(4)	2675(4)	1469(2)	62(2)	0.476(4)
O(51B)	1315(5)	4316(3)	5364(2)	75(2)	0.524(4)
C(52B)	899(7)	4533(5)	5758(3)	53(2)	0.524(4)
C(53B)	-22(8)	5292(7)	5909(5)	68(3)	0.524(4)
C(54B)	1385(15)	4504(15)	6255(7)	149(10)	0.524(4)
O(50B)	-123(5)	3726(6)	7096(2)	96(2)	0.524(4)

Table 3. Bond lengths [Å] and angles [°] for MLC03 (CCDC 629534).

Tb-O(7)	2.3467(14)	C(26)-C(27)	1.522(4)
Tb-O(5)	2.3573(15)	C(28)-C(29)	1.515(3)
Tb-O(1)	2.3879(15)	C(29)-C(30)	1.522(3)
Tb-O(3)	2.3987(15)	C(30)-C(31)	1.522(4)
Tb-N(1)	2.4918(19)	C(32)-C(33)	1.517(3)
Tb-N(5)	2.5564(18)	C(33)-C(34)	1.505(4)
Tb-N(3)	2.5657(18)	C(34)-C(35)	1.507(4)
Tb-N(2)	2.6437(17)	O(51A)-C(52A)	1.241(12)
Tb-N(4)	2.6550(18)	C(52A)-C(53A)	1.463(12)
O(1)-C(7)	1.267(3)	C(52A)-C(54A)	1.545(15)
O(2)-C(7)	1.234(3)	O(51B)-C(52B)	1.199(8)
O(3)-C(6)	1.259(3)	C(52B)-C(54B)	1.445(19)
O(4)-C(6)	1.241(3)	C(52B)-C(53B)	1.625(14)
O(5)-C(17)	1.272(2)		
O(6)-C(17)	1.250(2)	O(7)-Tb-O(5)	144.47(6)
O(7)-C(19)	1.276(2)	O(7)-Tb-O(1)	86.35(5)
O(8)-C(19)	1.245(2)	O(5)-Tb-O(1)	79.79(5)
N(1)-C(5)	1.332(3)	O(7)-Tb-O(3)	79.49(5)
N(1)-C(1)	1.332(3)	O(5)-Tb-O(3)	84.35(5)
N(2)-C(8)	1.475(3)	O(1)-Tb-O(3)	129.31(6)
N(2)-C(16)	1.475(3)	O(7)-Tb-N(1)	72.84(5)
N(2)-C(15)	1.491(3)	O(5)-Tb-N(1)	71.66(5)
N(3)-C(10)	1.466(3)	O(1)-Tb-N(1)	64.54(5)
N(3)-C(9)	1.489(3)	O(3)-Tb-N(1)	64.78(6)
N(4)-C(18)	1.483(3)	O(7)-Tb-N(5)	74.00(5)
N(4)-C(12)	1.482(3)	O(5)-Tb-N(5)	132.49(5)
N(4)-C(11)	1.478(3)	O(1)-Tb-N(5)	76.65(6)
N(5)-C(13)	1.482(3)	O(3)-Tb-N(5)	141.46(5)
N(5)-C(14)	1.475(3)	N(1)-Tb-N(5)	129.68(6)
C(1)-C(2)	1.389(3)	O(7)-Tb-N(3)	131.59(5)
C(1)-C(6)	1.525(3)	O(5)-Tb-N(3)	73.61(6)
C(2)-C(3)	1.390(4)	O(1)-Tb-N(3)	140.27(5)
C(3)-C(4)	1.389(4)	O(3)-Tb-N(3)	77.08(6)
C(4)-C(5)	1.384(3)	N(1)-Tb-N(3)	129.99(6)
C(5)-C(7)	1.525(3)	N(5)-Tb-N(3)	100.32(6)
C(8)-C(9)	1.513(3)	O(7)-Tb-N(2)	139.96(5)
C(10)-C(11)	1.526(3)	O(5)-Tb-N(2)	66.38(5)
C(12)-C(13)	1.515(3)	O(1)-Tb-N(2)	74.10(5)
C(14)-C(15)	1.510(3)	O(3)-Tb-N(2)	139.53(5)
C(16)-C(17)	1.522(3)	N(1)-Tb-N(2)	124.89(5)
C(18)-C(19)	1.517(3)	N(5)-Tb-N(2)	67.71(5)
N(6)-C(20)	1.518(3)	N(3)-Tb-N(2)	68.45(6)
N(6)-C(28)	1.528(3)	O(7)-Tb-N(4)	66.30(5)
N(6)-C(32)	1.522(3)	O(5)-Tb-N(4)	138.69(5)
N(6)-C(24)	1.526(3)	O(1)-Tb-N(4)	140.29(5)
C(20)-C(21)	1.524(3)	O(3)-Tb-N(4)	75.30(6)
C(21)-C(22)	1.518(4)	N(1)-Tb-N(4)	126.78(5)
C(22)-C(23)	1.538(4)	N(5)-Tb-N(4)	68.67(6)
C(24)-C(25)	1.519(3)	N(3)-Tb-N(4)	67.04(5)
C(25)-C(26)	1.513(4)	N(2)-Tb-N(4)	108.32(6)

C(7)-O(1)-Tb	125.87(15)	N(4)-C(18)-C(19)	113.87(17)
C(6)-O(3)-Tb	125.03(14)	O(8)-C(19)-O(7)	123.9(2)
C(17)-O(5)-Tb	122.63(14)	O(8)-C(19)-C(18)	118.11(19)
C(19)-O(7)-Tb	123.76(14)	O(7)-C(19)-C(18)	117.97(18)
C(5)-N(1)-C(1)	120.4(2)	C(20)-N(6)-C(28)	107.20(16)
C(5)-N(1)-Tb	119.92(14)	C(20)-N(6)-C(32)	111.30(18)
C(1)-N(1)-Tb	119.72(15)	C(28)-N(6)-C(32)	110.36(17)
C(8)-N(2)-C(16)	110.85(17)	C(20)-N(6)-C(24)	110.72(17)
C(8)-N(2)-C(15)	110.12(18)	C(28)-N(6)-C(24)	110.53(18)
C(16)-N(2)-C(15)	110.26(17)	C(32)-N(6)-C(24)	106.77(16)
C(8)-N(2)-Tb	110.80(13)	N(6)-C(20)-C(21)	115.28(18)
C(16)-N(2)-Tb	105.73(13)	C(20)-C(21)-C(22)	110.1(2)
C(15)-N(2)-Tb	108.99(12)	C(23)-C(22)-C(21)	110.8(2)
C(10)-N(3)-C(9)	112.04(18)	C(25)-C(24)-N(6)	115.25(18)
C(10)-N(3)-Tb	116.74(13)	C(26)-C(25)-C(24)	110.4(2)
C(9)-N(3)-Tb	112.29(13)	C(25)-C(26)-C(27)	112.2(2)
C(18)-N(4)-C(12)	110.54(17)	N(6)-C(28)-C(29)	115.84(18)
C(18)-N(4)-C(11)	110.08(17)	C(30)-C(29)-C(28)	110.94(19)
C(12)-N(4)-C(11)	110.32(19)	C(29)-C(30)-C(31)	113.0(2)
C(18)-N(4)-Tb	105.86(13)	C(33)-C(32)-N(6)	115.22(18)
C(12)-N(4)-Tb	110.24(12)	C(34)-C(33)-C(32)	111.0(2)
C(11)-N(4)-Tb	109.71(12)	C(33)-C(34)-C(35)	115.1(3)
C(13)-N(5)-C(14)	111.97(18)	O(51A)-C(52A)-C(53A)	124.1(10)
C(13)-N(5)-Tb	112.57(13)	O(51A)-C(52A)-C(54A)	123.9(11)
C(14)-N(5)-Tb	115.99(13)	C(53A)-C(52A)-C(54A)	106.9(8)
N(1)-C(1)-C(2)	121.7(2)	O(51B)-C(52B)-C(54B)	124.3(12)
N(1)-C(1)-C(6)	114.3(2)	O(51B)-C(52B)-C(53B)	134.0(8)
C(2)-C(1)-C(6)	124.0(2)	C(54B)-C(52B)-C(53B)	97.3(10)
C(1)-C(2)-C(3)	118.2(2)		
C(2)-C(3)-C(4)	119.5(2)		
C(5)-C(4)-C(3)	118.5(2)		
N(1)-C(5)-C(4)	121.7(2)		
N(1)-C(5)-C(7)	114.3(2)		
C(4)-C(5)-C(7)	124.0(2)		
O(4)-C(6)-O(3)	127.0(2)		
O(4)-C(6)-C(1)	117.3(2)		
O(3)-C(6)-C(1)	115.66(19)		
O(2)-C(7)-O(1)	127.5(2)		
O(2)-C(7)-C(5)	117.8(2)		
O(1)-C(7)-C(5)	114.7(2)		
N(2)-C(8)-C(9)	113.07(19)		
N(3)-C(9)-C(8)	110.25(17)		
N(3)-C(10)-C(11)	109.31(19)		
N(4)-C(11)-C(10)	111.82(18)		
N(4)-C(12)-C(13)	113.11(19)		
N(5)-C(13)-C(12)	110.81(17)		
N(5)-C(14)-C(15)	109.68(18)		
N(2)-C(15)-C(14)	112.02(18)		
N(2)-C(16)-C(17)	114.21(17)		
O(6)-C(17)-O(5)	124.0(2)		
O(6)-C(17)-C(16)	118.02(18)		
O(5)-C(17)-C(16)	117.91(18)		

Table 4. Anisotropic displacement parameters ($Å^2 x\ 10^4$) for MLC03 (CCDC 629534). The anisotropic displacement factor exponent takes the form: $-2\pi^2[h^2 a^{*2} U^{11} + ... + 2\ h\ k\ a^*\ b^*\ U^{12}]$

	U^{11}	U^{22}	U^{33}	U^{23}	U^{13}	U^{12}
Tb	118(1)	186(1)	123(1)	15(1)	-14(1)	-8(1)
O(1)	184(8)	233(9)	143(7)	17(6)	1(6)	7(7)
O(2)	338(10)	303(10)	234(9)	121(7)	73(7)	31(8)
O(3)	182(8)	248(9)	127(7)	6(6)	-12(6)	-19(6)
O(4)	580(13)	351(11)	155(8)	-71(8)	75(8)	-83(9)
O(5)	157(7)	258(9)	123(7)	-2(6)	-28(5)	12(6)
O(6)	174(8)	216(8)	168(7)	18(6)	-30(6)	-12(6)
O(7)	142(7)	244(8)	152(7)	29(6)	-22(5)	-2(6)
O(8)	246(9)	292(9)	166(7)	-15(7)	-65(6)	4(7)
N(1)	112(8)	239(9)	143(8)	14(6)	-35(7)	4(7)
N(2)	162(9)	207(10)	150(8)	0(7)	-30(7)	10(7)
N(3)	137(9)	215(10)	179(9)	2(8)	9(7)	-12(7)
N(4)	148(9)	247(10)	150(8)	37(7)	-10(7)	-20(7)
N(5)	141(9)	213(10)	170(9)	22(8)	6(7)	-13(7)
C(1)	136(10)	270(12)	171(10)	-17(9)	-36(8)	-6(9)
C(2)	243(12)	300(14)	303(13)	-69(11)	25(10)	2(10)
C(3)	416(17)	250(15)	478(17)	-55(13)	105(13)	-9(12)
C(4)	309(14)	267(14)	414(16)	83(12)	92(12)	10(11)
C(5)	151(10)	241(12)	216(11)	49(9)	-11(8)	12(9)
C(6)	152(10)	308(13)	155(10)	-2(10)	-30(8)	-32(9)
C(7)	113(10)	306(13)	201(11)	59(10)	-9(8)	32(9)
C(8)	181(11)	245(12)	216(11)	-46(9)	-26(8)	-44(9)
C(9)	167(11)	252(12)	226(11)	-6(10)	-36(9)	-66(9)
C(10)	201(11)	251(13)	259(12)	46(10)	-18(9)	-65(9)
C(11)	202(11)	276(13)	224(11)	72(10)	-2(9)	-38(9)
C(12)	220(12)	231(12)	256(12)	70(10)	-33(9)	32(9)
C(13)	160(11)	256(12)	226(11)	10(10)	-25(9)	27(9)
C(14)	160(11)	245(12)	254(12)	-14(10)	-6(9)	42(9)
C(15)	185(11)	235(12)	193(10)	-54(9)	-11(8)	11(9)
C(16)	182(10)	278(12)	133(9)	-11(8)	-38(7)	34(9)
C(17)	120(9)	208(11)	153(9)	13(9)	-13(7)	-45(8)
C(18)	204(11)	303(13)	146(10)	48(9)	-29(8)	-12(9)
C(19)	142(9)	238(12)	164(8)	-3(9)	-1(6)	54(9)
N(6)	151(9)	263(10)	176(9)	86(8)	15(7)	23(7)
C(20)	154(11)	300(13)	256(12)	139(10)	31(8)	18(9)
C(21)	173(12)	375(16)	332(13)	199(12)	14(9)	8(11)
C(22)	179(13)	740(20)	720(20)	480(19)	2(13)	-43(14)
C(23)	218(15)	720(20)	780(30)	370(20)	17(15)	-79(15)
C(24)	182(11)	271(12)	193(10)	86(9)	15(8)	44(9)
C(25)	316(14)	352(16)	221(12)	65(11)	2(10)	79(12)
C(26)	306(13)	332(15)	279(12)	26(11)	-14(9)	50(11)
C(27)	392(16)	448(17)	327(14)	-37(13)	0(11)	76(13)
C(28)	178(11)	324(14)	203(11)	101(10)	-22(8)	37(9)
C(29)	185(11)	420(15)	196(11)	95(10)	-20(8)	-9(10)
C(30)	261(13)	329(14)	255(12)	56(10)	-65(10)	-30(10)
C(31)	257(14)	410(17)	454(17)	71(13)	-97(12)	-50(12)

C(32)	183(11)	257(12)	197(10)	66(9)	6(8)	-12(9)
C(33)	340(14)	316(14)	303(13)	73(11)	26(11)	57(11)
C(34)	448(17)	310(16)	353(15)	-16(12)	75(12)	-32(13)
C(35)	660(20)	440(20)	630(20)	-129(18)	116(19)	70(18)
O(11)	356(9)	269(9)	183(7)	10(7)	-68(6)	64(8)
O(12)	394(11)	454(12)	199(8)	34(8)	-58(7)	154(9)
O(51A)	280(30)	400(30)	1260(100)	-200(40)	160(40)	-40(20)
C(52A)	350(40)	770(60)	800(60)	-360(50)	70(40)	60(40)
C(53A)	480(40)	610(50)	640(50)	-180(40)	20(40)	90(40)
C(54A)	510(70)	1300(130)	960(100)	200(90)	90(60)	60(80)
O(50A)	620(30)	720(40)	520(30)	140(30)	-120(20)	40(30)
O(51B)	1160(50)	330(30)	740(40)	70(20)	380(30)	-30(30)
C(52B)	800(60)	230(30)	550(40)	40(30)	210(40)	-90(30)
C(53B)	380(50)	750(70)	900(70)	180(60)	-60(40)	-20(40)
C(54B)	990(140)	2900(200)	550(60)	-610(100)	-160(70)	390(130)
O(50B)	1110(50)	1170(60)	580(40)	-170(40)	230(30)	-350(40)

Table 5. Hydrogen bonds for MLC03 (CCDC 629534) [Å and °].

D-H...A	d(D-H)	d(H...A)	d(D...A)	<(DHA)
N(3)-H(3)...O(5)#1	0.93	2.25	3.078(2)	148.5
N(3)-H(3)...O(6)#1	0.93	2.43	3.221(2)	142.2
N(5)-H(5)...O(7)#2	0.93	2.20	3.048(2)	150.4
N(5)-H(5)...O(8)#2	0.93	2.51	3.271(3)	139.4
O(11)-H(11A)...O(4)#3	1.00	1.87	2.867(2)	172.1
O(11)-H(11B)...O(6)#4	1.00	1.82	2.776(2)	159.2
O(12)-H(12A)...O(2)#1	1.00	1.88	2.868(3)	170.6
O(12)-H(12B)...O(8)#5	1.00	1.88	2.836(2)	159.2
Other possible H-O interactions:				
N(3)-H(3)...O(3)	0.93	2.76	3.096(2)	102.2
N(5)-H(5)...O(1)	0.93	2.75	3.069(2)	101.3

Symmetry transformations used to generate equivalent atoms:
#1 -x+1,-y,-z+1
#2 -x,-y,-z+1
#3 -x+1,y+1/2,-z+1/2
#4 x,-y+1/2,z-1/2
#5 x+1,y,z

CALIFORNIA INSTITUTE OF TECHNOLOGY

BECKMAN INSTITUTE

X-RAY CRYSTALLOGRAPHY LABORATORY

Date 11 April 2007

Crystal Structure Analysis of:

MLC06

(shown below)

For Investigator: Morgan Cable ext. (818) 354-4345

Advisor: A. Ponce/H. B. Gray ext. 6500

Account Number: API.HSARPA-1-DOI.000002

By Michael W. Day 116 Beckman ext. 2734

e-mail: mikeday@caltech.edu

Contents

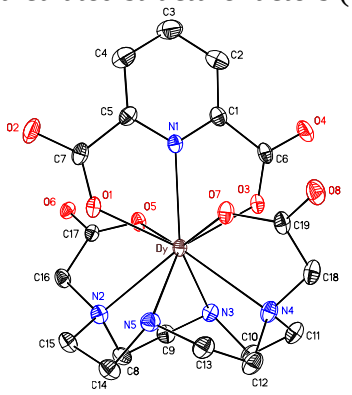

MLC06

Note: The crystallographic data have been deposited in the Cambridge Database (CCDC) and has been placed on hold pending further instructions from me. The deposition number is 643596. Ideally the CCDC would like the publication to contain a footnote of the type: "Crystallographic data have been deposited at the CCDC, 12 Union Road, Cambridge CB2 1EZ, UK and copies can be obtained on request, free of charge, by quoting the publication citation and the deposition number 643596."

Table 1. Crystal data and structure refinement for MLC06 (CCDC 643596).

Empirical formula	$[C_{19}H_{25}N_5O_8Dy]^-$ $[C_{16}H_{36}N]^+$ $2(C_3H_8O)$ $3(H_2O)$
Formula weight	966.51
Crystallization Solvent	Acetone/isopropanol/water
Crystal Habit	Prism
Crystal size	0.39 x 0.14 x 0.11 mm^3
Crystal color	Colorless

Data Collection

Type of diffractometer	Bruker SMART 1000
Wavelength	0.71073 Å MoKα
Data Collection Temperature	100(2) K
θ range for 28613 reflections used in lattice determination	2.19 to 40.17°
Unit cell dimensions	a = 13.1742(4) Å b = 13.1860(4) Å β= 90.3720(10)° c = 26.1130(8) Å
Volume	4536.1(2) $Å^3$
Z	4
Crystal system	Monoclinic
Space group	$P2_1/c$
Density (calculated)	1.415 Mg/m^3
F(000)	2012
θ range for data collection	1.55 to 40.83°
Completeness to θ = 40.83°	93.8 %
Index ranges	$-23 \le h \le 23$, $-23 \le k \le 23$, $-46 \le l \le 48$
Data collection scan type	ω scans at 7 ϕ settings
Reflections collected	139731
Independent reflections	27766 [R_{int}= 0.1106]
Absorption coefficient	1.710 mm^{-1}
Absorption correction	None
Max. and min. transmission	0.8342 and 0.5553

Table 1 (cont.)

Structure solution and Refinement

Structure solution program	SHELXS-97 (Sheldrick, 1990)
Primary solution method	Isomorphous method
Secondary solution method	Difference Fourier map
Hydrogen placement	Geometric positions
Structure refinement program	SHELXL-97 (Sheldrick, 1997)
Refinement method	Full matrix least-squares on F^2
Data / restraints / parameters	27766 / 10 / 548
Treatment of hydrogen atoms	Riding
Goodness-of-fit on F^2	1.029
Final R indices [$I>2\sigma(I)$, 14774 reflections]	R1 = 0.0408, *w*R2 = 0.0721
R indices (all data)	R1 = 0.0995, *w*R2 = 0.0806
Type of weighting scheme used	Sigma
Weighting scheme used	$w=1/\sigma^2(Fo^2)$
Max shift/error	0.009
Average shift/error	0.000
Largest diff. peak and hole	3.252 and -2.305 e.Å^{-3}

Special Refinement Details

The disordered solvent region was modeled as two acetone and one water.

Refinement of F^2 against ALL reflections. The weighted R-factor (*w*R) and goodness of fit (S) are based on F^2, conventional R-factors (R) are based on F, with F set to zero for negative F^2. The threshold expression of $F^2 > 2\sigma(F^2)$ is used only for calculating R-factors(gt) etc. and is not relevant to the choice of reflections for refinement. R-factors based on F^2 are statistically about twice as large as those based on F, and R-factors based on ALL data will be even larger.

All esds (except the esd in the dihedral angle between two l.s. planes) are estimated using the full covariance matrix. The cell esds are taken into account individually in the estimation of esds in distances, angles and torsion angles; correlations between esds in cell parameters are only used when they are defined by crystal symmetry. An approximate (isotropic) treatment of cell esds is used for estimating esds involving l.s. planes.

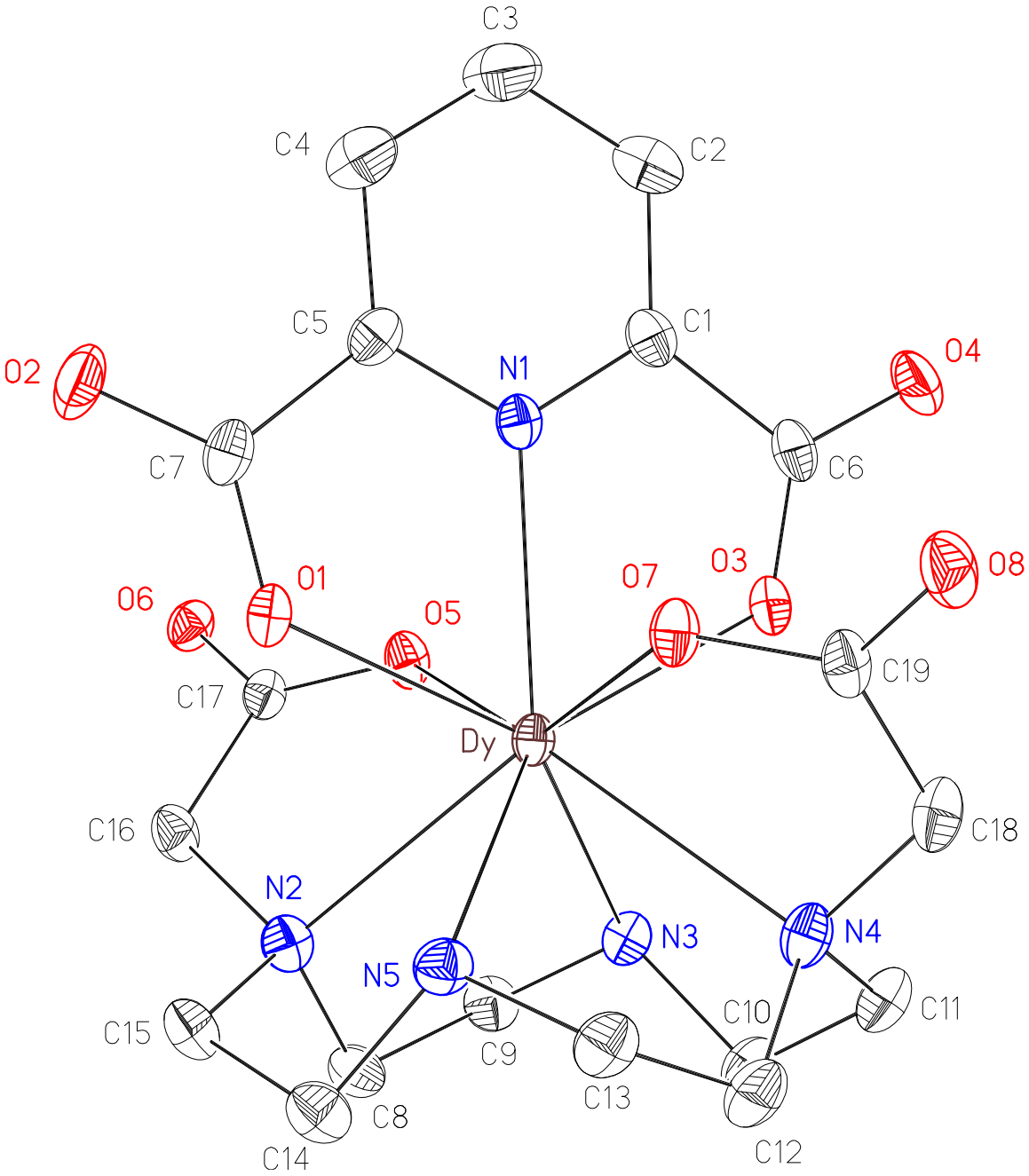
C3
C4
C2
C5
C1
O2
N1
O4
C7
C6
O6
O1
O5
O7
O3
O8
C17
C19
Dy
C16
C18
N2
N5
N3
N4
C15
C9
C10
C11
C8
C13
C14
C12

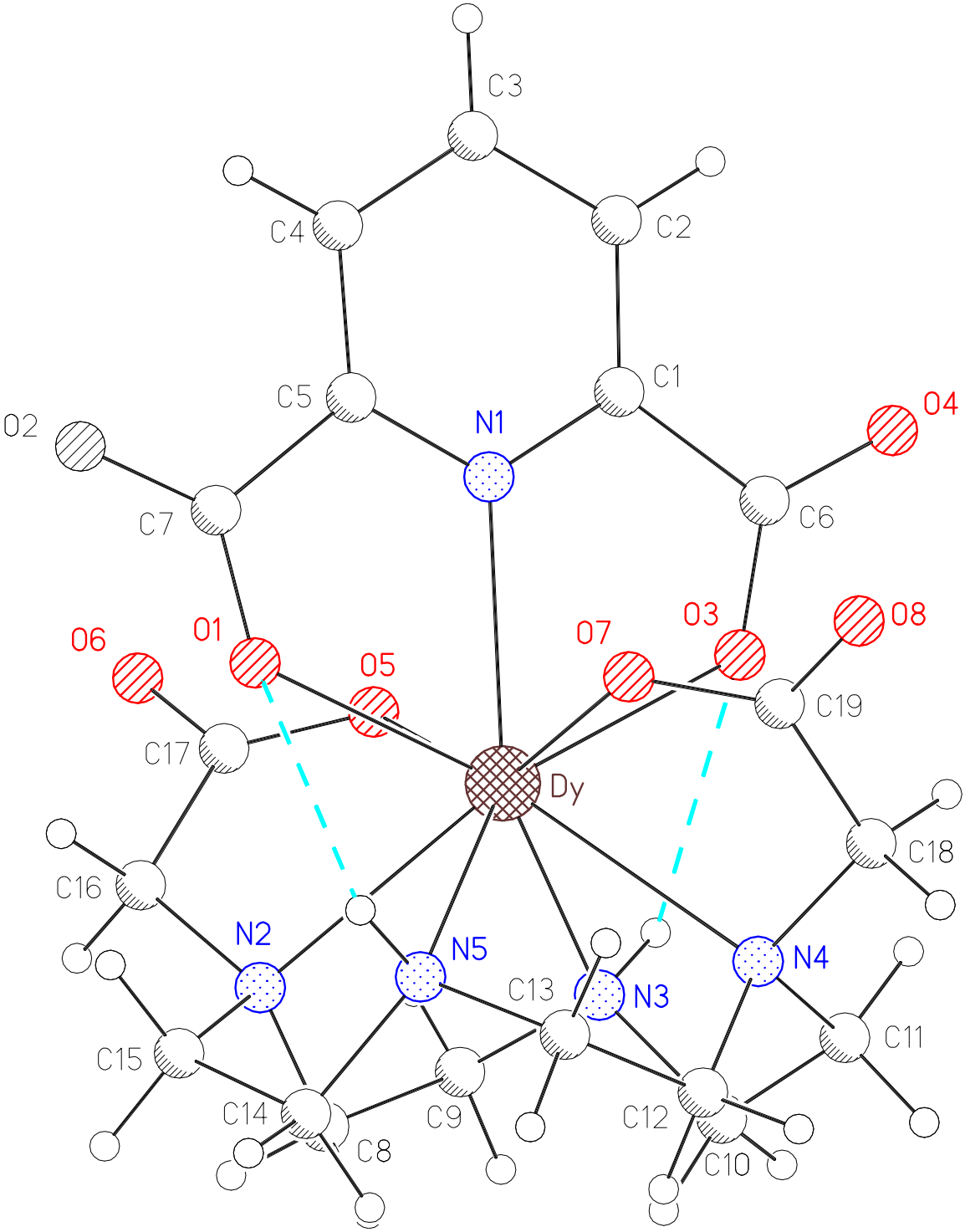
C3
C4
C2
C5
C1
O2
N1
O4
C7
C6
O6
O1
O7
O3
O8
O5
C19
C17
Dy
C18
C16
N2
N5
N4
C13
N3
C15
C11
C14
C9
C12
C8
C10

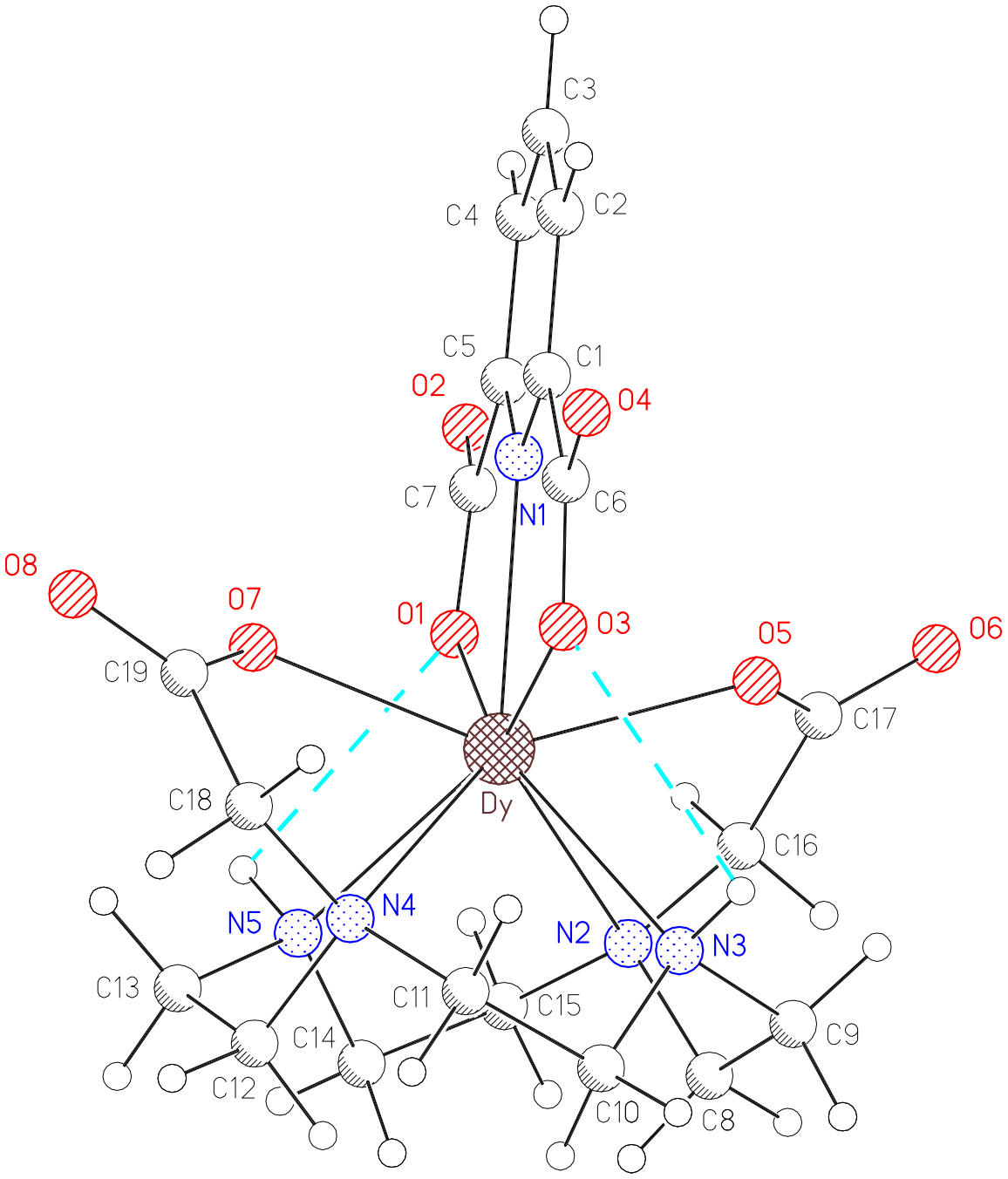
C3
C4
C2
C5
C1
O2
O4
C7
N1
C6
O8
O7
O1
O3
O5
O6
C19
C17
C18
Dy
C16
N5
N4
N2
N3
C13
C11
C15
C9
C14
C12
C10
C8

Table 2. Atomic coordinates (x 10^4) and equivalent isotropic displacement parameters ($Å^2$x 10^3) for MLC06 (CCDC 643596). U(eq) is defined as the trace of the orthogonalized U^{ij} tensor.

	x	y	z	U_{eq}	Occ
Dy	2482(1)	52(1)	4985(1)	13(1)	1
O(1)	1700(1)	-860(1)	5658(1)	18(1)	1
O(2)	1398(1)	-2314(1)	6082(1)	28(1)	1
O(3)	3299(1)	-554(1)	4233(1)	18(1)	1
O(4)	3669(2)	-1796(1)	3679(1)	32(1)	1
O(5)	3923(1)	-581(1)	5402(1)	17(1)	1
O(6)	4664(1)	-1044(1)	6137(1)	18(1)	1
O(7)	1061(1)	-396(1)	4497(1)	17(1)	1
O(8)	278(1)	-479(1)	3738(1)	24(1)	1
N(1)	2499(1)	-1818(1)	4889(1)	15(1)	1
N(2)	2945(1)	1039(1)	5836(1)	18(1)	1
N(3)	3905(1)	1341(1)	4839(1)	18(1)	1
N(4)	2017(1)	1390(1)	4267(1)	19(1)	1
N(5)	1062(1)	1229(1)	5270(1)	18(1)	1
C(1)	2900(2)	-2236(2)	4468(1)	18(1)	1
C(2)	2933(2)	-3279(2)	4400(1)	28(1)	1
C(3)	2551(2)	-3901(2)	4787(1)	33(1)	1
C(4)	2156(2)	-3459(2)	5224(1)	28(1)	1
C(5)	2131(2)	-2403(1)	5261(1)	18(1)	1
C(6)	3319(2)	-1469(2)	4089(1)	19(1)	1
C(7)	1708(2)	-1822(2)	5709(1)	19(1)	1
C(8)	3637(2)	1899(2)	5730(1)	21(1)	1
C(9)	4421(2)	1650(2)	5320(1)	20(1)	1
C(10)	3647(2)	2216(2)	4511(1)	22(1)	1
C(11)	2958(2)	1879(2)	4072(1)	23(1)	1
C(12)	1324(2)	2174(2)	4468(1)	24(1)	1
C(13)	548(2)	1740(2)	4835(1)	21(1)	1
C(14)	1310(2)	1939(2)	5691(1)	21(1)	1
C(15)	1999(2)	1417(2)	6078(1)	20(1)	1
C(16)	3442(2)	282(2)	6174(1)	19(1)	1
C(17)	4067(2)	-506(1)	5881(1)	15(1)	1
C(18)	1525(2)	808(2)	3849(1)	22(1)	1
C(19)	892(2)	-86(2)	4041(1)	18(1)	1
N(6)	6380(1)	2787(1)	2784(1)	18(1)	1
C(20)	7199(2)	3421(2)	2523(1)	22(1)	1
C(21)	8262(2)	3278(2)	2740(1)	26(1)	1
C(22)	8998(2)	4000(2)	2480(1)	43(1)	1
C(23)	10095(2)	3775(3)	2645(1)	50(1)	1
C(24)	6671(2)	1667(1)	2784(1)	19(1)	1
C(25)	6818(2)	1205(2)	2258(1)	28(1)	1
C(26)	7082(2)	90(2)	2304(1)	28(1)	1
C(27)	7269(2)	-403(2)	1785(1)	36(1)	1
C(28)	5401(2)	2948(2)	2482(1)	21(1)	1
C(29)	4478(2)	2390(2)	2684(1)	24(1)	1
C(30)	3646(2)	2345(2)	2273(1)	26(1)	1
C(31)	2688(2)	1817(2)	2460(1)	36(1)	1

C(32)	6254(2)	3092(1)	3339(1)	19(1)	1
C(33)	6040(2)	4211(2)	3433(1)	26(1)	1
C(34)	5666(2)	4370(2)	3973(1)	30(1)	1
C(35)	5617(3)	5479(2)	4128(1)	50(1)	1
O(11)	5754(1)	4997(1)	1877(1)	26(1)	1
O(12)	9152(2)	909(1)	3124(1)	34(1)	1
O(51A)	1469(2)	4414(3)	6177(2)	66(2)	0.747(4)
C(52A)	552(2)	4385(2)	6237(1)	54(1)	0.747(4)
C(53A)	-5(3)	3688(3)	6616(2)	58(1)	0.747(4)
C(54A)	-53(3)	5123(5)	5895(2)	109(4)	0.747(4)
O(50A)	-1170(50)	2500(50)	6430(30)	1940(70)	0.747(4)
O(51B)	1223(8)	4340(6)	5350(3)	61(3)	0.253(4)
C(52B)	765(6)	4521(6)	5744(3)	42(3)	0.253(4)
C(53B)	-371(7)	4792(16)	5766(5)	102(10)	0.253(4)
C(54B)	1399(9)	4464(15)	6241(3)	75(10)	0.253(4)
O(50B)	-58(8)	3751(8)	7120(4)	61(3)	0.253(4)

Table 3. Selected bond lengths [Å] and angles [°] for MLC06 (CCDC 643596).

Dy-O(7)	2.3333(14)	O(7)-Dy-O(5)	144.16(5)
Dy-O(5)	2.3370(14)	O(7)-Dy-O(1)	85.70(5)
Dy-O(1)	2.3708(15)	O(5)-Dy-O(1)	80.10(5)
Dy-O(3)	2.3817(15)	O(7)-Dy-O(3)	80.27(5)
Dy-N(1)	2.4786(15)	O(5)-Dy-O(3)	83.97(5)
Dy-N(5)	2.5458(18)	O(1)-Dy-O(3)	129.90(6)
Dy-N(3)	2.5602(18)	O(7)-Dy-N(1)	72.59(5)
Dy-N(4)	2.6436(17)	O(5)-Dy-N(1)	71.58(5)
Dy-N(2)	2.6452(17)	O(1)-Dy-N(1)	64.81(5)
		O(3)-Dy-N(1)	65.09(5)
		O(7)-Dy-N(5)	74.04(5)
		O(5)-Dy-N(5)	132.63(5)
		O(1)-Dy-N(5)	76.62(6)
		O(3)-Dy-N(5)	141.46(5)
		N(1)-Dy-N(5)	130.01(6)
		O(7)-Dy-N(3)	132.31(5)
		O(5)-Dy-N(3)	73.32(5)
		O(1)-Dy-N(3)	140.22(5)
		O(3)-Dy-N(3)	76.45(6)
		N(1)-Dy-N(3)	129.67(6)
		N(5)-Dy-N(3)	100.30(6)
		O(7)-Dy-N(4)	66.48(5)
		O(5)-Dy-N(4)	138.86(6)
		O(1)-Dy-N(4)	139.87(5)
		O(3)-Dy-N(4)	75.15(5)
		N(1)-Dy-N(4)	126.51(5)
		N(5)-Dy-N(4)	68.47(6)
		N(3)-Dy-N(4)	67.56(5)
		O(7)-Dy-N(2)	139.74(6)
		O(5)-Dy-N(2)	66.48(5)
		O(1)-Dy-N(2)	74.03(5)
		O(3)-Dy-N(2)	139.02(5)
		N(1)-Dy-N(2)	124.89(5)
		N(5)-Dy-N(2)	67.67(5)
		N(3)-Dy-N(2)	68.46(6)
		N(4)-Dy-N(2)	108.60(6)

Table 4. Bond lengths [Å] and angles [°] for MLC06 (CCDC 643596).

Dy-O(7)	2.3333(14)	C(26)-C(27)	1.525(3)
Dy-O(5)	2.3370(14)	C(28)-C(29)	1.519(3)
Dy-O(1)	2.3708(15)	C(29)-C(30)	1.531(3)
Dy-O(3)	2.3817(15)	C(30)-C(31)	1.526(4)
Dy-N(1)	2.4786(15)	C(32)-C(33)	1.523(3)
Dy-N(5)	2.5458(18)	C(33)-C(34)	1.510(4)
Dy-N(3)	2.5602(18)	C(34)-C(35)	1.519(4)
Dy-N(4)	2.6436(17)	O(51A)-C(52A)	1.2200
Dy-N(2)	2.6452(17)	C(52A)-C(53A)	1.5400
O(1)-C(7)	1.275(2)	C(52A)-C(54A)	1.5400
O(2)-C(7)	1.243(3)	O(51B)-C(52B)	1.2200
O(3)-C(6)	1.264(2)	C(52B)-C(53B)	1.5400
O(4)-C(6)	1.244(3)	C(52B)-C(54B)	1.5400
O(5)-C(17)	1.267(2)		
O(6)-C(17)	1.249(2)	O(7)-Dy-O(5)	144.16(5)
O(7)-C(19)	1.277(2)	O(7)-Dy-O(1)	85.70(5)
O(8)-C(19)	1.242(2)	O(5)-Dy-O(1)	80.10(5)
N(1)-C(5)	1.333(3)	O(7)-Dy-O(3)	80.27(5)
N(1)-C(1)	1.341(3)	O(5)-Dy-O(3)	83.97(5)
N(2)-C(16)	1.481(3)	O(1)-Dy-O(3)	129.90(6)
N(2)-C(8)	1.483(3)	O(7)-Dy-N(1)	72.59(5)
N(2)-C(15)	1.487(3)	O(5)-Dy-N(1)	71.58(5)
N(3)-C(10)	1.476(3)	O(1)-Dy-N(1)	64.81(5)
N(3)-C(9)	1.480(3)	O(3)-Dy-N(1)	65.09(5)
N(4)-C(12)	1.478(3)	O(7)-Dy-N(5)	74.04(5)
N(4)-C(18)	1.481(3)	O(5)-Dy-N(5)	132.63(5)
N(4)-C(11)	1.489(3)	O(1)-Dy-N(5)	76.62(6)
N(5)-C(14)	1.479(3)	O(3)-Dy-N(5)	141.46(5)
N(5)-C(13)	1.481(3)	N(1)-Dy-N(5)	130.01(6)
C(1)-C(2)	1.388(3)	O(7)-Dy-N(3)	132.31(5)
C(1)-C(6)	1.522(3)	O(5)-Dy-N(3)	73.32(5)
C(2)-C(3)	1.397(4)	O(1)-Dy-N(3)	140.22(5)
C(3)-C(4)	1.388(4)	O(3)-Dy-N(3)	76.45(6)
C(4)-C(5)	1.396(3)	N(1)-Dy-N(3)	129.67(6)
C(5)-C(7)	1.509(3)	N(5)-Dy-N(3)	100.30(6)
C(8)-C(9)	1.528(3)	O(7)-Dy-N(4)	66.48(5)
C(10)-C(11)	1.524(3)	O(5)-Dy-N(4)	138.86(6)
C(12)-C(13)	1.516(3)	O(1)-Dy-N(4)	139.87(5)
C(14)-C(15)	1.519(3)	O(3)-Dy-N(4)	75.15(5)
C(16)-C(17)	1.533(3)	N(1)-Dy-N(4)	126.51(5)
C(18)-C(19)	1.530(3)	N(5)-Dy-N(4)	68.47(6)
N(6)-C(32)	1.514(3)	N(3)-Dy-N(4)	67.56(5)
N(6)-C(24)	1.526(2)	O(7)-Dy-N(2)	139.74(6)
N(6)-C(28)	1.522(3)	O(5)-Dy-N(2)	66.48(5)
N(6)-C(20)	1.528(3)	O(1)-Dy-N(2)	74.03(5)
C(20)-C(21)	1.519(3)	O(3)-Dy-N(2)	139.02(5)
C(21)-C(22)	1.522(3)	N(1)-Dy-N(2)	124.89(5)
C(22)-C(23)	1.534(4)	N(5)-Dy-N(2)	67.67(5)
C(24)-C(25)	1.515(3)	N(3)-Dy-N(2)	68.46(6)
C(25)-C(26)	1.516(3)	N(4)-Dy-N(2)	108.60(6)

C(7)-O(1)-Dy	125.37(14)
C(6)-O(3)-Dy	125.23(14)
C(17)-O(5)-Dy	123.25(13)
C(19)-O(7)-Dy	124.15(13)
C(5)-N(1)-C(1)	120.45(18)
C(5)-N(1)-Dy	119.89(13)
C(1)-N(1)-Dy	119.65(13)
C(16)-N(2)-C(8)	110.95(16)
C(16)-N(2)-C(15)	110.00(17)
C(8)-N(2)-C(15)	109.94(16)
C(16)-N(2)-Dy	105.52(11)
C(8)-N(2)-Dy	110.95(13)
C(15)-N(2)-Dy	109.39(12)
C(10)-N(3)-C(9)	112.28(16)
C(10)-N(3)-Dy	116.04(13)
C(9)-N(3)-Dy	112.98(13)
C(12)-N(4)-C(18)	110.86(17)
C(12)-N(4)-C(11)	109.69(17)
C(18)-N(4)-C(11)	109.57(18)
C(12)-N(4)-Dy	110.79(13)
C(18)-N(4)-Dy	105.93(12)
C(11)-N(4)-Dy	109.94(12)
C(14)-N(5)-C(13)	112.28(16)
C(14)-N(5)-Dy	116.38(13)
C(13)-N(5)-Dy	112.75(14)
N(1)-C(1)-C(2)	121.6(2)
N(1)-C(1)-C(6)	114.04(17)
C(2)-C(1)-C(6)	124.3(2)
C(1)-C(2)-C(3)	118.5(2)
C(4)-C(3)-C(2)	119.2(2)
C(3)-C(4)-C(5)	118.9(2)
N(1)-C(5)-C(4)	121.2(2)
N(1)-C(5)-C(7)	114.14(17)
C(4)-C(5)-C(7)	124.6(2)
O(4)-C(6)-O(3)	126.6(2)
O(4)-C(6)-C(1)	117.84(19)
O(3)-C(6)-C(1)	115.54(19)
O(2)-C(7)-O(1)	126.8(2)
O(2)-C(7)-C(5)	117.94(19)
O(1)-C(7)-C(5)	115.25(18)
N(2)-C(8)-C(9)	112.71(17)
N(3)-C(9)-C(8)	110.15(18)
N(3)-C(10)-C(11)	110.04(17)
N(4)-C(11)-C(10)	111.27(19)
N(4)-C(12)-C(13)	112.47(17)
N(5)-C(13)-C(12)	110.43(18)
N(5)-C(14)-C(15)	109.63(16)
N(2)-C(15)-C(14)	111.69(18)
N(2)-C(16)-C(17)	113.33(17)
O(6)-C(17)-O(5)	124.8(2)
O(6)-C(17)-C(16)	117.21(17)
O(5)-C(17)-C(16)	117.91(16)
N(4)-C(18)-C(19)	113.25(17)
O(8)-C(19)-O(7)	124.7(2)
O(8)-C(19)-C(18)	117.81(18)
O(7)-C(19)-C(18)	117.47(17)
C(32)-N(6)-C(24)	106.59(15)
C(32)-N(6)-C(28)	111.09(17)
C(24)-N(6)-C(28)	110.34(16)
C(32)-N(6)-C(20)	111.30(16)
C(24)-N(6)-C(20)	110.60(17)
C(28)-N(6)-C(20)	106.96(15)
C(21)-C(20)-N(6)	114.65(16)
C(20)-C(21)-C(22)	110.15(18)
C(21)-C(22)-C(23)	110.9(2)
C(25)-C(24)-N(6)	115.00(17)
C(26)-C(25)-C(24)	110.45(18)
C(25)-C(26)-C(27)	112.5(2)
C(29)-C(28)-N(6)	115.51(16)
C(28)-C(29)-C(30)	110.20(19)
C(31)-C(30)-C(29)	112.4(2)
N(6)-C(32)-C(33)	115.72(17)
C(34)-C(33)-C(32)	110.34(18)
C(33)-C(34)-C(35)	113.4(2)
O(51A)-C(52A)-C(53A)	125.2
O(51A)-C(52A)-C(54A)	114.6
C(53A)-C(52A)-C(54A)	120.2
O(51B)-C(52B)-C(53B)	124.2
O(51B)-C(52B)-C(54B)	115.6
C(53B)-C(52B)-C(54B)	120.2

Table 5. Anisotropic displacement parameters ($Å^2 x\ 10^4$) for MLC06 (CCDC 643596). The anisotropic displacement factor exponent takes the form: $-2\pi^2[h^2 a^{*2} U^{11} + ... + 2\ h\ k\ a^*\ b^*\ U^{12}]$

	U^{11}	U^{22}	U^{33}	U^{23}	U^{13}	U^{12}
Dy	111(1)	169(1)	114(1)	13(1)	-13(1)	3(1)
O(1)	184(8)	225(7)	123(7)	34(5)	14(5)	0(5)
O(2)	363(10)	283(8)	201(8)	113(6)	67(7)	41(7)
O(3)	186(8)	236(7)	111(7)	1(5)	-7(5)	-9(5)
O(4)	477(12)	321(8)	154(8)	-80(6)	74(8)	-57(8)
O(5)	142(7)	241(7)	129(7)	-3(5)	-47(5)	26(5)
O(6)	180(7)	191(6)	160(7)	33(5)	-43(6)	-9(5)
O(7)	132(7)	250(7)	137(7)	26(5)	-27(5)	3(5)
O(8)	250(9)	304(8)	162(7)	-16(6)	-68(6)	26(6)
N(1)	122(7)	187(6)	128(8)	6(5)	-32(7)	14(5)
N(2)	154(9)	215(8)	172(8)	-7(6)	-15(7)	6(6)
N(3)	154(9)	193(7)	177(9)	26(6)	-2(7)	-4(6)
N(4)	152(9)	238(8)	175(9)	49(6)	-11(7)	5(6)
N(5)	178(9)	176(7)	195(9)	5(6)	-22(7)	12(6)
C(1)	146(10)	234(9)	163(10)	-23(7)	-34(7)	-6(7)
C(2)	271(13)	243(10)	310(13)	-82(8)	-1(10)	-5(8)
C(3)	363(15)	211(10)	419(15)	-8(9)	78(12)	-17(9)
C(4)	268(13)	222(10)	349(14)	50(9)	48(10)	9(8)
C(5)	151(10)	190(8)	195(10)	48(7)	-27(7)	17(6)
C(6)	164(10)	277(9)	131(9)	-26(7)	-41(8)	-9(7)
C(7)	144(10)	247(9)	166(10)	58(7)	-11(8)	15(7)
C(8)	211(11)	203(8)	216(11)	-44(7)	-14(8)	-16(7)
C(9)	159(10)	229(9)	219(11)	-14(7)	-26(8)	-38(7)
C(10)	199(11)	225(9)	248(11)	61(8)	3(9)	-35(7)
C(11)	216(11)	245(9)	229(11)	91(8)	6(9)	-20(8)
C(12)	220(11)	245(9)	247(12)	78(8)	-20(9)	52(8)
C(13)	165(10)	223(9)	230(11)	32(7)	-21(8)	39(7)
C(14)	170(11)	231(9)	228(11)	-35(8)	-10(8)	38(7)
C(15)	192(11)	245(9)	169(10)	-50(7)	-7(8)	20(7)
C(16)	199(10)	238(8)	134(9)	-20(6)	-45(7)	21(7)
C(17)	137(9)	185(8)	137(9)	17(6)	-21(7)	-32(6)
C(18)	203(11)	305(10)	164(10)	65(8)	-31(8)	-15(8)
C(19)	139(8)	254(9)	131(8)	-2(7)	-20(6)	68(7)
N(6)	160(9)	214(7)	167(9)	68(6)	-17(7)	5(6)
C(20)	187(11)	266(9)	197(11)	125(8)	21(8)	0(7)
C(21)	192(11)	340(11)	262(12)	139(9)	0(9)	-7(8)
C(22)	199(13)	557(17)	525(19)	336(14)	4(12)	-26(11)
C(23)	214(14)	608(19)	680(20)	299(17)	-30(14)	-84(12)
C(24)	199(10)	195(8)	179(10)	65(7)	0(8)	21(7)
C(25)	352(14)	275(10)	203(11)	32(8)	30(10)	54(9)
C(26)	322(12)	250(10)	272(11)	-7(9)	-32(9)	48(9)
C(27)	354(15)	385(13)	334(15)	-79(11)	-3(12)	77(11)
C(28)	180(10)	247(9)	189(10)	86(7)	-26(8)	29(7)
C(29)	178(11)	343(11)	196(11)	74(8)	-23(8)	-7(8)
C(30)	265(13)	288(10)	229(12)	34(8)	-64(10)	-20(8)
C(31)	245(14)	404(13)	431(17)	68(11)	-108(12)	-82(10)

C(32)	196(10)	200(8)	168(9)	57(7)	-7(8)	-4(7)
C(33)	290(13)	222(9)	259(12)	42(8)	34(9)	13(8)
C(34)	368(15)	241(10)	299(14)	-42(9)	22(11)	3(9)
C(35)	590(20)	342(15)	570(20)	-136(14)	145(17)	12(13)
O(11)	358(9)	240(7)	178(7)	14(6)	-72(6)	62(7)
O(12)	392(11)	400(10)	227(9)	9(7)	-97(8)	141(8)
O(51A)	380(30)	520(20)	1090(40)	-80(20)	10(30)	7(19)
C(52A)	360(30)	660(30)	600(30)	-230(20)	20(20)	90(20)
C(53A)	420(30)	610(30)	700(40)	-170(20)	-10(20)	50(20)
C(54A)	310(40)	2180(110)	800(50)	580(60)	40(30)	260(50)
O(51B)	1020(90)	270(40)	540(60)	80(40)	250(60)	-40(40)
C(52B)	730(90)	180(40)	360(60)	90(40)	80(60)	-90(40)
C(53B)	180(90)	1900(300)	1000(180)	360(170)	-120(90)	-10(120)
C(54B)	280(100)	1800(300)	130(60)	-250(90)	30(60)	-190(110)

Table 6. Hydrogen bonds for MLC06 (CCDC 643596) [Å and °].

D-H...A	d(D-H)	d(H...A)	d(D...A)	<(DHA)
N(3)-H(3)...O(5)#1	0.93	2.29	3.101(2)	146.1
N(3)-H(3)...O(6)#1	0.93	2.42	3.204(3)	141.4
N(5)-H(5)...O(7)#2	0.93	2.23	3.069(2)	149.4
N(5)-H(5)...O(8)#2	0.93	2.54	3.297(3)	138.2
O(11)-H(11A)...O(4)#3	0.99	1.89	2.879(2)	175.2
O(11)-H(11A)...O(3)#3	0.99	2.55	3.246(2)	126.5
O(11)-H(11B)...O(6)#4	0.99	1.83	2.7691(19)	155.9
O(12)-H(12A)...O(2)#1	1.00	1.89	2.875(3)	170.7
O(12)-H(12B)...O(8)#5	1.00	1.88	2.844(2)	160.8

Symmetry transformations used to generate equivalent atoms:
#1 -x+1,-y,-z+1
#2 -x,-y,-z+1
#3 -x+1,y+1/2,-z+1/2
#4 x,-y+1/2,z-1/2
#5 x+1,y,z

APPENDIX E

Crystallographic Data for TBA·Eu(DO2A)(DPA) Temperature Dependence

Temperature	Designation	CCDC	Page
100 K	MLC18	761599	E2
200 K	MLC17	762705	E17
300 K	MLC19	763335	E31

CALIFORNIA INSTITUTE OF TECHNOLOGY

BECKMAN INSTITUTE

X-RAY CRYSTALLOGRAPHY LABORATORY

Date 15 January 2010

Crystal Structure Analysis of:

MLC18

(shown below)

For Investigator: Morgan Cable ext. (818) 354-4345

Advisor: Adrian Ponce ext. (818) 354-8196

Account Number: AP1.HSARPA3-1-HSARPA.PONCE

By Michael W. Day 116 Beckman ext. 2734

e-mail: mikeday@caltech.edu

Contents

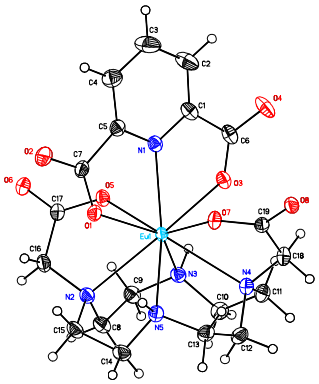

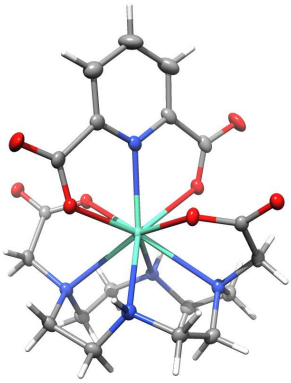

MLC18

Note: The crystallographic data have been deposited in the Cambridge Database (CCDC) and has been placed on hold pending further instructions from me. The deposition number is 761599. Ideally the CCDC would like the publication to contain a footnote of the type: "Crystallographic data have been deposited at the CCDC, 12 Union Road, Cambridge CB2 1EZ, UK and copies can be obtained on request, free of charge, by quoting the publication citation and the deposition number 761599."

Table 1. Crystal data and structure refinement for MLC18 (CCDC 761599).

Empirical formula	$[C_{19}H_{25}N_5O_8Eu]^-$ $[C_{16}H_{36}N]^+ \bullet C_3H_6O \bullet 3.68(H_2O)$
Formula weight	970.23
Crystallization Solvent	Acetone
Crystal Habit	Fragment
Crystal size	0.22 x 0.19 x 0.15 mm^3
Crystal color	Colorless

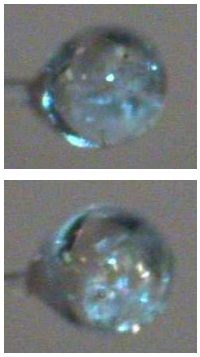

Data Collection

Type of diffractometer	Bruker KAPPA APEX II
Wavelength	0.71073 Å MoKα
Data Collection Temperature	100(2) K
θ range for 9759 reflections used in lattice determination	2.22 to 39.59°
Unit cell dimensions	a = 13.0309(5) Å b = 13.4740(5) Å β= 90.600(2)° c = 26.1088(9) Å
Volume	4583.9(3) $Å^3$
Z	4
Crystal system	Monoclinic
Space group	P $2_1/c$
Density (calculated)	1.406 Mg/m^3
F(000)	2035
θ range for data collection	1.56 to 40.90°
Completeness to θ = 40.90°	97.8 %
Index ranges	$-23 \le h \le 23$, $-24 \le k \le 23$, $-47 \le l \le 46$
Data collection scan type	ω scans; 19 settings
Reflections collected	219049
Independent reflections	29345 [R_{int}= 0.0420]
Absorption coefficient	1.432 mm^{-1}
Absorption correction	Semi-empirical from equivalents
Max. and min. transmission	0.7480 and 0.6761

Table 1 (cont.)

Structure solution and Refinement

Structure solution program	SHELXS-97 (Sheldrick, 2008)
Primary solution method	Direct methods
Secondary solution method	Difference Fourier map
Hydrogen placement	Geometric positions
Structure refinement program	SHELXL-97 (Sheldrick, 2008)
Refinement method	Full matrix least-squares on F^2
Data / restraints / parameters	29345 / 0 / 544
Treatment of hydrogen atoms	Riding
Goodness-of-fit on F^2	2.444
Final R indices [$I>2\sigma(I)$, 19989 reflections]	R1 = 0.0341, *w*R2 = 0.0624
R indices (all data)	R1 = 0.0648, *w*R2 = 0.0638
Type of weighting scheme used	Sigma
Weighting scheme used	$w=1/\sigma^2(Fo^2)$
Max shift/error	0.003
Average shift/error	0.000
Largest diff. peak and hole	3.339 and -2.101 e.Å^{-3}

Special Refinement Details

Crystals were mounted on a glass fiber using, coated with epoxy then placed on the diffractometer under a nitrogen stream at 100K.

The asymmetric unit contains acetone at one site that is disordered between two orientations. The major orientation (69%), O51-C53 is accompanied by a water molecule, O44, that is hydrogen bonded to two other waters, O42 and O43. The minor orientation does not contain a discernable water. Hydrogen atoms on water were located in the electron density difference map and were constrained to ride the appropriate oxygen. All other hydrogens were placed at geometric positions and refined as riding atoms. No other restraints were placed on the model.

Refinement of F^2 against ALL reflections. The weighted R-factor (*w*R) and goodness of fit (S) are based on F^2, conventional R-factors (R) are based on F, with F set to zero for negative F^2. The threshold expression of $F^2 > 2\sigma(F^2)$ is used only for calculating R-factors(gt) etc. and is not relevant to the choice of reflections for refinement. R-factors based on F^2 are statistically about twice as large as those based on F, and R-factors based on ALL data will be even larger.

All esds (except the esd in the dihedral angle between two l.s. planes) are estimated using the full covariance matrix. The cell esds are taken into account individually in the estimation of esds in distances, angles and torsion angles; correlations between esds in cell parameters are only used when they are defined by crystal symmetry. An approximate (isotropic) treatment of cell esds is used for estimating esds involving l.s. planes.

E5

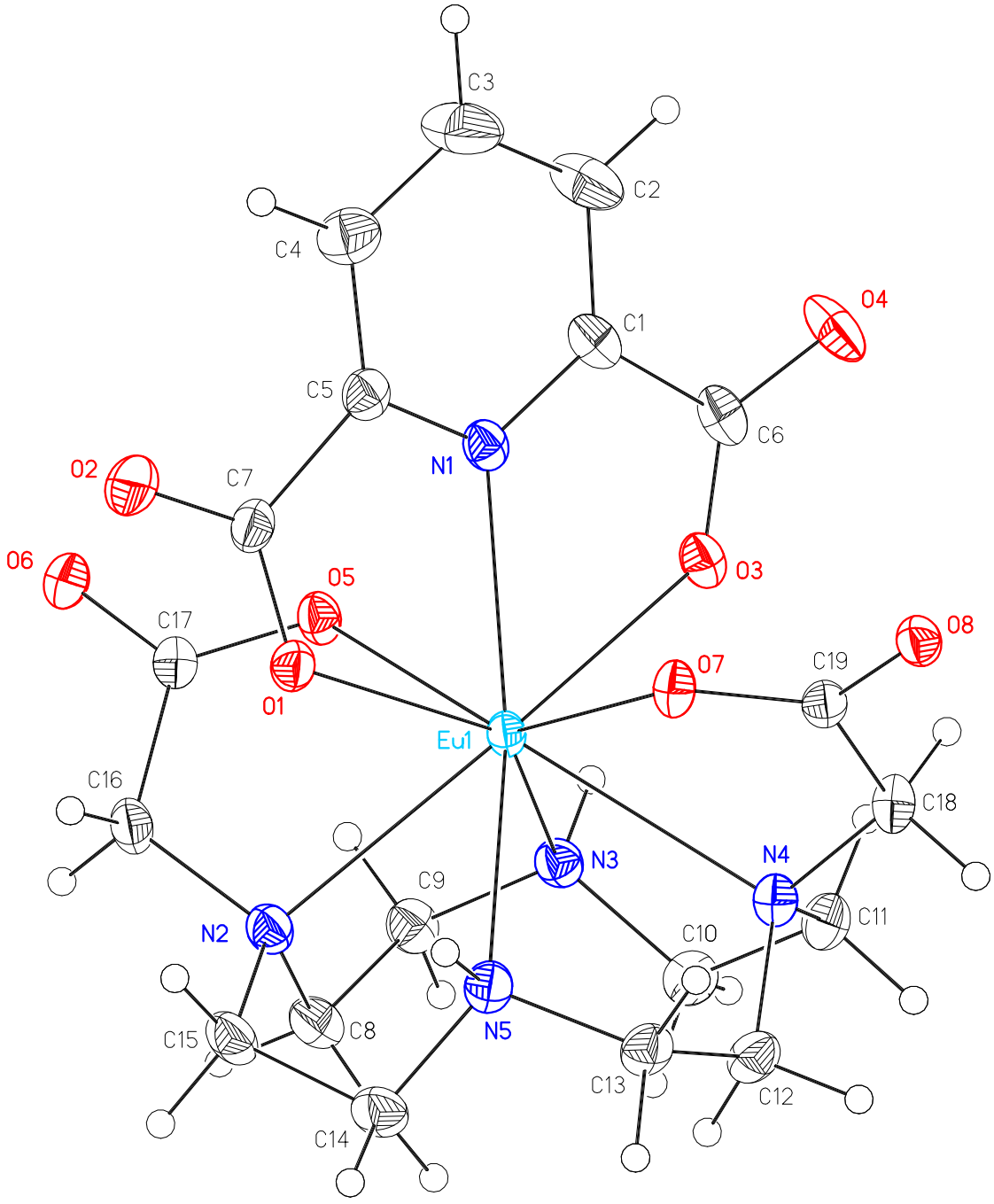
C3
C2
C4
C1
O4
C5
N1
C6
O2
C7
O6
O5
O3
C17
O8
O1
O7
C19
Eu1
C16
C18
N3
N4
C9
N2
C10
C11
C15
C8
N5
C13
C12
C14

E6

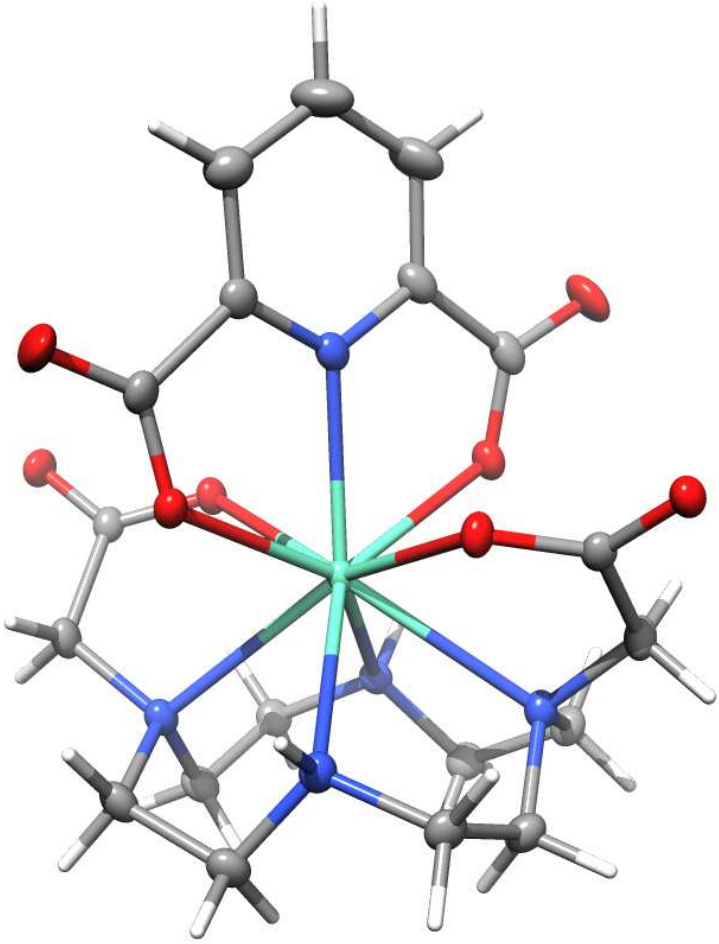

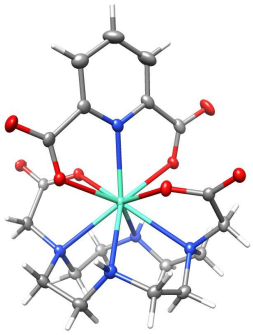

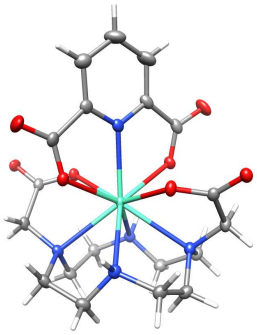

E7

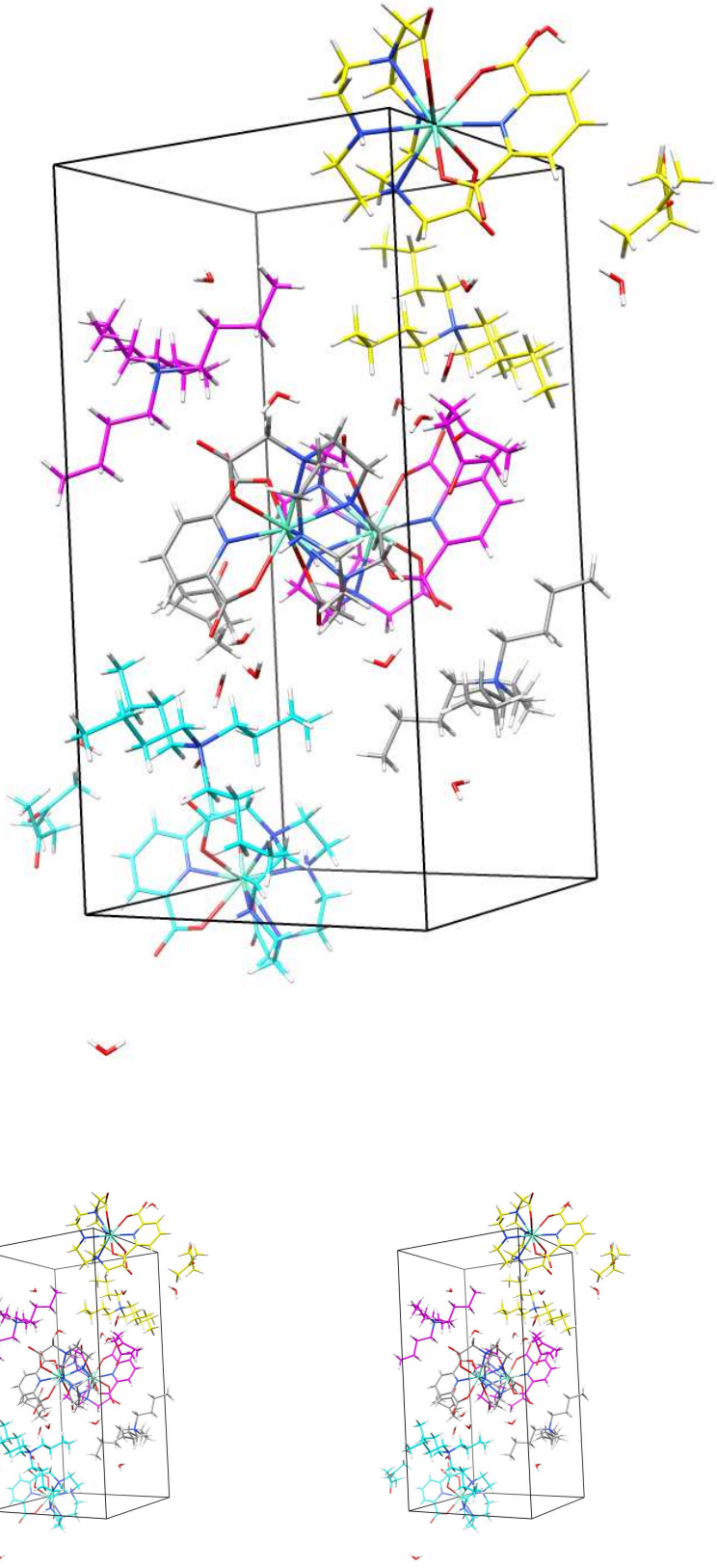

Table 2. Atomic coordinates (x 10^4) and equivalent isotropic displacement parameters ($Å^2$x 10^3) for MLC18 (CCDC 761599). U(eq) is defined as the trace of the orthogonalized U^{ij} tensor.

	x	y	z	U_{eq}	Occ
Eu(1)	7492(1)	4903(1)	4994(1)	14(1)	1
O(1)	8306(1)	5479(1)	5775(1)	18(1)	1
O(2)	8565(1)	6661(1)	6360(1)	42(1)	1
O(3)	6699(1)	5871(1)	4322(1)	19(1)	1
O(4)	6432(1)	7320(1)	3919(1)	31(1)	1
O(5)	6045(1)	5286(1)	5504(1)	18(1)	1
O(6)	5344(1)	5321(1)	6275(1)	23(1)	1
O(7)	8971(1)	5551(1)	4584(1)	18(1)	1
O(8)	9676(1)	6058(1)	3858(1)	18(1)	1
N(1)	7502(1)	6747(1)	5124(1)	17(1)	1
N(2)	7026(1)	3510(1)	5684(1)	18(1)	1
N(3)	6038(1)	3765(1)	4670(1)	18(1)	1
N(4)	7955(1)	3995(1)	4122(1)	17(1)	1
N(5)	8935(1)	3605(1)	5124(1)	18(1)	1
C(1)	7130(1)	7348(1)	4758(1)	20(1)	1
C(2)	7127(2)	8365(1)	4817(1)	32(1)	1
C(3)	7510(2)	8769(1)	5267(1)	37(1)	1
C(4)	7885(1)	8142(1)	5646(1)	26(1)	1
C(5)	7877(1)	7133(1)	5556(1)	18(1)	1
C(6)	6718(1)	6808(1)	4291(1)	21(1)	1
C(7)	8283(1)	6363(1)	5932(1)	20(1)	1
C(8)	6320(1)	2765(1)	5452(1)	22(1)	1
C(9)	5532(1)	3222(1)	5091(1)	20(1)	1
C(10)	6301(1)	3113(1)	4240(1)	21(1)	1
C(11)	6990(1)	3653(1)	3870(1)	20(1)	1
C(12)	8644(1)	3141(1)	4220(1)	21(1)	1
C(13)	9436(1)	3345(1)	4638(1)	20(1)	1
C(14)	8665(1)	2726(1)	5429(1)	23(1)	1
C(15)	7981(1)	3018(1)	5867(1)	22(1)	1
C(16)	6530(1)	4032(1)	6113(1)	20(1)	1
C(17)	5911(1)	4945(1)	5952(1)	16(1)	1
C(18)	8463(1)	4744(1)	3802(1)	20(1)	1
C(19)	9098(1)	5510(1)	4103(1)	16(1)	1
N(6)	1363(1)	2123(1)	7182(1)	20(1)	1
C(20)	1674(1)	3209(1)	7193(1)	21(1)	1
C(21)	1850(1)	3646(1)	7721(1)	28(1)	1
C(22)	2079(1)	4747(1)	7682(1)	29(1)	1
C(23)	2313(2)	5212(1)	8203(1)	39(1)	1
C(24)	2194(1)	1484(1)	7439(1)	25(1)	1
C(25)	3264(1)	1634(1)	7243(1)	30(1)	1
C(26)	3996(2)	873(2)	7480(1)	53(1)	1
C(27)	5107(2)	1117(2)	7360(1)	56(1)	1
C(28)	1228(1)	1845(1)	6622(1)	22(1)	1
C(29)	911(2)	773(1)	6522(1)	36(1)	1
C(30)	706(2)	582(1)	5967(1)	43(1)	1

C(31)	462(2)	-459(2)	5822(1)	63(1)	1
C(32)	380(1)	1958(1)	7474(1)	23(1)	1
C(33)	-555(1)	2516(1)	7273(1)	26(1)	1
C(34)	-1414(1)	2506(1)	7660(1)	27(1)	1
C(35)	-2376(1)	3033(1)	7471(1)	35(1)	1
O(41)	761(1)	5077(1)	3094(1)	28(1)	1
O(42)	4212(1)	3975(1)	6888(1)	37(1)	1
O(43)	3882(2)	2263(1)	8520(1)	92(1)	1
O(44)	5098(2)	8671(2)	7083(1)	69(1)	0.689(2)
O(51)	3588(2)	9313(1)	5364(1)	56(1)	0.689(2)
C(51)	3427(3)	9395(3)	6244(2)	57(1)	0.689(2)
C(52)	4006(3)	9500(2)	5753(1)	45(1)	0.689(2)
C(53)	5099(5)	9768(5)	5796(2)	111(2)	0.689(2)
O(61)	3597(11)	9491(10)	6027(5)	120(5)	0.311(2)
C(61)	4945(7)	8811(6)	6490(3)	71(2)	0.311(2)
C(62)	4450(9)	9449(7)	6180(4)	75(3)	0.311(2)
C(63)	5015(10)	10326(7)	5883(4)	66(3)	0.311(2)

Table 3. Selected bond lengths [Å] and angles [°] for MLC18 (CCDC 761599).

Eu(1)-O(5)	2.3747(10)	O(5)-Eu(1)-N(4)	140.15(3)
Eu(1)-O(7)	2.3813(10)	O(7)-Eu(1)-N(4)	65.88(3)
Eu(1)-O(3)	2.4104(8)	O(3)-Eu(1)-N(4)	74.06(3)
Eu(1)-O(1)	2.4156(8)	O(1)-Eu(1)-N(4)	140.21(4)
Eu(1)-N(1)	2.5067(11)	N(1)-Eu(1)-N(4)	124.77(3)
Eu(1)-N(3)	2.5728(11)	N(3)-Eu(1)-N(4)	67.50(4)
Eu(1)-N(5)	2.5882(11)	N(5)-Eu(1)-N(4)	68.26(3)
Eu(1)-N(4)	2.6595(11)	O(5)-Eu(1)-N(2)	65.70(3)
Eu(1)-N(2)	2.6759(11)	O(7)-Eu(1)-N(2)	138.66(3)
Eu(1)-C(19)	3.2513(14)	O(3)-Eu(1)-N(2)	140.46(4)
Eu(1)-C(17)	3.2569(14)	O(1)-Eu(1)-N(2)	76.02(3)
		N(1)-Eu(1)-N(2)	127.27(3)
O(5)-Eu(1)-O(7)	145.43(4)	N(3)-Eu(1)-N(2)	68.39(3)
O(5)-Eu(1)-O(3)	87.33(3)	N(5)-Eu(1)-N(2)	66.89(4)
O(7)-Eu(1)-O(3)	79.43(3)	N(4)-Eu(1)-N(2)	107.96(3)
O(5)-Eu(1)-O(1)	78.58(3)	O(5)-Eu(1)-C(19)	150.10(3)
O(7)-Eu(1)-O(1)	84.92(3)	O(3)-Eu(1)-C(19)	67.47(3)
O(3)-Eu(1)-O(1)	128.40(3)	O(1)-Eu(1)-C(19)	104.05(3)
O(5)-Eu(1)-N(1)	73.29(4)	N(1)-Eu(1)-C(19)	81.05(4)
O(7)-Eu(1)-N(1)	72.19(4)	N(3)-Eu(1)-C(19)	113.07(3)
O(3)-Eu(1)-N(1)	64.11(3)	N(5)-Eu(1)-C(19)	77.96(3)
O(1)-Eu(1)-N(1)	64.30(3)	N(4)-Eu(1)-C(19)	49.42(3)
O(5)-Eu(1)-N(3)	74.19(4)	N(2)-Eu(1)-C(19)	144.18(3)
O(7)-Eu(1)-N(3)	131.85(3)	O(7)-Eu(1)-C(17)	149.39(3)
O(3)-Eu(1)-N(3)	76.99(3)	O(3)-Eu(1)-C(17)	106.25(3)
O(1)-Eu(1)-N(3)	141.63(4)	O(1)-Eu(1)-C(17)	67.80(3)
N(1)-Eu(1)-N(3)	129.60(4)	N(1)-Eu(1)-C(17)	83.21(3)
O(5)-Eu(1)-N(5)	130.81(3)	N(3)-Eu(1)-C(17)	78.09(3)
O(7)-Eu(1)-N(5)	73.51(4)	N(5)-Eu(1)-C(17)	112.09(3)
O(3)-Eu(1)-N(5)	140.01(4)	N(4)-Eu(1)-C(17)	144.72(3)
O(1)-Eu(1)-N(5)	78.18(3)	N(2)-Eu(1)-C(17)	49.13(3)
N(1)-Eu(1)-N(5)	130.51(4)	C(19)-Eu(1)-C(17)	164.23(3)
N(3)-Eu(1)-N(5)	99.87(4)		

Symmetry transformations used to generate equivalent atoms:

Table 4. Bond lengths [Å] and angles [°] for MLC18 (CCDC 761599).

Eu(1)-O(5)	2.3747(10)	C(24)-C(25)	1.504(2)
Eu(1)-O(7)	2.3813(10)	C(25)-C(26)	1.525(2)
Eu(1)-O(3)	2.4104(8)	C(26)-C(27)	1.521(3)
Eu(1)-O(1)	2.4156(8)	C(28)-C(29)	1.525(2)
Eu(1)-N(1)	2.5067(11)	C(29)-C(30)	1.494(2)
Eu(1)-N(3)	2.5728(11)	C(30)-C(31)	1.487(3)
Eu(1)-N(5)	2.5882(11)	C(32)-C(33)	1.520(2)
Eu(1)-N(4)	2.6595(11)	C(33)-C(34)	1.517(2)
Eu(1)-N(2)	2.6759(11)	C(34)-C(35)	1.520(2)
Eu(1)-C(19)	3.2513(14)	O(51)-C(52)	1.174(3)
Eu(1)-C(17)	3.2569(14)	C(51)-C(52)	1.502(7)
O(1)-C(7)	1.2597(16)	C(52)-C(53)	1.473(7)
O(2)-C(7)	1.2386(15)	O(61)-C(62)	1.179(15)
O(3)-C(6)	1.2647(16)	C(61)-C(62)	1.341(11)
O(4)-C(6)	1.2447(15)	C(62)-C(63)	1.597(16)
O(5)-C(17)	1.2716(15)		
O(6)-C(17)	1.2353(17)	O(5)-Eu(1)-O(7)	145.43(4)
O(7)-C(19)	1.2696(15)	O(5)-Eu(1)-O(3)	87.33(3)
O(8)-C(19)	1.2375(17)	O(7)-Eu(1)-O(3)	79.43(3)
N(1)-C(5)	1.3316(16)	O(5)-Eu(1)-O(1)	78.58(3)
N(1)-C(1)	1.3389(16)	O(7)-Eu(1)-O(1)	84.92(3)
N(2)-C(16)	1.4762(18)	O(3)-Eu(1)-O(1)	128.40(3)
N(2)-C(15)	1.4849(18)	O(5)-Eu(1)-N(1)	73.29(4)
N(2)-C(8)	1.4862(18)	O(7)-Eu(1)-N(1)	72.19(4)
N(3)-C(10)	1.4701(18)	O(3)-Eu(1)-N(1)	64.11(3)
N(3)-C(9)	1.4805(19)	O(1)-Eu(1)-N(1)	64.30(3)
N(4)-C(18)	1.4740(18)	O(5)-Eu(1)-N(3)	74.19(4)
N(4)-C(12)	1.4794(18)	O(7)-Eu(1)-N(3)	131.85(3)
N(4)-C(11)	1.4867(17)	O(3)-Eu(1)-N(3)	76.99(3)
N(5)-C(14)	1.4712(18)	O(1)-Eu(1)-N(3)	141.63(4)
N(5)-C(13)	1.4752(19)	N(1)-Eu(1)-N(3)	129.60(4)
C(1)-C(2)	1.378(2)	O(5)-Eu(1)-N(5)	130.81(3)
C(1)-C(6)	1.5149(19)	O(7)-Eu(1)-N(5)	73.51(4)
C(2)-C(3)	1.382(2)	O(3)-Eu(1)-N(5)	140.01(4)
C(3)-C(4)	1.387(2)	O(1)-Eu(1)-N(5)	78.18(3)
C(4)-C(5)	1.381(2)	N(1)-Eu(1)-N(5)	130.51(4)
C(5)-C(7)	1.5204(19)	N(3)-Eu(1)-N(5)	99.87(4)
C(8)-C(9)	1.5165(19)	O(5)-Eu(1)-N(4)	140.15(3)
C(10)-C(11)	1.512(2)	O(7)-Eu(1)-N(4)	65.88(3)
C(12)-C(13)	1.5204(18)	O(3)-Eu(1)-N(4)	74.06(3)
C(14)-C(15)	1.510(2)	O(1)-Eu(1)-N(4)	140.21(4)
C(16)-C(17)	1.5274(18)	N(1)-Eu(1)-N(4)	124.77(3)
C(18)-C(19)	1.5346(19)	N(3)-Eu(1)-N(4)	67.50(4)
N(6)-C(32)	1.515(2)	N(5)-Eu(1)-N(4)	68.26(3)
N(6)-C(20)	1.5180(18)	O(5)-Eu(1)-N(2)	65.70(3)
N(6)-C(28)	1.5191(17)	O(7)-Eu(1)-N(2)	138.66(3)
N(6)-C(24)	1.5324(18)	O(3)-Eu(1)-N(2)	140.46(4)
C(20)-C(21)	1.515(2)	O(1)-Eu(1)-N(2)	76.02(3)
C(21)-C(22)	1.517(2)	N(1)-Eu(1)-N(2)	127.27(3)
C(22)-C(23)	1.525(2)	N(3)-Eu(1)-N(2)	68.39(3)

N(5)-Eu(1)-N(2)	66.89(4)	N(1)-C(5)-C(4)	122.14(12)
N(4)-Eu(1)-N(2)	107.96(3)	N(1)-C(5)-C(7)	113.81(11)
O(5)-Eu(1)-C(19)	150.10(3)	C(4)-C(5)-C(7)	124.05(12)
O(7)-Eu(1)-C(19)	19.13(3)	O(4)-C(6)-O(3)	126.74(13)
O(3)-Eu(1)-C(19)	67.47(3)	O(4)-C(6)-C(1)	117.54(12)
O(1)-Eu(1)-C(19)	104.05(3)	O(3)-C(6)-C(1)	115.72(11)
N(1)-Eu(1)-C(19)	81.05(4)	O(2)-C(7)-O(1)	126.38(12)
N(3)-Eu(1)-C(19)	113.07(3)	O(2)-C(7)-C(5)	117.34(12)
N(5)-Eu(1)-C(19)	77.96(3)	O(1)-C(7)-C(5)	116.27(11)
N(4)-Eu(1)-C(19)	49.42(3)	N(2)-C(8)-C(9)	113.08(11)
N(2)-Eu(1)-C(19)	144.18(3)	N(3)-C(9)-C(8)	110.90(12)
O(5)-Eu(1)-C(17)	18.95(3)	N(3)-C(10)-C(11)	110.18(11)
O(7)-Eu(1)-C(17)	149.39(3)	N(4)-C(11)-C(10)	111.80(10)
O(3)-Eu(1)-C(17)	106.25(3)	N(4)-C(12)-C(13)	112.87(11)
O(1)-Eu(1)-C(17)	67.80(3)	N(5)-C(13)-C(12)	110.92(12)
N(1)-Eu(1)-C(17)	83.21(3)	N(5)-C(14)-C(15)	110.31(11)
N(3)-Eu(1)-C(17)	78.09(3)	N(2)-C(15)-C(14)	111.81(10)
N(5)-Eu(1)-C(17)	112.09(3)	N(2)-C(16)-C(17)	114.22(10)
N(4)-Eu(1)-C(17)	144.72(3)	O(6)-C(17)-O(5)	124.68(12)
N(2)-Eu(1)-C(17)	49.13(3)	O(6)-C(17)-C(16)	117.48(11)
C(19)-Eu(1)-C(17)	164.23(3)	O(5)-C(17)-C(16)	117.78(12)
C(7)-O(1)-Eu(1)	124.58(8)	O(6)-C(17)-Eu(1)	156.72(9)
C(6)-O(3)-Eu(1)	125.38(8)	O(5)-C(17)-Eu(1)	37.35(7)
C(17)-O(5)-Eu(1)	123.70(9)	C(16)-C(17)-Eu(1)	81.98(8)
C(19)-O(7)-Eu(1)	122.95(9)	N(4)-C(18)-C(19)	114.36(10)
C(5)-N(1)-C(1)	119.64(12)	O(8)-C(19)-O(7)	124.83(12)
C(5)-N(1)-Eu(1)	120.17(8)	O(8)-C(19)-C(18)	117.69(11)
C(1)-N(1)-Eu(1)	120.18(9)	O(7)-C(19)-C(18)	117.46(12)
C(16)-N(2)-C(15)	109.96(10)	O(8)-C(19)-Eu(1)	156.91(9)
C(16)-N(2)-C(8)	110.94(12)	O(7)-C(19)-Eu(1)	37.92(7)
C(15)-N(2)-C(8)	110.07(11)	C(18)-C(19)-Eu(1)	81.39(8)
C(16)-N(2)-Eu(1)	106.26(8)	C(32)-N(6)-C(20)	111.11(12)
C(15)-N(2)-Eu(1)	109.53(9)	C(32)-N(6)-C(28)	111.06(11)
C(8)-N(2)-Eu(1)	110.01(7)	C(20)-N(6)-C(28)	106.47(10)
C(10)-N(3)-C(9)	112.36(11)	C(32)-N(6)-C(24)	107.12(10)
C(10)-N(3)-Eu(1)	115.53(9)	C(20)-N(6)-C(24)	110.25(11)
C(9)-N(3)-Eu(1)	112.53(8)	C(28)-N(6)-C(24)	110.88(12)
C(18)-N(4)-C(12)	110.77(12)	C(21)-C(20)-N(6)	115.37(11)
C(18)-N(4)-C(11)	110.10(10)	C(20)-C(21)-C(22)	110.29(12)
C(12)-N(4)-C(11)	110.11(10)	C(21)-C(22)-C(23)	112.28(13)
C(18)-N(4)-Eu(1)	106.19(7)	C(25)-C(24)-N(6)	115.44(11)
C(12)-N(4)-Eu(1)	110.73(7)	C(24)-C(25)-C(26)	110.51(13)
C(11)-N(4)-Eu(1)	108.86(8)	C(27)-C(26)-C(25)	111.36(15)
C(14)-N(5)-C(13)	112.65(11)	N(6)-C(28)-C(29)	115.23(11)
C(14)-N(5)-Eu(1)	115.90(9)	C(30)-C(29)-C(28)	111.91(13)
C(13)-N(5)-Eu(1)	112.07(7)	C(31)-C(30)-C(29)	116.42(16)
N(1)-C(1)-C(2)	121.55(12)	N(6)-C(32)-C(33)	115.56(11)
N(1)-C(1)-C(6)	113.93(12)	C(34)-C(33)-C(32)	111.05(11)
C(2)-C(1)-C(6)	124.52(12)	C(33)-C(34)-C(35)	113.03(12)
C(1)-C(2)-C(3)	119.04(13)	O(51)-C(52)-C(51)	119.1(4)
C(2)-C(3)-C(4)	119.21(14)	O(51)-C(52)-C(53)	123.9(4)
C(5)-C(4)-C(3)	118.41(13)	C(51)-C(52)-C(53)	116.9(3)

O(61)-C(62)-C(61)	133.0(12)
O(61)-C(62)-C(63)	103.8(10)
C(61)-C(62)-C(63)	123.0(10)

Table 5. Anisotropic displacement parameters ($Å^2 x\ 10^4$) for MLC18 (CCDC 761599). The anisotropic displacement factor exponent takes the form: $-2\pi^2[h^2 a^{*2} U^{11} + ... + 2\ h\ k\ a^*\ b^*\ U^{12}]$

	U^{11}	U^{22}	U^{33}	U^{23}	U^{13}	U^{12}
Eu(1)	130(1)	164(1)	114(1)	17(1)	11(1)	19(1)
O(1)	211(6)	207(5)	138(4)	-4(3)	-5(4)	36(4)
O(2)	816(11)	293(6)	152(5)	-67(4)	-98(6)	111(6)
O(3)	195(6)	228(5)	160(4)	42(3)	-11(4)	10(4)
O(4)	367(8)	291(6)	265(5)	151(4)	-89(5)	-43(5)
O(5)	161(5)	216(5)	149(4)	27(3)	25(3)	18(4)
O(6)	273(6)	239(5)	172(4)	-9(4)	71(4)	26(4)
O(7)	166(5)	248(5)	134(4)	-1(3)	19(3)	-3(4)
O(8)	197(6)	195(5)	162(4)	26(3)	32(4)	19(4)
N(1)	144(6)	195(5)	164(5)	28(3)	24(4)	7(4)
N(2)	181(6)	197(5)	168(5)	30(4)	10(4)	31(4)
N(3)	162(6)	184(5)	178(5)	19(4)	5(4)	18(4)
N(4)	158(6)	204(5)	146(5)	3(4)	6(4)	-2(4)
N(5)	162(6)	217(6)	168(5)	-2(4)	-2(4)	31(4)
C(1)	169(7)	218(7)	225(6)	67(5)	-2(5)	-5(5)
C(2)	359(11)	226(8)	389(9)	93(6)	-95(8)	6(7)
C(3)	440(12)	182(7)	478(10)	1(7)	-99(9)	0(7)
C(4)	266(9)	236(7)	294(7)	-34(5)	-17(6)	-7(6)
C(5)	158(7)	211(6)	183(6)	5(5)	34(5)	13(5)
C(6)	169(7)	262(7)	196(6)	75(5)	-2(5)	-19(5)
C(7)	223(8)	234(7)	147(5)	-12(5)	30(5)	37(5)
C(8)	240(8)	194(7)	236(6)	51(5)	11(6)	-5(5)
C(9)	172(7)	220(7)	217(6)	22(5)	24(5)	-12(5)
C(10)	183(8)	219(7)	224(6)	-21(5)	-2(5)	-21(5)
C(11)	191(8)	243(7)	170(6)	-27(5)	-11(5)	-10(5)
C(12)	192(8)	224(7)	207(6)	-39(5)	8(5)	42(5)
C(13)	163(7)	231(7)	211(6)	-16(5)	19(5)	49(5)
C(14)	221(8)	221(7)	250(7)	42(5)	7(6)	78(6)
C(15)	216(8)	235(7)	208(6)	76(5)	-2(5)	61(6)
C(16)	211(8)	254(7)	147(5)	44(5)	31(5)	43(5)
C(17)	140(6)	194(6)	146(5)	-1(4)	1(4)	-27(5)
C(18)	196(7)	253(7)	138(5)	-2(4)	18(5)	-23(5)
C(19)	145(7)	190(6)	155(5)	8(4)	9(4)	42(5)
N(6)	166(6)	242(6)	202(5)	101(4)	-22(4)	-20(5)
C(20)	199(8)	237(7)	200(6)	87(5)	-31(5)	-35(5)
C(21)	315(10)	316(8)	211(7)	66(6)	-41(6)	-58(7)
C(22)	309(10)	324(8)	242(7)	36(6)	-17(6)	-65(7)
C(23)	420(12)	418(10)	319(8)	-25(7)	-33(8)	-96(9)
C(24)	178(8)	298(8)	280(7)	168(6)	-37(6)	-5(6)
C(25)	187(8)	365(9)	331(8)	187(6)	-31(6)	-3(7)
C(26)	236(11)	624(13)	724(14)	446(11)	-39(10)	54(9)
C(27)	207(11)	664(14)	807(16)	367(12)	-17(10)	65(10)
C(28)	198(8)	252(7)	206(6)	65(5)	-20(5)	4(5)
C(29)	400(12)	300(9)	371(9)	41(6)	7(8)	-133(8)
C(30)	632(15)	268(9)	389(10)	-26(7)	-157(10)	63(9)

C(31)	686(19)	479(13)	734(16)	-205(11)	-45(14)	-157(12)
C(32)	180(8)	291(7)	225(6)	107(5)	-12(5)	-38(6)
C(33)	199(8)	355(8)	225(7)	109(6)	4(6)	18(6)
C(34)	258(9)	297(8)	252(7)	63(5)	48(6)	-2(6)
C(35)	269(10)	395(10)	394(9)	61(7)	86(7)	36(7)
O(41)	403(8)	249(5)	179(4)	-4(4)	64(4)	95(5)
O(42)	461(9)	430(7)	229(5)	46(5)	59(5)	-184(6)
O(43)	902(17)	1005(15)	850(13)	180(11)	175(12)	-21(13)
O(44)	850(20)	802(17)	423(12)	-117(11)	-116(12)	469(14)
O(51)	950(20)	216(9)	523(12)	40(8)	-274(13)	9(10)
C(51)	420(20)	750(30)	540(20)	-178(19)	-84(19)	166(18)
C(52)	740(30)	178(12)	422(16)	60(10)	-114(17)	127(13)
C(53)	920(50)	1500(60)	920(40)	550(40)	-370(30)	-390(50)

Table 6. Hydrogen bonds for MLC18 (CCDC 761599) [Å and °].

D-H...A	d(D-H)	d(H...A)	d(D...A)	<(DHA)
N(3)-H(3)...O(5)#1	0.93	2.18	3.0310(15)	151.2
N(3)-H(3)...O(6)#1	0.93	2.50	3.2799(14)	141.9
N(5)-H(5)...O(7)#2	0.93	2.20	3.0464(16)	150.6
N(5)-H(5)...O(8)#2	0.93	2.44	3.2325(13)	143.6
O(41)-H(41A)...O(8)#3	0.75	2.05	2.7908(15)	170.8
O(41)-H(41B)...O(2)#1	0.74	2.13	2.8745(14)	179.0
O(42)-H(42A)...O(6)	0.77	2.10	2.8418(16)	163.0
O(42)-H(42B)...O(4)#1	0.80	2.06	2.8542(15)	171.9
O(43)-H(43A)...O(6)#4	0.59	2.45	2.853(2)	128.9
O(43)-H(43B)...O(2)#4	0.94	2.40	3.309(3)	163.3
O(44)-H(44A)...O(42)#5	0.82	2.03	2.854(2)	177.2
O(44)-H(44B)...O(43)#5	0.81	2.01	2.808(3)	166.9

Symmetry transformations used to generate equivalent atoms:
#1 -x+1,-y+1,-z+1
#2 -x+2,-y+1,-z+1
#3 x-1,y,z
#4 -x+1,y-1/2,-z+3/2
#5 -x+1,y+1/2,-z+3/2

CALIFORNIA INSTITUTE OF TECHNOLOGY

BECKMAN INSTITUTE

X-RAY CRYSTALLOGRAPHY LABORATORY

Date 21 January 2010

Crystal Structure Analysis of:

MLC17

(shown below)

For Investigator: Morgan Cable ext. (818) 354-4345

Advisor: Adrian Ponce ext. (818) 354-8196

Account Number: AP1.HSARPA3-1-HSARPA.PONCE

By Michael W. Day 116 Beckman ext. 2734

e-mail: mikeday@caltech.edu

Contents

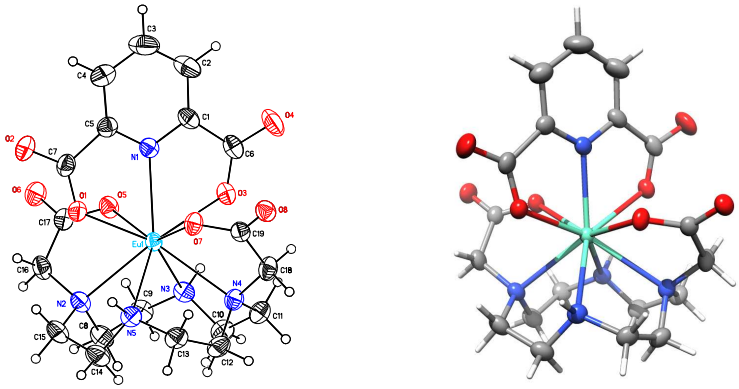

MLC17

Note: The crystallographic data have been deposited in the Cambridge Database (CCDC) and has been placed on hold pending further instructions from me. The deposition number is 762705. Ideally the CCDC would like the publication to contain a footnote of the type: "Crystallographic data have been deposited at the CCDC, 12 Union Road, Cambridge CB2 1EZ, UK and copies can be obtained on request, free of charge, by quoting the publication citation and the deposition number 762705."

Table 1. Crystal data and structure refinement for MLC18 (CCDC 762705).

Empirical formula	$[C_{19}H_{25}N_5O_8Eu]^-$ $[C_{16}H_{36}N]^+ \bullet C_3H_6O \bullet 3.68(H_2O)$
Formula weight	970.23
Crystallization Solvent	Acetone
Crystal Habit	Fragment
Crystal size	0.22 x 0.19 x 0.15 mm^3
Crystal color	Colorless

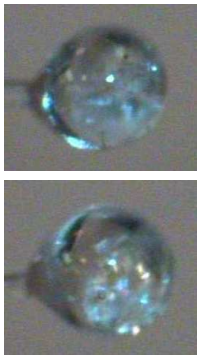

Data Collection

Type of diffractometer	Bruker KAPPA APEX II
Wavelength	0.71073 Å MoKα
Data Collection Temperature	200(2) K
θ range for 9964 reflections used in lattice determination	2.21 to 33.31°
Unit cell dimensions	a = 13.1516(5) Å b = 13.5276(5) Å β= 90.701(2)° c = 26.1946(9) Å
Volume	4659.9(3) $Å^3$
Z	4
Crystal system	Monoclinic
Space group	P $2_1/c$
Density (calculated)	1.383 Mg/m^3
F(000)	2035
θ range for data collection	1.55 to 39.51°
Completeness to θ = 39.51°	99.7 %
Index ranges	$-23 \le h \le 23$, $-24 \le k \le 23$, $-46 \le l \le 46$
Data collection scan type	ω scans; 17 settings
Reflections collected	197040
Independent reflections	27945 [R_{int}= 0.0446]
Absorption coefficient	1.409 mm^{-1}
Absorption correction	Semi-empirical from equivalents
Max. and min. transmission	0.7478 and 0.6642

Table 1 (cont.)

Structure solution and Refinement

Structure solution program	SHELXS-97 (Sheldrick, 2008)
Primary solution method	Direct methods
Secondary solution method	Difference Fourier map
Hydrogen placement	Geometric positions
Structure refinement program	SHELXL-97 (Sheldrick, 2008)
Refinement method	Full matrix least-squares on F^2
Data / restraints / parameters	27945 / 0 / 546
Treatment of hydrogen atoms	Riding
Goodness-of-fit on F^2	1.916
Final R indices [$I>2\sigma(I)$, 16515 reflections]	R1 = 0.0337, *w*R2 = 0.0550
R indices (all data)	R1 = 0.0775, *w*R2 = 0.0576
Type of weighting scheme used	Sigma
Weighting scheme used	$w=1/\sigma^2(Fo^2)$
Max shift/error	0.007
Average shift/error	0.000
Largest diff. peak and hole	1.688 and -2.002 e.Å^{-3}

Special Refinement Details

Crystals were mounted on a glass fiber using Paratone oil then coated in epoxy and placed on the diffractometer under a nitrogen stream at 200K.

This is the same exact crystal as MLC18. ∴ The asymmetric unit contains acetone at one site that is disordered between two orientations. **This acetone site was refined as a rigid body starting with the coordinates from MLC18.** The major orientation (69%), O51-C53 is accompanied by a water molecule, O44, that is hydrogen bonded to two other waters, O42 and O43. The minor orientation does not contain a discernable water. Hydrogen atoms on water were located in the electron density difference map and were constrained to ride the appropriate oxygen. All other hydrogens were placed at geometric positions and refined as riding atoms. No other restraints were placed on the model.

Refinement of F^2 against ALL reflections. The weighted R-factor (*w*R) and goodness of fit (S) are based on F^2, conventional R-factors (R) are based on F, with F set to zero for negative F^2. The threshold expression of $F^2 > 2\sigma(F^2)$ is used only for calculating R-factors(gt) etc. and is not relevant to the choice of reflections for refinement. R-factors based on F^2 are statistically about twice as large as those based on F, and R-factors based on ALL data will be even larger.

All esds (except the esd in the dihedral angle between two l.s. planes) are estimated using the full covariance matrix. The cell esds are taken into account individually in the estimation of esds in distances, angles and torsion angles; correlations between esds in cell parameters are only used when they are defined by crystal symmetry. An approximate (isotropic) treatment of cell esds is used for estimating esds involving l.s. planes.

E20

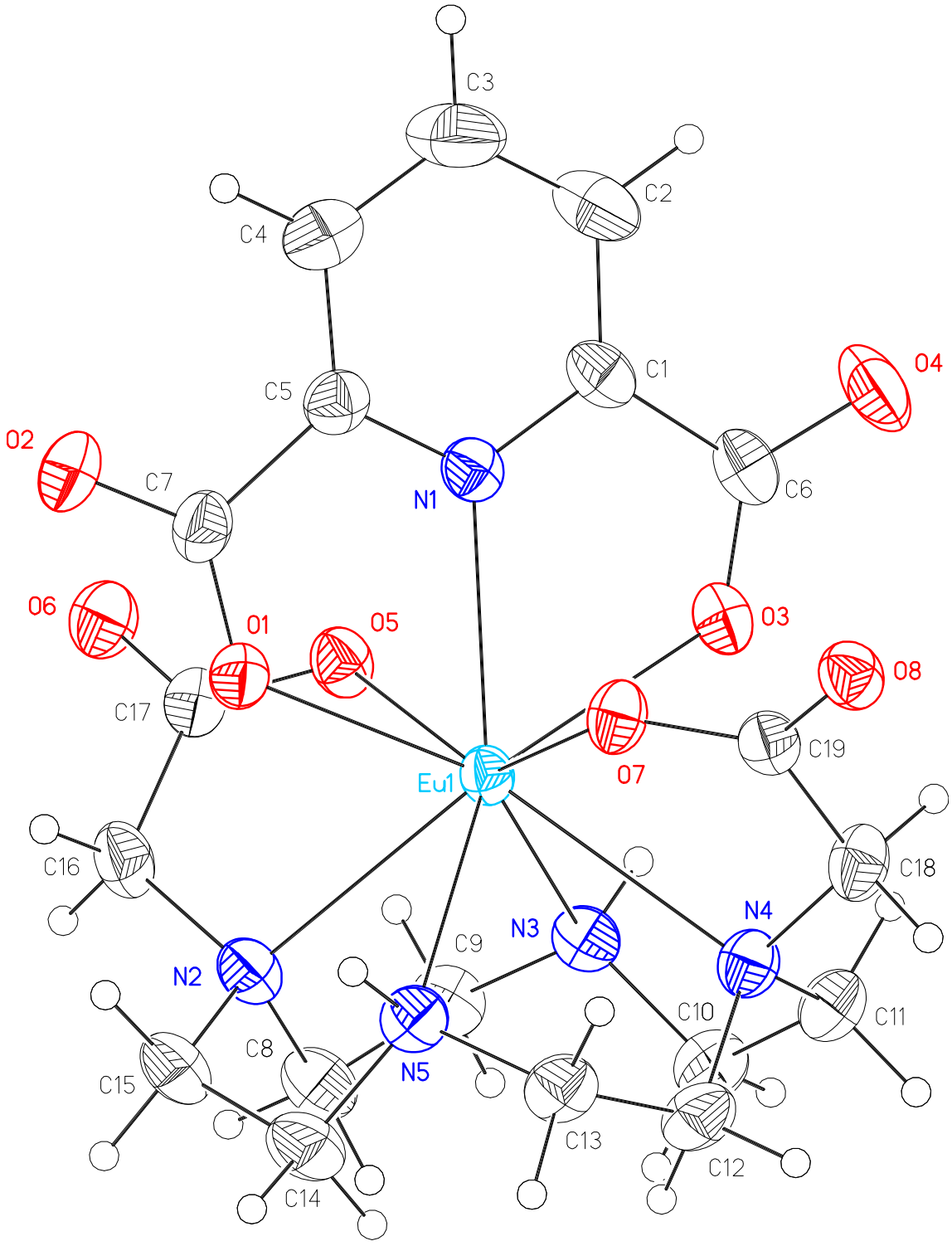
C3
C2
C4
C1
C5
O4
O2
C7
N1
C6
O6
O1
O5
O3
O8
C17
O7
C19
Eu1
C16
C18
N3
N4
N2
C9
C10
C11
C8
N5
C15
C13
C12
C14

E21

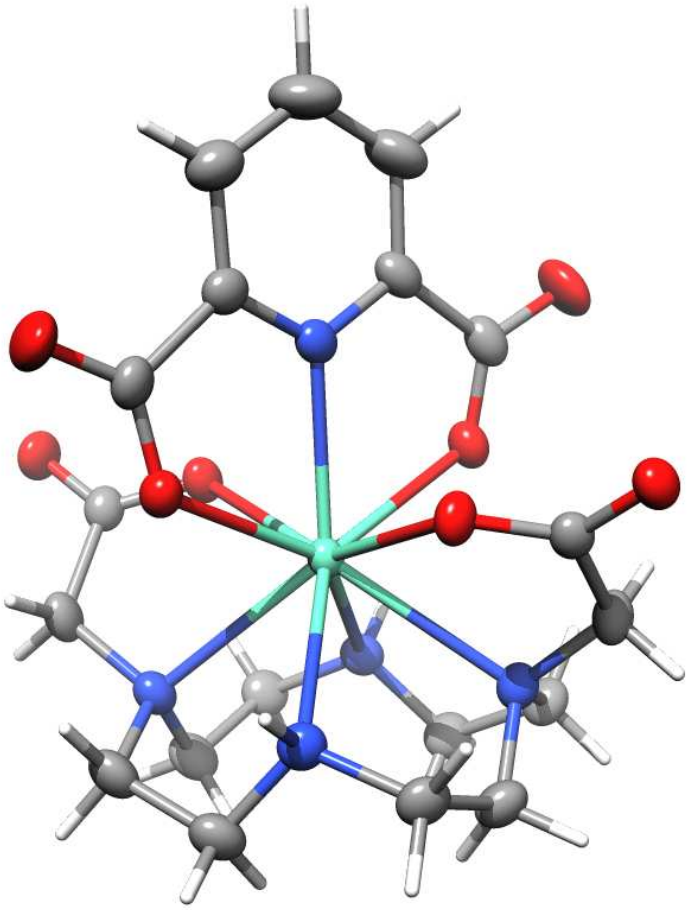

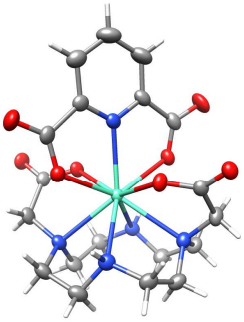

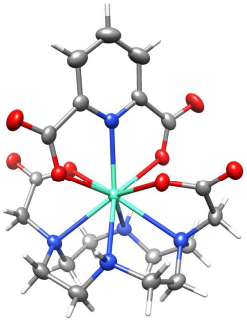

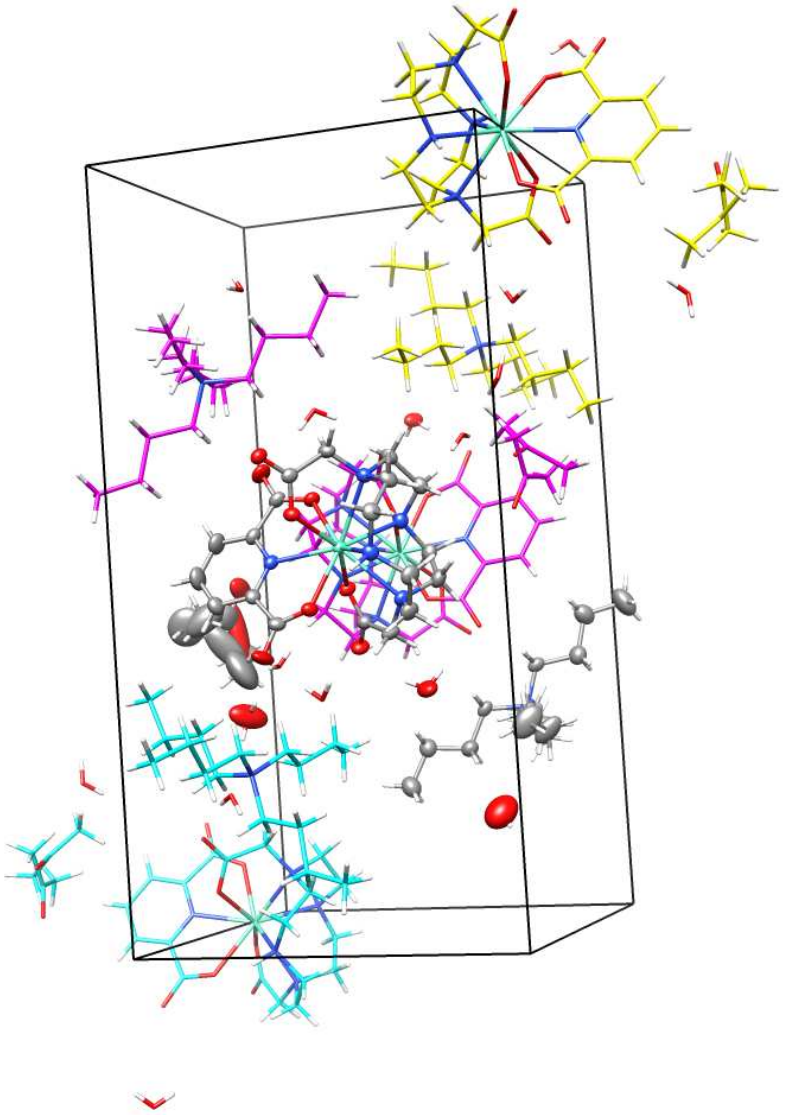

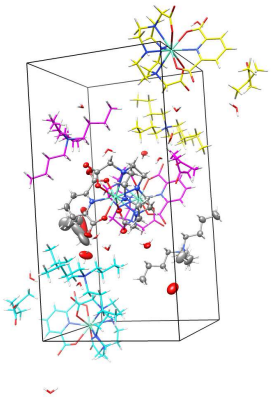

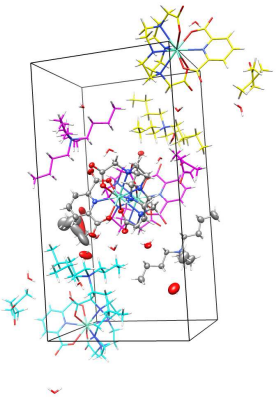

Table 2. Atomic coordinates (x 10^4) and equivalent isotropic displacement parameters ($Å^2$x 10^3) for MLC18 (CCDC 762705). U(eq) is defined as the trace of the orthogonalized U^{ij} tensor.

	x	y	z	U_{eq}	Occ
Eu(1)	7497(1)	4924(1)	5002(1)	22(1)	1
O(1)	8318(1)	5503(1)	5774(1)	30(1)	1
O(2)	8635(1)	6689(1)	6344(1)	57(1)	1
O(3)	6704(1)	5883(1)	4331(1)	31(1)	1
O(4)	6440(1)	7318(1)	3928(1)	49(1)	1
O(5)	6066(1)	5318(1)	5508(1)	30(1)	1
O(6)	5343(1)	5340(1)	6267(1)	38(1)	1
O(7)	8962(1)	5558(1)	4586(1)	29(1)	1
O(8)	9664(1)	6037(1)	3861(1)	31(1)	1
N(1)	7518(1)	6761(1)	5125(1)	26(1)	1
N(2)	7028(1)	3546(1)	5693(1)	30(1)	1
N(3)	6050(1)	3786(1)	4684(1)	29(1)	1
N(4)	7952(1)	3999(1)	4138(1)	28(1)	1
N(5)	8919(1)	3621(1)	5135(1)	29(1)	1
C(1)	7140(1)	7353(1)	4760(1)	31(1)	1
C(2)	7142(2)	8365(1)	4818(1)	47(1)	1
C(3)	7536(2)	8768(1)	5261(1)	54(1)	1
C(4)	7922(1)	8152(1)	5639(1)	41(1)	1
C(5)	7908(1)	7148(1)	5554(1)	29(1)	1
C(6)	6725(1)	6814(1)	4299(1)	32(1)	1
C(7)	8320(1)	6385(1)	5927(1)	32(1)	1
C(8)	6325(1)	2807(1)	5463(1)	37(1)	1
C(9)	5549(1)	3258(1)	5104(1)	34(1)	1
C(10)	6316(1)	3130(1)	4260(1)	34(1)	1
C(11)	6993(1)	3656(1)	3888(1)	33(1)	1
C(12)	8635(1)	3148(1)	4239(1)	35(1)	1
C(13)	9416(1)	3355(1)	4654(1)	33(1)	1
C(14)	8644(1)	2754(1)	5442(1)	37(1)	1
C(15)	7972(1)	3056(1)	5876(1)	36(1)	1
C(16)	6543(1)	4078(1)	6117(1)	34(1)	1
C(17)	5920(1)	4975(1)	5953(1)	28(1)	1
C(18)	8457(1)	4740(1)	3813(1)	32(1)	1
C(19)	9088(1)	5502(1)	4108(1)	26(1)	1
N(6)	1373(1)	2174(1)	7200(1)	32(1)	1
C(20)	1689(1)	3253(1)	7206(1)	35(1)	1
C(21)	1859(2)	3693(1)	7731(1)	47(1)	1
C(22)	2105(2)	4778(1)	7694(1)	51(1)	1
C(23)	2323(2)	5245(2)	8210(1)	67(1)	1
C(24)	2198(1)	1537(1)	7459(1)	38(1)	1
C(25)	3251(1)	1663(1)	7258(1)	46(1)	1
C(26)	3977(2)	916(2)	7495(1)	75(1)	1
C(27)	5075(2)	1135(2)	7364(1)	94(1)	1
C(28)	1239(1)	1888(1)	6643(1)	35(1)	1
C(29)	929(2)	818(1)	6546(1)	51(1)	1
C(30)	719(2)	622(1)	5996(1)	64(1)	1

C(31)	479(2)	-427(2)	5861(1)	98(1)	1
C(32)	401(1)	2017(1)	7491(1)	36(1)	1
C(33)	-522(1)	2572(1)	7294(1)	44(1)	1
C(34)	-1373(1)	2546(1)	7670(1)	47(1)	1
C(35)	-2331(2)	3068(2)	7492(1)	66(1)	1
O(41)	733(1)	5045(1)	3100(1)	48(1)	1
O(42)	4224(1)	3983(1)	6873(1)	64(1)	1
O(43)	3931(2)	2311(2)	8542(1)	141(1)	1
O(44)	5079(3)	8661(2)	7101(1)	125(1)	0.687(3)
O(51)	3577(2)	9293(1)	5363(1)	97(1)	0.687(3)
C(51)	3473(3)	9448(3)	6226(1)	112(2)	0.687(3)
C(52)	4047(2)	9495(1)	5753(1)	70(1)	0.687(3)
C(53)	5149(2)	9716(4)	5768(2)	172(4)	0.687(3)
O(61)	3595(2)	9410(2)	6019(1)	289(12)	0.313(3)
C(61)	4986(4)	8804(3)	6471(1)	184(7)	0.313(3)
C(62)	4456(2)	9461(2)	6145(1)	199(11)	0.313(3)
C(63)	5036(3)	10280(4)	5847(2)	173(9)	0.313(3)

Table 3. Selected bond lengths [Å] and angles [°] for MLC18 (CCDC 762705).

Eu(1)-O(5)	2.3757(11)	O(5)-Eu(1)-O(7)	145.56(3)
Eu(1)-O(7)	2.3837(10)	O(5)-Eu(1)-O(3)	86.96(3)
Eu(1)-O(3)	2.4098(8)	O(7)-Eu(1)-O(3)	79.58(3)
Eu(1)-O(1)	2.4126(8)	O(5)-Eu(1)-O(1)	78.97(3)
Eu(1)-N(1)	2.5051(10)	O(7)-Eu(1)-O(1)	84.90(3)
Eu(1)-N(3)	2.5785(11)	O(3)-Eu(1)-O(1)	128.47(3)
Eu(1)-N(5)	2.5907(11)	O(5)-Eu(1)-N(1)	73.33(4)
Eu(1)-N(4)	2.6606(11)	O(7)-Eu(1)-N(1)	72.26(4)
Eu(1)-N(2)	2.6758(11)	O(3)-Eu(1)-N(1)	64.19(3)
		O(1)-Eu(1)-N(1)	64.27(3)
		O(5)-Eu(1)-N(3)	74.15(4)
		O(7)-Eu(1)-N(3)	131.66(3)
		O(3)-Eu(1)-N(3)	76.99(3)
		O(1)-Eu(1)-N(3)	141.75(4)
		N(1)-Eu(1)-N(3)	129.84(4)
		O(5)-Eu(1)-N(5)	130.74(3)
		O(7)-Eu(1)-N(5)	73.75(4)
		O(3)-Eu(1)-N(5)	140.34(4)
		O(1)-Eu(1)-N(5)	78.05(3)
		N(1)-Eu(1)-N(5)	130.62(4)
		N(3)-Eu(1)-N(5)	99.53(4)
		O(5)-Eu(1)-N(4)	140.17(3)
		O(7)-Eu(1)-N(4)	65.73(3)
		O(3)-Eu(1)-N(4)	74.54(3)
		O(1)-Eu(1)-N(4)	139.74(4)
		N(1)-Eu(1)-N(4)	125.05(3)
		N(3)-Eu(1)-N(4)	67.51(4)
		N(5)-Eu(1)-N(4)	67.97(3)
		O(5)-Eu(1)-N(2)	65.64(3)
		O(7)-Eu(1)-N(2)	138.93(3)
		O(3)-Eu(1)-N(2)	140.00(4)
		O(1)-Eu(1)-N(2)	76.30(3)
		N(1)-Eu(1)-N(2)	127.27(4)
		N(3)-Eu(1)-N(2)	68.07(3)
		N(5)-Eu(1)-N(2)	66.85(4)
		N(4)-Eu(1)-N(2)	107.68(4)

Table 4. Bond lengths [Å] and angles [°] for MLC18 (CCDC 762705).

Eu(1)-O(5)	2.3757(11)	C(26)-C(27)	1.517(3)
Eu(1)-O(7)	2.3837(10)	C(28)-C(29)	1.525(2)
Eu(1)-O(3)	2.4098(8)	C(29)-C(30)	1.489(2)
Eu(1)-O(1)	2.4126(8)	C(30)-C(31)	1.496(3)
Eu(1)-N(1)	2.5051(10)	C(32)-C(33)	1.512(2)
Eu(1)-N(3)	2.5785(11)	C(33)-C(34)	1.500(3)
Eu(1)-N(5)	2.5907(11)	C(34)-C(35)	1.513(3)
Eu(1)-N(4)	2.6606(11)	O(51)-C(52)	1.2187
Eu(1)-N(2)	2.6758(11)	C(51)-C(52)	1.4609
O(1)-C(7)	1.2582(16)	C(52)-C(53)	1.4807
O(2)-C(7)	1.2348(15)	O(61)-C(62)	1.1779
O(3)-C(6)	1.2636(16)	C(61)-C(62)	1.4098
O(4)-C(6)	1.2407(15)	C(62)-C(63)	1.5596
O(5)-C(17)	1.2715(16)		
O(6)-C(17)	1.2309(18)	O(5)-Eu(1)-O(7)	145.56(3)
O(7)-C(19)	1.2668(16)	O(5)-Eu(1)-O(3)	86.96(3)
O(8)-C(19)	1.2358(17)	O(7)-Eu(1)-O(3)	79.58(3)
N(1)-C(5)	1.3351(16)	O(5)-Eu(1)-O(1)	78.97(3)
N(1)-C(1)	1.3381(16)	O(7)-Eu(1)-O(1)	84.90(3)
N(2)-C(16)	1.4759(19)	O(3)-Eu(1)-O(1)	128.47(3)
N(2)-C(8)	1.4840(18)	O(5)-Eu(1)-N(1)	73.33(4)
N(2)-C(15)	1.4837(18)	O(7)-Eu(1)-N(1)	72.26(4)
N(3)-C(10)	1.4676(19)	O(3)-Eu(1)-N(1)	64.19(3)
N(3)-C(9)	1.473(2)	O(1)-Eu(1)-N(1)	64.27(3)
N(4)-C(18)	1.4762(19)	O(5)-Eu(1)-N(3)	74.15(4)
N(4)-C(12)	1.4820(18)	O(7)-Eu(1)-N(3)	131.66(3)
N(4)-C(11)	1.4880(17)	O(3)-Eu(1)-N(3)	76.99(3)
N(5)-C(14)	1.4700(19)	O(1)-Eu(1)-N(3)	141.75(4)
N(5)-C(13)	1.471(2)	N(1)-Eu(1)-N(3)	129.84(4)
C(1)-C(2)	1.376(2)	O(5)-Eu(1)-N(5)	130.74(3)
C(1)-C(6)	1.509(2)	O(7)-Eu(1)-N(5)	73.75(4)
C(2)-C(3)	1.378(2)	O(3)-Eu(1)-N(5)	140.34(4)
C(3)-C(4)	1.384(2)	O(1)-Eu(1)-N(5)	78.05(3)
C(4)-C(5)	1.3764(19)	N(1)-Eu(1)-N(5)	130.62(4)
C(5)-C(7)	1.5171(19)	N(3)-Eu(1)-N(5)	99.53(4)
C(8)-C(9)	1.5087(19)	O(5)-Eu(1)-N(4)	140.17(3)
C(10)-C(11)	1.506(2)	O(7)-Eu(1)-N(4)	65.73(3)
C(12)-C(13)	1.5126(19)	O(3)-Eu(1)-N(4)	74.54(3)
C(14)-C(15)	1.506(2)	O(1)-Eu(1)-N(4)	139.74(4)
C(16)-C(17)	1.5231(19)	N(1)-Eu(1)-N(4)	125.05(3)
C(18)-C(19)	1.5271(19)	N(3)-Eu(1)-N(4)	67.51(4)
N(6)-C(28)	1.5164(18)	N(5)-Eu(1)-N(4)	67.97(3)
N(6)-C(20)	1.5185(17)	O(5)-Eu(1)-N(2)	65.64(3)
N(6)-C(32)	1.512(2)	O(7)-Eu(1)-N(2)	138.93(3)
N(6)-C(24)	1.5363(18)	O(3)-Eu(1)-N(2)	140.00(4)
C(20)-C(21)	1.514(2)	O(1)-Eu(1)-N(2)	76.30(3)
C(21)-C(22)	1.507(2)	N(1)-Eu(1)-N(2)	127.27(4)
C(22)-C(23)	1.516(3)	N(3)-Eu(1)-N(2)	68.07(3)
C(24)-C(25)	1.498(2)	N(5)-Eu(1)-N(2)	66.85(4)
C(25)-C(26)	1.518(2)	N(4)-Eu(1)-N(2)	107.68(4)

C(7)-O(1)-Eu(1)	124.94(8)	N(4)-C(18)-C(19)	114.39(11)
C(6)-O(3)-Eu(1)	125.18(8)	O(8)-C(19)-O(7)	124.80(13)
C(17)-O(5)-Eu(1)	124.03(9)	O(8)-C(19)-C(18)	117.64(12)
C(19)-O(7)-Eu(1)	123.11(9)	O(7)-C(19)-C(18)	117.54(13)
C(5)-N(1)-C(1)	120.01(11)	C(28)-N(6)-C(20)	106.45(10)
C(5)-N(1)-Eu(1)	120.09(8)	C(28)-N(6)-C(32)	111.17(11)
C(1)-N(1)-Eu(1)	119.90(8)	C(20)-N(6)-C(32)	111.27(12)
C(16)-N(2)-C(8)	111.13(13)	C(28)-N(6)-C(24)	110.81(12)
C(16)-N(2)-C(15)	109.96(10)	C(20)-N(6)-C(24)	110.02(11)
C(8)-N(2)-C(15)	110.17(11)	C(32)-N(6)-C(24)	107.16(10)
C(16)-N(2)-Eu(1)	106.02(8)	C(21)-C(20)-N(6)	115.13(11)
C(8)-N(2)-Eu(1)	110.09(8)	C(20)-C(21)-C(22)	110.72(13)
C(15)-N(2)-Eu(1)	109.38(9)	C(21)-C(22)-C(23)	112.73(15)
C(10)-N(3)-C(9)	112.60(11)	C(25)-C(24)-N(6)	115.61(12)
C(10)-N(3)-Eu(1)	115.08(9)	C(24)-C(25)-C(26)	111.09(14)
C(9)-N(3)-Eu(1)	112.59(8)	C(25)-C(26)-C(27)	111.85(17)
C(18)-N(4)-C(12)	110.76(13)	N(6)-C(28)-C(29)	115.41(12)
C(18)-N(4)-C(11)	110.10(10)	C(30)-C(29)-C(28)	112.05(14)
C(12)-N(4)-C(11)	110.16(10)	C(31)-C(30)-C(29)	115.69(18)
C(18)-N(4)-Eu(1)	106.11(8)	N(6)-C(32)-C(33)	116.01(12)
C(12)-N(4)-Eu(1)	110.86(8)	C(34)-C(33)-C(32)	111.51(13)
C(11)-N(4)-Eu(1)	108.76(9)	C(33)-C(34)-C(35)	114.37(14)
C(14)-N(5)-C(13)	112.86(11)	O(51)-C(52)-C(51)	116.1
C(14)-N(5)-Eu(1)	115.76(9)	O(51)-C(52)-C(53)	123.7
C(13)-N(5)-Eu(1)	112.23(8)	C(51)-C(52)-C(53)	120.1
N(1)-C(1)-C(2)	121.13(13)	O(61)-C(62)-C(61)	126.8
N(1)-C(1)-C(6)	114.23(11)	O(61)-C(62)-C(63)	112.0
C(2)-C(1)-C(6)	124.64(12)	C(61)-C(62)-C(63)	120.7
C(1)-C(2)-C(3)	119.07(14)		
C(2)-C(3)-C(4)	119.63(14)		
C(5)-C(4)-C(3)	118.29(14)		
N(1)-C(5)-C(4)	121.86(12)		
N(1)-C(5)-C(7)	113.87(11)		
C(4)-C(5)-C(7)	124.27(12)		
O(4)-C(6)-O(3)	126.46(13)		
O(4)-C(6)-C(1)	117.70(12)		
O(3)-C(6)-C(1)	115.83(11)		
O(2)-C(7)-O(1)	126.53(13)		
O(2)-C(7)-C(5)	117.24(12)		
O(1)-C(7)-C(5)	116.22(11)		
N(2)-C(8)-C(9)	113.17(11)		
N(3)-C(9)-C(8)	110.89(13)		
N(3)-C(10)-C(11)	110.58(11)		
N(4)-C(11)-C(10)	111.67(11)		
N(4)-C(12)-C(13)	112.87(11)		
N(5)-C(13)-C(12)	110.88(13)		
N(5)-C(14)-C(15)	110.35(12)		
N(2)-C(15)-C(14)	111.86(11)		
N(2)-C(16)-C(17)	114.26(11)		
O(6)-C(17)-O(5)	124.67(13)		
O(6)-C(17)-C(16)	117.67(12)		
O(5)-C(17)-C(16)	117.59(13)		

Table 5. Anisotropic displacement parameters ($Å^2 x\ 10^4$) for MLC18 (CCDC 762705). The anisotropic displacement factor exponent takes the form: $-2\pi^2[h^2 a^{*2} U^{11} + ... + 2\ h\ k\ a^*\ b^*\ U^{12}]$

	U^{11}	U^{22}	U^{33}	U^{23}	U^{13}	U^{12}
Eu(1)	220(1)	247(1)	202(1)	18(1)	16(1)	14(1)
O(1)	343(6)	308(5)	241(5)	-8(4)	-20(4)	38(4)
O(2)	970(12)	465(6)	264(5)	-98(5)	-133(6)	76(6)
O(3)	322(6)	341(5)	258(5)	56(4)	-26(4)	-3(4)
O(4)	621(9)	461(6)	397(6)	204(5)	-125(6)	-32(6)
O(5)	270(6)	347(5)	273(5)	49(4)	52(4)	37(4)
O(6)	413(7)	425(6)	310(5)	-5(4)	119(5)	37(5)
O(7)	266(6)	378(5)	239(5)	-15(4)	41(4)	-28(4)
O(8)	311(6)	315(5)	294(5)	45(4)	54(4)	5(4)
N(1)	242(6)	279(5)	266(6)	26(4)	52(5)	11(4)
N(2)	298(7)	297(6)	295(6)	59(4)	10(5)	31(5)
N(3)	245(7)	295(6)	325(6)	21(4)	-7(5)	10(5)
N(4)	259(7)	317(6)	258(5)	-18(4)	11(5)	-19(5)
N(5)	240(7)	317(6)	317(6)	-12(5)	-15(5)	28(5)
C(1)	274(8)	300(7)	343(7)	88(5)	30(6)	0(6)
C(2)	526(12)	319(8)	567(11)	123(7)	-49(9)	23(8)
C(3)	635(14)	274(8)	701(12)	-19(8)	-50(10)	3(8)
C(4)	448(11)	351(8)	439(9)	-79(6)	14(8)	-11(7)
C(5)	269(8)	299(7)	293(7)	-17(5)	53(6)	9(6)
C(6)	270(9)	380(8)	314(7)	102(6)	3(6)	-14(6)
C(7)	330(9)	378(8)	238(7)	-27(5)	40(6)	27(6)
C(8)	370(10)	332(7)	415(8)	93(6)	26(7)	-46(6)
C(9)	265(9)	349(7)	391(8)	23(6)	31(7)	-59(6)
C(10)	295(9)	346(7)	380(8)	-46(6)	-3(7)	-51(6)
C(11)	322(9)	366(7)	308(7)	-71(6)	-23(6)	-28(6)
C(12)	318(9)	354(7)	367(8)	-86(6)	18(7)	59(6)
C(13)	254(8)	352(7)	373(8)	-34(6)	32(6)	71(6)
C(14)	343(10)	335(7)	446(9)	76(6)	6(7)	93(6)
C(15)	358(10)	352(7)	372(8)	115(6)	-34(7)	66(6)
C(16)	343(9)	405(8)	262(7)	89(5)	56(6)	39(6)
C(17)	254(8)	327(7)	261(6)	-4(5)	9(5)	-42(6)
C(18)	324(9)	403(7)	245(6)	-17(5)	48(6)	-59(6)
C(19)	229(8)	296(7)	268(7)	22(5)	21(6)	48(5)
N(6)	306(7)	347(6)	314(6)	129(5)	-20(5)	-16(5)
C(20)	361(10)	346(7)	348(8)	129(6)	-24(7)	-36(6)
C(21)	566(13)	458(9)	379(9)	67(7)	-47(8)	-78(8)
C(22)	575(14)	467(9)	488(10)	15(7)	9(9)	-97(9)
C(23)	777(18)	605(11)	615(13)	-82(9)	-16(12)	-135(11)
C(24)	321(10)	421(8)	406(8)	196(6)	-38(7)	13(7)
C(25)	338(11)	555(10)	480(9)	221(8)	-13(8)	31(8)
C(26)	418(14)	920(15)	900(16)	495(12)	-22(12)	142(11)
C(27)	391(15)	1120(19)	1320(20)	518(17)	-2(15)	171(13)
C(28)	355(10)	394(8)	303(7)	89(6)	-7(7)	8(6)
C(29)	550(13)	469(9)	511(11)	41(7)	17(9)	-91(8)
C(30)	821(18)	528(11)	565(12)	-65(8)	-137(12)	43(10)

C(31)	1050(20)	800(16)	1070(20)	-354(15)	-104(18)	-162(16)
C(32)	324(9)	412(8)	341(8)	128(6)	13(7)	-39(7)
C(33)	356(10)	551(10)	413(9)	182(7)	31(8)	55(8)
C(34)	433(11)	515(10)	458(10)	98(7)	95(8)	31(8)
C(35)	462(14)	772(14)	759(14)	123(10)	166(11)	113(11)
O(41)	715(10)	407(6)	318(5)	5(4)	118(6)	149(5)
O(42)	807(11)	743(8)	372(7)	39(6)	117(7)	-313(8)
O(43)	1400(20)	1457(18)	1388(19)	312(14)	318(16)	85(16)
O(44)	1580(30)	1330(20)	850(20)	-283(16)	-280(20)	820(20)
O(51)	1740(30)	380(11)	776(17)	36(10)	-398(18)	42(13)
C(51)	900(50)	1790(60)	650(30)	-290(30)	-120(30)	450(40)
C(52)	940(40)	371(17)	790(20)	129(15)	-110(20)	176(18)
C(53)	960(60)	2630(90)	1580(60)	990(60)	80(50)	-210(50)
O(61)	990(100)	610(60)	7100(400)	-780(120)	-580(160)	-10(50)
C(61)	1850(170)	1490(110)	2180(180)	-900(110)	-110(130)	-230(100)
C(62)	1080(140)	2030(170)	2800(200)	-1370(170)	-1080(160)	660(120)
C(63)	950(130)	2190(180)	2030(180)	320(130)	-600(120)	-30(100)

Table 6. Hydrogen bonds for MLC18 (CCDC 762705) [Å and °].

D-H...A	d(D-H)	d(H...A)	d(D...A)	<(DHA)
N(3)-H(3)...O(5)#1	0.93	2.23	3.0715(15)	149.9
N(3)-H(3)...O(6)#1	0.93	2.51	3.2945(15)	142.0
N(5)-H(5)...O(7)#2	0.93	2.24	3.0801(15)	149.4
N(5)-H(5)...O(8)#2	0.93	2.44	3.2385(14)	144.6
O(41)-H(41A)...O(8)#3	0.76	2.05	2.7967(15)	171.2
O(41)-H(41B)...O(2)#1	0.74	2.14	2.8780(14)	178.4
O(42)-H(42A)...O(6)	0.77	2.10	2.8472(17)	163.6
O(42)-H(42B)...O(4)#1	0.80	2.07	2.8658(16)	172.1
O(43)-H(43A)...O(6)#4	0.59	2.47	2.873(2)	127.9
O(43)-H(43B)...O(2)#4	0.95	2.57	3.495(3)	164.4
O(44)-H(44A)...O(42)#5	0.83	2.04	2.864(3)	178.0
O(44)-H(44B)...O(43)#5	0.81	2.02	2.815(4)	165.6

Symmetry transformations used to generate equivalent atoms:
#1 -x+1,-y+1,-z+1
#2 -x+2,-y+1,-z+1
#3 x-1,y,z
#4 -x+1,y-1/2,-z+3/2
#5 -x+1,y+1/2,-z+3/2

E31

CALIFORNIA INSTITUTE OF TECHNOLOGY

BECKMAN INSTITUTE

X-RAY CRYSTALLOGRAPHY LABORATORY

Date 26 January 2010

Crystal Structure Analysis of:

MLC19

(shown below)

For Investigator: Morgan Cable ext. (818) 354-4345

Advisor: Adrian Ponce ext. (818) 354-8196

Account Number: AP1.HSARPA3-1-HSARPA.PONCE

By Michael W. Day 116 Beckman ext. 2734

e-mail: mikeday@caltech.edu

Contents

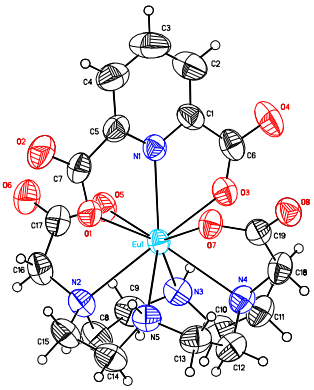

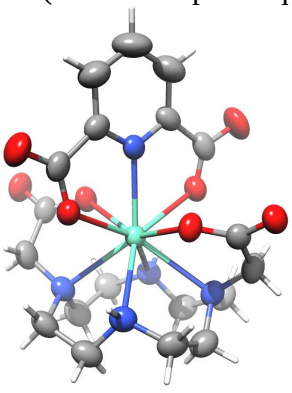

MLC19

Note: The crystallographic data have been deposited in the Cambridge Database (CCDC) and has been placed on hold pending further instructions from me. The deposition number is 763335. Ideally the CCDC would like the publication to contain a footnote of the type: "Crystallographic data have been deposited at the CCDC, 12 Union Road, Cambridge CB2 1EZ, UK and copies can be obtained on request, free of charge, by quoting the publication citation and the deposition number 763335."

Table 1. Crystal data and structure refinement for MLC19 (CCDC 763335).

Empirical formula	$[C_{19}H_{25}N_5O_8Eu]^-$ $[C_{16}H_{36}N]^+ \bullet C_3H_6O \bullet 2.50(H_2O)$
Formula weight	949.07
Crystallization Solvent	Acetone
Crystal Habit	Fragment
Crystal size	0.22 x 0.19 x 0.15 mm^3
Crystal color	Colorless

Data Collection

Type of diffractometer	Bruker KAPPA APEX II
Wavelength	0.71073 Å MoKα
Data Collection Temperature	300(2) K
θ range for 9548 reflections used in lattice determination	2.18 to 27.72°
Unit cell dimensions	a = 13.3306(9) Å b = 13.4557(9) Å β= 90.450(3)° c = 26.3443(17) Å
Volume	4725.3(5) $Å^3$
Z	4
Crystal system	Monoclinic
Space group	P $2_1/c$
Density (calculated)	1.334 Mg/m^3
F(000)	1988
θ range for data collection	1.53 to 39.59°
Completeness to θ = 39.59°	98.5 %
Index ranges	$-23 \le h \le 23$, $-24 \le k \le 23$, $-46 \le l \le 47$
Data collection scan type	ω scans; 19 settings
Reflections collected	220185
Independent reflections	28102 [R_{int}= 0.0620]
Absorption coefficient	1.386 mm^{-1}
Absorption correction	Semi-empirical from equivalents
Max. and min. transmission	0.7477 and 0.6515

Table 1 (cont.)

Structure solution and Refinement

Structure solution program	SHELXS-97 (Sheldrick, 2008)
Primary solution method	Direct methods
Secondary solution method	Difference Fourier map
Hydrogen placement	Geometric positions
Structure refinement program	SHELXL-97 (Sheldrick, 2008)
Refinement method	Full matrix least-squares on F^2
Data / restraints / parameters	28102 / 0 / 482
Treatment of hydrogen atoms	Riding
Goodness-of-fit on F^2	1.682
Final R indices [$I>2\sigma(I)$, 11411 reflections]	R1 = 0.0469, *w*R2 = 0.0623
R indices (all data)	R1 = 0.1399, *w*R2 = 0.0679
Type of weighting scheme used	Sigma
Weighting scheme used	$w=1/\sigma^2(Fo^2)$
Max shift/error	0.014
Average shift/error	0.000
Largest diff. peak and hole	2.053 and -1.042 e.Å^{-3}

Special Refinement Details

Crystals were mounted on a glass fiber using Paratone oil then coated in epoxy and placed on the diffractometer under a nitrogen stream at 300K.

This is the same exact crystal as MLC18. ∴ The asymmetric unit contains acetone at one site that is disordered between two orientations. **This acetone site was refined as a rigid body starting with the coordinates from MLC18.** The relative occupancies refine to different ratios than the lower temperature studies, with the major orientation (50.3%), O51-C53 accompanied by a water molecule, O44, that is hydrogen bonded to two other waters, O42 and O43. The minor orientation does not contain a discernable water. Hydrogen atoms on water were located in the electron density difference map and were constrained to ride the appropriate oxygen. All other hydrogens were placed at geometric positions and refined as riding atoms. No other restraints were placed on the model. **Note, one water molecule (O43) was removed from the model as the position appeared to become so diffuse as to disappear from maps.**

Refinement of F^2 against ALL reflections. The weighted R-factor (*w*R) and goodness of fit (S) are based on F^2, conventional R-factors (R) are based on F, with F set to zero for negative F^2. The threshold expression of $F^2 > 2\sigma(F^2)$ is used only for calculating R-factors(gt) etc. and is not relevant to the choice of reflections for refinement. R-factors based on F^2 are statistically about twice as large as those based on F, and R-factors based on ALL data will be even larger.

All esds (except the esd in the dihedral angle between two l.s. planes) are estimated using the full covariance matrix. The cell esds are taken into account individually in the estimation of esds in distances, angles and torsion angles; correlations between esds in cell parameters are only used when they are defined by crystal symmetry. An approximate (isotropic) treatment of cell esds is used for estimating esds involving l.s. planes.

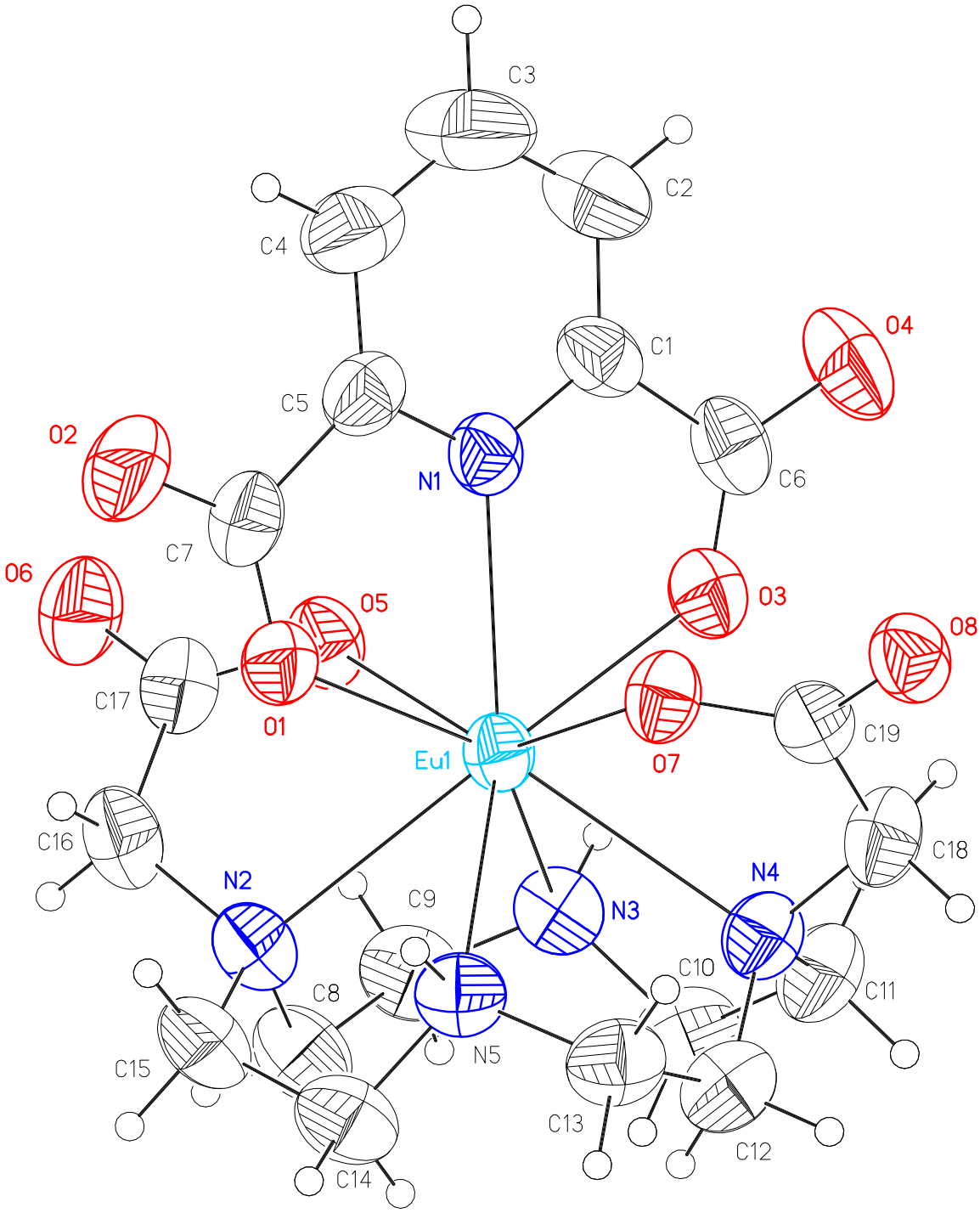
C3
C2
C4
C1
O4
C5
O2
N1
C6
C7
O6
O3
O5
O8
C17
O1
Eu1
O7
C19
C16
C18
N2
N4
C9
N3
C10
C11
C8
N5
C15
C13
C12
C14

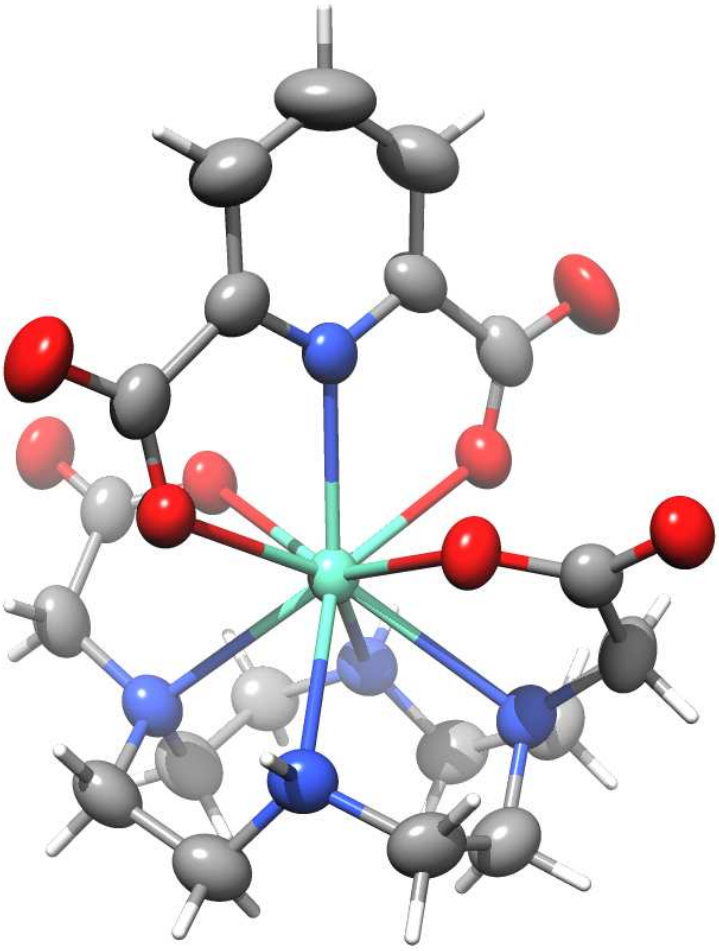

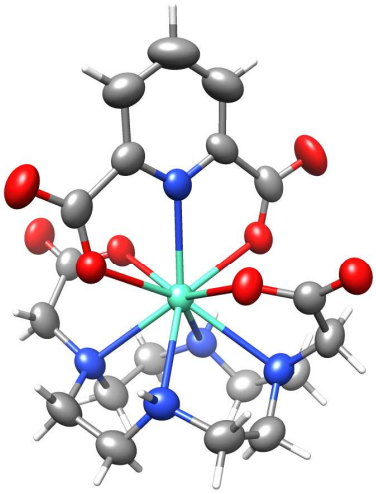

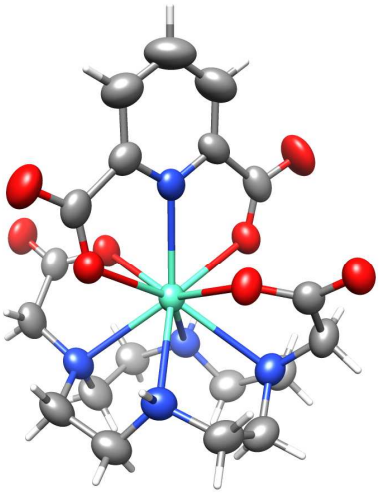

E36

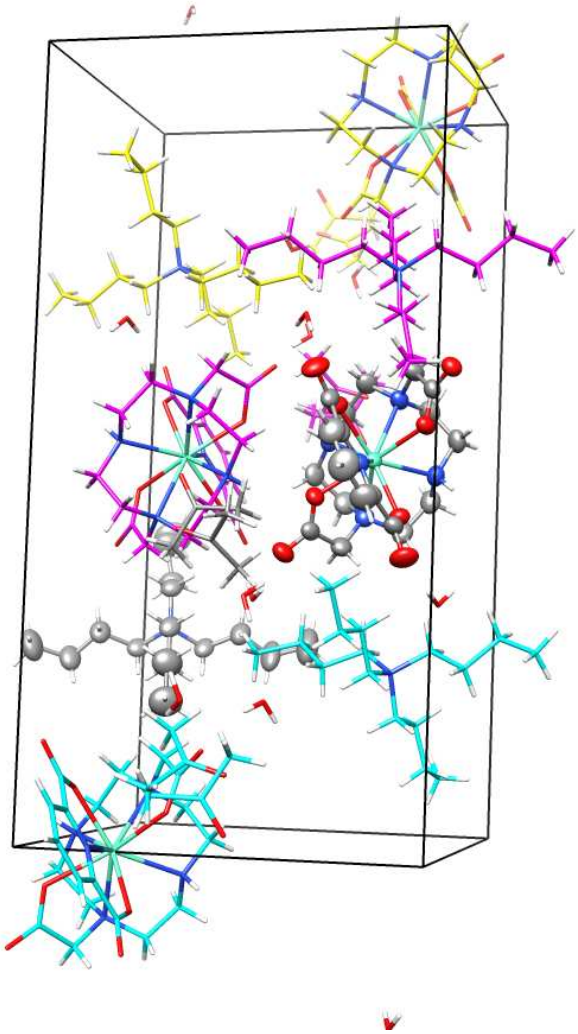

E37

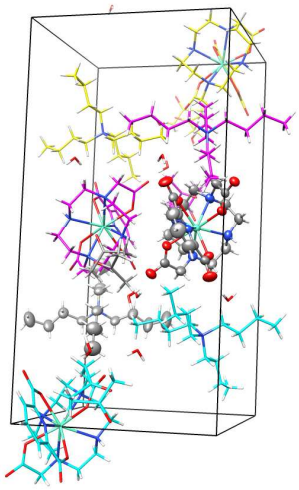

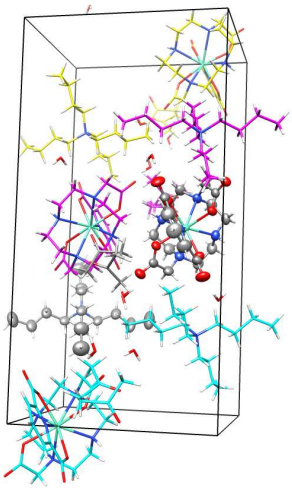

Table 2. Atomic coordinates (x 10^4) and equivalent isotropic displacement parameters ($Å^2$x 10^3) for MLC19 (CCDC 763335). U(eq) is defined as the trace of the orthogonalized U^{ij} tensor.

	x	y	z	U_{eq}	Occ
Eu(1)	7500(1)	4978(1)	5016(1)	40(1)	1
O(1)	8333(1)	5567(1)	5772(1)	51(1)	1
O(2)	8717(1)	6773(1)	6321(1)	79(1)	1
O(3)	6717(1)	5932(1)	4353(1)	51(1)	1
O(4)	6437(1)	7371(1)	3950(1)	81(1)	1
O(5)	6085(1)	5391(1)	5512(1)	51(1)	1
O(6)	5298(1)	5386(1)	6246(1)	66(1)	1
O(7)	8945(1)	5588(1)	4590(1)	49(1)	1
O(8)	9641(1)	6022(1)	3861(1)	53(1)	1
N(1)	7533(1)	6829(1)	5130(1)	44(1)	1
N(2)	7034(1)	3615(1)	5714(1)	53(1)	1
N(3)	6068(1)	3814(1)	4713(1)	51(1)	1
N(4)	7941(1)	4002(1)	4166(1)	49(1)	1
N(5)	8905(1)	3658(1)	5156(1)	51(1)	1
C(1)	7147(2)	7422(2)	4773(1)	50(1)	1
C(2)	7150(2)	8424(2)	4820(1)	78(1)	1
C(3)	7565(2)	8841(2)	5255(1)	95(1)	1
C(4)	7953(2)	8230(2)	5624(1)	75(1)	1
C(5)	7940(2)	7217(2)	5549(1)	51(1)	1
C(6)	6725(2)	6860(2)	4316(1)	54(1)	1
C(7)	8363(2)	6455(2)	5913(1)	53(1)	1
C(8)	6342(2)	2869(2)	5501(1)	68(1)	1
C(9)	5573(2)	3301(2)	5138(1)	61(1)	1
C(10)	6322(2)	3139(2)	4296(1)	64(1)	1
C(11)	6984(2)	3657(2)	3925(1)	61(1)	1
C(12)	8605(2)	3146(2)	4275(1)	63(1)	1
C(13)	9385(2)	3365(2)	4677(1)	59(1)	1
C(14)	8630(2)	2801(2)	5470(1)	65(1)	1
C(15)	7968(2)	3131(2)	5900(1)	63(1)	1
C(16)	6555(2)	4172(2)	6128(1)	62(1)	1
C(17)	5915(2)	5046(2)	5952(1)	50(1)	1
C(18)	8438(2)	4732(2)	3837(1)	58(1)	1
C(19)	9070(2)	5507(2)	4115(1)	46(1)	1
N(6)	1442(1)	2262(1)	7233(1)	56(1)	1
C(20)	1744(2)	3344(2)	7231(1)	63(1)	1
C(21)	1885(2)	3805(2)	7747(1)	80(1)	1
C(22)	2153(3)	4867(2)	7711(1)	100(1)	1
C(23)	2304(3)	5365(2)	8219(1)	119(1)	1
C(24)	2239(2)	1629(2)	7495(1)	62(1)	1
C(25)	3277(2)	1717(2)	7292(1)	79(1)	1
C(26)	3998(2)	1094(3)	7583(1)	129(1)	1
C(27)	5074(3)	1278(4)	7440(2)	170(2)	1
C(28)	1329(2)	1943(2)	6678(1)	62(1)	1
C(29)	1039(2)	878(2)	6587(1)	81(1)	1
C(30)	785(3)	670(3)	6048(1)	110(1)	1

C(31)	623(4)	-374(3)	5912(2)	159(2)	1
C(32)	477(2)	2107(2)	7518(1)	62(1)	1
C(33)	-437(2)	2661(2)	7319(1)	73(1)	1
C(34)	-1280(2)	2627(2)	7687(1)	88(1)	1
C(35)	-2221(3)	3137(3)	7525(1)	129(1)	1
O(41)	698(1)	4987(1)	3117(1)	77(1)	1
O(42)	4175(2)	4013(2)	6845(1)	106(1)	1
O(44)	5030(30)	8240(30)	6864(18)	1210(40)	0.503(5)
O(51)	3635(4)	9301(4)	5422(2)	192(3)	0.503(5)
C(51)	3518(4)	9433(4)	6286(2)	201(6)	0.503(5)
C(52)	4099(3)	9494(2)	5815(2)	123(3)	0.503(5)
C(53)	5201(3)	9717(6)	5836(2)	317(10)	0.503(5)
O(61)	3644(3)	9401(3)	6078(2)	344(8)	0.497(5)
C(61)	5029(6)	8785(5)	6531(2)	210(5)	0.497(5)
C(62)	4503(4)	9450(3)	6208(2)	142(3)	0.497(5)
C(63)	5085(4)	10278(5)	5918(3)	212(6)	0.497(5)

Table 3. Selected bond lengths [Å] and angles [°] for MLC19 (CCDC 763335).

Eu(1)-O(5)	2.3674(15)	O(7)-Eu(1)-N(4)	65.77(5)
Eu(1)-O(7)	2.3836(14)	O(3)-Eu(1)-N(4)	75.46(5)
Eu(1)-O(3)	2.4004(12)	O(1)-Eu(1)-N(4)	138.90(5)
Eu(1)-O(1)	2.4059(11)	N(1)-Eu(1)-N(4)	125.83(5)
Eu(1)-N(1)	2.5085(16)	N(3)-Eu(1)-N(4)	67.03(5)
Eu(1)-N(3)	2.5904(16)	N(5)-Eu(1)-N(4)	67.65(5)
Eu(1)-N(5)	2.6055(16)	O(5)-Eu(1)-N(2)	65.94(5)
Eu(1)-N(4)	2.6661(15)	O(7)-Eu(1)-N(2)	138.84(5)
Eu(1)-N(2)	2.6724(16)	O(3)-Eu(1)-N(2)	139.95(5)
Eu(1)-C(19)	3.256(2)	O(1)-Eu(1)-N(2)	76.44(5)
Eu(1)-C(17)	3.259(2)	N(1)-Eu(1)-N(2)	127.12(5)
		N(3)-Eu(1)-N(2)	67.84(5)
O(5)-Eu(1)-O(7)	146.00(5)	N(5)-Eu(1)-N(2)	66.75(6)
O(5)-Eu(1)-O(3)	86.12(5)	N(4)-Eu(1)-N(2)	107.05(6)
O(7)-Eu(1)-O(3)	79.73(5)	O(5)-Eu(1)-C(19)	150.44(5)
O(5)-Eu(1)-O(1)	80.31(5)	O(7)-Eu(1)-C(19)	19.03(4)
O(7)-Eu(1)-O(1)	84.61(4)	O(3)-Eu(1)-C(19)	68.32(5)
O(3)-Eu(1)-O(1)	128.45(5)	O(1)-Eu(1)-C(19)	103.63(5)
O(5)-Eu(1)-N(1)	73.42(5)	N(1)-Eu(1)-C(19)	81.90(5)
O(7)-Eu(1)-N(1)	72.59(5)	N(3)-Eu(1)-C(19)	112.55(5)
O(3)-Eu(1)-N(1)	64.11(4)	N(5)-Eu(1)-C(19)	77.67(5)
O(1)-Eu(1)-N(1)	64.35(4)	N(4)-Eu(1)-C(19)	49.30(5)
O(5)-Eu(1)-N(3)	73.97(5)	N(2)-Eu(1)-C(19)	143.62(5)
O(7)-Eu(1)-N(3)	131.25(5)	O(5)-Eu(1)-C(17)	18.76(5)
O(3)-Eu(1)-N(3)	77.47(5)	O(7)-Eu(1)-C(17)	151.34(5)
O(1)-Eu(1)-N(3)	142.07(5)	O(3)-Eu(1)-C(17)	104.77(5)
N(1)-Eu(1)-N(3)	130.47(5)	O(1)-Eu(1)-C(17)	70.33(5)
O(5)-Eu(1)-N(5)	131.07(5)	N(1)-Eu(1)-C(17)	83.86(6)
O(7)-Eu(1)-N(5)	73.64(5)	N(3)-Eu(1)-C(17)	76.70(5)
O(3)-Eu(1)-N(5)	140.82(5)	N(5)-Eu(1)-C(17)	112.44(5)
O(1)-Eu(1)-N(5)	77.34(5)	N(4)-Eu(1)-C(17)	142.89(5)
N(1)-Eu(1)-N(5)	130.41(5)	N(2)-Eu(1)-C(17)	49.03(6)
N(3)-Eu(1)-N(5)	99.12(6)	C(19)-Eu(1)-C(17)	165.75(6)
O(5)-Eu(1)-N(4)	139.51(5)		

Symmetry transformations used to generate equivalent atoms:

Table 4. Bond lengths [Å] and angles [°] for MLC19 (CCDC 763335).

Eu(1)-O(5)	2.3674(15)	C(24)-C(25)	1.492(3)
Eu(1)-O(7)	2.3836(14)	C(25)-C(26)	1.484(3)
Eu(1)-O(3)	2.4004(12)	C(26)-C(27)	1.506(5)
Eu(1)-O(1)	2.4059(11)	C(28)-C(29)	1.503(3)
Eu(1)-N(1)	2.5085(16)	C(29)-C(30)	1.483(3)
Eu(1)-N(3)	2.5904(16)	C(30)-C(31)	1.465(4)
Eu(1)-N(5)	2.6055(16)	C(32)-C(33)	1.519(3)
Eu(1)-N(4)	2.6661(15)	C(33)-C(34)	1.492(4)
Eu(1)-N(2)	2.6724(16)	C(34)-C(35)	1.489(4)
Eu(1)-C(19)	3.256(2)	O(51)-C(52)	1.2294
Eu(1)-C(17)	3.259(2)	C(51)-C(52)	1.4697
O(1)-C(7)	1.253(2)	C(52)-C(53)	1.4999
O(2)-C(7)	1.247(2)	O(61)-C(62)	1.1945
O(3)-C(6)	1.254(2)	C(61)-C(62)	1.4162
O(4)-C(6)	1.242(2)	C(62)-C(63)	1.5608
O(5)-C(17)	1.271(2)		
O(6)-C(17)	1.224(2)	O(5)-Eu(1)-O(7)	146.00(5)
O(7)-C(19)	1.269(2)	O(5)-Eu(1)-O(3)	86.12(5)
O(8)-C(19)	1.232(2)	O(7)-Eu(1)-O(3)	79.73(5)
N(1)-C(5)	1.333(2)	O(5)-Eu(1)-O(1)	80.31(5)
N(1)-C(1)	1.334(2)	O(7)-Eu(1)-O(1)	84.61(4)
N(2)-C(8)	1.472(3)	O(3)-Eu(1)-O(1)	128.45(5)
N(2)-C(16)	1.474(3)	O(5)-Eu(1)-N(1)	73.42(5)
N(2)-C(15)	1.484(3)	O(7)-Eu(1)-N(1)	72.59(5)
N(3)-C(10)	1.468(3)	O(3)-Eu(1)-N(1)	64.11(4)
N(3)-C(9)	1.476(3)	O(1)-Eu(1)-N(1)	64.35(4)
N(4)-C(18)	1.470(3)	O(5)-Eu(1)-N(3)	73.97(5)
N(4)-C(12)	1.479(3)	O(7)-Eu(1)-N(3)	131.25(5)
N(4)-C(11)	1.495(2)	O(3)-Eu(1)-N(3)	77.47(5)
N(5)-C(14)	1.467(3)	O(1)-Eu(1)-N(3)	142.07(5)
N(5)-C(13)	1.474(3)	N(1)-Eu(1)-N(3)	130.47(5)
C(1)-C(2)	1.354(3)	O(5)-Eu(1)-N(5)	131.07(5)
C(1)-C(6)	1.524(3)	O(7)-Eu(1)-N(5)	73.64(5)
C(2)-C(3)	1.387(3)	O(3)-Eu(1)-N(5)	140.82(5)
C(3)-C(4)	1.373(3)	O(1)-Eu(1)-N(5)	77.34(5)
C(4)-C(5)	1.378(3)	N(1)-Eu(1)-N(5)	130.41(5)
C(5)-C(7)	1.510(3)	N(3)-Eu(1)-N(5)	99.12(6)
C(8)-C(9)	1.512(3)	O(5)-Eu(1)-N(4)	139.51(5)
C(10)-C(11)	1.494(3)	O(7)-Eu(1)-N(4)	65.77(5)
C(12)-C(13)	1.507(3)	O(3)-Eu(1)-N(4)	75.46(5)
C(14)-C(15)	1.508(3)	O(1)-Eu(1)-N(4)	138.90(5)
C(16)-C(17)	1.522(3)	N(1)-Eu(1)-N(4)	125.83(5)
C(18)-C(19)	1.525(3)	N(3)-Eu(1)-N(4)	67.03(5)
N(6)-C(32)	1.510(3)	N(5)-Eu(1)-N(4)	67.65(5)
N(6)-C(20)	1.511(3)	O(5)-Eu(1)-N(2)	65.94(5)
N(6)-C(24)	1.524(3)	O(7)-Eu(1)-N(2)	138.84(5)
N(6)-C(28)	1.529(2)	O(3)-Eu(1)-N(2)	139.95(5)
C(20)-C(21)	1.506(3)	O(1)-Eu(1)-N(2)	76.44(5)
C(21)-C(22)	1.477(3)	N(1)-Eu(1)-N(2)	127.12(5)
C(22)-C(23)	1.509(4)	N(3)-Eu(1)-N(2)	67.84(5)

N(5)-Eu(1)-N(2)	66.75(6)	N(1)-C(5)-C(4)	120.79(19)
N(4)-Eu(1)-N(2)	107.05(6)	N(1)-C(5)-C(7)	114.04(18)
O(5)-Eu(1)-C(19)	150.44(5)	C(4)-C(5)-C(7)	125.17(18)
O(7)-Eu(1)-C(19)	19.03(4)	O(4)-C(6)-O(3)	127.5(2)
O(3)-Eu(1)-C(19)	68.32(5)	O(4)-C(6)-C(1)	116.7(2)
O(1)-Eu(1)-C(19)	103.63(5)	O(3)-C(6)-C(1)	115.87(16)
N(1)-Eu(1)-C(19)	81.90(5)	O(2)-C(7)-O(1)	126.47(19)
N(3)-Eu(1)-C(19)	112.55(5)	O(2)-C(7)-C(5)	116.9(2)
N(5)-Eu(1)-C(19)	77.67(5)	O(1)-C(7)-C(5)	116.67(16)
N(4)-Eu(1)-C(19)	49.30(5)	N(2)-C(8)-C(9)	113.52(18)
N(2)-Eu(1)-C(19)	143.62(5)	N(3)-C(9)-C(8)	110.76(19)
O(5)-Eu(1)-C(17)	18.76(5)	N(3)-C(10)-C(11)	109.99(18)
O(7)-Eu(1)-C(17)	151.34(5)	N(4)-C(11)-C(10)	111.92(16)
O(3)-Eu(1)-C(17)	104.77(5)	N(4)-C(12)-C(13)	113.12(17)
O(1)-Eu(1)-C(17)	70.33(5)	N(5)-C(13)-C(12)	110.62(18)
N(1)-Eu(1)-C(17)	83.86(6)	N(5)-C(14)-C(15)	109.97(19)
N(3)-Eu(1)-C(17)	76.70(5)	N(2)-C(15)-C(14)	112.03(16)
N(5)-Eu(1)-C(17)	112.44(5)	N(2)-C(16)-C(17)	114.37(15)
N(4)-Eu(1)-C(17)	142.89(5)	O(6)-C(17)-O(5)	124.6(2)
N(2)-Eu(1)-C(17)	49.03(6)	O(6)-C(17)-C(16)	118.24(17)
C(19)-Eu(1)-C(17)	165.75(6)	O(5)-C(17)-C(16)	117.17(19)
C(7)-O(1)-Eu(1)	124.96(11)	O(6)-C(17)-Eu(1)	158.82(17)
C(6)-O(3)-Eu(1)	125.81(12)	O(5)-C(17)-Eu(1)	36.80(10)
C(17)-O(5)-Eu(1)	124.44(13)	C(16)-C(17)-Eu(1)	81.03(12)
C(19)-O(7)-Eu(1)	123.21(12)	N(4)-C(18)-C(19)	115.07(15)
C(5)-N(1)-C(1)	120.16(18)	O(8)-C(19)-O(7)	125.14(19)
C(5)-N(1)-Eu(1)	119.63(12)	O(8)-C(19)-C(18)	117.70(17)
C(1)-N(1)-Eu(1)	120.21(12)	O(7)-C(19)-C(18)	117.13(19)
C(8)-N(2)-C(16)	110.77(19)	O(8)-C(19)-Eu(1)	157.45(15)
C(8)-N(2)-C(15)	110.44(17)	O(7)-C(19)-Eu(1)	37.76(10)
C(16)-N(2)-C(15)	110.23(15)	C(18)-C(19)-Eu(1)	81.03(12)
C(8)-N(2)-Eu(1)	110.75(11)	C(32)-N(6)-C(20)	111.29(18)
C(16)-N(2)-Eu(1)	105.29(12)	C(32)-N(6)-C(24)	106.86(15)
C(15)-N(2)-Eu(1)	109.25(13)	C(20)-N(6)-C(24)	110.81(16)
C(10)-N(3)-C(9)	112.69(17)	C(32)-N(6)-C(28)	111.00(16)
C(10)-N(3)-Eu(1)	115.57(14)	C(20)-N(6)-C(28)	106.97(14)
C(9)-N(3)-Eu(1)	112.42(11)	C(24)-N(6)-C(28)	109.94(17)
C(18)-N(4)-C(12)	111.21(18)	C(21)-C(20)-N(6)	115.17(16)
C(18)-N(4)-C(11)	110.09(15)	C(22)-C(21)-C(20)	111.6(2)
C(12)-N(4)-C(11)	110.38(16)	C(21)-C(22)-C(23)	113.8(2)
C(18)-N(4)-Eu(1)	105.64(11)	C(25)-C(24)-N(6)	115.90(17)
C(12)-N(4)-Eu(1)	110.89(11)	C(26)-C(25)-C(24)	111.6(2)
C(11)-N(4)-Eu(1)	108.49(12)	C(25)-C(26)-C(27)	113.1(3)
C(14)-N(5)-C(13)	112.64(17)	C(29)-C(28)-N(6)	116.35(17)
C(14)-N(5)-Eu(1)	115.69(14)	C(30)-C(29)-C(28)	113.0(2)
C(13)-N(5)-Eu(1)	112.20(11)	C(31)-C(30)-C(29)	116.5(3)
N(1)-C(1)-C(2)	121.95(19)	N(6)-C(32)-C(33)	116.40(17)
N(1)-C(1)-C(6)	113.48(18)	C(34)-C(33)-C(32)	111.48(19)
C(2)-C(1)-C(6)	124.57(19)	C(35)-C(34)-C(33)	115.9(2)
C(1)-C(2)-C(3)	118.7(2)	O(51)-C(52)-C(51)	115.8
C(4)-C(3)-C(2)	119.3(2)	O(51)-C(52)-C(53)	124.0
C(3)-C(4)-C(5)	119.1(2)	C(51)-C(52)-C(53)	120.1

O(61)-C(62)-C(61)	127.3
O(61)-C(62)-C(63)	112.2
C(61)-C(62)-C(63)	119.9

Table 5. Anisotropic displacement parameters ($Å^2 x\ 10^4$) for MLC19 (CCDC 763335). The anisotropic displacement factor exponent takes the form: $-2\pi^2[h^2 a^{*2} U^{11} + ... + 2\ h\ k\ a^*\ b^*\ U^{12}]$

	U^{11}	U^{22}	U^{33}	U^{23}	U^{13}	U^{12}
Eu(1)	375(1)	444(1)	371(1)	25(1)	26(1)	-2(1)
O(1)	593(10)	519(9)	406(6)	-13(6)	-48(6)	60(7)
O(2)	1034(15)	840(12)	486(8)	-184(7)	-161(9)	48(10)
O(3)	526(10)	569(9)	445(7)	63(6)	-44(6)	-20(7)
O(4)	964(15)	871(12)	599(9)	311(8)	-150(9)	18(10)
O(5)	455(9)	611(9)	465(7)	88(6)	78(6)	19(7)
O(6)	603(11)	867(12)	526(8)	-21(7)	157(7)	30(8)
O(7)	437(9)	611(9)	415(6)	-37(6)	44(6)	-62(7)
O(8)	527(10)	573(9)	502(7)	78(6)	99(6)	7(7)
N(1)	424(10)	491(10)	414(8)	30(6)	82(7)	13(8)
N(2)	502(12)	539(11)	537(9)	110(8)	21(8)	8(9)
N(3)	421(11)	541(11)	584(9)	31(8)	-23(8)	-25(8)
N(4)	446(11)	553(11)	480(8)	-57(7)	32(7)	-36(9)
N(5)	423(11)	523(11)	589(9)	2(8)	-27(8)	42(8)
C(1)	466(13)	468(12)	574(11)	123(9)	91(9)	20(10)
C(2)	890(20)	563(16)	878(16)	146(13)	-42(15)	48(15)
C(3)	1150(30)	465(16)	1230(20)	-46(16)	-90(20)	17(16)
C(4)	910(20)	571(15)	755(15)	-153(12)	-41(14)	23(14)
C(5)	506(14)	525(13)	502(11)	-74(9)	91(9)	-8(10)
C(6)	434(14)	693(16)	499(11)	163(10)	26(9)	-10(12)
C(7)	487(14)	688(16)	414(10)	-54(10)	54(9)	38(11)
C(8)	663(18)	624(15)	744(14)	175(11)	47(12)	-125(13)
C(9)	442(14)	622(15)	768(14)	43(11)	22(11)	-132(11)
C(10)	530(16)	605(15)	784(15)	-125(12)	-62(12)	-100(12)
C(11)	584(16)	704(16)	530(11)	-155(10)	-16(11)	-87(12)
C(12)	600(16)	632(15)	658(13)	-123(11)	48(11)	16(12)
C(13)	458(14)	593(14)	732(13)	-38(11)	70(11)	108(11)
C(14)	567(17)	581(15)	793(15)	123(12)	-23(12)	68(12)
C(15)	624(17)	602(15)	651(13)	202(11)	-34(12)	68(12)
C(16)	601(16)	761(16)	499(11)	153(10)	72(10)	20(13)
C(17)	411(11)	658(13)	442(8)	-27(12)	16(7)	-93(13)
C(18)	564(15)	727(17)	441(9)	-60(9)	85(9)	-71(11)
C(19)	385(12)	511(12)	483(10)	34(9)	45(9)	70(10)
N(6)	567(13)	601(12)	498(9)	189(8)	4(8)	-18(9)
C(20)	637(16)	640(15)	603(12)	214(10)	-4(11)	-40(12)
C(21)	980(20)	685(18)	736(15)	79(12)	-45(14)	-144(16)
C(22)	1160(30)	830(20)	999(19)	-49(16)	12(18)	-172(19)
C(23)	1430(40)	980(20)	1160(20)	-152(18)	-90(20)	-170(20)
C(24)	604(16)	711(16)	560(11)	241(11)	-22(11)	44(12)
C(25)	654(19)	980(20)	744(15)	281(14)	-8(13)	101(15)
C(26)	720(30)	1780(40)	1360(30)	710(30)	40(20)	410(20)
C(27)	790(30)	2290(50)	2010(40)	740(40)	20(30)	360(30)
C(28)	673(17)	699(16)	489(11)	140(10)	6(10)	35(13)
C(29)	940(20)	766(19)	724(15)	54(13)	30(14)	-32(16)
C(30)	1240(30)	1140(30)	920(20)	-177(18)	-90(20)	20(20)

C(31)	2150(50)	1170(30)	1460(30)	-490(30)	-230(30)	-190(30)
C(32)	657(17)	680(15)	520(11)	169(10)	29(11)	-44(13)
C(33)	641(18)	832(18)	714(14)	259(13)	81(13)	60(14)
C(34)	700(20)	1060(20)	897(18)	302(16)	175(15)	106(17)
C(35)	850(30)	1580(40)	1440(30)	240(20)	370(20)	270(20)

Table 6. Hydrogen bonds for MLC19 (CCDC 763335) [Å and °].

D-H...A	d(D-H)	d(H...A)	d(D...A)	<(DHA)
N(3)-H(3)...O(5)#1	0.91	2.30	3.115(2)	148.2
N(3)-H(3)...O(6)#1	0.91	2.53	3.284(2)	140.7
N(5)-H(5)...O(7)#2	0.91	2.30	3.108(2)	148.0
N(5)-H(5)...O(8)#2	0.91	2.47	3.2522(18)	144.3
O(41)-H(41A)...O(8)#3	0.76	2.04	2.795(2)	173.1
O(41)-H(41B)...O(2)#1	0.74	2.16	2.897(2)	176.5
O(42)-H(42A)...O(6)	0.77	2.11	2.859(3)	164.3
O(42)-H(42B)...O(4)#1	0.81	2.12	2.913(2)	168.7
O(44)-H(44A)...O(42)#4	0.83	2.88	3.70(4)	171.4

Symmetry transformations used to generate equivalent atoms:
#1 -x+1,-y+1,-z+1
#2 -x+2,-y+1,-z+1
#3 x-1,y,z
#4 -x+1,y+1/2,-z+3/2

APPENDIX F

Crystallographic Data for TBA·Tb(DO2A)(F-DPA)

CALIFORNIA INSTITUTE OF TECHNOLOGY

BECKMAN INSTITUTE

X-RAY CRYSTALLOGRAPHY LABORATORY

Date 11 January 2010

Crystal Structure Analysis of:

MLC23

(shown below)

For Investigator: Morgan Cable ext. (818) 354-4345

Advisor: Adrian Ponce ext. (818) 354-8196

Account Number: AP1.HSARPA3-1-HSARPA.PONCE

By Michael W. Day 116 Beckman ext. 2734

e-mail: mikeday@caltech.edu

Contents

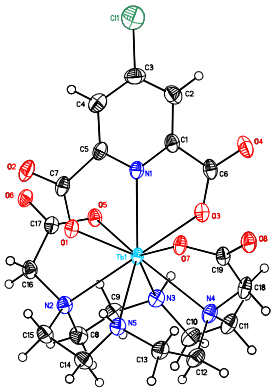

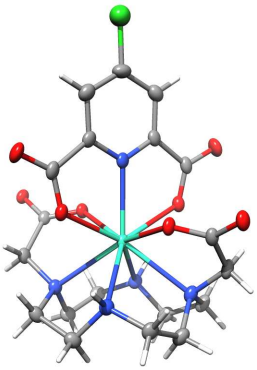

MLC23

Note: The crystallographic data have been deposited in the Cambridge Database (CCDC) and has been placed on hold pending further instructions from me. The deposition number is 761002. Ideally the CCDC would like the publication to contain a footnote of the type: "Crystallographic data have been deposited at the CCDC, 12 Union Road, Cambridge CB2 1EZ, UK and copies can be obtained on request, free of charge, by quoting the publication citation and the deposition number 761002."

Table 1. Crystal data and structure refinement for MLC23 (CCDC 761002).

Empirical formula	$[C_{19}H_{24}Cl_{0.63}F_{0.37}N_5O_8Tb]^-[C_{16}H_{36}N]^+ \bullet C_3H_6O \bullet 2(H_2O)$
Formula weight	975.45
Crystallization Solvent	Acetone/water
Crystal Habit	Trapezoidal
Crystal size	0.15 x 0.15 x 0.15 mm^3
Crystal color	Colorless

Data Collection

Type of diffractometer	Bruker KAPPA APEX II
Wavelength	0.71073 Å MoKα
Data Collection Temperature	100(2) K
θ range for 9873 reflections used in lattice determination	2.33 to 38.01°
Unit cell dimensions	a = 13.2324(6) Å b = 12.9812(6) Å β= 90.528(2)° c = 26.2126(11) Å
Volume	4502.4(3) $Å^3$
Z	4
Crystal system	Monoclinic
Space group	P $2_1/c$
Density (calculated)	1.439 Mg/m^3
F(000)	2028
θ range for data collection	1.54 to 39.88°
Completeness to θ = 39.88°	96.2 %
Index ranges	$-22 \le h \le 23$, $-23 \le k \le 21$, $-44 \le l \le 46$
Data collection scan type	ω scans; 16 settings
Reflections collected	172388
Independent reflections	26652 [R_{int}= 0.0331]
Absorption coefficient	1.671 mm^{-1}
Absorption correction	Semi-empirical from equivalents
Max. and min. transmission	0.7478 and 0.6753

Table 1 (cont.)

Structure solution and Refinement

Structure solution program	SHELXS-97 (Sheldrick, 2008)
Primary solution method	Direct methods
Secondary solution method	Difference Fourier map
Hydrogen placement	Geometric positions
Structure refinement program	SHELXL-97 (Sheldrick, 2008)
Refinement method	Full matrix least-squares on F^2
Data / restraints / parameters	26652 / 0 / 525
Treatment of hydrogen atoms	Riding
Goodness-of-fit on F^2	2.025
Final R indices [$I>2\sigma(I)$, 18685 reflections]	R1 = 0.0285, *w*R2 = 0.0499
R indices (all data)	R1 = 0.0534, *w*R2 = 0.0518
Type of weighting scheme used	Sigma
Weighting scheme used	$w=1/\sigma^2(Fo^2)$
Max shift/error	0.005
Average shift/error	0.000
Largest diff. peak and hole	2.226 and -1.457 e.Å^{-3}

Special Refinement Details

Crystals were mounted on a glass fiber using Paratone oil then placed on the diffractometer under a nitrogen stream at 100K.

The DPA ligand is disordered at the halogen site, composed of 63% Cl and 37% F. The fluorine was refined isotropically and the two were restrained to a total occupancy of unity

Hydrogen atoms on water were located in the map then assigned to ride the corresponding oxygen. All other hydrogen atoms were restrained as riding at calculated positions.

Refinement of F^2 against ALL reflections. The weighted R-factor (*w*R) and goodness of fit (S) are based on F^2, conventional R-factors (R) are based on F, with F set to zero for negative F^2. The threshold expression of $F^2 > 2\sigma(F^2)$ is used only for calculating R-factors(gt) etc. and is not relevant to the choice of reflections for refinement. R-factors based on F^2 are statistically about twice as large as those based on F, and R-factors based on ALL data will be even larger.

All esds (except the esd in the dihedral angle between two l.s. planes) are estimated using the full covariance matrix. The cell esds are taken into account individually in the estimation of esds in distances, angles and torsion angles; correlations between esds in cell parameters are only used when they are defined by crystal symmetry. An approximate (isotropic) treatment of cell esds is used for estimating esds involving l.s. planes.

F5

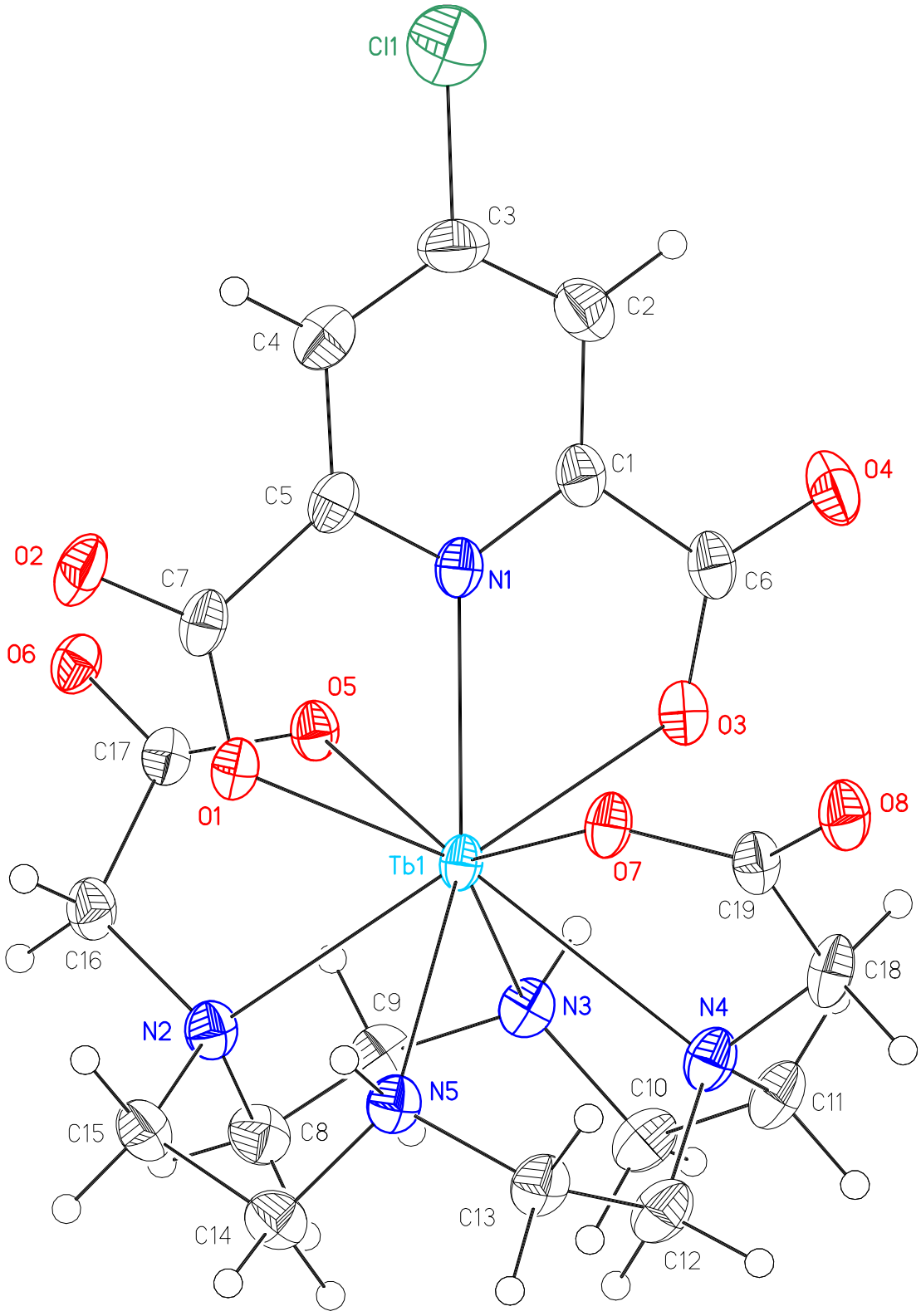
Cl1
C3
C2
C4
C1
O4
C5
O2
C7
N1
C6
O6
O5
O3
C17
O1
O8
Tb1
O7
C19
C16
C18
C9
N3
N4
N2
N5
C10
C11
C15
C8
C14
C13
C12

F6

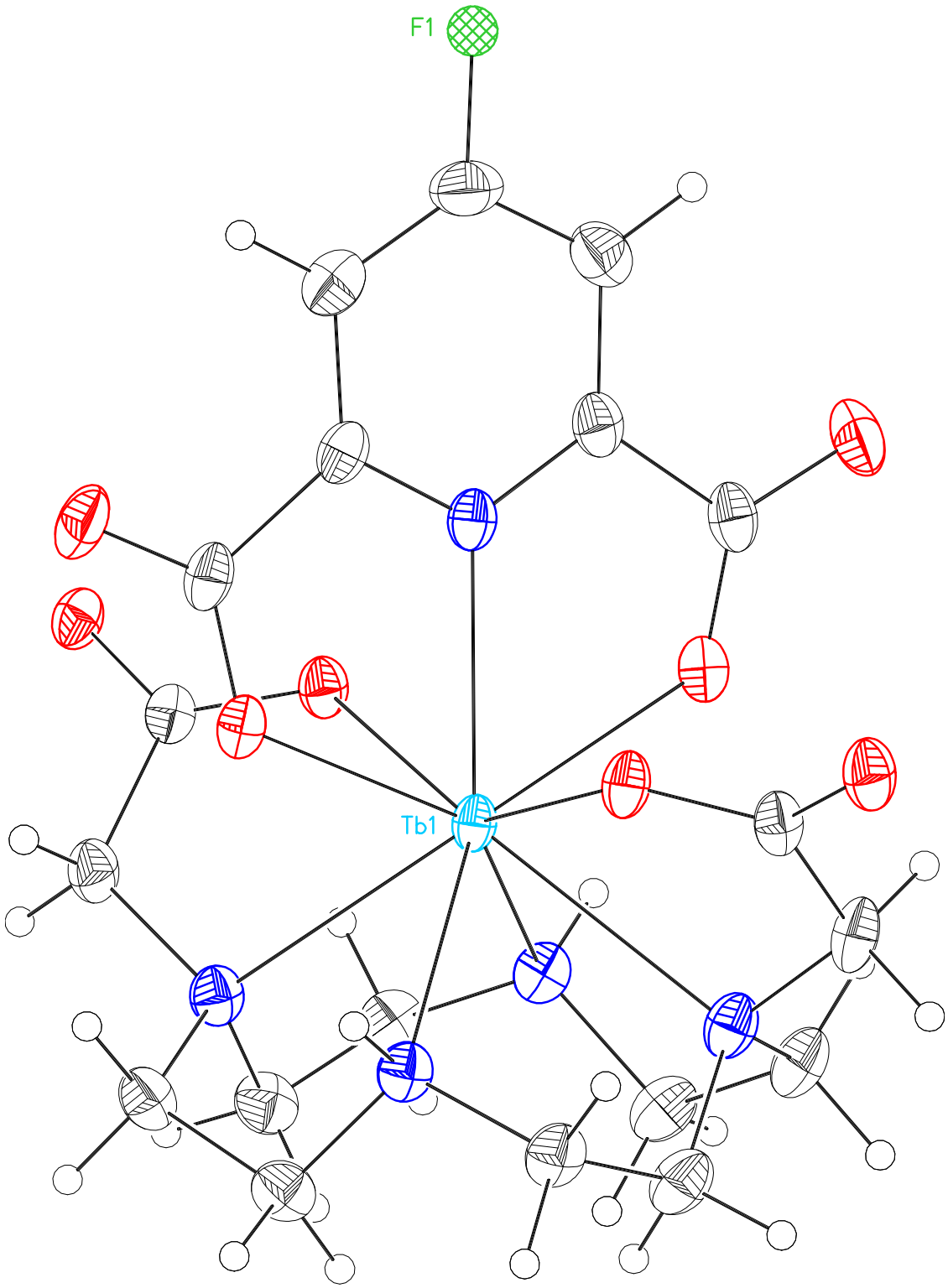

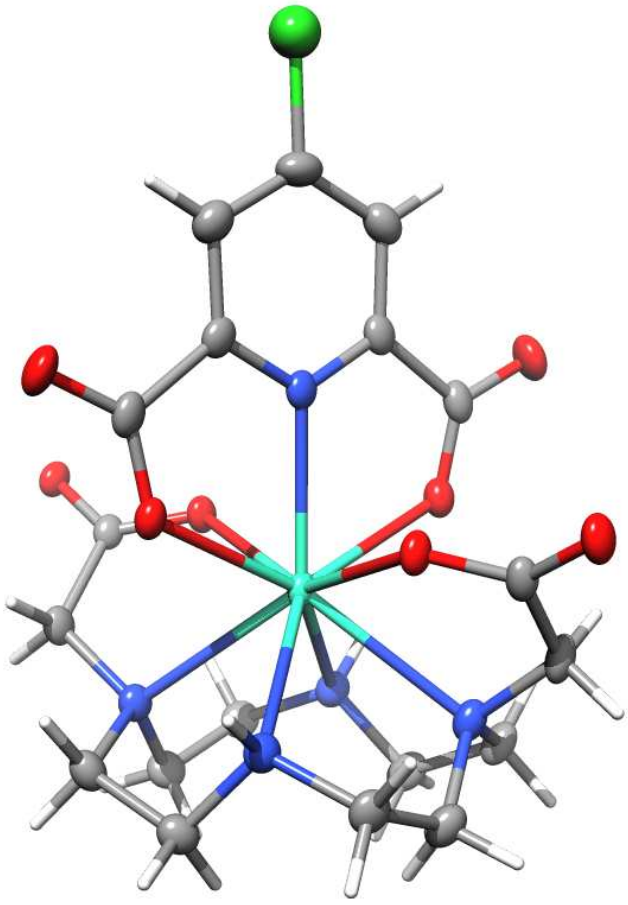

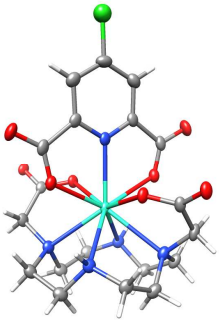

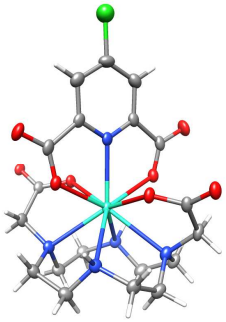

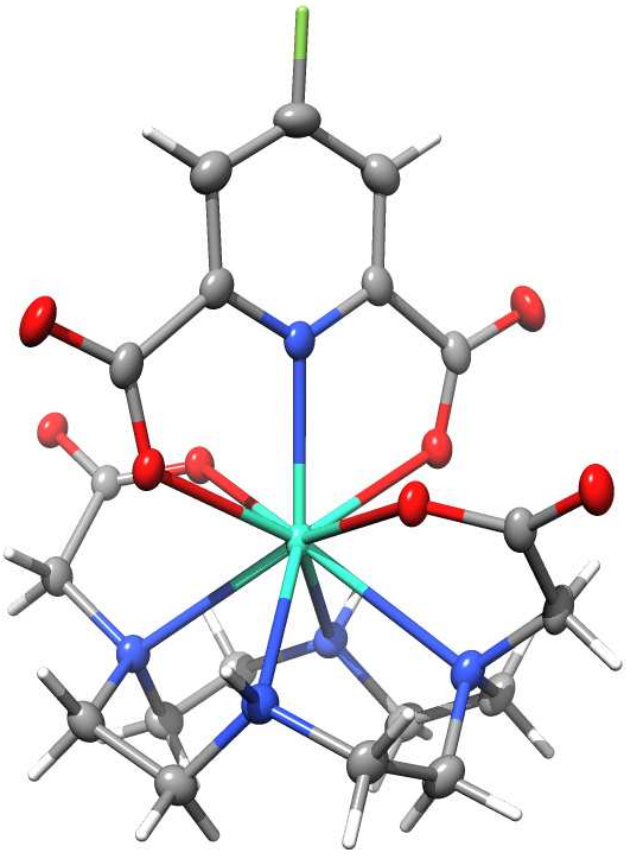

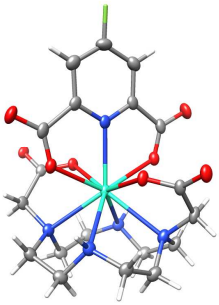

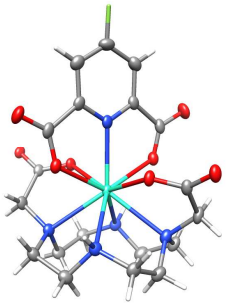

F9

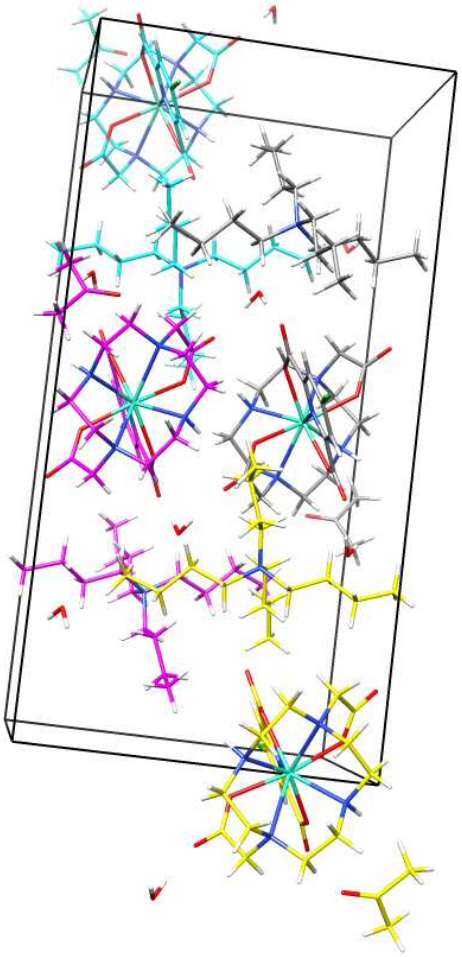

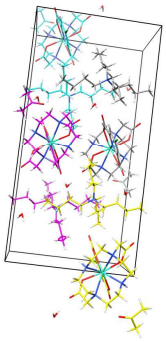

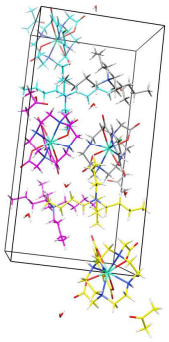

Table 2. Atomic coordinates (x 10^4) and equivalent isotropic displacement parameters ($Å^2$x 10^3) for MLC23 (CCDC 761002). U(eq) is defined as the trace of the orthogonalized U^{ij} tensor.

	x	y	z	U_{eq}	Occ
Tb(1)	2472(1)	5024(1)	4974(1)	16(1)	1
Cl(1)	2658(1)	-260(1)	4804(1)	54(1)	0.630(6)
F(1)	2514(4)	26(5)	4774(2)	50(2)	0.370(6)
O(1)	1696(1)	4120(1)	5658(1)	21(1)	1
O(2)	1372(1)	2667(1)	6091(1)	31(1)	1
O(3)	3290(1)	4354(1)	4236(1)	22(1)	1
O(4)	3678(1)	3059(1)	3708(1)	33(1)	1
O(5)	3911(1)	4403(1)	5406(1)	20(1)	1
O(6)	4661(1)	4001(1)	6142(1)	21(1)	1
O(7)	1048(1)	4548(1)	4494(1)	21(1)	1
O(8)	251(1)	4439(1)	3745(1)	26(1)	1
N(1)	2495(1)	3110(1)	4902(1)	19(1)	1
N(2)	2939(1)	6079(1)	5808(1)	21(1)	1
N(3)	3895(1)	6320(1)	4811(1)	22(1)	1
N(4)	2011(1)	6340(1)	4240(1)	22(1)	1
N(5)	1062(1)	6248(1)	5245(1)	21(1)	1
C(1)	2898(1)	2665(1)	4494(1)	22(1)	1
C(2)	2938(1)	1600(1)	4441(1)	28(1)	1
C(3)	2555(1)	1026(1)	4835(1)	32(1)	1
C(4)	2144(1)	1462(1)	5263(1)	28(1)	1
C(5)	2123(1)	2534(1)	5279(1)	21(1)	1
C(6)	3322(1)	3415(1)	4108(1)	23(1)	1
C(7)	1693(1)	3151(1)	5719(1)	23(1)	1
C(8)	3635(1)	6939(1)	5687(1)	25(1)	1
C(9)	4406(1)	6661(1)	5286(1)	24(1)	1
C(10)	3629(1)	7187(1)	4474(1)	27(1)	1
C(11)	2949(1)	6816(1)	4043(1)	26(1)	1
C(12)	1319(1)	7148(1)	4429(1)	27(1)	1
C(13)	554(1)	6744(1)	4804(1)	24(1)	1
C(14)	1323(1)	6993(1)	5649(1)	25(1)	1
C(15)	2004(1)	6487(1)	6043(1)	24(1)	1
C(16)	3432(1)	5334(1)	6155(1)	23(1)	1
C(17)	4057(1)	4520(1)	5881(1)	18(1)	1
C(18)	1513(1)	5724(1)	3834(1)	25(1)	1
C(19)	874(1)	4837(1)	4038(1)	21(1)	1
N(6)	3611(1)	2719(1)	2232(1)	19(1)	1
C(20)	3314(1)	1590(1)	2225(1)	21(1)	1
C(21)	3168(1)	1107(1)	2747(1)	30(1)	1
C(22)	2891(1)	-15(1)	2696(1)	31(1)	1
C(23)	2702(1)	-521(1)	3209(1)	38(1)	1
C(24)	4582(1)	2875(1)	2535(1)	22(1)	1
C(25)	5502(1)	2309(1)	2337(1)	26(1)	1
C(26)	6319(1)	2248(1)	2749(1)	27(1)	1
C(27)	7271(1)	1721(1)	2570(1)	36(1)	1
C(28)	3744(1)	3042(1)	1681(1)	21(1)	1

C(29)	3955(1)	4177(1)	1593(1)	26(1)	1
C(30)	4358(1)	4338(1)	1057(1)	29(1)	1
C(31)	4402(1)	5473(1)	908(1)	48(1)	1
C(32)	2798(1)	3365(1)	2488(1)	22(1)	1
C(33)	1746(1)	3240(1)	2265(1)	26(1)	1
C(34)	1004(1)	3960(1)	2523(1)	36(1)	1
C(35)	-72(1)	3767(1)	2336(1)	47(1)	1
O(41)	5766(1)	5083(1)	6854(1)	28(1)	1
O(42)	9136(1)	5853(1)	3129(1)	37(1)	1
O(51)	1422(1)	9456(1)	6247(1)	57(1)	1
C(51)	17(1)	8655(2)	6648(1)	61(1)	1
C(52)	525(1)	9313(1)	6258(1)	52(1)	1
C(53)	-148(2)	9784(3)	5859(1)	121(1)	1

Table 3. Selected bond lengths [Å] and angles [°] for MLC23 (CCDC 761002).

Tb(1)-O(7)	2.3392(8)	O(7)-Tb(1)-O(5)	144.47(3)
Tb(1)-O(5)	2.3492(7)	O(7)-Tb(1)-O(1)	85.65(3)
Tb(1)-O(1)	2.3835(7)	O(5)-Tb(1)-O(1)	79.68(3)
Tb(1)-O(3)	2.3889(8)	O(7)-Tb(1)-O(3)	80.64(3)
Tb(1)-N(1)	2.4924(9)	O(5)-Tb(1)-O(3)	83.90(3)
Tb(1)-N(5)	2.5562(9)	O(1)-Tb(1)-O(3)	129.13(3)
Tb(1)-N(3)	2.5634(9)	O(7)-Tb(1)-N(1)	72.93(3)
Tb(1)-N(4)	2.6409(9)	O(5)-Tb(1)-N(1)	71.54(3)
Tb(1)-N(2)	2.6476(9)	O(1)-Tb(1)-N(1)	64.62(3)
		O(3)-Tb(1)-N(1)	64.52(3)
		O(7)-Tb(1)-N(5)	74.14(3)
		O(5)-Tb(1)-N(5)	132.09(3)
		O(1)-Tb(1)-N(5)	77.12(3)
		O(3)-Tb(1)-N(5)	142.03(3)
		N(1)-Tb(1)-N(5)	130.57(3)
		O(7)-Tb(1)-N(3)	132.31(3)
		O(5)-Tb(1)-N(3)	73.28(3)
		O(1)-Tb(1)-N(3)	140.40(3)
		O(3)-Tb(1)-N(3)	76.41(3)
		N(1)-Tb(1)-N(3)	129.19(3)
		N(5)-Tb(1)-N(3)	100.23(3)
		O(7)-Tb(1)-N(4)	66.38(3)
		O(5)-Tb(1)-N(4)	138.96(3)
		O(1)-Tb(1)-N(4)	140.26(3)
		O(3)-Tb(1)-N(4)	75.45(3)
		N(1)-Tb(1)-N(4)	126.36(3)
		N(5)-Tb(1)-N(4)	68.64(3)
		N(3)-Tb(1)-N(4)	67.62(3)
		O(7)-Tb(1)-N(2)	139.59(3)
		O(5)-Tb(1)-N(2)	66.28(3)
		O(1)-Tb(1)-N(2)	74.50(3)
		O(3)-Tb(1)-N(2)	138.80(3)
		N(1)-Tb(1)-N(2)	125.11(3)
		N(5)-Tb(1)-N(2)	67.36(3)
		N(3)-Tb(1)-N(2)	68.39(3)
		N(4)-Tb(1)-N(2)	108.52(3)

Table 4. Bond lengths [Å] and angles [°] for MLC23 (CCDC 761002).

Tb(1)-O(7)	2.3392(8)	C(24)-C(25)	1.5179(16)
Tb(1)-O(5)	2.3492(7)	C(25)-C(26)	1.5223(17)
Tb(1)-O(1)	2.3835(7)	C(26)-C(27)	1.5126(18)
Tb(1)-O(3)	2.3889(8)	C(28)-C(29)	1.5171(16)
Tb(1)-N(1)	2.4924(9)	C(29)-C(30)	1.5225(17)
Tb(1)-N(5)	2.5562(9)	C(30)-C(31)	1.525(2)
Tb(1)-N(3)	2.5634(9)	C(32)-C(33)	1.5135(16)
Tb(1)-N(4)	2.6409(9)	C(33)-C(34)	1.5191(17)
Tb(1)-N(2)	2.6476(9)	C(34)-C(35)	1.5219(19)
Cl(1)-C(3)	1.676(2)	O(51)-C(52)	1.202(2)
F(1)-C(3)	1.309(6)	C(51)-C(52)	1.496(3)
O(1)-C(7)	1.2683(14)	C(52)-C(53)	1.500(3)
O(2)-C(7)	1.2385(13)		
O(3)-C(6)	1.2662(14)	O(7)-Tb(1)-O(5)	144.47(3)
O(4)-C(6)	1.2430(13)	O(7)-Tb(1)-O(1)	85.65(3)
O(5)-C(17)	1.2681(12)	O(5)-Tb(1)-O(1)	79.68(3)
O(6)-C(17)	1.2455(12)	O(7)-Tb(1)-O(3)	80.64(3)
O(7)-C(19)	1.2731(12)	O(5)-Tb(1)-O(3)	83.90(3)
O(8)-C(19)	1.2358(13)	O(1)-Tb(1)-O(3)	129.13(3)
N(1)-C(1)	1.3312(14)	O(7)-Tb(1)-N(1)	72.93(3)
N(1)-C(5)	1.3362(14)	O(5)-Tb(1)-N(1)	71.54(3)
N(2)-C(16)	1.4759(14)	O(1)-Tb(1)-N(1)	64.62(3)
N(2)-C(8)	1.4822(15)	O(3)-Tb(1)-N(1)	64.52(3)
N(2)-C(15)	1.4854(15)	O(7)-Tb(1)-N(5)	74.14(3)
N(3)-C(10)	1.4722(14)	O(5)-Tb(1)-N(5)	132.09(3)
N(3)-C(9)	1.4788(14)	O(1)-Tb(1)-N(5)	77.12(3)
N(4)-C(18)	1.4812(15)	O(3)-Tb(1)-N(5)	142.03(3)
N(4)-C(12)	1.4812(15)	N(1)-Tb(1)-N(5)	130.57(3)
N(4)-C(11)	1.4834(15)	O(7)-Tb(1)-N(3)	132.31(3)
N(5)-C(14)	1.4726(15)	O(5)-Tb(1)-N(3)	73.28(3)
N(5)-C(13)	1.4786(14)	O(1)-Tb(1)-N(3)	140.40(3)
C(1)-C(2)	1.3913(16)	O(3)-Tb(1)-N(3)	76.41(3)
C(1)-C(6)	1.5163(16)	N(1)-Tb(1)-N(3)	129.19(3)
C(2)-C(3)	1.3741(18)	N(5)-Tb(1)-N(3)	100.23(3)
C(3)-C(4)	1.3740(18)	O(7)-Tb(1)-N(4)	66.38(3)
C(4)-C(5)	1.3924(16)	O(5)-Tb(1)-N(4)	138.96(3)
C(5)-C(7)	1.5190(17)	O(1)-Tb(1)-N(4)	140.26(3)
C(8)-C(9)	1.5157(17)	O(3)-Tb(1)-N(4)	75.45(3)
C(10)-C(11)	1.5158(17)	N(1)-Tb(1)-N(4)	126.36(3)
C(12)-C(13)	1.5114(17)	N(5)-Tb(1)-N(4)	68.64(3)
C(14)-C(15)	1.5136(16)	N(3)-Tb(1)-N(4)	67.62(3)
C(16)-C(17)	1.5237(16)	O(7)-Tb(1)-N(2)	139.59(3)
C(18)-C(19)	1.5267(16)	O(5)-Tb(1)-N(2)	66.28(3)
N(6)-C(28)	1.5163(14)	O(1)-Tb(1)-N(2)	74.50(3)
N(6)-C(24)	1.5172(14)	O(3)-Tb(1)-N(2)	138.80(3)
N(6)-C(20)	1.5176(14)	N(1)-Tb(1)-N(2)	125.11(3)
N(6)-C(32)	1.5254(14)	N(5)-Tb(1)-N(2)	67.36(3)
C(20)-C(21)	1.5195(16)	N(3)-Tb(1)-N(2)	68.39(3)
C(21)-C(22)	1.5076(17)	N(4)-Tb(1)-N(2)	108.52(3)
C(22)-C(23)	1.5185(18)	C(7)-O(1)-Tb(1)	125.80(7)

C(6)-O(3)-Tb(1)	125.65(7)	N(2)-C(16)-C(17)	113.78(9)
C(17)-O(5)-Tb(1)	123.19(7)	O(6)-C(17)-O(5)	124.44(10)
C(19)-O(7)-Tb(1)	124.39(7)	O(6)-C(17)-C(16)	117.70(9)
C(1)-N(1)-C(5)	120.22(10)	O(5)-C(17)-C(16)	117.85(9)
C(1)-N(1)-Tb(1)	119.92(7)	N(4)-C(18)-C(19)	113.58(9)
C(5)-N(1)-Tb(1)	119.84(7)	O(8)-C(19)-O(7)	125.07(11)
C(16)-N(2)-C(8)	110.70(9)	O(8)-C(19)-C(18)	117.80(9)
C(16)-N(2)-C(15)	110.13(9)	O(7)-C(19)-C(18)	117.10(9)
C(8)-N(2)-C(15)	110.00(9)	C(28)-N(6)-C(24)	110.89(8)
C(16)-N(2)-Tb(1)	105.52(6)	C(28)-N(6)-C(20)	106.70(8)
C(8)-N(2)-Tb(1)	110.72(6)	C(24)-N(6)-C(20)	110.73(8)
C(15)-N(2)-Tb(1)	109.68(6)	C(28)-N(6)-C(32)	110.84(8)
C(10)-N(3)-C(9)	112.41(9)	C(24)-N(6)-C(32)	107.08(8)
C(10)-N(3)-Tb(1)	115.48(7)	C(20)-N(6)-C(32)	110.64(8)
C(9)-N(3)-Tb(1)	112.80(7)	N(6)-C(20)-C(21)	114.96(9)
C(18)-N(4)-C(12)	110.56(9)	C(22)-C(21)-C(20)	110.55(10)
C(18)-N(4)-C(11)	110.10(9)	C(21)-C(22)-C(23)	112.37(11)
C(12)-N(4)-C(11)	110.11(9)	N(6)-C(24)-C(25)	115.73(9)
C(18)-N(4)-Tb(1)	105.79(6)	C(24)-C(25)-C(26)	110.42(9)
C(12)-N(4)-Tb(1)	110.67(6)	C(27)-C(26)-C(25)	113.09(10)
C(11)-N(4)-Tb(1)	109.52(7)	N(6)-C(28)-C(29)	115.86(9)
C(14)-N(5)-C(13)	112.21(9)	C(28)-C(29)-C(30)	109.86(9)
C(14)-N(5)-Tb(1)	116.13(7)	C(29)-C(30)-C(31)	112.58(11)
C(13)-N(5)-Tb(1)	112.44(7)	C(33)-C(32)-N(6)	114.90(9)
N(1)-C(1)-C(2)	121.91(11)	C(32)-C(33)-C(34)	110.95(9)
N(1)-C(1)-C(6)	114.30(10)	C(33)-C(34)-C(35)	111.23(11)
C(2)-C(1)-C(6)	123.78(10)	O(51)-C(52)-C(51)	123.83(17)
C(3)-C(2)-C(1)	116.63(11)	O(51)-C(52)-C(53)	119.93(18)
F(1)-C(3)-C(4)	119.4(3)	C(51)-C(52)-C(53)	116.22(17)
F(1)-C(3)-C(2)	117.5(2)		
C(4)-C(3)-C(2)	122.86(11)		
F(1)-C(3)-Cl(1)	8.1(2)		
C(4)-C(3)-Cl(1)	118.84(11)		
C(2)-C(3)-Cl(1)	118.20(11)		
C(3)-C(4)-C(5)	116.35(11)		
N(1)-C(5)-C(4)	122.02(11)		
N(1)-C(5)-C(7)	114.13(10)		
C(4)-C(5)-C(7)	123.85(10)		
O(4)-C(6)-O(3)	126.63(11)		
O(4)-C(6)-C(1)	118.09(11)		
O(3)-C(6)-C(1)	115.27(9)		
O(2)-C(7)-O(1)	127.06(11)		
O(2)-C(7)-C(5)	117.71(10)		
O(1)-C(7)-C(5)	115.23(9)		
N(2)-C(8)-C(9)	113.13(9)		
N(3)-C(9)-C(8)	110.43(9)		
N(3)-C(10)-C(11)	109.95(9)		
N(4)-C(11)-C(10)	111.51(9)		
N(4)-C(12)-C(13)	113.09(9)		
N(5)-C(13)-C(12)	110.87(9)		
N(5)-C(14)-C(15)	109.87(9)		
N(2)-C(15)-C(14)	111.42(9)		

Table 5. Anisotropic displacement parameters ($Å^2 x\ 10^4$) for MLC23 (CCDC 761002). The anisotropic displacement factor exponent takes the form: $-2\pi^2[h^2 a^{*2} U^{11} + ... + 2\ h\ k\ a^*\ b^*\ U^{12}]$

	U^{11}	U^{22}	U^{33}	U^{23}	U^{13}	U^{12}
Tb(1)	134(1)	221(1)	136(1)	19(1)	-16(1)	-6(1)
Cl(1)	719(7)	453(7)	442(5)	9(4)	-18(4)	-15(5)
O(1)	200(4)	274(4)	165(3)	36(3)	1(3)	3(3)
O(2)	362(5)	360(5)	219(4)	127(3)	37(4)	14(4)
O(3)	207(4)	287(4)	170(3)	2(3)	2(3)	-23(3)
O(4)	401(5)	401(5)	189(4)	-69(3)	50(4)	-25(4)
O(5)	173(4)	266(4)	164(3)	-3(3)	-30(3)	5(3)
O(6)	199(4)	241(4)	188(3)	33(3)	-46(3)	-20(3)
O(7)	172(4)	301(4)	164(3)	33(3)	-32(3)	-15(3)
O(8)	234(4)	371(5)	186(4)	-9(3)	-52(3)	8(4)
N(1)	159(4)	254(4)	164(4)	10(3)	-44(3)	-9(4)
N(2)	179(4)	252(5)	197(4)	-4(3)	-25(3)	1(4)
N(3)	171(4)	246(5)	229(4)	25(4)	-5(3)	-9(4)
N(4)	176(4)	288(5)	209(4)	57(4)	-8(3)	1(4)
N(5)	174(4)	247(5)	212(4)	12(3)	-9(3)	6(4)
C(1)	181(5)	293(6)	176(5)	-17(4)	-44(4)	-3(4)
C(2)	282(6)	312(6)	256(6)	-61(5)	-25(5)	27(5)
C(3)	367(7)	202(6)	374(7)	-9(5)	-60(6)	15(5)
C(4)	280(6)	288(6)	286(6)	61(5)	-31(5)	-3(5)
C(5)	175(5)	265(6)	197(5)	48(4)	-46(4)	2(4)
C(6)	193(5)	339(6)	164(5)	-23(4)	-25(4)	-18(5)
C(7)	183(5)	322(6)	179(5)	56(4)	-31(4)	7(4)
C(8)	226(6)	258(6)	275(6)	-33(4)	-38(5)	-34(5)
C(9)	175(5)	263(6)	288(6)	4(4)	-36(4)	-41(4)
C(10)	208(6)	271(6)	322(6)	80(5)	-2(5)	-24(5)
C(11)	214(6)	320(6)	250(6)	109(5)	14(4)	-12(5)
C(12)	225(6)	299(6)	294(6)	81(5)	-9(5)	38(5)
C(13)	171(5)	301(6)	262(5)	32(4)	-24(4)	48(4)
C(14)	209(6)	272(6)	277(6)	-37(5)	-14(5)	26(5)
C(15)	211(5)	294(6)	218(5)	-49(4)	-1(4)	21(4)
C(16)	215(5)	293(6)	176(5)	-11(4)	-42(4)	14(4)
C(17)	148(5)	226(5)	175(5)	13(4)	-18(4)	-42(4)
C(18)	208(5)	380(7)	174(5)	80(4)	-32(4)	-9(5)
C(19)	151(4)	314(6)	164(4)	0(4)	-7(3)	42(4)
N(6)	181(4)	211(4)	175(4)	-56(3)	-2(3)	-8(3)
C(20)	209(5)	206(5)	215(5)	-51(4)	1(4)	-24(4)
C(21)	382(7)	267(6)	246(6)	-26(5)	44(5)	-44(5)
C(22)	352(6)	260(6)	322(6)	30(5)	-66(5)	-37(6)
C(23)	418(8)	316(7)	410(8)	91(6)	-44(6)	-23(6)
C(24)	189(5)	260(6)	195(5)	-47(4)	-18(4)	-20(4)
C(25)	201(6)	333(6)	244(6)	-66(5)	-26(4)	18(5)
C(26)	262(6)	280(6)	273(6)	-3(5)	-59(5)	14(5)
C(27)	248(7)	422(8)	420(8)	-25(6)	-78(6)	63(6)
C(28)	220(5)	231(5)	172(5)	-40(4)	3(4)	7(4)
C(29)	295(6)	231(6)	257(6)	-29(4)	25(5)	10(5)

C(30)	321(7)	280(6)	279(6)	16(5)	25(5)	0(5)
C(31)	585(11)	350(8)	514(9)	137(7)	132(8)	3(7)
C(32)	197(5)	248(5)	202(5)	-75(4)	17(4)	6(4)
C(33)	208(5)	329(6)	245(5)	-102(5)	-7(4)	9(5)
C(34)	224(6)	468(8)	396(7)	-181(6)	5(5)	50(6)
C(35)	214(7)	608(10)	576(10)	-195(8)	-3(6)	70(7)
O(41)	377(5)	274(4)	197(3)	-19(3)	-69(3)	-69(4)
O(42)	423(6)	442(5)	254(4)	-3(4)	-102(4)	145(4)
O(51)	382(7)	675(8)	643(8)	-57(6)	-31(6)	-51(6)
C(51)	461(10)	646(12)	725(12)	-19(10)	42(9)	22(9)
C(52)	399(9)	676(11)	480(9)	-122(8)	-12(8)	71(8)
C(53)	558(14)	2270(30)	808(17)	690(20)	19(13)	157(19)

Table 6. Hydrogen bonds for MLC23 (CCDC 761002) [Å and °].

D-H...A	d(D-H)	d(H...A)	d(D...A)	<(DHA)
N(3)-H(3)...O(5)#1	0.93	2.31	3.1089(12)	144.0
N(3)-H(3)...O(6)#1	0.93	2.41	3.1876(12)	141.2
N(5)-H(5)...O(7)#2	0.93	2.22	3.0600(12)	149.4
N(5)-H(5)...O(8)#2	0.93	2.55	3.3037(12)	137.9
O(41)-H(41A)...O(6)	0.83	1.92	2.7457(11)	172.4
O(41)-H(41B)...O(4)#1	0.87	2.05	2.9239(12)	176.6
O(42)-H(42A)...O(8)#3	0.81	2.04	2.8477(12)	171.1
O(42)-H(42B)...O(2)#1	0.85	2.04	2.8888(13)	175.5

Symmetry transformations used to generate equivalent atoms:
#1 -x+1,-y+1,-z+1
#2 -x,-y+1,-z+1
#3 x+1,y,z

APPENDIX G

Characterization of DOAAM Ligand

DOAAM = *1,4,7,10*-tetraazacyclododecane-*1*-acetate-*7*-amide

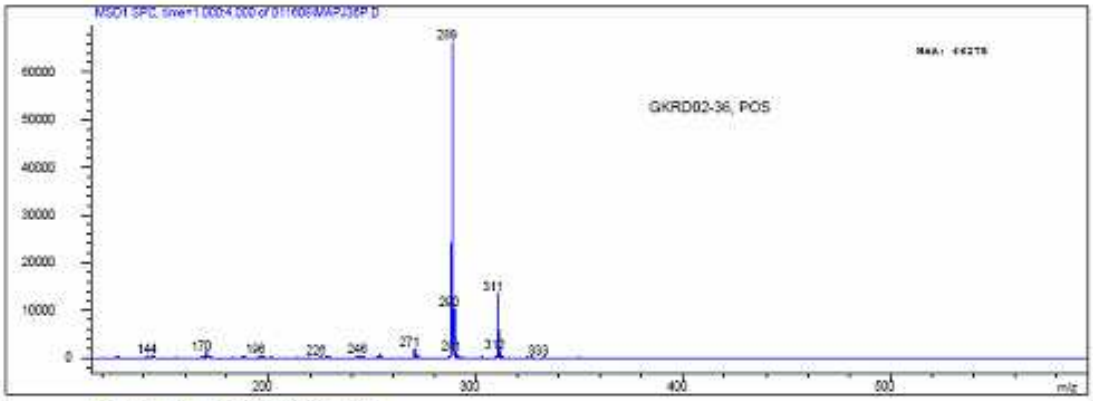

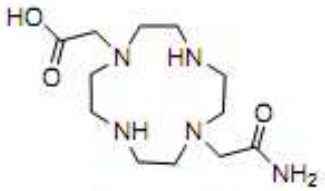

$C_{12}H_{25}N_5O_3$
Exact Mass: 287.2
m/e: 287.20 (100.0%), 288.20 (13.4%), 288.19 (1.8%), 289.20 (1.7%)

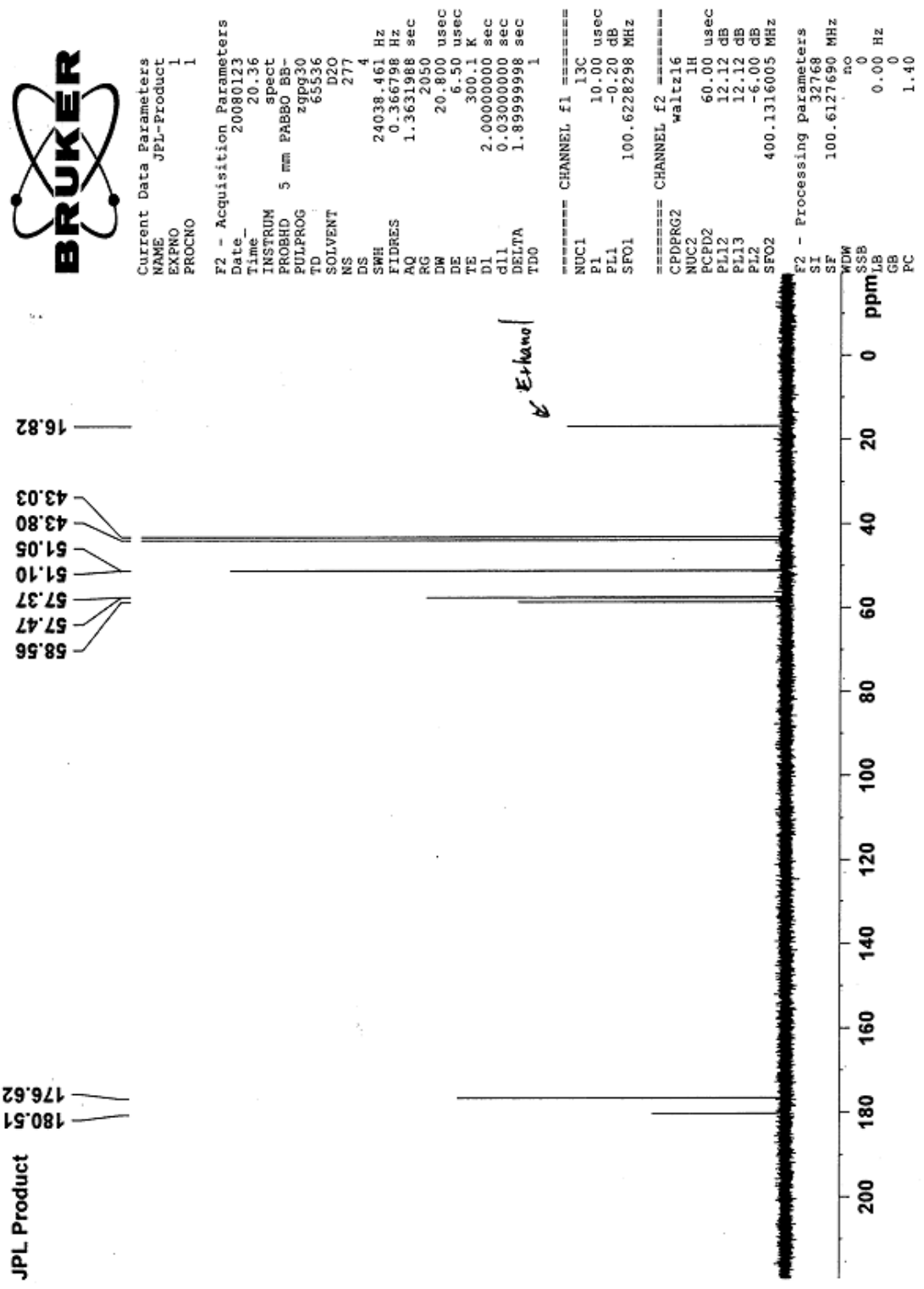
JPL Product
176.62
180.51
16.82
43.03
43.80
51.05
51.10
57.37
57.47
58.56
Ethanol
ppm
200
180
160
140
120
100
80
60
40
20
0
Current Data Parameters
NAME JPL-Product
EXPNO 1
PROCNO 1
F2 - Acquisition Parameters
Date_ 20080123
Time_ 20.36
INSTRUM spect
PROBHD 5 mm PABBO BB-
PULPROG zgpg30
TD 65536
SOLVENT D2O
NS 277
DS 4
SWH 24038.461 Hz
FIDRES 0.366798 Hz
AQ 1.3631988 sec
RG 2050
DW 20.800 usec
DE 6.50 usec
TE 300.1 K
D1 2.00000000 sec
d11 0.03000000 sec
DELTA 1.89999998 sec
TD0 1
======== CHANNEL f1 ========
NUC1 13C
P1 10.00 usec
PL1 -0.20 dB
SFO1 100.6228298 MHz
======== CHANNEL f2 ========
CPDPRG2 waltz16
NUC2 1H
PCPD2 60.00 usec
PL12 12.12 dB
PL13 12.12 dB
PL2 -6.00 dB
SFO2 400.1316005 MHz
F2 - Processing parameters
SI 32768
SF 100.6127690 MHz
WDW no
SSB 0
LB 0.00 Hz
GB 0
PC 1.40

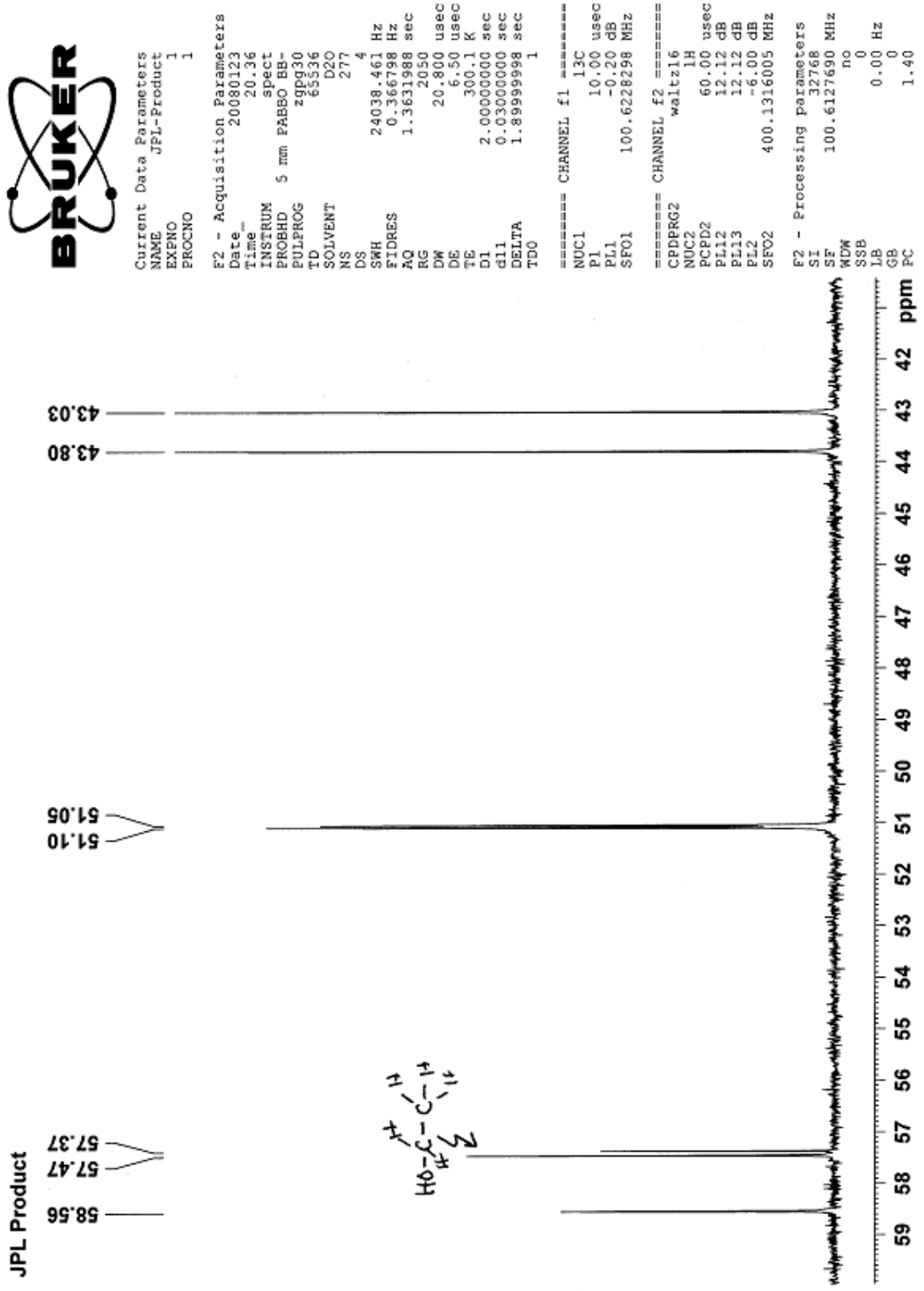
JPL Product
58.56
57.47
57.37
51.10
51.05
43.80
43.03
ppm
Current Data Parameters
NAME JPL-Product
EXPNO 1
PROCNO 1
F2 - Acquisition Parameters
Date_ 20080123
Time_ 20.36
INSTRUM spect
PROBHD 5 mm PABBO BB-
PULPROG zgpg30
TD 65536
SOLVENT D2O
NS 277
DS 4
SWH 24038.461 Hz
FIDRES 0.366798 Hz
AQ 1.3631988 sec
RG 2050
DW 20.800 usec
DE 6.50 usec
TE 300.1 K
D1 2.00000000 sec
d11 0.03000000 sec
DELTA 1.89999998 sec
TD0 1
======== CHANNEL f1 ========
NUC1 13C
P1 10.00 usec
PL1 -0.20 dB
SFO1 100.6228298 MHz
======== CHANNEL f2 ========
CPDPRG2 waltz16
NUC2 1H
PCPD2 60.00 usec
PL12 12.12 dB
PL13 12.12 dB
PL2 -6.00 dB
SFO2 400.1316005 MHz
F2 - Processing parameters
SI 32768
SF 100.6127690 MHz
WDW no
SSB 0
LB 0.00 Hz
GB 0
PC 1.40

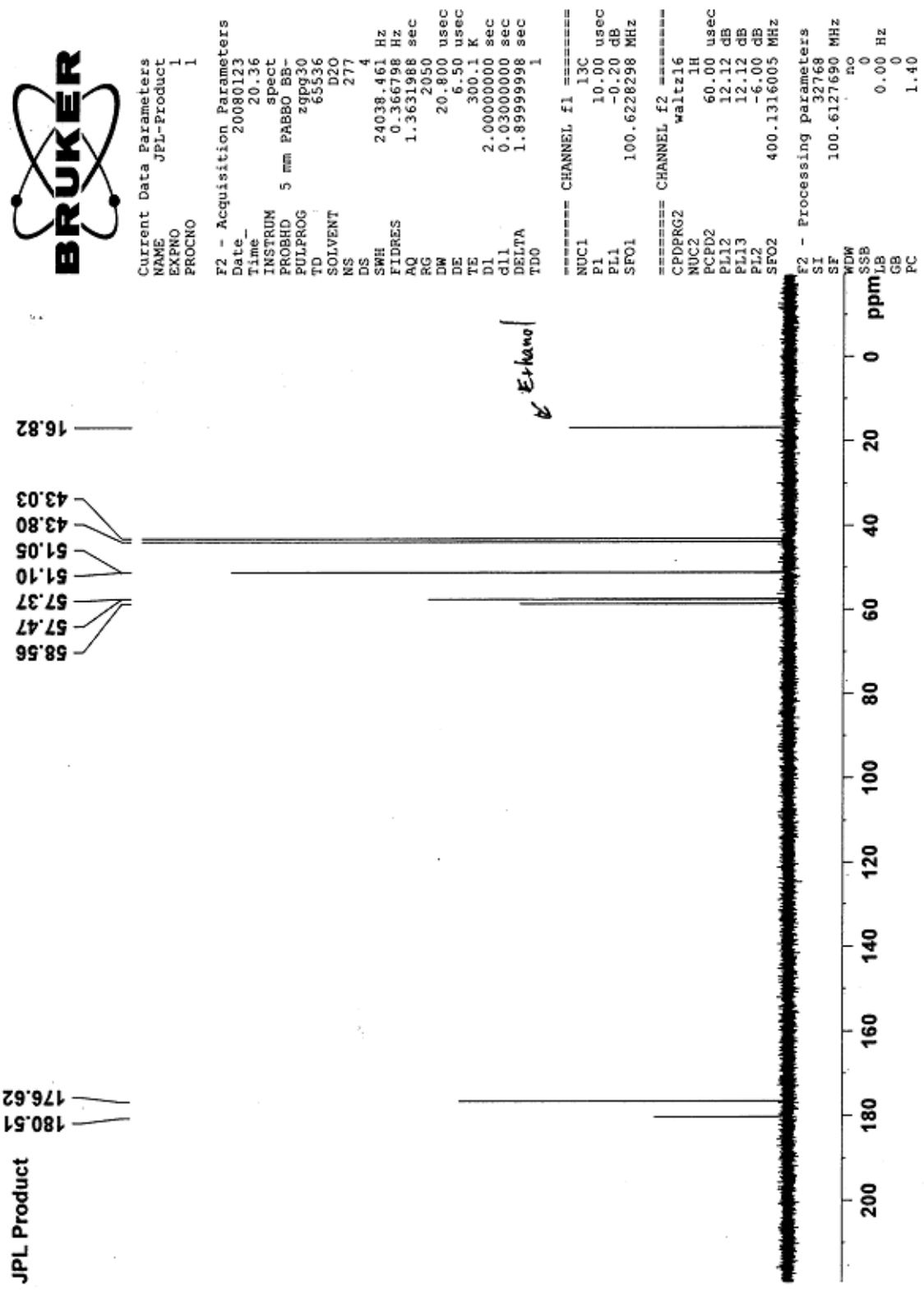
JPL Product
176.62
180.51
16.82
43.03
43.80
51.05
51.10
57.37
57.47
58.56
Ethanol
ppm
Current Data Parameters
NAME JPL-Product
EXPNO 1
PROCNO 1
F2 - Acquisition Parameters
Date_ 20080123
Time_ 20.36
INSTRUM spect
PROBHD 5 mm PABBO BB-
PULPROG zgpg30
TD 65536
SOLVENT D2O
NS 277
DS 4
SWH 24038.461 Hz
FIDRES 0.366798 Hz
AQ 1.3631988 sec
RG 2050
DW 20.800 usec
DE 6.50 usec
TE 300.1 K
D1 2.00000000 sec
d11 0.03000000 sec
DELTA 1.89999998 sec
TD0 1
======== CHANNEL f1 ========
NUC1 13C
P1 10.00 usec
PL1 -0.20 dB
SFO1 100.6228298 MHz
======== CHANNEL f2 ========
CPDPRG2 waltz16
NUC2 1H
PCPD2 60.00 usec
PL12 12.12 dB
PL13 12.12 dB
PL2 -6.00 dB
SFO2 400.1316005 MHz
F2 - Processing parameters
SI 32768
SF 100.6127690 MHz
WDW no
SSB 0
LB 0.00 Hz
GB 0
PC 1.40

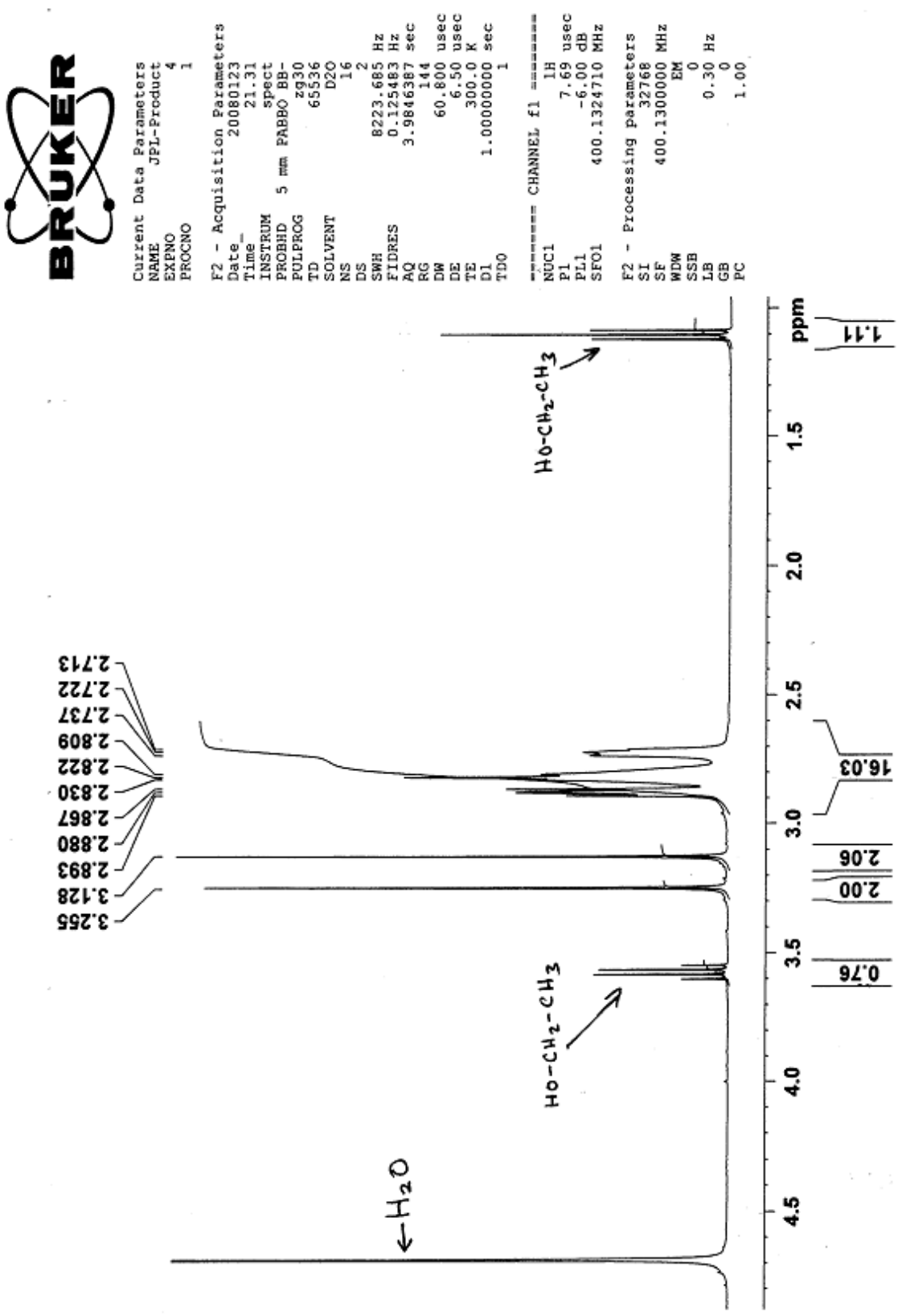
BRUKER
Current Data Parameters
NAME JPL-Product
EXPNO 4
PROCNO 1
F2 - Acquisition Parameters
Date_ 20080123
Time_ 21.31
INSTRUM spect
PROBHD 5 mm PABBO BB-
PULPROG zg30
TD 65536
SOLVENT D2O
NS 16
DS 2
SWH 8223.685 Hz
FIDRES 0.125483 Hz
AQ 3.9846387 sec
RG 144
DW 60.800 usec
DE 6.50 usec
TE 300.0 K
D1 1.00000000 sec
TD0 1
======== CHANNEL f1 ========
NUC1 1H
P1 7.69 usec
PL1 -6.00 dB
SFO1 400.1324710 MHz
F2 - Processing parameters
SI 32768
SF 400.1300000 MHz
WDW EM
SSB 0
LB 0.30 Hz
GB 0
PC 1.00
←H2O
HO-CH2-CH3
HO-CH2-CH3
3.255
3.128
2.893
2.880
2.867
2.830
2.822
2.809
2.737
2.722
2.713
4.5
4.0
3.5
3.0
2.5
2.0
1.5
ppm
0.76
2.00
2.06
16.03
1.11